

# INDIAN JOURNAL OF PHYSICS

VOL. 34

AND

## PROCEEDINGS

OF THE

Indian Association for the Cultivation of Science, Vol. 43

*(Published in Collaboration with the Indian Physical Society)*

( With Eleven Plates )

Printed by Kalipada Mukherjee, Eka Press, 204/1, B. T. Road, Calcutta  
and published by the Registrar, Indian Association for the Cultivation  
of Science, Jadavpur, Calcutta 32

**1960**

## BOARD OF EDITORS

K. BANERJEE	D. S. KOTHARI
D. M. BOSE	S. K. MITRA
S. N. BOSE	K. R. RAO
P. S. GILL	D. B. SINHA
S. R. KHASTGIR	S. C. SIKKAR ( <i>Secretary</i> )

B. N. SRIVASTAVA

## EDITORIAL COLLABORATORS

PROF. D. BASU, PH.D.
PROF. J. N. BHAR, D.Sc., F.N.I.
PROF. A. BOSH, D.Sc. F.N.I.
DR. K. DASGUPTA, PH.D.
PROF. N. N. DASGUPTA, PH.D., F.N.I.
PROF. A. K. DUTTA, D.Sc., F.N.I.
DR. S. N. GHOSH, D.Sc.
PROF. P. K. KICILU, D.Sc., F.N.I.
DR. K. S. KRISHNAN, D.Sc., F.R.S.
PROF. D. N. KUNDU, PH.D.
PROF. B. D. NAG CHOWDHURY, PH.D.
PROF. S. R. PALIT, D.Sc., F.R.I.C., F.N.I.
DR. H. RAKSHIT, D.Sc., F.N.I.
DR. R. GOPALAMURTY RAO.
PROF. A. SAHA, D.Sc., F.N.I.
DR. VIKRAM A. SARABHAI, M.A., PH.D.
DR. A. K. SENGUPTA, D.Sc.
DR. M. S. SINHA, D.Sc.
PROF. N. R. TAWDE, D.Sc., F.N.I.
DR. P. VENKATESWARLU.

ASSISTANT EDITOR

DR. MONOMOHAN MAZUMDER, M.Sc., D.Phil.

---

*Annual Subscription—*

Inland Rs. 25/-  
Foreign £ 2 10-0 or 7

## NOTICE

### TO INTENDING AUTHORS

1. Manuscripts for publication should be sent to the Assistant Editor, Indian Journal of Physics, Jadavpur, Calcutta-32.

2. The manuscripts submitted must be type-written with double space on thick foolscap paper with sufficient margin on the left and at the top. The original copy, and not the carbon copy, should be submitted. Each paper must contain an **ABSTRACT** at the beginning.

3. All **REFERENCES** should be given in the text by quoting the surname of the author, followed by year of publication, e.g., (Roy, 1958). The full **REFERENCE** should be given in a list at the end, arranged alphabetically, as follows; MAZUMDER, M. 1959, *Ind. J. Phys.*, **33**, 346.

4. Line diagrams should be drawn on white Bristol board or tracing paper with black Indian ink, and letters and numbers inside the diagrams should be written neatly in capital type with Indian ink. The size of the diagrams submitted and the lettering inside should be large enough so that it is legible after reduction to one-third the original size. A simple style of lettering such as gothic, with its uniform line width and no serifs should be used, e.g.,

A·B·E·F·G·M·P·T·W·

5. Photographs submitted for publication should be printed on glossy paper with somewhat more contrast than that desired in the reproduction.

6. Captions to all figures should be typed in a separate sheet and attached at the end of the paper.

7. The mathematical expressions should be written carefully by hand. Care should be taken to distinguish between capital and small letters and superscripts and subscripts. Repetition of a complex expression should be avoided by representing it by a symbol. Greek letters and unusual symbols should be identified in the margin. Fractional exponents should be used instead of root signs.

# INDIAN JOURNAL OF PHYSICS, 34, 1960

## CONTENTS

### No. 1. January

	PAGE
1. On the infrared Spectra of Mesitylene in the Vapour and liquid States and in Solutions—S. B. Banerjee and K. C. Medhi ... ..	1
2. A Preliminary Note on the Magnetic Anisotropy and Susceptibility of $\text{Fe}(\text{NH}_4\text{SO}_4)_2 \cdot 6\text{H}_2\text{O}$ —A. S. Chakravarty and R. Chatterjee ..	10
3. Infrared Absorption Spectra of Diamonds of Different Types—S. C. Sirkar ... ..	13
4. On the Variation of the Transport Factor of a Junction Transistor with Injected Carrier Concentration—A. N. Daw ... ..	20
5. Frequency of the Three-Phase R-C Coupled Oscillator. Part II. Inductive Anode Load Resistance—H. Rakshit and M. C. Mallik ...	36

#### LETTER TO THE EDITOR—

1. Dipole Moments of long Chain Dicarboxylic Acids—R. J. R. Mohan Rao and S. R. Palit ... ..	55
--	----

BOOK REVIEWS ... ..	57
---------------------	----

### No. 2. February

6. On the Electronic Spectra of $\alpha$ -Fluoronaphthalene in the Liquid and Solid States—S. B. Banerjee ... ..	61
7. On the $F_2$ -Region of the Ionosphere—S. Datta ... ..	66
8. Intermolecular Potential of Helium—A. K. Barua ... ..	76
9. M. U. F. Factor and Solar Activity—C. S. R. Rao and J. C. Bhargava	85
10. Fourth Order Meson Equation and Neutron-Proton Scattering—S. P. Misra ... ..	92

#### LETTER TO THE EDITOR :

2. Search for EO Transition in Zinc-68—M. K. Ramaswamy ...	98
--	----

BOOK REVIEWS ... ..	100
---------------------	-----

### No. 3. March

11. A Microwave Analogue for X-ray Diffraction. Part I. Effect of the Crystallite Size—G. B. Mitra and G. S. Sanyal ... ..	103
12. Oscillations of Rotating Cosmical Bodies in the Presence of Magnetic Field—J. N. Tandon ... ..	107
13. An Arc Type Water-Cooled Ion Source for Positive Ions—S. Z. R. Hashmi ... ..	118
14. The Emission Band System of Iodine in the Blue Violet—P. B. V. Haranath and T. A. Prasada Rao ... ..	123

	PAGE
15. On Zero Mass Meson-Meson Scattering—B. Deo ... ..	131
16. Force Constants for Unlike Molecular Interactions on Exp-six Model from Inter-Diffusion—R. Paul ... ..	141
LETTER TO THE EDITOR—	
3. Anisotropy of Water Cluster About the $\text{Cu}^{++}$ Ion—A. Mookherji and M. S. Chhonkar ... ..	147
4. Application of Sign Relations in the case of 4,1,3-Chloro-Dinitro- Benzene—E. M. Gopalakrishna ... ..	149
BOOK REVIEWS ... ..	152

### No. 4. April

17. Influence of Geomagnetic Field on Extensive Air Showers of Cosmic Radiation—A. Bhaskara Rao and P. S. Gill ... ..	153
18. On Fermion Loops of Two Vertices—B. Deo ... ..	159
19. Thermal Conductivity and Eucken-Type Factor for the Binary Mix- tures H-He, H-Ne, H-Kr and H-Xe—A. K. Barua ... ..	169
20. Statistical Structure of Anthrone—K. Banerjee and S. N. Srivastava ... ..	184
21. Optimum Conditions to Observe the New Light Effect—P. S. V. Setty ... ..	187

### LETTERS TO THE EDITOR—

5. Absorption Spectra of <i>O</i> -, <i>M</i> - and <i>P</i> -Hydroxy Benzaldehydes—I. Achyuta Rao and V. Ramakrishna Rao ... ..	196
6. Induced Lightning Strokes—S. D. Chatterjee and B. K. Dutta ... ..	198
7 The Near Ultraviolet Absorption Spectra of <i>M</i> - and <i>P</i> -Methyl Anisoles —K. V. Kameswara Rao and V. Ramakrishna Rao ... ..	200
BOOK REVIEWS ... ..	201

### No. 5. May

22. Penetration Factor in Alpha-Decay—S. K. Dutta, T. K. Mitra and N. C. Sil ... ..	205
23. Gravitational Field of Distant Rotating Masses—Ramesh V. Wagh ... ..	211
24. Dielectric Relaxation in Relation to Temperature II—J. Sobhanadri ... ..	217
25. Fourth Order Scattering Matrix Elements of Nucleons with a Fourth Order Meson Equation—S. P. Misra ... ..	221
26. Ultraviolet Absorption Spectra of Isomeric Fluorotoluenes in the Liquid and Solid States—S. K. Sen ... ..	237
27. Raman Spectra of Ortho- and Para-chloroanisole in the Solid State at $-180^{\circ}\text{C}$ —Krishna Kumar Deb ... ..	247
BOOK REVIEW ... ..	253



**No. 6. June**

28. Determination of the Elastic Constants of Tetragonal (4, 4, 4/m) Crystals from the Study of Diffuse X-Ray Reflections—R. C. Srivastava and S. C. Chakraborty	253
29. Splitting of Neutron Energy Levels Due to Spin-Orbit Coupling—Arundhati Ghosh	260
30. Space Groups of Crystals of Ortho, Meta and Paraxylene at—180°C—S. G. Biswas	263
31. Ultrasonic Velocity in Supercooled Liquids—S. Parthasarathy and V. N. Bindal	272
32. Ultraviolet Band Spectra of AsO and AsO <sup>+</sup> —S. V. J. Lakshman and P. Tiruvenganna Rao	278

**LETTERS TO THE EDITOR—**

8. The Near Ultraviolet Absorption Spectra of the Three Isomeric Methyl Phenetoles—K. V. Kameswara Rao and V. Ramakrishna Rao	289
9. Structure of Naphthazarin C <sub>10</sub> H <sub>4</sub> O <sub>2</sub> (CH) <sub>2</sub> —P. Srivastava	290

**No. 7. July**

33. Transistor Drive Circuits for Dekatrons—K. S. Patel and B. M. Banerjee	293
34. X-Ray Study of Crystallite Orientation in Agave Americana—Anand Prakash and V. D. Gupta	299
35. Some Observations on the Energy Spectrum of low Energy Bremsstrahlung from Electrons of Energy $\leq 10^{12}$ eV—P. K. Aditya	302
36. A High Intensity Neutron Generator—S. K. Mukherjee, N. K. Majumder and A. Ganguly	307
37. Infrared Spectra of Uranyl Phosphate, Oxalate and Salicylate in the Solid State—K. V. Narasimham	321
38. Singlet→Triplet Absorption in Halogen Substituted Toluenes—J. K. Roy	331

**LETTER TO THE EDITOR—**

10. Light Absorption in Paramagnetic Co <sup>++</sup> Ions in State of Solution A. Mookherji and N. S. Chhonkar	336
---	-----

**No. 8. August**

39. Nuclear Spin Echoes and Molecular Self-Diffusion in Liquids—S. K. Ghosh and S. K. Sinha	339
40. Absorption of Microwaves in Cyclohexanol and Cyclopentanol and their Solutions—T. J. Bhattacharyya	358

	PAGE
41. Light Absorption in Paramagnetic Ions in State of Solution Part II --Ni <sup>++</sup> ion—A. Mookherji and N. S. Chhonkar ...	363
42. On the Electronic Spectra of 2-Bromo and 3-Bromopyridine in Different States and in Solutions—T. N. Misra ...	381

LETTER TO THE EDITOR—

11. On Thermal Conductivity of Aluminium at Low Temperatures—H. N. Patil ...	395
--	-----

**No. 9. September**

43. Estimation of ( $\Delta E_g$ ) of an Electronic Band System—A New Method —N. R. Tawde and A. P. Walvekar ...	397
44. Raman Spectra of Fluorobenzene at Different Low Temperatures—Deb Kumar Mukherjee ...	402
45. A Two-Directional Focussing High-Intensity Mass-Spectrometer —S. B. Karmohapatro ...	407
46. Thermal Expansion of Some Alkali Halides by X-Ray Diffraction— P. D. Pathak and N. V. Pandya ...	416
47. Choice of Sampled Waves for Time-Division Multiplex Telephone Systems—P. N. Das ...	424

LETTERS TO THE EDITOR—

12. Force Constants of the Uranyl Ion by Wilson's F-G Matrix Method —K. V. Narasimham ...	432
13. Phase-Transitions in $\text{Cu}[(\text{NH}_4)\text{SO}_4]_2 \cdot 6\text{H}_2\text{O}$ —(Miss) Gouri Bhowmik ...	433
14. F-G Matrix Elements for Pyramidal $\text{XY}_2\text{Z}$ Molecules—P. Babu Rao and K. Sreeramamurty ...	434
BOOK REVIEWS ...	434

**No. 10. October**

48. An Isotope Effect in the Collection on the Charged Plates of ( $n, \gamma$ ) Recoil Products of Bromine—H. J. Arnika and A. Lal ...	441
49. Thermal Diffusion Factor for Hydrogen and Water Mixtures—S. C. Saxena ...	449
50. A Note on Heat Transfer and Film Boiling—R. D. Rao, H. S. Desai and D. V. Gogate ...	456
51. The Dielectric Properties of Copal Ester—A. K. Sen and G. N. Bhattacharya ...	461
52. The Lifetime of Hyperfragments—G. C. Deka ...	470
53. Impedance Matching by Re-entrant Stub Line—G. S. Sanyal ...	475
54. Some Studies on the Spread-F, Double-F and Forked-F Traces as Observed at Haringhata (Calcutta)—R. N. Datta ...	482

## *Contents*

PAGE

### **No. 11. November**

55. Day to Day Changes in the Daily Mean Intensity of Cosmic Rays— R. P. Kane, S. R. Kane and B. A. Holla ... ..	493
56. An X-ray Study of Silver-Cadmium Alloys—Md. Abdul Quader ... ..	506
57. Ionization of E-Layer by X-rays—S. N. Ghosh and Sharda Nand ... ..	516
58. Analysis of Random Fading Records—S. R. Khastgir and R. N. Singh ... ..	527

#### **LETTERS TO THE EDITOR—**

15. Latitude Dependence of Nucleonic intensity During August 24—September 20—Lekh Vir and P. S. Gill ... ..	531
16. Debye $\Theta$ of Some Crystals—S. K. Joshi and S. S. Mitra ... ..	532
17. Magnetism of the Iron Particles as Revealed by Electron Diffraction —S. Yamaguchi .. .. .	535
<b>BOOK REVIEWS</b> ... .. .	538

### **No. 12. December**

59. Intermolecular Potential and Properties of Argon—I. B. Srivastava ... ..	539
60. A Note on some Tunable Oscillators—N. B. Chakraborty and K. D. Dixit ... ..	549
61. Raman, Infrared and Luminescence Spectra of some Trisubstituted Benzenes—K. K. Deb and S. B. Banerjee ... ..	554
62. Ultrasonic Velocity in some Aqueous Solutions of Electrolytes—P. R. K. L. Padmini and B. Ramachandra Rao ... ..	565
63. Dipole Moment and Relaxation time of certain Tri-Substituted Benzenes —J. Sobhandari ... .. .	577
64. On the Singlet→Triplet Absorption in Aromatic Compounds in Gaseous State—S. C. Sirkar and J. K. Roy ... ..	581

#### **LETTER TO THE EDITOR—**

18. On the Variation of Electronic Transition moment $R_e$ in CN Violet band Systems—S. S. Prasad ... ..	584
<b>BOOK REVIEWS</b> ... .. .	586



# AUTHOR INDEX

AUTHOR	SUBJECT	PAGE
Aditya, P. K.	Some observations on the energy spectrum of low energy Bremsstrahlung from electrons of energy $\leq 10^{12}$ eV	302
Arunkar, H. J. and Lal, A.	An isotope effect in the collection on the charged plates of $(n, \gamma)$ recoil products of bromine	441
Bauerjee, B. M.	See Patel K. S.	
Banerjee, K. and Srivastava, S. N.	Statistical structure of anthrone	184
Banerjee, S. B.	On the electronic spectra of $\alpha$ -fluoronaphthalene in the liquid and solid state	61
Banerjee, S. B. and Medhi, K. C.	On the infrared spectra of mesitylene in the vapour and liquid states and in solutions	1
	See Deb K. K.	
Barua, A. K.	Intermolecular potential of Helium	76
	Thermal conductivity and Eucken-type factor for the binary mixtures H-He, H-Ne, H-Kr and H-Xe	169
Bhargava, J. C.	See Rao, C. S. R.	
Bhattacharya, G. N.	See Sen, A. K.	
Bhattacharyya, T. J.	Absorption of microwaves in cyclohexanol and cyclopentanol and their solutions	358
Bhowmik, (Miss) Gouri	Phase-transitions in $\text{Cu}[(\text{NH}_4)\text{SO}_4]_2 \cdot 6\text{H}_2\text{O}$ (L)	433
Bindal, V. N.	See Parthasarathy, S	
Biswas, S. G.	Space groups of crystals of ortho, meta and paraxylene at $-180^\circ\text{C}$	263
Chakravarty, A. S. and Chatterjee, R.	A preliminary note on the magnetic anisotropy and susceptibility of $\text{Fe}(\text{NH}_4\text{SO}_4)_2 \cdot 6\text{H}_2\text{O}$	10
Chakraborty, N. B. and Dixit, K. D.	A note on some tunable oscillators	549
Chakraborty, S. C.	See Srivastava, R. C.	
Chatterjee, R.	See Chakravarty, A. S.	
Chatterjee, S. D. and Dutta, B. K.	Induced lightning strokes (L)	198

AUTHOR	SUBJECT	PAGE
Chhonkar, N. S.	See Mookherji, A.	
Das, P. N.	Choice of sampled waves for time-division multiplex telephone systems	424
Datta, R. N.	Some studies on the Spread-F, Double-F and Forked-F traces as observed at Haringhata (Calcutta)	482
Datta, S.	On the F <sub>2</sub> -region of the ionosphere	66
Daw, A. N.	On the variation of the transport factor of a junction transistor with injected carrier concentration	20
Deb, Krisilua Kumar	Raman spectra of ortho- and para-chloroaniline in the solid state at -180°C	247
Deb, K. K. and Banerjee, S. B.	Raman, infrared and luminescence spectra of some trisubstituted benzenes	554
Deka, G. C.	The lifetime of hyperfragments	470
Deo, B.	On zero mass meson-meson scattering	131
"	On fermion loops of two vertices	159
Desai, H. S.,	See Rao, R. D.	
Dixit, K. D.	See Chakraborty, N. B.	
Dutta, B. K.	See Chatterjee, S. D.	
Dutta, S. K., Mitra, T. K. and Sil, N. C.	Penetration factor in alpha-decay	205
Ganguly, A.	See Mukherjee, S. K.	
Ghosh, Arundhati	Splitting of neutron energy levels due to spin-orbit coupling	260
Ghosh, S. K. and Sinha, S. K.	Nuclear spin echoes and molecular self-diffusion in liquids	339
Ghosh, S. N. and Nand, Sharda	Ionization of E-layer by X-rays	516
Gill, P. S.	See Rao Bhaskara, A.	
"	See Vir, Lekh	
Gogate, D. V.	See Rao, R. D.	
Gopalakrishna, E. M.	Application of sign relation in the case of 4, 1, 3-chloro-dinitrobenzene (L)	149
Gupta, V. D.	* See Prakash, Anand	
Haranath, P. B. V. and T. A. Prasad Rao	The emission band system of iodine in the blue violet	123
Hashmi, S. Z. R.	An arc type water-cooled ion source for positive ions	118

AUTHOR	SUBJECT	PAGE
Holla, B. A.	See Kane, R. P.	
Joshi, S. K. and Mitra, S. S.	Debye $\Theta$ of some crystals (L)	532
Kane, R. P., Kane, S. R. and Holla, B. A.	Day to day changes in the daily mean intensity of cosmic rays	493
Kane, S. R.	See Kane, R. P.	
Karmohapatro, S. B.	A two directional focussing high-intensity mass-spectrometer	407
Khastgir, S. R. and Singh, R. N.	Analysis of random feeding records	527
Lakshman, S. V. J. and P. Tiruvenganna Rao	Ultraviolet band spectra of $\text{AsO}$ and $\text{AsO}^+$	278
Lal, A.	See Arnikar, H. J.	
Mallik, M. C.	See Rakshit, H.	
Majumder, N. K.	See Mukherjee, S. K.	
Medhi, K. C.	See Banerjee, S. B.	
Misra, S. P.	Fourth order meson equation and neutron-proton scattering	92
	Fourth order scattering matrix elements of nucleons with a fourth order meson equation	221
Misra, T. N.	On the electronic spectra of 2-bromo and 3-bromopyridine in different states and in solutions	381
Mitra, G. B. and Sanyal, G. S.	A microwave analogue for X-ray diffraction. Part I. Effect of the crystallite size	103
Mitra, T. K.	See Dutta, S. K.	
Mitra, S. S.	See Joshi, S. K.	
Mookherji, A. and Chhonkar, N. S.	Anisotropy of water cluster about the $\text{Cu}^{++}$ ion (L)	147
	Light absorption in paramagnetic $\text{Co}^{++}$ ions in state of solution (L)	336
	Light absorption in paramagnetic ions in state of solution Part II $\text{Ni}^{++}$ ion	363
Mukherjee, Deb Kumar	Raman spectra of fluorobenzene at different low temperatures	402
Mukherjee, S. K., Majumder, N. K. and Ganguly, A.	A high intensity neutron generator	307
Nand, Sharda	See Ghosh, S. N.	
Narashimham, K. V.	Infrared spectra of uranyl phosphate, oxalate and salicylate in the solid state	321

AUTHOR	SUBJECT	PAGE
Narashinham, K. V.	Force constants of the uranyl ions by Wilson's F-G matrix method (L)	432
Padmini, P. R. K. L. and Rao, B. Ramachandra	Ultrasonic velocity in some aqueous solutions of electrolytes	565
Palit, S. R.	See Rao Mohan, R. J. R.	
Pandya, N. V.	See Pathak, P. D.	
Parthasarathy, S. and Bindal, V. N.	Ultrasonic velocity in supercooled liquids	272
Patel, K. S. and Banerjee, B. M.	Transistor drive circuits for dekatrons	293
Pathak, P. D. and Pandya, N. V.	Thermal expansion of some alkali halides by X-ray diffraction	416
Patil, H. N.	On thermal conductivity of aluminium at low temperature (L)	395
Paul, R.	Force constants for unlike molecular interactions on exp-six model from interdiffusion	141
Prakash, Anand and Gupta, V. D.	X-ray study of crystallite orientation in agave Americana	299
Parasad, S. S.	On the variation of electronic transition moment $R_e$ in CN violet band systems (L)	584
Quader, Md. Abdul	An X-ray study of silver-cadmium alloys	506
Rakshit, H. and Mallik, M. C.	Frequency of the three-phase R-C coupled oscillator. Part II. Inductive anode load resistance	36
Ramaswamy, M. K.	Search for EO transition in zinc-68 (L)	98
Rao, Achuta, I and Rao, V. Ramakrishna	Absorption spectra of <i>o</i> -, <i>m</i> - and <i>p</i> -hydroxy benzaldehydes (L)	196
Rao, Babu P. and K. Sroeramamurty	F-G matrix elements for pyramidal $XY_2Z$ molecule (L)	434
Rao Bhaskara, A. and Gill, P. S.	Influence of geomagnetic field on extensive air showers of cosmic radiation	153
Rao, C. S. R. and J. C. Bhargava	M.U.F. factor and solar activity	85
Rao, K. V. Kameswara and Rao, V. Ramakrishna	The near ultraviolet absorption spectra of <i>m</i> - and <i>p</i> -methyl anisoles (L)	200
Rao, Kameswara, K. T. and Rao V. Ramakrishna	The near ultraviolet absorption spectra of the three isomeric methyl phenetoles (L)	289



AUTHOR	SUBJECT	PAGE
Rao, Mohan, R. J. R. and Palit, S. R.	Dipole moments of long chain dicar- boxylic acids (L)	55
Rao, Prasada, T. A.	See Haranath, P. B. V.	
Rao, R. D., Desai, H. S. and Gogate, D. V.	A note on heat transfer and film boiling	456
Rao, Ramakrishna, V.	See Rao, Achuta. I. See Rao, Kameswara, K. V.	
	"	
Rao, Ramchandra. B.	See Padmini, P. R. K. L.	
Rao, Tiruvenganna, P.	See Lakshman, S. V. J.	
Roy, J. K.	Singlet→triplet absorption in halogen substituted toluenes	331
	See Sirkar, S. C.	
Sanyal, G. S.	See Mitra, G. B.	
"	Impedance matching by re-entrant stub line	475
Saxena, S. C.	Thermal diffusion factor for hydrogen and water mixtures	449
Sen, S. K.	Ultraviolet absorption spectra of iso- meric fluorotoluenes in the liquid and solid states	237
Sen, A. K. and Bhattacharyya, G. N.	The dielectric properties of Copal ester	461
Setty, P. S. V.	Optimum conditions to observe the new light effect	187
Sil, N. C.	See Dutta, S. K.	
Singh, R. N.	See Khastgir, S. R.	
Sinha, S. K.	See Ghosh, S. K.	
Sirkar, S. C.	Infrared absorption spectra of dia- monds of different types	13
Sirkar, S. C. and Roy, J. K.	On the singlet→triplet absorption in aromatic compounds in gaseous state	581
Sobhanadri, J.	Dielectric relaxation in relation to temperature. II. Dipolemoment and relaxation time of certain tri-substituted benzens	217 577
Sreeramamurty, K.	See Rao, Babu. P.	
Srivastava, I. B.	Intermolecular potential and pro- perties of argon	539
Srivastava, P.	Structure of naphthazarin $C_{10}H_4O_2$ (CH) <sub>2</sub> . (L)	290

AUTHOR	SUBJECT	PAGE
Srivastava, R. C. and Chakraborty, S. C.	Determination of the elastic constants of tetragonal (4, 4, 4/m) crystals from the study of diffuse X-ray reflections	253
Srivastava, S. N.	See Banerjee, K.	
Tandon, J. N.	Oscillations of rotating cosmical bodies in the presence of magnetic field	107
Tawde, N. R. and Walvekar, A. P.	Estimation of ( $\Delta r_0$ ) of an electronic band system—a new method	397
Vir, Lekh and Gill, P. S.	Latitude dependence of nucleonic intensity during August 24—September 20. (L)	531
Wagh, Ramesh. V.	Gravitational field of distant rotating masses	211
Walvekar, A. P.	See Tawde, N. R.	
Yamaguchi, S.	Magnetism of the iron particle as revealed by electron diffraction (L)	535

# SUBJECT INDEX

SUBJECT	AUTHOR	PAGE
Absorption of microwaves in cyclohexanol and cyclopentanol and their solutions	T. J. Bhattacharyya	358
Anisotropy of water cluster about the $Cu^{++}$ ion (L)	A. Mookherji and N. S. Chhonkar	147
Bremsstrahlung from electrons of energy $\lesssim 10^{12}$ eV. Some observations on the energy spectrum of low energy	P. K. Aditya	302
Daily mean intensity of cosmic ray. Day to day changes in the	R. P. Kane, S. R. Kane, and B. A. Holla	493
Debye $\Theta$ of some crystals (L)	S. K. Joshi and S. S. Mitra	532
Dielectric properties of copal ester. The	A. K. Sen and G. N. Bhattacharyya	461
Dielectric relaxation in relation to temperature. II	J. Sobhanadri	217
Dipole moments of long chain dicarboxylic acids (L)	R. J. R. Mohan Rao and S. R. Palit	55
Dipole moment and relaxation time of certain tri-substituted benzenes	J. Sobhanadri	577
Elastic constants of tetragonal (4, 4, 4/m) crystals from the study of diffuse X-ray reflections. Determination of the	R. C. Srivastava and S. C. Chakraborty	253
Electronic band system. Estimation of $(\Delta r_e)$ of an. A new method.	N. R. Tawde and A. P. Wulvekar	397
Electronic transition moment $R_e$ in CN violet band systems. On the variation of (L)	S. S. Prasad	584
EO-transition in Zinc-68. Search for (L)	M. K. Ramaswamy	98
Extensive air showers of cosmic radiation. Influence of Geomagnetic field on	A. Bhaskara Rao and P. S. Gill	153
Fermion loops of two vertices. On	B. Deo	159
F-G matrix elements for pyramidal $XY_2Z$ molecules (L)	P. Babu Rao and K. Sreeramamurthy	434
Force constants for unlike molecular interaction on exp-six model from inter-diffusions	R. Paul	141

## *Subject Index*

SUBJECT	AUTHOR	PAGE
Force constants of the uranyl ion by Wilson's F-G matrix method (L)	K. V. Narasimham	432
Fourth order meson equation and neutron-proton scattering.	S. P. Misra	92
Fourth order scattering matrix elements of nucleons with a fourth order meson equation	S. P. Misra	221
F <sub>2</sub> -region of the ionosphere. On the Gravitational field of distant rotating masses	S. Datta	66
	V. Ramesh Wagh	211
Heat transfer and film boiling. A note on	R. D. Rao, H. S. Desai and D. V. Gogate	456
Impedance matching by re-entrant stub line	G. S. Sanyal	475
Ion source for positive ions. An arc type water-cooled	S. Z. R. Hashmi	118
Intermolecular potential and properties of argon	I. B. Srivastava	539
Intermolecular potential of helium	A. K. Barua	76
Ionization of E-layer by X-rays	S. N. Ghosh and Sharda Nand	516
Isotope effect in the collection on the charge plates of ( $n, \gamma$ ) recoil products of bromine. An	H. J. Arnikaar and A. Lal	441
Junction transistor with injected carrier concentration. On the variation of the transport factor of a	A. N. Daw	20
Lifetime of hyperfragments. The	G. C. Deka	470
Lightning strokes. Induced, (L)	S. D. Chatterjee and B. K. Dutta	198
Magnetic anisotropy and susceptibility of Fe(NH <sub>4</sub> SO <sub>4</sub> ) <sub>2</sub> · 6H <sub>2</sub> O. A preliminary note on the	A. S. Chakravarty and R. Chatterjee	10
Magnetism of the iron particles as revealed by electron diffraction (L)	S. Yamaguchi	535
Mass-spectrometer. A two-directional focussing high-intensity	S. B. Karmohapatro	407
Meson-meson scattering. On zero mass	B. Deo	131
Multiplex telephone systems. Choice of sampled waves for time-division	P. N. Das	424
M.U.F. factor and solar activity	C. S. R. Rao and J. C. Bhargava	58

# Subject Index

xx

SUBJECT	AUTHOR	PAGE
Neutron energy levels due to spin-orbit coupling. Splitting of	Arundhati Ghosh	260
Neutron generator. A high intensity	S. K. Mukherjee, N. K. Mazumder and A. Ganguly	307
New light effect. Optimum conditions to observe the	P. S. V. Setty	187
Nuclear spin echoes and molecular self-diffusion in liquids	S. K. Ghosh and S. K. Sinha	339
Nucleonic intensity during August 24-September 20. Latitude dependence of (L)	Lekh Vir and P. S. Gill	531
Paramagnetic $\text{Co}^{++}$ ions in state of solution. Light absorption in	A. Mookherji and N. S. Chhonkar	336
Paramagnetic ions in state of solution. Light absorption in. Part II— $\text{Ni}^{++}$ ion.	A. Mookherji and N. S. Chhonkar	363
Penetration factor in alpha-decay	S. K. Dutta, T. K. Mitra and N. C. Sil	205
Phase-transitions in $\text{Cu}[(\text{NH}_4)\text{SO}_4]_2 \cdot 6\text{H}_2\text{O}$ (L)	(Miss) Gouri Bhownik	433
Random fading records. Analysis of	S. R. Khastgir and R. N. Singh	527
Rotating cosmical bodies in the presence of magnetic field Oscillations of	J. N. Tandon	107
Space groups of crystals of ortho, meta and paraxylene at $-180^\circ\text{C}$	S. G. Biswas	263
Spread-F, Double-F, and Forked-F traces as observed at Haringhata (Calcutta). Some studies on the	R. N. Datta	482
Sign relation in the case of 4, 1, 3-chlorodinitrobenzene. Application of	E. M. Gopalakrishna	149
Singlet→triplet absorption in halogen substituted toluenes	J. K. Roy	331
Singlet→triplet absorption in aromatic compounds in gaseous states. On the	S. C. Sirkar and J. K. Roy	581
<b>SPECTRA</b>		
Absorption spectra of <i>o</i> -, <i>m</i> - and <i>p</i> -hydroxy benzaldehydes (L)	I. Achyuta Rao and V. Ramakrishna Rao	196
Electronic spectra of $\alpha$ -fluoronaphthalene in the liquid and solid states. On the	S. B. Banerjee	61

SUBJECT	AUTHOR	PAGE
Electronic spectra of 2-bromo and 3-bromo-pyridine in different states in solutions. On the	T. N. Misra	381
Emission band system of iodine in the blue violet. The	P. B. V. Haranath and T. A. Prasada Rao	123
Infrared absorption spectra of diamonds of different types	S. C. Sirkar	13
Infrared spectra of mesitylene in the vapour and liquid states and in solutions. On the	S. B. Banerjee and K. C. Meelhi	1
Infrared spectra of uranyl phosphate, oxalate and salicylate in solid state	K. V. Narasimham	321
Raman spectra of fluorobenzene at different low temperatures	Deb Kumar Mukherjee	402
Raman, infrared and luminescence spectra of some trisubstituted benzenes	K. K. Deb and S. B. Banerjee	554
Raman spectra of ortho-, and para-chloroanisole in the solid state at $-180^{\circ}\text{C}$	Krishna Kumar Deb	247
Ultraviolet absorption spectra of <i>m</i> - and <i>p</i> -methyl anisoles. The near (L)	K. V. Kameswara Rao and V. Ramakrishna Rao	200
Ultraviolet absorption spectra of isomeric fluorotoluenes in the liquid and solid states	S. K. Sen	237
Ultraviolet absorption spectra of the three isomeric methyl phenetoles. The near (L)	K. V. Kameswara Rao and V. Ramakrishna Rao	289
Ultraviolet band spectra of AsO and AsO <sup>+</sup>	S. V. J. Lakshman and P. Tiruvenganna Rao	278
Structure of anthrone. Statistical	K. Banerjee and S. N. Srivastava	184
Structure of naphthazarin		
$\text{C}_{10}\text{H}_4\text{O}_2(\text{CH})_2$ (L)	P. Srivastava	290
Thermal conductivity and Eucken-type factor for the binary mixtures		
M.U.F. $^4\text{He}$ , H-Ne, H-Kr and H-Xe	A. K. Barua	160

# Subject Index

xvii

SUBJECT	AUTHOR	PAGE
Thermal conductivity of aluminium at low temperatures. On (L)	H. N. Patil	395
Thermal diffusion factor for hydrogen and water mixtures	S. C. Saxena	449
Thermal expansion of some alkali halides by X-ray diffraction	P. D. Pathak and N. V. Pandya	416
Three-phase R-C. coupled oscillator Frequency of the Part II. Inductive anode load resistance	H. Rakshit and M. C. Mallik	36
Transistor drive circuits for dekatrons	K. S. Patel and B. M. Banerjee	293
Tunable oscillators. A note on some	N. B. Chakraborty and K. D. Dixit	549
Ultrasonic velocity in some aqueous solutions of electrolytes	P. R. K. L. Padmini and B. Ramachandra Rao	565
Ultrasonic velocity in supercooled liquids	S. Parthasarathy and V. N. Bindal	272
X-ray diffraction Part I. Effect of the crystallite size. A microwave analogue for	G. B. Mitra and G. S. Sanyal	103
X-ray study of crystallite orientation in agave Americana	Anand Prakash and V. D. Gupta	299
X-ray study of silver-cadmium alloys. An	Md. Abdul Quader	506





# ON THE INFRARED SPECTRA OF MESITYLENE IN THE VAPOUR AND LIQUID STATES AND IN SOLUTIONS\*

S. B. BANERJEE and K. C. MEDHI

OPTICS DEPARTMENT, INDIAN ASSOCIATION FOR THE CULTIVATION OF SCIENCE,  
CALCUTTA-32

(Received, December 19, 1959)

**ABSTRACT.** The infrared absorption spectra of mesitylene in the vapour and liquid states and in solutions in different solvents have been investigated with a Perkin-Elmer Model 21 spectrophotometer and some of the assignments of the observed frequencies of the molecule made by previous workers have been critically examined. It has been observed that the frequencies due to a mode of aromatic C-H vibration and the CH vibration in the methyl group are affected with the change from the vapour to liquid state. These frequencies are further affected in different ways when the compound is dissolved in different solvents. Attempts have been made to interpret these results.

## INTRODUCTION

It was observed in some recent investigations that the 0-0 electronic transition is forbidden in the spectrum of mesitylene in the vapour state (Sponer and Stallcup, 1948), but this transition becomes allowed in the case of the liquid (Sen, 1959) and its solutions in some solvents (Roy, 1957). This was explained by the latter workers by assuming that the three-fold symmetry of the molecule is disturbed due to association of the molecules in the liquid state and in solutions. Information of such molecular association may be obtained from a comparative study of the infrared spectra of the substance in the vapour and liquid states and in solutions. Pitzer and Scott (1943) reported an analysis of the infrared spectrum of mesitylene, based on the data reported by previous workers. These data relate to the spectrum of the liquid or its solutions and it appears that no data are available for the vapour. Pitzer and Scott (1943) did not make any definite assignments of the vibrational frequencies of the molecule in the  $3000\text{ cm}^{-1}$  region because of lack of suitable experimental data. It would be expected that in analysing these and other frequencies the study of infrared spectrum of mesitylene in the vapour state would be helpful. With these objects in view an investigation of the infrared spectra of mesitylene in the liquid and vapour states and in solutions in different solvents was undertaken and the results have been discussed in the present paper.

\* Read in the symposium on Raman and Infrared Spectra held at Nainital in October 1959.

## EXPERIMENTAL

Pure samples of mesitylene and of the solvents chloroform and carbon tetrachloride obtained from B.D.H. were used after being distilled under reduced pressure. The infrared spectra were recorded with a Perkin-Elmer Model 21 spectrophotometer with sodium chloride optics. The absorption cell used for studying the spectrum of the vapour consisted of a pyrex tube 10 cm long and connected through a side tube to a small bulb containing the liquid. Two plane parallel sodium chloride plates at the two ends of the tube, held in position with the help of suitable gaskets and screws, served as the windows. A similar evacuated tube was placed in the path of the reference beam. Absorption cells of different thicknesses varying from .025 mm. to 0.1 mm. were used for studying the spectra of the solutions and a much thinner film was used in the case of the pure liquid. Suitable compensation cells were put in the reference beam to eliminate the bands due to the solvents in the case of the solutions. The calibration of the spectrophotometer was checked by noting the position of the  $\text{CO}_2$  band.

## RESULTS AND DISCUSSION

The infrared absorption curves are reproduced in Figs. 1, 2, 3 and 4 and the frequencies of the observed bands are given in Table I.

TABLE I  
Infrared spectrum of mesitylene

Vapour	Liquid	5% Solution in $\text{CHCl}_3$	5% Solution in $\text{CCl}_4$
682 (s)	682	685	683
832 (vs)	835	836	835
925 (w)	925	915	920
1040 (ms)	1038	1038	1035
1238 (vw)	1200 (?)	1210	1230 (v)
1378 (ms)	1378	1378	1378
1440 (ms)	1442	1440	1450
1460 (s)	1470	1470	— 1472
1612 (vs)	1610	1605	1610
2882 (s)	2860	2858	2870
2950 (s)	2918	2918	2930
3050 (s)	3025	3005	3035

(a) *Assignment of the observed frequencies :*

It can be seen from Figs. 1(a) and 1(b) that in the vapour state mesitylene exhibits several bands which correspond to fundamental modes of vibration in the benzene ring as well as vibrations in the methyl group and that the spectrum shows two bands of moderate intensities at  $3050$  and  $2950\text{ cm}^{-1}$  and a weaker band at  $2882\text{ cm}^{-1}$ . Of these, the band at  $3050\text{ cm}^{-1}$  is expected to be due to a CH vibration in the ring and the other bands to vibrations in the methyl group according to Pitzer and Scott (1943) who did not assign the band at  $3050\text{ cm}^{-1}$  to any particular mode and also proposed that both the symme-

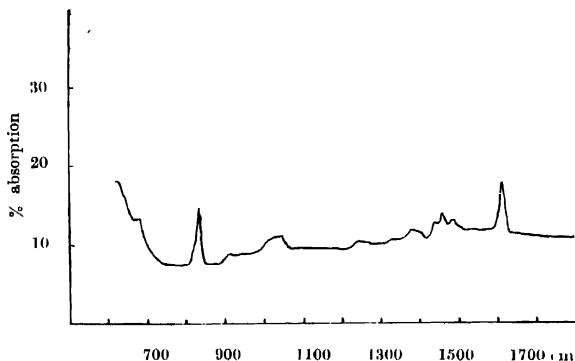


Fig. 1(a) Infrared spectrum of mesitylene (vapour at  $26^{\circ}\text{C}$ ).

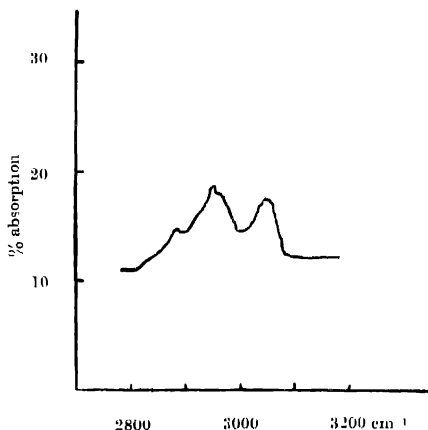


Fig. 1(b) Infrared spectrum of mesitylene (vapour at  $26^{\circ}\text{C}$ ).

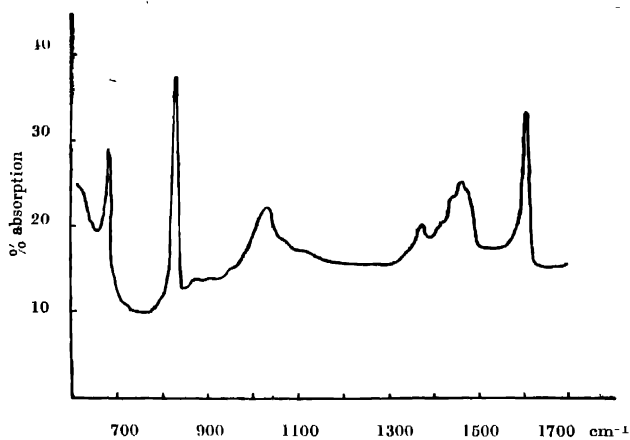


Fig. 2(a) Infrared spectrum of mesitylene (liquid at 26°C)

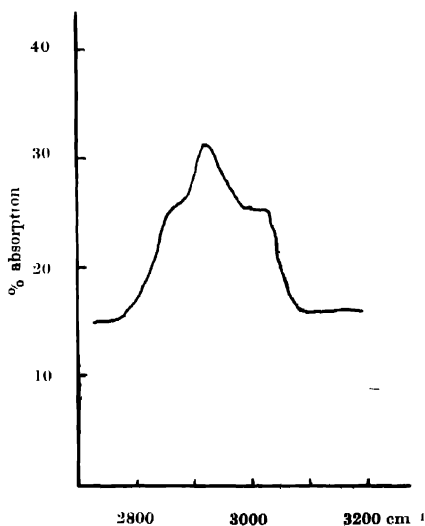


Fig. 2(b) Infrared spectrum of mesitylene (liquid at 26°C)

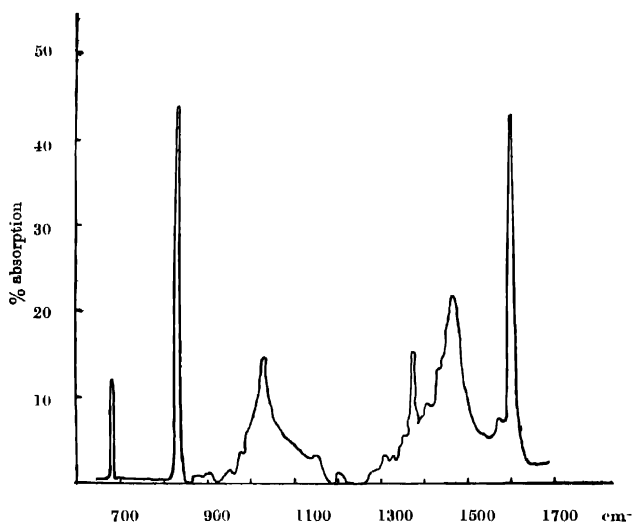


Fig. 3(a) Infrared spectrum of 5% solution of mesitylene in chloroform.

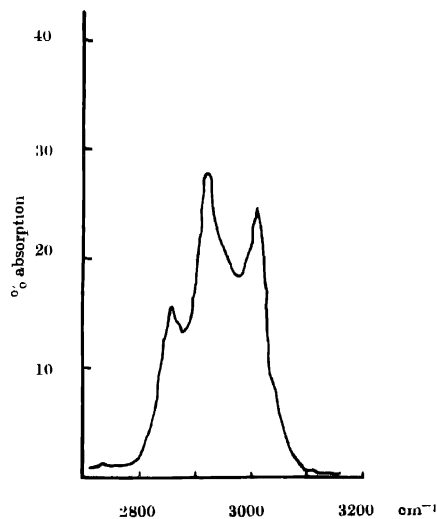


Fig. 3(b) Infrared spectrum of 5% solution of mesitylene in chloroform.

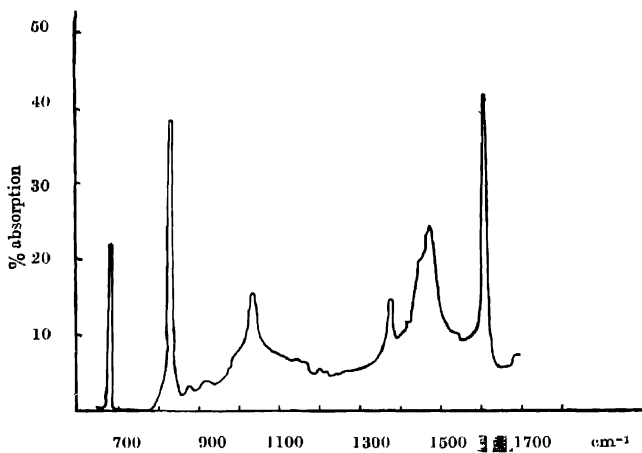


Fig. 4(a) Infrared spectrum of 5% solution of mesitylene in  $\text{CCl}_4$

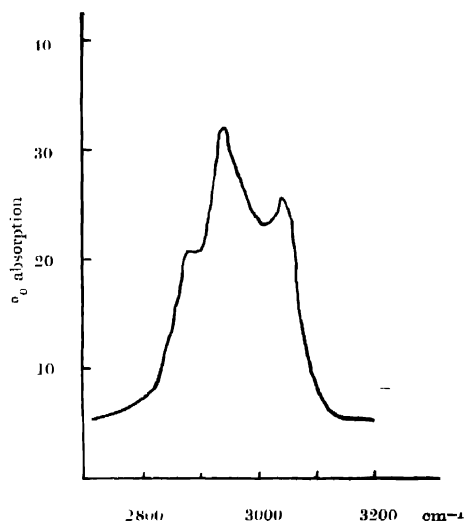
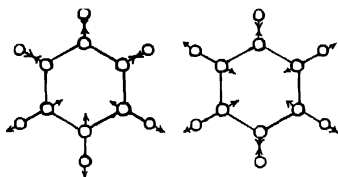


Fig. 4(b) Infrared spectrum of 5% solution of mesitylene in  $\text{CCl}_4$ .

tric and the asymmetric CH vibration in the methyl group would have the same frequency  $2950\text{ cm}^{-1}$ . But from a review of the general trend of vibrational frequencies of the methyl group (Sheppard and Simpson, 1953) it appears that it would be proper to assign the band at  $2950\text{ cm}^{-1}$  to asymmetric CH stretching vibration and that at  $2882\text{ cm}^{-1}$  to the symmetric CH stretching vibration in the methyl group.



(a). Fig. 5.

(b)

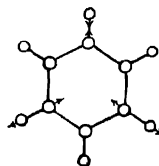


Fig. 6.

The large intensity of the band at  $3050\text{ cm}^{-1}$ , which is expected to correspond to a mode of CH oscillation of the ring, points to the fact that it cannot be due to any mode of symmetric vibration. In assigning this band to an asymmetric mode of CH stretching vibration, the assignment of the bands in the infrared spectrum of 1,3,5-trideuterobenzene by Bailey *et al* (1946) has been followed. They have shown that the doubly degenerate  $e_{2g}$  and  $e_{2u}$  modes in benzene of frequencies  $3047$  and  $3080\text{ cm}^{-1}$  shown in Figs. 5(a) and 5(b) respectively, interact with double decomposition into a nearly pure doubly degenerate stretching vibration of deuterium atom only and another almost pure doubly degenerate vibration of hydrogen atom only. In the present case of 1,3,5-trimethylbenzene similar argument would lead us to expect an almost pure CH vibration and another almost pure C-CH<sub>3</sub> vibration as shown in figure 6. In that case the band at  $3050\text{ cm}^{-1}$  would represent a CH vibration of symmetry class  $e'$  (Bailey *et al.*, 1946) and this band would be allowed in the infrared thus accounting for its observed intensity in the infrared spectrum. There is a weak band at  $1238\text{ cm}^{-1}$  in the spectrum of the vapour, which might represent the corresponding C-CH<sub>3</sub> vibration also of  $e'$ -class.

On the long wavelength side there are several bands due to fundamental vibrations which include CH deformation vibrations within the methyl group. It is known from studies of infrared spectra of methylated compounds (Sheppard and Simpson, 1953) that in the methyl group there may be a symmetric deformation oscillation of frequency below  $1400\text{ cm}^{-1}$  and two approximately doubly degenerate asymmetric modes of frequency near about  $1450\text{ cm}^{-1}$ . Thus, it would be appropriate to attribute the band at  $1378\text{ cm}^{-1}$  to the symmetric CH<sub>3</sub> bending, and the bands at  $1440$  and  $1470\text{ cm}^{-1}$  to the two modes of asymmetric bending as done by Pitzer and Scott (1943). In addition to these there is a band

at  $1040\text{ cm}^{-1}$  corresponding to wagging of the  $\text{CH}_3$  group (Pitzer and Scott, 1943; Sheppard *et al.*, 1953).

The other molecular frequencies may be assigned to different modes by following Bailey *et al.* (1946) who analysed the spectrum of 1,3,5-trideutero benzene. Pitzer and Scott (1943) also have analysed these bands. Thus the band at  $682\text{ cm}^{-1}$  may be attributed to a C-C deformation perpendicular to the plane of the molecule ( $a_2''$ ), that at  $835\text{ cm}^{-1}$  to an out of plane hydrogen deformation ( $e'$ ) and the band at  $1610\text{ cm}^{-1}$  to a mode of C-C stretching vibration ( $e'$ )

(b) *Changes observed in the spectrum with the change from the vapour to liquid state and in solutions :*

As discussed above, in the spectrum of mesitylene vapour there is a band at  $3050\text{ cm}^{-1}$  representing a CH stretching vibration in the benzene ring and two other bands at  $2950$  and  $2882\text{ cm}^{-1}$  which represent respectively the asymmetric CH stretching vibrations in the methyl group. When the vapour is liquefied these bands are found to shift to  $3025$ ,  $2918$  and  $2860\text{ cm}^{-1}$  respectively, while the positions of the other bands except that at  $1238\text{ cm}^{-1}$  remain unchanged. In the case of the solution in chloroform the band at  $3050\text{ cm}^{-1}$  is further shifted to  $3005\text{ cm}^{-1}$ . When the substance is dissolved in the non-polar solvent carbon tetrachloride the three bands shift respectively to  $2870$ ,  $2930$  and  $3035\text{ cm}^{-1}$  and the shifts are much smaller than those observed in the case of solution in chloroform. The presence of a permanent electric moment in the chloroform molecule is thus responsible for the large change in the frequencies.

The weak band at  $1238\text{ cm}^{-1}$  which has already been assigned to a  $\text{C-CH}_3$  vibrational mode in the vapour state is absent in the spectrum due to a thin film of the liquid. However, when a thicker film, of thickness of the order of  $0.025\text{ mm.}$ , is used a very weak band at  $1200\text{ cm}^{-1}$  is just perceptible. Also, in the case of solutions of chloroform and carbon tetrachloride a weak band at  $1210\text{ cm}^{-1}$  and  $1230\text{ cm}^{-1}$  respectively is observed, which may correspond to this mode of vibration. If the assignments of these bands due to the liquid and the solutions be correct then the  $\text{C-CH}_3$  vibrational frequency also appears to be affected by change of state and environment. In this case also the change observed in the case of the solution in  $\text{CCl}_4$  is small.

The shifts in the frequencies of the CH stretching vibration in the benzene ring and the CH stretching vibrations in the methyl group may indicate an association of the molecules in the liquid state through a virtual bond in which both the H-atoms of the ring and the  $\text{CH}_3$  groups are involved. The changes in the intensity and frequency of the  $\text{C-CH}_3$  vibration discussed above also support this conclusion. It is, however, unlikely that two  $\text{CH}_3$  groups of neighbouring molecules form associated bonds to suppress the  $\text{C-CH}_3$  vibration. Therefore we have to postulate that such association is due to the influence of



$\pi$ -electrons of the neighbouring molecules on the hydrogen atoms of the  $\text{CH}_3$  group. This is also in conformity with the fact that the symmetry of the  $\pi$ -electron is disturbed and the 0-0 band appears in the ultraviolet absorption spectrum of the compound when the vapour is liquefied (Sen 1959). That only the aromatic CH oscillation frequency is further affected in the case of the solution in chloroform shows that the chlorine atom is involved in an association only with the H-atom of the ring and not with the  $\text{CH}_3$  group

## ACKNOWLEDGMENT

The authors are indebted to Professor S. C. Sirkar, D.Sc., F.N.I., for his kind interest and helpful discussion.

## REFERENCES

- Bailey, C. R., Hale, J. B., Herzfeld, N., Ingold, C. K., Leckie, A. H. and Poole, H. G., 1946, *J. Chem. Soc.*, 255.  
Pitzer, K. S. and Scott, D. W., 1943, *J. Am. Chem. Soc.*, **65**, 803.  
Roy, S. B., 1957, *Ind. J. Phys.*, **31**, 588.  
Sen, S. K., 1959, *Ind. J. Phys.*, **33**, 41.  
Sheppard, N. and Simpson, D. M., 1953, *Quart. Revs.*, **7**, 19.  
Sponer, H. and Stallecup, M. J., 1958, Contribution a l'Etude de la Structure Moleculaire, Victor Henri Memorial volume. (Descor, hege), p. 222.

# A PRELIMINARY NOTE ON THE MAGNETIC ANISOTROPY AND SUSCEPTIBILITY OF $\text{Fe}(\text{NH}_4\text{SO}_4)_2 \cdot 6\text{H}_2\text{O}$

A. S. CHAKRAVARTY and R. CHATTERJEE

DEPARTMENT OF MAGNETISM, INDIAN ASSOCIATION FOR THE CULTIVATION OF SCIENCE,  
CALCUTTA-32

(Received, December 17, 1959)

**ABSTRACT.** The theory of magnetic anisotropy and susceptibility of  $\text{Fe}^{2+}$  in Tutton salts has been worked out on the basis of Abragam and Pryce's method. It is found that the anisotropic part of the crystal field changes with temperature due to the thermal expansion of the crystal lattice. The spin-orbit coupling coefficient has to be decreased by 20% from its free ion value of  $-103 \text{ cm}^{-1}$  which indicates some amount of overlap between the  $3d$  -  $\text{Fe}^{2+}$  and  $s$  and  $p$  -  $\text{O}^{2-}$  charge clouds. The agreement of the theoretical values with the experiment is excellent.

## INTRODUCTION

The five-fold degeneracy of the ground state  $3d^6, {}^5D$  of  $\text{Fe}^{2+}$  ion in the free state is split up by the predominant cubic component of the crystal field into an orbital doublet and a triplet, the latter being lower by about  $10^4 \text{ cm}^{-1}$ , in the octahedrally co-ordinated  $\text{Fe}^{2+}$  salts, e.g., the Tutton salts (van Vleck, 1932). In these salts the octahedron of six water molecules surrounding each  $\text{Fe}^{2+}$  ion has very nearly a tetragonal symmetry with the  $z$ -axis elongated as observed from paramagnetic resonance measurements (Tinkham, 1955). This tetragonal component of the electric field and the spin-orbit coupling acting together partly removes the remaining degeneracy of the orbital levels inclusive of the five-fold spin degeneracy of each orbital level. The complete secular problem is highly complicated and a complete theory of the susceptibility of  $\text{Fe}^{2+}$  salts has not yet been worked out. In the case of the trigonal symmetry, the expression for the susceptibility has been approximately worked out by Pryce (1957) and in some details by Palumbo (1958), but the agreement with Jackson's (1959) measurements in  $\text{Fe SiF}_6 \cdot 6\text{H}_2\text{O}$  is not very satisfactory at all ranges of temperature.

We have derived the theoretical expressions for the magnetic susceptibility and anisotropy in the tetragonal case i.e., for the  $\text{Fe}^{2+}$  Tutton salts on the basis of Abragam and Pryce's theory (1951) and compared these with the experimental results on  $\text{Fe}(\text{NH}_4\text{SO}_4)_2 \cdot 6\text{H}_2\text{O}$  of Bose (1947) and Jackson (1924) and also with the resonance data of Tinkham.

Since the  $\text{Fe}^{2+}$  ion is in the  $D$  state, we have assumed  $\alpha \approx \alpha' \approx 1$  (Abragam and Pryce) in this case. Under the action of the tetragonal field and the spin-orbit coupling, our fifteen order secular determinant breaks up into six  $|j| = 3$ , three  $|j| = 2$ , four  $|j| = 1$  and two  $|j| = 0$  levels, one of the six  $|j| = 1$  levels, lying lowest. All these levels lie within a span of about  $800 \text{ cm}^{-1}$ . We next apply magnetic perturbation on these levels and get the expression for the magnetic susceptibility and finally for the square of the effective moment

$$= \frac{3k}{N\beta^2}$$

converted into ionic values of  $P^2$ , taking two  $\text{Fe}^{2+}$  ions in the unit cell equally inclined to the crystallographic  $X_1$  axis, in the usual manner.

Here again we find that unless  $\Delta$  is varied appreciably as in  $\text{Ti}^{3+}$  (1959a) and  $\text{Co}^{2+}$  (1959b) salts, the agreement with experiment at all temperatures is impossible. Thus the crystal field changes quite appreciably due to thermal expansion of the crystal lattice. The facts that at high temperatures the spin-lattice relaxation time is very small making paramagnetic resonance lines too wide to be observable and that it increases sufficiently at about  $20^\circ\text{K}$  to give well-resolved lines are also indications that the crystal field changes considerably with temperature. Moreover, the spin-orbit coupling coefficient has to be decreased by 20% from its free ion value of  $103 \text{ cm}^{-1}$ . This indicates a corresponding overlap between the  $3d$   $\text{Fe}^{2+}$  and  $s$ - and  $p$ - $O^{2-}$  charge clouds.

TABLE I  
 $\text{Fe}(\text{NH}_4\text{SO}_4)_2 \cdot 6\text{H}_2\text{O}$  ( $\zeta = 80 \text{ cm}^{-1}$ )

Temp in $^\circ\text{K}$	$\Delta \text{ cm}^{-1}$	$P^2_{\parallel}$	$P^2_{\perp}$	$P^2 - P^2_{\perp}$	$g$ -values
300	650	36.26 (36.25)	26.31 (26.22)	9.95 (10.02)	—
160	500	44.12 (44.01)	24.72 (24.56)	19.39 (29.44)	—
90	400	51.80 (51.77)	21.28 (21.23)	30.51 (30.52)	—
20	270	—	—	—	$\left\{ \begin{array}{l} g_{\parallel} = 8.989 \\ \quad (8.97 \pm .02) \\ g_{\perp} = 0(0) \end{array} \right.$

The values in the parentheses indicate the mean of the experimental moment results of Jackson (1924) and Bose (1948). The  $g$ -values within parentheses are Tinkham's (1955).

The agreement with the magnetic anisotropies is quite excellent as can be seen in Table I, but the theoretical absolute  $P^2_{\perp}$ -values agree with the mean values of Jackson and Bose. The  $g$ -values given by Tinkham at  $20^\circ\text{K}$  also agree quite closely with our theoretical values.

The mathematical details will be published elsewhere shortly.

#### ACKNOWLEDGMENT

Authors wish to place their gratitude to Professor A. Bose for suggesting the problem and for his continued encouragement, criticism and suggestions.

#### REFERENCES

- Abragam, A. and Pryce, M. H. L., 1951, *Proc. Roy. Soc. A.*, **205**, 135.  
Bose, A., Chakravarty, A. S. and Chatterjee, R., 1959a, *Proc. Roy. Soc. A.*, (communicated), 1959b, *Proc. Roy. Soc. A.*, (communicated).  
Bose, A., 1948, *Ind. J. Phys.*, **22**, 483.  
Jackson, L. C., 1959, *Phil. Mag.*, **4**, No. 38, 269.  
Jackson, L. C., 1924, *Phil. Trans. Roy. Soc. A.*, **224**, 1.  
Pryce, M. H. L. and Lezoni di Varenna, in *Suppl. Nuovo Cim.*, **6**, 817.  
Palambo, D., 1958, *Nuovo. Cim.*, **8**, 271.  
Tinkham, M., 1955, *Proc. Phys. Soc. A*, **68**, 258.  
van Vleck, J. H., 1932, *Phys. Rev.*, **41**, 208.

# INFRARED ABSORPTION SPECTRA OF DIAMONDS OF DIFFERENT TYPES

S. C. SARKAR

OPTICS DEPARTMENT, INDIAN ASSOCIATION FOR THE CULTIVATION OF SCIENCE  
CALCUTTA-32

(Received, November 27, 1959)

**ABSTRACT.** The infrared absorption spectra of ten specimens of diamond of which the fluorescence and absorption spectra had been studied earlier were investigated using a Perkin-Elmer Model 21 spectrophotometer. Two of these diamonds transparent upto about  $2300 \text{ \AA}$  in the ultraviolet region and producing no fluorescence band at  $4156 \text{ \AA}$  exhibit only very weak infrared absorption in different regions while the other specimens show some or all the absorption bands reported by previous workers. It has been concluded from these results that these infrared bands excepting the band  $1360 \text{ cm}^{-1}$  are due to impurities and are not produced by characteristic vibrations of the diamond lattice. The band  $1360 \text{ cm}^{-1}$  has been assigned to the vibration in those portions of the lattice which are under strain due to presence of impurities.

## INTRODUCTION

The infrared absorption spectra of a large number of diamonds were investigated by Robertson, Fox and Martin (1934) along with many other properties of the crystal and it was observed by them that all the specimens showed bands in the regions  $2462\text{--}2491 \text{ cm}^{-1}$ ,  $2167\text{--}2187 \text{ cm}^{-1}$ ,  $2080\text{--}2106 \text{ cm}^{-1}$  and  $1992\text{--}2015 \text{ cm}^{-1}$ , but only the specimens of common type absorbing ultraviolet radiation beyond  $3000 \text{ \AA}$  showed another set of bands in the region  $1196\text{--}1387 \text{ cm}^{-1}$ . These latter bands were absent in the spectra due to the crystals transparent to ultraviolet radiation beyond  $3000 \text{ \AA}$ . From these results they concluded that the diamonds could be divided into two types, e.g., Type 1 showing the absorption bands at  $8\mu$  and also absorption of ultraviolet rays beyond  $3000 \text{ \AA}$  and Type 2 not showing any absorption in these two regions. They, however, classified under Type 2 some diamonds which were transparent to ultraviolet radiation beyond  $3000 \text{ \AA}$  but showed absorption bands in the region  $2351\text{--}2335 \text{ \AA}$ , as these diamonds also did not show any infrared absorption band in the region  $8\mu$ .

The study of the luminescence spectra of different specimens of diamond was later undertaken by Nayar (1941*a*, 1941*b*), Anna Mani (1944), Chandrasekharan (1948) and others. It was concluded by these workers that the luminescence is feeble in diamonds of Type 2 which show transparency in the ultraviolet region beyond  $3000 \text{ \AA}$  and that the absorption band at  $4156 \text{ \AA}$  and the

fluorescence band at this position were the characteristic bands of the diamond lattice Bishui (1950) pointed out, however, that the fluorescence band at  $4156\text{ \AA}$  exhibited by diamonds of Type 1 might be due to chemical impurities, as macroscopic strain in the crystal has no influence on the intensity of the band. He next studied (Bishui, 1952) quantitatively the intensity of the fluorescence band at  $4156\text{ \AA}$  relative to that of the Raman line at  $1332\text{ cm}^{-1}$  and also the ultraviolet absorption spectra of eight selected specimens of diamond and observed that the intensity of the fluorescence band at  $4156\text{ \AA}$  does not depend on the strength of the absorption band at the same place. He further observed that a specimen which is transparent to the visible region and to ultraviolet radiation upto  $2270\text{ \AA}$  and shows only two absorption bands at  $2360\text{ \AA}$  and  $2363.3\text{ \AA}$ , produces strong fluorescence band at  $4156\text{ \AA}$ , but those specimens which do not show any absorption bands in the visible or ultraviolet region upto  $2240\text{ \AA}$  do not produce the fluorescence band at  $4156\text{ \AA}$ . From these results he concluded that diamonds of these totally transparent type are pure diamonds and should be classified under Type 2, while all other specimens showing fluorescence band at  $4156\text{ \AA}$  are of Type 1 and that the fluorescence band at  $4156\text{ \AA}$  is due to the impurity which produces the ultraviolet absorption bands at  $2360\text{ \AA}$  and  $2363.3\text{ \AA}$ .

The infrared spectra of these specimens of diamond were not known and it was thought worthwhile to study the infrared spectra to find out whether the band at  $8\mu$  was a characteristic band of diamonds of Type 1 which show the fluorescence band at  $4156\text{ \AA}$  and also whether the other bands observed in the infrared spectra of diamonds of Type 2 by Robertson, Fox and Martin (1934) are exhibited by all the diamonds of both the types.

#### EXPERIMENTAL

As mentioned above some of the specimens of diamond used previously by Bishui (1950, 1952) for investigating the fluorescence yield and ultraviolet absorption spectra were used in the present investigation. The specimens selected are D 1, D 4, D 5, D 6, D 7, D 8, D 9, D 10, D 11 and D 13. Of these, D 4 and D 13 were classified by him under Type 2 and the rest under Type 1.

A Perkin-Elmer Model 21 infrared spectrophotometer was used to study the absorption spectra. As the diamonds were smaller than the full apertures in the two beams in the spectrophotometer two small apertures of the same size made in two discs of black paper were used in the paths of the two beams, so that the radiation in the sample beam could enter into the spectrophotometer only after passing through the specimen of diamond covering the aperture in this beam. The size of the aperture was not less than  $4.5\text{ mm} \times 6\text{ mm}$  in any case and the smallest diamond used could wholly cover this aperture. Even when a smaller aperture was used in the reference beam and the sample beam

was shut off the pen was driven to the position 1 instead of zero, so that the heights of the absorption peaks were not affected very much by the introduction of the apertures in the two beams.

# RESULTS AND DISCUSSIONS

The positions of the bands observed in the infrared absorption spectra of the specimens of diamond are given in Table I. The intensities are given as strong, medium, etc. The details about the ultraviolet absorption limit, intensities of fluorescence and absorption band at 1156 Å and the dimensions of the specimens are given in Table II. The absorption curve due to D 6 is reproduced in Fig. 1. The curves due to D 9 and D 10 are shown in Fig. 2. The curves due to D 5, D 7 and D 10 show bands similar to those given by D 6 but with

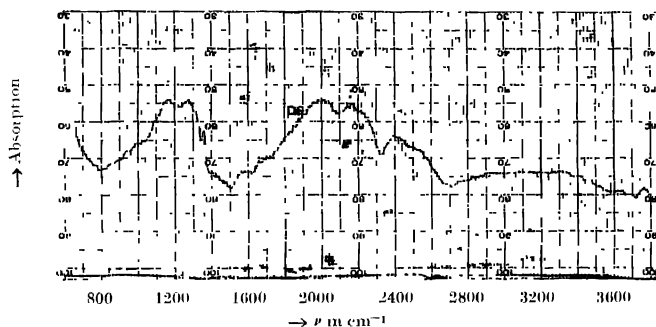


Fig. 1. Infrared absorption spectrum of D 6

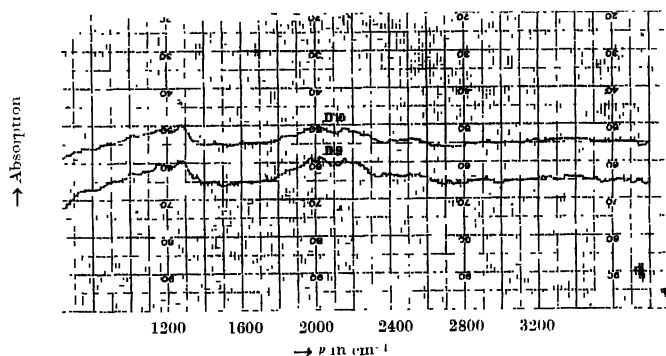


Fig. 2. Infrared absorption spectra of D 9 and D 10

smaller strengths of absorption, and therefore, these curves have not been reproduced. Fig. 3 shows the curve due to D 1, which is a rose diamond belonging to Type 1, along with the curves given by D 4 and D 13 which are of Type 2. The curve due to D 8 was found to be similar to that due to D 1 and it has not been reproduced. Fig. 4 shows the curve due to D 11 which is transparent upto 2270 Å but shows two absorption bands at 2360 Å and 2363.3 Å respectively.

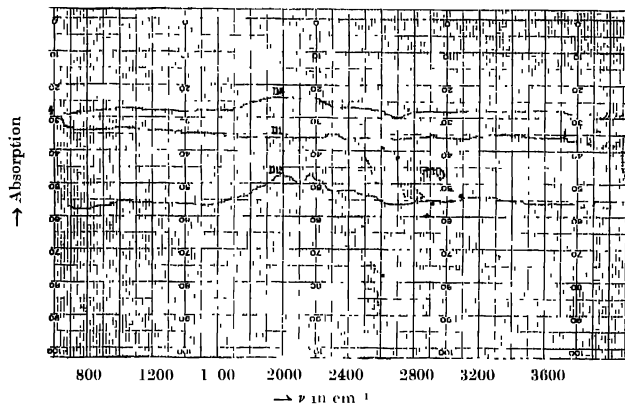


Fig. 3. Infrared absorption spectra of D 1, D 4 and D 13

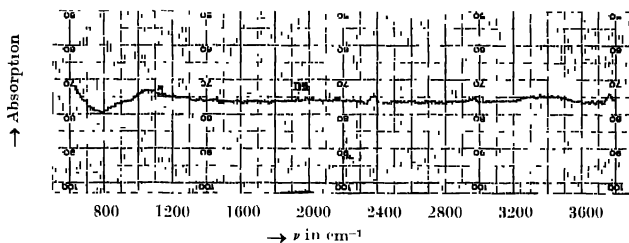


Fig. 4. Infrared absorption spectrum of D 11

It can be seen from the figures and the tables mentioned above that the diamonds D 5, D 6, D 7, D 9 and D 10 belonging to Type 1 produce similar absorption bands in the regions from 1000  $\text{cm}^{-1}$  to 1400  $\text{cm}^{-1}$  and from about 1900  $\text{cm}^{-1}$  to 2500  $\text{cm}^{-1}$ . All these specimens show a sharp band at 1360  $\text{cm}^{-1}$  besides the other broad bands, but the height of this sharp peak is different for the different specimens. On the other hand, the diamonds D 1 and D 8 which



TABLE I  
Infrared absorption bands of diamonds

Diamond No.	Frequencies of bands in $\text{cm}^{-1}$ and intensities									
	900-1300 (vw)	(very broad band)	—	—	—	—	—	—	—	—
D 1	—	—	—	1800-2200 (w)	(very broad band)	—	—	—	—	—
D 4	—	—	—	1800-2200 (w)	(very broad band)	—	—	—	—	—
D 5	1150 (m)	1270 (m)	1360 (vw)	2000 (mb)	2150 (mb)	2260 (w)	2400 (w)	2500 (w)	2900-3400 (wb)	2900-3400 (wb)
D 6	1160 (s)	1280 (s)	1360 (m)	2000 (s b)	2160 (s)	2240 (m)	2400 (w)	2500 (w)	2900-3400 (w)	2900-3400 (w)
D 7	1180 (m)	1280 (s)	1360 (w)	2000 (s, b)	2160 (s)	2230 (m)	—	2500 (w, b)	3000-3400 (vw)	3000-3400 (vw)
D 8	900-1400 (w, v, b)	—	—	—	—	—	—	—	—	—
D 9	1000 (w)	1160 (m)	1280 (m)	1360 (vw)	1980 (m)	2020 (m)	2160 (m)	2220 (w)	—	—
D 10	1000 (w)	1160 (m, b)	1280 (m)	1360 (vw)	1980 (m)	2020 (m)	2160 (m)	—	—	—
D 11	—	—	—	—	1930 (w)	2000 (w)	2150 (w)	2400 (vw)	—	—
D 13	—	—	—	—	2000 (w, b)	2150 (w)	2240 (vw)	2400 (vw)	—	—

TABLE II  
Properties of the specimens of diamond used

Diamond No.	Dimensions in mm.	Intensity of absorption band at	Intensity of fluorescence band at	Ultraviolet absorption limit	
		4152 Å at -180°C	4152 Å at -180°C		
D 1	9×7×1.5	strong	very strong	opaque beyond	3500 Å
D 4	11×8×1.5 (triangular)	zero	very weak	limit	2280 Å
D 5	10×8×2	weak	very strong	„	3000 Å
D 6	14×12×2	medium	very strong	„	3500 Å
D 7	9×7.5×1.35	weak	strong	„	2560 Å
D 8	9×5.5×1.3	medium	weak	„	3000 Å
D 9	6×5×0.8	weak	very strong	„	2550 Å
D 10	7.5×5.5×1.09	very weak	strong	„	2810 Å
D 11	7×5×0.95 (low pyramid)	weak	very strong	„	2270 Å bands at 2360 & 2363.3 Å
D 13	8×5×0.84 (low pyramid)	zero	zero	limit	2240 Å

also are of Type 1 and absorb all ultraviolet radiation of wavelengths shorter than 3000 Å, do not produce any discrete infrared absorption bands in the region from 2000  $\text{cm}^{-1}$  to 3500  $\text{cm}^{-1}$ , but each of them shows only a very weak continuous absorption in the region 900–1400  $\text{cm}^{-1}$ . The specimens D 4 and D 13 which belong to Type 2 and are transparent upto 2240 Å do not show any absorption band in the region 900–1400  $\text{cm}^{-1}$ , but although D 13 produces a few weak and broad bands in the region 2000–2400  $\text{cm}^{-1}$ , D 4 shows only very weak continuous absorption in the region 1800–2200  $\text{cm}^{-1}$ . The specimen D 11 produces strong fluorescence band at 4156 Å and unlike other diamonds of Type 1 it is transparent up to about 2240 Å but shows two absorption bands at 2360 Å and 2363.3 Å. It exhibits no absorption bands in the region 1000  $\text{cm}^{-1}$ –1400  $\text{cm}^{-1}$ .

It can be seen from the above results that all the diamonds opaque to ultraviolet radiation beyond 3000 Å and classified under Type 1 do not necessarily produce infrared absorption bands in the regions 2000–2260  $\text{cm}^{-1}$  and 2400  $\text{cm}^{-1}$ –2500  $\text{cm}^{-1}$ . D 1 and D 8 are examples of such diamonds not showing any infrared bands in these regions. Again, D 11, although classified under Type 1, does not show any band in the region 1000–1400  $\text{cm}^{-1}$ . Thus the intensity of the fluorescence band at 4156 Å cannot be correlated with infrared

absorption in any of the regions mentioned above. The fluorescence band was, however, ascribed to some impurities which produce the ultraviolet absorption bands at 2360 Å and 2363.3 Å by Bishui (1952). It appears from these facts that the infrared absorption in the regions shown in Table I are due to some impurities and they do not represent the characteristic frequencies of vibration of the diamond lattice.

It has to be pointed out, however, that the band at  $1360\text{ cm}^{-1}$  is much sharper than the other bands and its frequency is also very near to the frequency of the Raman line of diamond. The vibration of frequency  $1332\text{ cm}^{-1}$  giving the Raman line is forbidden in the infrared spectra. It appears, however, that in small microscopic regions in the diamond in which impurities are present the symmetry of the lattice is destroyed and the mode of vibration is made allowed with slightly increased frequency. The intensity of the infrared band produced in this way will depend on the percentage of the total volume of the crystal which is under strain due to the presence of the impurities. This may explain the difference in the intensities of this band observed in the different cases. The strength of the absorption at the  $1360\text{ cm}^{-1}$  band is in conformity with the fact that even a 0.025 mm thick film of 1% solution of any organic liquid produces large peaks in the infrared absorption spectra.

#### REFERENCES

- Anna Muni (Miss), 1944, *Proc. Ind. Acad. Sci.*, **19A**, 231  
Bishui, B. M., 1950, *Ind. J. Phys.*, **24**, 441  
Bishui, B. M., 1952, *Ind. J. Phys.*, **28**, 347.  
Chandrasekharan, V., 1948, *Proc. Ind. Acad. Sci.*, **27A**, 310  
Nayar, P. G. N., 1941a, *Proc. Ind. Acad. Sci.*, **13A**, 483  
Nayar, P. G. N., 1941b, *Proc. Ind. Acad. Sci.*, **14A**, 1.  
Robertson, R., Fox, J. J. and Martin, A. R., 1934, *Phil. Trans. Roy. Soc. A.*, **232**, 482.

# ON THE VARIATION OF THE TRANSPORT FACTOR OF A JUNCTION TRANSISTOR WITH INJECTED CARRIER CONCENTRATION

A. N. DAWI

INSTITUTE OF RADIO PHYSICS AND ELECTRONICS, CALCUTTA UNIVERSITY

(Received, November 27, 1959)

**ABSTRACT.** An attempt has been made to set up a general equation governing the distribution of injected carriers in the base region of a  $p-n-p$  junction transistor and hence to obtain an expression for the transport factor  $\beta$ . Subject to certain approximations, a relation is derived giving the emitter current density as a function of the concentration of injected carriers and with its help, the transport factor is expressed explicitly in terms of the latter. The expression is critically examined in the light of recombination process both on the surface and in the volume. The results are compared with those suggested by previous workers.

The possible effect of the presence of a significant electronic component of current, across the emitter-base junction on the expression for the transport factor is also considered. It is shown that the effect if any would be very small. An electronic component of current however, affects the value of the current amplification factor  $\alpha$  and a categorical experimental verdict in favour of one or the other of the different possible modes of recombination is not possible unless the so-called emitter efficiency term can be determined by independent experimental measurement.

## 1. INTRODUCTION

The current amplification factor of a junction transistor, as given approximately by the product of the so-called transport factor  $\beta$  and the emitter efficiency  $\gamma$ , is known to vary with the emitter current  $I_e$ . A large amount of work (Webster 1954, Rittner 1954, Giacoletto 1955, Misawa 1955, Fletcher 1956, Hauri 1956, Matz, 1598 and Kaufmann 1959) has already been done to account for this variation but a satisfactory answer has not yet been obtained. One reason for this is the fact that a rigorous solution of the diffusion equation of a junction transistor holding for all values of  $I_e$  is difficult to obtain and only approximate solutions for operation at high injection level have to be inferred by making use of the known results for that at low level and of certain plausible assumptions. The deductions are obviously rather crude and it is not known whether these may be applicable to the intermediate levels of operation. An attempt was therefore made to set up a general equation governing the distribution of carriers injected in the base region with a view particularly to obtain an expression for the transport factor  $\beta$  valid over a wide range of operation. In the present paper, an account

is given of the results thus obtained for three cases of general interest, viz., (i) when recombination of carriers is confined only to the surface; (ii) when recombination occurs only in the volume and (iii) when recombination occurs both on the surface and in the volume. The results are compared with the values given by the previous workers.

## 2. GENERAL EQUATION FOR THE DISTRIBUTION OF CARRIERS IN THE BASE REGION

The basic equations governing the one dimensional flow of minority carriers through the base region of a junction transistor are the following :

$$J_n = ne\mu_n E + eD_n \frac{dn}{dx} \quad \dots (1)$$

$$J_p = pe\mu_p E + eD_p \frac{dp}{dx} \quad \dots (2)$$

where  $J_n, J_p$  = electron and hole current densities across the emitter-base boundary.

$n, p$  = electron and hole concentrations in the base region,

$\mu_n, \mu_p$  = electron and hole mobilities,

$D_n, D_p$  = diffusion constants for electrons and holes

$E$  = electric field in the base region

and  $e$  = electronic charge

Confining to transistors of the  $p-n-p$  type we note that for high values of emitter efficiency,  $J_n \approx 0$ . The electric field  $E$  can now be eliminated (Webster 1954) between Eqs. (1) and (2) giving

$$J_p = -eD_p \left( 1 + \frac{p}{p+N_d} \right) \frac{dp}{dx} \quad \dots (3)$$

where  $N_d$  = equilibrium donor concentration in the base region.

When recombination is present, the time rate of decay of injected hole density in the base region is given by

$$\frac{dp}{dt} = -\frac{p-p_B}{\tau} - \frac{1}{e} \frac{dJ_p}{dx} \quad \dots (4)$$

where  $p_B$  = thermal equilibrium value of hole density in the base region, and  $\tau$  = effective lifetime of holes in the base region

Eliminating  $J_p$  from Eqs.(3) and (4) one obtains

$$\frac{dp}{dt} = -\frac{p-p_B}{\tau} + D_p \left( 1 + \frac{p}{p+N_d} \right) \frac{d^2p}{dx^2} + D_p \frac{N_d}{(p+N_d)^2} \cdot \left( \frac{dp}{dx} \right)^2 \quad \dots (5)$$

Eq. (4) assumes tacitly that the lifetime  $\tau$  is independent of the injected minority carrier concentration. This assumption is not, however, generally true. Experimental results on the variation of  $\tau$  with  $I_e$  are somewhat conflicting. Results of a recent work (Deb and Daw, 1958) show that in general, leaving out the case involving very low values of  $I_e$ , the effective lifetime  $\tau$  passes through a maximum as the injection level is increased from a low value. An analytical relation suggested to account for this variation is

$$\frac{1}{\tau} = \frac{1}{\tau_B} \left( 1 + \frac{p}{N_d} \right) + \frac{\nu_B \left( 1 + \frac{p}{N_d} \right)}{1 + \frac{2p}{N_d}} \quad \dots (6)$$

where  $\tau_B$  = volume recombination lifetime when  $p \ll N_d$ ,

and  $1/\nu_B$  = surface recombination lifetime when  $p_s \ll N_d$ ,

it being assumed that the volume recombination is bimolecular. Accepting Eq.(6) one obtains from Eq.(5).

$$\frac{dp}{dt} = -(p-p_B) \left\{ \frac{1}{\tau_B} \left( 1 + \frac{p}{N_d} \right) + \frac{\nu_B \left( 1 + \frac{p}{N_d} \right)}{1 + \frac{2p}{N_d}} \right\} + D_p \left( 1 + \frac{p}{p+N_d} \right) \frac{d^2 p}{dx^2} + D_p \left( \frac{dp}{dx} \right)^2 \frac{N_d}{(p+N_d)^2} \quad \dots (7)$$

Eq. (7) is the general form of diffusion equation valid for all values of  $I_e$ , provided the lifetime  $\tau$  follows the relation given by Eq.(6).

### 3. SOLUTION OF DIFFUSION EQUATION AND GENERAL EXPRESSION FOR THE TRANSPORT FACTOR

We now proceed to obtain a solution of Eq. (7) deduced in the preceding section. For simplicity, we assume the steady state operating condition. For

this,  $\frac{dp}{dt} = 0$  and

$$\left( 1 + \frac{p}{p+N_d} \right) \frac{d^2 p}{dx^2} + \frac{N_d}{(p+N_d)^2} \left( \frac{dp}{dx} \right)^2 - \frac{1}{D_p} \left\{ \frac{1}{\tau_B} \left( 1 + \frac{p}{N_d} \right) + \frac{\nu_B \left( 1 + \frac{p}{N_d} \right)}{1 + \frac{2p}{N_d}} \right\} = 0 \quad \dots (8)$$

This equation is of a standard form and can be integrated easily giving

$$Z \left( \frac{2p + N_d}{p + N_d} \right)^2 = -\frac{2}{D_p} \int \left\{ \frac{2p + N_d}{\tau_B N_d} (p - p_B) + v_B (p - p_B) \right\} dp + C$$

$$= -\frac{2}{D_p \tau_B} \left[ \frac{2p^3}{3N_d} + \left( \frac{1}{2} - \frac{p_B}{N_d} \right) p^2 - p \cdot p_B \right] + \frac{2v_B}{D_p} \left[ \frac{p^2}{2} - p \cdot p_B \right] + C \dots (9)$$

where  $Z = \left( \frac{dp}{dx} \right)^2$  and  $C$  is the constant of integration

Let us now introduce the variable  $y = \frac{p}{N_d}$  so that

$$Z = \left( \frac{dp}{dx} \right)^2 = N_d^2 \left( \frac{dy}{dx} \right)^2 \quad (10)$$

Substituting Eq. (10) in Eq. (9),

$$\left( \frac{dy}{dx} \right)^2 \left( \frac{1 + 2y}{1 + y} \right)^2 = \frac{2}{D_p \tau_B} \left[ \frac{2}{3} y^3 + \left( \frac{1}{2} - \frac{p_B}{N_d} \right) y^2 - \frac{p_B}{N_d} \cdot y \right]$$

$$+ \frac{2v_B}{D_p} \left[ \frac{y^2}{2} - \frac{p_B}{N_d} y \right] + C' \dots (11)$$

To evaluate  $C'$ , we utilise the condition that at the collector base junction, the minority carrier concentration is negligible so that

$$\left. \begin{aligned} &y = 0 \\ \text{and} \quad &\frac{dy}{dx} = \left( \frac{dy}{dx} \right)_c \text{ say} = - \frac{J_c}{e D_p N_d} \end{aligned} \right\} \dots (12)$$

where  $J_c$  is the collector current density. From Eqs. (11) and (12), we have

$$C' = \left( - \frac{J_c}{e D_p N_d} \right)^2 \dots (13)$$

Again, from Eq. (3), the emitter current density  $J_e = J_p$  is given by

$$J_e = -e D_p \left( 1 + \frac{p_e}{p_e + N_d} \right) \left( \frac{dp}{dx} \right)_e$$

$$= -e D_p N_d \left( \frac{1 + 2y_e}{1 + y_e} \right) \left( \frac{dy}{dx} \right)_e \dots (14)$$

where the subscript  $e$  refers to the emitter base junction.

From Eqs. (11), (13) and (14), one obtains

$$\left( \frac{J_e}{eD_p N_d} \right)^2 = \frac{2}{D_p \tau_B} \left[ \frac{2}{3} y_e^3 + \left( \frac{1}{2} - \frac{p_B}{N_d} \right) y_e^2 - \frac{p_B}{N_d} y_e \right] + \frac{2v_B}{D_p} \left[ \frac{y_e^2}{2} - \frac{p_B}{N_d} y_e \right] + \left( \frac{J_e}{eD_p N_d} \right)^2 \quad \dots \quad (15)$$

$$\text{on } J_e \text{ as } J_e \left[ 1 - \left( \frac{eD_p N_d}{J_e} \right)^2 \frac{2}{D_p \tau_B} \left\{ \frac{2}{3} y_e^3 + \left( \frac{1}{2} - \frac{p_B}{N_d} \right) y_e^2 - \frac{p_B}{N_d} y_e \right\} - \left( \frac{eD_p N_d}{J_e} \right)^2 \frac{2v_B}{D_p} \left\{ \frac{y_e^2}{2} - \frac{p_B}{N_d} y_e \right\} \right]^{-1} \quad \dots \quad (16)$$

Differentiating both sides of Eq. (16) with respect to  $J_e$  and noting that the transport factor  $\beta_{ce}$  for the grounded base mode is given by  $\beta_{ce} = - \frac{dJ_e}{dJ_e}$ , one obtains

$$\beta_{ce} = \frac{1 - \left[ \frac{1}{J_e} \frac{(eD_p N_d)^2}{D_p \tau_B} \left\{ 2y_e^3 + \left( 1 - 2\frac{p_B}{N_d} \right) y_e^2 - \frac{p_B}{N_d} y_e \right\} + \frac{1}{J_e} \frac{(eD_p N_d)^2 v_B}{D_p} \left\{ \frac{y_e^2}{2} - \frac{p_B}{N_d} y_e \right\} \right]}{\left[ 1 - \frac{2}{J_e^2} \frac{(eD_p N_d)^2}{D_p \tau_B} \left\{ \frac{2}{3} y_e^3 + \left( \frac{1}{2} - \frac{p_B}{N_d} \right) y_e^2 - \frac{p_B}{N_d} y_e \right\} - \frac{2}{J_e^2} \frac{(eD_p N_d)^2 v_B}{D_p} \left\{ \frac{y_e^2}{2} - \frac{p_B}{N_d} y_e \right\} \right]} \frac{dy_e}{dJ_e} \quad (17)$$

which is the general expression for  $\beta_{ce}$ .

#### 4 RELATION BETWEEN THE CURRENT DENSITY AND INJECTED CARRIER CONCENTRATION

The relation for  $\beta_{ce}$  given above [Eq. (17)] has the drawback that it involves both  $J_e$  and  $y_e$  and a precise relationship between these two parameters is needed to obtain  $\beta_{ce}$  explicitly in terms of either  $J_e$  or  $y_e$ . Unfortunately, however, a rigorous relation cannot be obtained readily and some approximations have to be made keeping in view, as far as possible, the peculiar conditions which arise under high level condition of operation. Thus noting that under high level



$\left(1 + \frac{y_e}{1 + y_e}\right)$ . Webster (1954) obtained, for the case when recombination in the base region is negligible, the relation

$$J_e = \frac{eD_p N_d}{W} \left\{ 2y_e - \ln(1 + y_e) \right\} = \frac{eD_p N_d P}{W} \quad \dots (18)$$

where  $P = 2y_e - \ln(1 + y_e)$  and  $W$  is the width of the base region of the transistor. In a practical transistor, however, some of the injected carriers are invariably lost by recombination in the base region and Eq (18) needs some modification to take this into account. A simple method of doing this is as follows.

We recall that in the presence of recombination the expression for  $J_e$  at low injection level is approximately given by

$$J'_e = \frac{eD_p p_B}{W} \exp\left(\frac{eV_e}{kT}\right) \frac{W}{\tanh \frac{W}{(D_p \tau)'}} \quad (19)$$

and that in the absence of recombination by

$$J'_e = \frac{eD_p p_B}{W} \exp\left(\frac{eV_e}{kT}\right), \quad \dots (20)$$

where  $J'_e$  is the emitter current density at low injection level and  $V_e$  the applied emitter to base d. c. potential. It is thus seen that the presence of recombination introduces a factor  $\frac{W}{(D_p \tau)' \tanh \frac{W}{(D_p \tau)'}}$  in the expression for  $J'_e$ . We assume that to a first approximation this also holds for high injection level. Eq (18) can then be modified as

$$J_e = \frac{eD_p N_d P}{W} \cdot \frac{W}{\tanh \frac{W}{(D_p \tau)'}} \quad \dots (21)$$

Next we argue that at high injection level the term  $\tau$  appearing in Eq. (21) is a function of  $y$  as given by Eq (6). From Eqs. (6) and (21) we then obtain

$$J_e = \frac{eD_p N_d P}{W} \cdot \frac{W \left( \frac{1 + y_e}{D_p \tau_B} \right)^{\frac{1}{2}}}{\tanh W \left( \frac{1 + y_e}{D_p \tau_B} \right)^{\frac{1}{2}}} \quad \dots (22)$$

when recombination occurs only in the volume and

$$J_e = \frac{eD_p N_d P}{W} \cdot \frac{W \left\{ \frac{v_B(1+y_e)}{D_p(1+2y_e)} \right\}^{\frac{1}{2}}}{\tanh W \left\{ \frac{v_B(1+y_e)}{D_p(1+2y_e)} \right\}^{\frac{1}{2}}} \quad \dots (23)$$

when recombination is confined only to the surface.

## 5. RECOMBINATION MECHANISM AND THE VALUE OF THE TRANSPORT FACTOR

An expression giving the value of the transport factor  $\beta_{ec}$  explicitly as a function of  $y_e$  can now be derived with the help of Eqs. (17), (22) and (23). It is, however, convenient at this stage to consider separately the effects of surface and volume recombinations. This procedure simplifies mathematical manipulation considerably and also helps to bring out clearly the role of the individual types of recombination processes on the operation of a transistor. Further, as will be shown presently, the results thus obtained are helpful in discussing the case when the two recombination processes are simultaneously operative. We consider first the case of surface recombination.

(i) *Recombination confined only to the surface.* When only surface recombination is operative,  $\tau_B = \alpha$ . Keeping this in mind and substituting in

Eq. (17) the value of  $J_e$  and  $\frac{dy_e}{dJ_e}$  as obtained from Eq. (23), one obtains

$$\beta_{ec} = \frac{1 - \left( \tanh^2 \frac{W}{L'_{BS}} \right) \frac{y_e}{P} \left[ 1 - \frac{P}{(1+2y_e)^2} \left\{ \frac{1}{2} - \frac{\frac{W}{L'_{BS}}}{\sinh \frac{2W}{L'_{BS}}} \right\} \right]^{-1}}{\left[ 1 - \left( \tanh^2 \frac{W}{L'_{BS}} \right) \frac{1+2y_e}{1+y_e} \cdot \frac{y_e^2}{P^2} \right]^{\frac{1}{2}}} \quad \dots (24)$$

where 
$$\frac{1}{L'_{BS}} = \left\{ \frac{v_B(1+y_e)}{D_p(1+2y_e)} \right\}^{\frac{1}{2}} \quad \dots (25)$$

For usual values of  $\frac{W}{L'}$ , the term

$$\left[ 1 - \frac{P}{(1+2y_e)^2} \left\{ \frac{1}{2} - \frac{\frac{W}{L'_{BS}}}{\sinh \frac{2W}{L'_{BS}}} \right\} \right]^{-1}$$

in the numerator of Eq. (24) is very nearly equal to unity. Eq. (24) can, therefore, be rewritten as

$$\beta_{ce} \approx \frac{1 - \frac{y_e}{P} \tanh^2 \frac{W}{L'_{BS}}}{\left[ 1 - \frac{y_e^2(1+2y_e)}{P^2(1+y_e)} \tanh^2 \frac{W}{L'_{BS}} \right]^{\frac{1}{2}}} \quad \dots (26)$$

Eq. (26) predicts a tendency for  $\beta_{ce}$  to increase with  $y_e$ , approaching a limiting value of

$$\beta_{ce} \approx 1 - \frac{W^2 v_B}{8 D_p} \quad \dots (27)$$

for  $y_e \gg 1$  and  $\frac{W^2 v_B}{D_p} \ll 1$ . For  $y_e \ll 1$ , Eq. (26) reduces to the form

$$\beta_{ce} \approx 1 - \frac{W^2 v_B}{2 D_p} \quad \dots (28)$$

If the right hand side of Eq. (26) is expanded binomially, one obtains, neglecting higher order terms,

$$\beta_{ce} \approx 1 - \left( \tanh^2 \frac{W}{L'_{BS}} \right) \left[ \frac{y_e}{P} - \frac{y_e^2 \left( \frac{1+2y_e}{1+y_e} \right)}{2P^2} \right] \quad \dots (29)$$

Using Eq. (29), the reciprocal of the transport factor  $\beta_{cb}$  for the grounded emitter mode of operation can be obtained as

$$\begin{aligned} \beta_{cb}^{-1} &= \left( \tanh^2 \frac{W}{L'_{BS}} \right) \left[ \frac{y_e}{P} - \frac{y_e^2 \left( \frac{1+2y_e}{1+y_e} \right)}{2P^2} \right] \\ &= \frac{W^2 v_B}{2 D_p} \left[ \frac{\tanh^2 \frac{W}{L'_{BS}}}{\frac{W^2 v_B}{D_p}} \left\{ \frac{2y_e}{P} - \frac{y_e^2 \left( \frac{1+2y_e}{1+y_e} \right)}{P^2} \right\} \right] \\ &= \frac{W^2 v_B}{2 D_p} \cdot k_1(z), \quad \dots (30) \end{aligned}$$

where

$$k_1(z) = \frac{\tanh^2 \frac{W}{L_{BS}}}{\frac{W^2 v_B}{D_p}} \left[ \frac{2y_e}{P} - y_e^2 \left( \frac{1 + 2y_e}{1 + y_e} \right) \right] \quad \dots (31)$$

It is easily shown that for  $W \ll L'$

$$k_1(z) \approx \frac{2y_e(1 + y_e)}{P(1 + 2y_e)} - \left( \frac{y_e}{P} \right)^2 \quad \dots (32)$$

$k_1(z)$  may be called the 'fall-off factor' and is analogous to the factors  $g(z)$  and  $m(z)$  of Webster (1954) and Hauri (1956) respectively. Like these latter factors,  $k_1(z)$  tends to unity for  $y_e \ll 1$  but for  $y_e \gg 1$ , the limiting value of this factor is 0.25 as compared to the value of 0.50 for both  $g(z)$  and  $m(z)$ .

In the analysis presented above it has been assumed that  $L'_B$  is a function of  $y_e$ . Webster has, however, suggested that the surface recombination lifetime is independent of  $y_e$  and has ascribed the observed increase in the value of  $\beta_{ce}$  to the increase in the value of the effective diffusion constant. Accepting this point of view, the modified expression for  $\beta_{ce}$  is found to be

$$\beta_{ce} = \frac{1 - \frac{y_e}{P} \tanh^2 \frac{W}{L_{BS}}}{\left[ 1 - \frac{2\{y_e^2 - y_e + \ln(1 + y_e)\}}{P^2} \tanh^2 \frac{W}{L_{BS}} \right]}, \quad \dots (33)$$

where

$$\frac{1}{L_{BS}} = \left( \frac{v_B}{D_p} \right)^{\frac{1}{2}}$$

For low values of  $y_e$  ( $y_e \ll 1$ ), Eq. (33) reduces to the form of Eq. (28) and for high values of  $y_e$  ( $y_e \gg 1$ ), Eq. (33) simplifies to

$$\beta_{ce} \approx 1 - \frac{W^2 v_B}{4D_p} \quad \dots (34)$$

which shows that the loss due to surface recombination is halved at high current densities. This is in accordance with the conclusions arrived at by both Webster and Hauri. For intermediate values of  $y_e$ , however, the nature of variation of

this term can be studied by considering the variation of the 'fall-off factor' which for this case may be written as

$$k_2(z) = \frac{\tanh^2 \frac{W}{L_{BS}}}{\left( \frac{W}{L_{RS}} \right)^2} \left[ \frac{2y_e}{P} - \frac{2\{y_e^2 - y_e + \ln(1 + y_e)\}}{P^2} \right] \quad \dots \quad (35)$$

$$\approx \frac{2y_e}{P} - \frac{2\{y_e^2 - y_e + \ln(1 + y_e)\}}{P^2} \quad \dots \quad (36)$$

It is easily seen from Eq (36) that the limiting values of the factor  $k_2(z)$  for  $y_e \ll 1$  and  $y_e \gg 1$  are 1 and 0.5 respectively in agreement with those of  $g(z)$  and  $m(z)$ . For intermediate values of  $y_e$ ,  $k_2(z)$  differs slightly from both. Table 1 compares these values.

TABLE I

Values of the factors  $g(z)$ ,  $m(z)$ ,  $k_1(z)$  and  $k_2(z)$ .

$y_e$	$g(z)$	$m(z)$	$k_1(z)$	$k_2(z)$
1	2	3	4	5
0.01	0.99	0.99	0.97	1.00
0.05	0.95	0.98	0.89	0.96
0.10	0.92	0.96	0.80	0.94
0.50	0.75	0.86	0.57	0.80
1.00	0.67	0.79	0.44	0.72
2.00	0.60	0.72	0.34	0.64
5.00	0.55	0.64	0.29	0.57
10.00	0.52	0.60	0.26	0.54

(ii) *Recombination confined only to the volume* When the volume recombination term in Eq.(17) plays the dominant role (i.e.  $v_B = 0$ ), one obtains with the help of Eq. (22) the following expression for  $\beta_{ee}$

$$\beta_{ee} = \frac{1 - \left( \tanh^2 \frac{W}{L_{BV'}} \right) \frac{y_e}{P} \left[ 1 - \frac{P}{1 + 2y_e} \left( \frac{1}{2} - \frac{L_{BV'}}{\sinh \frac{2W}{L_{BV'}}} \right) \right]}{\left[ 1 - \left( \tanh^2 \frac{W}{L_{BV'}} \right) \frac{y_e^2}{P^2} \left( 1 + \frac{4}{3} y_e \right) \right]^{\frac{1}{2}}}} \quad (37)$$

where

$$L_{BV'} = \left( \frac{1 + y_e}{D_p \tau_B} \right)^{\frac{1}{2}} \quad \dots \quad (38)$$

On making the same assumption as was made in deriving Eq. (26), Eq. (37) can be simplified to

$$\beta_{cb} \approx \frac{1 - \frac{y_e}{P} \tanh^2 \frac{W}{L_{BV'}}}{\left[ 1 - \left( \frac{y_e}{P} \right)^2 \left( 1 + \frac{4}{3} y_e \right) \tanh^2 \frac{W}{L_{BV'}} \right]} \quad \dots \quad (39)$$

From Eq (39) it is easily seen that for  $y_e \ll 1$ , the expression for  $\beta_{cb}$  reduces to

$$\beta_{cb} \approx 1 - \frac{1}{2} \tanh^2 \frac{W}{D_p \tau_B} \approx 1 - \frac{W^2}{2 D_p \tau_B} \quad \dots \quad (40)$$

which is the usual expression for low level condition of operation. When  $y_e \gg 1$ , the expression for  $\beta_{cb}$  takes the form

$$\beta_{cb} \approx 1 - \frac{1}{3} \left( \tanh^2 \frac{W}{D_p \tau_B} \right) y_e \quad \dots \quad (41)$$

provided  $\frac{W^2}{D_p \tau_B} \cdot y_e$

Assuming  $\frac{W}{L_{BV'}} \ll 1$ , one can obtain from Eq. (39) and approximate expression for  $\beta_{cb}^{-1}$  of the form

$$\beta_{cb}^{-1} = \frac{W^2}{D_p \tau_B} \left[ \frac{y_e}{P} (1 + y_e) \frac{y_e^2}{2 P^2} \left( 1 + \frac{4}{3} y_e \right) \right] \quad \dots \quad (42)$$

It may be noted here that Matz (1958) has suggested an expression for  $\beta_{cb}$  in the form of an integral which when evaluated gives a relation similar to Eq. (42).

From Eq (42) an expression for the 'fall off factor' for this case can be written down directly. Denoting this by the term  $k_3(z)$ , we have

$$k_3(z) = \frac{2 y_e (1 + y_e)}{P} - \frac{y_e^2}{P^2} \left( 1 + \frac{4}{3} y_e \right) \quad \dots \quad (43)$$

It is to be noted that  $k_3(z)$ , unlike the factors  $k_1(z)$  and  $k_2(z)$ , increases with  $y_e$  which shows that the transport factor  $\beta_{cb}$  actually decreases with increasing  $y_e$ . Thus the term 'fall off factor' is a misnomer for this case but has been retained for the sake of uniformity. From Eq. (43) it follows easily that  $k_3(z)$  is equal

to 1 for  $y_e \ll 1$  and is equal to  $\frac{2}{3}y_e$  for  $y_e \gg 1$ . Its values in the range  $.01 < y_e < 10$  are given in Table II.

TABLE II  
Values of the factors  $k_3(z)$ ,  $g'(z)$  and  $m'(z)$

$y_e$	$k_3(z)$	$g'(z)$	$m'(z)$
1	2	3	4
0.01	1.01	1.01	1.00
0.05	1.03	1.05	1.01
0.10	1.07	1.10	1.02
0.50	1.35	1.59	1.11
1.00	1.67	2.31	1.21
2.00	2.39	3.90	1.41
5.00	4.47	9.21	2.01
10.00	7.87	18.60	3.00

'Fall off factors' for the cases considered by Webster (1954) and Hauri (1956) may be derived easily by examining the expressions for  $\beta_{ce}^{-1}$  given by these authors and are found to be

$$\left. \begin{aligned} g'(z) &= 1 + P && [\text{Webster}] \\ m'(z) &= \{m(z)\{1 + \frac{2}{3}m(z)y_e\} && [\text{Hauri}] \end{aligned} \right\} \dots \quad (44)$$

Values of  $g'(z)$  and  $m'(z)$  as given by Eq. (44) for different values of  $y_e$  are given in columns 3 and 4 of Table II.

It should be noted however that the type of volume recombination discussed above is the bimolecular one. The other type of interest is monomolecular volume recombination in which the lifetime tends to become independent of  $y_e$ . A solution for this case may be obtained in the manner outlined above yielding for  $\beta_{ce}$  the expression

$$\beta_{ce} = \frac{1 - \frac{y_e}{P} \tanh^2 \frac{W}{L_{BV}}}{\left[ 1 - \frac{2(y_e^2 - y_e + \ln(1 + y_e))}{P^2} \tanh^2 \frac{W}{L_{BV}} \right]}, \quad \dots \quad (45)$$

where

$$L_{BV} = (D_p \tau_B)^{\frac{1}{2}}.$$

For the limiting case  $y_e \gg 1$ , Eq. (45) reduces to the form

$$\beta_{ce} \approx 1 - \frac{W^2}{4D_p \tau_B}, \quad \dots \quad (46)$$

showing that  $\beta_{ce}$ , after an initial increase with  $y_0$ , attains a limiting value. This is in agreement with the conclusions arrived at by both Webster (1954) and Hauri (1956). The increase of  $\beta_{ce}$  with  $y_0$  as is observed here is due to the apparent increase of the diffusion constant  $D_p$ .

As regards the 'fall off factor' for this case, the formal resemblance between Eq. (45) and Eq. (33) evidently suggests that this factor should be identical with the factor  $k_2(z)$ . A similar argument would show that the 'fall off factors' for the cases treated by Webster and Hauri are identical with the factors  $g(z)$  and  $m(z)$  respectively.

(iii) *Surface and volume recombination operative simultaneously.* So far the two types of recombination processes have been considered separately for reasons already mentioned. The concept of the "fall off factor", however, enables one to infer the law of variation of  $\beta_{ce}$  with  $y_0$  when both the processes are simultaneously operative. We recall (Webster 1954) that at low injection level the expression for  $\beta_{cb}^{-1}$  is given as the sum of three terms corresponding to the contributions of surface recombination, volume recombination and emitter efficiency. Assuming that the emitter efficiency is unity, the expression for  $\beta_{cb}^{-1}$  can be written as

$$\beta_{cb}^{-1} = a \cdot \left\{ \begin{array}{c} k_1(z) \\ k_2(z) \end{array} \right\} + b \cdot \left\{ \begin{array}{c} k_2(z) \\ k_3(z) \end{array} \right\}, \quad \dots \quad (47)$$

where  $a$  and  $b$  are constants depending on the low level values of the surface recombination term and the volume recombination term respectively. The terms within the parentheses in Eq. (47) take into account the possible alternative modes of recombination mentioned earlier.

## 6. EFFECT OF EMITTER EFFICIENCY ON THE TRANSPORT FACTOR

The analysis given in the preceding section has the drawback that it is based on the assumption  $\gamma = 1$ , i.e.  $J_n = 0$ . In a practical transistor, however, this is not so and the expression for  $J_p$  as given by Eq. (3) will consequently be inadequate. When  $J_n \neq 0$ , one obtains from Eqs. (1) and (2)

$$E = \frac{J_n - ebD_p \frac{dp}{dx}}{e\mu_n(p + N_d)}, \quad \dots \quad (48)$$

$$\text{and} \quad J_p = -eD_p \left( 1 + \frac{p}{N_d} \right) \left\{ 1 - \frac{p}{b} \frac{J_n}{J_p(p + N_d)} \right\}^{-1} \frac{dp}{dx} \quad \dots \quad (49)$$

where  $b = \frac{\mu_n}{\mu_p}.$



From Eqs (3) and (49), it is seen that the effective value of the diffusion constant in the latter case is larger than the value obtained with  $J_n = 0$ . This will make the value of  $\beta$  larger. In actual practice, however, this increase is not appreciable. Thus even if  $J_n$  becomes high enough to make  $\gamma = 0.9$ , the percentage increase in  $D_p'$  is not more than 5. The assumption  $J_n = 0$ , therefore, does not affect appreciably the results reported in Secs. 3–5.

## 7. DISCUSSION

To summarise the results obtained in the preceding sections we note that the values of the 'fall-off factors'  $g(z)$ ,  $m(z)$  and  $k_2(z)$  in Table I are in reasonable agreement while those of the factor  $k_1(z)$  are much smaller in magnitude for  $y_e \gg 1$ . This discrepancy arises because of the fact that in deriving Eq (26),  $L_{ps}'$  was assumed to be a function of  $y_e$ , its values increasing with increasing values of  $y_e$  whereas the other factors, viz.  $g(z)$ ,  $m(z)$  and  $k_2(z)$ , were not based on such assumption. A glance at Table I would show that an experimental test of the validity or otherwise of the aforesaid assumption is best made by measuring  $\beta$  at high level of operation. This is, however, difficult because of the increased importance of the emitter efficiency term and volume recombination at high level and of the lack of an accurate method of independent measurement of  $\gamma$  (Deb and Daw, 1958). In view of this we can make a check only for the low levels of operation even though at such levels the values of  $\beta$  as predicted by the different theoretical relations in Table I do not differ widely from each other. Let us consider the case when  $y_e$  is increased from 0 to 0.1. Table I would show that for this change in  $y_e$  the percentage increase in  $\beta$  as predicted by the fall off factors  $g(z)$ ,  $m(z)$ ,  $k_2(z)$  and  $k_1(z)$  are 8, 4, 6 and 20 respectively. Experimentally measured values of change in current amplification factor as obtained for transistor types OC70 and OC602 for the same conditions are 14% for the former and 8.5% for the latter. Bearing in mind the fact that the effects of the volume recombination and emitter efficiency terms would be to make the experimentally measured percentage change in current amplification factor lower than the true increase in the transport factor  $\beta$  it would appear that the assumption regarding the dependance of surface recombination lifetime on  $y_e$  is somewhat justified and that the factor  $k_1(z)$  gives the more correct value of fall-off factor than any of the other three.

Taking the case of volume recombination we find from Table II that the values of the factor  $k_3(z)$  agree quite well with those of  $g'(z)$  for  $y_e \leq 0.1$ . At higher values of  $y_e$ , however, the increase of  $g'(z)$  is faster than that of  $k_3(z)$ . This is understood if it is recalled that while in the present analysis the apparent increase in the diffusion constant of the minority carriers with the level of injection has been taken account of, Webster in his treatment had ignored it. As regards  $m'(z)$ , this factor has the slowest variation with  $y_e$  and consequently gives the highest value of  $\beta_{co}$ . This is because the assumed nature of bimolecular

recombination in this case is different from that given by Eq. (6). Thus in the limiting case  $y_e \gg 1$ , the approximate expressions for  $\beta_{es}$  as given by Webster, Hauri and Eq. (41) are as follows:

$$\beta_{es} \approx 1 - \frac{W^2}{2D_p \tau_B} y_e \quad (\text{Webster}) \quad \dots \quad (50)$$

$$\beta_{es} \approx 1 - \frac{W^2}{12D_p \tau_B} y_e \quad (\text{Hauri}) \quad \dots \quad (51)$$

$$\beta_{es} \approx 1 - \frac{W^2}{8\tau_B} y_e \quad (\text{obtained from Eq. 41}) \quad \dots \quad (52)$$

Here again a categorical experimental verdict in favour of the one or the other of these equations is difficult because of the increasing role of the emitter efficiency term  $\gamma$  under the limiting condition  $y_e \gg 1$ .

It is, however, to be noted that some earlier experimental results (Evans 1956, Deb and Daw 1958) indicate that the effective lifetime passes through a maximum as  $y_e$  is increased from a low value. Eq. (6) used in the present analysis is the only relation suggested so far which can account for such a variation. As such Eq. (47) undoubtedly deserves careful consideration. Assuming now that Eq. (6) is valid for a practical transistor, one obtains from Eqs. (32), (43) and (47) the following expression for  $\beta_{cb}^{-1}$

$$\beta_{cb}^{-1} = a \left[ \frac{2y_e(1+y_e)}{P(1+2y_e)} - \frac{y_e^2}{P^2} \right] + b \left[ \frac{2y_e}{P} (1+y_e) - \frac{y_e^2}{P^2} \left( 1 + \frac{1}{3} y_e \right) \right] \quad (53)$$

$$\text{where} \quad a = \frac{W^2 v_B}{2D_p} \quad \text{and} \quad b = \frac{W^2}{2D_p \tau} \quad \dots \quad (54)$$

A rough check on the validity of Eq. (53) may be made as follows. The values of  $\tau_B$  and  $v_B$  for types OC70 and OC602 transistors determined earlier (Deb and Daw, 1958) are given in columns 2 and 3 of Table III. In column 4 are given values of  $\beta_{ee}$  obtained from these values and Eqs. (53) and (54) for  $y_e = 1$ . Column 5 gives the experimental values of the current amplification factor  $\alpha$  and column 6 those of  $\gamma$  using the results of the preceding two columns. In the last column are given the values of  $\sigma_e L_e$  obtained from the relation

$$\frac{\sigma_e W}{\sigma_e L_e} = \frac{1 - \gamma}{\gamma} \quad \dots \quad (55)$$

These results are in reasonable agreement with the expected values (Early 1953, Webster 1954 and Kaufmann 1959) and lend support to the validity of Eq. (53)

TABLE III  
Values of  $\sigma_e L_e$  at  $y_e = 1$

Transistor type	$\tau_B$ $\mu\text{sec.}$	$1/\nu_B$ $\mu\text{sec.}$	$\beta_{ce}$	$\alpha$	$\gamma$	$\sigma_e L_e$ mhos
1	2	3	4	5	6	7
OC70	86.4	17.2	0.979	0.973	0.994	0.07
OC602	51.8	26.4	0.979	0.977	0.999	1.60

With regard to the role of the term  $\gamma$  it is found that this does not affect sensibly the utility of Eq (17). It is interesting to note that the presence of an appreciable electronic component of current—apart from decreasing  $\beta$  through a decreased  $\gamma$  value—also increases the same through an increased diffusion constant. In practice, however, the decrease in  $\gamma$  masks completely any increase arising out of this last effect.

#### ACKNOWLEDGMENTS

The author wishes to thank Professor J. N. Bhar for providing him with facilities for the work and constant encouragement. Thanks are also due to Dr. S. Deb for giving guidance throughout the progress of the work.

#### REFERENCES

- Deb, S. and Daw, A. N., 1958, *Jour. Elec. and Control.*, **5**, 514.  
 Early, J. M., 1953, *Bell Sys. Tech. Jour.*, **32**, 1271.  
 Fletcher, N. H., 1956, *Proc. I.R.E.*, **44**, 1475.  
 Gnaniotto, L. J., 1955, *Proc. I.R.E.*, **43**, 1529.  
 Hauri, E. R., 1956, *Technische Mitteilungen von der Schweizerischen Post-Telegraphen- und Telefonverwaltung*, **34**, 441.  
 Kaufmann, P., 1959, *Archiv. der Elektrischen Übertragung*, **13**, 141.  
 Matz, A. W., 1958, *Proc. I.R.E.*, **46**, 616.  
 Misawa, T., 1955, *Jour. Phys. Soc., Japan*, **10**, 362.  
 Rittner, E. S., 1954, *Phys. Rev*, **94**, 1161.  
 Webster, W. M., 1954, *Proc. I.R.E.*, **42**, 914.

# FREQUENCY OF THE THREE-PHASE R-C COUPLED OSCILLATOR PART II. INDUCTIVE ANODE LOAD RESISTANCE

H. RAKSHIT AND M. C. MALLIK

DEPARTMENT OF ELECTRONICS & ELECTRICAL COMMUNICATION ENGINEERING, INDIAN  
INSTITUTE OF TECHNOLOGY, KHARGPUR

(Received, December 12, 1959)

**ABSTRACT.** When the three stages of a conventional three phase R-C oscillator are identical, the oscillations normally produced are of radio frequency  $\omega = \sqrt{3/CR}$ , where  $R$  and  $C$  are tuning resistance and capacitance. It was shown in Part I (Rakshit and Mallik, 1955) that this simple formula holds when the load resistance is non-reactive and the cathode impedance is zero or resistive. The case of inductive anode resistance when cathode impedance is (i) resistive and (ii) reactive has been discussed in the present paper. For resistive cathode impedance an inductance in series with anode resistance  $R$  causes an increase in frequency over the  $\sqrt{3/CR}$  value up to a certain magnitude of the inductance but for still higher magnitudes the frequency goes on decreasing.

The effect of reactive cathode when the anode load is inductive is the same as that for non-reactive anode load resistance discussed in Part I. Inductive cathode impedance decreases the frequency of oscillation from the value for resistive cathode impedance while capacitive cathode impedance generally increases the same.

## INTRODUCTION

It has been shown in Part I that the frequency of the three phase R-C oscillator is dependent on the cathode circuit impedance. The simple expression for frequency  $\omega = \sqrt{3/CR}$  holds good, only when the cathode circuit impedance is zero or purely resistive and anode load resistance is non-reactive. When the cathode impedance is reactive the generated frequency will be greater or less than  $\sqrt{3/CR}$  depending upon whether the cathode impedance is capacitive or inductive. The effect of cathode impedance is prominent when the generated frequency is much below or much above the cathode resonant frequency.

In the present paper we shall discuss the condition when cathode impedance is zero, resistive, or reactive but anode load resistance is inductive. The addition of inductance with the load resistance increases the load impedance and makes it possible to maintain oscillation at comparatively low values of load resistance. In fact in our attempt to generate very high frequency it has been found that these inductances are essential for maintenance of oscillation (Rakshit and Mallik, 1953). Without the small inductance the oscillation frequency  $\omega =$

$\sqrt{3}/CR$  and the phase shift per stage is 120 degrees. The presence of the small inductance causes a decrease in phase shift at this frequency and as a result the frequency of the maintained oscillation is increased. This increase in frequency with increasing inductance continues up to a certain maximum value and thereafter the frequency goes on decreasing and finally for still larger values of inductance the frequency becomes less than  $\sqrt{3}/CR$  value.

#### THEORETICAL CONSIDERATION

In this case the anode load  $Z_0$  consists of the tuning capacitor  $C$  shunted by the series combination of  $R$  and its associated inductance  $L$ .

Hence,

$$Z_0 = \frac{R + j\omega\{L(1 - \omega^2 LC) - CR^2\}}{\omega^2 C^2 R^2 + (\omega^2 LC - 1)^2} \quad \dots (1)$$

The phase angle of the load is given by

$$\tan \theta = \frac{\omega\{L(1 - \omega^2 LC) - CR^2\}}{R}$$

and the frequency of the radio frequency oscillation is accordingly given by  $\tan \theta = -\sqrt{3}$  (Rakshit and Bhattacharyya, 1946)

$$\text{Or} \quad \omega^3 L^2 C^3 + \omega(CR^2 - L) - \sqrt{3}R = 0 \quad \dots (2)$$

This is a cubic equation with one real root, the other two being imaginary. The real value of  $\omega$  is given by

$$\omega = [P + (P^2 + Q^3)^{1/3}]^{1/3} + [P - (P^2 + Q^3)^{1/3}]^{1/3} \quad \dots (3)$$

where

$$P = \frac{\sqrt{3}R}{2L^2C} \quad \text{and} \quad Q = \frac{CR^2 - L}{3L^2C}$$

For convenience of numerical computation, this may be written in the following form by putting  $x$  for  $CR^2/L$ . We then have

$$\omega = \frac{x^{2/3}}{CR} \left[ \left\{ \frac{\sqrt{3}}{2} + \left( 0.75 + \frac{(x-1)^3}{27x} \right)^{1/3} \right\}^{1/3} + \left\{ \frac{\sqrt{3}}{2} - \left( 0.75 + \frac{(x-1)^3}{27x} \right)^{1/3} \right\}^{1/3} \right] \quad \dots (3a)$$

$$= \frac{K}{CR}, \quad \dots (3b)$$

$$\text{where } K = x^{2/3} \left[ \left\{ \frac{\sqrt{3}}{2} + \left( 0.75 + \frac{(x-1)^3}{27x} \right)^{1/3} \right\} + \left\{ \frac{\sqrt{3}}{2} - \left( 0.75 + \frac{(x-1)^3}{27x} \right)^{1/3} \right\} \right].$$

It is obvious that if a table giving  $K$  for different values of  $x$  according to this equation is available we can at once calculate  $\omega$  from Eqn. (3b) by first finding  $x$  for the particular combination of  $R$ ,  $L$  and  $C$ . For this purpose the calculated values of  $K$  for different values of  $x$  ranging from 0.01 to 100 have been given in Table 1. The results are also plotted in Fig. 1. For values of  $x > 100$  or  $<$

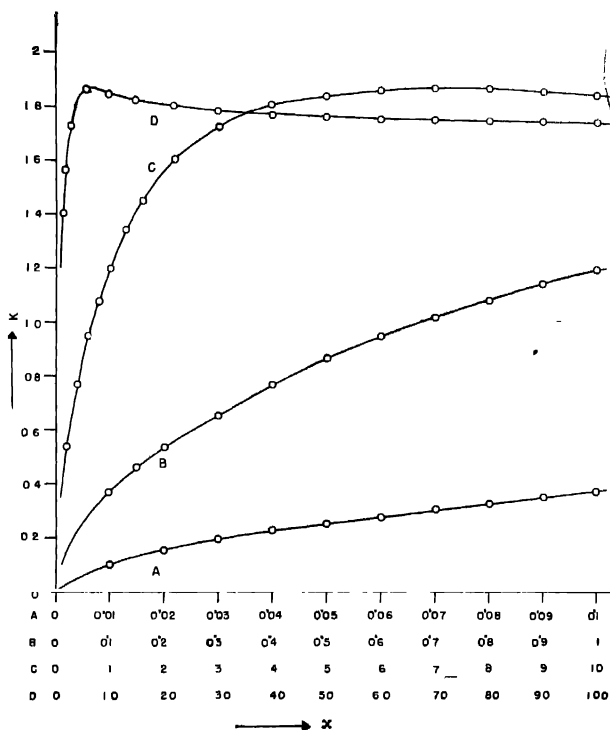


Fig. 1. Variation of  $K$  with  $x$ .

$< 0.01$  we can calculate the value of  $\omega$  after making some approximations leading to Eqns. (4a) and (7a). The error involved in these approximations is quite

small. Thus for  $x = 100$  if  $\omega$  is calculated by Eqn. (4a) instead of Eqn. (3a), the result is 0.117% greater than the exact value. For larger values of  $x$  the error due to approximation will gradually diminish. Similarly when  $x = 0.01$  if  $\omega$  is calculated by Eqn. (7a) the result is 1.2% greater than the exact value. For still smaller values of  $x$  the error due to approximation is still less.

TABLE I

 $x$  vs.  $K$ 

$x$	$K$	$x$	$K$	$x$	$K$
0.01	0.1073	1	1.2010	6	1.8633
0.02	0.1547	1.1	1.2486	7	1.8661
0.03	0.1930	1.2	1.2971	8	1.8637
0.04	0.2251	1.3	1.3389	9	1.8551
0.05	0.2540	1.4	1.3789	10	1.8537
0.06	0.2805	1.5	1.4154	11	1.8479
0.07	0.3049	1.6	1.4492	12	1.8416
0.08	0.3272	1.7	1.4804	13	1.8363
0.09	0.3495	1.8	1.5134	15	1.8263
0.1	0.3699	1.9	1.5363	22	1.8014
0.15	0.4606	2	1.5613	25	1.7945
0.20	0.5375	2.2	1.6062	30	1.7854
0.30	0.6556	2.5	1.6622	40	1.7735
0.40	0.7724	2.8	1.7108	50	1.7648
0.50	0.8660	3	1.7320	60	1.7559
0.60	0.9477	3.4	1.7718	70	1.7547
0.70	1.0217	3.7	1.7949	80	1.7534
0.80	1.0859	4	1.8137	90	1.7520
0.90	1.1445	5	1.8488	100	1.7472

It will be noted that when  $Q$  is negative and  $P^2 < |Q^3|$ ,  $\{P^2 + Q^3\}^{1/2}$  is imaginary and Eqn. (3) can be solved with the help of trigonometry but not algebraically.

The expression for  $\omega$  as given in Eqn. (3) can be reduced to a simpler approximate form when one of the terms under the square root becomes small in comparison with the other. Thus when  $CR^2 > L$ , i.e.  $Q$  is positive and  $P^2 \ll Q^3$

i.e.  $\frac{81CR^2}{4L} \left( \frac{CR^2}{L} - 1 \right)^3$ , we get (see Appendix I)

$$\omega = \frac{\sqrt{3}R}{CR^2 - L} \left[ 1 - \frac{3R^2 L^2 C}{(CR^2 - L)^3} \right] \quad \dots (4)$$

Or

$$\omega = \frac{\sqrt{3}x}{CR(x-1)} \left[ 1 - \frac{3x}{(x-1)^3} \right] \quad \dots (4a)$$

As a further approximation when  $CR^2 \gg L$  we may neglect the term

$\frac{3R^2L^2}{(CR^2 - L)^3}$  and Eqn (4) reduces to

$$\omega = \frac{\sqrt{3R}}{CR^2 - L} \quad \dots (5)$$

This shows that when  $L$  is so small that  $P^2 \ll Q^3$  the small inductance associated with the anode load resistance causes an increase in frequency. In the limit when  $L = 0$ , we get the simple expression  $\omega = \sqrt{3}/CR$

When  $Q$  is negative and  $P^2 < |Q^3|$ , solving Eqn. (3) trigonometrically gives

$$\omega = r^{1/3} 2 \cos \frac{\phi}{3} \quad \dots (6)$$

where  $r = |Q^{3/2}|$  and  $\cos \phi = P/Q^{3/2}$ . Substituting the values of  $P$  and  $Q$ ,

$$\omega = \left[ \frac{1}{3LC} \left( \frac{CR^2}{L} - 1 \right) \right]^{1/3} 2 \cos \frac{\cos^{-1} \left[ \frac{81CR^2}{4L \left( \frac{CR^2}{L} - 1 \right)^3} \right]}{3} \quad \dots (6a)$$

When  $R$  is very small Eqn (6) reduces to (see Appendix II)

$$\omega = \frac{1}{\sqrt{LC}} + \frac{\sqrt{3R}}{2L} \quad \dots (7)$$

Or in terms of  $x$ ,

$$\omega = \frac{\sqrt{x}}{CR} \left( 1 + \frac{\sqrt{3x}}{2} \right) = \frac{1}{\sqrt{LC}} \left( 1 + \frac{\sqrt{3x}}{2} \right) \quad \dots (7a)$$

This shows that when  $R$  is of the order of 0 the frequency generated by a 3-phase oscillator is approximately equal to the frequency generated by an orthodox  $L-C$  oscillator with same circuit parameters but always greater than  $1/\sqrt{LC}$ . The expression  $\omega = 1/\sqrt{LC}$  in case of 3-phase oscillator can also be obtained by putting  $R = 0$  in Eqn. (2) but from the expression for  $\tan \theta$  it is obvious that oscillations cannot be maintained when  $R = 0$ .

The above Eqn. (6) holds good in the case  $CR^2 < L$  upto the limit  $P^2 = |Q^3|$ . Under this limiting condition  $\cos \phi = 1$  and hence  $\cos \frac{\phi}{3} = 1$  and

$$\omega = 2 \left\{ \frac{\sqrt{3R}}{2L^2C} \right\}^{1/3} \quad \dots (8)$$



It will be noted that when the above condition holds,  $P^2 + Q^3 = 0$  and the same expression for  $\omega$  is also obtained directly from Eqn. (3).

When, on the other hand,  $P^2 \gg Q^3$

$[P + (P^2 + Q^3)]^{1/3}$  is of the order of  $(2P)^{1/3} + \frac{1}{12} \frac{Q^3}{P^2} (2P)^{1/3}$  and  $[P - (P^2 + Q^3)]^{1/3}$

is of the order of  $-\left(\frac{Q}{2P}\right)^{1/3}$ .

$$\therefore \omega = (2P)^{1/3} - \left(\frac{Q}{2P}\right)^{1/3} + \frac{1}{12} \frac{Q^3}{P^2} (2P)^{1/3} \quad \dots (9)$$

Or, in terms of  $x$ ,

$$\omega = \frac{1}{CR} \left[ (\sqrt{3}x^2)^{1/3} - \frac{x^{1/3}(x-1)}{3^{7/6}} + \frac{(x-1)^3}{x^{1/3}3^{29/6}} \right] \quad \dots (9a)$$

For generating very high frequency the magnitudes of  $R$ ,  $C$  and  $L$  should be very small;  $(CR^2 - L)$  is then usually a very small quantity. In the special case when  $CR^2 - L = 0$  i.e.  $x = 1$ , Eqn. (9a) reduces to

$$\omega = \frac{3^{1/6}}{CR} = \frac{1.201}{CR} \quad \dots (10)$$

#### Condition for Maintenance of Oscillation

We have so far considered the phase shift per stage necessary to produce oscillations. For maintenance of these oscillations the gain  $A$  per stage must at least be unity. If anode load impedance of each oscillator stage is  $Z_0$  as given in Eqn. (1), this means

$$g_m Z_0 = A \gg 1$$

where  $g_m$  is the mutual conductance of the oscillator valves. To evaluate  $Z_0$  from Eqn. (1) in terms of circuit parameters we have to substitute the value of  $\omega$  in terms of these parameters. Taking  $\omega$  as given by Eqn. (3b), we find

$$Z_0 = \frac{R \left[ 1 + \frac{K^2}{x^2} \left\{ 1 - \frac{K^2}{x} - x \right\}^2 \right]}{K^2 + \left( \frac{K^2}{x} - 1 \right)^2}$$

For a particular combination of  $C$ ,  $R$  and  $L$ , since  $x$  and  $K$  are pure numbers  $Z_0$  is obtained in terms of  $R$  only. It is easy to see that  $Z_0$  can likewise be expressed in terms of any one of the circuit parameters. The magnitude of  $Z_0$  in terms of  $R$  for various values of  $x$  and the condition that has to be satisfied to maintain oscillation in those cases are given in Table II and plotted in figure 2. It may be noted that when  $L = 0$  we have the simple  $R-C$  oscillator and  $\omega = \sqrt{3/CR}$ ,

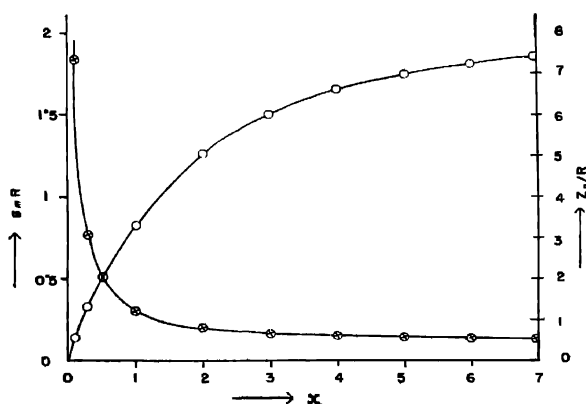


Fig. 2.  $Z_0$  in terms of  $R$ , and  $g_m R$  required for maintenance of oscillation, for different values of  $x$ .

TABLE II  
 $Z_0$  vs  $x$  and minimum  $g_m R$  for oscillation

$x$	$Z_0$	Min. $g_m R$	Remarks
$\infty$	0.5 R	2	Purely resistive load
6.964	0.53 R	1.866	$\frac{\partial \omega}{\partial L} = 0$
6	0.546 R	1.813	
5	0.568 R	1.759	
4	0.603 R	1.659	
3	0.666 R	1.50	$\omega_{RC} = \omega_{RLC}$
2	0.792 R	1.263	
1	1.221 R	0.818	$CR^2 = L$
0.5	2 R	0.5	$\frac{\partial \omega}{\partial R} = 0$
0.3	3.06 R	0.327	
0.1	7.342 R	0.136	

$Z_0 = R/2$  and condition for maintenance is  $g_m R \gg 2$ . When  $R = 0$ ,  $\omega$  is of the order of  $1/\sqrt{LC}$  (Eqn. 7),  $Z_0$  is very large and oscillation can be maintained with only a very small value of  $g_m$ .

#### NATURE OF VARIATION OF $\omega$ WITH THE TUNING PARAMETERS IN THE THREE-PHASE OSCILLATOR

The equations deduced above give the variations of  $\omega$  when the tuning parameters are changed. Some important results are obtained if we study the variation with any one parameter at a time.

##### (a) Variation of $\omega$ with $R$

1. In the case of the  $R-C$  oscillator the frequency is given by  $\omega = \sqrt{3/CR}$ .

$$\frac{\partial \omega}{\partial R} = -\frac{\sqrt{3}}{CR^2} \quad \dots (11)$$

and is always negative.

2. In the case of the  $R-L-C$  oscillator the real value of  $\omega$  is given by Eqn. (3), but it is rather difficult to find  $\partial \omega / \partial R$  from this expression for  $\omega$ . It is more convenient to find  $\partial \omega / \partial R$  starting from Eqn. (2). Thus if we put

$$\omega^3 L^2 C + \omega (CR^2 - L) - \sqrt{3}R = F$$

then

$$\frac{\partial \omega}{\partial R} = -\frac{\partial F}{\partial R} \bigg/ \frac{\partial F}{\partial \omega} = -\frac{2\omega CR - \sqrt{3}}{3\omega^2 L^2 C + (CR^2 - L)} \quad \dots (12)$$

For any particular set of values for  $R$ ,  $L$  and  $C$ , we find  $\omega$  from Eqn. (3) and substituting this value of  $\omega$  in Eqn. (12) we get  $\partial \omega / \partial R$ . Now from Eqn. (2),  $\omega^2 L^2 C + (CR^2 - L) = \frac{\sqrt{3}R}{\omega}$  and hence Eqn. (12) may be written as

$$\frac{\partial \omega}{\partial R} = \frac{\sqrt{3} - 2\omega CR}{2\omega^2 L^2 C + \frac{\sqrt{3}R}{\omega}} \quad \dots (12a)$$

The denominator being always positive, we see that the nature of variation of  $\omega$  is dependent upon whether  $2\omega CR$  is greater or less than  $\sqrt{3}$ . In the limit when  $L = 0$ , we have the simple  $R-C$  oscillator and  $\omega = \sqrt{3/CR}$  and Eqn. (12a) gives

$$\frac{\partial \omega}{\partial R} = -\frac{\sqrt{3}}{\sqrt{3}R/\omega} = -\frac{\omega}{R} = -\frac{\sqrt{3}}{CR^2}$$

exactly as in Eqn. (11a). Equation (12a) further shows that if the set of values of  $R$ ,  $L$  and  $C$  is such that  $\sqrt{3/2CR} > \omega$ ,  $\partial\omega/\partial R$  is positive for the  $R-L-C$  oscillator and not negative as is always the case with simple  $R-C$  oscillator. In fact for very small values of  $R$ ,  $\partial\omega/\partial R$  is always positive, since  $2CR\omega$  approaches zero as  $R$  becomes negligibly small.

Further if  $R$  is gradually increased, keeping the above magnitudes of  $L$  and  $C$  constant, we come to a value of  $\omega = \sqrt{3/2CR}$  for which  $\partial\omega/\partial R = 0$ . This maximum value of  $\omega$  for which  $\partial\omega/\partial R = 0$  may be calculated as follows : We have  $\omega_{max} = \sqrt{3/2CR_{max}}$ , where  $R_{max}$  is the value of  $R$  for which  $\partial\omega/\partial R = 0$ . Substituting this value of  $R$  in Eqn. (2), we have

$$\omega^3 L^2 C' - \frac{3}{4\omega C} - \omega L = 0$$

or

$$4\omega^4 L^2 C'^2 - 4\omega^3 L C' - 3 = 0$$

Solving as a quadratic in  $2\omega^2 L C'$ , we get

$$2\omega^2 L C' = 3 \text{ or } -1,$$

the negative value being obviously inadmissible

$$\omega_{max} = \left[ \frac{3}{2LC} \right]^{1/2} \quad \dots (13a)$$

and

$$R_{max} = \left[ \frac{L}{2C} \right]^{1/2} \quad \dots (13b)$$

These equations show that if the ratio  $L/C$  is kept constant, the maximum frequency for which  $\partial\omega/\partial R = 0$  will correspond to a fixed value of resistance irrespective of the individual magnitudes of  $L$  and  $C$ . The magnitude of the maximum frequency which depends on the product  $LC$  will however be different for different magnitudes of  $L$  and  $C$ .

For further increase in  $R$ ,  $\delta\omega/\partial R$  is negative and at a certain value of  $R$  the frequency of the  $R-L-C$  oscillator once again becomes equal to  $\sqrt{3/CR}$  as if  $L$  were not present. This value of  $R$  for which the presence or absence of  $L$  makes no difference in the frequency of the oscillations may be obtained by putting  $\omega = \sqrt{3/CR}$  in Eqn. (2). This gives

$$\frac{3\sqrt{3}L^2C}{C^3R^3} + \frac{\sqrt{3}CR^2}{CR} - \frac{\sqrt{3}L}{CR} - \sqrt{3}R = 0$$

or

$$\frac{\sqrt{3}L}{CR} \left( \frac{3L}{CR^2} - 1 \right) = 0$$

which is satisfied by

$$(i) \quad L = 0 \text{ and } (ii) \quad CR^2 = 3L \quad \dots (14)$$

Condition (i) is obvious and condition (ii) gives the desired value of  $R$ .

It is interesting to compare the value of  $\partial\omega/\partial R$  at the same value of  $\omega$ , for the two cases — (i)  $R$ - $C$  oscillator and (ii)  $R$ - $L$ - $C$  oscillator with  $R = [3L/C]^{\frac{1}{2}}$  i.e.,  $CR^2 = 3L$ . For case (i),  $\partial\omega/\partial R = -\sqrt{3}/CR^2$  as already seen. For case (ii), substituting  $\omega = \sqrt{3}/CR$  and  $L = CR^2/3$  in Eqn. (12) gives

$$\left(\frac{\partial\omega}{\partial R}\right)_{RLC} = -\frac{\sqrt{3}}{5CR^2} - \frac{3}{5}\left(\frac{\partial\omega}{\partial R}\right)_{RC} \quad (15)$$

This shows that for the same value of  $\omega$  with a particular value of  $R$  and  $C$  the stability of frequency with respect to variation in  $R$  is higher if an inductance  $L = CR^2/3$  is included in series with the anode load resistance

To minimise this type of frequency variation it is obviously best to work in the region where  $\partial\omega/\partial R = 0$ . Since we have two Eqns. (13a and 13b) and three quantities  $R_{max}$ ,  $L$  and  $C$  to be estimated for the desired value of  $\omega_{max}$  to be maintained, we have a wide choice in the selection of these parameters. From the point of view of reduction in frequency variation due to changes in valve inter-electrode capacitances we should select as large a value of  $C$  as is possible

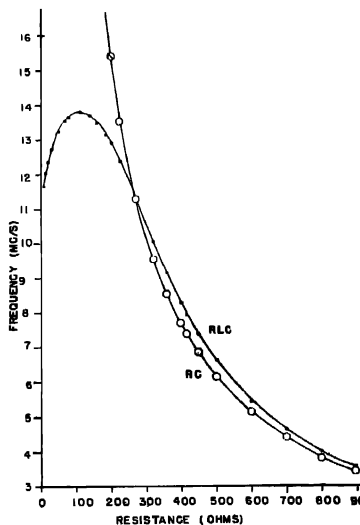


Fig. 3. Variation of Frequency with Resistance.

Thus if the desired frequency is 20 Mc/s. and is to be obtained with  $C = 100\mu F$ , Eqn. (13a) gives  $L$  is of the order of  $0.964\mu H$  and Eqn. (13b) gives  $R_{max}$  is of the order of 68.94 ohms.

The frequencies calculated according to Equ. (3) for different values of  $R$  and (i) with fixed values of  $L$  and  $C$  for  $R-L-C$  oscillator and (ii) fixed value of  $C$  for  $R-C$  oscillator are given in Table III and the variations of frequency with  $R$  are plotted in Fig. 3. The curves in Fig. 3 further show that for the typical values of  $L$  and  $C$  chosen in the example although  $\partial\omega/\partial R$  is negative in either case for values of  $R > [L/2C]^{\frac{1}{2}}$ , the magnitude of  $\partial\omega/\partial R$  is lower for the  $RLC$  case for moderate values of  $R$ . As  $R$  is further increased  $\partial\omega/\partial R$  becomes equal for the two cases and for still larger values of  $R$ ,  $\partial\omega/\partial R$  for the  $RLC$  case becomes higher than that for the  $RC$  case. Again for very high resistances the slopes tend towards equality.

TABLE III  
Variation of frequency with  $R$   
 $C = 89.4\mu\mu F$ ;  $L = 2.2277\mu H$

$R$ in ohms (Effective value)	Frequency in Mc/s		$f_{R-L-C} - f_{R-C}$ in Mc/s
	$R-L-C$	$R-C$	
5	11.672	Oscillation is not possible with valves having $g_m$ not greater than $10\text{mA/V}$	
13.5	12.02		
22	12.357		
32	12.717		
52	13.237		
70	13.55		
80	13.663		
100	13.802		
111.6	13.812		
138	13.723		
160	13.505		
185	13.413		
200	12.91	15.417	-2.507
228	12.348	13.520	1.172
273.5	11.27	11.27	0
323	10.044	9.562	+0.482
360	9.159	8.565	0.594
400	8.296	7.709	0.587
416	7.930	7.403	0.527
450	7.370	6.852	0.518
500	6.613	6.617	0.446
600	5.427	5.139	0.302
700	4.602	4.404	0.198
800	3.994	3.854	0.140
900	3.527	3.429	0.098
1000	3.155	3.083	0.072

(b) Variation of  $\omega$  with  $L$ .

This case applies only to the  $R-L-C$  oscillator and proceeding as already discussed we get

$$\frac{\partial \omega}{\partial L} = - \frac{\partial F}{\partial L} \bigg/ \frac{\partial F}{\partial \omega} = \frac{\omega(1 - 2LC'\omega^2)}{3\omega^2 L^2 C' + (C'R^2 - L)} = \frac{\omega(1 - 2LC'\omega^2)}{2\omega^2 L^2 C' + \frac{\sqrt{3}R}{\omega}} \dots (16)$$

Here also, as in case of variation of  $\omega$  with  $R$ , the nature of variation of  $\omega$  is dependent upon whether  $2LC'\omega^2$  is greater or less than unity. For negligibly small values of  $L$ ,  $\partial\omega/\partial L$  is positive and with increase of  $L$  the rate is gradually reduced to zero and thereafter  $\partial\omega/\partial L$  becomes negative. The maximum value of  $\omega$  when  $\partial\omega/\partial L = 0$  is given by  $\omega_{max} = 1/[2CL_{max}]^{1/2}$ , where  $L_{max}$  is the value of  $L$  for which  $\partial\omega/\partial L = 0$ . Substituting this value of  $L_{max}$  in Eqn. (2), we get

$$4\omega^2 C'^2 R^2 - 1\sqrt{3}\omega C'R - 1 = 0$$

$\therefore \omega_{max} = (\sqrt{3} \pm 2)/2C'R$ . The negative sign is obviously inadmissible and hence

$$\omega_{max} = 1.866/C'R \text{ and } L_{max} = 0.1435 CR^2 \dots (17)$$

After reaching maximum frequency for  $L = L_{max}$ ,  $\partial\omega/\partial L$  becomes negative with further increase in  $L$ . At a certain value of  $L$  greater than  $L_{max}$  the fre-

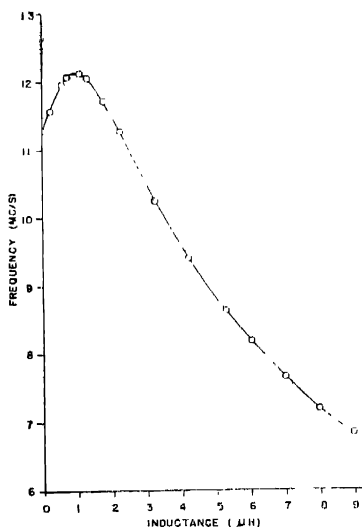


Fig. 4. Variation of frequency with inductance.

quency becomes equal to that of a simple  $R-C$  oscillator. This value of  $L$  is, as before, given by  $CR^2 = 3L$ .

The frequencies calculated according to Eqn. (3) for different values of  $L$  and with fixed values of  $R$  and  $C$  are given in Table IV and the results are plotted in Fig. 4.

TABLE IV  
Variation of frequency with  $L$   
 $C = 89.4 \mu\mu F$ ;  $R = 273.5 \Omega$

Inductance in $\mu H$	Frequency in Mc/s.	Inductance in $\mu H$ .	Frequency in Mc/s.
0.1937	11.580	6	8.1713
0.5444	11.979	7	7.665
0.7087	12.085	8	7.2042
0.9693	12.147	9	6.834
1.062	12.136	11.00	6.216
1.30	12.06	13.374	5.6063
1.749	11.725	15.00	5.3179
2.2277	11.27	17.00	4.979
3.2386	10.26	20.00	4.5958
4.1824	9.4155	30.00	3.677
5.2923	8.6261	40.00	3.1776

(c) Variation of  $\omega$  with  $C$ .

1. In case of  $R$ - $C$  oscillator  $\omega = \sqrt{3/CR}$  and

$$\frac{\partial \omega}{\partial C} = - \frac{\sqrt{3}}{C^2 R} \quad \dots \quad (18)$$

and is always negative.

2. In case of the  $R$ - $L$ - $C$  oscillator,

$$\frac{\partial \omega}{\partial C} = - \frac{\partial F}{\partial C} \bigg/ \frac{\partial F}{\partial \omega} = - \frac{\omega^3 L^2 + \omega R^2}{2\omega^2 L^2 C + \frac{\sqrt{3}R}{\omega}} \quad \dots \quad (19)$$

and is always negative. When  $C$  is negligibly small, Eqn. (2) reduces to  $\omega L + \sqrt{3}R = 0$ , i.e. oscillations are not possible with very small values of  $C$ . At a value of  $C = 3L/R^2$ ,  $\omega_{LO} = \omega_{RO} = \sqrt{3/CR} = R/\sqrt{3}L$ , and substituting  $\omega = \sqrt{3/CR}$  and  $L = CR^2/3$  in Eqn. (19) we get

$$\frac{\partial \omega}{\partial C} = - \frac{4}{5} \frac{\sqrt{3}}{C^2 R} = - \frac{4}{5} \left( \frac{\partial \omega}{\partial C} \right)_{RC} \quad \dots \quad (20)$$



This shows that with a particular combination of  $R$  and  $C$ , the stability of frequency with respect to variation in  $C$  is higher if an inductance  $L = CR^2/3$  is included in series with the anode load resistance. Equations (15) and (20) show that this inductance improves frequency stability with regard to variations in  $R$  as well as  $C$ .

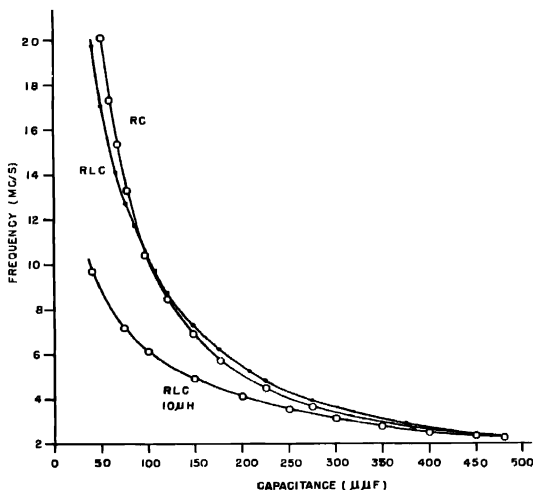


Fig. 5. Variation of frequency with capacitance

The frequencies calculated according to Equ (3) for different values of  $C$  and (i) with fixed values of  $L$  and  $R$  for  $R-L-C$  oscillator and (ii) with fixed value of  $R$  for the  $R-C$  oscillator are given in Table V and the results are plotted in Fig. 5. In the same figure the variation of frequency with capacity for same  $R$  but  $L = 10\mu H$  is also plotted.

#### EFFECT OF CATHODE CIRCUIT IMPEDANCE ON OSCILLATOR FREQUENCY

The impedance of the cathode circuit of an oscillator valve may be resistive, inductive or capacitive depending on the magnitude of cathode biasing capacitance and operating frequency. The nature of impedance of the cathode circuit at different frequencies with different circuit components has been discussed

in Part I in connection with  $R-C$  oscillator with non-inductive load resistance. It has been pointed out there that the effect of cathode impedance  $Z_k$  on the oscil-

TABLE V  
Variation of frequency with  $C$   
 $R = 273.50\Omega$  ;  $L = 2.2277\mu H$

Capacitance in $\mu\mu F$	Frequency in Mc/s		Capacitance in $\mu\mu F$	Frequency in Mc/s.	
	$R-L-C$	$R-C$		$R-L-C$	$R-C$
40	19.72	25.19	120	8.743	8.420
49.5	17.05	20.04	133	7.975	7.578
58	15.355	17.35	147	7.276	6.856
66	14.039	15.27	175	6.184	5.772
76	12.665	13.26	207.4	5.236	4.860
85	11.633	11.857	225	4.821	4.478
89.4	11.27	11.27	275	3.937	3.664
96	10.556	10.499	375	2.845	2.694
106	9.724	9.509	480	2.209	2.120

lator load is to change its effective value. When, for example, the screen is decoupled to ground the anode load  $Z_0$  is changed to (Sturley, 1949)

$$Z_{eff} = \frac{Z_0}{1 + g_k Z_k} \quad \dots (21)$$

where  $g_k = g_m + g_s$ ,  $g_s$  being screen current-grid voltage slope conductance.

The presence of some impedance in the cathode circuit also influences the input admittance of the valve which becomes perceptible only at high frequency. In the present case the effect of change in input admittance on the oscillator frequency which is very small, has been ignored.

Substituting the value of  $Z_0$  from Eqn. (1) we find, on simplification, that the phase angle  $\theta$  of the effective load is given by

$$\tan \theta = \frac{\omega\{L - \omega^2 L^2 C - CR^2\}\{1 + g_k r\} - g_k X R}{R(1 + g_k r) + \omega X g_k (L - \omega^2 L^2 C - CR^2)} \quad (22)$$

where  $r$  and  $X$  are the resistive and reactive parts of the cathode impedance. The frequency of the oscillation is given by  $\tan \theta = -\sqrt{3}$

$$\text{Or} \quad -\sqrt{3} = \frac{\{\omega L - \omega^3 L^3 C - \omega C R^2\}\{1 + g_k r\} - g_k X R}{R(1 + g_k r) + \omega X g_k (L - \omega^2 L^2 C - C R^2)} \quad (23)$$

Near about the resonant frequency of the cathode circuit the magnitude of the reactive component  $X$  is negligible and then the frequency of oscillation is given by

$$-\sqrt{3} = \frac{\{\omega L - \frac{\omega^3 L^2 (C - \omega^2 R^2)}{R(1 + g_k r)}\}}{R(1 + g_k r)}$$

or

$$\omega^3 L^2 (C + \omega(CR^2 - L)) - \sqrt{3}R = 0$$

which, as expected, is the same as Eqn. (2).

When the generated frequency is greater than the resonant frequency of the cathode circuit the cathode impedance will be inductive and we may put  $X = \omega_1 L'$ , where

$L'$  = effective inductance of the cathode circuit which is also a function of the generated frequency  $\omega_1$ .

Equation (23) then reduces to

$$\begin{aligned} & \sqrt{3}\omega_1^4 L^2 C L' g_k + \omega_1^4 L^2 C (1 + g_k r) + \omega_1(CR^2 - L)(1 + g_k r) \\ & - \sqrt{3}R(1 + g_k r) + \sqrt{3}\omega_1^2 L' g_k (CR^2 - L) + \omega_1 L' g_k R = 0 \quad \dots (24) \end{aligned}$$

This being a bi-quadratic equation in  $\omega_1$  it is not possible to have a simple solution. It can however be shown that when the cathode circuit is inductive the generated frequency decreases. This can be seen by comparing Eqn. (24) which may be put in the form

$$\omega_1^4 L^2 C + \omega_1(CR^2 - L) - \sqrt{3}R = \frac{4\omega_1 L' g_k R}{1 + g_k r + \sqrt{3}\omega_1 L' g_k} \quad (24a)$$

and Eqn. (2) according to which the generated frequency is  $\omega$  when the cathode circuit is resonant, given by

$$\omega^3 L^2 C + \omega(CR^2 - L) - \sqrt{3}R = 0$$

Since the right hand side of Eqn. (24a) is essentially a negative quantity,  $\omega_1 < \omega$  because the anode circuit parameters  $L$ ,  $C$  and  $R$  are maintained constant.

The absolute difference between  $\omega$  and  $\omega_1$  naturally depends upon the magnitude of  $4\omega_1 L' g_k R / (1 + g_k r + \sqrt{3}\omega_1 L' g_k)$ . When either  $g_k$  or  $R$  or both are small  $\omega - \omega_1$  is also small, i.e. the influence of cathode circuit on the oscillator frequency will be small.

Similarly when the cathode circuit is capacitive i.e. the generated frequency is less than the resonant frequency of the cathode circuit, we may put  $X = -1/\omega_2 C'$  where  $C'$  = effective capacitance of the cathode circuit which is of

course a function of the generated frequency  $\omega_2$ . Equation 23 then reduces to

$$\omega_2^3 L^2 C' + \omega_2 (CR^2 - L) - \sqrt{3}R = \frac{4g_k R}{\omega_2 C'(1 + g_k r) - \sqrt{3}g_k} \quad \dots \quad (25)$$

The right hand side of Eqn. (25) may be positive or negative depending mainly on the magnitude of  $C'$ . It may be mentioned here that in any practical case  $C'$  never reaches such a low value as to make  $\omega_2 C'(1 + g_k r)$  less than  $\sqrt{3}g_k$ . The right hand side of Eqn. (25) will then be positive. Now comparing Eqn. (25) with Eqn. (2) we at once see that  $\omega_2 > \omega$ , since the anode circuit parameters  $L$ ,  $C'$  and  $R$  are constant. The absolute difference between  $\omega_2$  and  $\omega$  being dependent on the magnitude of  $4g_k R / \{\omega_2 C'(1 + g_k r) - \sqrt{3}g_k\}$ , when either  $g_k$  or  $R$  or both are small,  $\omega_2 - \omega$  is also small, i.e. the influence of cathode circuit on oscillator frequency will be small.

#### CONCLUSION

The effect of an added inductance in series with the load resistance of the three-phase oscillator, and in such case the effect of cathode impedance, on the frequency of oscillation has been discussed in detail in the present paper. An interesting feature which has been observed is that  $\partial\omega/\partial R$  and  $\partial\omega/\partial L$  may have both positive and negative values. These features can be utilized to eliminate frequency variation of the oscillator due to change in temperature. The effect of cathode impedance on the oscillator frequency is very small unless the cathode circuit resonant frequency is far off from the generated frequency and  $Q$  factor of the anode circuit is very low. The conclusions arrived at different stages of this paper have been verified experimentally. The results of such observations and detailed design procedure for better frequency stability of the oscillator are being communicated separately.

#### APPENDIX I

$$\omega = [P + (P^2 + Q^3)^{1/2}]^{1/3} + [P - (P^2 + Q^3)^{1/2}]^{1/3}$$

where

$$P = \frac{\sqrt{3}R}{2L^2C'} \quad \text{and} \quad Q = \frac{CR^2 - L}{3L^2C'}.$$

When  $Q$  is positive and  $P^2 \ll Q^3$ ,

$$\begin{aligned} & [P + (P^2 + Q^3)^{1/2}]^{1/3} \\ &= \left[ P + Q^{3/2} \left\{ 1 + \frac{1}{2} \frac{P^2}{Q^3} - \frac{1}{8} \frac{P^4}{Q^6} + \dots \right\} \right]^{1/3} \\ &= Q^{1/2} \left[ 1 + \frac{P}{Q^{3/2}} + \frac{1}{2} \frac{P^2}{Q^3} - \frac{1}{8} \frac{P^4}{Q^6} + \dots \right]^{1/3}, \end{aligned}$$

neglecting other terms which are insignificant in magnitude.

$$-Q^{\frac{1}{2}} \left[ 1 + \frac{1}{3} \left( \frac{P}{Q^{3/2}} + \frac{1}{2} \frac{P^2}{Q^3} - \frac{1}{8} \frac{P^4}{Q^6} \right) - \frac{1}{9} \left( \frac{P}{Q^{3/2}} + \frac{1}{2} \frac{P^2}{Q^3} - \frac{1}{8} \frac{P^4}{Q^6} \right)^2 \right. \\ \left. + \frac{5}{81} \left( \frac{P}{Q^{3/2}} + \frac{1}{2} \frac{P^2}{Q^3} - \frac{1}{8} \frac{P^4}{Q^6} \right)^3 \dots \right]$$

$$\text{is of the order of } Q^{\frac{1}{2}} \left[ 1 + \frac{1}{3} \frac{P}{Q^{3/2}} + \frac{1}{18} \frac{P^2}{Q^3} - \frac{4}{81} \frac{P^3}{Q^{9/2}} + \frac{5}{216} \frac{P^4}{Q^6} \right].$$

$$\text{Similarly } [P - (P^2 + Q^3)^{\frac{1}{2}}]^{\frac{1}{3}}$$

$$\text{is of the order of } -Q^{\frac{1}{2}} \left[ 1 - \frac{1}{3} \frac{P}{Q^{3/2}} + \frac{1}{18} \frac{P^2}{Q^3} + \frac{4}{81} \frac{P^3}{Q^{9/2}} + \frac{5}{216} \frac{P^4}{Q^6} \right]$$

$$\therefore \omega = Q^{\frac{1}{2}} \left[ \frac{2}{3} \frac{P}{Q^{3/2}} - \frac{8}{81} \frac{P^3}{Q^{9/2}} \right] \text{ approximately}$$

$$\frac{2}{3} Q^{\frac{1}{2}} \left( 1 - \frac{4}{27} \frac{P^2}{Q^3} \right)$$

Substituting the values of  $P$  and  $Q$

$$\omega = \frac{\sqrt{3}R}{(CR^2 - L)} \left[ 1 - \frac{3R^2L^2C^2}{(CR^2 - L)^3} \right]$$

## APPENDIX II

When  $R$  is very small,  $CR^2 < L$  and  $P^2 < Q^3$

$$\text{Under these conditions } \cos \phi = \frac{P}{Q^{3/2}} = 0$$

and we may put  $\phi = \frac{\pi}{2} - \beta$ , where  $\beta$  is very small

$$\text{Then } \cos \frac{\phi}{3} = \cos \left( 30^\circ - \frac{\beta}{3} \right) \text{ is of the order of } \frac{\sqrt{3}}{2} + \frac{1}{2} \frac{\beta}{3}$$

$$\text{Now } Q = -\frac{1}{3LC} \left( 1 - \frac{CR^2}{L} \right) \text{ and } \left| Q^{3/2} \right| \text{ is of the order of } \frac{1}{(3LC)^{3/2}} \left( 1 - \frac{3}{2} \frac{CR^2}{L} \right)$$

$$\therefore \left| \frac{P}{Q^{3/2}} \right| = \frac{\sqrt{3}R}{2LC} \cdot \frac{(3LC)^{3/2}}{1 - \frac{3}{2} \frac{CR^2}{L}} \text{ is of the order of } \frac{9R}{2} \sqrt{L} \left( 1 + \frac{3}{2} \frac{CR^2}{L} \right).$$

Neglecting  $\frac{3}{2} \frac{CR^2}{L}$  which is very small in comparison to 1,

$$\cos \phi - \sin \beta = -\frac{9R}{2} \sqrt{\frac{C}{L}} \quad \text{or} \quad \frac{\beta}{3} = \frac{3R}{2} \frac{L}{C}$$

and hence 
$$\cos \frac{\phi}{3} = \frac{\sqrt{3}}{2} + \frac{1}{2} \frac{3R}{2} \sqrt{\frac{C}{L}} = \frac{1}{2} \left\{ \sqrt{3} + \frac{3R}{2} \sqrt{\frac{C}{L}} \right\}$$

Substituting this value of  $\cos \phi/3$  in Eqn. (6)

$$\omega = \frac{1}{\sqrt{LC}} + \frac{\sqrt{3}R}{2L}$$

#### REFERENCES

- Rakshit, H. and Bhattacharyya, K. K., 1946, *Ind. J. Phys.*, **20**, 171.  
 Rakshit, H. and Mallik, M. C., 1953, *Jour. Sci. & Ind. Res.*, **12B**, 30.  
 Rakshit, H. and Mallik, M. C., 1955, *Ind. J. Phys.*, **30**, 534.  
 Sturley, K. R., 1949, *Radio Receiver Design Part One*. (Chapman & Hall, London).

# Letters to the Editor

The Board of Editors will not hold itself responsible for opinions expressed in the letters published in this section. The notes containing reports of new work communicated for this section should not contain many figures and should not exceed 500 words in length. The contributions must reach the Assistant Editor not later than the 15th of the second month preceding that of the issue in which the paper is to appear. No proof will be sent to the authors.

## 1

### DIPOLE MOMENTS OF LONG CHAIN DICARBOXYLIC ACIDS

R. J. R. MOHAN RAO AND S. R. PALIT

DEPARTMENT OF PHYSICAL CHEMISTRY,

INDIAN ASSOCIATION FOR THE CULTIVATION OF SCIENCE, JADAVPUR, CALCUTTA-32

(Received, November 15, 1959)

The heterodyne beat apparatus used in our measurements has been designed and constructed by a modification of the circuit used by Stranathan (1934) and Terman (1947). The apparatus has been standardised by determining the dipole moments of known compounds and the values obtained are found to be in good agreement with the literature values.

All the substances are crystallised twice from alcohol and their purity checked by their m.p. The solvent *p*-dioxane is purified by the method adopted by Rieche and Milas (1955). The dipole moment is calculated by the following equation deduced by Palit (1952) from the data given in Table I

$$\mu_{2\mu} - \left[ \frac{3(\epsilon_1 - n_1^2)}{d_1(\epsilon_1 + 2)(n_1^2 + 2)} \left( 1 - \frac{\beta_0}{d_1} \right) \right] + \left[ \frac{3\alpha_0}{d_1(\epsilon_1 + 2)^2} \right] - \left[ \frac{6n_1\gamma_0}{d_1(n_1^2 + 2)^2} \right]$$

TABLE I

Solvent: <i>p</i> -Dioxane		Temp: 35°C.			
Substance	Formulae	$\alpha_0$	$\beta_0$	$\nu_0$	10 <sup>-18</sup> esu
Adipic acid	(CH <sub>2</sub> ) <sub>4</sub> .(COOH) <sub>2</sub>	3.4975	0.12434	-0.44899	2.50
Azelaic acid	(CH <sub>2</sub> ) <sub>7</sub> .(COOH) <sub>2</sub>	3.9027	0.89863	-0.17564	2.71
Sebacic acid	(CH <sub>2</sub> ) <sub>8</sub> .(COOH) <sub>2</sub>	3.9999	0.09292	-0.01901	2.49
Brassylic acid	(CH <sub>2</sub> ) <sub>11</sub> .(COOH) <sub>2</sub>	3.0822	0.49372	-0.09169	2.68
Tridecanoic acid	(CH <sub>2</sub> ) <sub>13</sub> .(COOH) <sub>2</sub>	2.8185	0.01382	-0.19709	2.35
Hexadecanoic acid	(CH <sub>2</sub> ) <sub>16</sub> .(COOH) <sub>2</sub>	2.6858	0.01691	0.009438	2.75

where  $\alpha_0$ ,  $\beta_0$  and  $\gamma_0$  are the concentration coefficients of  $\epsilon$ ,  $d$  and  $n$  respectively which were obtained by statistical least square evaluation for these quantities.

The observed dipole moment for the homologous series of dicarboxylic acids are found to be nearly a constant. This clearly shows that the dipole moment of dicarboxylic acids are independent of the number of  $(CH_2)$  groups attached in between the carboxylic acid groups. The dipole moment of adipic acid which we have determined is 2.50 in accordance with the homologous series of dicarboxylic acids where as the dipole moment of adipic acid given by Tseng-Sun-Yao (1944) is 4.04.

Thanks are due to The Director and Dr. S. S. Bhattacharya of National Chemical Laboratory, Poona, for supplying materials.

#### REFERENCES

- Palit, 1952, *J. Am. Chem. Soc.*, **74**, 3952.  
Stranathan, 1934, *Rev. Sci. Instr.*, **5**, 334.  
Terman, 1947, *Radio Engineering*, McGraw Hill.  
Tseng-Sun-Yao, 1944, *J. Chinese Chem. Soc.*, **5**, 236.  
Weissberger, 1955, *Technique of Organic Chemistry*, Vol. VII, Second edition, page 372.



## BOOK REVIEWS

**ELECTROMAGNETIC ISOTOPE SEPARATORS AND APPLICATIONS OF ELECTRO-MAGNETICALLY ENRICHED ISOTOPE**—By J. Koch (Editor). R. H. V. M. Dawton, M. L. Smith and W. Walcher. Pp. 314+ix. North-Holland Publishing Company. Amsterdam. 1958. Price 26.5 guilders.

This book gives an account of gradual development of the technique for separation of stable and radioactive isotopes in large quantities and also reveals the details of some methods which were guarded as close secrets during the last year. Starting from the earliest electromagnetic isotope separator constructed in 1934 by Oliphant, Shire and Crowther which provided isotopic samples of  $\text{Li}^6$  and  $\text{Li}^7$ , the authors proceed to describe other experiments for the separation of stable isotopes including the separation of  $\text{U}^{235}$  and  $\text{U}^{238}$  by Nier, Booth, Dunning and Grosse in 1940. In Chapter III a historical account of the development of the technique for the separation of artificial radioactive isotopes has been given. The assignment of mass number to half life of some fission isotopes by Hayden has also been discussed in this chapter. Next, the recent development of isotope separators for preparing stable and radioactive samples for nuclear research has been discussed in detail. Details of design of several such separators installed in laboratories in different places such as Stockholm, Uppsala, Gothenburg, Salcey, etc., have been given and photographs of the separators have been reproduced. The history of the United States and British projects for installation of plants for production of isotopes has been given in Chapter V. In the next few chapters photographs of such alpha- and beta-type production units have been reproduced and details of the construction of  $180^\circ$  and  $90^\circ$  separators at Harwell have been discussed with the help of illustrations.

Chapter IX dealing with operational experience in the electromagnetic separation of isotopes gives very useful information regarding the method of separation of different types of isotopes, such as gaseous, alkali and alkaline earth metals, elements with very volatile chlorides, sulphur, halogens, lanthanides, etc. A chapter has been devoted to application of electromagnetically enriched stable isotopes.

In part C comprising the last three chapters, Dr. W. Walcher has discussed the general treatment of some problems related to the design of modern isotope separators, such as mass analysing field systems, production of high current ion beams, space charge neutralisation in ion beams, etc. A complete bibliography has been given at the end of each chapter.

It will appear from the above brief review that the publication of this volume is a great boon to experimental physicists engaged in investigations in nuclear physics and the authors will certainly earn the gratitude of numerous workers in this field in different laboratories all over the world for taking the trouble of compiling and publishing this extremely useful store of information the part of which was not available in any existing literature. It may be safely predicted that every laboratory interested in nuclear physics will try to procure and use this book as a reference volume.

*S.C.S.*

#### PROCEEDINGS OF THE SYMPOSIUM ON ELECTRONIC WAVE GUIDES.

Edited by Jerome Fox, New York., April, 1958. Pp. 418 + xix. Interscience Publishers Inc 250 Fifth Avenue, New York. N.Y 1. Price \$5.00.

This volume constitutes a full record of the Proceedings indicated by the title and includes besides the original papers all the addresses and lectures delivered in the symposium arranged by the Microwave Research Institute of the Polytechnic Institute of Brooklyn and held in April, 1958. The topics of the symposium have been divided under five headings, *viz.*, State of the art, Background and recent developments, Plasmas, Mode and large signal theories, and Special phenomena and devices. There was also a round table discussion on 'Electron tubes and solid state devices—future trends' in the afternoon session on the last day of the symposium.

There are three papers on Traveling-wave tubes, New microwave devices and Dynamic of plasmas and electron beams respectively under the first topic and four similar papers under the second heading mentioned above. Six full papers have been contributed under the topic plasmas. Similarly, there are six papers under the heading Mode and large signal theories and six papers under Special phenomena and devices. In the paper entitled 'Travelling-wave tubes' Doehler has summarised the work on the application of principle of space charge waves in the manufacture of some travelling wave tubes.

Under the title 'New microwave devices' Kompfner has discussed the development of ammonia 'maser' and 'mavar' amplifiers for microwaves. In a third paper read in this session by Gross who has reviewed the work on dynamics of electron beams and plasmas in which one-particle velocity distribution functions have been described, a new collective method in which the ionised gas is treated in terms of density fluctuations has been discussed.

In the next session Marcuvitz read a paper entitled 'General electronic wave guides' in which he reviewed the analyses of propagation and diffraction

problems and the application of guided wave theory in which analysis in terms of cold modes is involved. He then presented an analysis in terms of orthogonal 'hot modes'. In another paper entitled "Electron beam waves in microwave tubes Haus reviewed the work on wave propagation along electron beams and interpreted the small-signal power theorem and the theorem for longitudinal beams and deduced the equations of the magnetron amplifier.

In a third paper Buneman has reviewed the work on the hydrodynamical theory of electron clouds and its application to axis symmetric or planar-startified systems. Similar work on fully randomized multi stream hot plasmas has then been reviewed. In the fourth paper of this session Allis has discussed the work on the theory of plasma oscillations.

In the next session Bradshaw discussed the results on experimental investigation on the phase shift and absorption experienced by a TEM microwave signal in transmission through a relatively long coaxial region containing space charge. Agdur discussed the theory of propagation of guided microwaves through an electron gas in the presence of a static magnetic field. In a third paper Whitmer discussed the theory of non-linear interaction of an electromagnetic wave with an anisotropic plasma and also the results of some experimental investigations in this line. In this session Rydbeck delivered a lecture on interaction between space charge waves and electromagnetic waves in an inhomogeneous ionized medium which has not been reproduced. In the fourth paper Gould and Trivelpiece discussed a new mode of wave propagation on electron beams. In the next paper Smullin and Chorney discussed the theory of propagation of electromagnetic waves in ion loaded wave guides.

In the first paper of the next session by Bernashevsky, Voronov, Iziumova and Tchernov the results of an experimental investigation of double stream amplifiers in the metre and 10 cm range have been discussed. In the next paper read in the session Hok discussed the theory of electrokinetic and electromagnetic noise waves in electronic waveguides and in another paper Kino discussed the theory of mode properties of passive transmission systems. The fourth paper of this session by Kluver deals with a representation of the boundary conditions at the surface of a slow wave circuit and in the fifth paper Wang and McIsaac discuss a fundamental formulation of interaction equation in electronic wave guides. The sixth paper of this session by Rowe deals with the analysis of non-linear O-type backward-wave oscillations.

In the next session the first paper read by Tchernov deals with the interaction of electromagnetic waves and electron beams in centrifugal electrostatic focusing systems. Feinstein read a paper on emission of space charge wave energy into electromagnetic radiation and another paper on space and time harmonics in electron beams was read by Muller. The theory of interaction

between an electron system and arc discharge plasma has been dealt with by Boyd, Field and Gould in the fourth paper of this session. In the next paper by Ettenberg and Targ the results of an experimental investigation on plasma and cyclotron oscillations have been discussed and the last paper by Weibel describes some new principles for achieving interactions of electrons with radiation under high magnetic field of the order of 1,000,000 gauss

It is evident that the papers read in the symposium cover the whole field of up-to-date development of theory and practical application of microwave technique and the Proceedings will be extremely useful to research workers in this line.

*S.C.S*

# ON THE ELECTRONIC SPECTRA OF $\alpha$ -FLUORONAPHTHALENE IN THE LIQUID AND SOLID STATES\*

S. B. BANERJEE

INDIAN ASSOCIATION FOR THE CULTIVATION OF SCIENCE, CALCUTTA-32

(Received, December 23, 1959)

**ABSTRACT.** The electronic absorption spectra of  $\alpha$ -fluoronaphthalene in the liquid and solid states have been analysed and compared with the spectrum of the compound in the vapour state reported by previous workers. The substance in different states is found to exhibit two systems of bands in the 3200–3000 A.U. and 2900–2600 A.U. regions. The 0,0 band of the first system shows a shift of  $442\text{ cm}^{-1}$  towards red when the vapour is liquefied. When the liquid is solidified and cooled to  $-180^\circ\text{C}$ , the 0,0 band is further displaced slightly towards longer wavelengths and the bands become sharper. The second system of bands due to the liquid consists of very broad bands and the 0,0 band is shifted towards red by about  $1100\text{ cm}^{-1}$  from its positions in the spectrum due to the vapour. With solidification of the liquid no further change is observed in this system.

## INTRODUCTION

Naphthalene and its monoderivatives are known to exhibit two systems of absorption bands in the near ultraviolet region. It was observed in previous investigations (Deb, 1954; Banerjee, 1956) that with change of state and temperature the bands of the two systems due to some monosubstituted naphthalene compounds undergo large changes indicating strong influence of intermolecular forces on the electronic energy state. Such an influence in the case of fluoronaphthalenes had not been studied before. The present work was therefore undertaken to study the absorption spectra of  $\alpha$ -fluoronaphthalene in the liquid and solid states and to compare the results with those due to the substance in the vapour state.

## EXPERIMENTAL

The sample of  $\alpha$ -fluoronaphthalene was obtained from Eastman Kodak Co. and was repeatedly distilled under reduced pressure before use. Thin films of the substance of thickness of the order of a few microns yielded the bands in the 2600–2900 A.U. region while much thicker film was required to obtain the bands of the first system on the longer wavelength side. The spectra were photographed on Ilford HP3 films with a Hilger E1 spectrograph. Microphotometric records

\* Communicated by Prof. S. C. Sarkar.

of the spectrograms were taken with a Kipp and Zonen type Moll microphotometer. The wavelengths of the absorption peaks were determined with the help of microphotometric records of iron arc lines photographed on each spectrogram by the method described in an earlier paper (Banerjee, 1956).

### RESULTS

The microphotometric records of the spectrograms are reproduced in Figs. 1 and 2 and the frequencies of the bands in  $\text{cm}^{-1}$  with probable assignments are

TABLE I  
Absorption bands of  $\alpha$ -fluoronaphthalene

Vapour* Ramanurthy <i>et al.</i> (1957)		Liquid at 28°C Present author		Solid at -180°C Present author		
Wave number (cm <sup>-1</sup> ) and intensity	Assignment	Wave number (cm <sup>-1</sup> ) and intensity	Assignment	Wave number (cm <sup>-1</sup> ) and intensity	Assignment	
First system	31872 s	0,0	31430 s	0,0	31348 s	0,0
	32281 m	0+409	32093 mb	0+663	31817 m	0+469
	32545 m	0+673	32500 m	0+1070	32042 s	0+694
	32710 vw	0+838	32866 s	0+1436	32416 m	0+1068
	32918	0+1046	33530 s	0+663+1436	32786 s	0+1438
	33307 m	0+1435			33092 w	0+1068+694
				33474 m	0+1438+694	
Second system	(Separation from 0,0)					
	35222	0	34100 wb	0,0	34158 m	0,0
	35399	177	35111 wvb	0+1011	34982 m	0+824
	35683	461	36132 wvb	0+2×1011	34158 m	0+1375
	36053	831			36370 w	0+1375+824
	36341	1119				
	36598	1376				
	36807	1585				
	37075	1853				
	37512	2200				
	38026	2804				
	38481	3259				

\*Bands corresponding to fundamental upper state frequencies only have been included.

given in Table I. The spectrum of the compound in the vapour state was studied earlier by Ramamurty *et al.* (1957), whose data have been included in the table for comparison. The compound in all the three states is found to exhibit two systems of bands in the regions 3200–3000 Å and 2900–2800 Å and these have been designated in this paper as the first and the second system respectively.

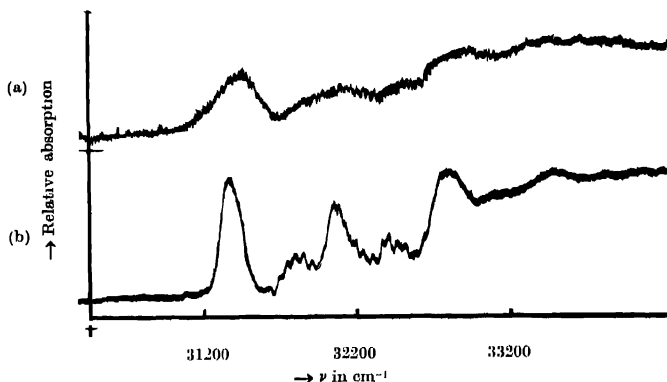


Fig. 1. Microphotometric records of the u. v. absorption spectra of  $\alpha$ -fluoronaphthalene (first system).

(a) Liquid at 28°C

(b) Solid at -180°C

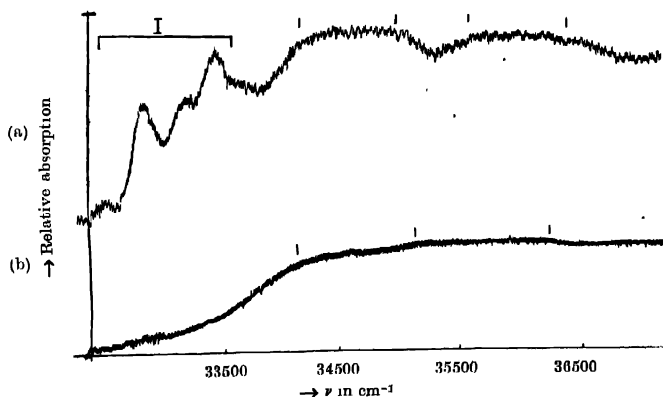


Fig. 2. Microphotometric records of the u. v. absorption spectra of  $\alpha$ -fluoronaphthalene (second system).

(a) Solid at -180°C

(b) Liquid at 28°C

(The bands marked I belong to the 1st system)

## DISCUSSION

(i) *Bands of the first system :*

The absorption spectrum of  $\alpha$ -fluoronaphthalene in the vapour state shows a number of bands with the 0,0 band of this system at  $31872\text{ cm}^{-1}$  (Ramamurty, Rao and Rao, 1957), the other band representing excited state vibrational frequencies 409, 673, 838, 1046 and  $1435\text{ cm}^{-1}$ . In the spectrum due to the liquid five bands are observed, the first band on the long wavelength side with its centre at  $31430\text{ cm}^{-1}$  being assigned as the 0,0 band (Fig. 1). This indicates a shift towards red of  $442\text{ cm}^{-1}$  of the 0,0 band with the liquefaction of the vapour. The other bands in the spectrum of the liquid are a little broad and are found to correspond to excited state fundamental frequencies 663, 1070 and  $1436\text{ cm}^{-1}$ . Owing to the broadening of the bands, the  $409\text{ cm}^{-1}$  band merges with the  $673\text{ cm}^{-1}$  band. In the spectrum of the solid at  $-180^\circ\text{C}$  seven bands are observed, which are sharper than those due to the liquid. The 0,0 band, which is the first and the most intense band of the system on the long wavelength side, is at  $31348\text{ cm}^{-1}$ , showing a further shift towards red by  $82\text{ cm}^{-1}$  with the solidification of the liquid. In the case of the solid, bands corresponding to the excited state vibrational frequencies 469, 694, 1068 and  $1438\text{ cm}^{-1}$  are observed.

The shifts in the position of the 0,0 band with change from vapour to liquid and from liquid to solid state are similar to those observed in the case of  $\alpha$ -chloro- and  $\alpha$ -bromonaphthalene (Deb, 1954). This indicates that in the case of this molecule also the excited electronic energy level is lowered by the intermolecular field in the condensed phases of the substance in the same way as observed in the spectra of the other two compounds.

(ii) *Bands of the second system .*

The bands in the spectrum of the liquid in this system are broad and are separated from each other by about  $1011\text{ cm}^{-1}$ . The long wavelength edge of the first band is at about  $34100\text{ cm}^{-1}$ . In the case of the vapour broad and diffuse bands have been reported by Ramamurty *et al.* (1957). The first band on the long wavelength side at  $35222\text{ cm}^{-1}$  has been taken to be the 0,0 band and this band is accompanied by two other bands on the short wavelength side separated from it by 177 and  $461\text{ cm}^{-1}$  respectively. Other bands in the spectrum of the vapour are also similarly grouped, the mean separation of  $461\text{ cm}^{-1}$  being quite prominent. In the liquid state the coalescence of the bands in each group perhaps produces the broad bands and the long wavelength edge at  $34100\text{ cm}^{-1}$  may be taken to be the position of the 0,0 band. Thus, the liquefaction of the vapour results in a large red shift of  $1122\text{ cm}^{-1}$  in the position of the 0,0 band. This shows that in the case of this compound the influence of intermolecular field in the liquid state is greater on the second system than on the first. In the spectrum of the solid at  $-180^\circ\text{C}$ , the bands are still broad and the position of the 0,0 band remains almost unaltered with solidification.



Thus the main changes in the spectra of both the systems are found to take place with change from the vapour to the liquid state. This probably indicates formation of strongly associated groups of the molecules in the liquid state due to the presence of highly active fluorine atom in the molecule.

#### ACKNOWLEDGMENT

The author's thanks are due to Professor S. C. Sirkar, D.Sc., F.N.I., for his kind interest in the work.

#### REFERENCES

- Banerjee, S. B., 1956, *Ind. J. Phys.*, **30**, 106.  
Deb, A. R., 1954, *Ind. J. Phys.*, **28**, 21.  
Ranamurty, S., Rao, M. J. and Rao, V. R., 1957, *Ind. J. Phys.*, **31**, 497.

ON THE  $F_2$ -REGION OF THE IONOSPHERE

S. DATTA

INSTITUTE OF RADIO PHYSICS AND ELECTRONICS, CALCUTTA

(Received, December 22, 1959)

**ABSTRACT.** Calculations of the total electron production rate in a column of unit cross-section extending from the "bottom" to the maximum electron density height and of the mean production rates in different parts of the  $F_2$ -region are made with the help of the attachment coefficient model suggested by Ratchffe *et al.* (1956). It is found that the results are consistent with those expected from the hypothesis of Bradbury for the formation of the  $F_2$ -region. The calculations are made by the method suggested by the author (1958).

## INTRODUCTION

The diurnal variation of electron density  $N$  at a given height in an ionized region, neglecting the effects of movements, is governed by the equation

$$\frac{dN}{dt} = q - KN^\eta \quad \dots (1)$$

where  $q$  = electron production rate

$K$  = electron loss coefficient

and  $\eta = 1$  or 2 depending on the electron loss process.

In the  $E$  and  $F_1$  regions the effects of movements are negligible. For these regions Eq. (1) may be utilised for calculating the production rate from the experimental values of  $\frac{dN}{dt}$  and  $N$  provided the loss process and the loss coefficient  $K$  are known. In the  $F_2$  region, however, movements of the electrons produce changes in electron density at a rate comparable to  $dN/dt$  of Eq. (1). Computations of production rate with the help of this equation cannot, therefore, yield reliable values. It is also not possible to take account of the effects of the movements in the computation as little is known about their nature and magnitude. Further, the height of the  $F_2$  region has large diurnal variations and its thickness also changes considerably at times. These difficulties notwithstanding, study of the production rates in different levels of the thick  $F_2$  region, is desirable for testing the theories of the formation of the  $F_2$  region.

A method of computation of such production rates was therefore proposed by the author of this paper. The method consists in dividing a column of unit cross-section of the region extending from the "bottom" to the height of maximum electron density into four sections of equal length. Mean production rate in

each of these sections (same as mean production rate in four different parts of the thick  $F_2$  region) is computed from the diurnal variation of the total number of electrons in it. The total production rate in the "unit column" of the  $F_2$  region and the mean production rate in the region are also computed. Such computations obviously minimise the effects of layer movement as a whole, movements of electrons, and layer contractions and dilutions due to thermal changes. There is, of course, the proviso that the fraction of the total number of electrons present in each of the four "unit" sections is not changed. Mean hourly values of  $N$  at a series of heights in the  $F_2$  region over Slough for the months of January and March, 1950 on international quiet days were utilised for the computation. "Tables of  $F_2$ -layer Electron Density on International Quiet Days" computed by Schmerling and Thomas (1955) were obtained from the Radio Group, Cavendish Laboratory, Cambridge, England. The height variation of the attachment coefficient as suggested by Ratcliffe *et al.* (1956) from night-time observations over Slough, Watheroo and Huancayo, was utilised.

In the paper of the author referred to above (Datta 1958) the diurnal variations of the production rates (as mentioned above) were delineated for the month of January, 1950. In the present paper, computations are made of the same parameters for the month of March of the same year. Values of the mean production rates have also been calculated on the basis of Bradbury's (1938) hypothesis for the formation of the  $F_2$  region. These are compared with the results for the two months, January and March, 1950 obtained by the suggested method of analysis.

## RESULTS

Fig. 2(a) depicts the diurnal variation of the total number of electrons  $n$  in a column of unit cross-section extending from the "bottom" to the height of maximum electron density in the  $F_2$  region over Slough for the month of March, 1950. Fig. 2(b) shows the diurnal variations for the same month of  $n_r$  ( $r = 1, 2, 3, 4$ ), the total number of the electrons in each of the four sections of the column taken in order from the "bottom". Hourly values of the number of electrons and the loss rates in each of the sections were calculated by Simpson's rule for numerical integration. Loss rates were calculated with the help of the height variation of the attachment coefficient as suggested by Ratcliffe *et al.* (1956) and extrapolated to a height of 200 Km. (Fig. 1). To obtain half

hourly values of  $\left( \frac{dn_r}{dt} \right)$  and  $n_r$ , a linear change between the hourly values of  $n_r$  was assumed. A quasi-equilibrium condition in each of the columns was assumed from 10 hrs. to 14 hrs. Such an assumption is justified in the neighbour-

hood of the midday when loss rate and production rate are much larger than  $\left( \frac{dn_r}{dt} \right)$ . The diurnal variations of mean production rate for the month of March,

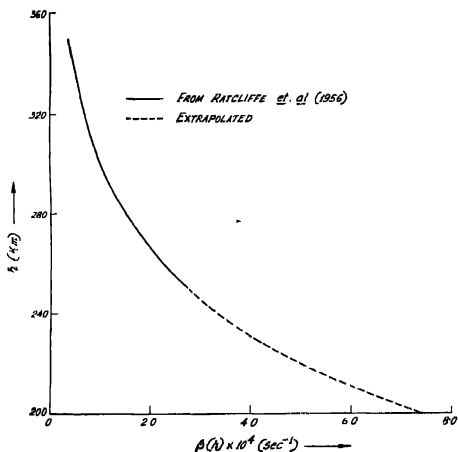


Fig. 1. Height variation of the attachment coefficient suggested by Ratcliffe *et al.* (1956).

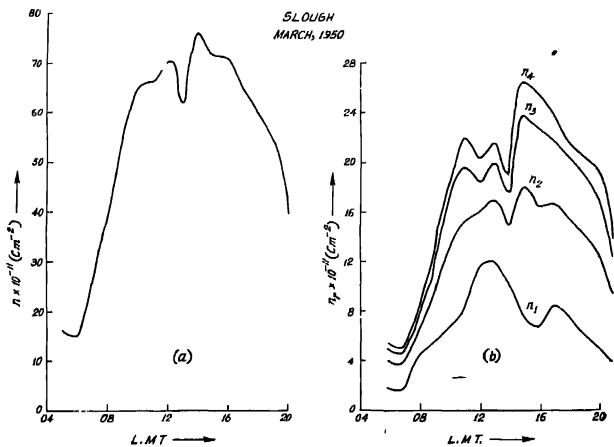


Fig. 2. (a) Diurnal variation of  $n$  in the  $F_2$  region for the month of March, 1950.  
(b) Diurnal variations of  $n_r$  ( $r = 1, 2, 3, 4$ ) in the  $F_2$  region for the month of March, 1950.

1950 over Slough are shown in Fig. 3. The diurnal variation of the mean production rate ( $q$ ) and the total production rate ( $Q$ ) in the whole column of unit

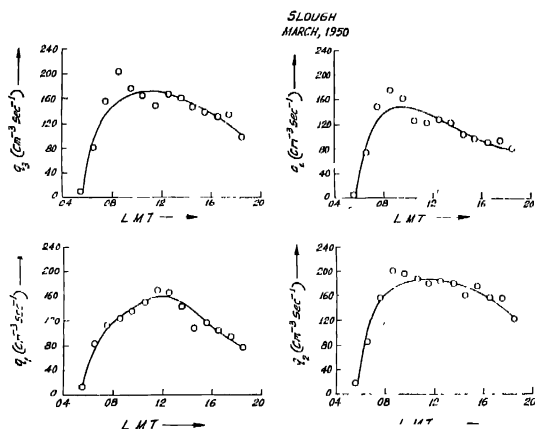


Fig. 3. Diurnal variations of  $q_r$  ( $r = 1, 2, 3, 4$ ) in the  $F_2$  region for the month of March, 1950.

cross-section extending from the "bottom" to the maximum electron density height in the  $F_2$  region for the months of January and March, 1950 over Slough, are shown by broken lines in Fig. 5 and Fig. 6 respectively.

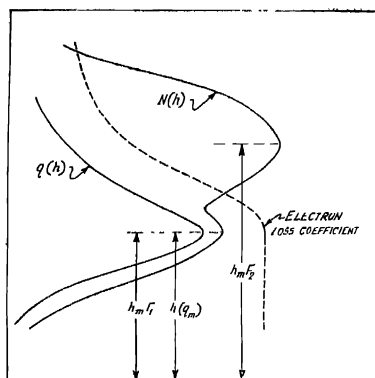


Fig. 4. Diagram illustrating the hypothesis of Bradbury for the formation of the  $F_2$  region.

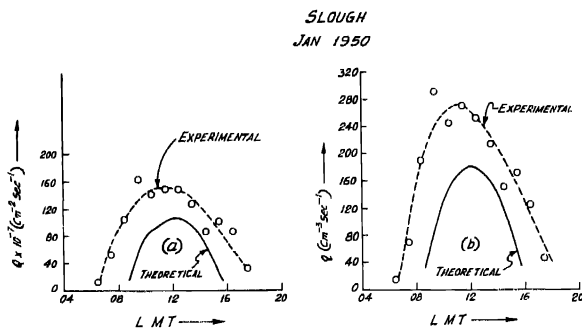


Fig. 5. Diurnal variation of  $Q$  and  $q$  (Experimental and theoretical) in the  $F_2$  region for the month of January, 1950.

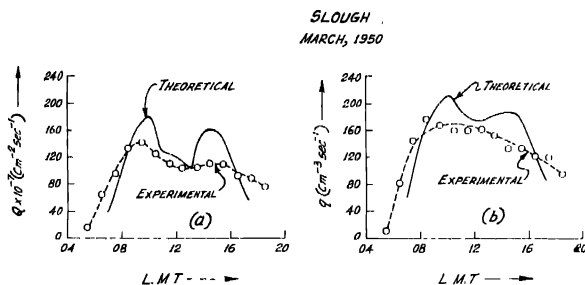


Fig. 6. Diurnal variation of  $Q$  and  $q$  (experimental and theoretical) in the  $F_2$  region for the month of March, 1950.

TABLE I

Half hourly values of  $q_r$  ( $r = 1, 2, 3, 4$ ),  $Q$  and  $q$ .

January 1950—Slough

Hour (L.M.T.)	$q_1$ $\text{cm}^{-3} \cdot \text{sec}^{-1}$	$q_2$ $\text{cm}^{-3} \cdot \text{sec}^{-1}$	$q_3$ $\text{cm}^{-3} \cdot \text{sec}^{-1}$	$q_4$ $\text{cm}^{-3} \cdot \text{sec}^{-1}$	$Q \times 10^{-7}$ $\text{cm}^{-3} \cdot \text{sec}^{-1}$	$q$ $\text{cm}^{-3} \cdot \text{sec}^{-1}$
0630	14	17	16	14	13	15
0730	37	70	84	89	51	70
0830	128	227	200	203	106	190
0930	205	332	314	317	163	292
1030	180	303	273	222	141	245
1130	193	319	306	262	151	270
1230	183	311	283	230	151	252
1330	173	255	231	191	127	213
1430	115	195	166	119	86	140
1530	135	208	190	151	102	171
1630	94	154	136	109	86	123
1730	60	69	40	7	33	44

TABLE II  
Half hourly values of  $q_r$  ( $r = 1, 2, 3, 4$ ),  $Q$  and  $q$ .  
March 1950—Slough

Hour (L.M.T.)	$q_1$ $\text{cm}^{-3}\text{sec.}^{-1}$	$q_2$ $\text{cm}^{-3}\text{sec.}^{-1}$	$q_3$ $\text{cm}^{-3}\text{sec.}^{-1}$	$q_4$ $\text{cm}^{-3}\text{sec.}^{-1}$	$Q \times 10^{-7}$ $\text{cm}^{-2}\text{sec.}^{-1}$	$q$ $\text{cm}^{-3}\text{sec.}^{-1}$
0530	12	18	10	4	11	11
0630	83	87	82	74	64	82
0730	113	160	159	150	96	145
0830	123	200	206	174	134	176
0930	135	196	177	161	142	167
1030	151	188	166	128	120	158
1130	169	179	150	124	106	156
1230	164	184	160	127	102	159
1330	144	181	160	122	108	152
1430	108	160	148	105	111	130
1530	114	175	139	96	109	131
1630	104	158	133	92	93	122
1730	94	160	138	97	90	122
1830	76	122	99	81	76	95

## COMPARISON WITH THEORY

For comparison, the values of  $Q$ ,  $q$  and  $q_r$  (mean production rate in the  $r$ th column) may be calculated from the hypothesis of Bradbury (1938) as follows:

If a gas of constant scale height  $H$  is ionized by monochromatic radiation, then the value of  $q(h)$ , when the solar zenithal angle is  $\chi$ , is given by the expression due to Chapman (1931).

$$q(h) = q_0 \exp(1 - Z - e^{-Z} \sec \chi) \quad \dots (2)$$

where  $Z = \frac{h - h_0}{H}$  and  $h_0$  is the height of maximum production rate  $q_0$  when  $\chi = 0$ .

According to Bradbury,  $F_1$  and  $F_2$  layers are both produced by the same ionization process. The ionizing radiation for the process, acting on a single ionizable gas constituent, has the height  $h(q_m)$  of peak production rate near the level of  $F_1$  layer peak ( $h_m F_1$ ); and, the  $F_2$  layer peak ( $h_m F_2$ ) is formed as a result of the rapid decrease of the electron loss coefficient above  $F_1$  layer, the loss coefficient in the  $F_1$  layer being independent of height. The hypothesis of Bradbury is illustrated in Fig 4. According to this hypothesis, when the solar zenith angle is  $\chi$ , the value of  $Q$ , the total electron production in a column of unit cross-section of the  $F_2$  region extending from the "bottom" ( $h_o F_2$ ) to the height of maximum density ( $h_m F_2$ ) is given by

$$Q = \int_{h_o F_2}^{h_m F_2} q(h) \cdot dh = q_0 H \cos \chi [\exp(1 - e^{-Z_2} \sec \chi) - \exp(1 - e^{-Z_1} \sec \chi)] \quad \dots (3)$$

$$= q \cdot T$$

where

$$Z_2 = \frac{h_m F_2}{H} - h_0$$

$$Z_1 = \frac{h_0 F_2}{H} - h_0$$

$$T = h_m F_2 - h_0 F_2$$

$q$  = mean production rate in the  $F_2$  layer and  $q_0$  = peak production rate.

The value of the peak production rate ( $q_0$ ) in the  $F_1$  region when the sun's rays are vertical may be estimated for the quasi-equilibrium conditions (production rate = loss rate) from the expression,

$$q_0 = \frac{\alpha N_m^2 F_1}{\cos \chi} \quad \dots (4)$$

where  $N_m F_1$  = maximum electron density in the  $F_1$  layer when the solar zenithal angle is  $\chi$  and  $\alpha$  = coefficient of recombination in the  $F_1$  layer.

Assuming  $\alpha = 5 \times 10^{-9} \text{ cm}^3. \text{ sec.}^{-1}$  [Bates and Massey (1946), Rydbeck (1946)], Ratcliffe *et al* found from an analysis of Slough and world-wide data that

$$q_0 = 280 (1 \pm 1.4 \times 10^{-2} R) \text{ cm}^{-3} \text{ sec.}^{-1} \quad \dots (5)$$

where  $R$  is the monthly average relative Zürich sunspot number.

It has been suggested (Bates and Massey 1948 and other authors) that the ionizable gas in the  $F$  region is atomic oxygen. The value of the scale height ( $H$ ) of atomic oxygen is about 50 km. between 200 km. and 400 km. according to the  $R$  model (based on rocket results) given by Bates (1954). This value of the scale height is consistent with the value ( $H = 45$  km.) accepted by Ratcliffe *et al.* after a critical examination of the experimental results and Bradbury's hypothesis. The value of  $h_0$  accepted by Ratcliffe *et al.* is 180 km. With these values of  $H$  and  $h_0$  (45 km. and 180 km. respectively) the hourly values of the total production rate ( $Q$ ) in the unit column and mean production rate ( $q$ ) in the  $F_2$  layer have been calculated with the help of Eq (3).

For comparison, the theoretical hourly values of  $Q$  and  $q$  (calculated on the assumption of Bradbury's hypothesis) and the hourly experimental values (from the mean curves in Fig. 5 and Fig. 6) are shown in Table III and Table IV.

To show how the values of the mean production rates  $q_r$  should fall with increasing order of the sectional column (first column being the lowest one) according to the hypothesis of Bradbury, values of the same have been calculated theoretically. This can be done with the help of the equation

$$q_r = \frac{x}{r} q_0 H \cos \chi [\exp (1 - e^{-Z_{2r} \sec \chi}) - \exp (1 - e^{-Z_{1r} \sec \chi})] \quad (6)$$



where  $Z_{2r}$  = reduced height of the upper boundary of the  $r$ th column,  
 $Z_{1r}$  = reduced height of the lower boundary of the  $r$ th column.

TABLE III

Hourly experimental and theoretical values of  $Q$  and  $q$ .

January 1950—Slough

Hour (L.M.T.)	$Q \times 10^{-7}$ $\text{cm}^{-2}, \text{sec.}^{-1}$ (Experimental)	$Q \times 10^{-7}$ $\text{cm}^{-2}, \text{sec.}^{-1}$ (Theoretical)	$q$ $\text{cm}^{-3}, \text{sec.}^{-1}$ (Experimental)	$q$ $\text{cm}^{-3}, \text{sec.}^{-1}$ (Theoretical)
09	120	27	220	51
10	144	81	256	133
11	152	94	272	168
12	150	106	260	183
13	140	102	238	170
14	126	85	206	144
15	100	46	168	84

TABLE IV

Hourly experimental and theoretical value of  $Q$  and  $q$

March 1950—Slough

Hour (L.M.T.)	$Q \times 10^{-7}$ $\text{cm}^{-2}, \text{sec.}^{-1}$ (Experimental)	$Q \times 10^{-7}$ $\text{cm}^{-2}, \text{sec.}^{-1}$ (Theoretical)	$q$ $\text{cm}^{-3}, \text{sec.}^{-1}$ (Experimental)	$q$ $\text{cm}^{-3}, \text{sec.}^{-1}$ (Theoretical)
07	80	40	116	61
08	118	101	150	149
09	140	156	162	184
10	132	180	168	212
11	116	128	168	191
12	106	120	164	174
13	104	103	158	178
14	108	157	150	187
15	110	158	138	186
16	104	117	128	146
17	92	67	116	94

Values of the mean production rates of the four sectional columns at midday [1200 hr. (L.M.T.)] as calculated are shown below in Table V for the month of January 1950 and March 1950 at Slough. The calculations were done with values of  $H$ ,  $h_0$  and  $q_0$  as stated earlier. It is to be noted that  $q_1 > q_2 > q_3 > q_4$ . This is as it should be, because, as the peak production rate is assumed to be near the  $F_1$  peak height, the mean production rate should decrease with increasing height of the column in the  $F_2$  region.

TABLE V

Theoretical values of  $q_r$  ( $r = 1, 2, 3, 4$ ) according to the hypothesis of Bradbury

Hr. — 1200 (L.M.T.)—Slough

1950 Month	$q_1$ $\text{cm}^{-3}, \text{sec.}^{-1}$	$q_2$ $\text{cm}^{-3}, \text{sec.}^{-1}$	$q_3$ $\text{cm}^{-3}, \text{sec.}^{-1}$	$q_4$ $\text{cm}^{-3}, \text{sec.}^{-1}$
January	201	197	173	166
March	247	206	129	124

## DISCUSSION

The computations of the diurnal variations of the mean production rates in the different sections of the  $F_2$  region by the method of analysis, suggested by the author, taking into account the height variation of the attachment coefficient after Ratcliffe *et al.* give consistent results. The diurnal variations are found to be more regular and symmetrical about noon for the winter month (January) than for the equinoctial month (March). The calculated values of the mean production rates for both the months as given in Table I and Table II, show that  $q_2 > q_3 > q_4$  for most of the half hourly values. This is in accordance with Table V, except that the experimental  $q_1$ 's are generally less instead of being greater than  $q_2$ 's. This may be due to the uncertainty in the correct determination of electron density near the "bottom" of the  $F_2$  region. This uncertainty affects the computed values of  $n_1$ . Another possible reason for this discrepancy may be due to the fact that the loss rates in the first column were often calculated from the extrapolated values (below 250 km) of attachment coefficient.

It may be noted from Table III that the theoretical values of  $Q$  and  $q$  are lower than the experimental values. The difference is smaller for the month of March than for the month of January. It must be mentioned in this connection that the magnitudes of  $Q$  and  $q$ , calculated theoretically on the assumption of Bradbury's hypothesis, depend on the assumed values of  $q_0$ ,  $h_0$  and  $H$ . The assumed value of  $q_0$ , again in its turn, is proportional [Eq. (4)] to the assumed values of the recombination coefficient ( $\alpha$ ) in the  $F_1$  region. The value of  $q_0$  utilized for the theoretical computation was obtained by Ratcliffe *et al.* by assuming  $\alpha = 5 \times 10^{-9} \text{ cm}^3 \text{ sec.}^{-1}$ . Higher values  $\alpha = 8 \times 10^{-9} \text{ cm}^3 \text{ sec.}^{-1}$ , however, has been suggested (Minnis, 1955). If this latter value is accepted, the theoretically calculated values of  $q$  and  $Q$  will be increased by about 50% provided the values of  $H$  and  $h_0$  are unaltered.

It may thus be concluded that with the height variation of the attachment coefficient suggested by Ratcliffe *et al.* the results as obtained by the method of analysis adopted are consistent with the hypothesis of Bradbury for the formation of the  $F_2$  region.

ACKNOWLEDGMENTS

The work forms part of the programme of Radio Research Committee of the Council of Scientific and Industrial Research, Government of India, and the author wishes to express his thanks to the Council for financial assistance.

The author is indebted to Professor J. N. Bhar, D.Sc., F.N.I., for his interest and encouragement throughout the progress of the work. Thanks are due to Dr. A. K. Saha for helpful discussions.

REFERENCES

- Bates, D. R., 1954, *Rocket Exploration of the Upper Atmosphere*, Pergamon Press, London, p. 347.
- Bates, D. R. and Massey, H. S. W., 1946, *Proc. Roy. Soc. A.*, **187**, 261.
- Bates, D. R. and Massey, H. S. W., 1948, *Proc. Roy. Soc. A.*, **192**, 1.
- Bradbury, N. E., 1938, *Terr. Magn. Atmos. Elect.*, **43**, 55.
- Chapman, S., 1931, *Proc. Phys. Soc.*, **43**, 26.
- Datta, S., 1958, *Indian J. Phys.*, **32**, 483.
- Munnis, C. M., 1955, *J. Atmos. Terr. Phys.*, **6**, 91.
- Ratcliffe, J. A., Schnerling, E. R., Sottly, C. S. G. K. and Thomas, J. O., 1956, *Phil. Trans. A.*, **248**, 621.
- Rydbeck, O. E. H., 1946, Chalmers. tek. Högsk. Handl. No. 53.
- Schmerling, E. R. and Thomas, J. O., 1955, *Tables of F2 layer Electron Density on International Quiet Days*, Cavendish Laboratory, Cambridge, England.
- Schmerling, E. R. and Thomas, J. O., 1956, *Phil. Trans. A.*, **248**, 609.

# INTERMOLECULAR POTENTIAL OF HELIUM

A. K. BARUA

INDIAN ASSOCIATION FOR THE CULTIVATION OF SCIENCE, CALCUTTA-32, INDIA

(Received, December 28, 1959)

**ABSTRACT.** The potential energy function for He-He interaction has been obtained on the exp 6-8 model which contains the dipole-quadrupole interaction term in addition to the dipole-dipole term in the attractive potential, by fitting in second virial and Joule-Thomson coefficient data over extensive range of temperatures. The necessary quantum corrections have been considered. Excellent agreement is obtained between the values calculated from the potential energy function determined and the experimental data. On the whole the exp. 6-8 potential gives better fit with the second virial and the Joule-Thomson coefficient data than either the exp-6 or the Lennard-Jones (12:6) potential.

## 1. INTRODUCTION

The potential energy function of molecules may be determined in two different ways. First, the potential energy function may be calculated directly from the atomic structure provided the molecules are sufficiently simple systems. The second method is to assume a carefully chosen potential form involving a number of constants whose values may be determined from accurate experimental data. Helium atom is particularly interesting in this respect for its simple structure and comparatively large quantum effects which play an important part up to temperatures of the order of 400°K.

The direct calculation of the interaction potential between two helium atoms results in a potential energy function of the form

$$\phi(r) = a \exp(-br) - (cr^{-6} + dr^{-8} + er^{-10} + \dots) \quad (1)$$

where  $\phi(r)$  is the potential energy between two molecules separated by a distance  $r$ . Slater and Kirkwood (1931) and Kirkwood and Keyes (1931) considered only the  $r^{-6}$  term in the attractive potential which represents dipole-dipole interaction. But Margenau (1931; 1939) showed that though the dipole interactions are the only appreciable ones when the molecules are far apart, the higher poles are to be considered at distances of the order of the kinetic theory radius. His calculations proved that although contributions from the  $r^{-10}$  term representing quadrupole-quadrupole interaction may be neglected, the  $r^{-8}$  term representing dipole-quadrupole interaction contributes a sizeable fraction of the total interaction energy. Margenau obtained for He the potential form

$$\phi(r) = \left( 770e^{-r/0.217} - 560e^{-r/0.187} - \frac{1.39}{r^6} - \frac{3.0}{r^8} \right) \times 10^{-12} \text{ erg.} \quad \dots \quad (2)$$

More recently the repulsive part of the interatomic potential of He has been calculated by Rosen (1950), Griffing and Welner (1955) and others more accurately. It has been observed by Yntema and Schneider (1950) that although the potential form derived by Kirkwood and Keyes (1931) gives somewhat fair agreement with their second virial data, generally the intermolecular potentials calculated directly from the atomic structures fail to explain the experimental data satisfactorily.

The alternative method of fitting the experimental data to suitably chosen potential forms has been tried by many workers (Buckingham, 1938, Massey, 1939; 1941; Lunbeck 1951, etc.). Second virial coefficient data have been fitted to the Buckingham and Lennard-Jones (12 : 6) potentials. Zero-pressure Joule-Thomson coefficient data have been used by Hirschfelder (1938) *et al.* to obtain the potential energy function for He on the Lennard-Jones (12 : 6) model. Recently Mason and Rice (1954) have fitted second virial and viscosity data to the modified exp-6 potential. Their determination of the intermolecular potential has the drawbacks that the  $r^{-8}$  term is not included in the potential form and both the first and the second quantum corrections have been taken from the exp-6-8 and the Lennard-Jones (12 : 6) potentials respectively which is not strictly justified especially as the first quantum correction for He is quite large at the lower temperatures. Moreover, it appears that at comparatively low temperatures the agreement between the experimental and the calculated values of the second virial coefficient is not very good and this disagreement is expected to be larger at the lower temperatures. Amdur (1954) and his co-workers have used molecular beam scattering method to obtain experimentally the repulsive part of the potential for He-He interactions. The theoretically calculated values of the repulsive energy for He-He interaction are consistently higher than the experimental values of Amdur *et al.*

Yntema and Schneider (1950) have tried to fit their experimental second virial data to an empirical potential of the form

$$\phi(r) = b \exp(-r/\rho) - (c_1/r^6) - (c_2/r^8). \quad \dots (3)$$

Though good agreement has been obtained with their experimental data they did not consider the quantum corrections.

In view of the above considerations, the most appropriate potential form for He seems to be exp-6-8 potential proposed by Buckingham and Corner (1947) which is given by

$$\phi(r) = c \left[ g_1(\alpha, \beta) \exp \alpha \left( 1 - \frac{r}{r_m} \right) - g_2(\alpha, \beta) \left( \frac{r_m}{r} \right)^6 \left( 1 + \beta \left( \frac{r_m}{r} \right)^2 \right) \right] \text{ for } r \geq r_m, \quad \dots (4)$$

$$\phi(r) = e \left[ g_1(\alpha, \beta) \exp \alpha \left( 1 - \frac{r}{r_m} \right) - g_2(\alpha, \beta) \left( \frac{r_m}{r} \right)^6 \left( 1 + \beta \left( \frac{r_m}{r} \right)^2 \right) \right. \\ \left. \exp \frac{1}{2} \left( 1 - \frac{r_m}{r} \right)^3 \right] \text{ for } r \leq r_m \dots \quad (5)$$

$$g_1(\alpha, \beta) = (6+8\beta)/[\alpha(1+\beta)-(6+8\beta)]$$

$$g_2(\alpha, \beta) = \alpha/[\alpha(1+\beta) - (6+8\beta)]$$

where  $c$  is the depth of the potential well,  $r_m$  the value of  $r$  for which  $\phi(r)$  has its minimum value,  $\alpha$  is the parameter which measures the steepness of exponential repulsion.

This potential form has the advantage that it not only includes an exponential repulsion term and the  $r^{-6}$  and  $r^{-8}$  terms but also the attractive term is provided with an exponential that prevents the appearance of a spurious maximum having no physical significance in the case of the exp-6 potential at  $r \approx 0.25 r_m$ . The first quantum correction for the second virial and the Joule-Thomson coefficient have been calculated accurately for the exp 6-8 model. In this paper second virial data over an extensive range of temperature and the zero-pressure Joule-Thomson coefficient data have been fitted to the exp 6-8 potential. It is expected that the potential form thus derived will be more reliable than those hitherto obtained. Force parameters on the exp 6-8 model has been determined by Corner (1948) for  $A$ ,  $Ne$  and for  $Kr$ ,  $Xe$  and  $C_2H_4$  by Barua (1959). In order to reproduce their low temperature diffusion data for  $He$ , Buckingham and Scriven (1952) have used Eq. (4) only and have chosen empirically the parameters  $\alpha = 13.5$ ,  $\beta = 0.2$ ,  $c/K = 10.18^\circ K$ ,  $r_m = 2.943 \text{ \AA}$ .

## 2 DETERMINATION OF THE PARAMETERS

Kirkwood (1933) and Uhlenbeck and Beth (1936) have shown that the second virial coefficient  $B(T)$  together with the quantum corrections may be written as

$$B(T) = \left[ B_{cl}(T) + \frac{h^2}{m} B_I(T) + \left( \frac{h^2}{m} \right)^2 B_{II}(T) + \dots \right] \quad (6)$$

where  $B_{cl}(T)$  is the classical expression for the second-virial coefficient and  $B_I(T)$  and  $B_{II}(T)$  are respectively the first and second quantum corrections,  $m$  is the mass of the molecule and  $h$  is the Planck's constant.

On the exp 6-8 model

$$B_{cl}(T) = 2\pi N r_m^3 F_0(\alpha, \beta, T^*), \quad \dots \quad (7)$$

$$B_I(T) = (N r_m^3 / kT) F_1(\alpha, \beta; T^*), \quad \dots \quad (8)$$

$$T^* = kT/\epsilon \quad \dots \quad (9)$$

where  $N$  is the Avogadro's number and  $k$  is the Boltzmann's constant. The second quantum correction  $B_{II}(T)$  has not been evaluated on the exp 6-8 model. Since the contribution of  $B_{II}(T)$  is not large (its contribution to the total  $B(T)$  at 100°K is about 1%), as has been done by Mason and Rice (1954), we may take the value of  $B_{II}(T)$  calculated by de Boer and Michels (1938) on the Lennard-Jones (12-6) model. Due to this uncertainty in the second quantum correction Eq. (6) cannot be used below 60°K.

Similarly, the zero pressure Joule-Thomson coefficient may be written as

$$\mu^0 = \left[ \mu_{cl}^0 + \frac{h^2}{m} \mu_I^0 + \left( \frac{h^2}{m} \right)^2 \mu_{II}^0 + \dots \right], \quad \dots \quad (10)$$

and on the exp 6-8 model

$$\mu_{cl}^0 = (2\pi N r_m^3 / C_p^0) G_0(\alpha, \beta; T^*) \quad (11)$$

$$C_p^0 \mu_I^0 = (N r_m / k T^*) G_1(\alpha, \beta; T^*) \quad (12)$$

where  $C_p^0$  is the value of the zero-pressure molar specific heat. The functions  $F_0, G_0, F_1, G_1$  have been tabulated by Buckingham and Corner (1947) for  $\alpha = 12.5$  to  $\alpha = 14.5$  and for  $\beta = 0$  and  $\beta = 0.2$ .

The force parameters  $\alpha, \beta, \epsilon/k, r_m$  can be determined from the experimental  $B(T)$  data by the method of translation of axes (Mason and Rice, 1954; Srivastava, 1957). In order to consider the quantum corrections, first one of the two values of  $\beta$  (either  $\beta = 0$  or  $\beta = 0.2$ ) is assumed and the quantum corrections  $B_I$  and  $B_{II}$  are taken to be zero and a set of values  $\alpha, \beta, \epsilon/k, r_m$  is obtained. With these parameters  $B_I$  and  $B_{II}$  are calculated which are then substituted in Eq. (6) to give  $\alpha, \beta, \epsilon/k, r_m$  to the second approximation. This procedure is to be repeated till the force parameters do not vary appreciably.

In Table I the force parameters obtained on the exp 6-8 model are given.  $\beta_M$  refers to the value of  $\beta$  as obtained by Margenau (1939) and  $\alpha, \epsilon/k$ , and  $r_m$  are assumed to vary linearly with  $\beta$  to find values corresponding to  $\beta_M$ . For the sake of comparison the force parameters for the exp-6 and the Lennard-Jones (12-6) potentials are also given in Table I.

### 3. COMPARISON WITH EXPERIMENT

An obvious test of the reliability of the intermolecular potential determined is a comparison of the values calculated from the potential energy function with the experimental data. A further test is the ability to reproduce more than one property with the same set of force parameters. The experimental second virial data over a temperature range of 90.2°K to 1473°K have been compared with the calculated values on the exp 6-8 model and the results are given in table II,

TABLE I  
Potential parameters for He

Potential form	$\alpha$	$\beta$	$\epsilon/k^\circ\text{K}$	$r_m \text{\AA}$	Ref. for data	
					2nd Virial	J-T Coeff.
Exp. 6-8 (Buckingham Corner)	11.4	0	9.45	3.13	v	j
	11.2	0.2	9.89	3.13		
	11.2	0.16 ( $-\beta_M$ )	9.82	3.13		
Exp 6*	12.4	.	9.16	3.136		
L-J (12 : 6)*		.	10.22	2.869		

\* (From Mason and Rice, 1954)

v Holborn and Otto (1926)

Michels and Wouters (1941)

Schneider and Duffie (1949)

Yutema and Schneider, (1950)

j. Roebuck and Osterberg (1933, 1934).

The second quantum correction which becomes important at the lower temperatures have been taken from the calculations of de Boer and Michels (1938) on the Lennard-Jones (12 : 6) model. Excellent agreement is obtained with the experimental data over the whole range of temperatures. Exp 6-8 potential gives better fit than the exp-6 potential (particularly at the lower temperatures) excepting at the highest temperatures. Throughout the temperature range exp 6-8; potential is found to reproduce the experimental data better than the Lennard-Jones (12 : 6) potential and this is very much marked at the higher temperatures. This confirms Mason and Rice's (1954) observation that helium atom is actually softer than that given by the Lennard-Jones (12 : 6) model.

The experimental and calculated values of the zero-pressure Joule-Thomson coefficient on the exp 6-8 and the Lennard-Jones (12 : 6) models are given in table III. Temperatures below 172°K have not been considered, for, at lower temperatures second quantum correction becomes important. The agreement on the exp-6-8 model is remarkably better than that obtained on the L-J (12 : 6) model. This single case perhaps cannot be taken as a proof of the superiority of the potential form with exponential repulsion term over the Lennard-Jones (12 : 6) potential. The fact that almost the same degree of agreement is obtained with the experimental data for both  $\beta = 0$  and  $\beta = 0.2$  confirms the observation of the earlier workers (Corner, 1948; Barua, 1959) that these equilibrium properties are not sensitive enough to measure the relative importance of the  $r^{-6}$  and  $r^{-8}$  terms. The third virial coefficient which is quite sensitive to the potential form chosen may serve the purpose. But no calculation for the third virial coefficient has been done for either exp-6 or exp-6-8 potentials.



TABLE II

Comparison of experimental and calculated values of  $B(T)$  of He.

T°K	$B(T)$ in cc/mole	exp 6-8		exp 6	Lennard- Jones (12-6)
		$\beta = 0$	$\beta = 0.2$		
90.2	10.45 <sup>a</sup>	10.55	10.34	11.40	10.43
123.2	11.42 <sup>a</sup>	11.36	11.27	11.60	10.76
173.2	11.92 <sup>a</sup>	11.82	11.78	12.34	11.31
223.2	11.94 <sup>a</sup>	11.90	11.84	12.21	11.59
	11.86 <sup>a</sup>				
273.2	11.87 <sup>b</sup> 11.77 <sup>c</sup>	11.70	11.69	12.11	11.50
298.2	11.74 <sup>b</sup>	11.60	11.57	11.99	11.46
323.2	11.74 <sup>b</sup> 11.58 <sup>b</sup>	11.47	11.53	11.86	11.39
348.2	11.43 <sup>b</sup>	11.37	11.42	11.73	11.30
	11.39 <sup>a</sup>				
373.2	11.35 <sup>b</sup> 11.42 <sup>c</sup>	11.25	11.30	11.60	11.22
398.2	11.24 <sup>b</sup>	11.14	11.16	11.48	11.07
423.2	11.07 <sup>b</sup>	11.07	11.09	11.36	11.01
473.2	11.07 <sup>a</sup> 11.08 <sup>c</sup>	10.95	10.98	11.12	10.90
573.2	10.50 <sup>a</sup> 10.76 <sup>c</sup>	10.30	10.44	10.71	10.65
673.2	10.14 <sup>a</sup> 10.45 <sup>c</sup>	10.01	10.05	10.33	10.41
773.2	10.14 <sup>c</sup>	9.74	9.75	9.99	10.22
873.2	9.82 <sup>c</sup> 9.80 <sup>d</sup>	9.52	9.57	9.68	10.03
1073.2	9.17 <sup>d</sup>	9.00	9.11	9.11	9.63
1273.2	8.66 <sup>d</sup>	8.78	8.85	8.69	9.50
1473.2	8.19 <sup>d</sup>	8.49	8.66	8.33	9.27

(a) Holborn and Otto (1926), (b) Michel and Wouters (1941), (c) Schneider and Duffie (1949); (d) Yntema and Schneider (1950).

TABLE III

Comparison of experimental and calculated values of  $\mu^0$  of He.

T°K	$\mu^0$ in deg at m <sup>-1</sup>	exp 6-8		Lennard- Jones (12:6)
		$\beta = 0$	$\beta = 0.2$	
172.1	-0.0557	-0.0556	-0.0556	-0.0506
273.1	-0.0599	-0.0608	-0.0611	-0.0579
297.5	-0.0601	-0.0613	-0.0614	-0.0587
374.2	-0.0621	-0.0617	-0.0622	-0.0593
472.5	-0.0616	-0.0615	-0.0624	-0.0593
575.5	-0.0568	-0.0596	-0.0608	-0.0589

#### 4. COMPARISON WITH THEORETICALLY CALCULATED POTENTIAL ENERGY FUNCTIONS

It has been shown by Margenau (1939) that the interaction energy of two He atoms may be represented as the sum of four terms

$$\phi(r) = \phi^{(val)} + \phi^{(ex, 2)} + \phi^{(dis, 6)} + \phi^{(dis, 8)} \quad \dots (13)$$

where  $\phi^{(val)}$  is the valence energy of repulsion obtained by the first-order perturbation calculation.  $\phi^{(ex, 2)}$  represents the second-order exchange terms and becomes important at distances where long and short-range forces meet. It is obtained in the second-order perturbation calculation of dispersion energy.  $\phi^{(dis, 6)}$ ,  $\phi^{(dis, 8)}$  are respectively the dispersion energy terms varying as the inverse sixth power and the inverse eighth power of separation.

The  $\phi^{(val)}$  term has been evaluated by various workers. Slater (1928) and Rosen (1950) and Sakamoto and Ishiguro (1956) used the valence bond method and later workers (Griffing and Wehner, 1955; Huzinaga, 1957) have applied LCAO MO method. For comparison with the potential energy curve obtained on the exp-6-8 model we shall take  $\phi^{(val)}$  calculated by Sakamoto and Ishiguro (1956) which is in good agreement with that of Griffing and Wehner (1955). The  $\phi^{(ex, 2)}$  and  $\phi^{(dis, 6)}$  terms have been obtained accurately by Margenau by the second-order perturbation calculation of dispersion energy. The  $\phi^{(dis, 8)}$  term has been obtained by Page (1938) by the variational method. Hence the potential energy function for He-He interaction becomes

$$\phi_{SI-M-P}(r) = \phi_{SI}^{(val)} + \phi_M^{(ex, 2)} + \phi_M^{(dis, 6)} + \phi_P^{(dis, 8)} \quad \dots (14)$$

$$= \left[ 655e^{-4.469r} - 560e^{-5.33r} - \frac{1.39}{r^6} - \frac{3.0}{r^8} \right] \times 10^{-12} \text{ erg.} \quad \dots (15)$$

The potential energy curve obtained from Eqs. (4) and (5) on the exp-6-8 model (taking the value of  $\beta = \beta_M$ ) by utilising the force parameters determined in the present investigation together with the theoretically obtained curve from Eq. (15) is shown in Fig. 1. For comparison the potential energy curve on the exp-6 model obtained by Mason and Rice (1954) is also shown.

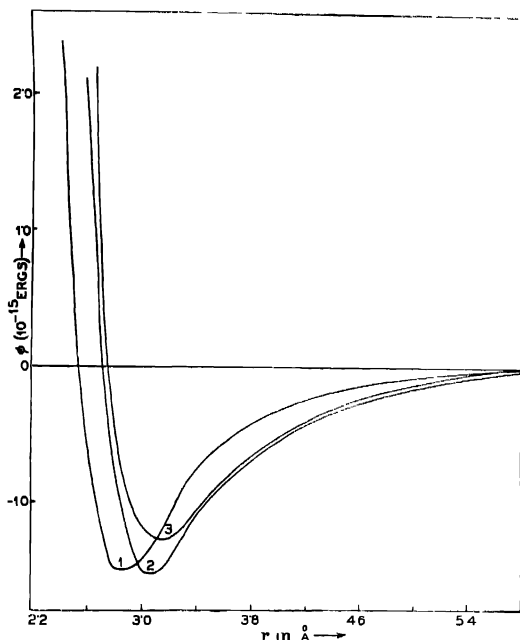


Fig. 1. Potential energy curves for He-He interaction (1) theoretical (Sakamoto-Ishiguro-Majgenau-Puge) (2) exp-6-8 (Buckingham-Corney) (3) exp-6 (Mason and Rice).

#### ACKNOWLEDGMENT

The author is grateful to Prof B N Srivastava, D.Sc., F.N.I., for his valuable suggestions and keen interest in the problem.

#### REFERENCES

- Amdur, I. and Harkness, A. L., 1954, *J. Chem. Phys.*, **22**, 664.
- Barua, A. K., 1959, *J. Chem. Phys.*, **31**, 957.
- Buckingham, R. A., 1938, *Proc. Roy. Soc. (Lond.)*, A **168**, 204.
- Buckingham, R. A. and Cornei, J., 1947, *Proc. Roy. Soc. (Lond.)*, A **189**, 118.

- Buckingham, R. A., Hamilton, J. and Massey, H. S. W., 1941, *Proc. Roy. Soc. (Lond.)*, A **179**, 103.
- Buckingham, R. A., and Scriven, R. A., 1952, *Proc. Phys. Soc. (Lond.)*, B **65**, 376.
- Corner, J., 1948, *Trans. Farad. Soc.*, **44**, 914.
- de Boer, J. and Michels, A., 1938, *Physica*, **5**, 945.
- Gripping, V. and Wehner, J. F., 1955, *J. Chem. Phys.*, **23**, 1024.
- Hirschfelder, J. O., Ewell, R. B. and Roebuck, J. R., 1938, *J. Chem. Phys.*, **6**, 205.
- Holborn, L. and Otto, J., 1920, *Z. Physik*, **38**, 359.
- Huzimaga, S., 1957, *Progr. Theo. Phys.*, **18**, 139.
- Kirkwood, J., 1933, *Phys. Rev.*, **44**, 31.
- Kirkwood, J. and Keyes, F. G., 1931, *Phys. Rev.*, **37**, 832.
- Lunbeck, R. J., 1951, Doctoral dissertation (Amsterdam).
- Margenau, H., 1931, *Phys. Rev.*, **38**, 747.
- Margenau, H., 1939, *Phys. Rev.*, **65**, 1000.
- Mason, E. A. and Rice, W. E., 1954, *J. Chem. Phys.*, **22**, 522.
- Massey, H. S. W. and Buckingham, R. A., 1939, *Proc. Roy. Soc. (Lond.)*, A **169**, 205.
- Michels, A. and Wouters, H., 1941, *Physica*, **8**, 923.
- Page, C. H., 1938, *Phys. Rev.*, **53**, 426.
- Roebuck, J. E. and Osterberg, H., 1933, *Phys. Rev.*, **43**, 60, *ibid.*, **45**, 332.
- Rosen, P., 1950, *J. Chem. Phys.*, **18**, 1152.
- Sakamoto, M. and Ishiguro, E., 1956, *Progr. Theo. Phys.*, **15**, 37.
- Schneider, W. G. and Duffie, J. A. H., 1949, *J. Chem. Phys.*, **17**, 751.
- Slater, J. C., 1928, *Phys. Rev.*, **32**, 349.
- Slater, J. C. and Kirkwood, J., 1931, *Phys. Rev.*, **37**, 682.
- Srivastava, K. P., 1957, *Ind. J. Phys.*, **31**, 404.
- Uhlenbeck, J. and Beth, E., 1936, *Physica*, **3**, 129.
- Yntema, J. L. and Schneider, W. G., 1950, *J. Chem. Phys.*, **18**, 646.

# M. U. F. FACTOR AND SOLAR ACTIVITY

C. S. R. RAO AND J. C. BHARGAVA

RESEARCH DEPARTMENT, ALL INDIA RADIO, NEW DELHI

(Received, December 23, 1959)

**ABSTRACT.** This paper deals with the variation of  $M(3000)F_2$  factor with sunspot activity. The ionospheric data for Delhi and Ahmedabad for the period 1950 to 1958 have been considered. The analysis indicates that a fairly good linear relationship exists between  $M(3000)F_2$  and sunspot number for both the places. A preliminary study of the variation of  $Y_m$  and  $h_o$  with sunspot activity (Ahmedabad) has also been made.

## I. INTRODUCTION

The variation of  $M(3000)F_2$ —the maximum usable frequency factor for distance of 3000 kms for transmission through the  $F_2$  layer—with sunspot activity has been studied recently by a few workers. Eyfrig (1951), following the variation of  $M(3000)F_2$  (related to the layer height), has observed that there exists a linear relationship. Rawer (1952) has stated that the variation of the factor  $M(3000)F_2$  can be taken as an index of altitude of the layer and that it is correlated with sunspot number. Allen (1953), however, has concluded that the variation of virtual heights is not related in any significant manner to either the sunspot cycle or the diurnal variation of  $f_oF_2$ . Theissen (1955) has attempted the evaluation of  $M(3000)F_2$  for every hour by use of charts and has also considered the possibility of a world-wide forecast of these factors. Eyfrig (1957) has followed up his previous study and has shown that an unambiguous relation of  $M(3000)F_2$  with change of solar activity exists for certain regions of the earth. He has, however, stressed therein, that the data is insufficient and sometimes contradictory to justify a world-wide examination.

The object of this paper is to study the variation of  $M(3000)F_2$  with sunspot activity as observed from the data at Delhi and Ahmedabad—two Indian stations where ionospheric sounding has been in progress for the last few years. For Delhi ( $28^{\circ}35'N$ ,  $77^{\circ}5'E$ ) data for years 1950 to 1958 and Ahmedabad ( $23^{\circ}0'N$ ,  $72^{\circ}40'E$ ) data for the years 1953 to 1958 have been analysed.

## II. CALCULATION OF $M(3000)F_2$

Over the last few years, a detailed analysis of the structure of the  $F_2$  layer has been made from the data from the different ionospheric stations in India. This analysis has shown that the assumption of a parabolic layer is a good approximation and for  $Y_m/h_o \geq 0.2$  (where  $Y_m$  is the semi-thickness of the layer and  $h_o$

is the height of the lower edge of the  $F_2$  layer), the variation of the factor  $M(3000)F_2$  with  $h_p F_2$  (height of maximum ionization density and equal to the height at 0.834 times  $f_o F_2$ ) can be represented by a curve, which appears to be a hyperbola (Fig. 1). This curve is obtained from a mass plot of  $M(3000)F_2$  factors. (after

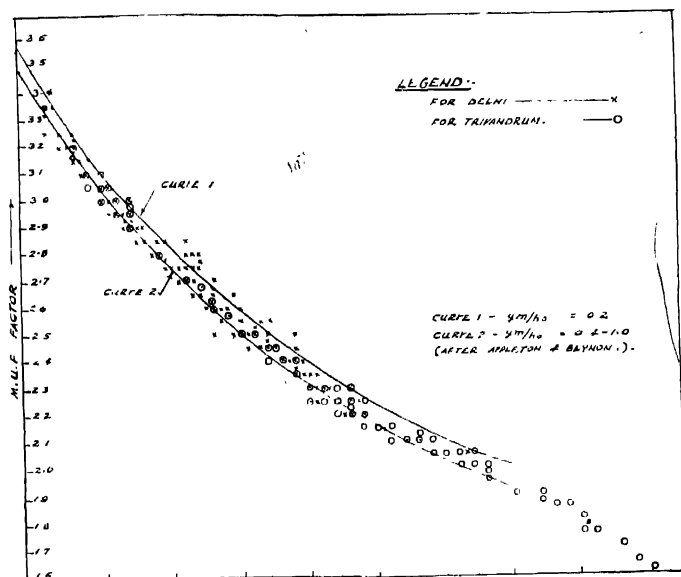


Fig. 1 Variation of  $M(3000)F_2$  with  $h_m$  for Delhi and Trivandrum.

Appleton and Beynon 1941, 1947) against height of maximum ionization for different values of  $M(3000)F_2$ . Bibl and others (1951) have also stated that  $h_p F_2$  may be related to  $M(3000)F_2$  and that the curve expressing the relationship appears to be a hyperbola. The curve corresponding to  $Y_m/h_o = 0.4$  in Fig. 1 fits in best with the data for Indian stations.

All the  $M(3000)F_2$  factors used in this paper have been obtained on the above basis.

The results of the analysis are discussed in the following sections.

### III. DIURNAL AND SEASONAL VARIATIONS OF $M(3000)F_2$

Fig. 2 shows the diurnal variation of  $M(3000)F_2$  for Delhi and Ahmedabad for sunspot minimum and maximum activity periods and for different seasons.

The predominance of the semidiurnal effect in the different seasons and in the different epochs of sunspot activity is quite evident. The effect of Solar tides in producing semi-diurnal variations of  $f_0F_2$  and  $h_pF_2$  has already been described earlier (Rao, 1956).

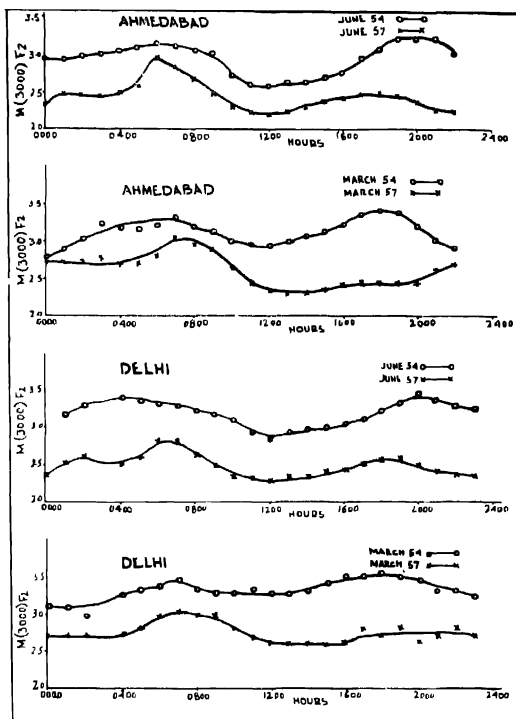


Fig. 2. Diurnal Variation of  $M(3000)F_2$  for Delhi and Ahmedabad.

#### IV VARIATION OF 'M' WITH SUNSPOT ACTIVITY

Fig. 3 shows the variations of the 12 monthly running averages of  $M(3000)F_2$  as observed at Delhi and Ahmedabad with the 12 monthly running average of relative sunspot numbers for 1200 hrs. A study of these graphs indicates that a linear relationship between the  $M(3000)F_2$  and sunspot number ( $R$ ) would be a good approximation

Assuming a relation of the type

$$M_R = M_0 - bR \quad \dots (1)$$

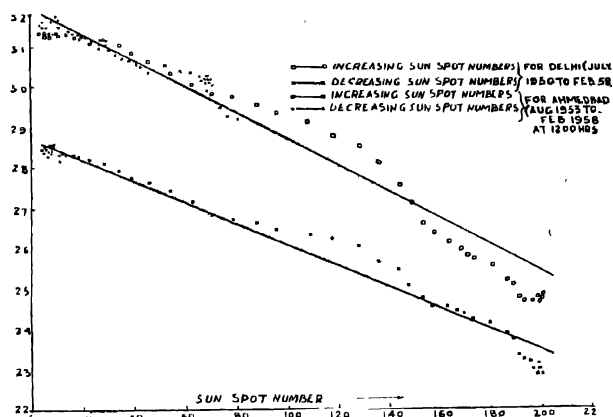


Fig. 3. Variation of running average of  $M(3000)F_2$  with running average Sunspot numl

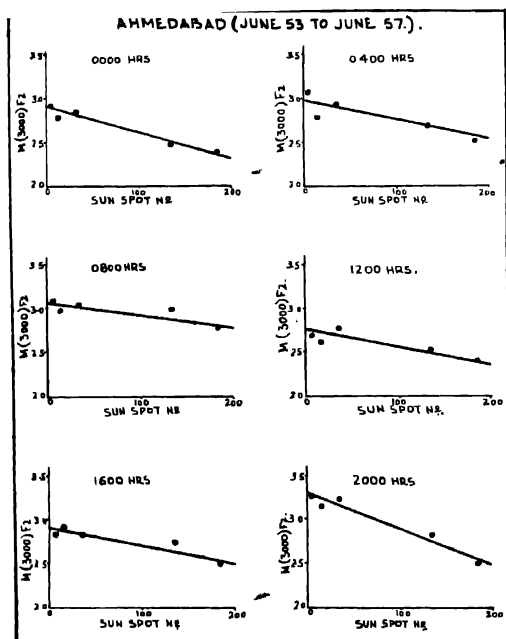


Fig. 4 Variation of  $M(3000)F_2$  with Sunspot number for different hours for Ahmedabad



where  $M_R$  is the  $M(3000)F_2$  factor for a sunspot number  $R$ ,  $M_0$  the same quantity for sunspot number zero and  $b$  the sunspot variation factor, the values of  $M_0$

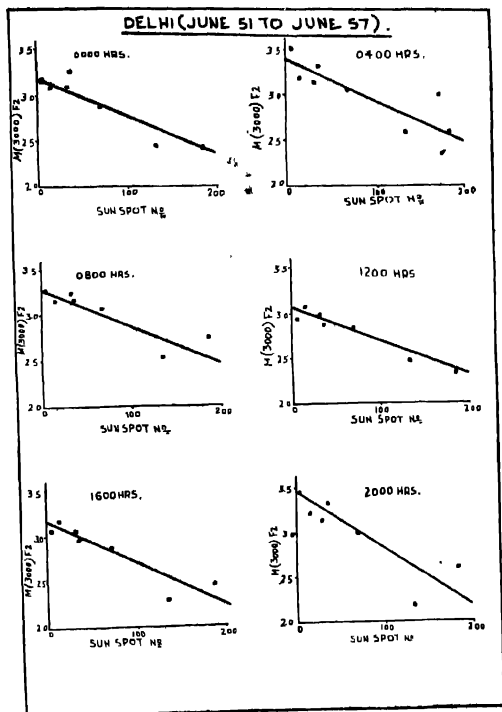


Fig. 5. Variation of  $M(3000)F_2$  with Sunspot number for different hours for Delhi.

and  $b$  and correlation co-efficient  $r$  between  $M_0$  and  $R$  have been obtained and are shown in Table I.

TABLE I

Station	$M_0$	$b$	$r$
Delhi	3.22	0.00360	0.990
Ahmedabad	2.87	0.00266	0.971

The slow variation of  $M$  with sunspot number is apparent from the values given in the above table and the high values of  $r$  obtained justify the linear relationship assumed in Eq. 1

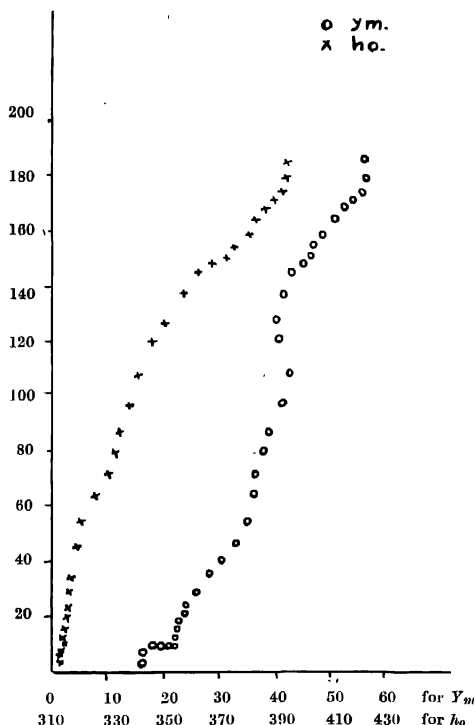


Fig. 6. Variation of  $Y_m$  and  $h_o$  with Sunspot number for Ahmedabad.

The variation of  $M(3000) F_2$  with sunspot number has also been studied for other hours. A few typical graphs showing the variations for Delhi and Ahmedabad for the month of June for different hours of the day are shown in Figs. 4 and 5 respectively. From these figures it is clear that the linear relationship assumed in Eq (1) can be extended to other hours of the day also.

#### V. VARIATION OF $Y_m$ AND $h_o$

An initial study of the variation of  $Y_m$  and  $h_o$  of the  $F_2$  layer at Ahmedabad with sunspot activity has been made. The data have been taken from those published by the Physical Research Laboratory, Ahmedabad. The variations

Fig. 4.

of  $Y_m$  and  $h_o$  (running average values of 12 months) with  $R$  are shown in Fig 6, from which it may be seen that both  $Y_m$  and  $h_o$  increase in a linear manner with increase in  $R$ .

From these graphs it is seen that the same ratio of  $Y_m/h_o$  is maintained throughout the sunspot cycle.

#### ACKNOWLEDGMENT

This work forms part of ionospheric research of the Research Department, All India Radio. The authors are grateful to the Director, Physical Research Laboratory, Ahmedabad for kindly supplying ionospheric data of Ahmedabad. The paper is published by permission of the Chief Engineer, All India Radio.

#### REFERENCES

- Allen, C. W., 1953, *J. Atmosph. Terr. Phys.*, **4**, 53.  
Appleton and Beynon, 1940, *Proc Phys. Soc*, **52**, 518  
Appleton and Beynon, 1947, *Proc Phys. Soc*, **59**, 59.  
Bibl, K., Rawer, K. and Thoissen, E., *Le rôle de J' occultation dans la pro-pagation des ondes decamétriques SP1M-R11* (December)  
Eyfrig, R., 1951, *Z. Angew Physik*, **3**, 96  
Eyfrig, R., 1957, *J Atmosph Phys.*, **11**, 163.  
Thoissen, E., 1955, *J. Atmosph. Phys.*, **6**, 243.  
Rao, C. S. R., 1957, *Ind. Jour. Phys.*, **31**, 516.  
Rawer, K., 1952, *Proc of the Macé Commission of the Ionosphere, Canberra 1952*, p. 145.

# FOURTH ORDER MESON EQUATION AND NEUTRON-PROTON SCATTERING

S. P. MISRA

MATHEMATICS DEPARTMENT, RAVENSHAW COLLEGE, CUTTACK-3

(Received, December 12, 1959)

**ABSTRACT.** We have obtained here the neutron-proton differential scattering cross-section with a fourth order meson equation proposed by Bhabha and Thirring, which was useful in explaining the anomalous magnetic moments of nucleons. We note that for moderate energies the results here disagree as violently with experiments as for conventional meson theory satisfying the Klein-Gordon equation.

## INTRODUCTION

It was noted in a previous paper (Misra and Deo, 1956) that the treatment of the anomalous magnetic moments of nucleons with a fourth order meson equation proposed by Bhabha (1950) and Thirring (1950) gives comparatively satisfactory agreement with experimental results. While proposing this equation, Bhabha had shown that the second order potential derived from this does not have the  $r^{-3}$  singularity. Because of this advantage and its previous success, we shall calculate the neutron-proton scattering cross-section in the second order perturbation theory.

The interaction hamiltonian in this case is given as

$$H_i(x) = if \bar{\Psi}(x) \gamma_5 \tau_k \psi(x) \phi_k(x). \quad \dots (1)$$

The interaction representation field-operators satisfy the equations

$$\begin{aligned} (\gamma_\mu \partial_\mu + \kappa_0) \psi(x) &= 0, \\ \partial_\mu \bar{\Psi}(x) \gamma_\mu - \kappa_0 \bar{\Psi}(x) &= 0 \end{aligned}$$

and

$$(\square - \kappa^2) \phi_k(x) = 0$$

The vacuum-expectation values of the  $P$ -products of the field operators are

$$\langle P(\phi_i(x) \phi_j(y)) \rangle_0 = \frac{\kappa^2}{2} \delta_{ij} D_F(x-y) \quad \dots (2)$$

where

$$D_F(x) = -\frac{2i}{(2\pi)^4} \int \frac{\exp(ikx)}{(k^2 + \kappa^2)^2} d^4k \quad \dots (2a)$$

and

$$\langle P(\psi(x)\bar{\psi}(y)) \rangle_0 = \frac{1}{2} S_F(x-y) \quad \dots (3)$$

where

$$S_F(x) = \frac{2i}{(2\pi)^4} \int \frac{i\gamma k + \kappa_0}{(k^2 + \kappa_0^2)} \exp(ikx) d^4k \quad \dots (3a)$$

As usual, integrals (2a) and (3a) are to be understood in the sense of Feynman.

In the perturbation calculations, the  $S$ -matrix is given as

$$S = 1 + \sum S_n$$

where

$$S_n = (-i)^n / (n!) \int d^4x_1 \dots d^4x_n P(H_i(x_1) \dots H_i(x_n)).$$

#### SECOND ORDER $S$ -MATRIX ELEMENT AND NEUTRON-PROTON SCATTERING

In the following, whenever we use the momentum space,  $p_1$  and  $p_2$  denote the four-momenta of the incoming proton and neutron and  $p_3$  and  $p_4$  denote the four-momenta of the outgoing proton and neutron respectively. Also, we use the expansion

$$\psi(x) = \frac{1}{(2\pi)^{3/2}} \int d^3p \sqrt{\kappa_0} \{ a_p u(p) e^{ipx} + b_p^* v(p) e^{-ipx} \} \quad \dots (4)$$

for the Dirac field operator where  $a_p$  and  $b_p^*$  represent respectively the annihilation and the creation operators of the particles and anti-particles.

The two Feynman diagrams that contribute to the second order matrix element are shown in Figs. 1(a) and 1(b).

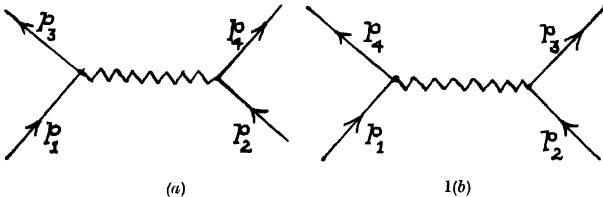


Fig. 1

These contribute to the second order matrix element, on using the expansion (4) and the results (2a) and (3), as,

$$\langle S_2 \rangle = -\frac{if^2\kappa^2}{(2\pi)^2} \delta(p_1 + p_2 - p_3 - p_4) \kappa_0^2 (p_{10} p_{20} p_{30} p_{40})^{-1/2}$$

$$\begin{aligned}
& |\bar{u}(p_3)\gamma_5\tau_i u(p_1)\bar{u}(p_4)\gamma_5\tau_i u(p_2)((p_1-p_3)^2+\kappa^2)^{-2} \\
& - \bar{u}(p_3)\gamma_5\tau_i u(p_2)\bar{u}(p_4)\gamma_5\tau_i u(p_1)((p_2-p_3)^2+\kappa^2)^{-2}]. \quad \dots \quad (5)
\end{aligned}$$

On carrying out summation over isotopic spin indices for the proton and neutron states, we obtain,

$$\begin{aligned}
\langle S_2 \rangle &= \frac{if^2k^2}{(2\pi)^2} \delta(p_1+p_2-p_3-p_4)\kappa_0^2(p_{10}p_{20}p_{30}p_{40})^{-1} \\
& |\bar{u}(p_3)\gamma_5 u(p_1)\bar{u}(p_4)\gamma_5 u(p_2)((p_1-p_3)^2+\kappa^2)^{-2} \\
& + 2\bar{u}(p_3)\gamma_5 u(p_2)\bar{u}(p_4)\gamma_5 u(p_1)((p_2-p_3)^2+\kappa^2)^{-2}]. \quad \dots \quad (6)
\end{aligned}$$

Now, we know that if the  $S$ -matrix element between the initial state  $|i\rangle$  and the final state  $|f\rangle$  is given as

$$\langle S \rangle = \delta(P_i - P_f) \langle f | M | i \rangle \quad \dots \quad (7)$$

where  $P_i$  and  $P_f$  are the total initial and final four-momenta respectively, then the total scattering cross-section is given as

$$\sigma = (2\pi)^2 \frac{p_{10}p_{20}}{((p_1p_2)^2 - \kappa_0^4)^{1/2}} \bar{S}_i S_f \{ \delta(P_i - P_f) | \langle f | M | i \rangle |^2 \}, \quad \dots \quad (8)$$

(Jauch and Rohrlich (1955)), where  $S_i$  stands for averaging over the initial states and  $S_f$  stands for the summation over all the final states. When we utilise the centre of mass coordinates, the equation (8) gives us the differential scattering cross-section as

$$\frac{d\sigma}{d\Omega} = \pi^2 E^2 S_i \Sigma | \langle f | M | i \rangle |^2, \quad \dots \quad (9)$$

where  $\Sigma$  stands for summation over final spin states.

For our problem, equations (6) and (7) give us

$$\begin{aligned}
\langle f | M_2 | i \rangle &= \frac{if^2k^2}{(2\pi)^2} \frac{\kappa_0^2}{E^2} [ \bar{u}(p_3)\gamma_5 u(p_1)\bar{u}(p_4)\gamma_5 u(p_2)((p_1-p_3)^2+\kappa^2)^{-2} \\
& + 2\bar{u}(p_3)\gamma_5 u(p_2)\bar{u}(p_4)\gamma_5 u(p_1)((p_2-p_3)^2+\kappa^2)^{-2}]. \quad \dots \quad (10)
\end{aligned}$$

The spin summation in equation (9) can be performed by using the projection operator  $\Lambda_+(p)$  to the positive energy states given as

$$\Lambda_+(p) = \frac{-i\gamma p + \kappa_0}{2E} \beta$$

Then we have, for equation (10),

$$\begin{aligned}
 S_i &= \Sigma |\dots f| M | i > |^2 \\
 &= \frac{1}{2} \frac{f^4 \kappa^4}{(2\pi)^4} \frac{\kappa_0^4}{E^4} [((p_1 - p_3)^2 + \kappa^2)^{-4} S p(\beta \gamma_5 \wedge_+(p_1) \gamma_5 \beta \wedge_+(p_3)) \times \\
 &\quad \times S p[\beta \gamma_5 \wedge_+(p_2) \gamma_5 \beta \wedge_+(p_4)] + 4((p_2 - p_3)^2 + \kappa^2)^{-4} S p[\beta \gamma_5 \wedge_+(p_2) \gamma_5 \beta \wedge_+(p_3)] \times \\
 &\quad \times S p[\beta \gamma_5 \wedge_-(p_1) \gamma_5 \beta \wedge_+(p_4)] + 2((p_1 - p_3)^2 + \kappa^2)^{-2} ((p_2 - p_3)^2 + \kappa^2)^{-2} \times \\
 &\quad \times \{S p[\beta \gamma_5 \wedge_+(p_1) \gamma_5 \beta \wedge_+ p_4 \beta \gamma_5 \wedge_+(p_2) \gamma_5 \beta \wedge_+(p_3)] + \text{hermitian conjugate expn.}\}] \\
 &= \frac{1}{2} \frac{f^4 \kappa^4}{(2\pi)^4} \frac{\kappa_0^4}{E^8} [((p_1 - p_3)^2 + \kappa^2)^{-4} ((p_1 p_3) + \kappa_0^2) ((p_2 p_4) + \kappa_0^2) \\
 &\quad + 4((p_2 - p_3)^2 + \kappa^2)^{-1} ((p_2 p_3) + \kappa_0^2) ((p_1 p_4) + \kappa_0^2) \\
 &\quad + ((p_1 - p_3)^2 + \kappa^2)^{-2} ((p_2 - p_3)^2 + \kappa^2)^{-2} ((p_1 p_4)(p_2 p_3) - (p_1 p_2)(p_3 p_4) + (p_1 p_3)(p_2 p_4) \\
 &\quad - \kappa_0^2((p_1 p_4) - (p_1 p_2) - (p_1 p_3) + (p_2 p_4) + (p_2 p_3) - (p_3 p_4)) + \kappa_0^4)] \dots \quad (11)
 \end{aligned}$$

We now remember that for the centre of mass system,

$$\begin{aligned}
 p_1 &= (\vec{P}, E), & p_2 &= (-\vec{P}, E) \\
 p_3 &= (\vec{P}', E), & p_4 &= (-\vec{P}', E), \dots \quad (12)
 \end{aligned}$$

and substitute

$$\vec{P}' = \vec{P} = P \cos \theta \quad \dots \quad (13)$$

This gives us, on simplification of the above equation (11) and by equation (9),

$$\begin{aligned}
 &\frac{d\sigma}{d\Omega} \\
 &= \left( \frac{f^2}{4\pi} \right)^2 \frac{2\kappa^4 \kappa_0^4}{E^6 P^4} \left[ \frac{\sin^4 \frac{\theta}{2}}{4 \sin^2 \frac{\theta}{2} + \lambda} + \frac{4 \cos^4 \frac{\theta}{2}}{4 \cos^2 \frac{\theta}{2} + \lambda} \right. \\
 &\quad \left. - \frac{2 \sin^2 \frac{\theta}{2} \cos^2 \frac{\theta}{2}}{\left( 4 \sin^2 \frac{\theta}{2} + \lambda \right)^2 \left( 4 \cos^2 \frac{\theta}{2} + \lambda \right)^2} \right] \dots \quad (14)
 \end{aligned}$$

Thus, for moderate energies, the differential scattering cross-section is given as

$$\frac{d\sigma}{d\Omega} = \left( \frac{f^2}{4\pi} \right)^2 \frac{2}{k_0^2} g(\theta)$$

where

$$g(\theta) = \lambda^2 \left[ \frac{\sin^4 \frac{\theta}{2}}{\left(4 \sin^2 \frac{\theta}{2} + \lambda\right)^4} + \frac{4 \cos^4 \frac{\theta}{2}}{\left(4 \cos^2 \frac{\theta}{2} + \lambda\right)^4} - \frac{2 \sin^2 \frac{\theta}{2} \cos^2 \frac{\theta}{2}}{\left(4 \sin^2 \frac{\theta}{2} + \lambda\right)^2 \left(4 \cos^2 \frac{\theta}{2} + \lambda\right)^2} \right],$$

with  $\lambda = (\kappa^2/P^2)$ . The laboratory energy is given here approximately as  $(42/\lambda)$  Mev.

Except for a multiplicative constant, the function  $g(\theta)$  above gives us the cross-section, and we have plotted this against  $\theta$  for  $\lambda = 1$  and  $\lambda = (1/2)$ , i.e., for laboratory energies 42 MeV and 84 MeV respectively (Fig. 2). It is noted that the nature of the curve obtained does not agree with the well-known experimental form, which should be rather symmetrical about  $90^\circ$  with a minimum at slightly less than that value. On the other hand, up to angle  $140^\circ$  the angular distribution is rather suggestive of the behaviour at higher energies. This leads to the suspicion that a smaller value of  $(1/\lambda)$  may give the experimental type of curve for lower energies. But in such cases the peak of the curve comes too near  $90^\circ$  for these to have any significance.

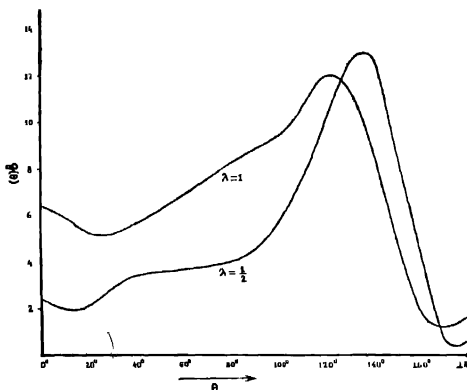


Fig. 2. The function of  $g(\theta)$  is plotted against the centre of mass angle  $\theta$  at laboratory energies 42 Mev ( $\lambda = 1$ ) and 84 Mev ( $\lambda = 0.5$ ).



A rough comparison of the scattering data with experiments gives, (on using  $1 \text{ Mev}^{-1} \approx 1.973 \cdot 10^{-11} \text{ cms}$ ), that,

$$\frac{f^2}{4\pi} \approx 16$$

Thus we note that this meson theory disagrees with experimental results for neutron-proton scattering as violently as the conventional one. Hence the fairly good agreement (Misra and Deo.) (1955)\* that was obtained for the treatment of the anomalous magnetic moments of nucleons may be regarded as accidental.

#### ACKNOWLEDGMENT

The author wishes to acknowledge his indebtedness to Prof. D. Basu for suggesting the problem.

#### REFERENCES

- Rubbia, H. J., 1950, *Phys. Rev.*, **77**, 665.  
 Jauch, J. M. and Rohrlich, F. 1955, *The Theory of Electrons and Photons*, Addison-Wesley Publishing Co.  
 Misra, S. P. and Deo, B. B., 1956, *Ind. J. Phys.*, **30**, 16.  
 Thuring, W., 1950, *Phil. Mag.*, **41**, 653.

---

\*There has been unfortunately a mistake in this paper in taking the meson field Lagrangian. This, as taken in the paper, should be multiplied by 2 so that it gives rise to the propagator quoted. This correction also gives better agreement with experiments with  $|\Delta^N/\Delta^P| = 1.6$  instead of 2.5.

# Letters to the Editor

*The Board of Editors will not hold itself responsible for opinions expressed in the letters published in this section. The notes containing reports of new work communicated for this section should not contain many figures and should not exceed 500 words in length. The contributions must reach the Assistant Editor not later than the 15th of the second month preceding that of the issue in which the paper is to appear. No proof will be sent to the authors.*

## 2

### SEARCH FOR EO TRANSITION IN ZINC-68

M. K. RAMASWAMY

DEPARTMENT OF PHYSICS, THE OHIO STATE UNIVERSITY COLUMBUS-10, OHIO (USA)

(Received, January 29, 1960)

The decay of Ga-68 has been recently reinvestigated by Horen (1959) who found evidence for levels in Zinc-68 at 1.07, 1.88 and 2.3 Mev. The levels were assigned the following spins and parities: 1.07( $2^+$ ), 1.88 ( $1^+$  or  $2^+$ ) and 2.3( $2^+$ ). No cross-over gamma transition was observed from the 2.3 Mev level to the  $0^+$  ground state. This fact together with the result of angular correlation studies on the 1.07-1.24 Mev gamma cascade led Horen to suggest  $2^+$  to the 2.3 Mev level. Since the errors on the angular correlation data were rather large, this spin assignment was considered to be far from ambiguous. It seemed attractive to assign  $0^+$  to this state and still be consistent with the observed data. In fact, the near harmonic model of Scharff-Goldhaber and Weneser (1955) predicts the existence of  $0^+$  levels at about twice the energy of the first excited state

$0-0$ . No gamma transitions are strictly forbidden because of the transverse nature of the photon. Hence the de-excitation of the state in question can proceed either through internal conversion or through internal pair formation. Since the internal positron spectrum from the 2.3 Mev level (end-point 1.28 Mev) would be superposed on a rather high background of positrons from the beta decay of Ga-68 (end-point 1.88 Mev), it was decided to look for internal conversion electrons of 2.3 Mev. In order to observe the small peak due to conversion it was necessary to reduce the background to a minimum. This was accomplished by the use of an anti-coincidence arrangement —

The Ga-68 source was sandwiched between two plastic scintillators each 1-1/2 cm high and 3 cm in diameter ensuring  $4\pi$  geometry, and mounted on the face of a Du Mont 6292 phototube. A second plastic scintillator surrounding the first one was mounted on another phototube and served as the anti-coincidence

counter. The sensitive volume of the counter was surrounded by 4" of lead. Pulses in counter 1 not accompanied by pulses in counter 2 operated a gate which admitted to the 20-channel analyzer any pulse in the beta-counter occurring in an interval of 3.5 microseconds. The end-point of the positron spectrum was determined to be  $1.89 \pm 0.05$  Mev, in agreement with the value reported by Daniel (1957). Phosphorus-32 with end-point energy of 1.72 Mev (Lidofsky, 1957) served as the calibration spectrum. The search for internal conversion electrons lasted 105 hours, during which time the apparatus was periodically checked. From the total number of counts observed in the region where the conversion electrons were expected and the total number of counts in the beta-spectrum, an upper limit of  $(5 \pm 25) \times 10^{-9}$  conversion electrons per Ga-68 decay could be set.

One can calculate the expected yield of 2.3 Mev internal conversion electrons as follows (assuming  $0^+$  level). The single-particle model gives the transition probability for the 1.24 Mev gamma-ray as  $W_{1.24} = 10^{11} \text{ sec}^{-1}$ . The  $K$ -conversion probability for the  $E0$  transition is expressed by Church and Weneser (1956) as  $W_K/\rho^2 = 7 \times 10^8 \text{ sec}^{-1}$  where  $\rho^2$  is a dimensionless parameter which measures the strength of the  $E0$  matrix element. We take  $\rho \sim 0.11$  in accordance with experiment (Alburger, 1958). The yield can then be written

$$N_K = \left[ (W_K/\rho^2) \rho^2 / \left( \frac{W_K}{\rho^2} \rho^2 + W_{1.24} \right) \right] fN$$

where  $N$  is the total number of disintegrations and  $f$  is the fraction of decays populating the 2.3 Mev level. From the data of Horen and the measured beta-spectrum  $Nf$  is about  $2 \times 10^5$ . The computed yield is  $84 \times 10^{-9}$  conversion electrons per decay, to be compared with the measured value  $(5 \pm 25) \times 10^{-9}$ .

If these estimates are indeed correct, then one can conclude that  $0^+$  is an unlikely assignment for the 2.3 Mev level. If, on the other hand, it turns out that the 1.24 Mev transition is 10 times faster than the single-particle estimate, by analogy with the situation in Ga-70, then our conclusions are somewhat weakened. Recent angular correlation measurements (Ramaswamy and Jastra, 1960) have indeed shown that the 2.3 Mev level is  $2^+$ .

The author is thankful to Professor L. Madansky of the Johns Hopkins University where this work was performed.

#### REFERENCES

- Alburger, D. E., 1958, *Phys. Rev.*, **109**, 1222.  
 Church, E. L. and Weneser, J., 1956, *Phys. Rev.*, **103**, 1035.  
 Daniel, H., 1957, *Zeit. Naturf.*, **12**, a, 363.  
 Horen, D. J., 1959, *Phys. Rev.*, **113**, 572; and private communication June 1958.  
 Lidofsky, L., 1957, *Revs. Mod. Phys.*, **29**, 773.  
 Ramaswamy, M. K. and Jastrani, P. S., 1960, *Nuclear Physics* (submitted).  
 Scharff-Goldhaber, G. and Weneser J., 1956, *Phys. Rev.*, **98**, 212.

## BOOK REVIEW

THEORIES OF FIGURES OF CELESTIAL BODIES—by W. S. Jardetzky.

Pages 186; 6×9 in. Inter-science Publishers—New York—London, 1958.

Price \$ 6.50.

One of the most important problems of any system of bodies is its evolution, that is, the sequence of changes it undergoes in time under the influence of its surroundings and internal variations. In the case of celestial bodies the problem has attracted the attention of a number of scientists. There are in general two fronts on which the problem is attacked. One is the physical state in which the study of internal constitution describes the run of the physical variables at different points inside the body. The other is the hydro-dynamical and kinematical state which describes the geometrical forms that a fluid body should acquire under the influence of the internal and external forces. In both these cases, the fast varying catastrophic changes are not included. It is assumed that the results conform to the situation which is established in due course of time when the final equilibrium is attained. For celestial objects it has become quite clear especially during recent years that the two fronts have to come very close and work together. Convection plays an important role in the study of the internal constitution. It is highly probable that the rotation is only a part of the general circulation of matter in a celestial body due to rotation as well as convection. It is believed in general that the probability of existence of a celestial body without currents of matter in its interior is practically zero. The general problem at present is still far from any complete solution.

On the interior side the active front was opened only during the present century. But the work on the dynamical front has been going on since the realization of the importance of Newton's Law of Gravitation. During these centuries quite a rigorous mathematical theory has been developed for the figures of the bodies in equilibrium by a number of great scientists like Maclaurin, Jacobi, Clairaut, Poincaré, Liapounov, Lichtenstein, Wavre, Mmeo, Jardetzky and others. All these studies are related to the equilibrium configurations under different forms of rotation for the bodies consisting of isolated, homogeneous or heterogeneous fluid masses or composite solid and fluid masses. Binaries and other complicated systems are also covered. Finally, this branch also deals with the possible sequence of equilibrium figures as a result of externally undisturbed evolution. In the last case possible atomic energy production inside the body cannot be taken into account as these studies are confined to hydrodynamical situations only under conservative forces, the forces depending upon velocities and the gyroscopical forces.

A general study of figures of equilibrium of fluid masses under the above mentioned forces is a problem of utmost importance specially to the celestial

mechanics. To have an idea of the importance of this branch we may note that when we look around we find that almost every thing in the universe rotates. The meteors, the asteroids, the planets, their satellites, the sun, the stars, the clusters, the nebulae and even the galaxies-all rotate in such a way that they have acquired over a long time a definite equilibrium distribution of velocities and a geometrical shape. Irregular forms of certain planetoids or nebulae are rather exceptions and the origin of these must be sought in some type of forces other than simple gravitation. The present position of the study of these dynamical conditions relates to rotation, pulsation, oscillations of some other type, progressing variations and rotation and revolution of two or more bodies. It is quite obvious that the problem of figures of equilibrium, though important, is quite difficult one. Some of them need very advanced mathematical tools for analysis. To-day the two important fields in this direction are: the small deformations of a gaseous mass and its stratification which have application in stars and the variation in viscosity, plasticity and the period of solidification which are important for the theories of the cold bodies like the planets. Observational confirmation of the theory can be available only for the limited cases of members of the solar system. The zonal rotation is important because it is actually observed in the case of planets like Jupiter and Saturn and also for the Sun. Law of variation of this zonal rotation from poles to the equator still remains an empirical one.

In view of what has been said above the book "Theories of Figures of Celestial Bodies" by W. S. Jardetzky, who has himself contributed a lot to this field, makes a very good addition to the existing literature, all the more so because majority of the original papers are in languages other than English. The book is well written. It is equally important to and can be appreciated by both beginners and advanced students in the field. In this book the phrase "equilibrium figures, of a body", has been used in a more general sense which includes the stratification. In the first part, in a few chapters, the author has developed the mathematical theory according to historical sequence. In the second part applications of the theory are made for explaining observed situations for the earth as well as other planets. The probable explanation of Saturn's rings is also suggested. The stratification studies which are applicable to stars and for which no observational check is possible has been dealt summarily. A brief account of the system of binaries is also given.

The order of the material is excellent. The book contains a bibliography of almost exhaustive references for further details on the subject. The study of this book can form a very good background for any student who wishes to work in this particular field. The printing and the quality of the paper make the book easy reading.

R. S. K.



# A MICROWAVE ANALOGUE FOR X-RAY DIFFRACTION

## PART I. EFFECT OF THE CRYSTALLITE SIZE

G. B. MITRA AND G. S. SANYAL

DEPARTMENTS OF PHYSICS AND ELECTRICAL COMMUNICATION ENGINEERING,  
INDIAN INSTITUTE OF TECHNOLOGY, Kharagpur

(Received, January 27, 1960)

**ABSTRACT.** Diffraction of X-rays by a crystal is analogous to that of microwaves by a three dimensional array of scatterers when the distance of one scatterer from another is of the same order of magnitude as the wave length of the microwaves. Thus all phenomena connected with the diffraction of X-rays by crystals are expected to be obtained due to the scattering of microwaves by a three dimensional arrangement of scatterers. To verify this, metallic scatterers in the form of small cylinders have been arranged to form the model of a crystal having tetragonal lattice parameter of  $a = 3.2$  cm and  $c = 4.8$  cm. A lattice of 900 such unit cells have been irradiated by microwaves of wavelength 3.2 cms. Bragg's law has been found to be valid for the (100) and (110) planes of the crystal model. The intensity distribution curves around these two reflection maxima have been studied for 10, 7 and 4 planes in the  $b$ -direction. The half intensity widths have been compared with the formula due to Scherrer. Scherrer formula has been found to agree fairly well with experimental data.

### INTRODUCTION

As is well known, all the phenomena concerning diffraction of X-rays by crystals have been explained on the basis of extremely short wavelength electromagnetic waves being scattered by atoms placed at the lattice points of a three dimensional periodic structure. The scattered electromagnetic waves interfere with each other and in the directions they reinforce each other there is obtained a diffraction maximum. The pattern of the diffraction maxima depends on the arrangement of the atoms in the crystal. Thus a study of the diffraction pattern of a crystal reveals the arrangement of atoms in it.

If a lattice is constructed with metal or dielectric scatterers at the lattice points, the lattice constants being of the order of centimeters, its behaviour towards centimetre wavelength microwaves should be exactly similar to that of a crystal to X-rays. Recently Allen (1955) described the verification of Bragg's law for 12-cm wave length microwaves and a model cubic structure of lattice constant 16 cm having metal discs mounted on wooden rods. The model was eight planes long, 4 planes high and two planes deep and so consisted of sixty-four unit cells only. Allen obtained diffraction maxima in the first order as well as in the second order for the (100) planes only. Since this is the first experiment of its kind, it

has been considered worth while to repeat the experiment for another crystallographic system, viz the tetragonal class with larger number of unit cells so that a crystal could be simulated more realistically. It has also been decided to study the effect of the crystal size on the width of the intensity distribution curves.

#### EXPERIMENTAL

A lattice containing nine hundred unit cells has been constructed with brass scatterers at the lattice points. The brass scatterers were cylinders having 1 cm diameter and 0.5 cm height and provided with a small hole in the middle for passing plastic threads through them. The plastic threads without scatterers were tested for their scattering power and were observed to have none or at least very little. This lattice was supported in a wooden structure provided with arrangements for quick rearrangement of the scatterers. The lattice constants in this case were  $a = 3.2$  cm,  $b = 3.2$  cm and  $c = 4.8$  cm.

The lattice was irradiated by a microwave horn and the diffraction pattern about the lattice was measured by another microwave horn. Both these horns could be rotated about a common vertical axis of the lattice. The microwave signal was generated by a klystron (723A/B) and was fed to the radiating horn. The second microwave horn, acting as a receiving antenna, picked up the diffracted signal and fed into a crystal detector. The klystron was square-wave modulated and the video square wave at the output of the detector was measured by an amplifier. The diffraction pattern was obtained by recording the output of the amplifier at various settings of the receiving horn for a pre-determined position of the transmitting horn. The scattering due to the wooden frame and the walls etc. of the room was first of all studied to determine the zero level of the signal received by the detector. This was made very low compared to the signal from the three dimensional array. The polar diagramme of the radiating horn was studied to find out the effect of instrumental broadening on the intensity distribution curves.

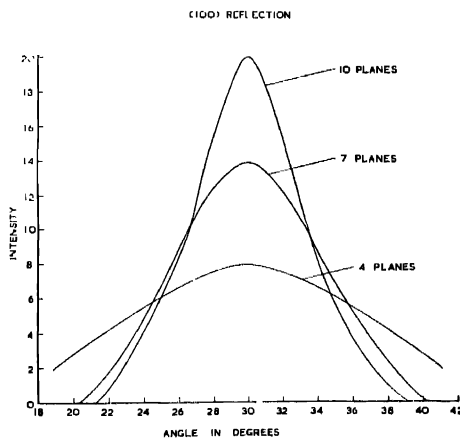
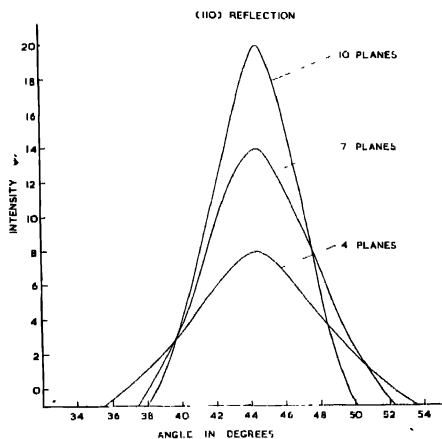
#### RESULTS AND DISCUSSIONS

The incident beam of microwaves was normal to the (001) direction and readings were taken only for the (100) and (110) planes. A diffraction maximum was obtained for both the incident as well as the diffracted beams making an angle of  $30^\circ$  with the planes parallel to the  $X$ -axis. This corresponds to the Bragg angle for the (100) plane of the lattice under investigation. Similarly, a diffraction maximum was again observed at  $44^\circ$  corresponding to the Bragg angle for the (110) planes. Thus Bragg law was found to be satisfied at least in these two cases.

Next the effect of particle size was investigated. The intensity vs angle curves in the vicinity of the  $44^\circ$  and  $30^\circ$  scattering maxima for 10, 7 and 4 planes in the  $b$ -direction were drawn and their half intensity angular widths were



determined after eliminating the instrumental broadening. The results are shown in Table I and in Figs. 1 and 2.



The measured half intensity widths have been compared with those calculated from the well-known Scherrer formula (1918). While calculating the half intensity width

$$\beta = \frac{\lambda}{t \cos \theta}$$

where  $\lambda$  is the wavelength,  $\theta$  the Bragg angle and  $t$  the crystallite size,  $t$  has been taken to be the thickness of the crystallite in the  $(hkl)$  direction. It is observed that the measured half intensity widths agree rather fairly well with the Scherrer formula. It is to be noted that all the planes normal to the (110) direction did not have the same number of scatterers in them. The end planes possessed very few scatterers. It is clear that it is necessary to have the intensity curves for the planes free from overlap from scatterings due to other planes. To achieve this, the lattice dimensions have been so taken that only two Bragg reflections, namely, at  $30^\circ$  and  $44^\circ 30'$  are possible for the given setting of the crystal model. Even then there has been certain overlap between these scatterings due to the two planes. The intensity distribution curves shown in figures 1 and 2 have been drawn after eliminating the effects due to such overlap. It must be noted that in calculating the half intensity widths the measurements of the parameters involved have been fairly accurate. The close agreement of the measured half intensity widths with Scherrer's formula is rather interesting.

#### ACKNOWLEDGMENT

Thanks are due to Dr H. Rakshit and to Dr K. Banerjee for their kind interest in this work.

TABLE I

Plane ( <i>hkl</i> )	Bragg angle $\theta$ degrees	Thickness of crystal in the ( <i>hkl</i> ) direction <i>t</i> cms.	Half intensity angular width calculated from Scherrer formula	Observed half intensity width $\beta$ in degrees
100	$30^\circ$	32.0	$6^\circ 36'$	$7^\circ$
		22.4	$9^\circ 48'$	$11^\circ$
		12.8	$16^\circ 32'$	$17^\circ$
110	$44^\circ 30'$	44.8	$5^\circ 44'$	$6^\circ$
		39.1	$6^\circ 34'$	$7^\circ$
		34.5	$7^\circ 28'$	$8^\circ$

#### REFERENCES

- Allen, R. A., 1955, *Am. J. Phys.*, **23**, 297.  
Scherrer, P., 1918, *Nachr. Göttingen Gesell.*, p. 98.

# OSCILLATIONS OF ROTATING COSMICAL BODIES IN THE PRESENCE OF MAGNETIC FIELD

J. N. TANDON

INDIAN NATIONAL COMMITTEE FOR THE IGY, NATIONAL PHYSICAL LABORATORY,  
DELHI

(Received, February 6, 1960)

**ABSTRACT.** The effect of rotation on the radial pulsations of cosmical fluid masses with special reference to spherical mass (magnetic variables) and cylindrical mass (spiral arm, solar-ion stream) has been investigated when the fluids are having volume electric currents. Two models of currents system are considered for cylindrical mass, viz., circular currents and line currents. It is found that for radial pulsations, rotation in general, helps in the dynamical stability of the cosmical bodies.

## 1. INTRODUCTION

Talwar and Tandon (1956) have earlier obtained an expression for the frequency of radial pulsations of spherical masses in the presence of magnetic field (magnetic variable stars). The magnetic field was assumed to be axially symmetric and derivable from volume currents flowing in the interior of the star. They also obtained an upper limit for the magnetic field above which the star will become dynamically unstable provided  $\Gamma > 4/3$  where  $\Gamma$  is the ratio of the two specific heats. Similar problem for radial pulsations of the infinitely long cylinder (spiral arm solar-ion streams etc.) having volume currents has also been investigated by Tandon and Talwar (1957). Two special cases, (1) circular currents and (2) line currents are investigated. It is found that the cylinder remains dynamically stable for both the models.

In this paper we have investigated the effect of rotation on the frequency of pulsations of the cosmical masses having volume currents. §2 deals with the radial pulsations of rotating spherical mass and is of great significance for magnetic variables. Ledoux (1945) has treated the similar problems for non-magnetic stars and has obtained the expression for frequency of radial pulsations. Our expression is similar to one obtained by Ledoux except that an additional term  $\int \mathbf{r} \cdot (\mathbf{J} \times \mathbf{H}) d\tau$  along with gravitational energy term  $\Omega$  has been obtained. It is also shown that rotation helps in the dynamical stability of the star provided  $\frac{1}{3} < \Gamma < \frac{5}{3}$ . In §3 we have considered the effects of the rotation on the radial pulsations of cylindrical fluid masses. The two special cases of the volume currents, viz., circular and line currents have been re-investigated. It is found that rotation helps in the dynamical stability of the cylinder also.

## 2 PULSATIONS OF ROTATING SPHERE WITH VOLUME CURRENTS

The equation of motion of a uniformly rotating fluid mass having an internal magnetic field arising from the volume currents can be written as

$$\frac{d\mathbf{u}}{dt} = -\frac{1}{\rho} \text{grad } p - \text{grad } V + \frac{1}{\rho} (\mathbf{J} \times \mathbf{H}) - \mathbf{w} \times (\mathbf{w} \times \mathbf{r}) - 2(\mathbf{w} \times \mathbf{u}) - \left( \frac{d\mathbf{w}}{dt} \times \mathbf{r} \right) \dots \quad (1)$$

where  $\rho$  denotes the fluid density,  $V$  the gravitational potential,  $p$  the pressure and  $\mathbf{w}$  the angular velocity at any point. The magnetic field  $\mathbf{H}$  and the current density  $\mathbf{j}$  satisfy the following relation inside

$$\text{curl } \mathbf{H} = 4\pi \mathbf{J} \dots \quad (2)$$

$$\text{div } \mathbf{H} = 0 \dots \quad (3)$$

and the field outside is continuous at the boundary.

Assuming axial symmetry,  $\mathbf{u}$  the fluid velocity vector will be in the meridian plane and the last two terms on the right hand side of eqn (1) are the only vector in this equation which are normal to this plane\*. Thus we should have

$$2(\mathbf{w} \times \mathbf{u}) + \left( \frac{d\mathbf{w}}{dt} \times \mathbf{r} \right) = 0 \dots \quad (4)$$

and

$$\frac{d\mathbf{u}}{dt} = -\frac{1}{\rho} \text{grad } p - \text{grad } V + \frac{1}{\rho} (\mathbf{J} \times \mathbf{H}) - \mathbf{w} \times (\mathbf{w} \times \mathbf{r}) \dots \quad (5)$$

We multiply equation (5) scalarly on a vector  $\mathbf{r}$  and integrate over the entire mass of the configuration. The left hand side of the equation becomes

$$\int \mathbf{r} \cdot \frac{d\mathbf{u}}{dt} dm = \int \mathbf{r} \cdot \frac{d^2\mathbf{r}}{dt^2} dm = \frac{1}{2} \frac{d^2}{dt^2} \int r^2 dm = \int |u|^2 dm \dots \quad (6)$$

where  $dm = \rho d\tau (= \rho dx_1 dx_2 dx_3)$

and the integration is effected over the entire mass,  $M$ , of the configuration.

\* It may be noted here that we are restricting ourselves to a case when the electro-magnetic force  $\mathbf{j} \times \mathbf{H}$  also lies only in the meridian plane.

Letting

$$I = \int_V r^2 dm$$

and

$$T = \frac{1}{2} \int_V |u|^2 d$$

denote the moment of inertia and kinetic energy of mass motion respectively, we have

$$\begin{aligned} \frac{1}{2} \frac{d^2 I}{dt^2} - 2T = & - \int_V \mathbf{r} \cdot \text{grad } p d\tau + \int_V \frac{1}{\rho} \mathbf{r} \cdot (\mathbf{j} \times \mathbf{H}) dm \\ & - \int_V \mathbf{r} \cdot (\text{grad } V) dm - \int_V \mathbf{r} \cdot \{\mathbf{w} \times (\mathbf{w} \times \mathbf{r})\} dm \quad \dots \quad (7) \end{aligned}$$

The third integral on the right hand side of this equation represents the gravitational potential energy  $\Omega$  of the configuration. Now

$$\int_V \mathbf{r} \cdot \text{grad } p d\tau = \int_S p \mathbf{r} \cdot d\mathbf{S} - \int_V p \text{ div } \mathbf{r} d\tau = -3 \int_V p d\tau \quad \dots \quad (8)$$

since the gas pressure vanishes at the boundary of the surface. Thus we should have

$$\int_V \mathbf{r} \cdot \text{grad } p d\tau = -3(\Gamma - 1)U \quad \dots \quad (9)$$

where  $U$  is the internal energy of the system. Now, since  $\mathbf{r} \cdot \mathbf{w} = 0$ , the last integral on the right hand side of equation (8) can be written as

$$\begin{aligned} \int_V \mathbf{r} \cdot \{\mathbf{w} \times (\mathbf{w} \times \mathbf{r})\} dm &= - \int_V w^2 (x^2 + y^2) dm \\ &= - \int_V w dm \\ &= - wW \end{aligned} \quad \dots \quad (10)$$

where  $W$  is the total angular momentum. Further, putting

$$\int_V \frac{1}{\rho} \mathbf{r} \cdot (\mathbf{j} \times \mathbf{H}) dm = E \quad \dots \quad (11)$$

the electromagnetic energy of the fluid, and substituting the values of various integrals in equation (8) we find

$$\frac{1}{2} \frac{d^2 I}{dt^2} = 2T + 3(\Gamma - 1)u + \Omega + E + wW \quad \dots \quad (12)$$

This is the Virial theorem for a system of rotating fluid subjected to electromagnetic field. We shall now apply this equation to the adiabatic pulsations of a rotating fluid in which there are body currents. In analysing this problem we shall adopt the Lagrangian mode of description and follow each element of mass,  $dm$ , as it moves.

Considering periodic oscillations with angular frequency we shall let  $\delta \mathbf{r} e^{i\omega t}$  denote the displacement of an element of mass  $dm$ , from its equilibrium position  $\mathbf{r}_0$ . Similarly, we shall denote by  $\delta p e^{i\omega t}$ ,  $\delta \rho e^{i\omega t}$ ,  $\delta \mathbf{H} e^{i\omega t}$ ,  $\delta \mathbf{j} e^{i\omega t}$  and  $\delta \mathbf{w} e^{i\omega t}$  the corresponding changes in the other physical variables as we follow the element,  $dm$ , during its motion. The assumption that oscillations take place adiabatically requires that the changes in pressure and density, as we follow the motion, should satisfy the relation

$$\delta p = \Gamma \frac{\delta \rho}{\rho} p \quad (13)$$

where  $\Gamma$  is the ratio of the specific heats (assumed to be constant in space and time) while the equation of continuity

$$\frac{\partial \rho}{\partial t} + \rho \operatorname{div} \mathbf{u} = 0$$

requires that

$$\frac{\delta \rho}{\rho} + \operatorname{div} \delta \mathbf{r} = 0 \quad (14)$$

Returning to equation (4) and assuming  $Z$ -axis as the axis of rotation we can write it in cylindrical coordinate system  $(\omega, \theta, z)$  as follows

$$2\omega r \frac{\partial \omega}{\partial t} + \omega \frac{\partial \omega}{\partial t} = 0 \quad \dots (15)$$

Upon integration this leads to the relation

$$\omega \omega^2 = \text{constant} \quad \dots (16)$$

which can also be expressed in cartesian as follows

$$w(x^2 + y^2) = \text{constant} \quad \dots (17)$$

Equation (4) simply expresses the conservation of angular momentum  $w$ .

Letting  $\delta I e^{i\omega t}$ ,  $\delta \Omega e^{i\omega t}$ ,  $\delta U e^{i\omega t}$ ,  $\delta E e^{i\omega t}$  and  $\delta(wW) e^{i\omega t}$  denote the changes in  $I$ ,  $\Omega$ ,  $U$ ,  $E$  and  $wW$  respectively we can write equation (12) as

$$\frac{1}{2} \sigma^2 \delta I = 3(\Gamma - 1) \delta U + \delta \Omega + \delta E + \delta(wW). \quad \dots (18)$$

Since to the first order in the displacement, the terms involved in  $T$  do not make any significant contribution,

Now

$$\begin{aligned}
 \delta I &= 2 \int_V \mathbf{r} \cdot \delta \mathbf{r} dm \\
 3(\Gamma - 1) \delta U &= 3 \int_V \delta(p/\rho) dm \\
 &= 3 \int_V \left( \frac{\delta p}{\rho} - \frac{p \delta \rho}{\rho^2} \right) dm \\
 &= 3(\Gamma - 1) \int_V \frac{p}{\rho} \frac{\delta \rho}{\rho} dm \\
 &= 3(\Gamma - 1) \int_V p \operatorname{div} \delta \mathbf{r} d\tau \\
 &= 3(\Gamma - 1) \left[ \int_S p \mathbf{r} \cdot d\mathbf{s} - \int_V \delta \mathbf{r} \cdot \operatorname{grad} p d\tau \right] \\
 &= 3(\Gamma - 1) \int_V \delta \mathbf{r} \cdot \operatorname{grad} p d\tau \quad \dots \quad (20)
 \end{aligned}$$

In obtaining equation (20) we have made use of the equations (13) and (14) and of the fact that the fluid pressure vanishes on the bounding surface. Further for the equilibrium configuration equation (5) gives

$$\operatorname{grad} p = -\rho \operatorname{grad} V + (\mathbf{J} \times \mathbf{H}) - \rho \mathbf{w} \cdot (\mathbf{w} \times \mathbf{r}) \quad (21)$$

Therefore

$$\begin{aligned}
 3(\Gamma - 1) \delta U &= 3(\Gamma - 1) \int_V \delta \mathbf{r} \cdot \operatorname{grad} p d\tau \\
 &= 3(\Gamma - 1) \left[ \int_V \delta \mathbf{r} \cdot \operatorname{grad} V dm \right. \\
 &\quad \left. + \int_V \delta r \cdot (\mathbf{J} \times \mathbf{H}) d\tau \right. \quad \dots \quad (22) \\
 &\quad \left. - \int_V \delta \mathbf{r} \cdot \{\mathbf{w} \times (\mathbf{w} \times \mathbf{r})\} dm \right]
 \end{aligned}$$

Further we have

$$\delta \Omega = - \int_V \delta \mathbf{r} \cdot \operatorname{grad} V dm \quad \dots \quad (23)$$

But

$$\begin{aligned}
 \mathcal{I} &= \delta \int^M \frac{1}{\rho} \mathbf{r} \cdot (\mathbf{J} \times \mathbf{H}) dm \\
 &= \int^M \left[ \left\{ \frac{\delta \mathbf{r}}{\rho} - \frac{\delta \rho}{\rho^2} \mathbf{r} \right\} (\mathbf{J} \times \mathbf{H}) \right. \\
 &\quad \left. + \mathbf{r} \cdot \{(\delta \mathbf{J} \times \mathbf{H}) + (\mathbf{J} \times \delta \mathbf{H})\} \right] dm \\
 &= \int [\{\delta \mathbf{r} + (\text{div } \delta \mathbf{r}) \cdot \mathbf{r}\} (\mathbf{J} \times \mathbf{H}) \\
 &\quad + \mathbf{r} \cdot \{(\delta \mathbf{J} \times \mathbf{H}) + (\mathbf{J} \times \delta \mathbf{H})\}] d\tau
 \end{aligned} \tag{24}$$

and since the total angular momentum is preserved during pulsations, we have

$$\delta(wW) = W\delta w \tag{25}$$

Substituting equations (19) to (25) in equation (18) we get

$$\begin{aligned}
 \int^M \mathbf{r} \cdot \delta \mathbf{r} dm &= -(3\Gamma - 4) \int^M \delta \mathbf{r} \cdot \text{grad } V dm \\
 &\quad + (3\Gamma - 2) \int_V \delta \mathbf{r} \cdot (\mathbf{J} \times \mathbf{H}) d\tau \\
 &\quad + \int_V (\text{div } \delta \mathbf{r}) \mathbf{r} \cdot (\mathbf{J} \times \mathbf{H}) d\tau \\
 &\quad + \int_V \mathbf{r} \cdot [(\delta \mathbf{J} \times \mathbf{H}) + (\mathbf{J} \times \delta \mathbf{H})] d\tau \\
 &\quad - 3(\Gamma - 1) \int^M \delta \mathbf{r} \cdot \{\mathbf{w} \times (\mathbf{w} \times \mathbf{r})\} dm \\
 &\quad + W \delta w
 \end{aligned} \tag{26}$$

This is the required integral formula for  $\sigma^2$ . The change  $\delta H$  following the motion is given by (Chandrasekhar and Fermi, 1953)

$$\delta \mathbf{H} = \text{curl } (\delta \mathbf{r} \times \mathbf{H}) + (\delta \mathbf{r} \cdot \text{grad}) \mathbf{H}$$

while  $\delta \mathbf{j}$  will be evaluated by substituting the value of this in equation (2) remembering that the independent variable is  $r_0$  and not  $r$  while following the motion.

To obtain the approximate relation for the frequency of pulsations we put,

$$\delta \mathbf{r} = \xi \mathbf{r} \quad \dots \tag{28}$$



where  $\xi$  is constant in space. Thus it can readily be seen that

$$\begin{aligned}\delta\mathbf{H} &= -2\xi\mathbf{H} \\ \delta\mathbf{j} &= -3\xi\mathbf{j} \\ \delta\mathbf{w} &= -2\xi\mathbf{w}\end{aligned}\quad \dots (29)$$

and

$$\int^M \delta\mathbf{r} \cdot \{\mathbf{w} \times (\mathbf{w} \times \mathbf{r})\} dm = -\xi w W$$

Substituting equations (28) and (29) in equation (27) we obtain after some reduction

$$\sigma^2 \int^M r^2 dm = -(3\Gamma - 4)[E + \Omega] + (5 - 3\Gamma)wW$$

or

$$\sigma^2 = -(3\Gamma - 4) \frac{E + \Omega}{I} + (5 - 3\Gamma) \frac{wW}{I} \quad \dots (30)$$

It is evident from equation (30) that rotation like gravitation helps in the dynamical stability of the sphere provided  $\frac{3}{4} < \Gamma < \frac{5}{2}$ . Also there exists an upper limit for the magnetic field set by the following equation, viz.

$$E = |\Omega| \leq \frac{3\Gamma - 5}{3\Gamma - 4} wW \quad \dots (31)$$

### 3. RADIAL PULSATIONS OF A ROTATING CYLINDER WITH VOLUME CURRENTS

Let us now consider an infinitely long cylinder, rotating with a constant angular velocity  $\mathbf{w}$  in which the currents are flowing. The equation of motion for the radial pulsation of such a configuration assuming axial symmetry can be written as follows\*

$$\begin{aligned}\frac{du_r}{dt} = & -\frac{1}{\rho} \frac{\partial p}{\partial \omega} - \frac{2Gm(\omega)}{\omega} + \frac{1}{\rho} (\mathbf{j} \times \mathbf{H})_{radial} \\ & - \{\mathbf{w} \times (\mathbf{w} \times \mathbf{r})\}_{radial}\end{aligned}\quad \dots (32)$$

and

$$2(\mathbf{w} \times \mathbf{u}) + \left( \frac{d\mathbf{w}}{dt} \times \mathbf{r} \right) = 0 \quad \dots (33)$$

Here  $m(\omega)$  is the mass of the unit length of the cylinder interior to  $\omega$ . Equation (33) with  $Z$ -axis of the cylindrical coordinate system  $(\omega, \theta, z)$  as the axis of the rotation can be written in the form (after integration)

$$w\omega^2 = \text{constant} \quad \dots (34)$$

---

\* Here we assume that  $\mathbf{j} \times \mathbf{H}$  has only radial component,

This equation simply expresses the conservation of angular momentum. Multiplying equation (32) by  $\omega$  and integrating over the entire mass of unit cylinder and proceeding exactly as in § 2, we find

$$\int \omega \frac{d\omega}{dt} dm = \frac{1}{2} \frac{d^2}{dt^2} \int \omega^2 dm = 2T \quad \dots (35)$$

where  $M$  is the mass of the unit cylinder and  $T$  is the kinetic energy of the mass motion. Also

$$\int \frac{\omega}{\rho} \frac{\partial p}{\partial \omega} dm = -2 \int_V p d\tau = -2(\Gamma - 1)U \quad \dots (36)$$

since  $\text{div } \omega = 2$ , for a 2 dimensional case and  $U$  is the internal energy per unit length of the configuration. For a homogeneous fluid mass we further have

$$\int \omega \cdot \frac{2Gm}{\omega} dm = GM^2 \quad \dots (37)$$

$$\int \frac{1}{\rho} \omega \cdot (\mathbf{J} \times \mathbf{H}) dm = E \quad \dots (38)$$

and

$$\int \omega \cdot \{\mathbf{w} \times (\mathbf{w} \times \omega)\} dm = \int w dW = wW \quad \dots (39)$$

where  $dW = w\omega^2$  and  $m$  is the angular momentum per unit length of the cylinder. Hence the Virial theorem for the study of radial pulsations of an rotating infinite cylinder having volume currents will be

$$\frac{1}{2} \frac{d^2}{dt^2} \int \omega^2 dm = 2T + 2(\Gamma - 1)U + GM^2 + E + wW \quad \dots (40)$$

To study the radial pulsations we adopt as before Lagrangian mode of description. Now consider periodic pulsations with the frequency  $\sigma$  and let  $\delta\omega e^{i\sigma t}$  denote the displacement of an element of mass,  $dm$ , from its equilibrium configuration,  $\omega_0$ . Similarly, denote the corresponding changes in other physical variables by  $\delta p e^{i\sigma t}$  etc. Further, the change in the pressure  $\delta p$  for adiabatic pulsations and the equation of continuity are represented by equations (13) and (14) respectively.

Letting  $\delta u e^{i\sigma t}$ ,  $\delta m e^{i\sigma t}$  and  $\delta(wW) e^{i\sigma t}$  denote the changes in quantities  $U$ ,  $E$  and  $wW$  we have from the Virial theorem

$$\sigma^2 \int \omega \delta\omega dm = 2(\Gamma - 1)\delta U + \delta E + \delta(wW) \quad \dots (41)$$

Since  $GM^2$  is constant and to the first order in the displacement, the terms in  $T$  will not make any contribution. Further,

$$2(\Gamma-1)\delta U = 2(\Gamma-1) \int_V \delta\omega \frac{\partial p}{\partial\omega} d\tau$$

since the pressure vanishes at the bounding surface. Now for the equilibrium configuration

$$\frac{\partial p}{\partial\omega} = - \frac{2Gm}{\omega} \rho^{-1} (\mathbf{J} \times \mathbf{H})_{radial} - \rho^{-1} \mathbf{w} \cdot (\mathbf{w} \times \boldsymbol{\omega})_{radial}$$

Multiplying this equation by  $\delta\omega$  and putting

$$\delta\omega = \xi\omega \tag{42}$$

we find

$$2(\Gamma-1)\delta U = 2(\Gamma-1) \int_V \xi Gm dm + \int_V \xi\omega \cdot (\mathbf{J} \times \mathbf{H}) d\tau + \int_V \xi w dW \tag{43}$$

Further

$$\delta E = \int \{ \xi + \text{div}(\xi\omega) \} \{ \omega \cdot (\mathbf{J} \times \mathbf{H}) \} d\tau + \int \omega \cdot [(\delta\mathbf{J} \times \mathbf{H}) + (\mathbf{J} \times \delta\mathbf{H})] d\tau \tag{44}$$

and

$$\delta(wW) = W \delta w \tag{45}$$

since the angular momentum is constant. Now from equation (34) we get

$$\delta w = -2\xi W$$

Therefore

$$\delta(wW) = -2\xi wW$$

Hence equation (41) with the help of equations (43) to (46) reduces to

$$-\sigma^2 \int_V \xi \omega^2 dm = -2(\Gamma-1) \left[ \int_V \xi 2Gm dm - \int_V \xi\omega \cdot (\mathbf{J} \times \mathbf{H}) d\tau \right]$$

$$\begin{aligned}
& - \int_V w \xi dm \Big] + \int_V [\xi + \text{div}(\xi \omega)] [\omega \cdot (\mathbf{J} \times \mathbf{H})] d\tau \\
& + \int_V \omega \cdot [(\delta \mathbf{j} \times \mathbf{H}) + (\mathbf{J} \times \delta \mathbf{H})] d\tau - 2\xi w W \quad \dots \quad (47)
\end{aligned}$$

This is the required integral formula for the frequency of radial pulsations of rotating infinitely long cylinder for all currents distribution having axial symmetry. The changes  $\delta \mathbf{H}$  in the magnetic field and  $\delta \mathbf{j}$  in the current density can easily be evaluated with the help of equations (27) and (2).

Let us now obtain the approximate expression for the frequency of pulsation for two special cases of magnetic fields, viz. poloidal and toroidal. Auluck and Kothari (1957) have discussed these two systems of fields in detail. Let us make use of the usual assumption made in the theory of adiabatic pulsations of stars, viz.,

$$\xi = \text{constant in space.} \quad \dots \quad (48)$$

Case (i) The magnetic field is poloidal

This poloidal magnetic field is derived from circular currents of the form

$$\mathbf{j} = \left\{ 0, -\frac{k\omega}{4\pi}, 0 \right\} \quad (49)$$

such that

$$\mathbf{H} = \left\{ 0, 0, \frac{k}{2}(\omega^2 - R^2) \right\} \quad \dots \quad (50)$$

where  $k$  is constant and  $R$  is the radius of the cylinder. For such a configuration, it was shown earlier by Tandon and Talwar (1957) that

$$\delta \mathbf{H} = -2\xi \mathbf{H}$$

and

$$\delta \mathbf{j} = -3\xi \mathbf{j} \quad \dots \quad (51)$$

The equation for the frequency of radial pulsations will then be

$$\begin{aligned}
\sigma^2 \int_V \omega^2 dm &= 2(\Gamma - 1)GM^2 - 2(\Gamma - 2) \int_V \omega \cdot (\mathbf{J} \times \mathbf{H}) d\tau \\
& - 2(\Gamma - 2)wW \quad \dots \quad (52)
\end{aligned}$$

or using the abbreviation

$$E' = \int_V \frac{H^2}{8\pi} d\tau \quad \dots \quad (53)$$

we get

$$\sigma^2 \int \omega^2 dm = 2(\Gamma - 1)GM^2 + 2(2 - \Gamma)[2E' + wW] \quad \dots (54)$$

Thus, in the case of rotation the term  $2E'$  of equation (25) of Tandon and Talwar has been replaced by  $2E' + wW$ . This clearly indicates that the rotation is similar to magnetic field and helps in the dynamical stability of the cylinder for radial pulsations in the presence of circular currents.

Case (ii)—The magnetic field is toroidal

For this case we consider a system in which there are line currents of constant value such that

$$\mathbf{j} = \left(0, 0, \frac{k}{2\pi}\right) \quad \dots (55)$$

and hence

$$\mathbf{H} = (0, k\omega, 0) \quad \dots (56)$$

where  $k$  is a constant. The change in the magnetic field  $\delta\mathbf{H}$  and the change in the current density  $\delta\mathbf{j}$  will then be given by

$$\begin{aligned} \delta\mathbf{H} &= -\xi\mathbf{H} \\ \text{and} \quad \delta\mathbf{j} &= -2\xi\mathbf{j} \end{aligned} \quad \dots (57)$$

The equation for the frequency of pulsations thus becomes

$$\sigma^2 \int \omega^2 dm = 2(\Gamma - 1)GM^2 - 2(\Gamma - 1) \int_V \omega \cdot (\mathbf{J} \times \mathbf{H}) d\tau - 2(\Gamma - 2)wW \quad \dots (58)$$

Further using the abbreviation represented by equation (53) we obtain

$$\sigma^2 \int \omega^2 dm = 2(\Gamma - 1)GM^2 + 8(\Gamma - 1)E' + 2(2 - \Gamma)wW \quad \dots (59)$$

This equation clearly indicates that the cylinder is stable for the radial pulsations in the presence of line currents as well.

## REFERENCES

- Auluck, F. C. and Kothari, D. S., 1957, *Z. Astrophys.*, **42**, 101.  
 Ledoun, P., 1945, *Astrophys. J.*, **102**.  
 Talwar, S. P. and Tandon, J. N., 1956, *Ind. J. Phys.*, **30**, 561  
 Tandon, J. N. and Talwar, S. P., 1958, *Ind. J. Phys.*, **32**, 317.

# AN ARC TYPE WATER-COOLED ION SOURCE FOR POSITIVE IONS\*

S. Z. R. HASHMI

NUCLEAR PHYSICS SECTION, HYDERABAD SCIENCE SOCIETY, AMENAGAR, HYDERABAD DN.

(Received, April 20, 1959)

**ABSTRACT** An arc type water-cooled ion source for positive ions of simple construction and reliable operation is described in which the anode-filament assembly can be readily changed. The characteristic curves of the source are given. Operating at an arc current of 0.4 amp a total beam current of 500 micro-amperes is produced with a probe potential of about 3000 volts.

## INTRODUCTION

A low voltage arc type ion source was installed in 1955 in connection with a 500 Kv Van de Graaff accelerator to provide positive ions for nuclear disintegration experiments. The ion source described here is the third one to be tried out. The first ion source was based on a design of Allen (1938)

The second ion source and the third, the present one incorporated improvements and simplifications on the original design. Attempts have been made to incorporate desirable features found in previous designs of various types of ion sources (Crane 1937; Timoshenko, 1938; Smith and Scott 1939; Livingston, Holloway & Baker 1939; Getting, Fisk & Vogt, 1939; Finkelstein, 1940; Allison 1948; Swann and Swingle, 1952; Goodwin 1953 and Barnett, Steir and Evans, 1953), e.g., reliability, long filament life, easy accessibility of parts etc. The source has been constructed of materials readily available in the laboratory.

## DESCRIPTION

The source is pictorially represented in Fig. 1. The construction of the source can be understood from Fig. 2. The body of the source is made of brass. The filament-anode assembly is mounted on a single plate (A) which can be readily replaced with a similarly constructed assembly. *a, b* and *c* are machine screws which hold the filament and anode assembly. They also serve as electric leads through the porcelain insulators, which are made vacuum tight by using lead gaskets. The hard glass envelope *D* confines the discharge, otherwise the arc spreads out and little current can be drawn by the probe voltage. During the experiment it was found that occasionally discharges would take place between

\* Communicated by Dr. J. C. Kameswar Rao.

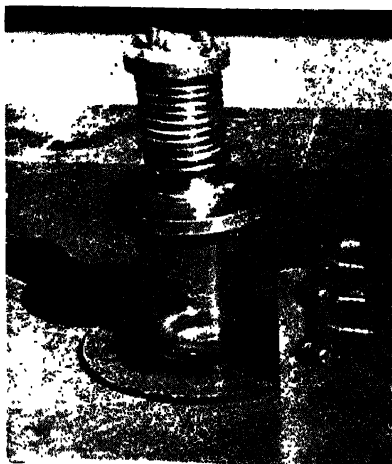


Fig. 1

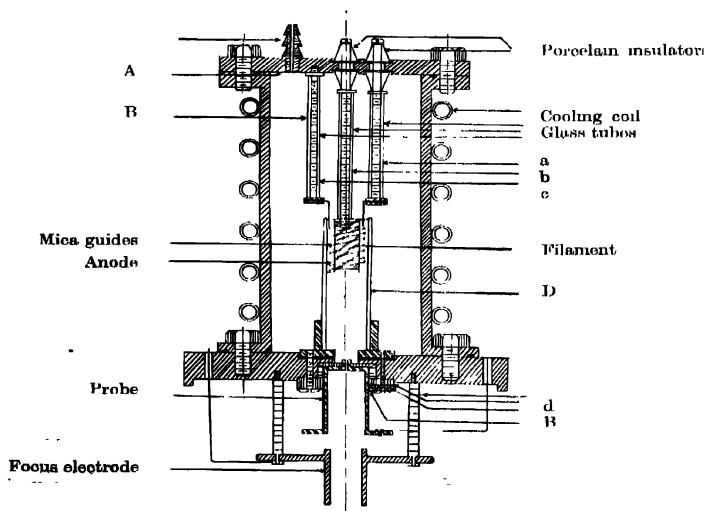


Fig. 2

the screws *a*, *b* and *c*, therefore, they have been covered with glass tubes to eliminate undesirable discharges. *B* is a Mycalex piece which holds the probe, which can be aligned by means of the screw *d*. The probe is made of steel and its front hole is drilled by No. 56 drill.

After considerable experience with tungsten-nickel combinations coated with alkaline earth oxides, we have decided on pure tungsten wire filaments. In the original design of Allen (1938) the distance between the anode and the filament was kept very small for easy starting of arc. Our experiments with close tungsten-nickel filaments coated with strontium and barium oxides have shown that although the arc would strike easily, sometimes the wire would break and would touch the anode thereby short-circuiting the power. Apart from this, unguided filaments are difficult to align with the result that the ion beam goes out of focus, as pointed out by Fulton and Gabrich (1952). In the new filaments, provision has been made to guide the helical form of the filament with three mica pieces. By using such guides the distance between the filament and the anode has been made uniformly as low as  $3/32$ ". The filament is a helix of  $\frac{1}{2}$  mm thick tungsten wire. It requires a current of 8-12 amps at about 8-12 volts. The striking voltage for the arc is about 250 volts, which is supplied from a 866A mercury vapour rectifier set.

The disappointing results with the oxide-coated tungsten-nickel filaments might be due to traces of oxygen present in hydrogen or vacuum system or due to non-trapping of organic vapours. However, pure tungsten filaments seem to be satisfactory except for heavy current consumption.

#### PERFORMANCE

The accelerator is operated with the ion source at ground potential, the accelerating tube being separate from the Van de Graaff generator. The usual electrical operating conditions of the ion source are given in Table I.

TABLE I

1. Arc current	400 mA
2. Starting voltage for arc.	250 volts
3. Voltage drop; anode to filament	88 volts
4. Filament current	11 amps
5. Filament voltage	9.5 volts
6. Probe voltage	3.2 Kv
7. Beam current	500 Micro-amp
8. Focus voltage*	10.4 KV

\* Applied while working the accelerator.



The curves of Fig. 3 show the beam current put out by the arc, and the current to the probe face, as a function of the probe voltage at various arc currents. The beam current is the current at the first electrode of the accelerating tube, next to the focus electrode (not shown here). There was no focussing voltage across the first gap during these measurements and the arc was operating on hydrogen gas.

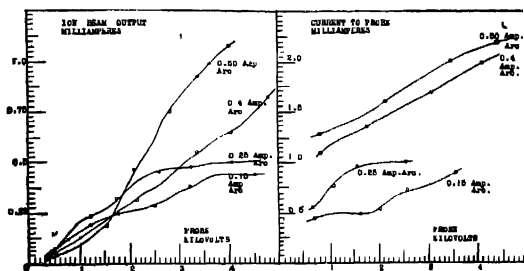


Fig. 3

Rough studies were made of the rate of consumption of the gas and the pressure when it was operating. The practice that has been followed is to adjust the leak till the pressure in the ion source rises to  $1.5 \times 10^{-3}$  mm of Hg, when measured with a gauge. The rate of consumption of the gas is then about 25 c.c. at atmospheric pressure per hour. The pumping speed on our accelerator as given by the manufacturers of the pumps and estimated from pump orifice dimensions is 40 litres per second.

We have two duplicate assemblies of the filaments made on another arc port plate. In order to change the filament assemblies, the diffusion pump is allowed to cool. With the fore pump in operation the entire plate is removed and the new plate inserted and tightened. The whole operation takes less than two minutes and the pressure rises a little through the probe canal. On the whole, the trouble due to any faults in the design has been negligible.

#### ACKNOWLEDGMENTS

The author wishes to express his indebtedness to the following

1. The Industrial Trust Fund of the erstwhile Hyderabad Government for financial aid to carry out this work.
2. Dr. J. C. Kameshwar Ray, our President, for his kind and continued interest throughout this work.
3. Dr. G. Randers of the Joint Establishment for Nuclear Research, Norway, for donating heavy water for the accelerator work, and
4. Mr. Sanjar Ali Khan for assisting in carrying out the work.

## REFERENCES

- Allon, J. S., 1938, *Rev. Sci. Instr.*, **9**, 160.  
Allison, S. K., 1948, *Rev. Sci. Instr.*, **19**, 291  
Barnett, C. F., Stear, P. M. and Evans, G. E., 1953, *Rev. Sci. Instr.*, **24**, 394.  
Crane, H. R., 1937, *Phys. Rev.*, **52**, 11.  
Finkelstein, A. T., 1940, *Rev. Sci. Instr.*, **11**, 94.  
Fulton, J. D., and Garbrich, 1952, *Rev. Sci. Instr.*, **23**, 309.  
Gottung, T. A., Fisk, J. B., and Vogt, H. G., 1939, *Phys. Rev.*, **56**, 1098.  
Goodwin, L. K., 1953, *Rev. Sci. Instr.*, **24**, 638.  
Livingston, M. S., Holloway, M. G., and Baker, C. P., 1939, *Rev. Sci. Instr.*, **10**, 63.  
Scott, G. W., Jr., 1939, *Phys. Rev.*, **55**, 954.  
Smith, L. P., and Scott, G. W., Jr., 1939, *Phys. Rev.*, **55**, 946.  
Swann, C. P. and Swinple, J. F., Jr., 1952, *Rev. Sci. Instr.*, **23**, 637.  
Timoshenko, G., 1938, *Rev. Sci. Instr.*, **9**, 187.

# THE EMISSION BAND SYSTEM OF IODINE IN THE BLUE VIOLET

P. B. V. HARANATH\* AND T. A. PRASADA RAO

PHYSICS DEPARTMENT, ANDHRA UNIVERSITY, WALTAIR

(Received, November 28, 1959)

## Plate I A & B

**ABSTRACT.** The D—B System of iodine molecule was found to be more extensively developed when the spectrum was excited in a condensed discharge from a high tension transformer. About 150 bands were newly classified as forming part of the previously known D—B system for which Waser and Wieland suggested the vibrational quantum formula.

## INTRODUCTION

Recent investigations on the spectra of halogens by Haranath and Rao (1958) have led to the discovery of a number of discrete band systems in the spectral region  $\lambda 2400$ — $\lambda 1400$ . Besides the above new results, a number of previously known systems in the visible and ultraviolet regions were also observed in the case of iodine, when the vapour was excited in a condensed discharge from a high tension transformer. The band system in the blue violet region  $\lambda 4400$ — $\lambda 4000$  was found to be more extensively developed than has been reported by previous workers. Only 40 bands obtained in fluorescence excitation by Elliot (1940) and about 80 in electrical excitation in the presence of argon by Venkateswarulu (1951) were known previously belonging to this system.

In the present work, the iodine spectrum excited at higher voltages of a condensed transformer revealed about 230 band heads some of which are clearly degraded towards longer wavelengths. This paper describes the results of the detailed investigations on the analysis of this band system attributed to neutral iodine molecule.

## RESULTS

Details of the experimental technique employed for the excitation of the emission band spectrum of iodine in a condensed transformer discharge was already described by Haranath and Rao (1958). In the present work, the spectrum extending in the region  $\lambda 4500$ — $\lambda 3900$  was photographed mainly on Hilger 3 prism glass Littrow and Fuess spectrographs, the times of exposures being of 10 and 5 minutes duration respectively.

National Research Fellow.

The appearance of the spectrum in the region  $\lambda 4500$ — $\lambda 3900$  photographed on Fuess instrument is shown in three strips *a*, *b* and *c* in Plate IA. They correspond respectively to spectra taken with different primary voltages 60, 100 and 140 of the transformer. At the lowest voltage the bands appear sharp and are clearly degraded towards red. On increasing the voltage, it was observed that many more new bands appear which are closely spaced. Under these conditions more atomic lines of iodine also appear simultaneously. Plate IB is the reproduction of the spectrum excited with 220 Volts of the primary of the transformer and was recorded on the Littrow spectrograph. Measurements of individual band heads in the region  $\lambda 4420$ — $\lambda 3965$  on a number of plates recorded on the above two instruments agree well with in  $2\text{ cm}^{-1}$ . Out of 230 band heads measured in this region, the data of about 80 band heads coincide very well with those reported by Venkateswarulu. In Table I are reported the wavenumber data of the newly recorded band heads about 150 in number with the visual estimates of their intensities

TABLE I

Authors wave number	Int.	Assignment $\nu', \nu''$	Calculated wave number	Obs. — Cal.
22623	1	1,33	22622	+1
22690	2	3,35	22696	—6
22726	1	0,30	22728	—2
22772	3	5,37	22775	—3
22798	1	4,35	22795	+3
22802	1	0,29	22802	0
22823	2	3,33	22823	0
22862	3	2,31	22859	+3
22878	2	0,28	22877	+1
22887	1	3,32	22890	—3
22895	2	5,35	22894	+1
22903	3	1,29	22903	0
22930	1	2,30	22931	—1
22960	3	3,31	22959	+1
22978	1	1,28	22979	—1
23005	3	2,29	23004	+1
23045	4	10,41	23048	—3
23050	6	11,43	23052	—2
23055	4	1,27	23056	—1
23072	4	8,37	23067	+5
23079	4	2,28	23079	0
23089	4	5,32	23089	0
23103	5	3,29	23104	—1
23115	7	0,25	23116	—1
23121	4	6,33	23120	+1
23144	4	11,41	23143	+1
23159	6	2,27	23157	+2
23178	8	3,28	23180	—2

TABLE I (contd.)

Authors wave number	Int.	Assignment $v', v''$	Calculated wave number	Obs - Cal.
23222	9	9,36	23222	0
23236	8	2,26	23237	-1
23244	10	11,39	23244	0
23284	10	0,23	23284	0
23287	10	7,32	23285	+2
23307	10	5,29	23302	+5
23329	7	6,30	23327	+2
23333	9	3,26	23337	-4
23355	10	4,27	23357	-2
23379	9	8,32	23381	-2
23391	8	12,38	23392	-1
23409	6	9,33	23410	-1
23415	8	11,36	23412	+3
23422	6	7,30	23425	-3
23430	5	13,39	23431	-1
23436	5	4,26	23436	0
23444	10	11,39	23444	0
23450	8	8,31	23450	0
23481	7	9,32	23477	+4
23499	7	3,24	23502	-3
23509	5	12,36	23506	+3
23518	6	4,25	23518	0
23526	8	14,39	23524	+2
23549	8	9,31	23546	+3
23560	7	15,40	23565	-5
23575	2	2,22	23575	0
23609	3	16,41	23607	+2
23653	2	1,20	23655	-2
23664	2	2,21	23665	-1
23676	6	3,22	23675	+1
23687	5	4,23	23687	0
23705	5	19,45	23703	+2
23711	3	6,25	23715	-4
23728	5	13,34	23723	+5
23733	3	7,26	23731	+2
23748	7	1,19	23749	-1
23753	3	14,35	23753	0
23758	3	2,20	23756	+2
23773	5	4,22	23775	-2
23799	2	6,24	23798	+1
23803	2	11,30	23808	-5
23827	8	12,31	23830	-3
23848	2	15,35	23845	+3
23851	3	2,19	23850	+1

TABLE I (ontd.)

Authors wave number	Int.	Assignment $\nu', \nu''$	Calculated wave number	Obs. - Cal.
23874	3	5,22	23874	0
23894	3	7,24	23896	-2
23900	2	12,30	23902	-2
23910	5	8,25	23909	+1
23917	5	20,42	23918	-1
23928	6	13,31	23924	+4
23934	6	16,35	23936	-2
23942	6	1,17	23941	+1
23947	2	2,18	23945	+2
23981	2	7,23	23982	-1
23996	4	13,30	23995	+1
24003	2	9,25	24005	-2
24010	3	20,40	24014	-4
24017	3	10,26	24019	-2
24032	5	11,27	24034	-2
24045	3	3,18	24046	0
24054	2	4,19	24049	+5
24062	2	6,21	24061	+1
24079	4	8,23	24079	0
24092	4	14,30	24088	+4
24115	2	11,26	24114	+1
24126	3	12,27	24128	-2
24145	5	4,18	24145	0
24149	5	5,19	24148	+1
24166	1	8,22	24166	0
24175	4	9,23	24175	0
24206	2	12,26	24208	-2
24223	3	13,27	24222	+1
24237	6	14,28	24237	0
24244	2	1,14	24244	0
24249	2	0,13	24246	+3
24254	2	7,20	24250	+4
24280	2	11,24	24279	+1
24291	2	17,31	24291	0
24302	2	13,26	24301	+1
24345	6	2,14	24344	+1
24350	4	1,13	24346	+4
24379	2	13,25	24383	-4
24396	1	14,26	24394	+2
24407	1	15,27	24406	+1
24422	3	20,33	24422	0
24447	5	3,14	24445	+2
24459	2	12,23	24459	0
24469	3	10,31	24470	-1

TABLE I (contd.)

Authors wave number	Int.	Assignment $v', v''$	Calculated wave number	(Obs. - Cal.)
24480	1	1,12	24484	-4
24490	2	15,26	24486	+4
24534	5	7,17	24536	-2
24543	5	4,14	24544	-1
24552	4	3,13	24549	+3
24561	4	1,11	24562	-1
24583	2	2,12	24585	-2
24637	3	6,15	24638	-1
24648	3	4,13	24649	-1
24669	1	1,10	24672	-3
24681	1	0,9	24682	-1
24688	1	3,12	24685	+3
24735	2	8,16	24732	+3
24749	1	5,13	24747	+2
24798	1	0,8	24795	+3
24819	2	11,18	24822	-3
24827	2	9,16	24828	-1
24831	3	8,15	24833	-2
24846	3	6,13	24845	+1
24874	2	3,10	24873	+1
24900	1	1,8	24896	+4
24966	2	4,10	24972	-6
24997	1	2,8	24997	0
25015	1	1,7	25011	+4
25032	1	9,14	25031	+1
25043	2	8,13	25040	+3
25071	1	5,10	25071	0
25084	1	4,9	25084	0
25097	1	3,8	25097	0
25112	1	2,7	25112	0
25180	1	5,9	25182	-2
25193	1	4,8	25196	-3
25212	1	3,7	25212	0

## ANALYSIS

Waser and Wieland (1947) were the first to propose the following vibrational quantum formula for the bands of iodine molecule in the blue violet region

$$\nu = 25757.2 - (101.88\nu' - 0.34\nu'^2) - (126.59\nu'' - 0.755\nu''^2 - 0.0033\nu''^3).$$

However, they have not published their experimental data or the vibrational analysis of the bands. Venkateswarulu (1951) reported the classification of about

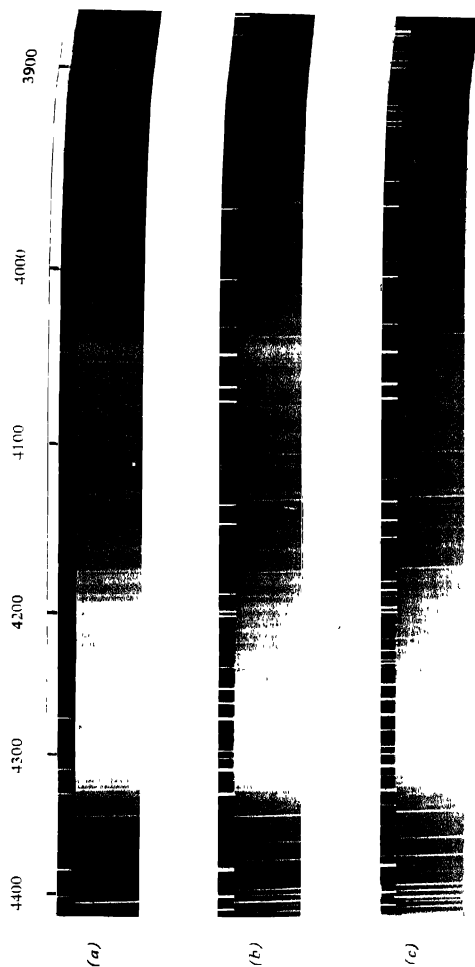
80 bands of this system on the basis of the above formula. In his analysis the scheme consists of assignments of bands with  $v' = 0$  to 11 and  $v'' = 9$  to 38. The wavenumbers of these bands are in close agreement with those obtained by the authors. Further, the agreement between the observed and calculated wavenumbers for all the 80 bands is remarkably good. Hence, it is concluded that the vibrational formula proposed by Waser and Wieland represents very well all the 80 bands assigned by Venkateswarulu. However, it is observed that there are a large number of gaps in the vibrational array proposed by him. It is possible to assume that the new bands, 150 in number, obtained in the present investigations could very well form part of this system. On this basis, the above vibrational scheme was extended to include the new bands. It was found possible that all the bands in the region  $\lambda 4420$ — $\lambda 3965$  could be analysed as belonging to a single system whose vibrational formula is the same as that proposed by Waser and Wieland. The vibrational assignments of these new bands were shown in column 4 of Table I. The observed wavenumbers of all these newly assigned band heads were compared with those calculated on the basis of the above formula and their differences were indicated in the last column. The extended vibrational analysis consists of assignments of bands with  $v' = 0$  to 20 and  $v'' = 7$  to 45.

The intensity distribution of bands of this system is indicated in Table II. It can be seen that most of the strongest bands of the system belong to  $v' = 0$  to 6 progressions and the progressions with  $v' = 0$  to 5 are more fully developed. The intensity distribution in the system closely corresponds to a typical Condon parabola which is to be expected for values of  $\omega_e' = 102.2 \text{ cm}^{-1}$  and  $\omega_e'' = 126.6$

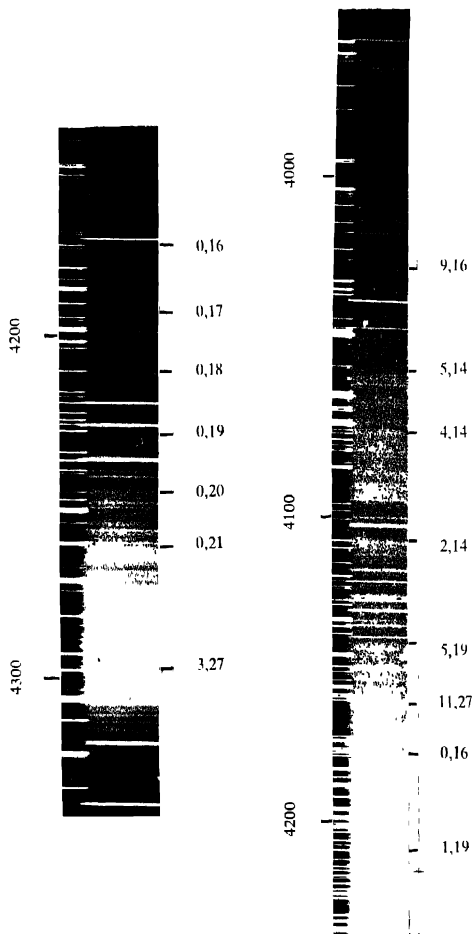
## ELECTRONIC STATES

The vibrational constants of the lower state of this system suggest that this is to be identified with the upper state  $^3\Pi_{ou}^+$  of the visible absorption bands. The upper state of the system was already attributed to the molecular electronic configuration  $\sigma_g^2\pi_g^2\pi_g^4\sigma_u^2-^3\Sigma_g^-, ^1\Sigma_g^+, ^1\Delta_g$  of which  $^3\Sigma_g^-$  is expected to be lower in energy. These states give rise to  $(0_g^+, 1_g)$ ,  $0_g^+$  and  $2_g$  respectively in Hund's case *C* coupling. This system designated as *D-B* was tentatively ascribed to the transition  $^1\Sigma_g^+(0_g^+)$  to  $^3\Pi_{ou}(0_u^+)$  by Haranath and Rao. Recently Mathieson and Rees have discussed the dissociation products of a group of electronic levels of iodine molecule lying at 40,000 to 55,000  $\text{cm}^{-1}$  by consideration of the ionic attractive forces operating. They found that the neighbouring states *E* and *D* (*D* and *C* according to Haranath and Rao) at  $\nu 41411$  and  $\nu 39293$  respectively dissociate into the same products of ions  $^3P_2(I^+)$  and  $^1S_0(I^-)$ . They assigned the state at  $\nu 41411$  the upper electronic level of the blue violet emission band system of iodine to the term  $^3\Sigma_g^-(0_g^+)$  arising out of the configuration (2242). Hence it seems reasonable to assign the *D-B* system to the electronic transition  $^3\Sigma_g^-(0_g^+)-$





Emission spectra of iodine excited in condensed discharge from a transformer at different primary voltages. Fues spectrograms (a) 60 volts (b) 100 volts (c) 140 volts.



## APPENDIX II

[illegible]

$^3\Pi_{00}+(0_0^+)$  in which case the selection rules of Hund's cases  $C$  and  $B$  couplings hold good simultaneously

## ACKNOWLEDGMENTS

The authors wish to express their grateful thanks to Dr P. Tiruvenganna Rao for his kind interest and valuable discussions on the work. The authors' thanks are also due to Prof K. R. Rao for his interest in this work.

## REFERENCES

- Elliot, A., 1940, *Proc. Roy. Soc. London*, **174A**, 273.  
Haranath, P. B. V. and Tiruvenganna Rao, P., 1958, *J. Mol. Spectroscopy*, **2**, 428.  
Mathieson, L. and Roes, A. L. G., 1956, *J. Chem. Phys.*, **25**, 753.  
Venkateswarulu, P., 1951, *Phys. Rev.*, **81**, 821.  
Waser, J. and Wieland, K., 1947, *Nature*, **160**, 643.

## ON ZERO MASS MESON-MESON SCATTERING

B. DEO

PHYSICS DEPARTMENT, RAVENSHAW COLLEGE, CUTTACK

(Received, December, 10, 1959)

**ABSTRACT.** The forward scattering matrix elements for the scattering of two mesons (zero mass) has been calculated from pair reproduction cross section by the method of analytic continuation. This has been compared with the Feynman matrix elements to the required order. By comparing the results of the two methods, the value of the counter  $\lambda\phi^4$  term has been evaluated.

## INTRODUCTION

Besides primitive divergencies, there is a class of divergences (comparable to photon-photon scattering divergence) peculiar to meson-nucleon interactions. The degree of divergence  $D$  for the process is determined by the well known relation

$$D = 4 - 3/2 F_e - B_e$$

where  $F_e$  = number of external fermion lines

$B_e$  = number of external Boson lines.

Thus closed loops of fermions with three and four vertices of bosons are divergent. For photons and pseudoscalar mesons which are of importance in physics, a closed loop with three vertices have zero matrix element. But the four-vertex diagram is permissible and also possible giving rise to processes like photon-photon or meson-meson scattering. Therefore, suitable counter term (i)  $\lambda A_\mu^4$  or (ii)  $\lambda\phi^4$ , where  $A_\mu$  is the photon and  $\phi$  the meson field operator, are to be added to the interaction Hamiltonian. For electrodynamics, gauge invariance forbids the occurrence of the term  $\lambda A_\mu^4$  in the Lagrangian; as a consequence, terms proportional to it can be dropped since they are non-gauge-invariant. Fortunately, however, if one calculates the matrix elements there is no divergence if the contribution for all the three basic diagrams are added up, as shown by Jauch and Rohrlich (1955).

But for meson-meson scattering, gauge invariance is not available. This is the first (and only) divergent process which is not eliminated by a renormalisation of mass or coupling constant in pseudoscalar theory. Therefore a counter term  $\lambda\phi^4$  is essential. However the exact value of  $\lambda$  even in the lowest order has not been calculated since no method exists as to its unambiguous evaluation, as has been pointed out by Schweber, Bethe and de' Hoffmann (1955). Therefore, it is interesting to be able to complete this counter term to see to what extent the absence of gauge invariance can be compensated by alternate mode of thought.

# FORMULATION OF THE PROBLEM

We shall use natural units  $\hbar = c = 1$ .

Let a pseudoscalar boson field  $\phi$  and a fermi field  $\psi$  interact, the Hamiltonian in interaction representation being given by,

$$H_{int} = ig \int d^3x \bar{\psi} \gamma_5 \psi \phi$$

The fourth-order term of  $S$ -matrix which describes the effects under consideration is given by the Feynman diagram, (Fig. 1)

or by the integral

$$S^{(4)} = -\frac{1}{64} g^4 \int \int \int \int d^4x_1 d^4x_2 d^4x_3 d^4x_4 \phi(x_1) \phi(x_2) \phi(x_3) \phi(x_4)$$

$$T_r \{ \gamma_5 S_F(x_2 - x_1) \gamma_5 S_F(x_3 - x_2) \gamma_5 S_F(x_4 - x_3) \gamma_5 S_F(x_1 - x_4) \} \quad \dots (1)$$

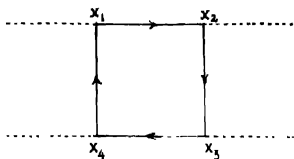


Fig- 1

$S_F(x)$  being the propagation function of the fermi field (mass =  $m$ )

$$S_F(x) = -\frac{2i}{(2\pi)^4} \text{Lt}_{\epsilon \rightarrow 0^+} + \int d^4p \dots \frac{i\gamma \cdot p - m}{p^2 - m^2 - i\epsilon} e^{-ip \cdot x}$$

$$p \cdot x = p \cdot r - p_0 x_0.$$

The transition to momentum space with

$$\phi(x) = \int \phi(k) e^{ik \cdot x} d^4k \quad \dots (1a)$$

yields,

$$S^{(4)} = -\frac{i}{2} \left( \frac{g^2}{4\pi} \right)^2 \int d^4x \int d^4k_1 \int d^4k_2 \int d^4k_3 \int d^4k_4 \phi(k_1) \phi(k_2) \phi(k_3) \phi(k_4).$$

$$e^{i(k_1 + k_2 + k_3 + k_4) \cdot x} \frac{1}{3} G(k_1 k_2 k_3 k_4) \quad \dots (2)$$

where

$$G(1234) = T^{(1)}(1234) + T^{(2)}(1, 2, 4, 3) + T^{(3)}(1, 3, 24) \quad \dots (2a)$$

and

$$T^{(1)}(1234) = \frac{1}{i\pi^2} \int d^4p \cdot Tr. \{ \gamma_5 S_F(p) \gamma_5 S_F(p-k_2) \gamma_5 S_F(p-k_2-k_3) \gamma_5 S_F(p-k_2-k_3-k_4) \}$$

$$T^{(2)} = T^{(1)}(k_2 \longleftrightarrow k_4)$$

$$T^{(3)} = T^{(1)}(k_2 \longleftrightarrow k_3) \quad \dots \quad (3)$$

It is easily seen that the divergent term is entirely contained in the terms proportional to  $(p^2)^2$  in the numerator and is logarithmically divergent. Therefore subtraction any term whatsoever, containing the log-divergent term shall eliminate this divergence.

To get round this difficulty we first note that the quantity we wish to subtract is essentially a constant independent of the scattering angle. So our problem will be considerably simplified if we can compute the matrix elements for forward scattering only. We let,

$$k_1 = k; \quad k_3 = -q; \quad k_2 = -k; \quad k_4 = q$$

Then only invariant that can be constructed is  $k.q$ , and in a c.m. system,  $k.q = -2\omega^2$  for forward scattering. So we write,

$$G(k, q) = G(k.q) = G(\omega^2, 0) = G(t, 0) \quad \dots \quad (4)$$

where  $t = w^2/m^2$  for convenience.

The matrix element is a function of the invariant  $t = -2k.q/4m^2$ . We can further separate the real and imaginary part of the Function

$$G(t, 0) = a_1(t) + ia_2(t) \quad \dots \quad (5)$$

The imaginary part  $a_2(t)$  is related to the pair production cross-section.

The unitarity of  $S$ -matrix, makes it possible to write the total transition probability for the production of a pair of fermions by two mesons.

$$P = -2R_e[\psi_i, S^{(A)}\psi_i]$$

$$= -\left[ \frac{2}{i\pi^2} \int d^4x \right] \left( \frac{q^2}{4\pi} \right)^2 \frac{1}{t} \text{Im. } G(t, 0) \quad \dots \quad (6)$$

This is evaluated by the usual substitution, (See reference R. Karplus and M. Neuman (1951)).

$$\vec{\phi}(\vec{k}, k_0) \rightarrow V(2|k|V)^{-1} [a(\vec{k})\delta(k_0 - |\vec{k}|) + a^\dagger(-\vec{k})\delta(k_0 + |\vec{k}|)]$$

$$\int d\vec{k} \rightarrow \frac{1}{V} \sum_{\vec{k}}$$

where  $\vec{a}(\vec{k})$  and  $\vec{a}^\dagger(-\vec{k})$  are the annihilation and creation operators and  $V$  a large but finite volume. The total cross-section of pair production by two mesons of momentum

$$\vec{k}_1 = \vec{k}; \quad \vec{k}_2 = -\vec{k}; \quad |\vec{k}_1| = |\vec{k}_2| = \omega \quad \text{is then}$$

$$\sigma_{pair}(t) = \frac{2(g^2/4\pi)^2}{m^2 t} \text{Im } G(t, 0)$$

Thus

$$a_s(t) = \frac{1}{(g^2/4\pi)^2} \frac{m^2 t}{2} \sigma_{pair}(t) \quad \dots \quad (7)$$

Following the same procedure, the probability for meson-meson scattering is

$$P = \left[ \frac{2}{V^2} \int d^4x \right] \left( \frac{g^2}{4\pi} \right)^4 \frac{1}{128\pi^2} \frac{1}{m^2 t} \int d\Omega(\vec{k}) |G(t)|^2 \quad \dots \quad (8)$$

when the diff. scattering cross-section in the forward direction in c.m. system is

$$\begin{aligned} \frac{d\sigma}{d\Omega}(t, 0) &= \left( \frac{g^2}{4\pi} \right)^4 \frac{1}{64\pi^2 m^2 t} |G(t, 0)|^2 \\ &= \left( \frac{g^2}{4\pi} \right)^4 \frac{1}{64\pi^2 m^2 t} |a_1 + ia_2|^2 \quad \dots \quad (9) \end{aligned}$$

We see that pair production cross-section  $\sigma_{pair}(t)$  shall enable us to write  $a_s(0, t)$ . We shall then resort to the method of analytic continuation, suggested by Toll (1952) and calculate  $a_s(t, 0)$ .

#### PAIR PRODUCTION CROSS-SECTION

The matrix element for pair production is

$$\begin{aligned} \langle p, p' | M | k_1 k_2 \rangle &= - \frac{ig^2}{(2\pi)^2} \sqrt{e_{pk_1} e_{pk_2}} \frac{m}{2\omega_1 2\omega_2} \\ u(p) \left[ \gamma_5 \frac{\not{p} - \not{k}_1 - m}{2p \cdot k_1} \gamma_5 + \gamma_5 \frac{\not{p} - \not{k}_2 - m}{2p \cdot k_2} \gamma_5 \right] v(p') \quad \dots \quad (10) \end{aligned}$$



arising from the crossed and uncrossed Feynman diagrams. The total scattering cross-section can be evaluated in standard way and one gets,

$$\sigma_{\text{pair}}(t) = 8\pi \left( \frac{g^2}{4\pi} \right)^2 \frac{1}{m^2 t} \left[ \log \frac{1 + \left( 1 - \frac{1}{t} \right)^{1/2}}{1 - \left( 1 - \frac{1}{t} \right)^{1/2}} - 2 \left( 1 - \frac{1}{t} \right)^{1/2} \right], \quad t > 1$$

$$= 0 \quad t < 1 \quad (11)$$

Equation (7) now gives

$$\alpha_2(t) = -4\pi \left[ \log \frac{1 + \left( 1 - \frac{1}{t} \right)^{1/2}}{1 - \left( 1 - \frac{1}{t} \right)^{1/2}} - 2 \left( 1 - \frac{1}{t} \right)^{1/2} \right], \quad t > 1$$

$$= 0, \quad t < 1 \quad (12)$$

However, these expressions hold good only for positive and real  $t$ .

For the use of analytic continuation we must know the value of  $\text{Im } G(t, 0)$  for  $t < 0$ . To find this out we resort to the Feynman diagrams as depicted in Figs 2(a), 2(b), and 2(c) which gives respectively  $T^{(1)}$ ,  $T^{(2)}$  and  $T^{(3)}$  of equation 2(a) with  $k_1 = -k_2 = k$ ,  $k_3 = k_4 = q$

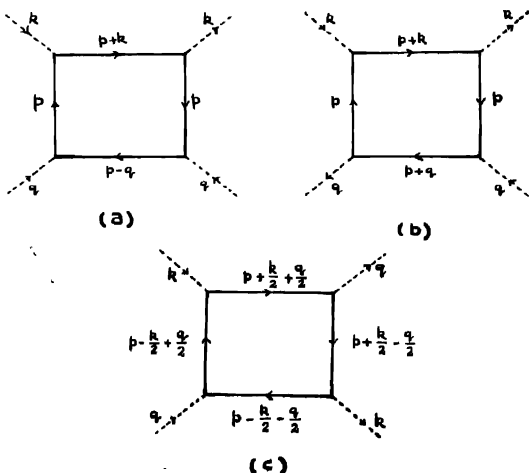


Fig. 2

From general four-momentum conservation we label the integral fermion lines as shown. Figure 2(c) we have shifted the value of ' $p$ ' which does not bring in any surface term, since the matrix element is only log. divergent. Inspection of Figs. 2(a) and 2(b) shows that

$$T^{(1)} = T^{(1)}(k, q) \quad (13a)$$

$$T^{(2)} = T^{(1)}(k, -q) = T^{(1)}(-k, q) \quad (13b)$$

$$T^{(1)} + T^{(2)} = T^{(1)}(k, q) + T^{(1)}(-k, q) \quad (13c)$$

This means that the matrix elements of  $T^{(2)}(k, q)$  can be obtained from  $T^{(1)}(k, q)$  by replacing  $q$  by  $-q$ . Since the contribution from each diagram must be a function of the only available invariant  $k \cdot q$ , equations 13(b) and 13(c) follows.

In diagram, Fig. 2(c), we note immediately that,

$$T^{(3)}(k, q) = T^{(3)}(k, -q) = T^{(3)}(-k, q) \quad (14)$$

Thus

$$G(t, 0) = G(-t, 0) \quad (15)$$

These symmetry properties are adequate to calculate the Matrix elements for forward scattering from pair production cross-section by analytic continuation. The  $S$ -matrix matrix elements can also be computed directly by Feynman method. The results from these two methods shall be compared. Retaining only those terms that can be obtained from analytic continuation, the counter renormalisation term for a finite  $S$ -matrix can be found out. We shall first make the necessary analytic continuation, in the next section and in the succeeding section, find the  $S$ -matrix elements.

#### METHOD OF ANALYTIC CONTINUATION

Following Rohrlich and Gluckstern (1952), we consider Cauchy's Theorem,

$$f(x) = \frac{1}{2\pi i} \oint \frac{f(z')}{z' - x} dz' \quad \dots (16)$$

Let  $z$  be on the real axis,  $z = t$  and assume that  $f(z)$  is regular for  $\text{Im}(z) > -\epsilon$ ;  $\epsilon > 0$ . We can choose the path of integration as shown in Fig. 3 and write

$$f(t) = \frac{1}{2\pi i} P \int_{-R}^{+R} \frac{f(t')}{t' - t} dt' + \frac{1}{2} f(t) + \frac{1}{2\pi i} \int_{-} \frac{f(z')}{z'} dz' \quad \dots (17)$$

where in the last integral  $t$  has been neglected in the denominator, since for the contour  $R$ ;  $|z'| \gg t$  everywhere. We further assume that  $f(z')/z'$  is regular at  $z' = 0$ , so that

$$\frac{f(z')}{z'} dz' = - \int_{-\infty}^{+\infty} \frac{f(t')}{t'} dt' \quad \dots (18)$$

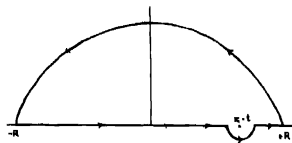


Fig. 3

Separating  $f(t)$  into its real and imaginary parts, we obtain with  $R \rightarrow \infty$

$$\operatorname{Re} f(t) = \frac{t}{\pi} P \int_{-\infty}^{+\infty} \frac{\operatorname{Im} f(t')}{t'(t'-t)} dt' \quad (19)$$

We identify  $f(t)$  with  $G(0, t)$  and since,

$$G(0, t) = G(0 - t)$$

we get

$$\operatorname{Re} G(0, t) = 2t^2 \frac{P}{\pi} \int_0^{\infty} \frac{\operatorname{Im} G(0, t')}{t'^2 - t^2} \cdot \frac{dt'}{t'} \quad \dots (20)$$

Thus we get

$$\begin{aligned} a_1(t) &= -8t^2 P \int_1^{\infty} \left[ \log \frac{1 + \left(1 - \frac{1}{t'}\right)^{\frac{1}{2}}}{1 - \left(1 - \frac{1}{t'}\right)^{\frac{1}{2}}} - 2 \left(1 - \frac{1}{t'}\right)^{\frac{1}{2}} \right] \frac{dt'}{t'} \cdot \frac{1}{t'^2 - t^2} \\ &= 8t^2 P \int_0^1 \frac{p' dp'}{1 - t^2 p'^2} \left[ \log \frac{1 - (1 - p')^{\frac{1}{2}}}{1 + (1 - p')^{\frac{1}{2}}} + 2(1 - p')^{\frac{1}{2}} \right] \quad \dots (21) \end{aligned}$$

where we have put  $t' = \frac{1}{p'}$

These integrals can be evaluated in straight forward way. But for sake of comparison, we shall make the following substitutions.

Integrating by parts,

$$a_1(t) = 4P \int_0^1 \left( \frac{1}{(1-p')^2 p'} - \frac{1}{(1-p')^4} \right) \log(1-t^2 p'^2) dp'$$

Letting

$$\sqrt{1-p'} = u, \quad -\frac{1}{2} \frac{dp'}{\sqrt{1-p'}} = du$$

$$\begin{aligned} a_1(t) &= 8P \int_{0+2}^1 \left( \frac{1}{1-u^2} - 1 \right) \log \left[ 1 - 16t^2 \left( \frac{1-u^2}{4} \right)^2 \right] du \\ &= 4P \int_{-1}^+ \left( \frac{1}{1-u^2} - 1 \right) \log \left[ 1 - 16t^2 \left( \frac{1-u^2}{4} \right)^2 \right] du \\ &= 8P \int_0^1 \left( \frac{1}{4x} - 1 \right) [\log(1 - 4tx(1-x)) + \log(1 + 4tx(1-x))] \\ &\quad \text{with} \quad x = \frac{1+u}{2}, \end{aligned} \quad (22)$$

Evaluating

$$\begin{aligned} \frac{1}{8} a_1(0, \omega) &= \left( \sinh^{-1} \frac{\omega}{m} \right)^2 - 2 \left( 1 + \frac{m}{\omega} \right)^{\frac{1}{2}} \sinh^{-1} \frac{\omega}{m} \\ &+ \begin{cases} - \left( \sinh^{-1} \frac{\omega}{m} \right)^4 - 2 \left( \frac{m^2}{\omega^2} - 1 \right)^{\frac{1}{2}} \sinh^{-1} \frac{\omega}{m} ; & 0 < \omega < m \\ \left( \cosh^{-1} \frac{\omega}{m} \right)^2 - \frac{\pi^2}{4} - 2 \left( 1 - \frac{m^2}{\omega^2} \right)^{\frac{1}{2}} \cosh^{-1} \frac{\omega}{m} ; & \omega > m. \end{cases} \quad (23) \\ \frac{1}{8} a_2(0, \omega) &= -\pi \left\{ \cosh^{-1} \frac{\omega}{m} - \left( 1 - \frac{m^2}{\omega^2} \right)^{\frac{1}{2}} \right\} ; \quad \omega > m \\ &= 0 \quad ; \quad \omega < m. \quad (24) \end{aligned}$$

Using equation (9), one can now calculate meson-meson scattering cross-section in the forward direction. This is what a physicist would have done, had Feynman method not been known, analytic continuation methods were known.

## DIRECT EVALUATION OF MATRIX ELEMENTS

One now proceeds to calculate directly Matrix elements  $G(kq)$  of equation (2), using the Feynman's diagrams Figs. 2(a), (b) and (c). Even in case of forward scattering, the calculations are extremely lengthy and tedious. The procedure and details of calculation have been outlined by Jost, Luttinger and Slotnick (1950). We merely quote the results, (the details of calculations can be supplied on request),

$$G(k_1q) = 12D_\infty + 8 \int_0^1 \left( \frac{1}{4y} - 1 \right) \log \left( 1 - \frac{2kq}{m^2} y(1-y) \right) \\ + 8 \int_0^1 \left( \frac{1}{4y} - 1 \right) \log \left( 1 + \frac{2kq}{m^2} y(1-y) \right)$$

$$\text{where } D_\infty = \frac{1}{i\pi^2} \int d^4p \cdot \frac{(p^2)^2 + 2m^2 p^2 + m^4}{(p^2 + m^2)^4} \quad (25)$$

Letting  $2kq = -4\omega^2 = -4m^2t$ , we see that  $G(k, q) - 12D_\infty = G_f$  gives correctly the values of  $a_1$  and  $a_2$  deduced before. Referring to equation (2) we see that, in general,

$$S^{(4)} = - \frac{i}{12} \left( \frac{g^2}{4\pi} \right)^2 \int d^4x \int d^4k_1 \dots d^4k_4 e^{i(k_1+k_2+k_3+k_4) \cdot x} \phi(k_1)\phi(k_2)\phi(k_3)\phi(k_4) \\ [12D_\infty + G_f(k_1 k_2 k_3 k_4)] \quad \dots \quad (26)$$

The first term (which is divergent) is  $-i \left( \frac{g^2}{6\pi} \right)^2 D_\infty \int d^4x \phi^4(x)$  since the momentum space transform is given by (1a).

Thus if we start with the interaction Hamiltonian density

$$H_{int} = ig \bar{\psi} \gamma_5 \psi \phi = \left( \frac{g^2}{4\pi} \right)^2 D_\infty \phi^4(x) \quad \dots \quad (27)$$

then, the contribution due to the second term in the first order is

$$\frac{(-i)}{12} \left( \frac{g^2}{4\pi} \right)^2 D_\infty \int \phi^4(x) d^4x = +i \left( \frac{g^2}{4\pi} \right)^2 D_\infty \int d^4x \phi^4(x)$$

which cancels the first term in (26). So the finite  $S^{(4)}$  is now given by

$$S^{(4)} = - \frac{i}{12} \left( \frac{g^2}{4\pi} \right)^2 \int d^4x \dots G_f(k_1 k_2 k_3 k_4)$$

This  $G_f$  in the forward direction shall now give

$$G_f(0, t) = a_1 + ia_2$$

which can be derived by analytic continuation method.

Thus the contact renormalisation term  $\lambda\phi^4$  that must be subtracted from the interaction Hamiltonian density is unambiguously determined with

$$\begin{aligned} \lambda &= \left(\frac{g^2}{4\pi}\right)^2 \frac{1}{i\pi^2} \int \frac{d^4p}{(p^2+m^2-i\epsilon)^4} ((p^2)^2 + 2m^2p^2 + m^4) \\ &= \left(\frac{g^2}{4\pi}\right)^2 \left[ \lim_{\Delta \rightarrow \infty} \alpha t \log \frac{\Delta^2 + m^2}{m^2} - 1 \right] \end{aligned}$$

The low energy theorem then turns out to be

$$\lim_{t \rightarrow 0} \alpha t G(0, t) = 0$$

We have used the method of analytic continuation which can also be derived from dispersion relations. Thus it seems that the causality requirements may as well provide the clue for a low energy theorem for meson-meson scattering. An application of the general dispersion relation to evaluate the low energy limit for  $\pi-\pi$  scattering is in progress.

#### ACKNOWLEDGMENTS

Author's thanks are due to Dr. T. Pradhan and Shri S. P. Misra for many helpful discussions.

#### REFERENCES

- Jauch, J. M. and Rohrlich, F., 1955, *The theory of Electrons and photons*, Addison and Wesley Publishing Co.  
 Jost, R., Luttinger, J. and Slotnick, M., 1950, *Phys. Rev.*, **80**, 189.  
 Karplus, R. and Neuman, M., 1951, *Phys. Rev.*, **83**, 776.  
 Rohrlich, F. and Glucksern, R., 1952, *Phys. Rev.*, **86**, 1.  
 Schweber, S. S., Betho, H. A. and de Hoffman, F., 1955, *Mesons and Fields*, Vol. I, Row Peterson & Co.  
 Toll, J. S., 1952, Thesis, Princeton University.

# FORCE CONSTANTS FOR UNLIKE MOLECULAR INTERACTIONS ON EXP-SIX MODEL FROM INTER-DIFFUSION

R. PAUL

INDIAN ASSOCIATION FOR THE CULTIVATION OF SCIENCE, CALCUTTA-32

(Received, February 11, 1960)

**ABSTRACT.** Force constants for unlike molecular interactions for the systems Ne-A, Ne-Kr, A-Kr, He-A, A-Xe, He-Xe, He-Kr and Ne-Xe have been determined on the exponential six model from temperature dependence of inter-diffusion coefficients. To simplify matters, the values of  $a_{12}$  were taken to be those obtained from the temperature dependence of thermal diffusion or from the combination rules and the method of interaction was employed to give  $r_{12}$  and  $(r_m)_{12}$ . The force constants, thus obtained, have been compared with the values obtained from other methods and satisfactory agreement has been obtained. These force constants have been used to calculate the thermal diffusion factors at different temperatures and reasonable agreement has been obtained except in the case of A-Kr.

## INTRODUCTION

The inter-molecular potentials for like molecules have been determined accurately for many molecules by a large number of workers. For this purpose, various transport properties of gases, specially viscosity, have been utilised. However, there is considerable uncertainty in the values of unlike force constants for most of the molecular pairs, as there is lack of suitable accurate experimental data over a large temperature range. The transport properties of gas mixtures depend on both like and unlike force parameters, and in cases of viscosity and thermal conductivity the like molecular interaction tends to mask the effect of unlike interactions. In case of thermal diffusion, the masking is reduced, and for inter-diffusion it is insignificant. Unfortunately, until quite recently, sufficiently accurate inter-diffusion data were not available over an extended temperature range. On the other hand, thermal diffusion data being readily available, have been utilised by Srivastava and Madan (1953), Saxena (1955), Srivastava and Srivastava (1957), and Srivastava (1957), for the calculation of the unlike force parameters. Srivastava and Srivastava (1959), and Barua (1959) combined inter-diffusion data with viscosity data to evaluate unlike force constants, which enables even one or two values of the diffusion constant to be utilised.

Recently, several workers (Strehlow, 1953; Bunde 1955; Rumpel, 1955; Srivastava and Srivastava, 1959; Srivastava, 1959; Srivastava and Barua 1959)

have determined  $D_{12}$  over a wide range of temperatures and utilised it to determine the unlike force constants on Lennard-Jones 12.6 model. In the present paper the values of inter-diffusion coefficients by Srivastava and Srivastava (1959), Srivastava (1959), and Srivastava and Barua (1959) have been used to determine unlike force parameters on the exp-six model. This is of considerable importance as the combination rules so far given are largely empirical and cannot therefore be considered satisfactory.

#### DETERMINATION OF THE FORCE PARAMETERS

On the Exp-Six model, the potential  $\phi(r)$  between two molecules, when separated by a distance  $r$ , is given by

$$\phi(r) = \frac{\epsilon}{1 - \frac{6}{\alpha}} \left[ \frac{6}{\alpha} e^{\frac{\alpha}{r_m} \left(1 - \frac{r}{r_m}\right)} - \left(\frac{r_m}{r}\right)^6 \right] \quad \dots (1)$$

where  $\epsilon$  is the depth of the potential energy minimum,  $r_m$  is the separation distance for the energy minimum and  $\alpha$  is the parameter which gives the steepness of the repulsion energy. The molecular parameters are denoted by  $\epsilon_{ij}$ ,  $(r_m)_{ij}$  and  $\alpha_{ij}$ , where  $i, j$  denote the two interacting molecules.

Two sets of combination rules have been recently proposed which enable us to calculate the unlike force parameters in terms of like parameters. The combination rules given by Mason and Rice (1954) are

$$\left[ \frac{\epsilon_{12}}{1 - \frac{6}{\alpha_{12}}} \cdot \frac{6}{\alpha_{12}} e^{\frac{\alpha_{12}}{r_m}} \right] = \left[ \left\{ \frac{\epsilon_{11}}{1 - \frac{6}{\alpha_{11}}} \cdot \frac{6}{\alpha_{11}} e^{\frac{\alpha_{11}}{r_m}} \right\} \left\{ \frac{\epsilon_{22}}{1 - \frac{6}{\alpha_{22}}} \cdot \frac{6}{\alpha_{22}} e^{\frac{\alpha_{22}}{r_m}} \right\} \right]^{\frac{1}{2}}$$

$$\frac{\alpha_{12}}{(r_m)_{12}} = \frac{1}{2} \left[ \frac{\alpha_{11}}{(r_m)_{11}} + \frac{\alpha_{22}}{(r_m)_{22}} \right] \quad \dots (2)$$

$$\frac{\epsilon_{12}(r_m)_{12}^6}{1 - \frac{6}{\alpha_{12}}} = \left[ \frac{\epsilon_{11}(r_m)_{11}^6}{1 - \frac{6}{\alpha_{11}}} \cdot \frac{\epsilon_{22}(r_m)_{22}^6}{1 - \frac{6}{\alpha_{22}}} \right]^{\frac{1}{2}}$$

while the following are given by Srivastava and Srivastava (1957)

$$\frac{\alpha_{12}}{(r_m)_{12}} = \frac{1}{2} \left[ \frac{\alpha_{11}}{(r_m)_{11}} + \frac{\alpha_{22}}{(r_m)_{22}} \right]$$

$$\epsilon_{12} = (\epsilon_{11} \cdot \epsilon_{22})^{\frac{1}{2}}$$

$$\frac{\epsilon_{12}(r_m)_{12}^6}{1 - \frac{6}{\alpha_{12}}} = \left[ \frac{\epsilon_{11}(r_m)_{11}^6}{1 - \frac{6}{\alpha_{11}}} \cdot \frac{\epsilon_{22}(r_m)_{22}^6}{1 - \frac{6}{\alpha_{22}}} \right]^{\frac{1}{2}} \quad \dots (3)$$



These have been used to yield value of  $\alpha_{12}$  where this value was not known from the thermal diffusion data.

The procedure adopted for calculating the force constants is as follows :—

The experimental value of  $D_{12}$  at different temperatures were plotted and four smoothed out values of  $D_{12}$  were taken. Theoretically,  $D_{12}$  is given by

$$D_{12} = .002628 \frac{T^{3/2}}{p(r_m)_{12}^2 \Omega_{12}^{(11)} (T_{12}^*)} \left[ \frac{M_1 + M_2}{2M_1M_2} \right]^{1/2} \quad (4)$$

where  $p$  is the pressure in atmospheres,  $T_{12}^* = \frac{kT}{\epsilon_{12}}$ ,  $k$  being the Boltzmann's

constant; and  $\Omega_{12}^{(11)}$  is a reduced collision integral tabulated by Mason (1954), other symbols having their usual meanings. The values of  $\alpha_{12}$  were taken from the previous determinations from thermal diffusion data, where available. In other cases it was calculated from the combination rules given by Srivastava and Srivastava (1957).

From equation (4), substituting a set of values for  $\epsilon_{12}$ , the corresponding values of  $(r_m)_{12}$  were found out using the value of  $D_{12}$  at a certain temperature. This was repeated with values of  $D_{12}$  at other temperatures, and in this way the values of  $(r_m)_{12}$  against  $\epsilon_{12}$  were plotted and curves were drawn corresponding to each temperature. Since the values of  $\epsilon_{12}$  and  $(r_m)_{12}$  should not vary with temperature, these curves should intersect at a single point. However, due to experimental error, several intersection points occur, fairly close to each other. The mean of all these values gives the required set of force parameters.

In the case where viscosity data on mixture were available, the values of force constants were also determined by combining the viscosity data with inter-diffusion data. The method used for this purpose is essentially the same as that used by Srivastava and Srivastava (1959). Viscosity data were taken from Rietveld, Iitterbeek and vanDen Berg (1953) and Trautz and Binkele (1930).

## RESULTS

For easy reference the smoothed out values of the inter-diffusion coefficient are recorded in Table I.

In Table II, are tabulated the values of the force constants obtained by the method indicated above, together with the values obtained from a combination of viscosity and mutual diffusion, and from the temperature variation of thermal

diffusion. The respective values from the different combination rules are also given for the sake of comparison

TABLE I  
Experimental values of the coefficients of inter-diffusion

Gas pairs	273°K	288°K	303°K	318°K
A-He	0.640	0.701	0.760	0.825
A-Xe	0.0943	0.102	0.114	0.128
He-Xe	0.501	0.550	0.604	0.655
Ne-A	0.276	0.300	0.327	0.357
Ne-Kr	0.223	0.240	0.266	0.284
A-Kr	0.119	0.128	0.140	0.153
He-Kr	0.556	0.605	0.659	0.720
Ne-Xe	0.186	0.202	0.221	0.244

TABLE II  
Force Parameters

Gas pair	From intersection	From viscosity and diffusion	From thermal diffusion	Combination rule Srivastava & Srivastava (1957)	Combination rules Mason and Rice (1954)
Ne-A	$\alpha_{12}$ 14.18	14.18	14.18	14.35	14.17
	$\epsilon_{12}/k$ 64.5	66.6	67.6	68.42	73.7
	$(r_m)_{12}$ 3.511	3.497	3.504	3.491	3.443
Ne-Kr	$\alpha_{12}$ 13.84		13.81	14.15	13.55
	$\epsilon_{12}/k$ 68.75		73.4	71.71	89.54
	$(r_m)_{12}$ 3.725		3.720	3.710	3.549
A-Kr	$\alpha_{12}$ 13.61			13.61	13.52
	$\epsilon_{12}/k$ 128.25			129.2	132.8
	$(r_m)_{12}$ 4.123			4.101	4.072
He-A	$\alpha_{12}$ 13.5	13.5	13.5	13.20	13.21
	$\epsilon_{12}/k$ 29.3	31.5	33.4	33.59	33.40
	$(r_m)_{12}$ 3.523	3.504	3.471	3.484	3.488
A-Xe	$\alpha_{12}$ 13.4		13.4	13.58	13.44
	$\epsilon_{12}/k$ 173.25		170.5	168.8	178.5
	$(r_m)_{12}$ 4.200		4.158	4.153	4.108
He-Xe	$\alpha_{12}$ 12.86	12.86		12.86	12.56
	$\epsilon_{12}/k$ 44.2	39.8		46.03	57.88
	$(r_m)_{12}$ 3.756	3.803		3.743	3.653
He-Kr	$\alpha_{12}$ 12.89			12.89	12.64
	$\epsilon_{12}/k$ 35.0			35.23	38.73
	$(r_m)_{12}$ 3.690			3.696	3.625
Ne-Xe	$\alpha_{12}$ 14.0		14.0	14.15	13.45
	$\epsilon_{12}/k$ 88.88		80.0	93.74	121.8
	$(r_m)_{12}$ 3.837		3.799	3.758	3.574

## COMPARISON WITH EXPERIMENT

The force constants obtained by the method of intersection are utilised to calculate the thermal diffusion factor at different temperatures. Table III gives the values of  $\alpha_T$ , thus obtained, together with the experimental values as determined by Grew (1947) and Grew, Johnson and Neal (1954).

TABLE III  
Comparison with experimental values of  $\alpha_T$

Gas Pairs	185°K		293°K		465°K	
	Cale	Expt	Cale	Expt	Cale	Expt.
Ne-A	142	148	176	174	194	191(a)
Ne-Kr	220	210	284	290	319	320(b)
A-Kr	040	032 038	108	060 .075	121	080(a) .149(b)
He-A	368	360	381	380	.	(b)
A-Xe	016	063	100	087	179	176(b)
He-Xe	.	.	426	434	441	434(b)
U-Kr	397	130	128	448	440	448(b)
Ne-Xe	.205	260	301	300	359	370(b)

Experimental values are of (a) Grew *et al.* (1954) and (b) Grew (1947)

## REMARKS

It will be seen that the agreement between the calculated and experimental values is very satisfactory except in the case of A-Kr. This may be due to some errors in the assumed values of the force parameters for Kr in the calculation of  $\alpha_T$ . For A-Xe and Ne-Xe the agreement becomes poor at 185°K which seems to be due to Xe approaching its liquefaction point.

## ACKNOWLEDGMENT

The author is grateful to Prof. B. N. Srivastava, D.Sc., F.N.I., for suggesting the problem and for his valuable guidance throughout the progress of the work, and to Council of Scientific and Industrial Research, New Delhi, for financial assistance.

## REFERENCES

- Barua, A. K., 1959, *Ind. J. Phys.*, **33**, 221.  
 Bunde, R. W., 1955, Univ. of Wisconsin, CM-850, 8 Aug.  
 Grew, K. W., 1947, *Proc. Roy. Soc. A*, **189**, 402.

- Grew, K. E., Johnson, F. A and Neal, W. E. T., 1954, *Proc. Roy. Soc.* **A224**.  
Mason, E. A., 1954, *J. Chem. Phys.*, **22**, 169.  
Mason, E. A. and Rice, W. E., 1954, *J. Chem. Phys.*, **22**, 522.  
Rietveld, A. O., Van Itterbeek, A. and Van Den Berg, G. J., 1953, *Physica*, **19**, 517.  
Rimpel, W. F., 1955, Univ. of Wisconsin, CM-851, 1 Aug.  
Saxena, S. C., 1955, *Ind. J. Phys.*, **29**, 131.  
Srivastava, B. N. and Madan, M. P., 1953, *J. Chem. Phys.*, **21**, 807.  
Srivastava, B. N. and Srivastava, K. P., 1957, *Physica*, **23**, 103.  
Srivastava, B. N. and Srivastava, K. P., 1959, *J. Chem. Phys.*, **30**, 984.  
Srivastava, K. P., 1957, *J. Chem. Phys.*, **26**, 579.  
Srivastava, K. P., 1959, *Physica*, **25**, 571.  
Srivastava, K. P. and Bana, A. K., 1959, *Ind. J. Phys.*, **33**, 229.  
Strehlow, R. A., 1953, *J. Chem. Phys.*, **21**, 2101.  
Trautz, M. and Binkelo, H. F., 1930, *Ann. der Phys.*, **5**, 561.

# Letters to the Editor

The Board of Editors will not hold itself responsible for opinions expressed in the letters published in this section. The notes containing reports of new work communicated for this section should not contain many figures and should not exceed 500 words in length. The contributions must reach the Assistant Editor not later than the 15th of the second month preceding that of the issue in which the paper is to appear. No proof will be sent to the authors.

## 3

### ANISOTROPY OF WATER CLUSTER ABOUT THE $\text{Cu}^{++}$ ION

A. MOOKHERJI AND M. S. CHHONKAR

PHYSICS LABORATORY, AGRA COLLEGE, AGRA

(Received, January 9, 1960)

The ground state of  $\text{Cu}^{++}$  ion ( $3d^9 \ ^2D_{5/2}$ ) in octahedrally co-ordinated salts under the influence of the usual type of cubic crystalline electric field with positive coefficient (Van Vleck, 1932, Schlapp and Penney, 1932 and Gorter, 1942) splits into an orbital doublet and triplet above it.

Beevers and Lipson (1934) have shown that the water cluster about the  $\text{Cu}^{++}$  ion has the approximate tetragonal symmetry and hence according to the theories of Polder (1942), Abragam and Pryce (1951), Bleaney *et al.* (1955) and Bose *et al.* (1957) the ionic magnetic anisotropy of the  $\text{Cu}^{++}$  ion is given by

$$K_{\parallel} - K_{\perp} - \Delta K = \frac{2N\beta^2}{kT} (\lambda + kT) \cdot D' - \frac{2N\beta^2}{kT} (\lambda + kT) \cdot D f^2$$

where  $K_{\parallel}$  and  $K_{\perp}$  are the ionic susceptibilities parallel and normal to the tetragonal axis respectively;  $D = \left( \frac{4}{E_{\parallel}} - \frac{1}{E_{\perp}} \right)$ , where  $E_{\parallel}$  and  $E_{\perp}$  are the energy differences of the lowest basic doublet and the two tetragonal levels respectively of the triplet, and  $f^2$  is the covalency factor (Owen, 1955).

Our measurements of the absorption spectra of  $\text{Cu}^{++}$  ion in copper sulphate in aqueous solution at first sight show that there is only one band having maximum at  $12,400 \text{ cm}^{-1}$ , but a closer examination of the absorption curves (fig.1) shows that there is another maximum at about  $12,000 \text{ cm}^{-1}$ . The second maximum is directly noticeable, though it is not very prominent. There is a great deal of experimental evidences (Ballhausen and Jorgensen, 1954) that the absorption

curves of cupric ion in aqueous solution in different amino copper complexes consist of at least two discernible bands

If this separation is taken to be due to the tetragonal component of the crystal field then one can calculate  $D$ , which when substituted in the above expression will give  $\Delta K/f^2$ . Now according to Owen's findings and also of ours (Mookherji and Chhonkar, 1959)  $f^2$  in  $\text{CuSO}_4$  aqueous solution is 0.85 which gives directly  $\Delta K$  in solution state for the water cluster about the  $\text{Cu}^{++}$  ion. Since we have found in our studies of nickel salts (Mookherji and Chhonkar, in course of publication)  $\Delta K$  in state of solution and in crystalline state does not differ appreciably and hence our evaluated value of  $\Delta K$  in case of  $\text{CuSO}_4$  solution should agree with that of crystal value of  $\Delta K$  (Bose *et al.*, 1957) provided that our optical findings are correct.  $\Delta K = 548.4 \times 10^{-6}$  at  $300^\circ\text{K}$  as obtained by Bose *et al.* (1957) from magnetic studies agrees well with our calculated value of  $\Delta K = 548 \times 10^{-6}$  at the same temperature and hence we conclude that the first and second maxima are due to tetragonal splitting.

Since our assignment agrees well with the magnetic findings we have calculated  $f^2$  evaluating  $\Delta K$  from our optical measurements and utilising Bose *et al.* (1957) magnetic  $\Delta K$  - values. They are given in Table I. We find that  $f^2$  - values are of the right order and almost the same for all the salts studied in agreement with the suggestions of Bose *et al.* (1957) for these salts.

TABLE I

Sulphate series					
Pentahydrate	K	$\text{NH}_4$	Rb	Ti	Zn-K
0.85	0.88	0.76	0.875	0.81	0.88
Selenate series					
Pentahydrate	K	$\text{NH}_4$			
0.865	0.88	0.83			

## REFERENCES

- Abragam, A. and Pryce, M. H. L., 1951, *Proc. Roy. Soc.*, **A206**, 165.  
 Bleaney, B., Bowers, K. D. and Pryce, 1955, *Proc. Roy. Soc.*, **228**, 166.  
 Bose, A., Mitra, S. K. and Dutta, S. K., 1957, *Proc. Roy. Soc.*, **239**, 165.  
 Bjerrum, J., Bullhausen, C. J. and Jorgensen, 1954, *Acta Chem. Scand.*, **8**, 1275.  
 Beever, C. A. and Lipson, H., 1934, *Proc. Roy. Soc.*, **A146**, 570.  
 Gorter, C. J., 1932, *Phys. Rev.*, **42**, 437.  
 Mookherji, A. and Chhonkar, N. S., 1959, *Ind. Jour. Phys.*, **33**, 74.  
 Polder, D., 1942, *Physika*, **9**, 713.  
 Schlapp and Peacey, 1932, *Phys. Rev.*, **41** & **42**, 194 & 666.  
 VanCleave, J. H., 1932, *The Theory of electric and magnetic susceptibilities*, Oxford Press.

# APPLICATION OF SIGN RELATIONS IN THE CASE OF 4, 1, 3-CHLORO-DINITRO-BENZENE

E. M. GOPALAKRISHNA

INDIAN ASSOCIATION FOR THE CULTIVATION OF SCIENCE, CALCUTTA-32, INDIA

(Received, February 11, 1960)

The method of systematic application of sign relations as developed and described by Grant, Howells and Rogers (1957) was tried for the sign determination of the structure factors of (*okl*) reflections from (4, 1, 3) chloro-dinitro-benzene and found to be very successful.

(4, 1, 3) chloro-dinitro-benzene ( $\alpha$ -modification) belongs to orthorhombic space group  $Pn\bar{c}2_1$  with  $a = 8.96$ ,  $b = 11.08$ ,  $c = 15.73$  Å and with eight molecules per unit cell [Gopalakrishna (1959)]. The (100) projection is of pmg symmetry.

Of the 96 observed  $|F(okl)|$ 's, 40 with larger  $|U|$  values were used in the process which gave rise to 300 distinct triple sign relations of the type

$$S(h')S(h^{-1}h') \approx S(h)$$

and about 100 sign coincidences from different pairs of triple sign relations of the type

$$S(A)S(B)S(C_1) \approx \pm 1$$

$$S(A)S(B)S(C_2) \approx \pm 1$$

The signs of seven structure factors (of  $k = \text{even}$ ,  $l = \text{even}$ ) were obtained from the sign relation of the type

$$S(o, 2k, 2l) \approx S(okl)S(o\bar{k}\bar{l}) = +1$$

$$S(o, 2k, o) \approx S(okl)S(okl) = (-1)^k$$

and

$$S(o, o, 2l) \approx S(okl)S(o\bar{k}\bar{l}) = (-1)^k$$

Starting with the signs of these seven structure factors and using the sign coincidences, all the forty terms were assigned signs. The iterative process corrected 13 signs out of those 40 after four cycles of the process, when all the signs were consistent with each other. The electron density map calculated with these forty factors gave out the position of chlorine atom and the approximate orientation of the molecule. Later, the signs of another 15 terms were determined from the triple sign relations. When the contribution due to these fifteen terms was added to the previous map, the approximate positions of all the atoms became

evident. Using these positions and calculating the structure factors, the  $R$ -value was about 0.40. Fig. 1 shows the electron density synthesised with 90 terms. When the structure factors were calculated using the atomic co-ordinates from this figure, only one was found to be not correct among the previously determined 55 signs.

The  $|U|$  values were calculated from intensities measured by visual comparison and were on an arbitrary scale. They were not corrected for absorption nor for temperature effect

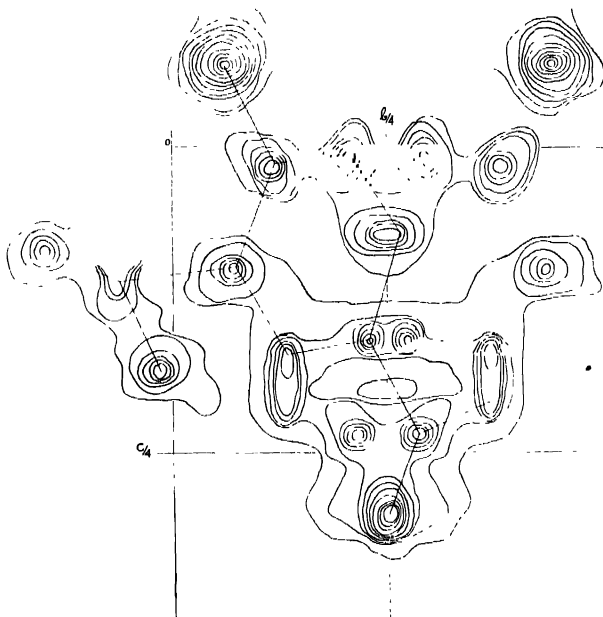


Fig. 1. Electron density map (100) projection calculated with 90 terms

The results obtained in this case show that the method under favourable conditions yields a tentative solution even without any previous knowledge of the stereo chemistry of the molecule or of any signs of the structure factors.

The presence of the chlorine atom among the lighter ones does not prevent the method from yielding a solution. The random and systematic errors in  $|U|$  values do not seriously affect the sign determination by this method.



TABLE I  
 $y$  and  $z$  co-ordinates of atoms (without refinement)

	$y/a$	$z/c$		$y/a$	$z/c$
Cl	.063	— .070	C	.208	.007
C	.117	.017	N	.263	.233
C	.067	.103	O	.250	.300
			O	.371	.210
C	.133	.175	N	— .054	.113
C	.229	.163	O	— .017	.183
C	.241	.075	O	— .154	.068

The complete structure analysis after refinement will be published later.

The author wishes to express his deep indebtedness to Prof. B. N. Srivastava, D.Sc., F.N.I., for his keen interest and valuable discussions. He expresses his gratefulness to Dr. B. V. R. Murty for suggesting this work and guiding.

#### REFERENCES

- Grant, D. F., Howells, R. G and Rogers, D., 1957, *Acta Cryst.*, **10**, 489  
 Gopala Krishna, E. M., 1959, *Zeit. f. Krist.*, **111**, 159

## R E V I E W

### RUSSIAN-ENGLISH GLOSSARY OF ACOUSTICS AND ULTRASONICS.

Pp. 170+xxiii. Consultant Bureau Inc. 227 West 17th Street, New York, N.Y. 1958. Price 10.00.

This volume gives the English-equivalents of all the words and phrases which are expected to be found in the literature dealing with topics on acoustics and ultrasonics. The words in Russian are written in Russian alphabet. Many of words and phrases are also found in the literature dealing with topics on other branches of physics. An index of Russian-equivalents of names of all the authors who have published papers in acoustics and ultrasonics has also been included.

It is needless to mention that the glossary will be extremely helpful to the workers who want to translate papers on these topics published in Russian journals. The volume is not bound, but the printing paper used is of high quality.

*S. C. S.*

# INFLUENCE OF GEOMAGNETIC FIELD ON EXTENSIVE AIR SHOWERS OF COSMIC RADIATION

A. BHASKARA RAO AND P. S. GILL

DEPARTMENT OF PHYSICS, MUSLIM UNIVERSITY, ALIGARH

(Received, February 10, 1960)

**ABSTRACT.** G. Cocconi (1954) pointed out that the deflection of air shower particles in the earth's magnetic field should produce some ellipticity of shower structure, and hence the lateral distribution of electrons around the shower axis should not be circular, but elliptical, with the major axis in the East-West direction. This effect was investigated at Gulmarg (alt. 2710 m  $24^{\circ}$ – $36^{\circ}$  N-geomagnetic lat.) with two G. M. counter telescopes, for three separations 10 m, 25 m, and 40 m. The results show that there is a significant difference between the shower rates from East-West and North-South directions. This asymmetry in the shower rates is found to increase with the separation, and the zenith angle of the telescopes.

## INTRODUCTION

G. Cocconi (1954) pointed out that  $D_m$ , the displacement of air shower particles due to the earth's magnetic field is not negligible in comparison with  $D_s$ , the projected lateral displacement due to multiple coulomb scattering, and this effect might be large enough to be detected as an asymmetry in the lateral distribution of electrons in air showers. It means the electrons are distributed elliptically, around the shower axis.

It has been evaluated in the first approximation, that the ratio of the two displacements is given by

$$D_m/D_s = 0.22 \cos \lambda / P$$

Where  $\lambda$  is geomagnetic latitude, and

$P$  is air pressure in atmospheres.

The combined displacement is  $D_{m+s} = [D_m^2 + D_s^2]^{1/2}$  : so that

$$\begin{aligned} D_{m+s} &= D_s \left[ 1 + \left( \frac{0.22 \cos \lambda}{P} \right)^2 \right]^{1/2} \\ &\approx D_s \left[ 1 + \frac{0.024 \cos^2 \lambda}{P^2} \right] \end{aligned}$$

P. Chaloupka (July, 1954) measured this effect on the top of "Lommicky Stit" (alt. 2634 m :  $48^{\circ}$  N. geomagnetic latitude) with two G. M. counter teles-

scopes. The separation of the telescopes was 7 m. The telescopes were inclined at  $45^\circ$  zenith angle and successively directed towards East, West, South, and North. Fourfold coincidences were taken. He reported nearly 20% more showers arriving from the E-W direction than from N-S direction. Due to large statistical errors he did not draw any conclusion. Later Dubinsky, Chaloupka, *et al.* (1956) continued the investigation (alt. 1778 m:  $48^\circ$ N. geomagnetic lat.) in which they fixed up the position of the shower core, and measured the particle densities to the West and South of the core, at three distances 15.5 m, 30 m, and 50 m. Though they did not find any variation for 15.5 m, they observed 40% and 60% greater densities in the West direction than in the South for 30 m, and 50 m distances respectively. Even in this case the statistical errors were large. The present investigation was carried out at Gulmarg (alt. 2710 m:  $24^\circ 36'$  N. geomagnetic lat.) with improved statistics.

#### EXPERIMENTAL

The experimental arrangement was similar to that of Chaloupka, and the block diagram is shown in Fig. 1. It consisted of two G. M. counter telescope  $T_1, T_2$ , with two trays in each. In each tray there were four counters (size  $52 \times 584$  mm) filled with Argon and petroleum-ether. The separation of the counter trays in the telescopes was 950 mm. The pulses from the trays were carried to the cathode-follower and from there to the coincidence circuit, through a low impedance coaxial cable, type KD-49. Only fourfold coincidences were recorded by the recording unit. The counter trays were mounted on an aluminium frame, which was fixed to a wooden stand in such a way that the telescope can be fixed at any particular zenith angle.

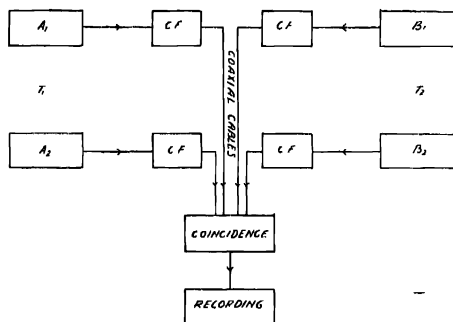


Fig. 1.

The asymmetry in the rate of showers was measured for three distances 10 m, 25 m, and 40 m between the telescopes. The telescopes were directed towards East, West, South, and North at zenith angles  $0^\circ, 15^\circ, 30^\circ, 45^\circ$ , and  $60^\circ$

and fourfold coincidences were recorded. Counters with a minimum plateau of 200 V were used in the experiment, and they were tested every day before starting the apparatus.

## RESULTS AND DISCUSSION

The results of the experiment are given in Tables I, II, and III, for the three separations 10 m, 25 m, and 40 m. In any direction if the total number of counts recorded is  $M$ , during the total time  $T$  hours, then the shower rate in that direction is  $M/T$  per hour. The error in the shower rate is taken as  $M^{1/2}/T$ .

The first table represents the shower rates from East, West, South, and North directions with the corresponding errors. In Table II the average shower rate from East-West directions is taken as  $x$  and the average shower rate from North-South directions as  $y$ . Next, the ratio  $x/y$  is calculated for the three separations and all the zenith angles as shown. If the circular symmetry of electrons around the shower axis is to be correct, the ratio  $x/y$  should be unity. But it can be seen that in all the cases, without exception, the ratio is larger than unity and far beyond the statistical errors. This clearly indicates that electrons in extensive air

TABLE I

Counting rates of showers from East, West, South, and North directions with corresponding errors

	Zenith angle $Z$	Showers per hour from the East $N_e \pm \Sigma_e$	Showers per hour from the West $N_w \pm \Sigma_w$	Showers per hour from the South $N_s \pm \Sigma_s$	Showers per hour from the North $N_n \pm \Sigma_n$
10 m	0°	94.4 ± 2.5	—	87.0 ± 2.3	—
	15°	79.4 ± 1.9	81.5 ± 1.9	72.1 ± 1.7	72.1 ± 1.7
	30°	69.5 ± 1.5	75.0 ± 1.9	63.0 ± 1.5	61.2 ± 1.5
	45°	60.4 ± 1.5	66.1 ± 1.7	52.9 ± 1.3	53.8 ± 1.3
	60°	50.9 ± 1.3	58.0 ± 1.5	45.6 ± 1.2	47.4 ± 1.2
25 m	0°	58.9 ± 1.9	—	52.5 ± 1.6	—
	15°	49.5 ± 1.5	54.9 ± 1.7	40.0 ± 1.3	40.6 ± 1.2
	30°	45.0 ± 1.0	48.2 ± 1.5	33.2 ± 1.0	33.3 ± 1.0
	45°	40.2 ± 1.2	45.2 ± 1.5	28.2 ± 0.9	28.7 ± 0.9
	60°	35.0 ± 1.0	37.1 ± 1.2	22.4 ± 0.7	23.3 ± 0.7
40 m	0°	38.4 ± 1.5	—	30.0 ± 1.2	—
	15°	32.6 ± 1.2	35.3 ± 1.3	24.7 ± 1.0	24.9 ± 1.0
	30°	29.7 ± 1.2	32.6 ± 1.3	20.6 ± 0.9	20.2 ± 0.7
	45°	26.5 ± 1.0	29.5 ± 1.2	16.5 ± 0.6	16.5 ± 0.6
	60°	24.5 ± 0.9	25.9 ± 1.0	13.3 ± 0.6	13.3 ± 0.6

TABLE II

Ellipticity and percentage asymmetry of extensive air showers

	Zenith angle $Z$	Average shower rate from E-W $x \pm \Sigma_x$	Average shower rate from N-S $y \pm \Sigma_y$	Ellipticity $x \pm \Sigma_x$ $y \pm \Sigma_y$	Percentage- asymmetry $F = \frac{2(x-y)}{(x+y)} \times 100\%$
10 m	0°	94.4 ± 1.8	87.0 ± 1.6	1.09 ± .029	8.2 ± 2.6
	15°	80.5 ± 1.4	72.1 ± 1.2	1.12 ± .027	11.0 ± 2.4
	30°	72.3 ± 1.2	62.1 ± 1.1	1.16 ± .028	15.2 ± 2.4
	45°	63.3 ± 1.1	53.4 ± 0.9	1.19 ± .029	17.0 ± 2.4
	60°	54.5 ± 1.0	46.5 ± 0.9	1.17 ± .031	15.8 ± 2.7
25 m	0°	58.9 ± 1.4	52.5 ± 1.1	1.12 ± .036	11.5 ± 3.2
	15°	52.2 ± 1.1	40.3 ± 0.9	1.30 ± .040	25.7 ± 3.0
	30°	46.6 ± 0.9	33.3 ± 0.7	1.40 ± .040	33.3 ± 2.8
	45°	42.7 ± 1.0	28.5 ± 0.7	1.50 ± .051	39.9 ± 3.3
	60°	36.1 ± 0.8	22.9 ± 0.5	1.58 ± .049	44.7 ± 3.0
40 m	0°	38.4 ± 1.1	30.0 ± 0.9	1.28 ± .053	24.6 ± 4.1
	15°	34.0 ± 0.9	24.8 ± 0.7	1.37 ± .053	31.3 ± 3.8
	30°	31.2 ± 0.9	20.4 ± 0.6	1.53 ± .063	41.9 ± 3.9
	45°	28.0 ± 0.8	16.5 ± 0.4	1.70 ± .064	51.7 ± 3.5
	60°	25.2 ± 0.7	13.3 ± 0.4	1.89 ± .078	61.8 ± 3.7

TABLE III

East-West percentage asymmetry of extensive air showers

Zenith angle $Z$	East-West asymmetry of extensive air showers		
	10 m	25 m	40 m
0°			
15°	2.61 ± 3.34	10.34 ± 4.32	7.95 ± 5.38
30°	7.61 ± 3.32	6.86 ± 3.82	9.30 ± 5.70
45°	9.01 ± 3.57	11.70 ± 4.45	10.71 ± 5.53
60°	13.03 ± 5.87	5.82 ± 4.31	5.55 ± 5.32

showers are distributed elliptically around the shower axis. The percentage asymmetry between the shower rates from E-W and N-S directions is given in the last column of Table II.

The errors in the ellipticity and the percentage asymmetries are calculated as follows :-

If ( $F$ ) is a function of both  $x$  and  $y$  then the error in  $F$  is given by

$$\Sigma^2 = \left[ \frac{d(F)}{dx} \right]^2 \Sigma_x^2 + \left[ \frac{d(F)}{dy} \right]^2 \Sigma_y^2$$

where  $\Sigma_x$  and  $\Sigma_y$  are errors in ( $x$ ) and ( $y$ ), and  $\Sigma$  is the error in the function ( $F$ ).

Then a graph is drawn with the zenith angles along the abscissa and the percentage asymmetries along the ordinate for the three separations of the telescopes. From the graph it is clear that there is a systematic increase in the asymmetry with zenith angle. It can also be seen that at any particular zenith angle the asymmetry increases with the separations of the telescopes. Of course the same arguments hold good for ellipticity also. The percentage asymmetry and ellipticity will increase by about 4 or 5% if the counting rates of showers only from West and South are taken into consideration, because the average shower rate from *E-W* is less than the individual shower rate from West, though the shower rates from North or South are exactly the same.

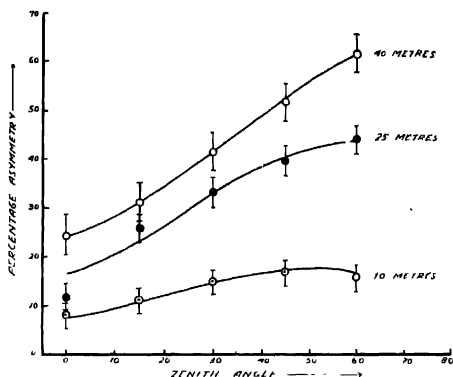


Fig. 2. Zenith angle versus percentage asymmetry.

Though the main aim of the investigation is to find out the geomagnetic effect on extensive air showers, there is one more interesting point. At all zenith angles from  $15^{\circ}$ - $60^{\circ}$  for the three separations 10 m, 25 m, and 40 m, the shower rate is slightly more from West than from East direction. This East-West asymmetry of extensive air showers is shown in Table III. In view of the very large statistical errors, and very poor angular resolution of the telescopes, it is felt better not to draw any definite conclusion. But it appears that there is some East-West asymmetry for extensive air showers also. From Table III it can be seen that for 10 m separation the asymmetry gradually increases from  $15^{\circ}$  to  $60^{\circ}$  zenith, whereas for 25 m, and 40 m, it reaches a maximum at  $45^{\circ}$  zenith and then comes down. To arrive at any conclusion regarding this East-West asymmetry of extensive air showers, more data are needed.

#### CONCLUSION

At moderate latitudes and mountain altitudes the geomagnetic field has a considerable and well detectable influence on the density distribution of extensive

air showers. The percentage asymmetry between the shower rates from E-W and N-S increases not only with the separation of the two telescopes but also with the zenith angle at which the telescopes are inclined. There appears to be 5 to 10% East-West asymmetry also for Extensive air showers.

#### ACKNOWLEDGMENTS

One of the authors (A. B. Rao) wishes to thank 'The Scientific Research Committee, Government of U.P.' for the financial help he received under the scheme "The Study of Extensive Air Showers." He thanks all the staff and the scholars of Gulmarg Observatory for their friendly help and suggestions. His thanks are also due to Mr Ajit Singh (Department of Physics, Muslim University, Aligarh) for his liberal co-operation while preparing the G. M. counters.

#### REFERENCES

- Chaloupka, P., 1954, *Phys. Rev.*, **96**, 1709.  
Cocconi, G., 1954, *Phys. Rev.*, **93**, 646; *Phys. Rev.*, **94**, 796; *Phys. Rev.*, **95**, 1705 (Errata)  
Dubinsky, J. et al., 1956, *Czechosl. Journ. Phys.*, **6**, 1, 29.  
Galbraith, W., 1958, Extensive Air Showers; Butterworths Scientific Publications, 66.



## ON FERMION LOOPS OF TWO VERTICES

B. DEO

PHYSICS DEPARTMENT, RAVENSHAW COLLEGE, CUTTACK

(Received, December 10, 1959)

**ABSTRACT.** The imaginary part of the retarded matrix element for a closed loop two vertices has been deduced by perturbation theory. It has been used to evaluate the photon and meson vacuum polarisation effects by assuming dispersion relations. Some difficulties regarding the meson vacuum polarisation have been shown to be removed by considering the vertex correction.

The formulae have been applied to deduce the decay rates of some fundamental particles and the results obtained are in good agreement with experiments.

## INTRODUCTION

Much interest is attached to explain the decay of fundamental particles by weak universal fermi interaction and the known strong/medium strong interactions. In most of the decay processes, a closed loop has to be inserted in Feynman diagram to bring in the four-fermion vertex, a convenient example being the charged pion decay. Since the decay probability is proportional to the weak coupling constant ( $10^{-14}$  n. u.) squared, one would expect that a straightforward perturbation analysis using Dyson's  $S$ -Matrix expansion will give us the correct decay rates. However, the closed loops intervening the initial and final states bring in infinite constants. They cannot be renormalised in a formal way i.e. we cannot absorb the infinite constants as unobservable constants associated with mass and coupling constant. Most of the fundamental-particle-decay studies have, therefore, been confined to the ratio of decay rates and the like. And only very recently  $\pi^{\pm} \rightarrow \mu^{\pm} + \nu(\bar{\nu})$  has been studied with considerable success by Goldberger and Trieman (1958).

To get rid of the infinite constants we shall calculate the imaginary part of the retarded matrix elements. This part is usually free from infinities and the real part can be evaluated from it by dispersion relations. In fact we shall show that the observable finite matrix elements can be unambiguously obtained from the imaginary part alone. Of course, one has to make a few subtractions, a procedure reminiscent of Pauli-Villars Regularisation Scheme.

## MATRIX ELEMENT OF A LOOP

Let us take a loop with two vertices ( $g_1\Gamma_1$ ;  $g_2\Gamma_2$ );  $g_1g_2$  denoting the coupling strength and  $\Gamma_1$  and  $\Gamma_2$  may consist of matrices. Referring to the Feynman

diagram in Fig. 1, the contribution to the matrix element can be written as

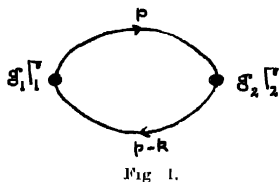
$$F_{12}(k) \propto \frac{g_1 g_2}{i\pi^2} \int d^4 p \frac{\text{Tr}[\Gamma_1(i\gamma \cdot p - m) \Gamma_2(i\gamma \cdot p - k - m)]}{(p^2 + m^2 - i\epsilon)(p - k)^2 + m^2 - i\epsilon} \quad \dots (1)$$

where  $m$  is the mass of the fermion. Evaluating the trace and combining the denominators we get

$$F_{12}(k) \propto \frac{g_2 g_1}{i\pi^2} \int_0^1 dx \int d^4 p \frac{A p^2 + B_{\mu\nu} k_\mu k_\nu x(1-x) - \frac{1}{2}(C_\mu - D_\mu) i m k_\mu + E m^2}{(p^2 + k^2 x(1-x) + m^2 - i\epsilon)^2} \quad \dots (2)$$

where

$$\begin{aligned} A &= -\frac{1}{4} s p (\Gamma_1 \gamma_\mu \Gamma_2 \gamma_\mu) \\ B_{\mu\nu} &= s p (\Gamma_1 \gamma_\mu \Gamma_2 \gamma_\nu) \\ C_\mu &= s p (\Gamma_1 \gamma_\mu \Gamma_2) \\ D_\mu &= s p (\Gamma_1 \Gamma_2 \gamma_\mu) \\ E &= s p \cdot (\Gamma_1 \Gamma_2) \end{aligned} \quad \dots (2a)$$



After partial integration over 'x',  $F_{12}(k)$  can be written as (omitting  $g_1, g_2$ )

$$\begin{aligned} F_{12}(k) = & \frac{A}{i\pi^2} \int \frac{d^4 p}{p^2 + m^2 - i\epsilon} + \left( \frac{1}{6} B_{\mu\nu} k_\mu k_\nu - \frac{1}{3} A k^2 - \frac{1}{2} i m k_\mu (C_\mu - D_\mu) \right. \\ & \left. + (E - A) m^2 \right) \frac{1}{i\pi^2} \int \frac{d^4 p}{(p^2 + m^2 - i\epsilon)^2} + \int_0^1 dx \left\{ B_{\mu\nu} k_\mu k_\nu \left( \frac{x^2}{2} - \frac{x^3}{3} \right) \right. \\ & \left. - A k^2 \frac{x^3}{3} - \frac{1}{2} (C_\mu - D_\mu) i m k_\mu x + (E - A) m^2 x \right\} \frac{k^2 (1 - 2x)}{k^2 x(1-x) + m^2 - i\epsilon} \quad \dots (3) \end{aligned}$$

It is easily seen that the last term alone has an imaginary part, since

$$\frac{1}{a - i\epsilon} = \frac{\rho}{a} + i\pi \delta(a)$$

$$Im . F_{12}(k^2) = +\pi \int_0^1 dx \delta(k^2 x(1-x) + m^2) k^2(1-2x) .$$

(expression in { } of Eqn. 3) ... (4)

In part of the retarded  $F_{12}(k^2)$  can be obtained by multiplying  $\epsilon(k_0)$ ,

since 
$$\Delta_F(k) = \frac{1}{k_\mu^2 + a^2 - i\epsilon} = \frac{\rho}{k^2 + a^2} + i\pi \delta(k^2 + a^2)$$

and 
$$\Delta_R(k) = \frac{1}{k^2 - (k_0 + i\epsilon)^2 + Q^2} = \frac{\rho}{k^2 + i\epsilon} + i\pi c(k_0) \delta(k^2 + a)$$

with 
$$\begin{aligned} \epsilon(k_0) &= +1, & k_0 > 0 \\ &= 0; & k_0 = 0 \\ &= -1; & k_0 < 0 \end{aligned} \quad \dots (5)$$

Our task is now to integrate over  $x$  with proper care to the delta function.

To this end we write

$$\delta(k^2 x(1-x) + m^2) = \frac{1}{4m^2 x(1-x)} \delta\left(\frac{k^2}{4m^2} + \frac{1}{x(1-x)}\right) .$$

and make the transformation  $u = \frac{1+x}{2}$ . The resulting integration is symmetrical and we get

$$\begin{aligned} Im . F_{12}^R(k^2) &= 4\pi c(k_0) \int_0^1 \delta\left(\frac{k^2}{4m^2} + \frac{1}{1-u^2}\right) \frac{k^2}{4m^2} \frac{u^2}{1-u^2} \left\{ \frac{1}{12} B_{\mu\nu} k_\mu k_\nu \left(1 + \frac{1-u^2}{2}\right) \right. \\ &\quad \left. + \frac{1}{6} A k^2 \left(\frac{1-u^2}{4} - 1\right) - \frac{1}{4} (C_\mu - D_\mu) i m k_\mu + \frac{1}{2} (E-A) m^2 \right\} du \quad \dots (6) \end{aligned}$$

Letting  $z = \frac{1}{1-u^2}$  with the help of a theta function

$$\begin{aligned} \theta(x) &= 1; & x > 0 \\ &= 0, & x < 0 \end{aligned}$$

$$\begin{aligned} Im . F_{12}^R(k^2) &= 4\pi \epsilon(k_0) \int_{-\infty}^{+\infty} \theta(z-1) \delta\left(\frac{k^2}{4m^2} + z\right) \frac{k^2}{4m^2} \frac{dz}{2z} \sqrt{1-\frac{1}{z}} \left\{ \frac{1}{12} B_{\mu\nu} k_\mu k_\nu \right. \\ &\quad \left. \left(1 + \frac{1}{2z}\right) + \frac{1}{6} A k^2 \left(\frac{1}{4z} - 1\right) - \frac{1}{4} (C_\mu - D_\mu) i m k_\mu + \frac{1}{2} (E-A) m^2 \right\} \\ &= -\frac{\pi}{2} \epsilon(k_0) 40 \left(-\frac{k^2}{4m^2} - 1\right) \sqrt{1 + \frac{4m^2}{k^2}} \left\{ \frac{1}{12} B_{\mu\nu} k_\mu k_\nu \left(1 - \frac{2m^2}{k^2}\right) \right. \\ &\quad \left. - \frac{1}{6} A k^2 \left(\frac{m^2}{k^2} + 1\right) - \frac{1}{4} i m k_\mu (C_\mu - D_\mu) + \frac{1}{2} (E-A) m^2 \right\} \quad \dots (7) \end{aligned}$$

This, then, is the divergence-free retrace matrix element contribution and small correspond to the imaginary part of the total matrix element.

#### PHOTON VACUUM POLARISATION

The vacuum polarisation tensor  $\Pi_{\mu\nu}$  of a photon for electron loop is given by

$$\Pi_{\mu\nu} = \frac{ie^2}{(2\pi)^4} \int d^4p \text{Tr.} \left\{ \gamma_\mu \frac{i\gamma \cdot p - m}{(p-k)^2 - m^2 - i\epsilon} \gamma_\nu \frac{i\gamma \cdot p - m}{p^2 + m^2 - i\epsilon} \right\}$$

Thus

$$\Gamma_1 = \gamma_\mu; \quad \Gamma_2 = \gamma_\nu$$

$$A = 2g_{\mu\nu}; \quad B_{\lambda\sigma} = 4(g_{\lambda\mu}g_{\sigma\nu} - g_{\mu\nu}g_{\lambda\sigma} + g_{\lambda\nu}g_{\mu\sigma}); \quad C_\mu = D_\mu = 0; \quad E = 4g_{\mu\nu}.$$

So we can write

$$\begin{aligned} \text{Im. } \pi^R_{\mu\nu}(k^2) &= (k_\mu k_\nu - g_{\mu\nu} k^2) \quad \text{Im. } \pi^R(k^2) \\ \text{Im. } \pi^R(k^2) &= -\frac{\alpha}{3} \theta\left(-\frac{k^2}{4m^2} - 1\right) \sqrt{1 + \frac{4m^2}{k^2}} \left(1 - \frac{2m^2}{k^2}\right) \epsilon(k_0) \quad \dots (8) \end{aligned}$$

For large  $k^2$  this imaginary part of  $\pi^R(k^2)$  approaches a constant value, so the Hilbert transform will be logarithmically divergent, necessitating one subtraction.

$$\begin{aligned} \text{Re } \pi_f(k^2) &= \text{Re. } [\pi(k^2) - \pi(0)] = -\frac{\alpha}{3\pi} k^2 \mu \int_{4m^2}^{\infty} \frac{\left(1 + \frac{4m^2}{x}\right)^{\frac{1}{2}} \left(1 - \frac{2m^2}{x}\right)}{x(x-k^2)} dx \\ &= -\frac{\alpha}{3\pi} \left[ \frac{5}{3} - \frac{4m^2}{k^2} - \left(1 - \frac{2m^2}{k^2}\right) \sqrt{1 + \frac{4m^2}{k^2}} \log \frac{\sqrt{1 + \frac{4m^2}{k^2}} + 1}{\sqrt{1 + \frac{4m^2}{k^2}} - 1} \right] \dots (9) \end{aligned}$$

which is the correct result.

#### MESIC VACUUM POLARISATION

Here  $\Gamma_1 = \Gamma_2 = \gamma_5$  for a pseudoscalar coupling.

$$\begin{aligned} A &= -4; & B_{\mu\nu} &= 4g_{\mu\nu} \\ C_\mu &= D_\mu = 0; & E &= -4 \end{aligned}$$

Denoting the polarisation by  $F(k^2)$  we have

$$\text{Im. part of } F(k^2) = -\frac{\alpha^2}{4\pi} \theta\left(\frac{k^2}{4m^2} - 1\right) \sqrt{1 + \frac{4m^2}{k^2}} \left(\frac{1}{8} k^2\right)$$

This diverges linearly with  $k^2 \rightarrow \infty$ .

## On Fermion Loops of Two Vertices

Hence the real part is quadratically divergent. Two subtractions are needed. The net observable effect is therefore contained in the integral

$$(G^2/4\pi) \cdot \frac{\rho}{\pi} \int \frac{\sqrt{1 - \frac{4m^2}{x}} \frac{1}{8} x}{4m^2 (x + \mu^2)^2 (x - k^2)} (k^2 + \mu^2)^2 dx. \quad \dots \quad (11)$$

Evaluation of this integral will lead directly to the finite part of the meson propagation function.

### EFFECT OF VERTEX CORRECTION ON THE CLOSED LOOP

In this section we shall study the correction due to the two vertices of the loop. Imaginary parts as given in equations (9) and (8) represent the effect of real pairs in the intermediate states. It should be obvious, therefore, the matrix elements of the vertex should be evaluated for real intermediate states; but for all values of  $k^2$  subject to the condition that  $k^2 \leq -4m^2$ . For electro-dynamics, this amounts to a negligible correction. But for mesons coupled to nucleons this amounts to a large correction. It should be noted that since the charge states of the nucleons are fixed, the correction for charged pion vertex is solely due to emission and absorption of  $\pi^0$  mesons. The details of evaluation have been given in the Appendix. The result obtained is to replace  $\gamma_5$  by a new function.

$$\Gamma'_5 = \frac{\gamma_5}{1 - \lambda \frac{k^2}{4m_p^2}} \quad \text{where } \lambda = \frac{g^2}{24\pi} \left( \frac{m_p}{\mu} \right)^2 \quad \dots \quad (12)$$

$$g^2 = \frac{G^2}{4\pi}.$$

Taking  $g^2 = 15$ ; the coefficient  $\lambda \simeq B$ . This amounts to a large reduction to the real pair formation at the vertex. Even at threshold,  $k^2 = -4m_p^2$ ; this is as large as 90%.

### DECAY OF FUNDAMENTAL PARTICLES

We are now in a position to calculate the absolute decay rates which involve a close loop of which one vertex representing a strong  $\gamma_5$  interaction. Let us take first the decay

$$\pi^+ \rightarrow \mu^+ + \nu$$

$$\pi^- \rightarrow \mu^- + \bar{\nu}$$

The Lagrangian density describing these decays is

$$\begin{aligned} \alpha_{int} = & f_A (\bar{\Psi}_r (1 - \gamma_5) i \gamma_\lambda \gamma_5 \psi_\mu) (\bar{\Psi}_\eta i \gamma_\lambda \gamma_5 \psi_p) \\ & + f_V (\bar{\Psi}_r (1 - \gamma_5) \gamma_\lambda \psi_\mu) (\bar{\Psi}_\eta \gamma_\lambda \psi_p) + i \sqrt{2} G (\bar{\Psi}_r \gamma_5 \psi_p \phi_\pi + \\ & + i G \bar{\Psi}_r \gamma_5 \psi_p \phi_{\pi^0} \\ & + \text{Hermitian conjugate.} \end{aligned} \quad \dots \quad (13)$$

Applying perturbation we shall take the Fermi coupling once and correct for the strong coupling vertex. First we note the vector coupling gives zero, due to the 'spur', so we have

$$\Gamma_1 = \gamma_5 : \quad \Gamma_2 = \gamma_\lambda \gamma_5$$

for the charged pion decay.

$$\begin{aligned} A &= 0 \\ B &= 0 \\ E &= 0 \\ C_\mu &= -D_\mu = 4g_{\mu\lambda}. \end{aligned}$$

Equation (7) takes the form

$$Im . F_{12}(k^2) = 4im_p k_\lambda \pi \epsilon(k_0) \theta \left( -\frac{k^2}{4m_p^2} - 1 \right) \sqrt{1 + \frac{4m_p^2}{k^2}}$$

The factor  $ik_\lambda$  is to be contracted  $i\gamma_\lambda k_\lambda$  with the free particle ( $\mu, \nu$ ) spinors yielding  $m_\mu$ , the mass of the muon. Thus

$$F(k^2) = 4im_p k_\lambda \pi \int_{4m_p^2}^{\infty} \frac{\sqrt{1 - \frac{4m_p^2}{x}}}{x - k^2} dx \quad \dots \quad (14)$$

which is log-divergent. However, if the correction at the vertex 1 is taken into account as given by (12),

$$F(k^2) = 4im_p k_\lambda \int_{4m_p^2}^{\infty} \frac{\sqrt{1 - \frac{4m_p^2}{X}}}{\left(1 + \frac{\lambda}{4m_p^2} X\right) (X - k^2)} dX \quad \dots \quad (15)$$

which is convergent. We get

$$F(k^2) = im_p k_\lambda \cdot \frac{4m^2/k^2}{\lambda + \frac{4m^2}{k^2}} \cdot \left[ (1+\lambda) \ln \cdot \frac{(1+\lambda)^{\frac{1}{2}} + 1}{(1+\lambda)^{\frac{1}{2}} - 1} \right] \\ - \left( 1 + \frac{4m^2}{k^2} \right)^{\frac{1}{2}} \log \left[ \frac{\left( 1 + \frac{4m^2}{k^2} \right)^{\frac{1}{2}} + 1}{\left( 1 + \frac{4m^2}{k^2} \right)^{\frac{1}{2}} - 1} \right] \quad \dots \quad (16)$$

We shall frequently use this result in evaluating decay rates. For convenience we write

$$F(-\mu^2) = 8im_p k_\lambda G(-\mu^2) \quad \dots \quad (17)$$

where

$$G(-\mu^2) = \frac{1}{2} \frac{4m^2/\mu^2}{4m^2/\mu^2 - \lambda} \left[ (1+\lambda) \ln \cdot \frac{(1+\lambda)^{\frac{1}{2}} + 1}{(1+\lambda)^{\frac{1}{2}} - 1} \right] \\ - \left( 1 + \frac{4m^2}{\mu^2} \right)^{\frac{1}{2}} \ln \cdot \left[ \frac{\left( 1 + \frac{4m^2}{\mu^2} \right)^{\frac{1}{2}} + 1}{\left( 1 + \frac{4m^2}{\mu^2} \right)^{\frac{1}{2}} - 1} \right] \quad \dots \quad (17a)$$

We can estimate  $G(-\mu^2)$  by noting

$$4m^2/\mu^2 \gg \lambda > 1.$$

Expanding the logarithms and retaining the first leading term, we obtain

$$G(-\mu^2) = \frac{1}{1+\lambda} \quad \dots \quad (18)$$

which depends only on the damping at the vertex.

Returning to the calculation of the decay rate we note the matrix element is in understandable notation

$$\langle \mu^+, \bar{\nu} | M | \pi^+ \rangle = - \frac{\sqrt{2} G g_A}{(2\pi)^{3/2}} \frac{1}{\sqrt{2\omega_\pi}} \sqrt{\frac{m_\mu}{\epsilon_\mu \epsilon_\nu}} \bar{u}_\mu(p_\mu) (i\gamma \cdot k_\pi) (1 + \gamma_5) v_\nu(p_\nu) \cdot \\ 8m_p \pi^2 G(-\mu^2). \quad \dots \quad (19)$$

with four momentum conservation.

This leads to the following decay rate in a familiar way,

$$\omega = \frac{m_\pi}{2\pi^4} \left( \frac{m_\mu}{m_\pi} \right)^2 \left( \frac{m_p}{m_\pi} \right)^2 \left( 1 - \frac{m_\mu^2}{m_\pi^2} \right)^2 \left( \frac{G^2}{4\pi} \right) \cdot (g_A m_\mu^2)^2 [G(-\mu^2)]^2 \quad (20)$$

If we take  $G^2/4\pi = 15$  and if we adopt for  $g_A$  the value of the Gamow-Teller coupling constant, we then find from the known pion life time that

$$G(-\mu^2) = 0.13. \quad (21)$$

whereas equation (18) gives

$$G(-\mu^2)|_{\text{theory}} = 0.11. \quad (22)$$

Thus the agreement can be considered extremely satisfactory. We emphasize again the influence of vertex damping as has been pointed out by Goldberger and Trieman (1958); they have, however, made a phase-shift analysis whereas we have just corrected for the vertex.

One would naturally be tempted to apply similar considerations to  $K \rightarrow \mu + \nu$  decays. Ignoring strangeness considerations, the decay rate is not very different from what one would expect. The value of  $\lambda$ , however, is about 10 times smaller, and the full expression (17a) is to be used. One cannot compare the life time with experiment since there are many channels of decay for the  $K$ -meson.

We shall extend our calculations to the decay modes

$$\Delta \rightarrow \begin{cases} p + \pi^- \\ n + \pi^0 \end{cases} \quad \dots (23a)$$

$$\dots (23b)$$

The simplest possible graphs leading to pionic  $\Delta$ -decay are shown in Fig. 2.

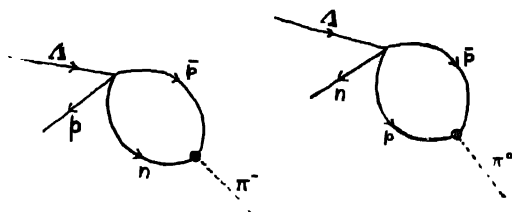


Fig. 2.

The decay rates are

$$\omega(\Delta \rightarrow p + \pi^-) = g_A^2 \frac{G^2}{4\pi} \frac{1}{2\pi^4} [G(-\mu^2)]^2 m_p^3 (m_\Delta - m_p)^2 (m_\Delta^2 + m_p^2 - \mu^2) \frac{1}{m_\Delta^3} \cdot [(m_\Delta - m_p)^2 - \mu^2]^{\frac{1}{2}} [(m_\Delta + m_p)^2 - \mu^2]^{\frac{1}{2}}$$

$$\frac{\omega(\Delta \rightarrow p + \pi^0)}{\omega(\Delta \rightarrow p + \pi^-)} = 0.5.$$



which is very near the observed ratio  $0.59 \pm 0.07$ . In deducing this we have tacitly assumed that  $(p, p)$  are the only intermediate virtual pair for the decay involving the neutral meson.

# ACKNOWLEDGMENT

The author wishes to record his thanks to his colleagues Dr. T. Pradhan and S. P. Misra for many interesting discussions.

# APPENDIX

Here we shall deduce the correction to a vertex as shown in Fig. 3, so that all the corrections due to pulling out the vertex in the direction of the boson line are accounted for.

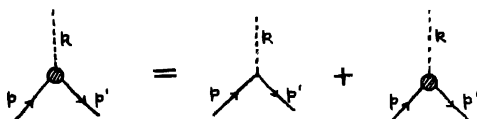


Fig. 3.

The function  $\Gamma_5$  for such processes as depicted is

$$\Gamma_5 = \gamma_5 + \frac{iG^2}{(2\pi)^4} \int d^4l \cdot \frac{\gamma_5(ir \cdot p - l + m_p) \Gamma_5(ir \cdot p' - l + m_p) \gamma_5}{(l^2 + \mu^2)((p-l)^2 + m_p^2)((p'-l)^2 + m_p^2)}$$

Since  $\Gamma_5$  is proportional to odd powers of  $\gamma_5$  we can anticommute it through the  $\gamma$ -matrices. The denominators can be combined by the well-known Feynman method and we obtain,

$$\Gamma_5 = \gamma_5 + \frac{iG^2}{(2\pi)^4} 2 \int_0^1 dx \int_0^x dy \int d^4l \cdot \frac{(ir \cdot p - l + m_p) \Gamma_5(ir \cdot p' - l + m_p)}{[(l - px - ky)^2 + a^2]^3}$$

where

$$a^2 = m_p^2 x^2 + \mu^2(1-x-y)(x-y) + (p^2 + m^2)(x-y)(1-x) + (p'^2 + m^2)(1-x)y + (k^2 + \mu^2)y(x-y)$$

Shifting the origin of 'l' integration, we can write,

$$\Gamma_5 = \gamma_5 + \frac{iG^2}{(2\pi)^4} 2 \int_0^1 dx \int_0^x dy \int d^4l \cdot \frac{K - (l^2 - m_p^2 x - \mu^2 y)(x-y) \Gamma_5}{(l^2 + a^2)^3}$$

where,

$$K = -(ir \cdot p' + m_p) \Gamma_5 (ir \cdot p + m_p - ir \cdot pX - ir \cdot kY) \\ + (ir \cdot pX + ir \cdot kY) \Gamma_5 (ir \cdot p + m_p) - (p^2 + m_p^2) x(x-y) \Gamma_5 + (p'^2 + m_p^2) xy \Gamma_5 \\ - (k^2 \mu^2) Y(X - Y) \Gamma_5.$$

One can now renormalize in the conventional way, by writing,

$$\Gamma_5(p', p) = \gamma_5(1 + L) + \Gamma_{5f}(p', p)$$

where  $L$  is determined by the equation

$$\Gamma_{5f}(p, p) = 0 \quad \text{for } ir \cdot p' = ir \cdot p = -m_p.$$

For our case,  $\Gamma_{5f}(p', p) = \Gamma_5 I(k^2)$  with  $ir \cdot p' = ir \cdot p = -m_p$ , but for arbitrary value of  $k^2$ .

Performing the necessary 'I' integration and estimating the major contributions from  $y$  and  $x$  integrations, we obtain the equation (12) given in the text.

#### REFERENCE

Goldberger M. L. and Treiman, S. B., 1958 *Phys. Rev.*, **110**, 1178

# THERMAL CONDUCTIVITY AND EUCKEN-TYPE FACTOR FOR THE BINARY MIXTURES H-He, H-Ne, H-Kr and H-Xe

A. K. BARUA

INDIAN ASSOCIATION FOR THE CULTIVATION OF SCIENCE, CALCUTTA-32

(Received, February 28, 1960)

**ABSTRACT.** In order to test the recent formulae for the thermal conductivity of polyatomic gas mixtures, the thermal conductivity of  $H_2$ -He,  $H_2$ -Ne,  $H_2$ -Kr and  $H_2$ -Xe mixtures have been measured at 30°C and 45°C by using the thick-wire variant of the hot-wire method. The experimental values of the thermal conductivity of the pure gases and then binary mixtures is lower than those given by Hirschfelder's theory based on the local chemical equilibrium assumption. It has been suggested that this discrepancy between theory and experiments at the temperatures under consideration is due to the non-validity of the condition of local chemical equilibrium. Apart from this drawback Hirschfelder's theory has been found to represent the concentration dependence of the thermal conductivity of polyatomic gas mixtures quite satisfactorily. The more rigorously derived formula of Hirschfelder has been found to represent the thermal conductivity of gas mixtures better than the approximate equation of Mason and Saxena.

## 1. INTRODUCTION

The problem of heat transfer in multicomponent mixtures of monatomic and polyatomic gases has recently attracted considerable attention. Though Curtiss and Hirschfelder (1949) has obtained expressions for the thermal conductivity of multicomponent mixture of monatomic gases by an extension of the Chapman-Enskog treatment for a binary mixture which is correct to the first approximation, their formula requires too much laborious calculations. In an attempt to overcome this difficulty, Mason (1958), Curtiss and Muckenfuss (1958) and Brokaw (1958) have obtained simpler expressions for the thermal conductivity of multicomponent mixtures of monatomic gases. The difficulty in treating the monatomic gases is only computational but the problem of heat transfer in polyatomic gases and gas mixtures is much more interesting as in this case the exchange of energy between the translational and the internal energies of the molecules need be considered. Eucken (1913) first suggested a correction to the thermal conductivity of polyatomic gases which was based on simple intuitive arguments whose inadequacy was later pointed out by several workers (Chapman and Cowling, 1952; K. Schafer, 1943). Recently, Hirschfelder (1957a) has obtained an expression for the thermal conductivity of a pure polyatomic gas by a formal

treatment in which the molecules in different states of excitation are treated as separate chemical species in local chemical equilibrium. The treatment for a pure polyatomic gas has been extended by Hirschfelder (1957b) to the case of the polyatomic gas mixtures. Mason and Saxena (1958) have made a number of approximations to simplify Hirschfelder's formula for the mixture conductivities. As accurate data on the thermal conductivity of gas mixtures are not extensive elaborate comparison of the experimental data with the recent theories cannot be made. Recently, Srivastava and his co-workers (1959, 1960a, 1960b) have measured the thermal conductivity of a number of binary mixtures of diatomic and monatomic gases and compared their data with the theory. In order to test further the expression for the thermal conductivity of gas mixtures and also to verify the suggestion of the non-validity of the condition of local chemical equilibrium in the present investigation the paper values of thermal conductivity of  $H_2$ -He,  $H_2$ -Ne,  $H_2$ -Kr and  $H_2$ -Xe mixtures at 30°C and 45°C have reported.

## 2. EXPERIMENT

The apparatus and the procedure adopted for the experiment are similar to those described by Srivastava and Barua (1960) and the constants of the conductivity cell are given in Table I.

TABLE I  
Constants of the conductivity cell

	At 30°C	At 45°C
Length of the cell wire ( $2l$ )	5.9978 cm	5.9987 cm.
Radius of the cell wire ( $r_1$ )	0.00500 „	0.00500 „
Internal diameter of the tube ( $2r_2$ )	0.3048 „	0.3048 „
External diameter of the tube ( $2r_3$ )	0.5915 „	0.5915 „
Resistance of the cell wire ( $R_0$ )	0.83518 $\Omega$	0.88012 $\Omega$
Temperature coefficient of resistance $\alpha$ of the platinum wire	0.00360°C <sup>-1</sup>	0.00358°C <sup>-1</sup>
Thermal conductivity $\lambda$ of the platinum wire in cal. cm <sup>-1</sup> . sec <sup>-1</sup> . °C <sup>-1</sup>	0.167	0.168
Cell constant (1-C)	0.9942	0.9941

As shown by Kannuliik and Martin (1934) the solution of the differential equation for heat flow is given by

$$f(\beta l) = \frac{1}{(\beta l)^2} \left( 1 - \frac{\tanh \beta l}{\beta l} \right) = \frac{2\pi r_1^2 \lambda J(R-R_0)}{R_0 \alpha l I^2} \quad (1)$$

with

$$\beta^2 = \frac{2h}{r_1 \lambda} - \frac{I^2 R_0 \alpha}{2\pi r_1^2 \lambda J l}, \quad h = \frac{K u}{r_1 \ln(r_2/r_1)} \quad (2)$$

where  $R$  is the resistance of the wire when a current of  $I$  amp. is flowing through it,  $R_0$  is the resistance of the cell wire at the bath temperature for  $I = 0$ ,  $\lambda$ ,  $K_u$  are the thermal conductivities of the wire and the gas respectively.

In Table II are shown the observations taken for  $H_2$ -He mixtures at  $30^\circ C$  which may serve as an example for the observations taken for other mixtures. In the Tables  $K_u$  has been calculated from Eq. (1) and (2),  $K_u'$  is the value of  $K_u$  reduced to the bath temperature and  $K'$  is the value of the conductivity when temperature jump and wall effect are corrected for and  $K$  is the value obtained after correcting for the asymmetry in the construction of the cell given by the relation  $K = K'(1-C)$ . In Tables III and IV are given the observed values of the thermal conductivity of the mixtures  $H_2$ -He,  $H_2$ -Ne,  $H_2$ -Kr and  $H_2$ -Xe at  $30^\circ C$  and  $45^\circ C$  which are plotted in Figs. 1 and 2.

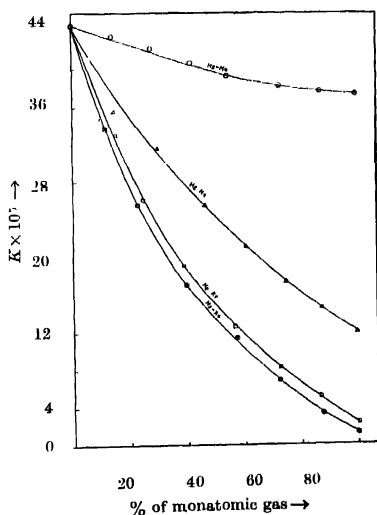


Fig. 1. Thermal conductivity  $K$  of  $H_2$ -He,  $H_2$ -Ne,  $H_2$ -Kr and  $H_2$ -Xe mixtures of different compositions at  $30^\circ C$ .

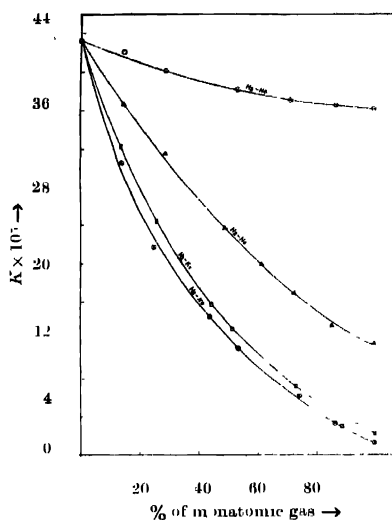


Fig. 2. Thermal conductivity  $K$  of  $H_2$ -He,  $H_2$ -Ne,  $H_2$ -Kr and  $H_2$ -Xe mixtures of different compositions at  $45^\circ C$

TABLE II

Thermal conductivity  $K$  of  $H_2$ -He mixtures  
cal.  $cm^{-1} sec^{-1} ^\circ C^{-1}$  at  $30^\circ C$

% of He	$T$ in $mK$	$R-R_0$ in $m\Omega$	$K_H \times 10^5$	$K_{H'} \times 10^5$	$K' \times 10^5$	$K \times 10^5$
100	208.42	6.247	36.89	36.79	36.49	36.32
87.13	207.68	6.023	37.24	37.14	36.84	36.63
71.36	209.78	6.040	37.88	37.78	37.39	37.17
53.28	214.62	6.125	39.06	38.95	38.58	38.36
45.62	213.75	6.008	39.59	39.49	39.18	38.95
28.91	212.31	5.690	41.25	41.13	40.75	40.52
14.64	210.16	5.323	43.24	43.12	42.72	42.47
0	213.48	5.289	44.99	44.89	43.49	43.20

TABLE III

Thermal conductivity  $K$  of H-He, H-Ne, H-Kr and H-Xe mixtures at 30°C

Gas Mixture	H <sub>2</sub> -He		H <sub>2</sub> -Ne		H <sub>2</sub> -Kr		H <sub>2</sub> -Xe	
	% of He	$K \times 10^5$	% of Ne	$K \times 10^5$	% of Kr	$K \times 10^5$	% of Xe	$K \times 10^5$
100	36.32		100	11.65	100	2.256	100	1.261
87.13	36.63		85.61	13.52	88.62	3.011	86.24	3.374
71.36	37.17		72.83	17.04	73.26	7.254	74.31	6.205
53.28	38.36		61.31	20.01	51.39	13.31	54.62	11.15
45.62	38.95		48.93	23.70	44.62	15.82	43.79	14.40
28.91	40.52		28.93	31.62	25.84	24.39	25.68	21.78
14.64	42.47		14.82	36.05	13.63	32.27	14.31	30.62
0	43.20		0	43.16	0	43.91	0	43.16

TABLE IV

Thermal conductivity  $K$  of H-He, H-Ne, H-Kr and H-Xe mixtures at 45°C

Gas Mixture	H-He		H-Ne		H-Kr		H-Xe	
	% of He	$K \times 10^5$	% of Ne	$K \times 10^5$	% of Kr	$K \times 10^5$	% of Xe	$K \times 10^5$
100	37.31		100	12.00	100	2.347	100	1.322
86.75	37.66		86.71	14.61	85.62	5.074	87.45	3.283
73.21	38.31		74.86	17.31	72.41	8.208	72.31	6.945
54.62	39.25		60.41	21.16	56.39	12.57	57.62	11.48
41.36	40.40		46.54	25.55	38.64	16.04	40.39	17.10
27.81	42.35		29.83	31.52	24.31	26.06	22.61	25.80
14.69	44.03		14.62	35.05	15.42	33.01	12.86	33.78
0	44.75		0	44.84	0	44.79	0	44.77

### 3. COMPARISON WITH THEORY

The simple Eucken (1913) expression for the thermal conductivity of a pure polyatomic gas may be written as

$$K = \frac{\eta}{M} [f_{trans} C_{v_{trans}} + f_{int} C_{v_{int}}], \quad \dots (3)$$

where  $K$  is the thermal conductivity,  $\eta$  the viscosity,  $M$  the molecular weight,  $C_{v_{trans}}$ ,  $C_{v_{int}}$  are the molar specific heats at constant volume corresponding to the translational and the internal degrees of freedom.  $f_{trans}=2.5$  and  $f_{int}$  indicate the transfer factors for the translational and the internal motions respectively. For simplicity Eucken put  $f_{int} = 1$ , so that Eq. (3) becomes

$$K = K_{mon} [(4/15)C_v/R + 3/5], \quad \dots (4)$$

where  $K_{mon}$  is the thermal conductivity of the gas when it is taken to be monatomic. Actually, however, internal energy is transported by a diffusion mechanism (Chapman and Cowling, 1952, Schäfer, 1943) so that  $f_{int} = 1$  should be replaced by  $f_{int} = \rho D/\eta$  (where  $\rho$  is the density,  $D$  the self-diffusion coefficient and  $\eta$  the viscosity) and Eq. (4) becomes,

$$K = \frac{\eta}{M} \left[ 2.5 C_{v_{trans}} + (\rho D/\eta) C_{v_{int}} \right] \quad \dots (5)$$

Hirschfelder (1957a) has obtained the following expression for the thermal conductivity of a pure polyatomic gas by considering the molecules in different states of excitation as separate chemical species which are in local chemical equilibrium,

$$K/K_{mon} = (1 - \delta_f) + \delta_f \rho D C_{pf}/C_{pf} \quad \dots (6)$$

where  $\delta_f = \rho D C_{pf}/K_{mon}$ ,  $C_{pf} = 5R/2$ . The values of  $\delta_f$  has been tabulated for several molecular models and it has been shown that  $\delta_f$  varies very little with temperature and it is possible to assign to  $\delta_f$  an average value of 0.885 so that Eq. (6) becomes

$$K/K_{mon} = 0.354 C_v/R + 0.469 \quad \dots (7)$$

By extending the treatment applied to a pure polyatomic gas Hirschfelder (1957b) has obtained the following expression for the thermal conductivity of a binary mixture of polyatomic gases

$$K_{mix} = K_{mix(mon)} + [K_1 - K_{1mon}] [1 + (x_2/x_1)(D_{11}/D_{12})]^{-1} \quad \dots (8) \\ + [K_2 - K_{2mon}] [1 + (x_1/x_2)(D_{22}/D_{12})]^{-1}$$

where  $K_1$ ,  $K_2$  are the thermal conductivities,  $D_{11}$ ,  $D_{22}$  are the coefficients of self-diffusion and  $x_1$ ,  $x_2$  are the molefractions for the components 1 and 2 of the mixture.  $D_{12}$  represents the coefficient of inter-diffusion.

In the present case the gas mixture consists of a diatomic gas denoted by the subscript 1 and a monatomic gas denoted by the subscript 2 so that Eq. (8) becomes

$$K_{mix} = K_{mix(mon)} + [K_1 - K_{1mon}] [1 + (x_2/x_1)(D_{11}/D_{12})]^{-1} \quad \dots (9)$$



The calculation of  $K_{mix}$  from Eq. (8) involves laborious computation and the knowledge of force laws between the molecules is necessary which is not easily available. Mason and Saxena (1958) have however tried to simplify Eq. (8) by a number of approximations and their formula may be written as,

$$K_{mix} = \sum_{i=1}^n K_i \left[ 1 + \sum_{\substack{j=1 \\ j \neq i}}^n G_{ij} \frac{x_j}{x_i} \right]^{-1} \quad \dots (10)$$

with

$$G_{ij} = \frac{1.065}{2 \sqrt{2}} \left( 1 + \frac{M_i}{M_j} \right)^{-1} \left[ 1 + \left( \frac{K_i^0}{K_j^0} \right)^{\frac{1}{2}} \left( \frac{M_i}{M_j} \right)^{1/4} \right]^2 \quad \dots (11)$$

where  $x_i, x_j$  are the molefractions,  $M_i, M_j$  the molecular weights of the components  $i$  and  $j$  respectively,  $K_i^0, K_j^0$  are the thermal conductivities when the gases are treated as monatomic and are related to the viscosities  $\eta_i, \eta_j$  by the relation

$$K_i^0/K_j^0 = \frac{\eta_i M_j}{\eta_j M_i} \quad \dots (12)$$

When  $\eta_i$  and  $\eta_j$  are known experimentally,  $K_i^0/K_j^0$  may be calculated from Eq. (12). In case the experimental viscosity data are not available, specific heat data may be used to obtain  $K_i^0/K_j^0$ . In order to compute  $K_{mix}$  from Eq. (10) the experimental values of  $K_i$  and  $K_j$  are to be used.

For comparing with the theory  $K_{1 mon}$  was calculated to the first approximation on the Lennard-Jones (12 : 6) model from the expression

$$K_{1 mon} = \frac{1989.1 \sqrt{T/M}}{\Omega^{(2,2)*}(T^*) \sigma^2} \quad \dots (13)$$

where  $\Omega^{(2,2)*}(T^*)$  is a collision integral which has been tabulated (Hirschfelder, Curtiss and Bird, 1954) as a function of  $T^* = kT/\epsilon$ ,  $\sigma$  and  $\epsilon/k$  being the potential parameters in Å and °K respectively. When  $K_{mon}$  is known, the experimental value of the Eucken factor  $K_{exp}/K_{mon}$  can be calculated. In order to calculate  $K/K_{mon}$  from Hirschfelder's Eq (6),  $\delta_f$  was taken from the tables (Hirschfelder 1957a) and specific heat data were obtained from the recent Tables published by the National Bureau of Standards (1955). By knowing  $K_{exp}/K_{mon}$ , the experimental value of  $\delta_f$  may be calculated from Eq.(6) and the corresponding value of  $f_{int}$  from the relation  $f_{int} = 3/2\delta_f$ . Similar calculations were done for the data obtained by other workers. The results of these calculations are indicated in Table V.

In order to calculate  $K_{mix}$  from Eq. (9),  $K_{mix(mon)}$ ,  $D_{11}$ ,  $D_{12}$  were calculated on the Lennard-Jones (12 : 6) model from the expressions obtained on the Chapman-Enskog theory (Hirschfelder, Curtiss and Bird, 1954). The force constants were taken as those determined from viscosity data except in the case of Kr for

which the force constants determined by Saxena (1957) from thermal conductivity data were used. The results of these calculations are given in Tables VI-XIII.

TABLE V  
Eucken factor and  $f_{int}$  for  $H_2$

T°K	$K_{exp}$ given by	Eucken factor			$f_{int} = \frac{1}{2} \delta f$	
		$\frac{K_{exp}}{K_{mon}}$	$\frac{K/K_{mon}}{\text{from Eq. (6)}}$	$\frac{K/K_{mon}}{\text{from Eq. (4)}}$	From expt	From Table
303.2	Present Work	1.312	1.343	1.259	1.121	1.330
318.2	—do—	1.314	1.348	1.261	1.162	1.331
273.2	Keyes (1952)	1.289	1.326	1.251	1.155	1.328
300.2	Johnston & Grilly (1946)	1.286	1.345	1.259	1.103	1.330
320.2	—	1.288	1.348	1.262	1.112	1.331
311.2	Srivastava & Srivastava (1959)	1.296	1.344	1.259	1.142	1.331

In column 3,  $K_H$  is the value of  $K_{mix}$  calculated from Eq. (9) with the theoretical value of  $\delta_f$  and  $K'_H$  in column 4 are those obtained with the experimental value of  $\delta_f$ . For calculating  $K_{mix}$  from Eq. (10), viscosity data were used for  $H_2$ -He, and  $H_2$ -Ne and specific heat data for  $H_2$ -Kr and  $H_2$ -Xe. These calculated values are indicated as  $K_{MS}$  in column 5 of Tables VI-XIII. Columns 6 and 7 give the values of the Eucken-type factors for the mixtures  $K_{exp}/K_{mix(mon)}$  and  $K'_H/K_{mix(mon)}$ . The experimental values of  $K_{mix}$  were read from suitable interpolation graphs.

An interesting test of the algebraic form of Hirschfelder formula for the gas mixture may be made in the following way.

Eq. (9) may be written as

$$K_{mix} - K_{mix(mon)} = \frac{K_1 - K_{1(mon)}}{(x_2/x_1)(D_{11}/D_{12})} \quad (14)$$

or  $y = mx + C$

where  $y = 1/(K_{mix} - K_{mix(mon)})$ ;  $x = x_2/x_1$ ;  $m = (D_{11}/D_{12})/(K_1 - K_{1(mon)})$ ;

$$C = 1/K_1 - (K_{1(mon)})$$

so that a plot of  $y$  vs  $x$  should be a straight line. The  $y$ - $x$  values for the different gas mixtures have been given in columns 8 and 9 of the Tables VI-XIII and

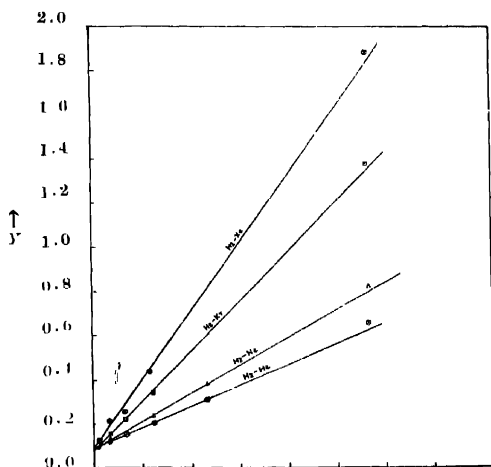


Fig. 3.  $x$ - $y$  graphs for  $H_2-He$ ,  $H_2-Ne$ ,  $H_2-Kr$  and  $H_2-Xe$  at  $30^\circ C$ .

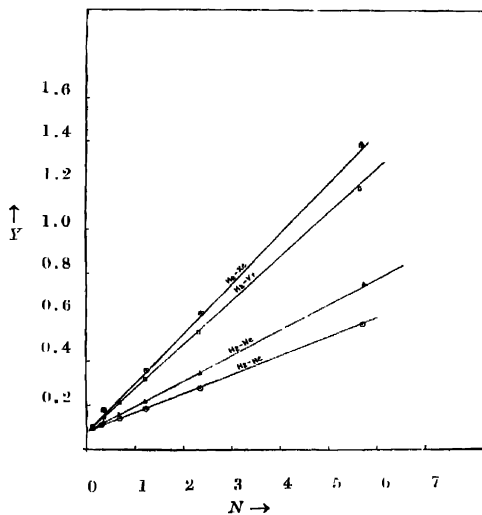


Fig. 4.  $x$ - $y$  graphs for  $H_2-He$ ,  $H_2-Ne$ ,  $H_2-Kr$  and  $H_2-Xe$  at  $45^\circ C$ .

are plotted in Figs. 3 and 4. The intercept on the  $y$ -axis gives the value of  $K_1$  and the slope gives the value of  $D_{11}/D_{12}$  from which  $D_{12}$  can be obtained by knowing  $D_{11}$ .

TABLE VI

Thermal conductivity and Eucken-type factor for  $H_2$ -He mixture at 30°C

% of He	$K_{exp} \times 10^5$	$K_H \times 10^5$ from Eq.(9)	$K'_H \times 10^5$ from Eq.(9)	$K_{MS} \times 10^5$ from Eq.(10)	$K_{exp}$ $K_{mix(mon)}$	$K'_H$ $K_{mix(mon)}$	$\eta$	$\alpha$
100	36.32	36.32	36.32	36.32	1.000	1.000		
85	36.80	37.12	37.06	37.01	1.038	1.046	0.719	5.666
70	37.44	37.58	37.45	37.86	1.096	1.096	0.306	2.333
55	38.29	38.55	38.36	38.88	1.145	1.148	0.206	1.223
40	39.45	39.80	39.55	40.05	1.195	1.199	0.155	0.667
25	40.96	41.37	41.06	41.39	1.246	1.249	0.123	0.333
10	42.73	43.25	42.88	42.88	1.293	1.298	0.103	0.111
0	43.30	44.42	43.20	43.20	1.312	1.312		

TABLE VII

Thermal conductivity and Eucken-type factor for  $H_2$ -He mixture at 45°C

% of He	$K_{exp} \times 10^5$	$K_H \times 10^5$ from Eq.(9)	$K'_H \times 10^5$ from Eq.(9)	$K_{MS} \times 10^5$ from Eq.(10)	$K_{exp}$ $K_{mix(mon)}$	$K'_H$ $K_{mix(mon)}$	$\eta$	$\alpha$
100	37.31	37.31	37.31	37.31	1.000	1.000		
85	37.92	38.07	37.95	38.13	1.045	1.046	0.599	5.667
70	38.60	38.73	38.47	39.11	1.105	1.101	0.275	2.333
55	39.55	39.77	39.62	40.25	1.157	1.160	0.186	1.223
40	40.88	41.12	40.82	41.56	1.212	1.210	0.140	0.667
25	42.57	42.79	42.47	43.03	1.264	1.261	0.113	0.333
10	44.46	44.89	44.56	44.57	1.304	1.307	0.097	0.111
0	44.75	46.03	44.75	44.75	1.314	1.314		

TABLE VIII

Thermal conductivity and Eucken-type factor for  $H_2$ -Ne mixture at 30°C

% of Ne	$K_{exp} \times 10^5$	$K_H \times 10^5$ from Eq.(9)	$K'_H \times 10^5$ from Eq.(9)	$K_{MS} \times 10^5$ from Eq.(10)	$K_{exp}$ ----- $K_{mix(mon)}$	$K'_H$ ----- $K_{mix(mon)}$	$y$	$x$
100	11.65	11.65	11.65	11.65	1.000	1.000	.	.
85	14.25	14.25	14.23	15.52	1.081	1.080	0.822	5.067
70	17.74	17.97	17.83	20.07	1.174	1.180	0.380	2.333
55	21.80	22.01	21.80	24.69	1.240	1.240	0.237	1.223
40	26.58	26.78	26.49	28.68	1.287	1.282	0.169	0.667
25	32.24	32.47	32.09	34.71	1.315	1.309	0.129	0.333
10	38.88	39.18	38.71	40.02	1.319	1.316	0.104	0.111
0	43.16	44.42	43.16	43.16	1.311	1.311	.	.

TABLE IX

Thermal conductivity and Eucken-type factor for  $H_2$ -Ne mixture at 45°C

% of Ne	$K_{exp} \times 10^5$	$K_H \times 10^5$ from Eq.(9)	$K'_H \times 10^5$ from Eq.(9)	$K_{MS} \times 10^5$ from Eq.(10)	$K_{exp}$ ----- $K_{mix(mon)}$	$K'_H$ ----- $K_{mix(mon)}$	$y$	$x$
100	12.00	12.00	12.00	12.00	1.000	1.000	.	...
85	14.94	15.06	15.00	16.10	1.098	1.102	0.752	5.667
70	18.59	18.68	18.57	20.91	1.185	1.183	0.345	2.333
55	22.71	22.87	22.69	25.81	1.246	1.245	0.223	1.223
40	27.81	28.00	27.74	30.03	1.292	1.289	0.159	0.667
25	33.52	33.72	33.39	36.43	1.321	1.316	0.123	0.333
10	40.56	40.68	40.37	42.09	1.340	1.334	0.0971	0.111
0	44.84	46.03	44.84	44.84	1.317	1.317	....	....

TABLE X

Thermal conductivity and Eucken-type factor for H<sub>2</sub>-Kr mixture at 30°C

% of Kr	$K_{exp} \times 10^5$	$K_H \times 10^5$ from Eq. (9)	$K'_H \times 10^5$ from Eq. (9)	$K_{MS} \times 10^5$ from Eq. (10)	$K_{exp}$ $K_{mix(mon)}$	$K'_H$ $K_{mix(mon)}$	$y$	$x$
100	2.256	2.256	2.256	2.265	1.000	1.000	.	.
85	4.602	4.903	4.876	5.324	1.168	1.216	1.390	5.667
70	9.016	8.299	8.240	8.901	1.264	1.299	0.597	2.333
55	12.20	12.53	12.43	13.36	1.311	1.336	0.345	1.223
40	17.62	17.95	17.80	18.96	1.343	1.338	0.224	0.607
25	24.84	25.13	24.72	26.18	1.345	1.344	0.155	0.333
10	35.02	35.25	34.97	35.75	1.346	1.344	0.111	0.111
0	43.21	44.42	43.88	43.21	1.312	1.312	.	.

TABLE XI

Thermal conductivity and Eucken-type factor for H<sub>2</sub>-Kr mixture at 45°C

% of Kr	$K_{exp} \times 10^5$	$K_H \times 10^5$ from Eq. (9)	$K'_H \times 10^5$ from Eq. (9)	$K_{MS} \times 10^5$ from Eq. (10)	$K_{exp}$ $K_{mix(mon)}$	$K'_H$ $K_{mix(mon)}$	$y$	$x$
100	2.347	2.347	2.347	2.347	1.000	1.000	.	.
85	5.160	5.281	5.246	5.510	1.195	1.214	1.191	5.667
70	8.600	8.775	8.695	9.310	1.280	1.294	0.531	2.333
55	12.86	13.15	13.01	13.99	1.317	1.334	0.322	1.223
40	18.31	18.74	18.54	19.83	1.350	1.352	0.217	0.667
25	25.66	26.04	25.76	27.35	1.351	1.358	0.156	0.333
10	36.40	37.60	36.50	37.32	1.355	1.359	0.105	0.111
0	44.79	46.03	44.79	44.79	1.315	1.315	.	.

TABLE XII

Thermal conductivity and Eucken-type factor for H<sub>2</sub>-Xe mixture at 30°C

$\frac{\%}{\text{of}}$ Xe	$K_{exp} \times 10^5$	$K_H \times 10^5$ from Eq. (9)	$K'_H \times 10^5$ from Eq. (9)	$K_{MS} \times 10^5$ Eq. (10)	$K_{exp}$ $K_{mix(mon)}$	$K'_H$ $K_{mix(mon)}$	$\eta$	$r$
100	1.261	1.261	1.261	1.261	1.000	1.000		
85	3.745	3.807	4.779	3.722	1.176	1.231	1.898	5.067
70	6.812	6.864	6.803	6.787	1.318	1.316	0.814	2.333
55	10.61	10.77	10.67	10.71	1.340	1.347	0.398	1.223
40	15.81	16.14	15.99	15.91	1.338	1.353	0.253	0.667
25	21.68	21.92	21.74	23.85	1.283	1.287	0.211	0.333
10	33.49	33.79	33.74	34.22	1.347	1.346	0.155	0.111
0	43.16	44.42	43.16	43.16	1.311	1.311		

TABLE XIII

Thermal conductivity and Eucken-type factor for H<sub>2</sub>-Xe mixture at 45°C

$\frac{\%}{\text{of}}$ Xe	$K_{exp} \times 10^5$	$K_H \times 10^5$ from Eq. (9)	$K'_H \times 10^5$ from Eq. (9)	$K_{MS} \times 10^5$ Eq. (10)	$K_{exp}$ $K_{mix(mon)}$	$K'_H$ $K_{mix(mon)}$	$\eta$	$r$
100	1.322	1.322	1.322	1.322	1.000	1.000		
85	3.936	3.988	3.931	3.916	1.245	1.243	1.293	5.667
70	7.062	7.191	7.066	7.142	1.315	1.316	0.590	2.333
55	11.05	11.27	11.06	11.26	1.345	1.346	0.353	1.223
40	16.31	16.71	16.40	17.61	1.348	1.355	0.238	0.667
25	23.58	24.13	23.68	24.24	1.349	1.355	0.164	0.333
10	34.35	35.12	34.48	35.25	1.336	1.342	0.116	0.111
0	44.77	46.03	44.77	44.77	1.315	1.315		

The values of  $K_1$  and  $D_{12}$  obtained from the graphs have been recorded in Table XIV together with the value of  $K_{1\text{exp}}$  and the values of  $D_{12}$  calculated on the Lenard-Jones (12 : 6) model.

TABLE XIV

Thermal conductivity and inter-diffusion coefficients from graphs

T°K	Gas Mixture	$K_1 \times 10^5$		$D_{12}$	
		from graph	from expt.	from graph	calculated on the $L-J$ (12:6) model
303.2	H <sub>2</sub> -He	43.79		1.332	1.592
	H <sub>2</sub> -Ne	43.65	43.20	1.143	1.152
	H <sub>2</sub> -Kr	43.45		0.654	0.724
	H <sub>2</sub> -Xe	42.87		0.021	0.618
318.2	H <sub>2</sub> -He	44.09		1.620	1.729
	H <sub>2</sub> -Ne	45.24	44.75	1.184	1.193
	H <sub>2</sub> -Kr	45.32		0.678	0.785
	H <sub>2</sub> -Xe	44.98		0.659	0.672

## DISCUSSION OF RESULTS

For pure H<sub>2</sub>, it may be seen from Table V, that all the experimental measurements of the thermal conductivity is consistently less than those given by Hirschfelder's Eq. (6) based on local chemical equilibrium assumption and so the experimental values of  $f_{int}$  are also less than the limiting value of  $\sim 1.3$ . This discrepancy between theory and experiments as has already been suggested (Srivastava and Barua, 1960) may be due to comparatively slow rate of rotational-translational transfer of energy. It is also to be noted that Waelbroeck and Zuckerbrodt (1958) have also reached the same conclusion from their measurements on the thermal conductivity of O<sub>2</sub> and H<sub>2</sub> down to very low pressures. Actual measurements (e.g. Stewart and Stewart, 1948) show that for H<sub>2</sub> about 1 collision out of 300 brings about a rotational-translational transfer of energy whereas practically every collision brings about a translational-translational transfer. On the other hand Eucken's derivation (i.e.  $f_{int} = 1$ ) is based on the assumption that the rotational-translational transfer rate is negligible. The actual cases are in between the conditions imposed upon by Hirschfelder's and Eucken's derivations. Hence it is to be expected that  $f_{int}$  should lie between 1 and 1.3 which is actually found to be so.

In Tables VI—XIII it can be seen that the calculated values of  $K_{mix}$  from Hirschfelder's Eq. (9) are always higher than the experimental values. At least a part of this disagreement must be due to the higher value of the thermal conductivity of pure H<sub>2</sub> given by the Hirschfelder's theory. When this is corrected for by taking the experimental value of  $K_1$  in calculating  $K_{mix}$ , it is seen that the agreement between the experimental and the calculated values of the mixture



conductivities becomes excellent. This points to the conclusion that Hirschfelder's Eq.(9) is capable of predicting correctly the concentration dependence of the mixture conductivities. A further support to this conclusion is given by the nearly straight line character of the  $x-y$  graphs for the various mixtures (Figs. 3 and 4). The approximate formula of Mason and Saxena (1958) Eq. (10) is found to represent the experimental data much worse than the more rigorous formula of Hirschfelder which is apparently due to the number of approximations made in the derivation of Eq. (10).

#### ACKNOWLEDGMENT

The author is grateful to Prof. B. N. Srivastava for his valuable guidance and keen interest in the work presented here.

#### REFERENCES

- Barua, A. K., 1960, *Physica* **25**, 1275.  
 Prokaw, R. S., 1958, *J. Chem. Phys.*, **28**, 391.  
 Chapman, S. and Cowling, T. G., 1952, *The Mathematical Theory of Non-uniform Gases*, Cambridge University Press.  
 Curtiss, C. F. and Hirschfelder, J. O., 1949, *J. Chem. Phys.*, **17**, 550.  
 Curtiss, C. F. and Muckenfuss, C., 1958, *J. Chem. Phys.*, **29**, 1273.  
 Eucken, A., 1913, *Phys. Zeit.*, **14**, 324.  
 Hirschfelder, J. O., 1957a, *J. Chem. Phys.*, **26**, 274, 282.  
 Hirschfelder, J. O., 1957b, Sixth International Symposium on Combustion, (Reinhold Publishing Corp., N.Y.), p. 351.  
 Hirschfelder, J. O., Curtiss, C. F. and Bird, R. B., 1954, *Molecular Theory of Gases and Liquids*, J. Wiley & Sons, N.Y.  
 Johnston, H. L. and Grilly, E. R., 1946, *J. Chem. Phys.*, **14**, 223.  
 Kennelink, W. G. and Martin, L. H., 1934 *Proc. Roy. Soc.*, **A141**, 144, *ibid.*, **A144**, 406.  
 Koyas, F. G., 1952 (April), *SQUID Tech. Rep.*, M.I.T.  
 Mason, E. A., 1958, *J. Chem. Phys.*, **28**, 1000.  
 Mason, E. A. and Saxena, S. C., 1958, *Phys. Fluids*, **1**, 301.  
 National Bur. of Standards (U.S.), 1955, *Circ.*, 561.  
 Saxena, S. C., 1957, *Ind. J. Phys.*, **31**, 404.  
 Schaler, K., 1943, *Z. Physik Chem.*, **B53**, 143.  
 Srivastava, B. N. and Barua, A. K., 1960, *J. Chem. Phys.*, **32**, 427.  
 Srivastava, B. N. and Srivastava, R. C., 1959, *J. Chem. Phys.*, **30**, 1200.  
 Stewart, J. and Stewart, E., 1948, *J. Acoust. Soc. Am.*, **20**, 21, 171.  
 Woolbroeck, F. and Zuckorbrodt, P., 1958, *J. Chem. Phys.*, **28**, 524.

## STATISTICAL STRUCTURE OF ANTHRONE

K. BANERJEE AND S. N. SRIVASTAVA,

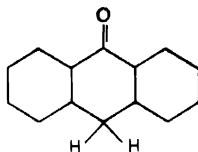
PHYSICS DEPARTMENT, ALLAHABAD UNIVERSITY, ALLAHABAD

(Received, March 22, 1960)

## Plate II

**ABSTRACT** The space group of anthrone was found by Srivastava to be  $P2_1/a$  with 2 molecules per unit cell. This requires a molecular centre of symmetry. The chemical formula of anthrone molecule does not possess any centre of symmetry. In the rotation photographs of anthrone crystal about the symmetry axis, there occur diffuse blackenings midway between layer lines. These are also corroborated by diffuse blackenings in appropriate positions in Weissenberg photographs. A statistical structure of anthrone crystal is proposed in order to explain these apparent anomalies.

Anthrone belongs to space group  $P2_1/a$  (Srivastava, 1957) with only two molecules per unit cell and having no symmetry centre in the structural formula.



Theoretically, such a situation is untenable, but very long exposure such as 130 hrs. at 30KV, 25 mA failed to show any exception to the systematic absences on which the space-group determination was based. Moreover, there appeared diffused layer lines in between the regular layer lines when the crystal was rotated about the symmetry axis  $b$ , (Fig. 1).

The position of these diffused layers were such as would have been occupied by the odd regular layer lines had the  $b$  axis been double. A Weissenberg photograph for the same rotation axis in which the first of such diffuse layer is allowed through is given in Fig. 2. In this photograph the diffuse reflections are brought clearer.

One would naturally be tempted to assume a unit cell of double this size so that the unit cell may contain four molecules, which is also the necessary number of asymmetric units needed for this space group. With the undoubled cell, the consecutive molecules along  $b$  axis should be identical as they are derived

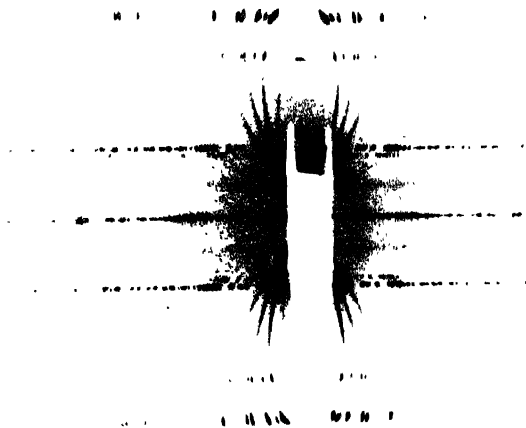


Fig. 1. Rotation about  $b$ -axis



Fig. 2. Weissenberg photograph of the first diffuse layer line



by transh but in the doubled cell it is possible to assume the position of O interchanged with H H' in the adjacent molecule. With such picture can see that the contribution for  $hkl$  planes, where  $k$  is odd, can come only from the difference in the scattering powers of an oxygen atom and two hydrogen atoms attached to D and D' respectively (Fig. 1).

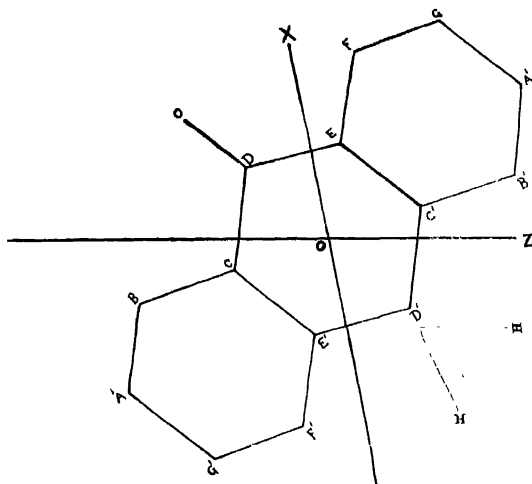


Fig. 3 (The symbol O refers to the oxygen atom and all other letters refer to carbon atoms.)

One could imagine that due to some loose bonding occurring among the O and 2H of the consecutive anthrone molecules along the  $b$  axis their bonding with the carbon atoms to which they are attached might be weakened considerably, resulting in large thermal vibrations of this group of oxygen and hydrogen atoms. This should cause irregularities in arrangements of those atoms. This deviation from regular arrangement may be argued as reason for the appearance of diffuse layer lines for  $k$  odd values. But the diffuseness that is observed is of a much higher order than one would expect from thermal oscillations about certain mean positions. Further, diffuseness if caused in that way would also be found in spots on the regular layer lines, which is against observation. The only possible structure that can explain the facts is that of random interchange between O and 2H atoms attached to the D and D' carbon atoms. The structure is similar to that of anthraquinone with half of the oxygen atoms replaced by 2H atoms. The phenomenon is thus quite akin to that of order-disorder phenomenon in alloys. Thus each molecule of anthrone can now be considered

statistically to have half of oxygen and half of H, H' attached to the D carbon atom and the other half to D' for the purpose of calculating the structure factor for the sharp reflections. Consequently, the centre of symmetry that is necessary to be assumed to explain the X-ray diffraction spots is a statistical effect in which the oxygen and the hydrogen pair interchange positions in a random way keeping the statistical ratio the same.

The diffraction effect of such a structure can be visualised in the following way. The anthrone molecules less the oxygen and hydrogen atoms in the positions in question are arranged in the regular lattice corresponding to the space-group  $P2_1/a$  and hence will give rise to diffraction maxima sharply only in the directions satisfying Laue equations corresponding to this space-group. An oxygen atom and a pair of hydrogen atoms are thus left over corresponding to each molecule. Had there been complete randomness these oxygen and hydrogen could give rise to some general scattering. The diffuse layers in between the regular layer lines show that there must be a preponderance of a periodicity double the axis length  $b$ . This can happen if the oxygen atoms as well as the hydrogen pairs have a tendency to face similar atoms rather than those of the opposite kind or that the anthrone crystal consists of a 1 : 1 combination of anthraquinone and 9, 10-dihydro-anthracene and occur at random throughout the structure while maintaining the basic lattice as given above and the proportion statistically with a considerable bias for the two types occurring in alternate layers. The first alternative is, however, improbable as it would mean that the attractions between the two oxygens and also of the two hydrogen pairs of the neighbouring molecules should be stronger than those between the oxygen of one molecule with the hydrogen pair of its neighbour. The second alternative, therefore, seems to be the correct solution. The intensity distributions in the diffuse layers are being studied with a view to knowing the domains of regularities and the nature of their distributions. The structure of 9, 10-dihydro-anthracene crystal is also under investigation as it is expected that it should have an isomorphous structure with anthraquinone, if our conclusions are correct.

#### REFERENCE

Srivastava, S. N., 1957, *Ind. J. Phys.*, **31**, 644.

# OPTIMUM CONDITIONS TO OBSERVE THE NEW LIGHT EFFECT\*

P. S. V. SETTY

NATIONAL RESEARCH FELLOW, DEPARTMENT OF PHYSICS, CENTRAL COLLEGE, BANGALORE

(Received, October 3, 1950; after revision, February 25, 1960)

**ABSTRACT.** Some experimental results with electrodeless discharge tubes containing iodine vapour are conducted with special reference to ageing. The results have shown that the effect of ageing is only the removal of occluded gases and vapours from the glass wall of the discharge tube. As a consequence of these experiments a new apparatus called the 'envelope tube' has been devised to obtain consistent results without waiting for ageing. From these results the optimum conditions for observing the new light effect have been worked out to be (a) ageing the envelope tube under low external pressure or heating it to a high temperature in vacuum till standard current voltage characteristics as shown are obtained; (b) sealing it under the above condition.

However, the cleaning up procedure recommended in this paper refers only to the external surface of the discharge tube.

## 1. INTRODUCTION

A glance through the vast literature on the new light effect discloses that consistent results have not been observed for the same substance by different experimenters. It might also be noted that none of the workers in that field has stated precisely the optimum conditions under which the effect can be observed. Moreover, the standard forms of the current voltage characteristics have not been worked out. In the present paper the inconsistency of results has been traced to the influence of occluded gases and water vapour in the glass wall of the discharge tube.

It has been observed that ageing of the discharge tube influences the effect considerably, sometimes increasing (Joshi and Bhat, 1942 and Deo, 1944) the percentage effect and sometimes reducing (Arnikar, 1944) it. In the case of mercury vapour (Prasad and Venkateswarlu, 1949) even ageing of the discharge tubes for a long period of 424 hours could not show any light effect, whereas one discharge tube with a preliminary heating upto 200°C. for 4 hours gave an effect of 60%. This shows that ageing alone is not sufficient for observing the effect. Secondly, while investigating the new light effect, it has been observed very often, that the discharge tubes which exhibited a good light effect suddenly became inactive under certain external conditions.

---

\* Communicated by Prof. N. R. Tawde.

The present paper concerns itself with the study of conditions under which reproducible and steady light effect can be observed. The necessary optimum conditions have been found to be (1) 'ageing' which is a cleaning up of the external surface of the discharge tube to remove the occluded water vapour as a result of passing the discharge for a long time through the tube and (2) securing a dry atmosphere surrounding the experimental tube.

## 2. INVESTIGATION OF OPTIMUM CONDITIONS

### (a) *Experiments on humidity :*

A glass chamber was used in these experiments. Anhydrous calcium chloride granules were placed inside the chamber. A small paper hygrometer (Edney) was also placed inside the chamber. By adjusting the quantity of calcium chloride, the percentage humidity inside the glass chamber could be maintained at any required value. The discharge tube containing iodine vapour, at saturated vapour pressure (3 mm of mercury at 40°C), fitted with external sleeve electrodes was placed inside such a chamber. The saturated iodine vapour pressure was maintained by sealing the discharge tube with some solid iodine inside it. A 500 Watt incandescent lamp kept inside a projection lantern at a distance of 6 feet was used for irradiating the discharge tube. Precautions were taken to see that the intensity of light emitted was constant throughout the experiment. The light effect was observed with varying humidity of the air surrounding the discharge tube. The  $\Delta i$  values i.e. the difference between the current in dark and current under light were studied. The results are shown in Fig. 1.

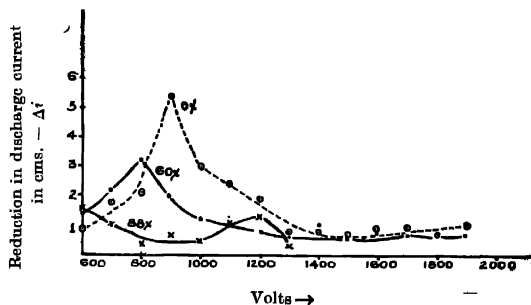


Fig. 1. Negative light effect under different humidity conditions.

The results in general have shown that the light effect and the voltage limits, in which this light effect occurs, increase as the percentage humidity of the surrounding air decreases. This shows the profound influence of humidity on the light effect.



(b) *Bell-jar experiments :*

A discharge tube containing iodine vapour at its saturated vapour pressure (3mm of Hg at 40°C) was fitted with two sleeve electrodes, of a few turns of copper wire each, kept at about 5 cm apart. This discharge tube was suspended inside a bell-jar of volume 4000 cc. by means of two copper wires connected to the sleeve electrodes. The bell-jar was kept on a bed plate with arrangements for removing air from or introducing dry air into the bell-jar.

To dry the atmospheric air a system consisting of drying agents, anhydrous calcium chloride, concentrated sulphuric acid, and phosphorus pentoxide in series was rigged up. The air, after passing through these drying agents, was introduced into the bell jar whenever necessary.

A Cenco hyvac pump was used to evacuate the bell-jar

A paper hygrometer (Edney) which gave the relative humidity of the air directly was kept inside the bell-jar to read the humidity. A mercury manometer was attached to the system to read the pressure inside the bell jar

### 3. EXPERIMENTAL PROCEDURE AND RESULTS

The experiment consisted in removing the humid air from inside the bell-jar and filling it again with dry air whenever necessary. Under these conditions readings for the light effect were taken using the conventional circuit. The results of a typical experiment are given below in Table I.

TABLE I

Date	Time	Ageing	% Humidity	Maximum % light effect	Remarks
20-10-58	1 00 P.M.	—	53	Nil	No effect
„	1 30 P.M.	30 Min.	53	Nil	„
„	1 40 P.M.	—	0 (Dry air)	18	Small & irregular
„	2 15 P.M.	15 Min.	0	15.4	Fairly regular
30-10-58	12 Noon	—	25	16.6	Small & regular
31-10-58	12 Noon	—	30	12	„
„	1 15 P.M.	75 Min.	30	12	Not good
„	3 00 P.M.	—	20	18	Better results
1-11-58	12 Noon	—	24	16	„
„	1 30 P.M.	90 Min.	24	23	„
„	2 00 P.M.	Kept under low atm. pr. for 30 Min.	—	26	„
4-11-58	12 Noon	—	0 (Dry air)	23	„

At this stage the maximum improvement of the light effect by the reduction of humidity alone was reached. In order to remove occluded water vapour the pressure of air in the bell-jar was reduced, from 68 cm of Hg to 8 cm of Hg, in steps of 10 cm of Hg and at each step the readings for light effect were taken. As the pressure of the air decreased the light effect was found to improve gradually. After each series of experiments the bell-jar was filled with dry air. This experiment was repeated for about 3 or 4 days. By then the discharge tube had developed a large and regular light effect. The experimental results after this date are given in Table II.

TABLE II

Date	Time	% Humidity	Maximum % light effect	Remarks
7-11-58	12 Noon	0 (Dry air)	52	Large & regular
12-11-58	"	30	61	A bit irregular
14-11-58	"	0 (Dry air)	65	Large & regular
17-11-58	2.00 P.M.	23.5	50	Reduced
"	3.00 P.M.	0 (Dry air)	68	Better results
18-11-58	12 Noon	0	69	"
19-11-58	"	0	65	"
21-11-58	"	26	69	Consistent reproducible results (shown in Fig. 3).

The current voltage characteristic and the  $\Delta i$  voltage characteristic as obtained till November 19, 1958 are shown by a set of typical curves in Fig. 2.

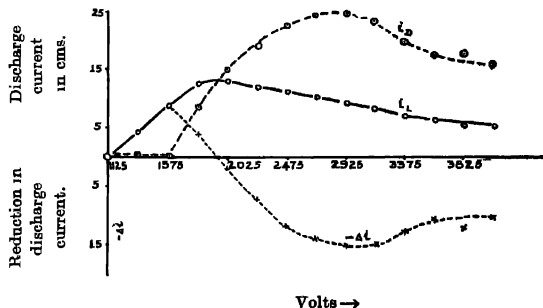


Fig. 2. Characteristic curves not under optimum conditions.

The readings for light effect taken after reaching the steady state showed a definite change in current voltage characteristics giving the standard forms of these curves. They are shown in Fig. 3 from which it is obvious that an ageing process extended over about a fortnight enabled consistent results to be obtained with the tube inside the bell-jar. It is interesting to note that when the discharge tube was removed from the bell-jar the same characteristics could not be obtained.

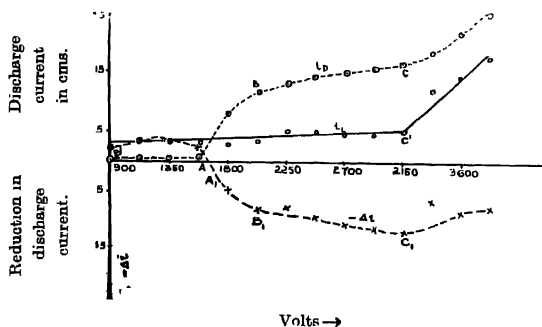


Fig. 3. Characteristic curves under optimum conditions.

The above account shows that consistent results can be obtained by the removal of occluded water vapour from the walls of the discharge tube after a tedious process extending over a large period. To obviate this difficulty a new apparatus was devised which may be called 'envelope tube' whose description and working is given below.

#### 4 ENVELOPE TUBE EXPERIMENT

A short note giving a preliminary description of the envelope tube and its working was published recently (Setty, 1959). The discharge tube (Fig. 4) is a co-axial double tube in which the space between the inner and the outer could be evacuated while the inner tube serves as the discharge tube. The sleeve

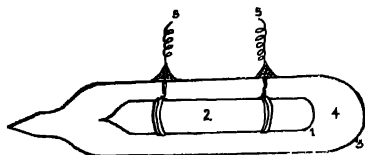


Fig. 4. Envelope Tube.

- (1) Discharge tube. (2) Iodine vapour. (3) Envelope. (4) Perfectly dry air in between discharge tube and envelope (5) Electrodes.

electrodes wound round the discharge tube were brought out by sealing them through the glass envelope. The whole apparatus was heated to a temperature

of 400°C and the envelope was evacuated using an oil diffusion pump for sufficient period and then refilled with dry air to the required pressure and sealed off. In some tubes the space was left as a vacuum. After the discharge tube cooled to the room temperature it was tried for the light effect. Results obtained with both types of tubes agree. A typical result obtained under these conditions is given in Fig. 5 which resembles Fig. 3 pertaining to bell-jar experiments in every respect.

## 5. EXPERIMENTAL RESULTS

A comparison of Figs. 3 and 5 shows that both of them are almost identical. But a distinct difference is observed between these and results in Fig. 2.

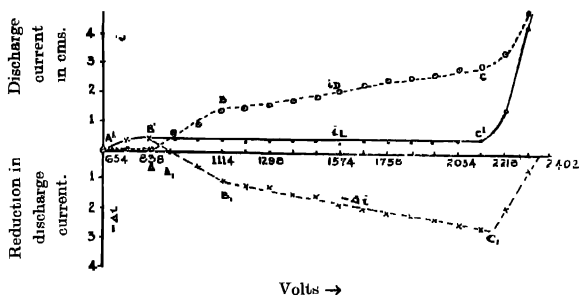


Fig. 5 Characteristic curves under optimum conditions with envelope tube.

In Fig. 2 all the characteristics ( $i_D$ ,  $i_L$  and  $-\Delta i$ ) start at some particular voltage and reach a maximum at a higher voltage beyond which they diminish considerably.

In Figs. 3 and 5 the characteristic  $i_D$  starts at a particular voltage  $A$ , increases rapidly upto a higher voltage  $B$ , beyond which the increase is gradual throughout the voltage up to  $C'$ . After this point  $C'$  the characteristic  $i_D$  suddenly shoots up. The characteristic  $i_L$  starts at a particular voltage  $A'$ , increases rapidly upto a higher voltage  $B'$  beyond which it is almost parallel to  $X$  axis till the point  $C'$ . After the point  $C'$  this also shoots up and meets  $i_D$  characteristic. Thus  $i_D$  and  $i_L$  do not show any tendency of diminishing at any voltage.

$-\Delta i$  characteristic starts at a particular voltage  $A_1$ , increases rapidly upto the point  $B_1$  beyond which the increase is gradual upto  $C_1$ . But after  $C_1$  it suddenly diminishes and meets the  $X$  axis showing the absence of light effect.

## 6. DISCUSSION

The first set of experiments with the tube inside the glass chamber reveals that the humidity of the atmosphere surrounding the tube brings down the light

effect in accordance with Fig. 1. It is clear from Fig. 1 that the maximum value of the negative light effect ( $-\Delta i$ ) goes on decreasing with the increase of the percentage humidity of the surrounding atmosphere. The second peak for 88% humidity at 1200 volts is a non-repeatable one, showing that the conditions for observing the light effect are not optimum. The second set of experiments points out the influence of gases and vapours occluded in the walls of the discharge tube, the results on the releasing of which is indicated in Figs. 2 and 3. The curves in Fig. 2 establish beyond doubt that as the occluded gases and vapours are removed from the walls of the discharge tube, the light effect observed not only goes on increasing but the voltage limits in which it occurs also increase enormously. That the process of ageing heats the discharge tube is supported by Mackinnon (1928) and Viswanathan (1951). That the occluded gases and

TABLE III

Percentage light effect observed with the Envelope Tube at different intervals

Volts	% light effect			
	11-2-59 (I)	11-2-59 (II)	19-2-59	25-2-59
1001	54.5	44.4	—	38.0
1092	69.7	63.0	50.0	60.0
1183	70.0	69.7	59.3	68.0
1274	73.5	74.4	63.0	71.4
1365	74.5	70.8	65.5	73.8
1456	75.5	74.5	67.0	75.2
1547	76.0	78.4	70.5	74.4
1638	78.4	78.0	71.6	74.0
1729	76.8	75.4	75.0	74.0
1820	75.4	72.9	75.7	71.4
1911	75.0	73.0	76.0	69.4
2002	74.0	71.7	79.4	72.0
2093	74.3	73.6	80.5	71.7
2184	67.0	69.0	77.4	70.0
2275	45.8	39.0	67.4	67.6
2366	0	0	53.2	53.1
2457	0	0	0	0

vapours are liberated when heated in vacuum is supported by Jnanananda (1947) Hence it might be gathered that the removal of water vapour and occluded gases is a pre-requisite for obtaining consistent results in light effect experiments. Reproducibility of results becomes difficult because one has to wait for ageing each time the experiment is started.

The new apparatus devised remove the above difficulty of ageing once and for all. The envelope tube can be used at any time and consistent results are obtained without any preliminary drying or ageing. The consistency of the results are considered here only from the point of view of the form of the curves and not from the voltage characteristics as the thickness of the wall of the discharge tube may interfere with the voltage. The readings of the percentage light effect observed with the envelope tube at different intervals but under the same experimental conditions shown in Table III clearly indicate that the results are consistent.

It is suggested that much of the previous work (Joshi and Bhat, 1942, Arnikar, 1949; Deo, 1944, Prasad and Venkateswarlu, 1949; Joshi and Kuppuswamy, 1941, Joshi and Deshmukh, 1942; Joshi and Murty, 1942, and Gopalaswamy and Viswanathan, 1949) yielding somewhat contradictory results be repeated with this new apparatus so that a theoretical explanation of the light effect becomes possible.

Thus the optimum conditions for the observation of the new light effect in A/C silent discharges are the following :

1. The envelope tube should either be aged under low external pressure or heated in a vacuum till it gives most likely the standard characteristics as shown in Fig. 5
2. Under the above condition the envelop is sealed with a perfectly dry air at the required pressure or sealed with a perfect vacuum.

#### 7. ACKNOWLEDGMENT

Author's grateful thanks are due to Prof. S. B. Bondade for his kind help, encouragement and interest in the work. The author also wishes to take this opportunity of expressing his gratitude to Sri H. K. Vittal Rao for preparing the necessary discharge tubes, to Sri H.S. Venkataramiah for his valuable suggestions and to the Ministry of Scientific Research and Cultural Affairs for awarding a National Research Fellowship to him.

#### REFERENCES

- Arnikar, H. J., 1949, *Proc. Indian Science Congress, Part III*, p. 16.  
 Deo, P. G., 1944, *Proc. Ind. Acad. Sci.*, **A21**, 77.  
 Gopalaswamy, N. and Viswanathan, K. S., 1949, *Proc. Indian Science Congress, Part III*, p. 48.

- Jnanananda, 1947, "High Vacua", D. Von Nostrand Company Inc., New York, pp. 129 & 294.
- Joshi, S. S. and Kuppaswamy, 1941, *Proc. Indian Science Congress*, Part III, p. 54.
- Joshi, S. S. and Bhat, N. M., 1942, *Proc. Indian Science Congress*, Part III, p. 65.
- Joshi, S. S. and Deshmukh, 1942, *Proc. Indian Science Congress*, Part III, p. 31.
- Joshi, S. S. and Murthy, 1942, *Proc. Indian Science Congress*, Abst. No. 67.
- Mackinnon, 1928, *Phil. Mag.*, **8**, 605.
- Prasad, B. N. and Venkateswarlu, V., 1949, *Proc. Indian Science Congress*, Part III, p. 23.
- Setty, P. S. V., 1959, *Quar. Sci.*, **28**, 195.
- Viswanathan, *et al.*, 1951, *J. Sci. Res., B.H.U.*, **2**, 80

# Letters to the Editor

The Board of Editors will not hold itself responsible for opinions expressed in the letters published in this section. The notes containing reports of new work communicated for this section should not contain many figures and should not exceed 500 words in length. The contributions must reach the Assistant Editor not later than the 15th of the second month preceding that of the issue in which the paper is to appear. No proof will be sent to the authors.

## 5

### ABSORPTION SPECTRA OF *O*-, *M*-and *P*-HYDROXY-BENZALDEHYDES

I. ACHYUTA RAO AND V. RAMAKRISHNA RAO

DEPARTMENT OF PHYSICS, ANDHRA UNIVERSITY, WALTAIR

(Received, January 29, 1960)

The near ultraviolet absorption spectra of ortho, meta and para hydroxy benzaldehydes have been studied in the vapour phase. Earlier workers (Morton and Stubbs, 1940) studied mainly the absorption spectra of their solutions in various solvents and reported band data for the vapour spectra also, but no vibrational analysis was made.

In the present work, two systems of bands have been observed in each of the ortho and meta isomers (only one system of bands was reported earlier (Morton and Stubbs, 1940) and one system in the para isomer, in the regions indicated below :

Ortho :—3630—3270A (System I)  
          2670—2330 A (System II)  
Meta :— 3125—2890A (System I)  
          2500—2395A (System II)  
Para :— 2915—2660A

The band data also have been extended and a systematic vibrational analysis has been made.

*Ortho* : In System I about fifty bands are measured. The 0, 0 band is chosen at 3537.6A ( $28260\text{ cm}^{-1}$ ). The bands are interpreted on the basis of three (269, 426 and  $558\text{ cm}^{-1}$ ) ground state fundamentals and seven (263, 410, 523, 671, 937, 1013 and  $1201\text{ cm}^{-1}$ ) upper state fundamentals.

In System II about One hundred and thirty bands are measured (only thirty-three were reported earlier) . The 0, 0 band is chosen at 2524.6A ( $39598\text{ cm}^{-1}$ ).



The bands are interpreted on the basis of seven (263, 437, 562, 776, 1032, 1232 and 1689  $\text{cm}^{-1}$ ) ground state fundamentals and eight (245, 440, 518, 763, 943, 1161, 1198 and 1503  $\text{cm}^{-1}$ ) upper state fundamentals.

*Meta* : In System I about twenty-five bands are measured. The 0,0 band is chosen at 3092A (32332  $\text{cm}^{-1}$ ). The bands are interpreted on the basis of one (249  $\text{cm}^{-1}$ ) ground state fundamental and three (189, 392 and 947  $\text{cm}^{-1}$ ) upper state fundamentals.

In System II about thirty bands are measured (only nine were reported earlier). The 0,0 band is chosen at 2478Å (40343  $\text{cm}^{-1}$ ). The bands are interpreted on the basis of one (243  $\text{cm}^{-1}$ ) ground state fundamental and six (213, 428, 494, 628, 814 and 967  $\text{cm}^{-1}$ ) upper state fundamentals

*Para* : In this case only one system was found. About thirty bands are measured (only eleven were reported earlier). The 0,0 band is chosen at 2836A (35251  $\text{cm}^{-1}$ ). The bands are interpreted on the basis of three (394, 635 and 861  $\text{cm}^{-1}$ ) ground state fundamentals and eight (174, 326, 529, 787, 996, 1142, 1181 and 1267  $\text{cm}^{-1}$ ) upper state fundamentals.

The upper state and lower state fundamentals observed in the three isomers have been correlated with the Raman data reported by Kohlrausch (1938).

Details will be published shortly

#### REFERENCES

- Kohlrausch, K. W. F., 1938, *Zeits. Physik. Chem.*, **38**, 119  
Morton, R. A. and Stubbs, A. L. 1940, *J. Chem. Soc.*, 1347.

## INDUCED LIGHTNING STROKES

S. D. CHATTERJEE AND B. K. DUTTA

DEPARTMENT OF PHYSICS, JADAVPUR UNIVERSITY, CALCUTTA-32

(Received, March 11, 1960)

The mechanism of direct cloud-to-ground lightning strokes have been extensively studied by Schonland (1950), McEachron (1939) and others from photographs taken with modified Boys camera. The surges of direct lightning strokes to the power and telephone lines, and induced effects due to charge induced on the line by an overhead thundercloud have also been subjected to careful analysis by Peek (1924). And yet direct photographic evidences of induced lightning strokes are rare.

During the monsoon season at Calcutta, two interesting still shots of induced lightning strokes were taken from the same spot on two consecutive evenings. It appears that the local terrain produces great localised variations in storm and lightning-stroke density.

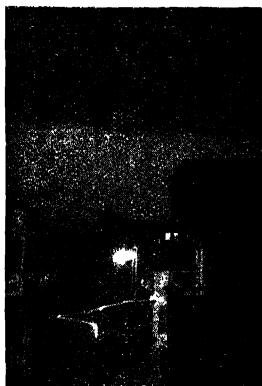


Fig. 1: Two cloud-to-ground direct lightning strokes accompanied by a fencing post-to-ground induced lightning stroke. Sprouting positive streamers on the ground.

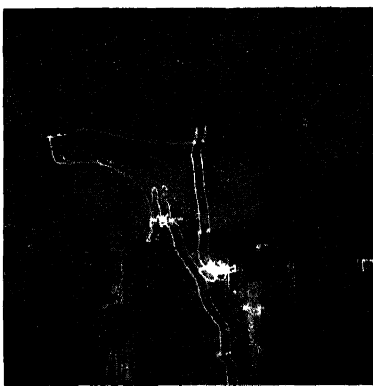


Fig. 2: Induced double lightning stroke from two incandescent lamps mounted on lamp posts to the ground. Faintly luminous tracks of an earlier double flash over in the background. Zig-zag "St. Elmo's fire" from a receiving aerial on the roof of a double storeyed building on the right.

Fig. 1 depicts two cloud-to-ground direct strokes accompanied by an induced stroke which links a barbed-wire-fencing post with the ground. The high luminosity of the latter suggests that it is probably a return stroke which follows the junction of a stepped leader with a positive streamer coming from the ground. Some faint points of luminiscence on the ground in the neighbourhood of the flash may be other sprouting positive streamers which failed to connect with the leader.

Fig. 2 shows a tantalizing photograph, which was taken on the second evening amidst a crescendo of lightning flashes and peels of thunder, occurring within a couple of hundred feet of the camera. It seems that a violent, swiftly oncoming storm, unaccompanied by rain, induced a heavy charge density upon the ground surface. As the magnitude of the ground gradient rapidly increased, the accumulated electric stress between the ground and two street lamps caused almost simultaneously a double flash-over. The electric lamps were mounted on two eighteen feet high steel posts carrying overhead supply lines and were situated at a distance of ninety feet from each other. An earlier double flash-over between the ground and two other incandescent electric lamps protruding from the walls of a building is revealed by a faintly luminous double streak in the background. Presumably the earlier flash-over had taken place within 0.5 second before the opening of the camera shutter. Malan and Collens (1938) have reported data on luminiscence of heavy discharges whose duration ranges in extreme cases from a few hundred microseconds to half a second. Although the electrostatic lines of force from the origin of the stroke to the ground should form essentially smooth curves, the picture shows tortuous paths interspersed with loops. These may be attributed to some variable condition at the head of the discharge, this condition being either variations in the head itself or variations in space ionization. However, the strict parallelism of the two sets of double strokes indicate preponderance of the latter factor. It is indeed amazing that even the corona or "St. Elmo's fire" emanating from a receiving aerial on the roof of a right-hand-side building exhibits an analogous zig zag pattern.

Assuming 5000 volts per cm as a fairly acceptable value (Creighton, 1937) for the average gradient at the surface of the earth for spark-over between two sharp points, the maximum induced potential on each of the street lamps should be about two million volts, while that on the verandah lamps about half of this value. Nevertheless, the length of the individual luminous paths indicates that the induced voltage is of the order of 12 million volts.

#### REFERENCES

- Creighton, E. E. F., 1937, *A.I.E.E. Lightning reference book*, 106.  
Malan, D. J. and Collens, E. E. F., 1938, *Proc. Roy. Soc., A*, **164**, 132.  
McEachron, K. B., 1939, *Jour. Frank. Inst.*, **227**.  
Peck Jr. F. W., 1924, *Transactions A.I.E.E.*, **48**, 1205.  
Schonland, B. F. G., 1950, "The flight of thunderbolts", Clarendon Press, Oxford.

# THE NEAR ULTRAVIOLET ABSORPTION SPECTRA OF *M*-and *P*-METHYL ANISOLES

K. V. KAMESWARA RAO AND V. RAMAKRISHNA RAO

DEPARTMENT OF PHYSICS, ANDHRA UNIVERSITY

(Received, January 29, 1960)

The near ultraviolet absorption spectra of meta- and para methyl anisoles were investigated in the vapour, liquid and solid phases.

*m*-Methyl anisole. In vapour absorption about 45 bands were measured and the intense band at  $2773.3 \text{ \AA}$  ( $36048 \text{ cm}^{-1}$ ) was taken as the (0, 0) band. The spectrum could be interpreted on the basis of seven fundamental frequencies in the upper state (210, 676, 824, 952, 1092, 1164 and  $1228 \text{ cm}^{-1}$ ) and two fundamentals in the ground state (206, and  $725 \text{ cm}^{-1}$ ). There is agreement with Raman data reported by Reitz and Ypsilanti (1935).

In liquid absorption four bands were obtained and the intense band at  $2807 \text{ \AA}$  ( $35615 \text{ cm}^{-1}$ ) was taken as the (0, 0) band. The spectrum could be interpreted on the basis of one upper state fundamental  $911 \text{ cm}^{-1}$ .

In solid absorption three bands were obtained and the intense band at  $2805 \text{ \AA}$  ( $35640 \text{ cm}^{-1}$ ) was taken as the (0, 0) band. The spectrum could be interpreted on the basis of one upper state fundamental  $926 \text{ cm}^{-1}$ .

*p*-Methyl anisole. In vapour absorption about 32 bands were measured and the intense band at  $2824.1 \text{ \AA}$  ( $35399 \text{ cm}^{-1}$ ) was taken as the (0, 0) band. The spectrum could be interpreted on the basis of six fundamentals in the upper state (379, 480, 544, 789, 1176 and  $1259 \text{ cm}^{-1}$ ) and two fundamentals in the ground state (530 and  $839 \text{ cm}^{-1}$ ). There is agreement with Raman data reported by Reitz and Ypsilanti (1935).

In liquid absorption two bands were obtained and the intense band at  $2869 \text{ \AA}$  ( $34845 \text{ cm}^{-1}$ ) was taken as the (0, 0) band. The other band was interpreted as the upper state fundamental  $795 \text{ cm}^{-1}$ .

In solid absorption about ten bands were obtained and the intense band at  $2872 \text{ \AA}$  ( $34809 \text{ cm}^{-1}$ ) was taken as the (0, 0) band. The spectrum could be interpreted on the basis of two upper state fundamentals (780 and  $1229 \text{ cm}^{-1}$ ).

The details will be published shortly.

## REFERENCE

Reitz, A. W. and Ypsilanti, G. P., 1935, *Monats. Fur. Chem.*, **66**, 304.

## BOOK REVIEWS

ADVANCES IN CHEMICAL PHYSICS, VOLUME II. Edited by I. Prigogine.  
Pp. 412+viii. Interscience Publishers, New York; London, 1959. Price  
\$11.50.

This volume consists of nine articles on different topics contributed by different authors. The first article entitled Clathrate solutions contributed by J.H. Van der Waals and J. C. Platteeuw starts with the discovery and designation of these compounds and then gives a statistical theory of formation of the compounds. The third section deals with hydroquinone clathrates in binary and tertiary systems. The article includes a list of 58 references.

The second article by K. S. Pitzer is on inter- and intra-molecular forces and molecular polarizability. Wave mechanical theory for many-electron systems has been discussed first and the results predicted by the theories have been next compared with experimental results. Finally, intramolecular applications and anisotropic effects have been dealt with in detail. The list of references includes 42 papers.

The third article by J. S. Rowlinson and M. J. Richardson deals with solubility of solids in compressed gases. Recent work on 17 simple systems has been discussed in detail and a brief outline of the theory has been given. A list of 90 references has been included at the end of the article.

In the fourth article entitled 'Thermodynamics of metallic solutions' R. A. Oriani has reviewed the work done in this line since the discovery of superlattices in 1919. A list of 71 references has been given in this article.

The fifth article by M. Szwarc deals with recent advances in polymer chemistry. The topics discussed are Addition polymerization, Initiation of polymerization, Propagation of polymerization and Termination. A list of 57 references has been included.

The sixth article entitled Nuclear Quadrupole Resonance in Irradiated Crystals contributed by Jules Duchesne deals mainly with the effect of high energy radiation on solids as studied by quadrupole resonance. A list of 34 references is included in this review.

The seventh review by Per-olov Löwdin deals with correlation problem in Many-Electron Quantum Mechanics. This is a lengthy review covering a wide field of theoretical work in this line. Starting with Schrodinger Equation for an electronic system, the article deals with the effect of two-particle repulsion and

then gives in detail the Hartree-Fock scheme. The theory is then applied to specific cases, such as, He, alkali metals, etc. Extended Hartree-Fock scheme for constructing pure spin functions has also been discussed. The article includes a list of 42 references.

The eighth article is also of the same title in which Hiroyuki Yoshizumi has made a bibliographical survey of the historical development of the subject

In the last article by Bright Wilson Jr. "the Problem of Barriers to Internal Rotation in Molecules" has been discussed and different methods for the measurement of the potential barriers have been described. A list of 35 references has been given in this review.

It can be seen from the above paragraphs that the book is extremely useful to physicists as well as chemists interested in the modern theories about the different phenomena covered in the articles

S. C. S.

ADVANCES IN SPECTROSCOPY, VOLUME I. Edited by H. W. Thompson. Pp 363+viii. 15cm×23cm. Interscience Publishers Inc., New York, 1959. Price \$ 12.50.

This volume contains eight articles reviewing work done in eight different selected lines of research in spectroscopy. The review entitled "The spectra of polyatomic free radicals" by D. A. Ramsay deals with the different methods of producing free polyatomic radicals. The spectrograms of a few such radicals have been reproduced in this article. The results of analysis of a large number of triatomic and a few polyatomic free radicals have been discussed in details. An exhaustive list of references has been given at the end of the review.

In the review of work on "Spectroscopy in the vacuum ultraviolet" written by W. C. Price the author has dealt with the experimental arrangement for studying the spectra in this region of atoms and molecules and a list of references has been given. No discussion of experimental results has been included in this review.

D. H. Rank has briefly discussed in two separate articles the Index of refraction of air and Determination of velocity of light

The fifth article on High resolution Raman spectroscopy" by B. P. Stoicheff deals mainly with the Raman spectra of polyatomic molecules in the gaseous state at high resolution. Many beautiful rotational Raman spectra of vapours obtained by the author himself using a new technique developed by him have

been reproduced. The results obtained for symmetric and asymmetric top molecules have been discussed in detail.

Under the title 'Modern infrared detectors' T. S. Moss has discussed the properties of thermal detectors, photo-conduction infrared detectors and indium antimonide detectors.

The infrared spectra of polymers have been discussed by A. Elliott who has given a complete bibliography of the papers published on this subject at the end of the review.

Finally, N. Sheppard has discussed the rotational isomerism about C—C bonds in saturated molecules as studied with the help of infrared and Raman spectra. He has also given an exhaustive list of references.

The book is very useful to research workers interested in the branches of spectroscopy mentioned above. The set-up is excellent.

*S.C.S.*





# PENETRATION FACTOR IN ALPHA-DECAY

S. K. DUTTA, T. K. MITRA AND N. C. SIL

DEPARTMENT OF THEORETICAL PHYSICS,  
INDIAN ASSOCIATION FOR THE CULTIVATION OF SCIENCE, JADAVPUR, CALCUTTA

(Received, April 4, 1960)

**ABSTRACT.** In this paper we have calculated the penetration probability of  $\alpha$ -particle through a potential barrier by using the Lanczos method of solving the Schrödinger equation near the nuclear boundary. We have chosen the Woods-Saxon potential for the nuclear field. The value of the half-life of  ${}^{212}_{84}\text{Po}$  calculated from this penetration factor comes out to be twice the experimental value.

## INTRODUCTION

The various calculations of the penetration factor in the process of  $\alpha$ -decay that have been made till recently according to one-body model, give different results which indicate that there is room for finding out a reasonably accurate approximation method. As for the potential for such calculations we have used the Woods-Saxons' diffuse potential model near the nuclear surface, since we feel it approaches reality more than others; outside the nuclear potential Coulomb field predominates. The calculation of the wave function in the region where only Coulomb potential is present has been made by the Riccati method as given by Abramowitz (1949) (cf. Froberg, 1955). So we get an accurate solution of the Schrödinger equation for the Coulomb region. In solving the Schrödinger equation in the neighbourhood of the nuclear boundary we have employed, instead of the WKB approximation, the method of solution given by Lanczos (1938), according to which the differential equation has been equated to an error term which is proportional to Tshelysheff's polynomial of a given order. Consequently the equation admits of a finite power series solution. The error term vanishes at the zero points of the Tshelysheff's polynomial and thus an interpolating power series solution has been obtained. In this case the error term is of an oscillatory character, and the maximum error at any point of the range is less than that of the Taylor's series solution with the same number of terms.

The penetration factor has been calculated from the value of the wave function at the point near the nuclear boundary where the potential energy is equal to the kinetic energy of the emitted  $\alpha$ -particle ( $r = r_0$ ).

We have next estimated the half-life from the calculated value of the penetration factor.

## MATHEMATICAL FORMULATION

The equation for  $u$ , which is  $r$  times the wave function of the radial part of the Schrödinger equation can be written as

$$\frac{d^2 u}{dr^2} + \frac{2m}{\hbar^2} [E - W(r)]u = 0 \quad \dots (1)$$

where  $W(r)$  for  $l = 0$  takes the form as

$$W(r) = U(r) + V(r).$$

where 
$$U(r) = \frac{2(Z-2)e^2}{r} \quad \text{for } r > r_1$$

$$= U(r_1) = \text{constant} \quad \text{for } r < r_1,$$

and 
$$V(r) = - \frac{V_0}{1 + e^{\frac{r-r_1}{a}}} \quad \text{for } r < r_1$$

$$= 0, \quad \text{for } r > r_1.$$

$r_1$  is taken as the point where the nuclear potential drops to  $-\frac{V_0}{100}$ . For  $r < r_1$ , the Coulomb potential is assumed to have a constant value.

To solve equation (1) in the region  $R \ll r \ll r_1$  we write it in the form

$$\frac{d^2 u}{dx^2} + \left\{ \frac{\lambda^2}{1 + \beta e^x} - k^2 \right\} u = 0 \quad \dots (2)$$

where, 
$$x = \frac{r}{a}, \quad \lambda^2 = \frac{2m}{\hbar^2} V_0 a^2$$

$$\beta = e^{-R/a}, \quad k^2 = \frac{2m}{\hbar^2} (U - E) a^2$$

we now seek solutions of the above differential equation of the form

$$u \sim e^{\mp kx} \cdot F_{\mp}$$

Substituting  $z = e^{-x}$ , we get,

$$z(z+\beta) \frac{d^2 F}{dz^2} + (z+\beta)(1 \pm 2k) \frac{dF}{dz} + \lambda^2 F = 0 \quad \dots (3)$$

For our later calculations the independent variable occurring as the argument of the Tshebysheff's polynomial has to be normalised such that it varies from zero to one; so we make the transformation

$$p = \frac{z - z_1}{z_2 - z_1}.$$

We get from equation (3)

$$(p+\mu)(p+\nu) \frac{d^2 F}{dp^2} + (p+\nu)(1 \pm 2k) \frac{dF}{dp} + \lambda^2 F = 0, \quad \dots \quad (4)$$

where

$$\mu = \frac{z_1}{z_2 - z_1} \quad \text{and} \quad \nu = \frac{z_1 + \beta}{z_2 - z_1}.$$

we now replace  $F$  by a polynomial of finite degree  $n$  and following Lanczos equate the differential equation to a term proportional to Tshebysheff's polynomial of order  $n$ . We write

$$D(F) = \tau T_n(p)$$

where

$$D \equiv (p+\mu)(p+\nu) \frac{d^2}{dp^2} + (p+\nu)(1 \pm 2k) \frac{d}{dp} + \lambda^2$$

Let

$$F = \sum_{i=0}^n a_i p^i \quad \text{where} \quad a_0 = 1.$$

$$T_n = \sum_{i=0}^n B_i p^i \quad (\text{for values of } B \text{ vide Lanczos p. 140}).$$

Substituting the above expressions for  $F$  and  $T$  in the differential equation (4) we get the recursion formulae by comparing the coefficients of the same power of  $p$  on both sides of the equation.

$$\tau B_r = a_{r+2}[\mu\nu(r+1)(r+2)] + a_{r+1}[(\mu+\nu)r(r+1) + \delta\nu(r+1)] + a_r[r(r-1) + \delta r + \lambda^2].$$

$$\tau B_n = a_n[\lambda^2 + \delta n + n(n-1)]$$

$$\tau B_{n-1} = a_n[n(n-1)(\mu+\nu) + n\delta\nu] + a_{n-1}[(n-1)(n-2) + (n-1)\delta + \lambda^2].$$

where

$$\delta = \begin{cases} 1+2k \\ 1-2k \end{cases}$$

Therefore the solution of the differential equation is known from the recursion formulae except for an arbitrary constant multiplier. The two values of  $\delta$  give

two solutions. We write therefore for the solution near the surface of the nucleus ( $r < r_1$ )

$$u = Ae^{-kz}F_-(\rho) + Be^{+kz}F_+(\rho). \quad \dots (5)$$

Now for the outside region ( $r > r_1$ ) only Coulomb potential is effective. We can write for this region,

$$\frac{d^2u}{d\rho^2} + \left(1 - \frac{2\eta}{\rho}\right) u = 0, \quad \dots (6)$$

where

$$\rho = \alpha r = \sqrt{\frac{2mE}{\hbar^2}} \cdot r$$

$$2\eta = \frac{2m}{\hbar^2} \cdot \frac{2(Z-2)e^2}{\alpha}$$

We must seek the appropriate solution of the above equation (6) near the boundary ( $r = r_1$ ) where the inner solution ( $r < r_1$ ) is to be matched with the outer solution ( $r > r_1$ ).

The equation has solutions  $F_0, G_0$  the asymptotic behaviour of which is given by

$$F_0 \sim \sin \theta$$

$$G_0 \sim \cos \theta,$$

as

$$\rho \rightarrow \infty,$$

where

$$\theta = \rho - \eta \log 2\rho + \sigma, \quad \text{and} \quad \sigma = \arg \Gamma(i\eta + 1).$$

The combination  $G_0 + iF_0$  will satisfy our boundary condition that at infinity the  $\alpha$ -particle should behave as a free outgoing particle. Now for different ranges defined by values of  $\rho$  and  $\eta$ , different representations of  $F_0$  and  $G_0$  are given. In our region ( $\rho < 2\eta$ ) we take the representation of  $F_0$  and  $G_0$  given by Abramowitz, based on Riccati's method as quoted by C. G. Froberg (1955),

$$F_0 = \frac{1}{2}e^{\psi(t,\eta)},$$

$$G_0 = e^{\psi(t,\eta)},$$

where

$$t = \frac{\rho}{2\eta}$$

$$Q(t, \eta) = 2\eta g_0 + g_1 + (2\eta)^{-1}g_2 + (2\eta)^{-2}g_3 + \dots$$

$$\psi(t, \eta) = -2\eta g_0 + g_1 - (2\eta)^{-1}g_2 + (2\eta)^2g_3 - \dots$$

From continuity of  $u$  and  $\frac{du}{dr}$  at the point  $r = r_1$ , we fix the constants  $A$  and  $B$  of equation (5). It is found that  $F_0$  and  $\frac{dF_0}{dr}$  are negligible in comparison with  $G_0$  and  $\frac{dG_0}{dr}$  at  $r = r_1$ . The values of  $u$  at  $r = r_2$  where  $R < r_2 < r_1$ , is next calculated from equation (5) and the penetration factor as defined by Blatt and Weisskopf (1954) is as follows

$$P = \frac{1}{|u(r_2)|^2}$$

To the probability of penetration per second we write

$$\lambda = nP$$

where  $n$  is the number of times the  $\alpha$ -particle hits the barrier wall. If the  $\alpha$ -particle moves with a velocity  $v$  within the crater of the nucleus of radius  $R$ , then  $n = \frac{v}{2R}$ , further we take the de Broglie wavelength to be equal to  $2R$ , we obtain (Max Born, 1951).

$$n = \frac{h}{4mR^2}$$

Now the half-life can be calculated from the expression

$$T = \frac{\log_e 2}{\lambda} = \frac{0.6931}{\lambda}$$

# RESULT AND DISCUSSION

The numerical calculations are made for Polonium (RaC') with  $A = 214$ ,  $Z = 84$ . The values of parameters are the same as used by Igo and Thaler (1957).

$$R = 1.35A^{1/3} + 1.3 \text{ in Fermi} = 8.32 \times 10^{-13} \text{ cm}$$

$$a = 0.5 \times 10^{-13} \text{ cm}, \quad V_0 = 45 \text{ Mev.}$$

$$m = 6.52 \times 10^{-24} \text{ gm.}$$

$$E = 7.714 \text{ Mev.}$$

We have found the value of  $P = .059 \times 10^{-16}$ . With the same values of the parameters and applying WKB method Rassmussen (1959) found the value of  $\alpha$ -emission width  $\delta^2 \sim 15$ , from which the penetration factor  $P$  comes out to be  $\sim 1.17 \times 10^{-16}$ . Our value is thus about 20 times smaller than this. It is worth while to

mention here that we have taken  $U(r)$  as constant equal to  $U(r_1)$  for the inner solutions whereas the actual Coulomb contribution for that part would be somewhat larger. Consequently the value of  $P$  is expected to be less than the value we have obtained. With our calculated value of the penetration factor the half-life comes out to be

$$T = 3.201 \times 10^{-4} \text{ sec.}$$

which is about twice the experimental value (Rasmussen, 1959)

$$T = 1.636 \times 10^{-4} \text{ sec.}$$

In view of the uncertainty of the values of the parameters, this agreement may be considered quite satisfactory.

The accuracy of WKB method has often been doubted (Blatt, and Weisskopf, 1954). That is why we have not used it and tried Lanczos' method. The result obtained here gives appreciably better agreement than that given by the WKB method.

The application of this technique to the excited states ( $l \neq 0$ ) is under progress.

#### ACKNOWLEDGMENTS

Authors are indebted to Prof. D. Basu for suggesting the problem and for helpful discussions.

#### REFERENCES

- Abramowitz, M., 1949, *Quart. Appl. Math.*, **7**, 75.  
 Blatt & Weisskopf, 1954, *Theoretical Nuclear Physics*, p. 332 & 362, John Wiley & Sons, N.Y.  
 Froberg, C. E., 1955, *Rev. Mod. Phys.* **27**, 405.  
 Igo, G. & Thaler, R. M., 1957, *Phys. Rev.*, **106**, 126.  
 Lanczos, C., 1938, *Jour. Math. Phys.*, **17**, 123.  
 Max Born 1951, *Atomic Phys.* 5th Edn. p. 392.  
 Rasmussen, J. O., 1959, *Phys. Rev.* **113**, 1953

# GRAVITATIONAL FIELD OF DISTANT ROTATING MASSES

RAMESH. V. WAGH.

APPLIED PHYSICS DEPARTMENT, GOVERNMENT POLYTECHNIC, POONA-5

(Received, October 31, 1959; after revision February 2, 1960)

**ABSTRACT.** In 1958, Thirring calculated the gravitational field near the centre of a rotating spherical shell. The case can be generalised to that of a rotating mass, where the field away from the mass can be determined. Thirring assumed

$$T^{\mu\nu} = \rho v^{\mu} v^{\nu} \quad (i)$$

But it can be shown that, starting from a Galilean field we can build up the case a non-Galilean field by introducing some small term in the metric tensor whose Galilean value is unity. Then by a straight forward process, we calculate  $T^{\mu\nu}$  given by

$$T^{\mu\nu} = (p_0 + \rho_{00})v^{\mu}v^{\nu} - p_0 g^{\mu\nu} \quad (ii)$$

By the introduction of a rotating mass in the galilean field, which now slightly deviates from its original characteristics is given by the metric tensor

$$g_{11}, g_{22}, g_{33} = -(1+\alpha)(1, r^2, r^2 \sin^2 \theta) \\ \text{and } g_{44} = (1-\alpha) \quad (iii)$$

The energy-momentum tensor is then calculated with  $\alpha = m(1-r^2 \sin^2 \theta \omega^2)$  and it is shown that this satisfies the conditions of mechanics. It is incidentally shown that there is no necessity of introducing  $E^{\mu\nu}$  in the expression for  $T^{\mu\nu}$ , as recently done by Bass and Pirani (1955). The desired results are obtained without making such assumptions.

## 1. INTRODUCTION AND DERIVATION OF ENERGY— MOMENTUM TENSOR

In a recent paper, Bass and Pirani (1955) and others (1956) have discussed corrections to Thirring's calculations of the gravitational field near the centre of a rotating spherical shell by introducing an additional term  $E^{\mu\nu}$  representing the elastic interaction between particles of the shell, in the expression for energy momentum tensor  $T^{\mu\nu} = \rho v^{\mu} v^{\nu}$ , where the symbols on the right hand side have their usual meanings. The method followed by them is an indirect one in so far as addition of  $E^{\mu\nu}$  is made to derive the expression for the energy momentum tensor and then certain assumptions are made as to the behaviour of  $E^{\mu\nu}$  with reference to the rotating shell. We can however derive the more general expression for the energy—momentum tensor in the form

$$T^{\mu\nu} = (p_0 + \rho_{00})v^{\mu}v^{\nu} - g^{\mu\nu}p_0 \quad (1)$$

wherein we can still assume Galilean values for  $g_{\mu\nu}$  or  $g^{\mu\nu}$ . With this and the modifications introduced in the field by the rotating mass, the whole problem can be worked out in a more straight forward manner as given below.

Accordingly, the flat space-time as envisaged in the general theory of relativity defined by the line-element,

$$ds^2 = -\{(dx_0^1)^2 + (dx_0^2)^2 + (dx_0^3)^2 + (dx_0^4)^2\} \quad (2)$$

or its analogue in spherical polar co-ordinates namely,

$$ds^2 = -(dx_0^1)^2 - r^2(dx_0^2)^2 - r^2 \sin^2\theta(dx_0^3)^2 - (dx_0^4)^2 \quad (2')$$

We shall use this in preference to (2) and remove the dashes in the equations that follow. By suitable transformation of  $dx_0^4$  the 'negative' sign for  $\rho_{00}$  which may otherwise appear can be avoided. Energy-momentum tensor can be expressed as :

$$T_0^{\alpha\beta} = \begin{vmatrix} -p_0 & 0 & 0 & 0 \\ 0 & -p_0 & 0 & 0 \\ 0 & 0 & -p_0 & 0 \\ 0 & 0 & 0 & \rho_{00} \end{vmatrix} \quad \dots \quad (3)$$

where  $p_{xx}^0 = -p_0$ ,

$p_{xy}^0 = 0$  etc, etc. as given in equation 85.1, p. 215 of Tolman's Relativity Thermodynamics and Cosmology (1934). If by the appearance of the rotating spherical mass at great distances from the point of interest, the metric for the gravitational field is given by

$$ds^2 = g_{\mu\nu} dx^\mu dx^\nu \quad \dots \quad (4)$$

then the energy-momentum tensor for this case can be written down in accordance with the usual transformation law as

$$T^{\mu\nu} = \frac{\partial x^\mu}{\partial x_0^\alpha} \cdot \frac{\partial x^\nu}{\partial x_0^\beta} \cdot T_0^{\alpha\beta} \quad \dots \quad (5)$$

Considering Eqns. (2), (3) and (5) we have,

$$T^{\mu\nu} = - \frac{\partial x^\mu}{\partial x_0^1} \cdot \frac{\partial x^\nu}{\partial x_0^1} p_0 - \frac{\partial x^\mu}{\partial x_0^2} \cdot \frac{\partial x^\nu}{\partial x_0^2} p_0 - \frac{\partial x^\mu}{\partial x_0^3} \cdot \frac{\partial x^\nu}{\partial x_0^3} p_0 + \rho_{00} \frac{\partial x^\mu}{\partial x_0^4} \cdot \frac{\partial x^\nu}{\partial x_0^4} \quad \dots \quad (6)$$

Here, the continuity of the  $g_{\mu\nu}$  in the sense of three spaces in space-time has not been considered. (See, for instance a paper "Discontinuities in spherically sym-



metric gravitational fields and shells of radiation" by W. Israel where reference in the subject are given.)

Let  $R_0$  be the radius of the rotating shell thus formed and let  $\Omega$  be its angular velocity of rotation. It may also be assumed that due to the presence of the rotating masses the field deviates only slightly from that in a flat space-time. This will be satisfied approximately if  $\alpha$  is considered to be a small quantity of first order.

$$v_0^1 = \frac{dx_0^1}{ds} = 0; \quad v_0^2 = \frac{dx_0^2}{ds} = 0; \quad \left. \begin{matrix} v_0^3 = \Omega \\ v_0^4 = i \end{matrix} \right\} \quad \dots \quad (7)$$

Initially, we have and  $(v_0^4)^2 + R_0^2 \sin^2 \theta (v_0^3)^2 = -1$

where 
$$v_0^3 = \frac{dx_0^3}{ds} \quad \text{and} \quad v_0^4 = \frac{dx_0^4}{ds}$$

The third and the fourth of Eq. (7) above give

$$\left. \begin{matrix} v_0^3 = \Omega (1 - R_0^2 \Omega^2 \sin^2 \theta)^{-1} \\ v_0^4 = i(1 - R_0^2 \Omega^2 \sin^2 \theta)^{-1} \end{matrix} \right\} \quad \dots \quad (8)$$

The metric tensor is now given by the transformation

$$g^{\mu\nu} = \frac{\partial x^\mu}{\partial x_0^\alpha} \cdot \frac{\partial x^\nu}{\partial x_0^\beta} \cdot g_0^{\alpha\beta}$$

which for  $g_0^{\alpha\beta}$  given by the metric (2) reduces to

$$g^{\mu\nu} = - \frac{\partial x^\mu}{\partial x_0^1} \cdot \frac{\partial x^\nu}{\partial x_0^1} - \frac{\partial x^\mu}{\partial x_0^2} \cdot \frac{\partial x^\nu}{\partial x_0^2} - \frac{\partial x^\mu}{\partial x_0^3} \cdot \frac{\partial x^\nu}{\partial x_0^3} - \frac{\partial x^\mu}{\partial x_0^4} \cdot \frac{\partial x^\nu}{\partial x_0^4} \quad \dots \quad (9)$$

We can also write the velocity components as

$$\frac{dx^\mu}{ds} = \frac{\partial x^\mu}{\partial x_0^\alpha} \cdot \frac{dx_0^\alpha}{ds} = \frac{\partial x^\mu}{\partial x_0^\alpha} \cdot v_0^\alpha$$

substituting for  $v_0^\alpha$  from Eq. (7) we get

$$\frac{dx^\mu}{ds} = 2i(1 - R_0^2 \Omega^2 \sin^2 \theta)^{-1} \frac{\partial x^\mu}{\partial x_0^4} \quad \dots \quad (10)$$

with the help of Eqs. (6) and (9) the energy-momentum tensor can now be written as

$$T^{\mu\nu} = (p_0 + \rho_{00}) \frac{\partial x^\mu}{\partial x_0^4} \cdot \frac{\partial x^\nu}{\partial x_0^4} + g^{\mu\nu} p_0 \quad \dots \quad (11)$$

The positive sign for the second term on the right hand side is due to the particular choice of the metric tensor as indicated in Eq. (2). Substituting for  $\frac{\partial x^\mu}{\partial x_0^4}$  in Eq. (11), we get

$$T^{\mu\nu} = -\frac{1}{2}(p_0 + \rho_{00})(1 - R_0^2 \Omega^2 \sin^2 \theta) v^\mu v^\nu + g^{\mu\nu} p_0 \quad \dots \quad (12)$$

It is usual to put  $idt = dx_0^4$  and  $t' = t$ , where  $t'$  is the time for the modified metric. We can, therefore, rewrite Eq. (10) as

$$\frac{dx^\mu}{ds} = 2(1 - R_0^2 \Omega^2 \sin^2 \theta_0)^{-1} \frac{\partial x^\mu}{\partial t} \quad \dots \quad (13)$$

Where  $\theta_0$  is a certain given value of  $\theta$ .

## 2. THE METRIC

It is assumed that the metric inside the rotating mass is only slightly modified and it does not differ very much from the Galilean field. We may, therefore, write

$$ds^2 = -(1 + \alpha)(dz^2 + r^2 d\theta^2 + r^2 \sin^2 \theta d\phi^2) + (1 - \alpha) dt^2 \quad \dots \quad (14)$$

where  $\alpha = \alpha(r, \theta, t)$ .  $\alpha$  is an infinitesimal of the first order and its first and second order variations are also small. Their products are infinitesimals of higher order. In the following derivation these are neglected.

It would appear that the solution may be similar to that obtained from Schwarzschild's exterior line-element where it is assumed that at large distances from the central particle the space would have symmetrical and isotropic properties. We now proceed to obtain the solution in this case.

For the metric given by (14) the energy-momentum tensor has the following surviving components to the first order of small quantities :

$$KT^1_1 = \frac{1}{r} \frac{\partial \alpha}{\partial r} + \frac{\partial^2 \alpha}{\partial t^2} \quad \dots \quad (15)$$

$$KT^2_2 = KT^3_3 = -\frac{1}{r} \frac{\partial \alpha}{\partial r} + \frac{\partial^2 \alpha}{\partial t^2} \quad \dots \quad (16)$$

$$KT_4^4 = \frac{\partial^2 \alpha}{\partial r^2} + \frac{3}{r} \frac{\partial \alpha}{\partial r} + \frac{1}{r^2} \left( \frac{\partial^2 \alpha}{\partial \theta^2} + \cot \theta \frac{\partial \alpha}{\partial \theta} \right) \quad \dots \quad (17)$$

$$-KT_2^1 = -r^2 KT_1^2 = \frac{1}{2} \frac{\partial^2 \alpha}{\partial r \partial \theta} - \frac{1}{r} \frac{\partial \alpha}{\partial \theta} \quad \dots \quad (18)$$

$$-KT_4^1 = +KT_1^4 = \frac{1}{2} \frac{\partial^2 \alpha}{\partial r \partial t} \quad \dots \quad (19)$$

$$\text{and} \quad -r^2 KT_4^2 = KT_4^2 = \frac{\partial^2 \alpha}{\partial \theta \partial t} - \frac{1}{2} \cot \theta \frac{\partial \alpha}{\partial t} \quad \dots \quad (20)$$

Only first-order infinitesimals are retained in these expressions as  $\alpha$  and its derivatives are of the first order. It is also considered that at the point of interest which is at a large distance from the rotating masses the space-time is symmetrical and conditions of isotropy are also satisfied. We have, therefore,  $T_1^1 = T_2^2 = T_3^3$ ,

which give  $\frac{\partial \alpha}{\partial r} = 0$ . Also, if  $T_2^1 = 0 = T_1^2$ ,  $\frac{\partial \alpha}{\partial \theta} = 0$ . These latter three relations give  $\alpha = 4\chi^2 + \text{constant}$  ... (21)

so that the metric will be given

$$ds^2 = -(1 + \chi^2)(dr^2 + r^2 d\theta^2 + r^2 \sin^2 \theta d\phi^2) + (1 - 4\chi^2)dt^2 \quad \dots \quad (22)$$

As  $\chi^2$  is a function of  $t$  only, the transformed metric is;

$$ds^2 = -(1 + 4[x(t^*)]^2)(dr^2 + r^2 d\theta^2 + r^2 \sin^2 \theta d\phi^2) + dt^{*2} \quad \dots \quad (22')$$

### 3 ANOTHER FORM OF METRIC

The condition that the pressure should be isotropic gives

$$-KT_\nu{}^\mu = \begin{vmatrix} \frac{\partial^2 \alpha}{\partial t^2} & 0 & 0 & 0 \\ 0 & \frac{\partial^2 \alpha}{\partial t^2} & 0 & \frac{\cot^2 \theta}{2r^2} \frac{\partial \alpha}{\partial t} \\ 0 & 0 & \frac{\partial^2 \alpha}{\partial t^2} & 0 \\ 0 & -\frac{\cot \theta}{2} \frac{\partial \alpha}{\partial t} & 0 & 0 \end{vmatrix} \quad \dots \quad (23)$$

where  $\alpha = 4\chi^2 + \text{constant}$ ;  $\chi^2 = \frac{1}{1 - R_0^2 \sin^2 \theta \Omega^2}$ ;  $\frac{\partial \alpha}{\partial t} = 8R_0^2 \sin^2 \theta \chi^4 \Omega \dot{\Omega}$ ; and

$$\frac{\partial^2 \alpha}{\partial t^2} = 8\dot{R}_0^2 \sin^2 \theta \chi^4 \{ \Omega \ddot{\Omega} - 3\dot{\Omega}^2 + 4\dot{\Omega}^2 \chi^2 \}$$

The density  $\rho_{00}$  turns out to be zero to a first approximation as would naturally be expected. We may however consider that the condition of isotropy is not strictly satisfied and that  $T_2^1 = 0 = T_1^2$ , then, a particular solution can be found viz.,

$$\alpha = m(1 - r^2 \sin^2 \theta \cdot \dot{\omega}^2) \quad \dots (24)$$

where  $m$  is an infinitesimal constant and we may take to depend upon time. Obviously  $\omega$  may be considered as the angular velocity. The energy-momentum tensor can now be written as

$$-KT_{\mu\nu} = \begin{vmatrix} 2m \sin^2 \theta \{ \dot{\omega}^2 - r^2 (\ddot{\omega} \dot{\omega} + \dot{\omega}^2) \}, & 0 & 0 & 2mr \sin^2 \theta \dot{\omega} \dot{\omega} \\ 0 & -2mr^2 \sin^2 \theta \{ \dot{\omega}^2 - r^2 (\ddot{\omega} \dot{\omega} + \dot{\omega}^2) \}, & 0 & 3mr^2 \sin \theta \cos \theta \dot{\omega} \dot{\omega} \\ 0 & 0, & -2mr^2 \sin^4 \theta \{ \dot{\omega}^2 - r^2 (\ddot{\omega} \dot{\omega} + \dot{\omega}^2) \}, & 0 \\ 2mr \sin^2 \theta \dot{\omega} \dot{\omega}, & 3mr^2 \sin \theta \cos \theta \dot{\omega} \dot{\omega}, & 0 & , & 2m \{ \dot{\omega}^2 - r^2 \sin^2 \theta (\ddot{\omega} \dot{\omega} + \dot{\omega}^2) \} \end{vmatrix} \quad (25)$$

The mechanical relation which must be satisfied by the energy-momentum tensor is given by  $\frac{\partial T^{\mu\nu}}{\partial x^\nu} = 0$ . It will be seen that this gives  $\frac{\partial T^{33}}{\partial \phi} = 0$ , which is satisfied in the present case. The other relations are :

$$\left. \begin{aligned} \frac{\partial T^{11}}{\partial r} + \frac{\partial T^{14}}{\partial t} &= 0 \\ \frac{\partial T^{22}}{\partial \theta} + \frac{\partial T^{24}}{\partial t} &= 0 \\ \text{and } \frac{\partial T^{44}}{\partial t} + \frac{\partial T^{41}}{\partial r} + \frac{\partial T^{42}}{\partial \theta} &= 0 \end{aligned} \right\} \quad \dots (26)$$

which gives a differential equation for the determination of  $\omega$  namely,

$$\ddot{\omega} + a \dot{\omega}^2 + b \omega^2 = 0 \quad \dots (27)$$

where  $a$  and  $b$  are constant coefficients.

#### REFERENCES

- Bass and Pirani, 1955, *Phil. Mag.*, **17**, 850.  
 Honl and Maue, 1956, *Zeit fur Physik*, **144**, 152.  
 Israel, W., 1958, *Proc. Roy. Soc.*, **248**, 404.  
 Tolman, R. C., *Rel. Thermodynamics and cosmology.* pp.215.

# DIELECTRIC RELAXATION IN RELATION TO TEMPERATURE. II

J. SOBHANADRI

PHYSICS DEPARTMENT, ANDHRA UNIVERSITY, WALTAIR

(Received, April 11, 1960)

**ABSTRACT.** In continuation of the previous work, the effect of temperature on the relaxation time  $\tau$  of three more polar molecules in the non-polar solvent heptane was studied adopting now the Cole-Cole arc plot method for finding  $\tau$ . The molecules investigated are 2, 3-dichloro nitrobenzene, 2, 5-dichloro nitrobenzene, and 6-chloro 2-nitrotoluene for which the results are newly obtained. The results are examined in the light of Eyring's theory.

In the previous paper (Sobhanadri, 1959) describing the results of experiments on the effect of temperature on dielectric relaxation in six molecules it was shown with reference to Eyring's equation

$$\tau = A/T \cdot e^{E\tau/kT} = h/kT \cdot e^{E\tau/kT}$$

(1) that the factor  $A$  for a given liquid remains constant and independent of temperature, (2) that its value is considerably higher than that calculated from the equation above, namely  $h/k$ , (3) that it is different for different liquids and (4) that the value of  $E$  is less than the corresponding value of  $E\eta$ .

These conclusions were drawn from experimental determinations of  $\tau$  based on Whiffen and Thompson's (1946) method of observation at a single frequency. However, as pointed out already, it is necessary in the work of this kind to determine  $\tau$  with as high an accuracy as is possible and perhaps Cole and Cole's (1941) method based on measurements at different frequencies is the most suitable. It is, therefore, thought worthwhile carrying out further investigations using this method. The purpose of this paper is to describe such investigations on the three molecules 2, 5-dichloro nitrobenzene, 2, 3-dichloronitrobenzene, and 6-chloro 2-nitrotoluene making measurements on solutions in heptane at 1.22 cm, 3.26 cm and 4.36 cm.

The experimental arrangement is the same as at 1.22 cm described in the previous paper Sobhanadri (1959). A solution of known concentration is taken in the dielectric cell. The temperature is varied between 0°C and 52°C. In order to avoid errors arising from divergences and variations in the concentration, the experimental determination of  $x_0$ ,  $\Delta x$  and  $c_0$  are made with the same prepared solution in rapid succession at the three wavelengths.

The values of  $\epsilon'$  and  $\epsilon''$  at the different wavelengths together with the static value  $\epsilon_0$  of the solution (measured at 1 Mc/sec) are presented in Table I for different temperatures for each liquid. The plots for each substance at different temperatures are shown in Figs. 1 to 3.

It is seen that the conclusions referred to in the previous experiments are confirmed by the present results that (1) for a given liquid there is no systematic

TABLE I  
(1) 6-chloro 2-nitrotoluene

Temp °C	1.22 cm			3.26 cm		4.36 cm		$\tau \times 10^{12}$	
	$\epsilon_0$	$\epsilon'$	$\epsilon''$	$\epsilon'$	$\epsilon''$	$\epsilon'$	$\epsilon''$	sec	$A \times 10^{11}$
0	2.029	1.948	0.026	1.975	0.044	1.991	0.043	20.13	10.71
20	2.018	1.950	0.029	1.980	0.036	1.993	0.025	15.33	11.41
30	2.007	1.949	0.026	1.979	0.033	1.993	0.033	12.19	10.96
39	2.001	1.956	0.029	1.980	0.032	1.991	0.029	10.88	10.14
52	1.993	1.958	0.029	1.979	0.026	1.989	0.024	8.26	11.39
Mean				$A = 10.92 \times 10^{-11}$		$E_T = 1.31 \times 10^{-13}$ ergs			

(2) 2, 3-dichloro nitrobenzene

0	2.092	1.949	0.036	1.988	0.071	2.009	0.076	25.60	22.40
18	2.078	1.956	0.045	2.008	0.069	2.029	0.067	17.61	22.00
30	2.063	1.958	0.046	2.011	0.066	2.030	0.061	15.93	22.33
40	2.044	1.960	0.048	2.017	0.061	2.033	0.055	13.81	25.80
52	2.027	1.968	0.046	2.023	0.055	2.036	0.047	11.58	20.30
Mean				$A = 22.57 \times 10^{-11}$		$E_T = 1.33 \times 10^{-13}$ ergs			

(2) 2, 5-dichloro nitrobenzene

0	2.056	1.948	0.030	1.981	0.055	1.998	0.058	23.43	17.13
20	2.041	1.940	0.031	1.989	0.051	2.004	0.049	17.61	17.69
30	2.036	1.945	0.033	1.984	0.047	1.998	0.044	16.32	18.23
40	2.022	1.948	0.033	1.984	0.041	1.995	0.036	14.28	17.94
54	2.014	1.948	0.034	1.984	0.037	1.993	0.032	12.76	18.16
Mean				$A = 17.83 \times 10^{-11}$		$E_T = 1.33 \times 10^{-13}$ ergs			

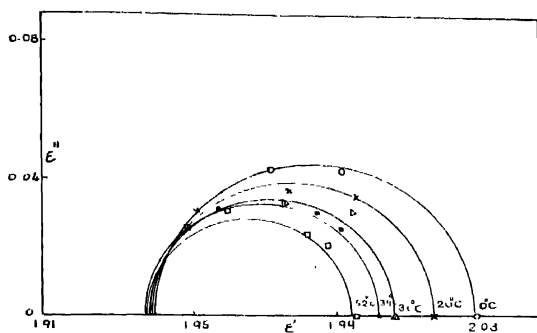


Fig. 1. 6-Chloro 2-nitrotoluene.

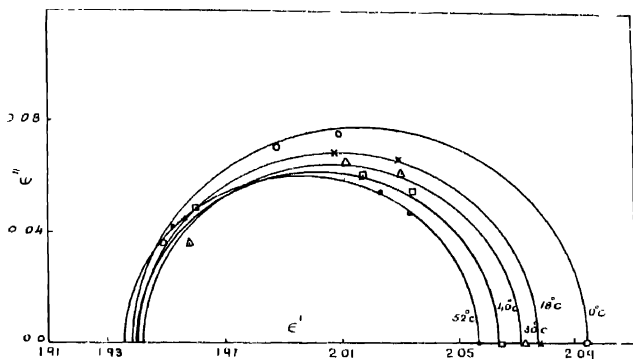


Fig. 2. 2,3-Dichloro nitrobenzene.

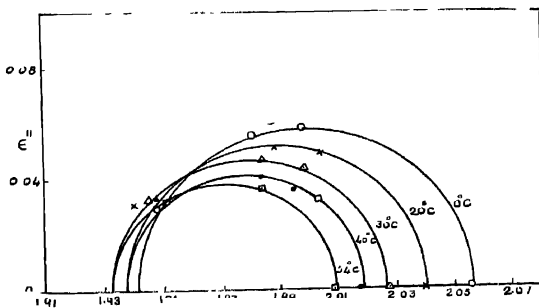


Fig. 3. 2,5-Dichloro nitrobenzene.

variation in  $A$ , its constancy may be assumed, (2) the values are considerably higher than the theoretical value  $4.5 \times 10^{-11}$  and (3)  $A$  is different for different liquids.

#### ACKNOWLEDGMENTS

The author is deeply indebted to Prof. K. R. Rao for his kind and valuable guidance throughout the progress of the work. He is also grateful to the government of India for the award of a scholarship.

#### REFERENCES

- Cole, R. H. and Cole, K. S., 1941, *J. Chem. Phys.*, **9**, 341.  
Sobhanadri, J., 1959, *Ind. J. Phys.*, **33**, 511.  
Whiffen, D. H. and Thompson, H. W., 1946, *Trans. Farad. Soc.*, **42A**, 114.



# FOURTH ORDER SCATTERING MATRIX ELEMENTS OF NUCLEONS WITH A FOURTH ORDER MESON EQUATION

S. P. MISRA

MATHEMATICS DEPARTMENT, RAVENSHAW COLLEGE, CUTTACK

(Received, February 2, 1960)

**ABSTRACT.** In this paper the important fourth order matrix elements with a fourth order meson equation have been calculated. It is noted that the charge renormalisation that we obtain with this theory is finite and small for a reasonable value of the coupling constant. But the contribution from the meson self-energy diagram remains unaltered and thus contains an infinity. A consistent interpretation of this term as meson mass renormalisation is obtained only if the bare meson has two different rest-masses.

## INTRODUCTION

In two previous papers, we have considered a fourth order meson equation proposed by Bhabha (1950) and Thirring (1950). It has been noted that this theory is fairly successful for the explanation of the anomalous magnetic moments of nucleons (Misra and Deo, 1956), but fails to give experimental results for neutron-proton scattering (Misra, 1960). However, the principal advantage of this theory is the finiteness of many matrix elements that are divergent in conventional meson theory. For example, Thirring noted that the self-energy of the nucleon in this theory was finite and fairly small for a reasonable value of the coupling constant. These are well illustrated when we consider the fourth order matrix elements for nucleon-nucleon scattering. It is the purpose of the present paper to calculate these matrix elements.

It is noted here that the charge renormalisation that we obtain in this theory from the vertex diagram is finite and small. But, the contribution from the meson self-energy diagram remains unaltered, and thus contains an infinity. This happens since the nucleon propagator, on which this depends, remains the same here. The interpretation of this term as mass renormalisation, however, presents serious difficulty, and this infinite renormalisation has been carried out in the appendix. We find that this mass renormalisation can be consistently done to give rise to unique renormalised mass only if the bare mesons had two different rest-masses. On the other hand, a single mass of the bare meson would give rise to two different renormalised masses. This aspect of the problem would be inter-

esting if the renormalisation terms were finite, which unfortunately is not the case here.

We now proceed to evaluate the fourth order matrix elements. The notation here will be the same as in the previous paper (Misra, 1960). We only note that the nucleon propagator is given as

$$\langle P(\psi(x)\bar{\psi}(y)) \rangle_0 = \frac{i}{(2\pi)^4} \int \frac{i\gamma k + \kappa_0}{(k^2 + \kappa_0^2)} \exp(ik(x-y)) d^4k \quad (1)$$

and the meson propagator, as

$$\langle P(\phi^i(x)\phi^j(y)) \rangle_0 = -\frac{i\kappa^2}{(2\pi)^4} \delta_{ij} \int \frac{\exp(ik(x-y))}{(k^2 + \kappa^2)^2} d^4k \quad (2)$$

#### FOURTH ORDER S-MATRIX ELEMENTS

Here we have,

$$\langle S_4 \rangle = \frac{f^4}{4!} \int d^4x_1 \dots \int d^4x_4 \langle P\bar{\psi}(x_1)\gamma_5\tau_i\psi(x_1)\phi^i(x_1)\dots \bar{\psi}(x_4)\gamma_5\tau_l\psi(x_4)\phi^l(x_4) \rangle \dots \quad (3)$$

where the expectation value is to be taken between initial and final two-nucleon states with four momenta  $p_1, p_2$  and  $p_3, p_4$  respectively. This gives rise to different Feynman diagrams which we consider separately.

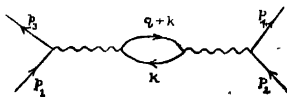


Fig. 1(a)

(a) Vacuum polarisation :

Here we obtain

$$\begin{aligned} \langle S_4 \rangle = & \frac{f^4 \kappa^4}{4!} \cdot 4! \cdot 2 \cdot \frac{\kappa_0^2}{(2\pi)^8 (p_{10}p_{20}p_{30}p_{40})^{\frac{1}{2}}} \delta(p_1 + p_2 - p_3 - p_4) \\ & \times \bar{u}(p_3)\gamma_5\tau_i u(p_1)\bar{u}(p_4)\gamma_5\tau_j u(p_2) \int d^4k \{ Sp[\gamma_5\tau_i(i\gamma(q+k) - \kappa_0)\gamma_5\tau_j(i\gamma k - \kappa_0)] \\ & (q^2 + \kappa^2)^{-4}((q+k)^2 + \kappa_0^2)^{-1}(k^2 + \kappa_0^2)^{-1} \}. \end{aligned}$$

which simplifies to

$$\begin{aligned} S_4^{(a)} = & \frac{4f^4\kappa^4\kappa_0^2}{(2\pi)^8 (p_{10}p_{20}p_{30}p_{40})^{\frac{1}{2}}} \delta(p_1 + p_2 - p_3 - p_4)(q^2 + \kappa^2)^{-4} I \\ & \times \bar{u}(p_3)\gamma_5\tau_i\psi(p_1)\bar{\psi}(p_4)\gamma_5\tau_j\psi(p_2) \dots \quad (4) \end{aligned}$$

where

$$I = \int d^4k \frac{(k^2 + qk + \kappa_0^2)}{(k^2 + 2qk + q^2 + \kappa_0^2)(k^2 + \kappa_0^2)}$$

The above integral is divergent, and we can write, as has been shown in the appendix.

$$I = I(q^2) = A + (q^2 + \kappa^2)B + (q^2 + \kappa^2)^2 I_c(q^2) \quad \dots \quad (6)$$

where  $A$  and  $B$  are respectively quadratically and logarithmically divergent constants, and  $I_c(q^2)$  gives rise to a finite contribution. We shall also show in the appendix that both  $A$  and  $B$  go as mass renormalisation terms. We note that the same constants also occur in conventional meson theory; but there the interpretation is different,  $A$  alone going as mass renormalisation, and  $B$  giving rise to coupling constant renormalisation (Schweber, Bethe and Hoffman, 1955).

After renormalisation, the (finite) contribution from this diagram has been evaluated in the appendix as

$$\begin{aligned} (S^{(4)}_4)_{rn} = & \frac{4f^4\kappa_0^2\kappa^4}{(2\pi)^6(p_{10}p_{20}p_{30}p_{40})^{1/2}} \delta(p_1 + p_2 - p_3 - p_4) \\ & \times \bar{u}(p_3)\gamma_5\tau_3u(p_1) \quad \bar{u}(p_4)\gamma_5\tau_3u(p_2)(q^2 + \kappa^2)^{-2} \\ & \times \pi^2 \int_0^1 dx \int_0^1 dy \int_0^1 dz \quad x^2(1-x)^2y^2\{3(\kappa_0^2 + q^2x(1-x)yz \\ & - \kappa^2x(1-x)(1-yz))^{-1} + 2\kappa_0^2(\kappa_0^2 + q^2x(1-x)yz - \kappa^2x(1-x)(1-yz)^{-1}) \dots \quad (7) \end{aligned}$$

In the nonrelativistic approximation, neglecting terms of the order of  $(q^2/\kappa_0^2)$  and  $(\kappa^2/\kappa_0^2)$  as compared to unity, we get

$$\begin{aligned} (S^{(4)}_4)_{rn} = & \frac{2i\pi^2f^4\kappa^4}{9\kappa_0^2(2\pi)^6} \delta(p_1 + p_2 - p_3 - p_4)(q^2 + \kappa^2)^{-2} \times \\ & \times \bar{u}(p_3)\gamma_5\tau_3u(p_1)\bar{u}(p_4)\gamma_5\tau_3u(p_2). \end{aligned}$$

Thus we find that this contribution, which is of the same type as the second order matrix element, is of the order of  $(f\kappa/\kappa_0)^2$  times the second order matrix element.

(b) *Vertex diagram :*

We see that the contribution from the vertex diagram (Fig. 1b) is

$$\begin{aligned}
S^{(b)}_4 = & \frac{f^4 \kappa^4 \kappa_0^2}{(2\pi)^6 (p_{10} p_{20} p_{30} p_{40})^{\frac{1}{2}}} \delta(p_1 + p_2 + p_3 + p_4) (q^2 + \kappa^2)^{-2} \int d^4 k \{ \bar{u}(p_3) \gamma_5 \tau_4 \\
& \times (i\gamma(p_3 - k) - \kappa_0) \gamma_5 \tau_3 (i\gamma(p_1 - k) - \kappa_0) \gamma_5 \tau_4 u(p_1) (k^2 + \kappa^2)^{-2} \\
& \times ((k - p_3)^2 + \kappa_0^2)^{-1} ((k - p_1)^2 + \kappa_0^2)^{-1} \bar{u}(p_4) \gamma_5 \tau_3 u(p_2) \}.
\end{aligned}$$

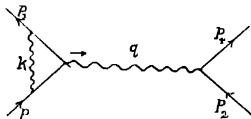


Fig. 1(b)

which simplifies to

$$\begin{aligned}
S^{(b)}_4 = & \frac{f^4 \kappa^4 \kappa_0^2}{(2\pi)^6 (p_{10} p_{20} p_{30} p_{40})^{\frac{1}{2}}} \delta(p_1 + p_2 + p_3 + p_4) \bar{u}(p_3) \gamma_5 \tau_3 u(p_1) \bar{u}(p_4) \gamma_5 \tau_3 u(p_2) \\
& \times (q^2 + \kappa^2)^{-2} U \quad \dots \quad (8)
\end{aligned}$$

where

$$U = \int \frac{k^2 d^4 k}{(k^2 - 2kp_1)(k^2 - 2kp_3)(k^2 + \kappa^2)^{-2}} \quad (9)$$

The above integral  $U$  is convergent. To evaluate it, we use

$$1/(abc^2) = \int_0^1 dx \int_0^1 dy \, 6y(1-y) \{ (ax + b(1-x))y + c(1-y) \}^{-4},$$

and thus obtain, on integrating for the momentum variable,

$$U = i\pi^2 \int_0^1 dx \int_0^1 dy \, y(1-y) \frac{y^2(\kappa_0^2 + q^2 x(1-x)) + 2\kappa^2(1-y)}{(y^2(\kappa_0^2 + q^2 x(1-x)) + \kappa^2(1-y))^2} \quad \dots \quad (10)$$

We can carry out charge renormalisation by writing

$$\begin{aligned}
U = & i\pi^2 \int_0^1 dx \int_0^1 dy \, y(1-y) \{ (y^2 \kappa_0^2 + \kappa^2(1-y))^{-1} + \kappa^2(1-y) (y^2 \kappa_0^2 + \kappa^2(1-y))^{-2} \} \\
& + i\pi^2 \int_0^1 dx \int_0^1 dy \, y(1-y) \{ (y^2(\kappa_0^2 + q^2 x(1-x)) + \kappa^2(1-y))^{-1} \\
& - (y^2 \kappa_0^2 + \kappa^2(1-y))^{-1} - \kappa^2(1-y) (y^2 \kappa_0^2 + \kappa^2(1-y))^{-2} \\
& + \kappa^2(1-y) (y^2(\kappa_0^2 + q^2 x(1-x)) + \kappa^2(1-y))^{-2} \}
\end{aligned}$$

$$\begin{aligned}
&= i\pi^2 \int dx \int dy y(1-y) \frac{y^2\kappa_0^2 + 2\kappa^2(1-y)}{(y^2\kappa_0^2 + \kappa^2(1-y))^2} - i\pi^2 q^2 \int dx \int dy \int dz y(1-y) \\
&\quad \times x(1-x) \{ (y^2\kappa_0^2 + q^2x(1-x)y^2z + \kappa^2(1-y))^{-2} \\
&\quad + 2\kappa^2(1-y)(y^2\kappa_0^2 + q^2x(1-x)y^2z + \kappa^2(1-y))^{-3} \} . \quad \dots \quad (11)
\end{aligned}$$

In deducing the above result we have utilised the equation

$$\frac{1}{\alpha^n} - \frac{1}{\beta^n} = \int_0^1 \frac{n(\beta - \alpha)}{\{\alpha z + \beta(1-z)\}^{n+1}} dz . \quad \dots \quad (12)$$

The first term on the right hand side of Eq. (11) may be regarded as the charge renormalisation term to be included in the second order contribution. This is because we assume that when there is no change in momentum, the contribution from the vertex diagram should vanish. The second term of the same equation gives us the physically important contribution from this process. For non-relativistic regions, neglecting  $q^2$  as compared to  $\kappa_0^2$  and making the substitution  $\lambda = \kappa^2/\kappa_0^2$ , the second term of Eq. (11) is seen to be

$$\begin{aligned}
&\simeq -i\pi^2 q^2 \frac{1}{6\kappa_0^4} \int_0^1 \left\{ \frac{y(1-y)dy}{(y^2 + \lambda(1-y))^2} + \frac{2\lambda y(1-y)^2 dy}{(y^2 + \lambda(1-y))^3} \right\} \\
&\simeq -i\pi^2 q^2 \left[ \frac{1}{6\kappa_0^4} \left[ \frac{1}{\lambda} - \frac{3}{8\lambda^{\frac{3}{2}}} \cos^{-1}(\frac{1}{2}\lambda^{\frac{1}{2}}) \right] \right]
\end{aligned}$$

Thus we have,  $U = O\left(\frac{q^2}{\kappa_0^2 \kappa^2}\right)$ , and hence, substituting in Eq. (8) and comparing with the second order contribution, the physical part of the contribution from the vertex diagram is found to be of the order of  $f^2 q^2/\kappa_0^2$  times the second order contribution.

We shall now see the order of magnitude of the renormalisation term. This term, on the right hand side of Eq. (11), is

$$\begin{aligned}
&\frac{i\pi^2}{\kappa_0^2} \left[ \int_0^1 \frac{y^3(1-y)}{(y^2 + \lambda(1-y))^2} dy + 2\lambda \int_0^1 \frac{y(1-y)^2}{(y^2 + \lambda(1-y))^2} dy \right] \\
&\simeq \frac{i\pi^2}{\kappa_0^2} [0.8 + 0.7] = \frac{i\pi^2}{\kappa_0^2} \times 1.5.
\end{aligned}$$

Thus, by Eqns. (8) and (11), the part of  $S^{(b)}_4$  that goes as renormalisation term is

$$\begin{aligned}
&-\frac{f^4 \kappa^4 \kappa_0^2}{(2\pi)^6 (p_{10} p_{20} p_{30} p_{40})^{\frac{1}{2}}} \frac{i\pi^2}{\kappa_0^2} \times 1.5 \times \delta(p_1 + p_2 - p_3 - p_4) (q^2 + \kappa^2)^{-2} \\
&\quad \times \bar{u}(p_3) \gamma_5 \tau_3 u(p_1) \bar{u}(p_4) \gamma_5 \tau_3 u(p_2).
\end{aligned}$$

Hence, on comparing with the second order contribution, we obtain,

$$\begin{aligned} f^2(\text{renormalised}) - f^2 \left[ 1 + \frac{f^2 \kappa^2}{16\pi^2 \kappa_0^2} \times 1.5 \right] \\ = f^2 [1 + f^2 \times 2.14 \times 10^{-4}]. \end{aligned}$$

This gives us that the renormalisation of the coupling constant is small for any reasonable value of the bare coupling constant, which in this case must be finite. We note that here the bare coupling constant is not an abstraction to be discarded later on, but is a meaningful quantity that can be determined to any degree of accuracy in terms of the physical or renormalised coupling constant.

(c) *Nucleon self-energy* :

The contribution from the nucleon self-energy graph (Fig. 1c) is to be treated just the same way as for ordinary mesons theory, and is to be taken along with the contribution from the diagram Fig. 1c'. We may note that the contribution from both the diagrams gives rise to an ambiguous expression and to get meaningful results we may assume some form of periodic damping explicitly. For example, we may take our interaction Hamiltonian as (Schweber, Bethe and de Hoffman, 1955, p. 286)

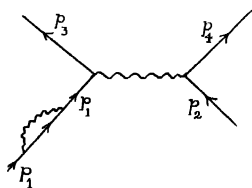


Fig. 1(c)

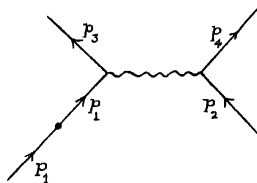


Fig. 1(c')

$$H_s(x) = if g(t) \bar{\psi}(x) \gamma_5 \tau_i \psi(x) \phi^i(x) - \delta \kappa_0 (g(t))^2 \bar{\psi}(x) \psi(x) \quad (13)$$

where

$$g(t) = \int_{-\infty}^{\infty} G(\Gamma_0) e^{-i\Gamma_0 t} d\Gamma_0 = \int_{-\infty}^{\infty} G(\Gamma_0) e^{+i\Gamma_0 x} d\Gamma_0 \quad \dots (14)$$

with  $\Gamma = (\Gamma_0, 0, 0, 0)$  and

$$g(0) = \int_{-\infty}^{\infty} G(\Gamma_0) d\Gamma_0 = 1. \quad -$$

As an example of a function of such a type, we can take

$$g(t) = (T/t) \sin(t/T) \quad \dots (15)$$

such that

$$G(\Gamma_0) = \begin{cases} T/2 & \text{when } -1/T \leq \Gamma_0 \leq 1/T \\ 0 & \text{otherwise.} \end{cases}$$

Clearly, in the limit  $T$  approaches infinity,  $G(\Gamma_0)$  approaches a  $\delta$ -function, and for any finite time,  $g(t)$  approaches unity.

Let us now consider the contribution from the self-energy diagram in the general case, with  $p$  not the momentum of an external line, given as

$$\begin{aligned}\Sigma(p) &= \frac{3if^2\kappa^2}{(2\pi)^4} \int \frac{i\gamma(p-k) - \kappa_0}{((p-k)^2 + \kappa_0^2(k^2 + \kappa^2)^2)} d^4k \\ &= A + B(i\gamma p + \kappa_0) + (i\gamma p + \kappa_0)^2 \Sigma_c(p), \text{ say.} \quad \dots (16)\end{aligned}$$

Now, when we recalculate the contributions from the Figs 1(c) and 1(c') with the Hamiltonian given by Eq. (13), by interpretation of the term for mass renormalisation, the constant  $A$  in Eq. (16) will exactly cancel with the term before going the limit  $T \rightarrow \infty$ . Also, the constant  $B$  in this equation, which at the outset is ambiguous, becomes now well-defined and gives rise to the wave-function renormalisation (also vide Juch and Rohrich, 1955, p. 185). Again, since in this case we have an external line, the contribution with  $\Sigma_c$  will not be there.

Thus, with such diagrams, the contribution goes only to a mass renormalisation (which is finite and has been calculated by Thirring (1950)) and to a wave-function renormalisation, which also is finite and can be calculated in the standard way), and there is no contribution to the scattering process.

(d) Successive and crossed exchange of two mesons.

As in the previous cases, the contribution from the Feynman diagram Fig. 1(d) for the case of successive exchange of two mesons becomes, on using the equations with  $p_1$  and  $p_2$  as the four-momenta of free particles,

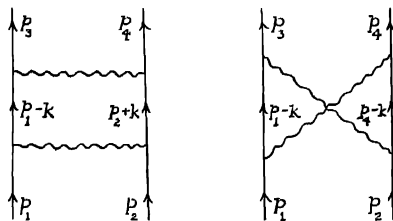


Fig. 1(d)

Fig. 1(e)

$$\begin{aligned}S_4^{(d)} &= \frac{f^4 \kappa^4 \kappa_0^2}{(2\pi)^4 (p_{10} p_{20} p_{30} p_{40})^{\frac{1}{2}}} V_{\mu\nu} \\ &\times \bar{u}(p_3) \tau_i \tau_j \gamma_\mu^{(1)} u(p_1) \bar{u}(p_4) \tau_i \tau_j \gamma_\nu^{(2)} u(p_2), \quad \dots (17)\end{aligned}$$

where

$$V_{\mu\nu} = \int d^4k \frac{k_\mu k_\nu}{(k^2 + 2kp_2)(k^2 - 2kp_1)((k^2 - q^2 + \kappa^2)^2(k^2 + \kappa^2)^2)} \quad \dots \quad (18)$$

Using representation with subsidiary variables and carrying out integration over the momentum variable, we obtain, on simplification,

$$\begin{aligned} V_{\mu\nu} = & 120 \int_0^1 dx \int_0^1 dy \int_0^1 dz \, z(1-z) x(1-x)^3 \int d^4k \, k_\mu k_\nu [k^2 - 2k(p_1x(1-y) \\ & - p_2xy + qz(1-x)) + q^2z(1-x) + \kappa^2(1-x)]^{-6} \\ & - i\pi^2 \int_0^1 dx \int_0^1 dy \int_0^1 dz \, x(1-x)^3 z(1-z) \left[ \frac{6Q_\mu Q_\nu}{D^4} + \frac{g_{\mu\nu}}{D^3} \right], \quad \dots \quad (19) \end{aligned}$$

where

$$Q = p_1x(1-y) - p_2xy + qz(1-x) \quad \dots \quad (20)$$

and

$$D = \kappa_0^2 x^2(1-2y)^2 + \kappa^2(1-x) + q^2z(1-z)(1-x)^2 - p^2x^2y(1-y). \quad (21)$$

Substituting the value of  $Q$  from equation (20), we see that in equation (17),

$$\gamma_\mu^{(1)} \gamma_\nu^{(2)} Q_\mu Q_\nu \simeq -\kappa_0^2 x^2(1-2y)^2$$

in the nonrelativistic approximation. Also, in this approximation,

$$\gamma_\mu^{(1)} \gamma_\nu^{(2)} g_{\mu\nu} \simeq 1.$$

Hence we have in Eqns. (17) and (19),

$$\gamma_\mu^{(1)} \gamma_\nu^{(2)} V_{\mu\nu} = i\pi^2 \int_0^1 dx \int_0^1 dy \int_0^1 dz \, x(1-x)^3 z(1-z) \times \left\{ -\frac{6\kappa_0^2 x^2(1-2y)^2}{D^4} + \frac{1}{D^3} \right\} \quad (22)$$

where  $D$  is given by eqn. (21).

The evaluation of the above integral even in the non-relativistic approximation requires special care, since the denominator vanishes for certain values of the auxiliary variables  $x$  and  $y$ . The singularity here is to be dealt with by adding a small negative imaginary part to the mass of the meson. The integral to be evaluated is

$$I = \int_0^1 dx \int_0^1 dy \int_0^1 dz \, x(1-x)^3 z(1-z) \left\{ -\frac{6\kappa_0^2 x^2(1-2y)^2}{D^4} + \frac{1}{D^3} \right\},$$

where, for Eq. (21), we can take

$$D \simeq \kappa_0^2 x^2(1-2y)^2 + \kappa^2(1-x) + q^2z(1-z)(1-x)^2 - \frac{1}{4}p^2x^2 \quad \dots \quad (23)$$



We now note that

$$I = \frac{\partial}{\partial q^2} \frac{\partial}{\partial \kappa^2} I_0, \quad \dots \quad (24)$$

where

$$I_0 = \int_0^1 dz \int_0^1 dx \int_0^1 dy \left\{ - \frac{\kappa_0^2 x^2 (1-2y)^2}{p^2} + \frac{1}{2} D^{-1} \right\} \quad \dots \quad (24')$$

We now put for brevity

$$\phi(x, z) = \kappa^2(1-x) + q^2 z(1-x)^2 - \frac{1}{4} p^2 x^2 \quad \dots \quad (25)$$

and put  $s = \kappa_0 x(1-2y)$  as the integration variable instead of  $y$ . Then we get,

$$I_0 = \int_0^1 dz \int_0^1 dx \int_0^{\kappa_0 x} ds \left\{ -s^2/(s^2 + \phi(x, z))^{-2} + \frac{1}{2}(s^2 + \phi(x, z))^{-1} \right\}. \quad (26)$$

Since  $p^2$  and  $q^2$  are positive definite constants, (they are positive definite in the centre of mass system), we have, in Eq. (25),  $\phi(x, z)$  is a monotonically diminishing function of  $x$  for any given value of  $z$ , and is positive when  $x = 0$  and negative when  $x = 1$ . Hence  $\phi(x, z)$  vanishes for one value  $\xi = \xi(z)$  of  $x$ , with  $0 < \xi < 1$ , and we have

$$\begin{aligned} \phi(x, z) &> 0 \text{ when } 0 < x < \xi \\ \phi(x, z) &< 0 \text{ when } \xi < x < 1. \end{aligned}$$

In the second case above, the singularity for the  $s$ -integration is to be treated by the addition of a small negative imaginary part. Separating the region of integration of  $x$  into  $(0, \xi)$  and  $(\xi, 1)$  and performing the  $s$ -integration for these regions separately, we obtain, after some lengthy but straightforward calculations,

$$I_0 = \frac{1}{2} \int_0^1 dz \int_0^1 dx \frac{x}{[\kappa_0^2 x^2 + \kappa^2(1-x) + q^2 z(1-x)^2 - \frac{1}{4} p^2 x^2]} \quad \dots \quad (27)$$

Thus, by Eqns. (24) and (24'),

$$I \simeq \int_0^1 dz \int_0^1 dx \frac{x(1-x)^2 z(1-x)}{[\kappa_0^2 x^2 + \kappa^2(1-x) + q^2 z(1-x)^2]^3}, \quad \dots \quad (28)$$

where we have again neglected  $\frac{1}{4} p^2$  as compared to  $\kappa_0^2$ .

Now, in Eq. (28), we note that when  $x$  in  $(1-x)$  of the denominator becomes significant, the term  $\kappa_0^2 x^2$  becomes large compared with the other terms whereas, for small values of  $x$  the terms  $\kappa^2$  and  $q^2$  predominate in the denominator. Hence in the denominator, we can write 1 instead of  $(1-x)$  for the factors of  $\kappa^2$  and  $q^2$ . Again, we can omit  $x$  in  $(1-x)^3$  in the numerator, since, when  $x$  is comparable with unity, the  $\kappa_0$  in the denominator makes the contribution anyhow small even without this factor, and thus the change thus introduced is negligible. Thus we can write

$$I \simeq \int_0^1 dz \int_0^1 dx \frac{x(1-z)z}{[\kappa_0^2 x^2 + \kappa^2 + q^2 z(1-z)]^3} \quad \dots (29)$$

The above heuristic argument, however, does not give us the degree of error in taking the value (29) instead of (28). We can estimate this by taking the difference of the right hand sides of Eqns (28) and (29). Using Eq. (12) we can show that this difference is of the order of

$$\int_0^1 \frac{x^2 dx}{[\kappa_0^2 x^2 - Ax + B]^3} + O(\kappa^2) \int_0^1 \frac{x^2 dx}{[\kappa_0^2 x^2 - Ax + B]^4} \quad \dots (30)$$

where the quantities  $A$  and  $B$  do not depend on  $x$  and are of the order of  $\kappa^2$  with  $B > A$ . Starting with the result

$$J = \int_0^1 \frac{dx}{[\kappa_0^2 x^2 - Ax + B]} = \frac{2}{\sqrt{4\kappa_0^2 B - A^2}} \tan^{-1} \left( \frac{\sqrt{4\kappa_0^2 B - A^2}}{2B - A} \right),$$

we get, by differentiating,

$$\int_0^1 \frac{x^2 dx}{[\kappa_0^2 x^2 - Ax + B]^3} \simeq \frac{1}{16\kappa_0^3 B^{3/2}} \tan^{-1} \left( \frac{2\kappa_0 \sqrt{B}}{2B - A} \right) \quad \dots (31a)$$

and

$$\int_0^1 \frac{x^2 dx}{[\kappa_0^2 x^2 - Ax + B]^4} \simeq \frac{1}{32\kappa_0^2 B^{5/2}} \tan^{-1} \left( \frac{2\kappa_0 \sqrt{B}}{2B - A} \right) \quad \dots (31b)$$

Thus we find the difference in the approximations (28) and (29) of the integral  $I$  as  $O\left(\frac{1}{\kappa_0^3 \kappa^3}\right)$ . On the other hand we find that the integral (29) is  $O(1/\kappa_0^2 \kappa^4)$ , such that we have neglected a term of the order of  $(\kappa/\kappa_0)$  higher than the leading

term when we have written down Eq. (29). The small values of the coefficients of the leading terms in Eq. (31) further justify this approximation.

Now performing the  $x$ -integration in Eq. (29) and retaining the main contribution, we get,

$$I \simeq \frac{1}{4\kappa_0^2} \int_0^1 \frac{z(1-z)dz}{[\kappa^2 + q^2z(1-z)]^2}, \quad \dots \quad (32)$$

which on direct evaluation gives us

$$I \simeq \frac{1}{4\kappa_0^2} \left\{ \frac{2\kappa^2 + q^2}{4(q^2)^{3/2}(\kappa^2 + \frac{1}{4}q^2)^{3/2}} \log \left( \frac{\sqrt{\kappa^2 + \frac{1}{4}q^2} + \frac{1}{2}(q^2)^{1/2}}{\sqrt{\kappa^2 + \frac{1}{4}q^2} - \frac{1}{2}(q^2)^{1/2}} \right) - \frac{1}{2q^2(\kappa^2 + \frac{1}{4}q^2)} \right\}, \quad \dots \quad (33)$$

such that by Eqs. (17) and (29),

$$S_4^{(d)} = \frac{i\pi^2 f^4 \kappa^4 \kappa_0^2}{(2\pi)^6 (p_{10} p_{20} p_{30} p_{40})^{1/2}} \delta(p_1 + p_2 - p_3 - p_4) \bar{u}(p_3) \tau_i \tau_j u(p_1) \bar{u}(p_4) \tau_i \tau_j u(p_2), \quad \dots \quad (34)$$

For crossed exchange of two mesons, we have, from Fig. 1(e),

$$S_4^{(e)} = -f^4 \kappa^4 (2\pi)^{-6} \kappa_0^2 (p_{10} p_{20} p_{30} p_{40})^{-1/2} \delta(p_1 + p_2 - p_3 - p_4) V'_{\mu\nu} \\ < \bar{u}(p_3) \tau_i \tau_j \gamma_\mu^{(1)} u(p_1) \bar{u}(p_4) \tau_j \tau_i \gamma_\nu^{(2)} u(p_2), \quad \dots \quad (35)$$

where

$$V'_{\mu\nu} = \int d^4k \frac{k_\mu k_\nu}{(\bar{k}^2 - 2k p_4)(k^2 - 2k p_1)(k^2 - 2k q + q^2 + \kappa^2)(k^2 + \kappa^2)} \quad \dots \quad (36)$$

Proceeding as in the case of successive exchange of two mesons, we obtain,

$$V'_{\mu\nu} = i\pi^2 \int_0^1 dx \int_0^1 dy \int_0^1 dz \, x(1-x)^2 z(1-z) \left\{ \frac{6Q'_\mu Q'_\nu}{D'^4} + \frac{g_{\mu\nu}}{D'^3} \right\} \quad \dots \quad (37)$$

where

$$Q'_\mu = p_{1\mu}x(1-y) + p_{4\mu}xy + q_\mu z(1-x) \quad \dots \quad (38)$$

and

$$D' = \kappa_0^2 x^2 + \kappa^2(1-x) + p^2 x^2 y(1-y) + q^2 z(1-z)(1-x)^2 + q^2 x^2 y(1-y) \\ \simeq \kappa_0^2 x^2 + \kappa^2(1-x) + q^2 z(1-z)(1-x)^2. \quad \dots \quad (39)$$

In the further nonrelativistic approximation, we have, in Eq. (35),

$$\begin{aligned}\gamma_\mu^{(1)}\gamma_\nu^{(2)}V'_{\mu\nu} &= i\pi^2 \int_0^1 dx \int_0^1 dz \ x(1-x)z(1-z) \left\{ -\frac{6\kappa_0^2 x^2}{D'^4} + \frac{1}{D'^3} \right\} \\ &= i\pi^2 I' \quad \text{say.} \quad \dots (40)\end{aligned}$$

We note that  $D'$  is positive definite and hence the integration above does not have the complications of the previous case.

For the evaluation of the integral (40), we make the same approximation as was made in the previous case in going from Eqn. (28) to (29). We have seen that this is strictly valid upto an order  $(\kappa/\kappa_0)$ . With this approximation we have, on carrying out the  $x$ -integration,

$$I' = -\frac{1}{4\kappa_0^2} \int_0^1 \frac{z(1-z)dz}{[\kappa^2 + q^2 z(1-z)]^2} \quad \dots (41)$$

A comparison of the above Eq. with Eq. (32) shows that

$$I' = -I.$$

Hence, by Eqns. (34), (35) and (49) and (41), we obtain, with  $I$  given by Eq. (33).

$$S_4^{(d)} + S_4^{(e)} \simeq 6i\pi^2 f^4 \kappa^4 (2\pi)^{-6} \delta(p_1 + p_2 - p_3 - p_4) \bar{I} u(p_3) u(p_1) \bar{u}(p_4) u(p_2).$$

A comparison with the other terms of the fourth order also shows us that the major contribution in the fourth order arises from the successive and crossed exchange of two mesons. This can also be seen from physical reasons. For  $\gamma_\mu$  coupling, a transition from particle to antiparticle states will give us the maximum contribution, which is possible for the above type of diagrams.

#### APPENDIX

*Meson mass renormalisation* In order to interpret certain terms arising from Eq (4) as mass renormalisation, we have to first write the integral (5) occurring there in the form (6). We notice that this integral, written as

$$I = \int_0^1 dx \int d^4k \frac{k^2 + qk + \kappa_0^2}{(k^2 + 2kqx + q^2x + \kappa_0^2)^2} \quad \dots (A1)$$

is quadratically divergent, and thus requires care even in the change of momentum variables to be integrated. Using well-known methods (Jauch and Rohrlich 1955, also Eq (12)), we obtain, for a shift of the origin,

$$I = \int_0^1 dx \int d^4k \frac{k^2 - q^2x(1-x) + \kappa_0^2}{(k^2 + q^2x(1-x) + \kappa_0^2)^2} - \frac{i\pi^2}{4} q^2 \quad (A2)$$

In order to write the integral  $I$  of (A2) in the form (6), we repeatedly make use of the identity (Eq. (12))

$$\frac{1}{\alpha^n} - \frac{1}{\beta^n} = \int_0^1 \frac{n(\beta - \alpha)}{(\alpha z + \beta(1-z))^{\overline{n+1}}} dz$$

This gives us, after some lengthy calculation and comparing with Eq. (6), the values of the constants  $A$  and  $B$  as

$$A = \int_0^1 dx \int d^4k \frac{k^2 + \kappa^2 x(1-x) + \kappa_0^2}{(k^2 - \kappa^2 x(1-x) + \kappa_0^2)^2} = \frac{\pi^2}{4} \kappa^2 \quad \dots \quad (\text{A3})$$

and

$$B = \int_0^1 dx \int d^4k \left\{ \frac{4x(1-x)(k^2 + \kappa_0^2)}{(k^2 - \kappa^2 x(1-x) + \kappa_0^2)^2} - \frac{x(1-x)}{(k^2 - \kappa^2 x(1-x) + \kappa_0^2)^2} \right\} = \frac{\pi^2}{4} \quad \dots \quad (\text{A4})$$

Also, after momentum integration, the finite integral  $I_\sigma(q^2)$  is given as

$$I_\sigma(q^2) = i\pi^2 \int_0^1 dx \int_0^1 dy \int_0^1 dz \ x^2(1-x)^2 y \times \{ 3(\kappa_0^2 + q^2 x(1-x)yz - \kappa^2 x(1-x)(1-yz))^{-1} \\ + 2\kappa_0^2(\kappa_0^2 + q^2 x(1-x)yz - \kappa^2 x(1-x)(1-yz))^{-2} \}. \quad \dots \quad (\text{A5})$$

We shall now see how the divergent constants  $A$  and  $B$  may be interpreted as mass renormalisation terms. For this purpose, we write the meson field Lagrangian and the interaction Lagrangian in the Heisenberg representation as

$$\underline{L}_m + \underline{L}_i \\ = -\frac{1}{2} [(\underline{\square}\underline{\phi})(\underline{\square}\underline{\phi}^\dagger) + (\kappa_1^2 + \delta\kappa_1^2 + \kappa_2^2 + \delta\kappa_2^2)(\partial_\mu \underline{\phi})(\partial_\mu \underline{\phi}^\dagger) \\ + (\kappa_1^2 + \delta\kappa_1^2)(\kappa_2^2 + \delta\kappa_2^2)\underline{\phi}^\dagger \underline{\phi}] - i f \underline{\bar{\Psi}} \gamma_5 \tau_3 \underline{\Psi} \underline{\phi}^\dagger \\ + \frac{1}{2\kappa_2} [(\delta\kappa_1^2 + \delta\kappa_2^2)(\partial_\mu \underline{\phi}^\dagger)(\partial_\mu \underline{\phi}^\dagger) + (\kappa_1^2 \delta\kappa_2^2 + \kappa_2^2 \delta\kappa_1^2 + \delta\kappa_1^2 \delta\kappa_2^2)\underline{\phi}^\dagger \underline{\phi}^\dagger], \quad \dots \quad (\text{A6})$$

where the line below the operators means the corresponding quantities in Heisenberg representation. In the above,  $\kappa_1$  and  $\kappa_2$  are unrenormalised masses and  $\delta\kappa_1^2$  and  $\delta\kappa_2^2$  are the renormalisation terms, such that the observed mass is given the equations

$$\kappa_1^2 + \delta\kappa_1^2 + \kappa_2^2 + \delta\kappa_2^2 = 2\kappa^2, \\ (\kappa_1^2 + \delta\kappa_1^2)(\kappa_2^2 + \delta\kappa_2^2) = \kappa^4 \quad (\text{A7})$$

We now have to set up the interaction representation and to do this, we proceed as in Umezawa (1956).

Using Eq. (A7), the meson field equation becomes

$$(\square - \kappa^2)^2 \phi^i(x) = -i \int \kappa^2 \bar{\psi}(x) \gamma_5 \tau_3 \psi(x) + (\kappa_1^2 \delta \kappa_2^2 + \kappa_2^2 \delta + \kappa_1^2 \delta \kappa_2^2) \phi^i(x) - (\delta \kappa_1^2 + \delta \kappa_2^2) \square \phi^i(x) \quad \dots \quad (\text{A8})$$

We now solve the above equation with the retarded Green's function  $G_R(x-x')$  satisfying the equation

$$(\square - \kappa^2)^2 G_R(x-x') = -\delta_4(x-x')$$

and  $G_R(x-x') = 0$  when  $x_0 < x'_0$  and the function  $G(x) = G_R(x) - G_R(-x)$ . Then, a partial integration with the assumption that the interaction (and hence the renormalisation terms) vanish at infinite past sufficiently rapidly, gives us,

$$\phi^i(x) = \phi^i(x) + \frac{1}{\square} \int_{-\infty}^{\infty} d^4 x' (1 - \epsilon(x-x')) \{ G(x-x') [i \kappa^2 \bar{\psi}(x') \gamma_5 \tau_3 \psi(x') - (\kappa_1^2 \delta \kappa_2^2 + \kappa_2^2 \delta + \kappa_1^2 \delta \kappa_2^2) \phi^i(x') - (\delta \kappa_1^2 + \delta \kappa_2^2) (\partial'_\mu G(x-x')) (\partial'_\mu \phi^i(x')) \} \} \quad (\text{A9})$$

where  $\phi^i(x)$  is a field operator satisfying the equation

$$(\square - \kappa^2)^2 \phi^i(x) = 0 \quad \dots \quad (\text{A10})$$

and  $\epsilon(x-x') = 1$  or  $-1$  according as  $x'$  is earlier or later than  $x$ . The words "earlier" and "later" refer to space-like surfaces on which  $c(x-x')$  has a discontinuity.

Now, let the interaction representation state-vector  $\underline{\psi}(\sigma)$  be given in terms of the Heisenberg state-vector  $\Phi$  as  $\Phi(\sigma) = S(\sigma)\Phi$ ,  $S(-\infty) = 1$ . Then we have,

$$i \frac{\delta S(\sigma)}{\delta \sigma(x)} = H(x, \sigma) S(\sigma) \quad (\text{A11})$$

and the integrability condition

$$\frac{\delta H(x', \sigma)}{\delta \sigma(x)} - \frac{\delta H(x, \sigma)}{\delta \sigma(x')} = i [H(x', \sigma), H(x, \sigma)] \quad (\text{A12})$$

where  $x$  and  $x'$  are any two points lying on the surface  $\sigma$ .

We now define auxiliary field operators  $\phi^i(x, \sigma)$  given by

$$\begin{aligned} \phi^i(x, \sigma) = & \phi^i(x) + \int_{-\infty}^{\sigma} \{ G(x-x') [i \kappa^2 \bar{\psi}(x') \gamma_5 \tau_3 \psi(x') \\ & - (\kappa_1^2 \delta \kappa_2^2 + \kappa_2^2 \delta + \kappa_1^2 \delta \kappa_2^2) \phi^i(x') \\ & - (\delta \kappa_1^2 + \delta \kappa_2^2) (\partial'_\mu G(x-x')) (\partial'_\mu \phi^i(x')) \} d^4 x', \end{aligned} \quad (\text{A13})$$

and proceed exactly as in Umezawa (1956). Then we obtain that the interaction Hamiltonian is given by the equation

$$\begin{aligned} |\phi(x), H(x', \sigma)| &= iU(x-x')S(\sigma)if\kappa^2\bar{\psi}(x')\gamma_5\tau_i\psi(x') \\ &\quad -(\kappa_1^2\delta\kappa_2^2 + \kappa_2^2\delta\kappa_1^2 + \delta\kappa_1^2\delta\kappa_2^2)\phi^i(x')S^{-1}(\sigma) \\ &\quad -S(\sigma)(\delta^{-1} + \delta^{-2})(\partial'_\mu U(x-x'))(\partial'_\mu\phi^i(x'))S^{-1}(\sigma), \end{aligned} \quad \dots \quad (A14)$$

where clearly  $x'$  lies on  $\sigma$ . Using this, and that  $U(x-x')$  and its first order space-time derivatives vanish for space-like separation of the points, Eq. (A14) may be seen to reduce to

$$\begin{aligned} |\phi^i(x), H(x', \sigma)| &= i\kappa^2U(x-x')if\bar{\phi}(x')\gamma_5\tau_i\psi(x') \\ &\quad -(\kappa_1^2\delta\kappa_2^2 + \kappa_2^2\delta\kappa_1^2 + \delta\kappa_1^2\delta\kappa_2^2)iU(x-x')\phi^i(x') \\ &\quad -(\delta\kappa_1^2 + \delta\kappa_2^2)i(\partial'_\mu U(x-x'))(\partial'_\mu\phi^i(x')) \end{aligned} \quad \dots \quad (A15)$$

Since the field operators in Eq. (A15) satisfy free field commutation relations

$$[\phi^i(x), \phi^j(x')] = i\kappa^2\delta_{ij}U(x-x'),$$

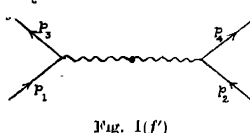
we obtain

$$\begin{aligned} H(x', \sigma) &= if\bar{\psi}(x')\gamma_5\tau_i\psi(x')\phi^i(x) - \frac{1}{2}\kappa^2(\kappa_1^2\delta\kappa_2^2 + \kappa_2^2\delta\kappa_1^2 + \delta\kappa_1^2\delta\kappa_2^2)\phi^i(x')\phi^i(x') \\ &\quad - \frac{1}{2}\kappa^2(\delta\kappa_1^2 + \delta\kappa_2^2)(\partial'_\mu\phi^i(x'))(\partial'_\mu\phi^i(x')) \end{aligned} \quad \dots \quad (A16)$$

We note that the presence of derivatives of field operations in the self-coupling of the meson fields *does not* introduce terms depending on the normal to the surface

The above interaction Hamiltonian clearly satisfies the integrability condition (A12).

The presence of second and third terms in  $H(x, \sigma)$  of Eq. (A16) gives rise to vertices with only two meson lines. Consideration of the corresponding Feynman diagram (Fig. 1f') gives us, with



$$\begin{aligned} A_1 &= \frac{1}{2}\kappa^2(\kappa_1^2\delta\kappa_2^2 + \kappa_2^2\delta\kappa_1^2 + \delta\kappa_1^2\delta\kappa_2^2) \\ B_1 &= \frac{1}{2}\kappa^2(\delta\kappa_1^2 + \delta\kappa_2^2) \end{aligned} \quad \dots \quad (A17)$$

the contribution as

$$\begin{aligned} S_2^{(a')} &= -if^2\kappa^4(2\pi)^{-2}\delta(p_1+p_2-p_3-p_4)\kappa_0^4(p_{10}p_{20}p_{30}p_{40})^{-\frac{1}{2}} \\ &\quad \times \bar{u}(p_3)\gamma_5\tau_i u(p_1)\bar{u}(p_4)\gamma_5\tau_i u(p_2)[(A_1-B_1\kappa^2)(q^2+\kappa^2)^{-4} + B_1(q^2+\kappa^2)^{-3}]. \end{aligned} \quad \dots \quad (A18)$$

Comparison of Eqs. (A17), (4) and (6) shows that the contributions with the divergent constants  $A$  and  $B$  are cancelled provided

$$4f^4\kappa^4A = if^2\kappa^4(2\pi)^4(A_1 - B_1\kappa^2),$$

$$4f^4\kappa^4B = if^2\kappa^4(2\pi)^4B_1.$$

Remembering substitution (17), the last equation gives the bare masses and the renormalisation terms with  $A$  and  $B$  given by equations (A3) and (A4). We note that the interpretation of the constants  $A$  and  $B$  in conventional meson theory went to both mass and coupling constant renormalisation, which is not possible here. Also, two bare masses were needed to interpret two divergent constants as renormalisation terms. On the other hand, if we had started with a bare particle of unique mass, and had considered interaction, the corresponding mass renormalisation would have given rise to a splitting of the mass. This result is interesting, but such a splitting is useless to investigate so long as the equations that determine the splitting, and thus the physical masses, contain infinite constants.

#### ACKNOWLEDGMENT

The author wishes to express his sincere thanks to Prof. D. Basu for suggesting the problem and to Dr. B. B. Deo for many interesting discussions.

#### REFERENCES

- Bhabha, H. J., 1950, *Phys. Rev.*, **77**, 665.  
 Jauch, J. M. and Rohrlich, F., 1955, *The theory of Electrons and Photons*, Addison Wesley Publ. & Co.  
 Misra S. P. and Deo B. B., 1956, *Ind. J. Phys.*, **30**, 16.  
 Misra, S. P., 1960, *Ind. J. Phys.*, **34**, 92.  
 Schweber, S. S., Bethe, H. A. and de Hoffman, F., 1955, *Mesons and Fields*, Vol. 1, Row, Peterson & Co.  
 Thirring, W., 1950, *Phil. Mag.*, **41**, 653.  
 Umezawa H., 1956, *Quantum Field Theory*, North Holl. Publ. & Co.



# ULTRAVIOLET ABSORPTION SPECTRA OF ISOMERIC FLUOROTOLUENES IN THE LIQUID AND SOLID STATES\*

S. K. Sen

OPTICS DEPARTMENT, INDIAN ASSOCIATION FOR THE CULTIVATION OF SCIENCE, JADAVPUR,  
CALCUTTA-32

(Received, February 29, 1960)

**ABSTRACT.** The ultraviolet absorption spectra of isomeric fluorotoluenes in the liquid and solid states have been analysed and the results have been compared with those for the substances in the vapour state reported by previous workers.

The spectrum due to liquid state of *o*-fluorotoluene exhibits broad bands, the 0,0 band being shifted towards longer wavelengths by  $238\text{ cm}^{-1}$  with respect to that due to vapour. The bands become sharper and shift towards shorter wavelengths when the liquid is solidified and cooled to  $-180^\circ\text{C}$ .

The spectrum due to the liquid *m*-fluorotoluene appears to consist of two series of broad bands which have been assigned to monomers and dimers respectively. Only one system of bands is given by the substance in the solid state at  $-180^\circ\text{C}$ . It has been shown that these results can be explained if it is assumed that all the molecules are transformed into dimers in the solid state at  $-180^\circ\text{C}$ .

The spectrum due to *p*-fluorotoluene in the solid state at  $-180^\circ\text{C}$  seems to consist of two series of bands. It has been possible to analyse them on the supposition that the excited electronic energy level is split up into two components. The shift of the 0,0 band on liquefaction is observed to be larger in the case of the para compound than in the case of the ortho compound. It has therefore been concluded that the larger shift may be due to the formation of dimers even in the liquid state. The cause of the splitting has been discussed.

## INTRODUCTION

Investigations on the influence of intermolecular field on the absorption spectra of some halogen substituted benzene compounds in the state of aggregation at low temperature by Swamy (1952, 1953) revealed some interesting facts. Splitting of the electronic energy level into three components was observed in the case of *o*- and *m*-chlorotoluene, *o*-dichlorobenzene and *o*-bromotoluene when the substances were solidified and cooled to  $-180^\circ\text{C}$ . No splitting was, however, observed in the case of the para compounds. Similar changes in the spectra were observed later in the case of *m*-bromotoluene and *m*-dichlorobenzene by the present author (Sen, 1957). Thus, unsymmetrical disubstituted benzenes containing halogen atoms as substituents showed the splitting of the energy level.

\*Communicated by Prof. S. C. Sarker.

The electronic absorption spectra of free molecules of isomeric fluorotoluenes in the vapour state have been investigated by Cave and Thompson (1950) and the spectra of solutions of isomeric fluorotoluenes in *n*-heptane have been reported by Miller and Thompson (1949). They observed higher extinction co-efficient for *p*-fluorotoluene than in the case of *o*- and *m*-fluorotoluene.

Previous investigations on the influence of intermolecular field on the absorption spectra of halogen substituted benzenes have been confined only to compounds having either chlorine or bromine atom as a substituent. As the fluorine atom is more strongly active than the chlorine or bromine atom, it was thought worthwhile to extend the investigations to isomeric fluorotoluenes. With this object, the ultraviolet absorption spectra of *o*-, *m*- and *p*-fluorotoluene in the liquid state and in the solid state at  $-180^{\circ}\text{C}$  have been studied in the present investigation. The results have been discussed and compared with those for the other halogen substituted benzene compounds in the states of aggregation reported by previous workers.

#### EXPERIMENTAL

Chemically pure samples of *o*-, *m*- and *p*-fluorotoluene (Fisher) were distilled repeatedly under reduced pressure before being used in the present investigation.

The experimental set up was the same as in an earlier investigation by the author (Sen, 1955). Spectrograms were taken on Ilford HP3 films with Hilger EI quartz spectrograph having a dispersion of 3 Å.U per mm in the region of 2600 Å. Very thin films of thicknesses of the order of a few microns were required to produce the bands due to the liquid state and the time of exposure varied from 10 to 15 minutes. The corresponding spectra due to the substances in the frozen state at low temperature were recorded with a time of exposure of about 1 hr. Iron arc spectrum was taken in each spectrogram as comparison. Microphotometric records were obtained with a self-recording microphotometer of Kipp and Zonen type. The frequencies of the bands were measured using the microphotometric records of iron lines as in an earlier investigation (Sen, 1956). The slit width was 0.3 mm ( $\approx 15\text{ cm}^{-1}$ ) in the region of 2600 Å.

#### RESULTS

The microphotometric records of the spectra are reproduced in Figs. 1, 2 and 3 and the wave numbers of the bands with approximate intensities and probable assignments are given in Tables I—III.

#### DISCUSSION

##### (a) *o*-Fluorotoluene ( $\text{C}_6\text{H}_4\text{CH}_3\text{F}$ ):

The absorption spectrum of *o*-fluorotoluene in the vapour state had earlier been photographed by Cave and Thompson (1950). The 0,0 band was taken at

37576  $\text{cm}^{-1}$ . The rest of the bands were explained as due to progressions of excited state vibration frequencies 707, 924, 1230  $\text{cm}^{-1}$  and their combinations.

They pointed out that on the longer wavelength side of the 0,0 band there is a very strong band, but they did not explain why the feebler band was taken as the 0,0 band. On examining the spectrogram reproduced by them, it is found that if the 0,0 band be identified with the strong band at 37484  $\text{cm}^{-1}$ , two very sharp and weak bands at 37414  $\text{cm}^{-1}$  and 37554  $\text{cm}^{-1}$  yield a vibration frequency 70  $\text{cm}^{-1}$  both in the ground and excited states. These two frequencies seem to be coupled with all other stronger bands giving progressions of frequencies 707  $\text{cm}^{-1}$ , 804  $\text{cm}^{-1}$ , 929  $\text{cm}^{-1}$  and 1230  $\text{cm}^{-1}$ . Also, a band giving an excited frequency 498  $\text{cm}^{-1}$  is observed in the spectrum due to the vapour state and this band is observed in the spectrum due to crystals at  $-180^\circ\text{C}$ . Hence the 0,0 band due to the vapour is fixed at 37484  $\text{cm}^{-1}$ .

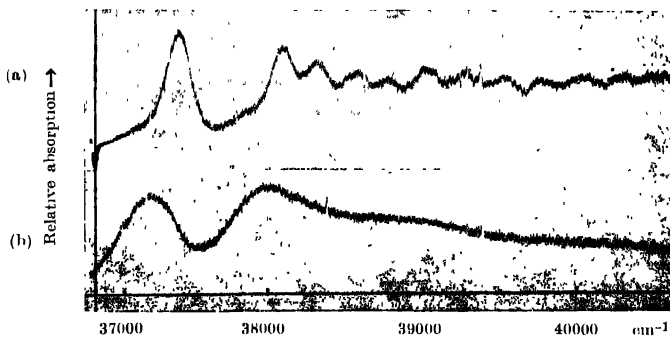


Fig. 1. Microphotometric records of the ultraviolet absorption spectra of *o*-fluorotoluene.  
(a) Solid at  $-180^\circ\text{C}$ . (b) Liquid at  $30^\circ\text{C}$ .

Four broad bands have been observed in the spectrum due to liquid state, the centre of the 0,0 band being at 37246  $\text{cm}^{-1}$ . The 0,0 band thus shifts towards longer wavelengths by 238  $\text{cm}^{-1}$  with liquefaction of vapour. Such a shift may be explained on the supposition that intermolecular field acting on the molecules in the liquid state lowers the excited electronic energy state. The broadness of the bands may be due to fluctuation of intermolecular field by thermal motion of molecules. The succeeding bands represent progressions of excited state vibration frequencies 707  $\text{cm}^{-1}$  and 924  $\text{cm}^{-1}$ , which are not different from the corresponding frequencies observed in the vapour state.

TABLE I

Absorption bands of *o*-fluorotoluene in the liquid and solid states

Vapour Cave and Thompson (1950) (Prominent bands)		Present author on the basis of spectrogram repro- duced by Cave & Thompson (1950) (Prominent bands)		Liquid at 30°C.		Solid at -180°C.	
$\nu$ in cm <sup>-1</sup>	Assign- ment	$\nu$ in cm <sup>-1</sup>	Assign- ment	$\nu$ in cm <sup>-1</sup>	Assign- ment	$\nu$ in cm <sup>-1</sup>	Assign- ment
36827	0-749	37351(vw)	0-133				
37302	0-274	37414(w, very sharp)	0-70				
37576	0,0	37484(vs)	0,0	37246(s,b)	0,0	37400(vs)	0,0
38283	0+707	37554(w, very sharp)	0+70	37953(s,b)	0+707	37896(m)	0+496
38500	0+924	37982(w)	0+498	38170(m,b)	0+924	38107(s)	0+707
38806	0+1230	38121(w, very sharp)	0+707 -70	38877(w,b)	0+707+924	38324(s)	0+924
		38191(s)	0+707			38630(m)	0+1230
		38260(w, very sharp)	0+707+70			38815(m)	0+707×2
		38218(w, very sharp)	0+804-70			39035(m)	0+707+924
		38288(s)	0+804			39127(m)	0+496+1230
		38358(w, very sharp)	0+804+70			39250(m)	0+924×2
		38413(s)	0+929			39552(m)	0+924+1230
		38714(m)	0+1230			39741(m)	0+707×2+924
						40044(m)	0+707×2+1230
						40261(w)	0+707+924+1230

On solidification and cooling of the substance to -180°C, the spectrum yields a sharper system of bands with the 0,0 band at 37400 cm<sup>-1</sup> shifted by 154 cm<sup>-1</sup> towards shorter wavelengths with respect to its position in the liquid state. Progressions of excited state vibration frequencies 496, 707, 924, 1230 cm<sup>-1</sup> have been observed. As mentioned earlier, the frequency 496 cm<sup>-1</sup> also appears in the vapour state and it may correspond to the ground state vibration frequency 530 cm<sup>-1</sup>. *o*-Fluorotoluene does not seem to exhibit any splitting of electronic energy level unlike orthochloro- and orthobromotoluene.

(b) *m*-Fluorotoluene ( $C_6H_4CH_3F$ )

The ultraviolet absorption spectrum due to vapour state of *m*-fluorotoluene was analysed by Cave and Thompson (1950). They found a large number of feeble bands within a distance of  $240\text{ cm}^{-1}$  from the 0,0 band at  $37398\text{ cm}^{-1}$  on the shorter wavelength side and a set of strong bands on the longer wavelength side. The latter bands were assigned to  $v \rightarrow 0$  transitions with ground state vibration frequencies 70, 184, 253, 311, 520 and  $726\text{ cm}^{-1}$ .

In the liquid state the first band appears to consist of two unresolved broad bands with centres at  $36965\text{ cm}^{-1}$  and  $37212\text{ cm}^{-1}$ . The next two prominent bands have a separation of  $685\text{ cm}^{-1}$  from the first two bands respectively. The succeeding bands are very broad having no structure.

TABLE II

 Absorption bands of *m*-fluorotoluene in the liquid and solid states

Vapour Cave & Thompson (1950) (Prominent bands)		Liquid at $30^\circ\text{C}$		Solid at $-180^\circ\text{C}$ .	
$\nu$ in $\text{cm}^{-1}$	Assignment	$\nu$ in $\text{cm}^{-1}$	Assignment	$\nu$ in $\text{cm}^{-1}$	Assignment
36935	0—1003				
36672	0—726				
36878	0—520				
37087	0—311				
37145	0—184—70				
37176	0—253				
37214	0—184				
37243					
37273	0—70				
37325					
37346					
37368					
37398	0,0	36965 (s)	$A_g$	37239 (s)	0,0
37486	0 + 684—520	37212 (s)	$B_g$	37924 (s)	0 + 685
37496	—70	37650 (s)	$A_g + 685$	38163 (s)	0 + 924
37535		37896 (s)	$B_g + 685$	38485 (s)	0 + 1246
37558	0 + 684—520				
37573				38853 (m)	0 + 685 + 924
37631	0 + 965—726			39087 (m)	0 + 924 $\times$ 2
37680	0 + 282			39412 (m)	0 + 924 + 1246
37892	0 + 457			39733 (w)	0 + 1246 $\times$ 2
38082	0 + 684			40331 (w)	0 + 924 $\times$ 2 + 1246
38363	0 + 965				
38659	0 + 1261				

The spectrum seems to consist of two series of bands separated by  $247\text{ cm}^{-1}$  and one of these series seems to disappear with solidification of the liquid. Hence it has been assumed that the two series are produced respectively by the monomers and dimers present in the liquid and that in the solid state at  $-180^\circ\text{C}$ , all the molecules are transformed into dimers.

When the liquid is solidified and cooled to  $-180^\circ\text{C}$ , the first band becomes narrower and appears to consist of only one broad band with its centre at  $37239\text{ cm}^{-1}$ . However, the 0,0 band due to the frozen mass at  $-180^\circ\text{C}$  is not sharp but it has a width of about  $100\text{ cm}^{-1}$ . This cannot be due to the presence of unresolved bands due to  $0 \rightarrow v$  transitions by the side of the 0,0 band on the shorter wavelength side because the first band is quite symmetrical throughout the whole width, and similarly, all the succeeding bands on the short wavelength side are equally wide. It appears, therefore, that these widths of the bands are due to perturbation produced by neighbouring molecules in the crystal on the electronic energy level of the molecule. This perturbation being small, there is no observable splitting into three components as observed in other cases of halogen substituted meta compounds. It appears from Fig. 2(a) and Table II, that in the spec-

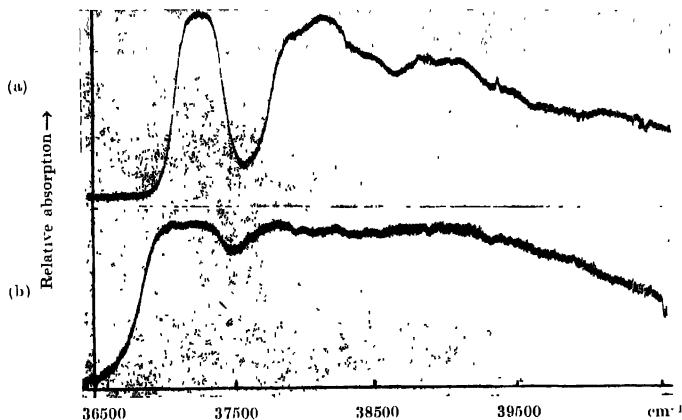


Fig. 2. Microphotometric records of the ultraviolet absorption spectra of *m*-fluorotoluene.  
(a) Solid at  $-180^\circ\text{C}$ . (b) Liquid at  $30^\circ\text{C}$ .

trum due to solidified *m*-fluorotoluene at  $-180^\circ\text{C}$ , there are bands due to vibrational transitions of excited state frequencies 685, 924 and  $1246\text{ cm}^{-1}$ . While the first frequency remains unaltered with change of state, the latter two correspond to the frequencies 965 and  $1261\text{ cm}^{-1}$  observed in the vapour state. The fact that the first band due to solid state at  $-180^\circ\text{C}$  is displaced towards shorter wavelengths from the position of the first band due to the liquid state confirms the assignment

indicated above, because generally with solidification and cooling of the crystals to  $-180^{\circ}\text{C}$ , the 0,0 band shifts towards shorter wavelengths. In the present case the 0,0 band at  $36965\text{ cm}^{-1}$  due to the dimers shifts towards shorter wavelengths with solidification of the liquid.

The assignment of the bands on both sides of the 0,0 band due to vapour state made by Cave and Thompson (1950) is confirmed by the fact that these bands disappear at low temperature.

(c) *p*-Fluorotoluene ( $\text{C}_6\text{H}_4\text{CH}_3\text{F}$ )

The analysis of the spectrum due to para compound in the vapour state made by Cave and Thompson (1950) shows the 0,0 band to be at  $36876\text{ cm}^{-1}$  and the succeeding bands are assigned to progressions of excited state frequencies 185, 398, 584, 794, 843, 1014, 1194 and  $1229\text{ cm}^{-1}$ . In the liquid state broad bands have been observed with the 0,0 band at  $36517\text{ cm}^{-1}$ . Thus, there is a shift of the 0,0 band by  $359\text{ cm}^{-1}$  towards longer wavelengths on liquefaction of vapour. The succeeding bands represent transitions corresponding to vibrational frequencies 843 and  $1230\text{ cm}^{-1}$  not different from the corresponding frequencies observed for the vapour state.

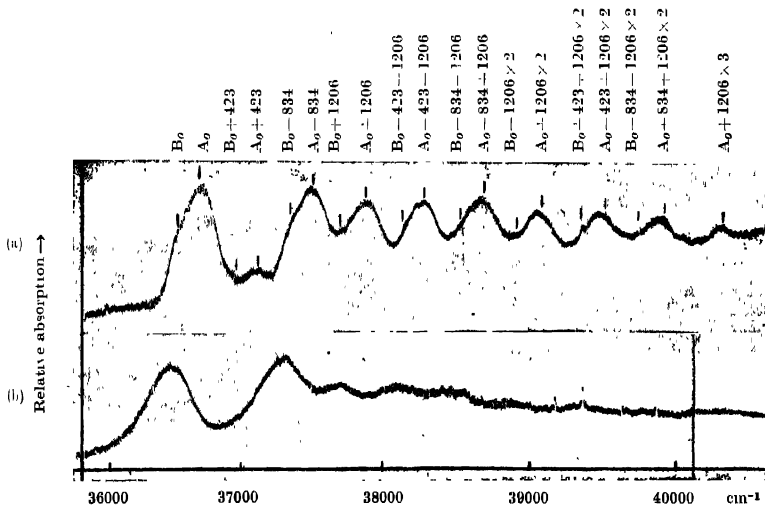


Fig. 3. Microphotometric records of the ultraviolet absorption spectra of *p*-fluorotoluene.

(a) Solid at  $-180^{\circ}\text{C}$ .

(b) Liquid at  $30^{\circ}\text{C}$ .

It is evident from Fig. 3(a) and Table III that in the spectrum due to solid state at  $-180^{\circ}\text{C}$ , each strong band is accompanied by a weaker one on the longer wavelength side. The first weak band cannot be due to a  $v \rightarrow 0$  transition, because the corresponding band due to  $0 \rightarrow v$  transition is absent. Hence, it is concluded that there is a splitting of the bands in the solid state. The distance between the components is observed to be  $188\text{ cm}^{-1}$  and assignments of the bands have been made on the assumption that the excited electronic energy level is split up into two components with a separation of  $188\text{ cm}^{-1}$ .

The excited state vibrational frequencies are observed to be 423, 834 and  $1206\text{ cm}^{-1}$ . The new excited state frequency  $423\text{ cm}^{-1}$  does not seem to have been observed in the vapour state and the other two frequencies may correspond to the frequencies  $843\text{ cm}^{-1}$  and  $1229\text{ cm}^{-1}$  observed in the spectrum due to the vapour. The intense component of the 0,0 band is shifted towards shorter wavelengths by  $223\text{ cm}^{-1}$ .

A comparison of the spectra due to the vapours of the ortho- and para dichlorobenzene shows that the 0,0 band shifts to longer wave lengths by about  $450\text{ cm}^{-1}$  with the change from the ortho to the para configuration. In the present case a similar shift of about  $608\text{ cm}^{-1}$  is observed with the change from ortho to the para position of the fluorine atom. When the vapour is liquefied the 0,0 band again shifts towards longer wavelengths by about  $359\text{ cm}^{-1}$  while in the case of the ortho compound the shift with liquefaction of vapour is only  $238\text{ cm}^{-1}$ . Hence this larger shift in the case of the para compound may be due to formation of dimers in the liquid state.

In the case of *o*-chlorotoluene, *o*-dichlorobenzene and *m*-dichlorobenzene (Swamy, 1952, 1953, Sen, 1957) each band was found to be split up into three components, the central component being the strongest. In the spectra of *m*-chlorotoluene (Swamy, 1952), *o*-bromotoluene (Swamy, 1953) and *m*-bromotoluene (Sen, 1957) in the solid state the strongest of the three components is on the short wavelength side of the other two components. In the case of *p*-fluorotoluene also, the weaker component is on the longer wavelength side of the stronger component in each of the bands.

It has already been pointed out by Sirkar and Misra (1959) that the so called Davydov splitting is not observed in the case of certain crystals owing probably to the fact that the contribution of only a few neighbours predominates in the interaction of transition moments of neighbouring molecules on the energy of any particular molecule, and therefore, the oscillator strength determined with a large number of molecules in the absorbing path cannot be used in this case. They also pointed out that when the transition takes place in the field of the permanent dipoles surrounding any molecule in the crystal there may be a splitting of the bands. Probably in the case of *p*-fluorotoluene also, the splitting is due to the interaction of such dipoles on the electronic transition in the molecule.



TABLE III

 Absorption bands of *p*-fluorotoluene in the liquid and solid states

Vapour Cavo & Thompson (1950) (Prominent bands)		Liquid at 30°C.		Solid at -180°C.	
$\nu$ in $\text{cm}^{-1}$	Assignment	$\nu$ in $\text{cm}^{-1}$	Assignment	$\nu$ in $\text{cm}^{-1}$	Assignment
35720	0-1156				
36632	0-844				
36051	0-825				
36235	0-641				
36423	0-453				
36539	0-337				
36565	0-311				
36659	0-217				
36780	0-96				
36831	0-40			36552 (w)	$B_u$
36876	0,0	36517 (s,b)	0,0	36740 (s)	$A_g$
36906	0-185-96	37360 (s,b)	0-843	36975 (w)	$B_g$ - 423
37001	0-584-453	37747 (m,b)	0-1230	37163 (m)	$A_g$ - 423
37061	0-185	38200 (m,b)	0-843 $\times 2$	37386 (m)	$B_g$ - 834
37175	0-398-96	38591 (w,b)	0-843-1230	37568 (s)	$A_g$ - 834
37218	0-398-40	39135 (w,b)	0-843 $\times 2$ -1230	37758 (w)	$B_g$ - 1206
37231				37948 (s)	$A_g$ - 1206
37274	0-398			38185 (w)	$B_g$ - 423-1206
37460	0-584			38368 (s)	$A_g$ - 423-1206
37670	0-794 0-398 $\times 2$			38598 (w)	$B_g$ - 834 - 1206
37719	0-843			38778 (s)	$A_g$ - 834-1206
37890	0-1014			38968 (w)	$B_g$ - 1206 $\times 2$
38070	0-1194			39157 (s)	$A_g$ - 1206 $\times 2$
38105	0-1229			39389 (w)	$B_g$ - 423-1206 $\times 2$
				39576 (s)	$A_g$ - 423-1206 $\times 2$
				39796 (w)	$B_g$ - 834-1206 $\times 2$
				39989 (s)	$A_g$ - 834 - 1206 $\times 2$
				40359 (m)	$A_g$ - 1206 $\times 3$

## ACKNOWLEDGMENT

The author is indebted to Professor S. C. Sirkar, D.Sc., F.N.I., for his kind interest and constant guidance throughout the progress of the work.

## REFERENCES

- Cave, W. T. and Thompson, H. W., 1950, *Discussions Faraday Society*, 9, 41.  
Miller, C. H. and Thompson, H. W., 1949, *J. Chem. Phys.*, 17, 845-6.  
Sen, S. K., 1955, *Ind. J. Phys.*, 29, 561.  
„ 1956, *Ind. J. Phys.*, 30, 56.  
„ 1957, *Ind. J. Phys.*, 31, 99.  
Sirkar, S. C. and Misra, T. N., 1959, *Ind. J. Phys.*, 33, 45-50.  
Swamy, H. N., 1952c, *Ind. J. Phys.*, 26, 445.  
„ 1953a, *Ind. J. Phys.*, 27, 55.  
„ 1953b, *Ind. J. Phys.*, 27, 119.

# RAMAN SPECTRA OF ORTHO- AND PARACHLORO-ANISOLE IN THE SOLID STATE AT $-180^{\circ}\text{C}^*$

KRISHNA KUMAR DEB

OPTICS DEPARTMENT, INDIAN ASSOCIATION FOR THE CULTIVATION OF SCIENCE, JADAVPUR,  
CALCUTTA-32

(Received, February 2, 1960)

## Plate III

**ABSTRACT.** The Raman spectra of ortho- and parachloroanisole have been studied in the liquid state and in the solid state at  $-180^{\circ}\text{C}$ . It has been observed that in the case of parachloroanisole the components of each of the doublets  $625$  and  $638\text{ cm}^{-1}$  and  $1584$  and  $1596\text{ cm}^{-1}$  coalesce to form a single line of Raman shift  $640\text{ cm}^{-1}$  in the former case and  $1603\text{ cm}^{-1}$  in the latter case. When the liquid is solidified a new line  $3026\text{ cm}^{-1}$  also appears in the spectrum. Besides these changes three new low frequency Raman lines  $60$ ,  $92$  and  $132\text{ cm}^{-1}$  also appear with solidification of the liquid.

In the case of orthochloroanisole no appreciable changes take place in the spectrum and no new low frequency lines appear with the solidification of the liquid. It has been concluded from these results that in the case of the ortho compound the  $\text{OCH}_3$  group is probably chelated to the adjacent chlorine atom and therefore the formation of associated groups is not possible in the solid state. Such groups are, however, formed when the para compound is solidified and the new low frequency lines observed in this case are attributed to such groups of molecules.

## INTRODUCTION

Since the discovery of new low-frequency Raman lines in the Raman spectra of some substituted benzene compounds in the solid state by Gross and Vuks (1936) many workers have investigated the Raman spectra of a large number of such solidified benzene compounds at different temperatures (Sirkar, 1937; Mazumder, 1949, Ray, 1950a,b, 1951, 1952, Biswas, 1954,a,b,c, 1955a,b,c, 1956a; and others). It has been concluded by these workers from the results obtained by them that the low-frequency Raman lines originate from vibrations in small groups of molecules formed by the attachment of the individual molecules to neighbouring molecules through weak linkages and that these lines cannot be attributed either to angular oscillations of the molecules about their axes as suggested by Kastler and Rousset (1941) and by Bhagavantam (1941) or to translational lattice oscillation as suggested by Gross and Vuks (1936). Generally, halogen substituted benzene compounds yield strong low-frequency Raman lines in the solid state and it has been pointed out that the formation of weak intermolecular bonds is more probable in such cases than in the molecules in which no such halogen atom

\*Communicated by Prof. S. C. Sirkar.

is present as a substituent. In certain disubstituted benzene compounds, such as chlorophenol, chloroanisole, etc., there is rotational freedom of the OH or  $\text{OCH}_3$  group about the C—O bond, but the relative positions of the halogen atom and the other substituent have influence on such rotational freedom. It would be interesting to find out whether the formation of intermolecular linkages in the solid state and the consequent production of low-frequency Raman lines are influenced by relative positions of the two substituents in such cases. As a preliminary investigation of this problem, the Raman spectra of ortho- and parachloroanisole in the solid state at  $-180^\circ\text{C}$  have been studied and the results have been compared with those for the liquids.

#### EXPERIMENTAL

The liquids were of chemically pure quality supplied by British Drug House. They were further purified by distillation under reduced pressure. While recording the spectra due to the liquids a strong continuous fluorescence in the visible region was observed. Hence, to reduce the intensity of this fluorescence a second photograph of the spectrum was taken in each case using Rhodamine 6 GBN filters which cut off  $4046\text{\AA}$  group of mercury lines. The fluorescence was found to be stronger in the case of orthochloroanisole than in the case of the para compound.

In order to record the Raman spectra of the compounds in the solid state attempt was made to obtain a homogeneous solid mass by cooling the liquid slowly so that the stray light due to diffuse reflection from the inner portion of the solid could be reduced considerably. The experimental arrangement in this case was the same as that used by Biswas (1954). The Raman spectra were recorded on Ilford Zenith plates using a Fuess glass spectrograph giving a dispersion of about  $11\text{\AA}$  in the region of  $4046\text{\AA}$ . The polarisation of the Raman lines due to each of the compounds was also studied in the usual manner, but in the case of the ortho compound a freshly prepared 5%  $\text{NaNO}_2$  solution was used as a filter in order to avoid the continuous fluorescence in the regions from  $4358\text{\AA}$  to  $4916\text{\AA}$ .

#### RESULTS AND DISCUSSION

The spectrograms are reproduced in Plate III. The Raman frequencies of the lines are given in Tables I and II. The frequencies reported for the liquids by previous workers are also included in the tables. The states of polarisation of the Raman lines due to the compounds are indicated in the respective tables by the usual symbols  $D(\rho \geq 6/7)$  and  $P(\rho < 6/7)$ ,  $\rho$  being the depolarisation factor.

##### (a) Parachloroanisole :

It can be seen from Table I and Figs. 1(a) and 1(b) that the following changes take place when this liquid is solidified and cooled to  $-180^\circ\text{C}$ .

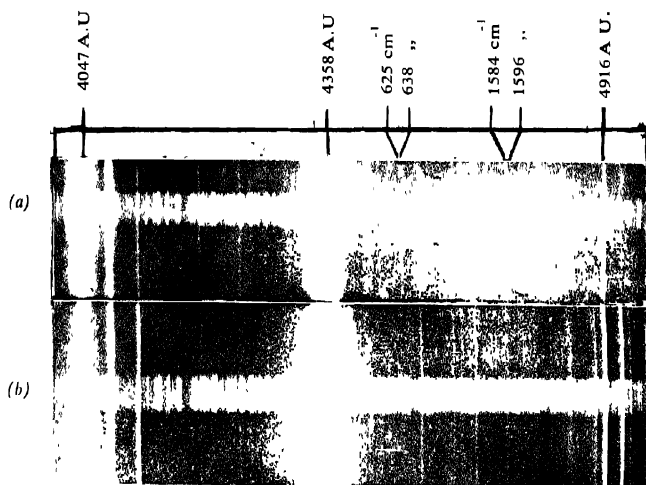


Fig. 1

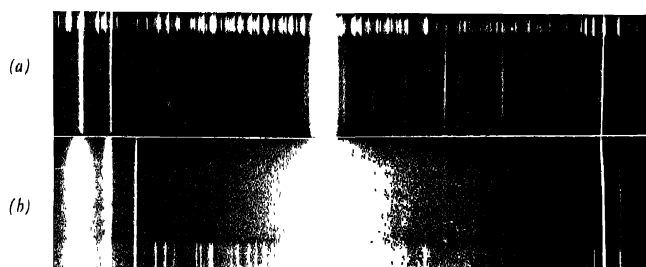


Fig. 2

- Fig. 1. (a) Raman spectra of parachloroanisole liquid at 30°C  
 (b) „ „ parachloroanisole solid at -180°C  
 Fig. 2. (a) „ „ orthochloroanisole liquid at 30°C  
 (b) „ „ orthochloroanisole solid at -180°C

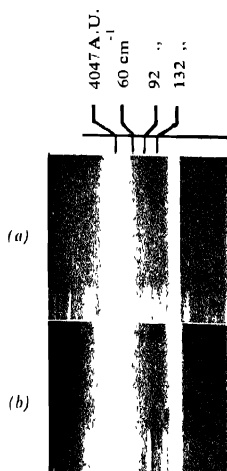


Fig. 3

Fig. 3. (a) Raman spectra of parachloroanisole solid at  $-180^\circ\text{C}$ , showing low-frequency lines

(b) orthochloroanisole solid at  $-180^\circ\text{C}$

Three new Raman lines with Raman shifts 60, 92 and 132  $\text{cm}^{-1}$  appear in the spectra due to the solid (Fig. 3a), the line 92  $\text{cm}^{-1}$  being the strongest. Further, some of the prominent Raman lines of the molecule undergo changes in position and intensity with the solidification. The intensity of the doublet 625  $\text{cm}^{-1}$  and 638  $\text{cm}^{-1}$  is reduced appreciably and the two lines coalesce to form a single line 640  $\text{cm}^{-1}$ . The line 799  $\text{cm}^{-1}$  shifts to 804  $\text{cm}^{-1}$  and the lines 1584  $\text{cm}^{-1}$  and 1596  $\text{cm}^{-1}$  coalesce to form a single line at 1603  $\text{cm}^{-1}$ . Finally, a new strong line at 3026  $\text{cm}^{-1}$  appears in the spectrum due to the solid.

The diminution in the number of Raman lines with the solidification of the liquid may be due to the fact that there exist in the liquid state two types

TABLE I  
Parachloroanisole.  $\Delta\nu$  in  $\text{cm}^{-1}$

Liquid		Solid at $-180^\circ\text{C}$
Hertz (1947)	Present author	Present author
		60 (3)
		92 (8b)
		132 (3)
143 (3) ?	150 (0) ?	145 (3)
212 (3)	218 (1b) P	225 (0)
309 (4)	313 (3) P	313 (2)
335 (4)	335 (4) D	335 (1)
366 (5)	367 (4) P	367 (2)
498 (1)		
625 (5)	625 (5) P	
636 (5)	638 (3b) P	640 (1)
698 (3)	695 (0) D	695 (0)
797 (10)	799 (10) P	804 (10)
829 (1)	826 (0) P	
1006 (3)	1005 (1) P	1005 (1)
1034 (1)	1035 (0) P	
1091 (8)	1091 (8) P	1094 (3)
1100 (1)		
1168 (3)	1170 (4b) P	1169 (2)
1181 (3)	1182 (3) P	1188 (1)
1244 (3)	1243 (3) P	1250 (0)
1292 (3)	1293 (4b) P	1299 (2)
1404 (1)		
1440 (3)	1443 (2) P	
1458 (3)	1459 (3b) P	1458 (1)
1492 (1)		
1580 (4)	1584 (3) D	
1594 (7)	1596 (6b) D	1603 (5)
2836 (4)	2844 (4) P	2844 (2)
2937 (2)	2938 (2) P	2838 (1)
3010 (1)		3026 (5)
3064 (6b)	3064 (4b) P	3064 (5)
3075 (6b)	3073 (5) P	3073 (4)

of molecules, namely, monomers and dimers, the latter being formed through weak intermolecular bonds between two neighbouring molecules. When the liquid is solidified probably all the molecules are transformed into small groups of molecules formed by association of the monomers and dimers through virtual linkages. The fact that the lines  $625\text{ cm}^{-1}$  and  $638\text{ cm}^{-1}$  change to a single line  $640\text{ cm}^{-1}$  with the solidification of the liquid shows that these virtual linkages take place between Cl and H atoms of the two neighbouring molecules respectively. As an example of such small splitting of some of the Raman lines with formation of dimers, mention can be made of the change in the Raman spectra of the solution of pyridine with dissolution in alcohol (Kastha, 1956). The spectra due to pure pyridine gives two Raman lines at  $995\text{ cm}^{-1}$  and  $1029\text{ cm}^{-1}$  of almost the same intensity, but when the liquid is dissolved in alcohol the former line becomes very weak. This is due to the fact that the non-bonding electron of the N-atom of pyridine forms a bond with the OH-group of the neighbouring alcohol molecules. In the present case also of the two lines  $625\text{ cm}^{-1}$  and  $638\text{ cm}^{-1}$ , the first one may be due to the monomers and the second one due to the dimers, and with solidification the former line disappears owing to formation of groups of molecules. It is also found that a new line  $3026\text{ cm}^{-1}$  is produced when the liquid is solidified. This shows that probably the H-atom attached to the benzene ring is responsible for the formation of virtual linkages with the Cl-atom of the neighbouring molecules. The disappearance of the line  $1584\text{ cm}^{-1}$  also leads to the conclusion that this line is due to monomers while the other line  $1596\text{ cm}^{-1}$  which persists in the solid state is due to the dimers.

(b) *Orthochloroanisole* :

On examination of the Raman spectra of orthochloroanisole in the liquid and solid states (Figs. 2a and 2b) it is found that no appreciable change takes place in the spectrum when the liquid is solidified. Hence, the formation of dimers in the liquid is not observed in this case. This may be due to the fact that the Cl-atom, which is the reactive atom for the formation of the dimers, is chelated to the  $\text{OCH}_3$  group, and therefore, it is no longer able to form a virtual bond with neighbouring molecules.

Tables I and II and also Figs. 3a and 3b show that *p*-chloroanisole produces three strong new low-frequency lines 60, 92 and  $132\text{ cm}^{-1}$  in the solid state at  $-180^\circ\text{C}$  while the ortho compound under the same condition does not produce any new line in this region. It has already been pointed out that in the para compound groups of molecules are formed while in the case of the ortho compound even in the solid state all the molecules remain as monomers. These facts show that the new lines in the low frequency region produced by the para compound in the solid state are due to groups of molecules. Had these lines been due to lattice vibrations they would also be produced by the ortho compound. The



TABLE II  
Orthochloroanisole.  $\Delta\nu$  in  $\text{cm}^{-1}$ 

Liquid		Solid at $-180^{\circ}\text{C}$
Hertz (1946)	Present author	Present author
160 (5bd)	160 (6b) D	165 (2b)
204 (3b)	202 (4) D	202 (2b)
288 (1)	290 (2vb)P	
410 (5b)	407 (8) P	407 (2)
444 (1)	440 (0)	
493 (6)	493 (8) P	493 (3)
546 (0)	550 (0) P	
576 (1b)	573 (3) D	573 (0b)
685 (8)	687 (8) P	692 (6)
712 (1)	708 (0) D	
753 (1b)	756 (1b) D	
785 (1)		
796 (7)	798 (b) P	798 (8)
844 (6)		
925 (0)		
995 (2)	995 (1)	
1025 (2)	1025 (1) P	
1041 (10)	1038 (10) P	1038 (8)
1065 (1)		
1092 (1)	1091 (0)	
1133 (1)	1130 (1)	
1162 (5)	1164 (6) D	1164 (1b)
1183 (3)	1181 (2d) P	1180 (0)
1208 (0)		
1250 (6)	1253 (5) P	1257 (2)
1274 (2)	1271 (2) P	
1300 (3)	1299 (3) P	1302 (1)
1360 (0)		
1436 (1)		
1463 (1)	1462 (2) D	
1486 (2)	1485 (3) P	1484 (1b)
1576 (5)	1576 (7) D	1576 (3)
1588 (5)	1588 (7) D	1586 (3)
2831 (2b)	2833 (3b) P	2833 (0)
2948 (2)	2948 (2b) P	
3004 (8)		
3068 (8)	3071 (9vb)P	3073 (6)
3076 (7b)		

results thus lead to the conclusion that the low frequency lines are due to vibrations in groups of molecules.

## ACKNOWLEDGMENT

The author is indebted to Professor S. C. Sirkar, D.Sc., F.N.I. for his keen interest and constant guidance throughout the progress of the work.

## REFERENCES

- Bhagavantham, S., 1941, *Proc. Ind. Acad. Sc.*, **13A**, 543.  
Biswas, D. C., 1954a, *Indian J. Phys.*, **28**, 85.  
    ,, 1954b, *Ind. J. Phys.*, **28**, 303.  
    ,, 1954c, *Ind. J. Phys.*, **28**, 423.  
    ,, 1955a, *Ind. J. Phys.*, **29**, 179.  
    ,, 1955b, *Ind. J. Phys.*, **29**, 257.  
    ,, 1955c, *Ind. J. Phys.*, **29**, 503.  
    ,, 1956, *Ind. J. Phys.*, **30**, 530.  
Gross and Vuks, 1936, *Comptes Rendus*, **1**, 73.  
Hertz, E., 1946, *Monatsh*, **76**, 1-26.  
Hertz, E., Kohlrausch and Vogel, 1947, *Monatsh*, **76**, 200-14.  
Kastler and Roussot, A., 1941, *Comptes Rendus*, **212**, 645.  
Kastha, G. S., 1956, *Ind. J. Phys.*, **30**, 313.  
Mazumdar, N., 1949, *Ind. J. Phys.*, **23**, 253.  
Ray, A. K., 1950a, *Ind. J. Phys.*, **24**, 111.  
    ,, 1950b, *Ind. J. Phys.*, **24**, 539.  
    ,, 1951a, *Ind. J. Phys.*, **25**, 131.  
    ,, 1951b, *Ind. J. Phys.*, **25**, 549.  
    ,, 1952, *Ind. J. Phys.*, **26**, 226.  
Sirkar, S. C., 1937, *Ind. J. Phys.*, **11**, 343.

## BOOK REVIEW

NUCLEAR ELECTRONICS I (SESSIONS 1-5)... pp 452 Being the Proceedings of the International Symposium on Nuclear Electronics organised by the French Society of Radioelectricians held in Paris 1958.

In September, 1958 the French Society of Radioelectricians organised a Colloquium on Nuclear Electronics in Paris. The publication under review is an edited version of the papers and discussions of this Colloquium published by the International Atomic Energy Agency from Vienna. The major part of the papers and discussions in this Colloquium was divided into five sessions, three of them devoted to scintillation counters and to fast counting techniques in the region of milli-micro seconds or less using photomultipliers. The fourth session was devoted mainly to pulse height and time analysers and the fifth to reactor instrumentation and reactor control techniques.

It is interesting to note that papers from many lands and different laboratories show parallel developments in the field of scintillation counting techniques. The papers also reflect the general attitude that one is fast approaching the limit of conventional electronic tubes in speed and pulse amplification. This is demonstrated by the general search for techniques for the elimination of ordinary electronic tubes in the achievement of improved measurements of fast pulses. The study of scintillation processes in many phosphors is also discussed in several papers as a prelude to attempts to use the fast initial component of the light pulse.

The field of pulse height and time analysers covered in the 4th session describes current efforts in this field. The necessity of using fast pulses has given rise to a few techniques different from the conventional pulse height analysers which have proved unsuitable for very fast pulses. The topic is well covered in a preliminary review paper followed by several more or less detailed contributions on different schemes. The last group of papers on reactor instrumentation and control reflect mostly problems encountered in the control and instrumentation of the French Reactors and do not describe the techniques connected with the operation control of the novel fast reactors involving more difficult problems of reactor control.

It is interesting to find contributions on the use of digital computer techniques and standardised transistor circuitry for reactor control. Their greater reliability under radiation had been foreseen earlier and these techniques are likely to play an important role in future reactor instrumentation.

The IAEA venture of publishing proceedings of Symposia is, the reviewer feels, a timely and useful step in the dissemination of technical information and deserves our congratulations. The proceedings are well printed and the illustrations are clear and profuse.

*B. D. N. C.*

# DETERMINATION OF THE ELASTIC CONSTANTS OF TETRAGONAL (4, 4, 4/m) CRYSTALS FROM THE STUDY OF DIFFUSE X-RAY REFLECTIONS

R. C. SRIVASTAVA AND S. C. CHAKRABORTY

PHYSICS DEPARTMENT, UNIVERSITY OF ALLAHABAD, ALLAHABAD

(Received, April 10, 1960)

**ABSTRACT.** Theoretical relationships connecting diffusely scattered X-ray intensities from crystals with its elastic constants have been derived for tetragonal crystals of classes 4, 4 and 4/m. Methods of evaluation of all the seven elastic constants for these types of crystals from a quantitative measurement of diffuse X-ray scattering only, have been described and the results are being used to determine elastic constants of single crystals of Penta-erythritol (Tetragonal 4)

The elastic properties of tetragonal crystals belonging to the point groups 4,  $\bar{4}$ , 4/m are defined by the matrix (according to the classical theory of elasticity)

$$\begin{array}{ccccc} C_{12} & C_{13} & 0 & 0 & C_1 \\ C_{11} & C_{33} & 0 & 0 & -C_1 \\ & C_{33} & 0 & 0 & 0 \\ & & C_{44} & 0 & 0 \\ & & & C_{44} & 0 \\ & & & & C_{66} \end{array}$$

where  $C_{11}$ , etc are the elastic constants of the crystal.

The relations for the evaluation of the elastic constants of the tetragonal crystals of more symmetrical point groups (namely, 42,  $\bar{4}2m$ , 4/mmm) from the intensity measurement of thermal diffuse scattering of X-rays, have been derived by Prasad and Wooster (1955). The intensity of diffuse X-ray scattering (1st order only) from a small element of volume of the crystal along a line passing through a reciprocal lattice point ( $hkl$ ) which is responsible for the diffuse scattering, is proportional to the value of the expression  $K[uvw]_{hkl}$  (designated as rekha constant by Ramchandran and Wooster, 1951)

where,

$$K[uvw]_{hkl} = L^2 A^{-1}_{11} + M^2 A^{-1}_{22} + N^2 A^{-1}_{33} + 2MNA^{-1}_{23} + 2NLA^{-1}_{31} + 2LMA^{-1}_{22}$$

where  $L, M, N$ , are the direction cosines of the reciprocal lattice vector with respect to the crystal axes (the elastic axes also coincide with the crystal axes for these cases) and  $u, v, w$  are the direction cosines of the thermal wave vector and  $A^{-1}_{11}$  etc. are the elements of the matrix inverse to the matrix  $A_{ij}$  whose elements for tetragonal crystals of classes 42,  $\bar{4}2m$ , 4mm and 4/mmm are given by

$$A_{11} = C'_{11}u^2 + C'_{66}v^2 + C'_{44}w^2$$

$$A_{22} = C'_{66}u^2 + C'_{11}v^2 + C'_{44}w^2$$

$$A_{33} = C'_{44}(u^2 + v^2) + C'_{33}w^2$$

$$A_{23} = mv(C'_{44} + C'_{13})$$

$$A_{31} = wu(C'_{44} + C'_{13})$$

$$A_{12} = vu(C'_{66} + C'_{12})$$

Prasad and Wooster have also indicated that for very simple and elementary directions of the reciprocal lattice vector and the thermal wave vector, the values of  $K[u, v, w]_{hkl}$  depend on one or two elastic constants only. Consequently, in principle, all the elastic constants can be evaluated without difficulty from the measurements of the intensities of the diffusely scattered X-rays along these directions. Since  $C'_{16} = -C'_{26} \neq 0$  for the crystal classes which have been dealt with in this paper (whereas  $C'_{16} = C'_{26} = 0$  for the classes considered by Prasad and Wooster) the values of  $K[uvw]_{hkl}$  involve many elastic constants even for simple reciprocal lattice vectors and simple directions of thermal wave vectors. Hence determination of all the elastic constants from X-ray measurements is apparently quite difficult, as will be evident from the succeeding text where the relationships and the method to be applied in such cases have been described. It can be shown that the elements of the matrix  $A_{ij}$  for tetragonal crystals of classes 4,  $\bar{4}$ , and 4/m are given by

$$A_{11} = C'_{11}u^2 + C'_{66}v^2 + C'_{44}w^2 + 2uvC'_{16}$$

$$A_{22} = C'_{66}u^2 + C'_{11}v^2 + C'_{44}w^2 - 2uvC'_{16}$$

$$A_{33} = C'_{44}(u^2 + v^2) + C'_{33}w^2$$

$$A_{23} = mv(C'_{44} + C'_{13})$$

$$A_{31} = wu(C'_{44} + C'_{13})$$

$$A_{12} = (u^2 - v^2)C'_{16} + uv(C'_{66} + C'_{12})$$

Values of the  $K[uvw]_{hkl}$  derived for the present cases for some reciprocal lattice points and some simple directions of propagation of the thermal waves are given in Table I.

It can be seen from Table I that the constants  $C'_{44}$  and  $C'_{33}$  can be determined independently from observations along  $[001]_{h00}$  and  $[001]_{00l}$  yielding the values

TABLE I  
K values for the tetragonal crystal classes (4,  $\bar{2}$  and 4/m)

Direction cosines $(u, v, w)$ of the direction of propa- tion of the thermal wave.	hoo	Index of the reciprocal lattice points	hlo	hol
100	$\left[ \frac{C_{66}}{C_{11}} (C_{11}C_{66} - C_{16}^2) \right]$	$1/C_{44}$	$\left[ \frac{L^2 C_{66} + M^2 C_{11} - 2LM(C_{16})}{(C_{11}C_{66} - C_{16}^2)} \right]$	$\left[ L^2 C_{66} (C_{11}C_{66} - C_{16}^2) + N^2 C_{44} \right]$
010	$\left[ \frac{C_{11}}{C_{11}(C_{11}C_{66} - C_{16}^2)} \right]$	$1/C_{44}$	$\left[ \frac{L^2 C_{11} + M^2 C_{66} - 2LM(C_{16})}{(C_{11}C_{66} - C_{16}^2)} \right]$	$\left[ L^2 C_{11} (C_{11}C_{66} - C_{16}^2) + N^2 C_{44} \right]$
001	$1/C_{44}$	$1/C_{33}$	$(L^2 + M^2)/C_{44}$	$\left[ L^2 C_{44} + N^2 C_{33} \right]$
$\left( \frac{1}{\sqrt{2}}, 0, \frac{1}{\sqrt{2}} \right)$	$\frac{2[(C_{66} + C_{44})(C_{44} - C_{33})]}{\Delta}$	$\frac{2[(C_{66} + C_{44})(C_{44} - C_{33}) - C_{16}^2]}{\Delta}$	$L^2 K \left[ \frac{1}{\sqrt{2}}, 0, \frac{1}{\sqrt{2}} \right]_{hoo}$	$-N^2 K \left[ \frac{1}{\sqrt{2}}, 0, \frac{1}{\sqrt{2}} \right]_{ool}$ + $\frac{4NL}{\Delta} (C_{44} + C_{11})(C_{44} + C_{33})$
$\left( -\frac{1}{\sqrt{2}}, 0, \frac{1}{\sqrt{2}} \right)$ or $\left( \frac{1}{\sqrt{2}}, 0, -\frac{1}{\sqrt{2}} \right)$	"	"	$L^2 K \left[ \frac{1}{\sqrt{2}}, 0, \frac{1}{\sqrt{2}} \right]_{hoo}$	$-N^2 K \left[ \frac{1}{\sqrt{2}}, 0, \frac{1}{\sqrt{2}} \right]_{ool}$ - $\frac{4NL}{\Delta} (C_{44} - C_{33})(C_{44} + C_{33})$

where  $\Delta = [(C_{44} + C_{11})(C_{66} + C_{44})(C_{44} + C_{33}) - C_{16}^2(C_{44} + C_{33}) - (C_{44} - C_{33})^2(C_{66} - C_{44})]$

TABLE I (contd.)  
K values for the tetragonal crystal classes (4,  $\bar{1}$  and 4/m)

Direction cosines ( $u, v, w$ ) of the direction of propaga- tion of the thermal wave.	Index of the reciprocal lattice points		
	hoo	ool	hko
$\left(\frac{1}{\sqrt{2}}, \frac{1}{\sqrt{2}}, 0\right)$	$\left[ \frac{2(C_{66} + C_{11})}{C_{11}^2 + 2C_{66}} \right. \\ \left. \frac{-2C_{10}}{(C_{11} - C_{12}) - C_{12}^2 - 4C_{10}^2} \right]$	$1/C_{14}$	
$\left(-\frac{1}{\sqrt{2}}, \frac{1}{\sqrt{2}}, 0\right)$ or $\left(\frac{1}{\sqrt{2}}, -\frac{1}{\sqrt{2}}, 0\right)$	$\left[ \frac{2(C_{66} + C_{11})}{C_{11}^2 + 2C_{66}} \right. \\ \left. \frac{-2C_{16}}{(C_{11} - C_{12}) - C_{12}^2 - 4C_{16}^2} \right]$	$1/C_{14}$	
$\left(0, \frac{1}{\sqrt{2}}, \frac{1}{\sqrt{2}}\right)$ or $\left(0, -\frac{1}{\sqrt{2}}, \frac{1}{\sqrt{2}}\right)$ or $\left(0, \frac{1}{\sqrt{2}}, -\frac{1}{\sqrt{2}}\right)$	$\frac{2[(C_{44} + C_{33})(C_{11} + C_{44})]}{1 - (C_{44} + C_{11})^2} \\ \Delta$	$\frac{2[(C_{66} - C_{44})(C_{11} + C_{44}) - C_{11}^2 - C_{44}^2]}{\Delta}$	

where  $\Delta = [(C_{44} + C_{11})(C_{66} - C_{44})(C_{44} + C_{33}) - C_{16}^2(C_{44} + C_{33}) - (C_{44} - C_{13})^2(C_{66} - C_{44})]$



of  $K[001]_{hoo}$  and  $K[001]_{hoi}$  respectively. The value of  $C'_{44}$  can also be evaluated from observations along  $[001]$  for different  $(hko)$  reciprocal lattice nodes and also from  $K[010]_{001}$ . Further, the values of  $C'_{44}$  and  $C'_{33}$  can be simultaneously obtained from observations along  $[001]$  for at least two different  $(hol)$  reciprocal lattice nodes. Since such determined values of  $C'_{44}$  and  $C'_{33}$  are dependent on two observed  $K$ -values, its accuracy of determination is theoretically less than that mentioned at the beginning. Again, by substituting the value of  $C'_{44}$  in the observed value of  $K[001]$ , the value of  $C'_{33}$  can be determined easily considering one  $(hol)$  reciprocal lattice node only at a time. To increase the accuracy of thus determined value of  $C'_{33}$ , we are to choose a reciprocal lattice node for which the value of  $L$  is very low compared to that of  $N$ , i.e. a node whose  $l$  index is much higher than its  $h$  index; in such condition the value of  $K[001]_{hol} = |L^2/C'_{44} + N^2C'_{33}|$  will be guided primarily by the value of  $N^2/C'_{33}$ . The value of  $C'_{44}$  can further be determined by combining the observed value of  $K[100]_{hol}$  with  $K[100]_{hoo}$  and  $K[010]_{hoi}$  with  $K[010]_{hoo}$ . Alternatively, by substituting the value of  $C'_{44}$  in  $K[100]_{hol}$  and  $K[010]_{hol}$ , the values of  $(C'_{11}C'_{66} - C'^2_{16})$  and  $(C'_{11}C'_{66} - C'^3_{16})$  can be obtained respectively from which we can get the ratio  $C'_{11}/C'_{66}$ . It will be seen further that solution of more than one relation only gives the values of the ratio of the constants (viz.  $C'_{11}/C'_{66}$ , etc.) and  $C'_{11}$ ,  $C'_{66}$  and  $C'_{16}$  cannot be determined independently and directly. For determining the absolute values of these three constants, the method of successive approximation suggested is as follows:

From the Table I, we have

$$K[100]_{hoo} = \left( C'_{11} - \frac{C'^2_{16}}{C'_{66}} \right) \quad \dots (1)$$

$$K[010]_{hoo} = \left( C'_{66} - \frac{C'^2_{16}}{C'_{11}} \right) \quad \dots (2)$$

and

$$K[100]_{hko} = \frac{(L^2C'_{66} + M^2C'_{11} - 2MLC'_{16})}{C'_{11}K[010]} \quad (3)$$

Substituting the experimentally determined values of  $1/K[100]_{hoo}$  and  $1/K[010]_{hoo}$  for  $C'_{11}$  and  $C'_{66}$  respectively in the relation (3), we can thus get some value for  $C'_{16}$ . Let us now substitute in relation (1) this value of  $C'_{16}$  along with the experimentally determined value of  $1/K[010]$  for  $C'_{66}$ . We thus get some value for  $C'_{11}$ . These values of  $C'_{11}$  and  $C'_{16}$  may be substituted in the relation (2) to give a better value for  $C'_{66}$ . These values of  $C'_{11}$  and  $C'_{66}$  can now be substituted in relation (3) to yield a better value for  $C'_{16}$ . This value for  $C'_{16}$  and  $C'_{66}$  on substitution in relation (1) gives a better value for  $C'_{11}$  and so on. We can in this way go on repeating the process again and again till further refinements do not change

the values of  $C'_{11}$ ,  $C'_{66}$  and  $C'_{16}$ . The smaller the value of  $C'_{16}$  as compared to  $C'_{11}$  and  $C'_{66}$ , the lesser would be the number of repetitions needed. It should be remarked that this method of successive approximation does not assume anything regarding the relative values of the constants involved. Actually a numerical example assuming tentatively  $C'_{11} = 2C'_{66} = 4C'_{16}$  required about four repetitions whereas in another example in which  $C'_{11} = 2C'_{66} = 2C'_{16}$ , about eight repetitions were found to suffice. In fact the constant  $C'_{16}$  relates an external stress to shear strain, therefore it would be expected for most of the cases to be smaller than the constants  $C'_{44}$ ,  $C'_{55}$ ,  $C'_{66}$  which relate a shear stress to a shear strain in the same plane and considerably smaller than the constants  $C'_{11}$ ,  $C'_{22}$ ,  $C'_{33}$  which relate an extentional stress to a collinear extentional strain. So in general not many repetitions will be required for getting the correct value of  $C'_{11}$ ,  $C'_{66}$ , and  $C'_{16}$ . Since we are to use three observational intensities each of which depends on these constants namely,  $C'_{11}$ ,  $C'_{66}$  and  $C'_{16}$  the values of  $C'_{11}$ ,  $C'_{66}$ ,  $C'_{16}$  will be theoretically less accurate than the values of the constants  $C'_{44}$  and  $C'_{33}$  which have been derived from intensities depending on one constant only. But in practical cases, the determination of a particular elastic constant derived by using different value of  $K[u, v, w]_{hkl}$ ,  $K[u', v', w']_{h'k'l'}$  does not appreciably reduce the accuracy of its determination. Once we obtain the absolute values of the constants  $C'_{11}$  and  $C'_{66}$  by substituting the value of  $C'_{11}$  in the ratio  $C'_{11}/C'_{66}$  which is obtained from different sources (as mentioned earlier), the value of  $C'_{66}$  can be determined or vice versa. The constant  $C'_{16}$  with proper sign can also be evaluated from the observed value of

$$K \left[ \frac{1}{\sqrt{2}}, \frac{1}{\sqrt{2}}, 0 \right]_{h00} - \frac{(C'_{11} + C'_{66} - 2C'_{16})}{(C'_{11} + C'_{66} + 2C'_{16})} \\ K \left[ -\frac{1}{\sqrt{2}}, \frac{1}{\sqrt{2}}, 0 \right]_{h00} \text{ or } K \left[ \frac{1}{\sqrt{2}}, -\frac{1}{\sqrt{2}}, 0 \right]_{h00}$$

when the values of  $C'_{11}$  and  $C'_{66}$  are substituted there. Similarly from observations

$$\left[ \frac{K \left[ \frac{1}{\sqrt{2}}, 0, \frac{1}{\sqrt{2}} \right]_{h0l}}{K \left[ \frac{1}{\sqrt{2}}, 0, \frac{1}{\sqrt{2}} \right]_{h0l} \text{ or } K \left[ \frac{1}{\sqrt{2}}, 0, -\frac{1}{\sqrt{2}} \right]_{h0l}} \right]$$

one obtains the value of the ratio

$$\frac{L^2[(C'_{66} + C'_{44})(C'_{44} + C'_{33}) + N^2[(C'_{55} + C'_{44})(C'_{44} + C'_{11}) - C'_{16}^2] + 2LN(C'_{44} + C'_{33})(C'_{33} + C'_{13})]}{L^2[(C'_{66} + C'_{44})(C'_{44} + C'_{33}) + N^2[(C'_{66} + C'_{44})(C'_{44} + C'_{11}) - C'_{16}^2] - 2LN(C'_{44} + C'_{33})(C'_{33} + C'_{13})]}$$

which, when the values of  $C'_{11}$ ,  $C'_{33}$ ,  $C'_{44}$ ,  $C'_{66}$  and  $C'_{16}$  are substituted, gives the value of  $C'_{13}$  with proper sign. Again, if we substitute the values of  $C'_{11}$ ,  $C'_{33}$ ,  $C'_{66}$

and  $C'_{10}$  in the observed values of  $K \left[ -\frac{1}{\sqrt{2}}, 0, \frac{1}{\sqrt{2}} \right]_{hoo}$ ,  $K \left[ \frac{1}{\sqrt{2}}, 0, \frac{1}{\sqrt{2}} \right]_{ool}$ ,  $K \left[ 0, \frac{1}{\sqrt{2}}, \frac{1}{\sqrt{2}} \right]_{hoo}$  and  $K \left[ 0, \frac{1}{\sqrt{2}}, \frac{1}{\sqrt{2}} \right]_{ool}$  each of which gives a second degree equation in  $C'_{13}$  and retain only the positive value of the solution under the surd, the value of the constant  $C'_{13}$  can be evaluated with proper sign. The remaining constant  $C'_{12}$  can be determined from the observed values of  $K \left[ \frac{1}{\sqrt{2}}, \frac{1}{\sqrt{2}}, 0 \right]_{hoo}$  and  $K \left[ \frac{1}{\sqrt{2}}, 0, -\frac{1}{\sqrt{2}} \right]_{hoo}$  or  $K \left[ -\frac{1}{\sqrt{2}}, 0, \frac{1}{\sqrt{2}} \right]_{hoo}$  each of which gives a second degree equation in  $C'_{12}$  on substitution of the values of  $C'_{11}$ ,  $C'_{66}$  and  $C'_{16}$ ; retaining only the positive values of the solution under the surd  $C'_{12}$  with proper sign can be evaluated. Other more complex directions of observations can be taken for which  $K$  values depend on  $C'_{12}$  in combination with the other constants and  $C'_{12}$  can be evaluated from those expressions just proceeding in the same manner as before.

The relations derived and the method of evaluation of the elastic constants indicated above are being used for the determination of the seven elastic constants ( $C'_{11}$ ,  $C'_{33}$ ,  $C'_{44}$ ,  $C'_{66}$ ,  $C'_{12}$ ,  $C'_{13}$  and  $C'_{16}$ ) of crystals of Pentaerythritol (Point Group 4) using the photographic method as developed by Chakraborty and Sen (1958) and the complete experimental results will be published in near future.

#### ACKNOWLEDGEMENTS

The authors are indebted to Prof. K. Banerjee, Director, Indian Association for the Cultivation of Science, Calcutta, for his keen interest and encouragement during the progress of the work and thankful to Dr. R. K. Sen, Physicist, Technological Research Laboratories (I.C.J.C.), Tollygunge, Calcutta, for his helpful criticism of the manuscript and also thankful to Council of Scientific and Industrial Research for financial assistance.

#### REFERENCES

- Chakraborty, S. C. and Sen, R. K., 1958, *Proceedings of the Symposium on Crystal Physics, Nat. Inst. Sci. Ind., Bulletin No. 14*, 20-35.  
 Prasad, S. C. and Wooster, W. A., 1955, *Acta, Cryst.*, **3**, 614.  
 Ramachandran, G. N. and Wooster, W. A., 1951, *Acta Cryst.*, **4**, 351.

# SPLITTING OF NEUTRON ENERGY LEVELS DUE TO SPIN-ORBIT COUPLING

ARUNDHATI GHOSH

DEPARTMENT OF THEORETICAL PHYSICS

INDIAN ASSOCIATION FOR THE CULTIVATION OF SCIENCE JADAVPUR

CALCUTTA-32

(Received, April 4, 1960)

**ABSTRACT.** Due to the spin-orbit interaction the splitting of the energy levels of neutrons moving in the potential  $V = V(r) + \alpha \frac{\hbar^2}{M^2 c^2} \frac{1}{r} \frac{dV}{dr} \vec{\sigma} \cdot \vec{l}$  is calculated for  $p$ -states for atomic mass 200. The effect of the spin-orbit coupling is calculated by the perturbation method with the unperturbed wave functions as obtained by (Ghosh and Sil (in course of publication) by the technique of Lanczos.

For the calculation of energy levels of neutrons moving in the nucleus we choose the nuclear potential as of the form

$$V = V(r) + \alpha \frac{\hbar^2}{M^2 c^2} \frac{1}{r} \frac{dV}{dr} \vec{\sigma} \cdot \vec{l}$$

where  $V(r) = -V_0[1 + e^{(r-R)/a}]^{-1}$  and  $\alpha = -\frac{15}{2}$

The constant  $\alpha$  is the same as taken by Fermi (1954) for polarization of high energy protons scattered by nuclei. The operator  $\vec{\sigma} \cdot \vec{l}$  in the above expression can be replaced by its eigen values (cf. Mayer and Jensen, 1955). Thus

$$\begin{aligned} V &= V(r) + \alpha \frac{\hbar^2}{M^2 c^2} \frac{1}{r} \frac{dV}{dr} l \quad \text{for } j = l + \frac{1}{2} \\ &= V(r) - \alpha \frac{\hbar^2}{M^2 c^2} \frac{1}{r} \frac{dV}{dr} (l+1) \quad j = l - \frac{1}{2} \end{aligned}$$

We shall consider the splitting of the energy levels due to the spin-orbit coupling term by the usual perturbation method; to obtain the unperturbed solutions, we neglect this term in the Schrodinger equation and solve it by a method due to Lanczos (1934). This procedure is previously (Ghosh and Sil, 1960) adopted in obtaining the single particle bound states of neutrons moving in the

# Splitting of Neutron Energy Levels Due to Spin-Orbit Coupling 261

potential  $V(r) = -V_0[1 + e^{(r-R)/a}]^{-1}$ . The separation of the perturbed state from the unperturbed level is given by

$$\Delta E = \int \psi^* H \psi d\tau$$

when  $H$  represents the perturbation and  $\psi$  is the unperturbed wave function (normalized)

Since the operator  $\sigma \cdot \vec{l}$  in the perturbation has been replaced by its eigen values we need consider only the radial part of the integral. The range of the above integration is split up into four regions which are as follows. *I.*  $0 < r \leq r_1 = R - a \log_e 9$ , *II.*  $r_1 \leq r \leq R$ , *III.*  $R \leq r \leq r_2 = R + a \log_e 9$  and *IV.*  $r_2 \leq r < \infty$ . The limits of  $r_1$  and  $r_2$  are so chosen that the nuclear potential drops respectively to 9/10 and 1/10 of its value at  $r = 0$ .

The unperturbed wave functions of the neutron in the four regions are :

$$\psi_I = j_l(\gamma x)$$

$$\psi_{II} = \frac{1}{x} [A e^{\gamma' x} F'(q) + A^* e^{-\gamma' x} F(q)]$$

$$\psi_{III} = \frac{1}{x} [A' e^{k' x} F'(p) + A'' e^{-k' x} F''(p)]$$

and 
$$\psi_{IV} = h_l^{(1)}(ikx)$$

where  $j_l$  and  $h_l$  are respectively the spherical Bessel and Hankel function of order  $l$ ,  $F$ 's are polynomials in  $p$  or  $q$ , further

$$p = \frac{1}{8} (9e^{(R-r)/a} - 1)$$

$$q = \frac{1}{8} (9e^{(r-R)/a} - 1)$$

$$\gamma = \sqrt{\lambda^2 - k^2}, \quad \gamma' = \sqrt{\lambda^2 - k'^2}$$

where 
$$\lambda^2 = \frac{2M}{\hbar^2} V_0 a^2; \quad k^2 = \frac{2M}{\hbar^2} |E| a^2$$

$$k'^2 = k^2 + \frac{l(l+1)}{2} a^2 \left[ \left( \frac{1}{R} \right)^2 + \left( \frac{1}{R+a \log_e 9} \right)^2 \right]$$

$$k''^2 = k^2 + \frac{l(l+1)}{2} a^2 \left[ \left( \frac{1}{R} \right)^2 + \left( \frac{1}{R-a \log_e 9} \right)^2 \right]$$

The constants  $A$ ,  $A^*$ ,  $A^+$ ,  $A^-$  and  $C$  of the unperturbed wave functions are determined by the usual matching of  $\psi_I$ ,  $\psi_{II}$  and their derivatives at  $r = r_1$ ,  $\psi_{II}$ ,  $\psi_{IV}$  and their derivatives at  $r = r_2$  and finally  $\psi_{II}$ ,  $\psi_{III}$  and their derivatives at  $r = R$ . Since the spin-orbit interaction is only a surface effect, in this paper we have evaluated the perturbation integral only in the two short ranges  $r_1$  to  $R$  and  $R$  to  $r_2$  near the boundary. In these two short ranges we have evaluated the integral numerically applying Simpson's rule

The parameters in the central part of the potential are  $V_0 = 52$  Mev,  $R = (1.15A^{1/3} + 0.4)10^{-13}$  cm,  $a = 0.57 \times 10^{-13}$  cm. The calculated values of the separation of the levels for  $j = 1/2$  and  $j = 3/2$  for atomic mass 200 are shown in Table I.

TABLE I

State	Separation between the states $j = 1/2$ and $j = 3/2$
1p	0.69 MeV
2p	0.70 MeV
3p	0.83 MeV

In conclusion we may mention that for atomic mass 208 Ross *et al.* (1956) have obtained a separation of nearly 0.9 Mev. between  $3p_{1/2}$  and  $3p_{3/2}$  states. In our case for  $A = 200$  we have obtained a separation of 0.8 MeV.

## ACKNOWLEDGMENT

The author is greatly indebted to Professor D. Basu for a critical reading of the manuscript and to Dr. N. C. Sil for his many helpful comments.

## REFERENCES

- Fermi, E., 1954, *Nuovo Cimento*, **11**, 407.  
 Ghosh, A. and Sil, N. C., *Nuclear Physics*, (in course of publication).  
 Lanczos, C., 1938, *Journal of Mathematics & Physics*, **17**.  
 Mayer, M. G., Hans, J. and Jensen, D., 1955, *Elementary theory of nuclear Shell Structure*, 231.  
 Ross, Hans Mark and Lawson, R. D., 1956, *Phys. Rev.* **101**, 1613.

# SPACE GROUPS OF CRYSTALS OF ORTHO, META AND PARAXYLENE AT $-180^{\circ}\text{C}^*$

S. G. BISWAS

OPTICS DEPARTMENT, INDIAN ASSOCIATION FOR THE CULTIVATION OF SCIENCE, CALCUTTA-32

(Received, May 5, 1960)

## Plate IV

**ABSTRACT** The Debye-Scherrer patterns of *o*-xylene, *m*-xylene and *p*-xylene frozen and cooled to  $-180^{\circ}\text{C}$  have been photographed and analysed. The analysis has given the unit cell dimensions which explain all the reflections. The densities of the substances have been determined and have been found to be 1.032, 1.030 and 1.006  $\text{gm cm}^{-3}$  respectively for the ortho-, meta- and para compound. From these data the space group has been found in each case. The crystals of *o*-xylene belong to the orthorhombic system with  $a = 8.77$ ,  $b = 10.20$  and  $c = 14.55$  Å. The number of molecules per unit cell is 8 and the space group is  $Pmmm$ . The crystals of *m*-xylene also belong to the orthorhombic system. The dimensions of the unit cell are  $a = 7.77$ ,  $b = 8.45$ ,  $c = 10.47$  Å. The number of molecules per unit cell is 4. The space group is  $P2_12_12$ . The crystals of *p*-xylene belong to the monoclinic system with  $a = 7.56$ ,  $b = 8.45$ ,  $c = 11.11$  Å,  $\beta = 98^{\circ}57'$ . The number of molecules per unit cell is 4. The space group is  $P2_1/m$ .

## INTRODUCTION

In continuation of the previous work on the analysis of the Debye-Scherrer patterns of crystals of toluene (Biswas and Surkar, 1957), pyridine (Biswas, 1958), chlorobenzene and bromobenzene (Biswas, 1958) and 1,3,5-trichlorobenzene (Biswas, 1959) the present investigation was undertaken to study the Debye-Scherrer patterns of *o*-xylene, *m*-xylene and *p*-xylene in the frozen state at  $-180^{\circ}\text{C}$  to find out the dimensions of the unit cell, number of molecules per unit cell and the space group. Such data throw much light on the influence of intermolecular field on the individual molecules and are helpful in understanding the changes which take place in the electronic spectra of these molecules with the change from the liquid to the solid state.

## EXPERIMENTAL

The chemicals *o*-xylene, *m*-xylene and *p*-xylene used in the investigation were of chemically pure quality supplied by Fisher and Co.. Debye-Scherrer patterns of the substances were taken with a low-temperature camera of special design discussed earlier (Biswas, 1958). The radius of the camera was derived from the Debye-Scherrer pattern of Al powder, and it was found to be

\* Communicated by Prof. S. C. Surkar.

4.50 cm. The specimen in the form of liquid was introduced in a Lindemann glass capillary tube of bore 0.3mm and frozen with liquid oxygen. A Seifert X-ray tube running at 32 Kv and 26 mA was used to photograph the patterns. An exposure of three and a half hours was sufficient to record the pattern with appropriate density, using  $\text{Cu } K_{\alpha}$  radiation. The densities of the frozen substances at  $-180^{\circ}\text{C}$  were measured by the method described earlier (Biswas and Sirkar, 1957). For the ortho variety the density was found to be  $1.030 \text{ gm cm}^{-3}$ , for the para compound  $1.006 \text{ gm cm}^{-3}$ , and for the meta compound  $1.030 \text{ gm cm}^{-3}$ .

## RESULTS AND DISCUSSION

### (a) *Meta-xylene at $-180^{\circ}\text{C}$ :*

The Debye-Scherrer pattern is reproduced in Fig. 1, Plate IV. In the determination of unit cell dimensions of ortho, meta and para xylene from the Debye-Scherrer patterns, Lipson's method (Lipson, 1949) was first tried and when this method showed the lattice to be other than orthorhombic, Ito's method (Ito, 1950) was applied. The patterns could not be assigned to any lattice having a symmetry higher than that of the orthorhombic.

The values of  $\sin^2\theta$  for the rings in the Debye-Scherrer pattern due to *m*-xylene crystals are given in column 1 of Table I, and with these values the difference diagram was drawn according to Lipson's method. It was found from the diagram that the determination of the values of A, B, C from the equation

$$\sin^2\theta = Ah^2 + Bk^2 + Cl^2 \quad \dots (1)$$

$$(A = \lambda^2/4a^2, \quad B = \lambda^2/4b^2 \quad C = \lambda^2/4c^2).$$

was quite easy and all the rings could be indexed quite satisfactorily. The values of A, B, C determined in this way are  $A = .0098$ ,  $B = .0083$  and  $C = .0054$ . The axial lengths calculated from these values of A, B, C are:  $a = 7.77$ ,  $b = 8.45$ ,  $c = 10.47 \text{ \AA}$ . The values of  $\sin^2\theta$  calculated with these axial lengths, the intensities of the Debye-Scherrer rings, the spacings and the indices are given in Table I, and it can be seen that the discrepancies between the calculated and observed values lie within the experimental error.

With these values of the dimensions of the unit cell and the value of the density determined in this investigation the number of molecules per unit cell was calculated and found to be 4.

The conditions limiting possible reflections indicated by Table I are

$$\left. \begin{array}{l} hkl \\ hko \\ hol \\ oko \end{array} \right\} \quad \begin{array}{ll} \text{No condition} & hoo : h = 2n \\ & ool : l = 2n \end{array}$$



Fig. 1.

Fig. 2 (a).

Fig. 2 (b).

Fig. 3.

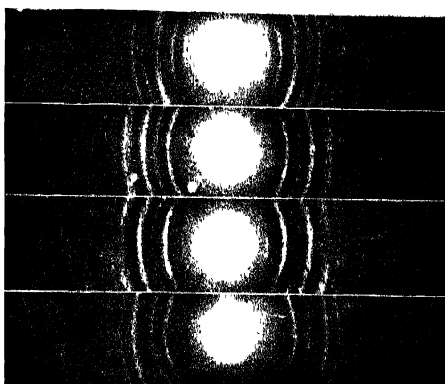


Fig. 1, Debye-Scherrer pattern of frozen *m*-xylene at  $-180^{\circ}\text{C}$

Fig. 2 (a). Fibre like pattern of frozen *o*-xylene at  $-180^{\circ}\text{C}$

Fig. 2 (b). Debye-Scherrer pattern of frozen *o*-xylene at  $-180^{\circ}\text{C}$

Fig. 3 Debye-Scherrer pattern of frozen *p*-xylene at  $-180^{\circ}\text{C}$



TABLE I  
*m*-Xylene at  $-180^{\circ}\text{C}$

$\sin^2\theta$ (observed)	$\sin^2\theta$ (calculated)	Spacings ( $\text{\AA}$ ) (observed)	Indices
.0083 (s)	.0083	8.45	010
.0137 (s)	.0137	6.58	011
.0184 (vw)	.0181	5.08	110
.0215 (m)	.0216	5.24	002
.0236 (m)	.0235	5.02	111
.0302 (m)	.0299	4.43	012
.0330 (w)	.0332	4.24	020
.0392 (s)	.0392 .0397	3.80	200 112
.0478 (m)	.0475 .0484		210 121
.0530 (w)	.0529	3.34	211
.0547 (w)	.0548	3.25	022
.0606 (m)	.0608	3.13	202
.0648 (vw)	.0646	3.02	122
.0750 (vw)	.0747	2.81	030
.0801 (m)	.0801	2.72	031
.0865 (m)	.0864	2.62	004
.0938 (vw)	.0936 .0940	2.52	301 222
.1020 (vw)	.1019	2.41	311
.1170 (w)	.1173	2.25	231
.1290 (w)	.1294	2.14	124
.1332 (m)	.1328 .1339	2.11	040 214
.1430 (w)	.1430 .1433	2.04	322 015
.1484 (w)	.1480	2.00	141
.1427 (w)	.1430	1.97	115
.1572 (vw)	.1568	1.94	400
.1746 (m)	.1746	1.84	304

Since the crystal belongs to the orthorhombic system and the unit cell contains molecules, the crystal belongs to the space group  $P2_1 2_1 2$  or  $D_2^3$ .

It can be seen from the above discussions that the number of molecules in the unit cell is the same as that required in the case of asymmetric molecules. The molecule may have either a plane of reflection perpendicular to its plane or a two-fold axis in its own plane. The plane cannot be utilised in the space group mentioned above and it is evident that the two-fold axis, if it is actually possessed by the molecule, does not coincide with any of the crystallographic axes.

(b) *Ortho-xylene* at  $180^\circ C$

One of the many Debye-Scherrer patterns photographed for frozen *o*-xylene was found to be analogous to a pattern due to a fibre while the other photographs showed continuous rings. Figs. 2(a) and 2(b) plate III show these two types of photographs. The former type helped the correct assignment of the indices.

Lipson's method applied in this case also indicated the lattice to be orthorhombic. It was found, however, that while two of the axial lengths were identical with those for the *m*-xylene lattice, the primitive translation along the third axis had to be taken as almost double that for the meta compound in order to index all the reflections in the powder pattern.

The values of  $\sin^2\theta$  observed in the pattern and those calculated from the values of A, B, C determined from the difference diagram, the spacings and the indices are given in Table II. It can be easily seen from Table II that the agreement between the observed and the calculated values of  $\sin^2\theta$  is very satisfactory. The correctness of the indices has been verified by examining the positions of the maxima in the rings due to the fibrous specimen [Fig. 2(b)]. The values of A, B, C in this case are  $A = .0028$ ,  $B = .0077$ ,  $C = .0057$ , from which the dimensions of the unit cell have been calculated and found to be  $a = 14.55$ ,  $b = 10.20$  and  $c = 8.77 \text{ \AA}$ .

From the value of the density mentioned earlier and the axial lengths given above the number of molecules per unit cell was calculated and found to be 8. The values of  $\sin^2\theta$  and the indices of the corresponding planes given in Table II show that there is no restriction limiting any reflection. So, the space group assigned to the crystal is  $Pmmm$  or  $D_2^3$ .

The molecule of *o*-xylene may have a plane of reflection perpendicular to the plane of the molecule and a two-fold axis in the plane of the molecule if the two  $\text{CH}_3$  groups in the molecule form mirror images of each other in a vertical plane between them owing to their mutual orientation produced by steric repulsion. If the plane were parallel to any of the crystallographic plane the number of molecules per unit cell would be reduced to 4, but actually the number is 8.

Hence the plane of the molecule is inclined to the crystallographic axis forming a complicated structure.

TABLE II  
o-Xylene at 180° C

$\sin^2 \theta$ (observed)	$\sin^2 \theta$ (calculated)	Spacings (Å) (observed)	Indices
0076 (ms)	0077	8.83	100
0086 (ms)	0085	8.30	011
0112 (vw)	0111	7.28	002
0162 (vw)	0162	6.09	111
0170 (vs)	0168	5.90	012
0228 (s)	0228	5.10	020
0248 (s)	0245 0250	4.89	112 003
0310 (vs)	0308	4.37	200
0338 (vs)	0336 0339	4.19	201 022
0442 (s)	0445	3.66	004
0478 (s)	0476	3.52	212
0507 (m)	0502 0512	3.42	014 300
0574 (m)	0579	3.21	114
0644 (w)	0646	3.03	222
0724 (vw)	0721	2.86	301
0812 (s)	0810	2.70	214
0866 (w)	0862	2.62	312
0916 (vw)	0914	2.54	040
1034 (ms)	1033 1035	2.40	322 134
1174 (ms)	1171	2.25	323
1314 (ms)	1310	2.12	206
1438 (vs)	1434	2.03	144
1595 (vs)	1591	1.93	136
1778 (vs)	1780 1773	1.83	008 431
1835 (w)	1837	1.80	018
2012 (w)	2008 2010	1.72	028 511
2048 (w)	2050	1.70	344
2408 (vw)	2403	1.57	523

(c) *paraxylene* at  $-180^{\circ}\text{C}$ .

The Debye-Scherrer pattern is reproduced in Fig. 3, Plate I. In determining the dimensions of the unit cell of the para compound it was noticed that the difference diagram did not yield sufficient number of constant differences. Hence Ito's method (Ito, 1950) was applied to index the pattern.

In order to select the axial lengths  $a^*$ ,  $b^*$ ,  $c^*$  of the reciprocal unit cell it was observed that all the spacings of the planes  $hoo$ ,  $oko$ ,  $ool$  with  $h, k, l$  even observed in the case of the *m*-xylene crystal were also present in the Debye-Scherrer pattern due to the para compound. These reflections were first utilised in selecting the values of  $a^*$ ,  $b^*$ ,  $c^*$ . The values are -

$$a^{*2} = 1/d_{100}^2 = 0083, \quad b^{*2} = 1/d_{010}^2 = .0138, \quad c^{*2} = 1/d_{001}^2 = .0180$$

In order to select the reciprocal cell angles  $\alpha^*$ ,  $\beta^*$ ,  $\gamma^*$ , ( $hko$ ), ( $hol$ ) and ( $okl$ ) reflections were carefully examined and it was observed that some ( $hko$ ) and ( $okl$ ) reflections were present if the angles  $a^* \wedge b^*$  and  $b^* \wedge c^*$  were taken to be  $90^\circ$ , and the angle  $a^* \wedge c^*$  was calculated by studying some pairs of ( $hol$ ) and ( $hok$ ) reflections according to the equation

$$\cos \beta^* = \frac{1/d_{hol}^2 - 1/d_{hok}^2}{4hla^*c^*} \quad \dots \quad (2)$$

where  $d_{hkl}$  is the spacing in the direct lattice

Thus the reciprocal cell-dimensions were calculated and found to be

$$\begin{array}{ll} a^* = .0911 & \alpha^* = 90^\circ \\ b^* = .1174 & \beta^* = 81^\circ 3' \\ c^* = .1339 & \gamma^* = 90^\circ \end{array}$$

With these values of the cell dimensions all the reflections in the powder pattern of the para xylene crystals were indexed according to the equation

$$1/d_{hkl}^2 = h^2a^{*2} + k^2b^{*2} + l^2c^{*2} + 2hla^*c^* \cos \beta^* \quad \dots \quad (3)$$

and the agreement was found to be satisfactory. The values of  $1/d^2$  observed from the photograph and those calculated with the help of Eqn.(3), the intensities, and the indices are given in Table III. The real cell corresponding to the reciprocal cell defines a lattice which is definitely the lattice of the crystal. The dimensions of the cell are

$$\begin{array}{l} a = 7.56 \text{ \AA} \\ b = 8.45 \text{ \AA} \\ c = 11.11 \text{ \AA} \\ \beta = 98^\circ 57' \end{array}$$

TABLE III  
*p*-Xylene at -180°C

$1/d^2$ (observed)	$1/d^2$ (calculated)	Indices
.0224 (vw)	0225	101
	0221	110
0301 (s)	0301	101
.0332 (m)	0332	200
.0366 (w)	0363	111
0437 (m)	0436	201
	0439	111
.0470 (s)	0470	210
.0550 (vs)	0552	020
.0720 (vs)	0722	002
0730 (w)	0732	021
	0729	102
0813 (w)	0813	301
.0886 (vs)	0884	220
	0885	310
	0881	102
0900 (vs)	0902	202
0994 (w)	0998	221
1032 (w)	1031	301
1138 (s)	1140	221
1204 (w)	1206	202
.1242 (s)	1241	302
1324 (m)	1328	400
2066 (s)	2065	501
	2060	303
2208 (w)	2208	040
	2212	421
	2213	510
	2207	023
	2215	203
2432 (vw)	2433	111
2595 (vw)	2593	511
2750 (vw)	2744	303
.2925 (s)	2930	012
.3116 (vw)	3110	242
	3126	610
3445 (vw)	3440	024
3608 (w)	3608	404
3830 (w)	3834	143

Now it has to be found out whether this cell can be reduced further

Let the primitive cell in the direct lattice have edges  $a, b, c$  written in order of increasing dimensions, corresponding to reciprocal lattice obtained from Ito's method. Every translation  $\mathbf{t}$  in the real lattice can be written in the form

$$\mathbf{t} = u\mathbf{a} + v\mathbf{b} + w\mathbf{c}$$

where  $u, v, w$  are integers, positive or negative. The problem of finding out the reduced cell is simply that of finding three shortest non-coplanar  $\mathbf{t}$ 's with the values of  $a, b, c$  determined from  $a^*, b^*, c^*$  and  $\beta^*$ . These three  $\mathbf{t}$ 's then become the edges of the reduced cell. This can be easily done by computation after assigning different values to  $u, v, w$ , both positive and negative, and it has been found that the arbitrary cell itself, initially chosen for indexing the pattern, is the reduced cell. Again, since the edges of a reduced face of a unit cell in the direct lattice are the shortest translations of the net, they are shorter than either of the two diagonals of the cell. For this reason the projection of either of the cell edges on the other cannot be greater than half the other edge (Buerger, 1957). As a consequence of this it follows that in a reduced plane cell,

$$\left| a \cos \gamma \right| \leq \frac{b}{2} \quad \text{and} \quad \left| b \cos \gamma \right| \leq \frac{a}{2}$$

$$\left| ab \cos \gamma \right| \leq \frac{b^2}{2} \quad \text{and} \quad \left| ab \cos \gamma \right| \leq \frac{a^2}{2}$$

These relations also apply to the reduced three-dimensional cell

The six scalar products  $\mathbf{a} \cdot \mathbf{a}, \mathbf{b} \cdot \mathbf{b}, \mathbf{c} \cdot \mathbf{c}, \mathbf{b} \cdot \mathbf{c}, \mathbf{c} \cdot \mathbf{a}, \mathbf{a} \cdot \mathbf{b}$  have been taken as an exact representation of the cell, since the six parameters  $a, b, c, \alpha, \beta, \gamma$  can readily be derived from them. For the purpose of identification, these six scalar products are set down in a form of rectangular matrix to represent the reduced cell as follows

$$\begin{pmatrix} \mathbf{a} \cdot \mathbf{a} & \mathbf{b} \cdot \mathbf{b} & \mathbf{c} \cdot \mathbf{c} \\ \mathbf{b} \cdot \mathbf{c} & \mathbf{c} \cdot \mathbf{a} & \mathbf{a} \cdot \mathbf{b} \end{pmatrix} = \begin{pmatrix} s_{11} & s_{22} & s_{33} \\ s_{23} & s_{31} & s_{12} \end{pmatrix}$$

Matrix representation of the direct cell of *p*-xylene crystal is found to be

$$\begin{pmatrix} 57.15 & 71.42 & 123.40 \\ 0.00 & -12.92 & 0.00 \end{pmatrix} \quad \dots \quad (7)$$

From representation (7) it can be seen that  $\mathbf{a} \cdot \mathbf{c}$  is less than either  $\frac{1}{2} \mathbf{a} \cdot \mathbf{b}$  or  $\frac{1}{2} \mathbf{b} \cdot \mathbf{b}$ . Hence according to (5) no further reduction is possible. From (7) it can also be seen that  $s_{11} \neq s_{22} \neq s_{33}$ , and since zero is regarded as negative ( $90^\circ$  is regarded as obtuse angle for the purpose of identification) the standard cell is a primitive monoclinic one as indicated by Azaroff and Buerger (1958). With



the values of the dimensions of the unit cell given earlier and the density of the substance at  $-180^{\circ}\text{C}$  determined experimentally the number of molecules per unit cell has been calculated and found to be 4

The conditions limiting possible reflections for *p*-xylene crystals are

*hkl* No condition

*hol* No condition

*oko*  $k = 2n$

So the space group  $P2_1/m$  has been assigned to the crystal

The *p*-xylene molecule may have a plane of symmetry perpendicular to the plane of the molecule and also a centre of symmetry with the two  $\text{CH}_3$  groups oriented in a particular way. As regards the plane of reflection this particular space group cannot utilise the symmetry element as in that case the number of molecules would be reduced to two. Again the contribution of the hydrogen atom in X-ray scattering is almost negligible. Therefore, the centre of symmetry could have been utilised by the molecule to form the lattice and in that case the number of molecules per unit cell would be 2. Actually, however, the unit cell contains 4 molecules. Hence it appears that the molecule does not possess the centre of symmetry in the solid state at  $-180^{\circ}\text{C}$ .

#### ACKNOWLEDGMENTS

The author is indebted to Professor S. C. Sirkar, D.Sc., F.N.I. for his kind interest and guidance during the progress of this work. The author is also indebted to the Council of Scientific and Industrial Research for financing the scheme under which this work was done.

#### REFERENCES

- Azartoff, L. V. and Buenger, M. J., 1958, *Powder Method*, p. 150.  
 Biswas, S. G., and Sirkar, S. C., 1957, *Ind. J. Phys.*, **31**, 141.  
 Biswas, S. G., 1958, *Ind. J. Phys.*, **32**, 13.  
 Biswas, S. G., 1958, *Acta Cryst.*, **11**, 882.  
 Biswas, S. G., 1959, *Ind. J. Phys.*, **33**, 371.  
 Buenger, M. J., 1957, *Zeitschrift für Kristallographie*, Bd. 109, S. 42-60.  
 Lapson, H., 1949, *Acta Cryst.*, **2**, 43-45.  
 Ito, T., 1950, X-ray studies on polymorphism, (Muruzen Co. Ltd., Tokyo), (210-214).

## ULTRASONIC VELOCITY IN SUPERCOOLED LIQUIDS

S. PARTHASARATHY AND V. N. BINDAL

NATIONAL PHYSICAL LABORATORY OF INDIA NEW DELHI, INDIA

(Received, February 21, 1960)

**ABSTRACT.** Velocity of ultrasonic waves has been studied over a range of temperatures extending into the supercooled region in five liquids, viz., thymol, phenol, salol, benzophenone, and diphenylamine.

It is observed that the temperature coefficient of velocity  $1/v (dv/dt)$ , does not remain the same on either side of the melting points in thymol and benzophenone. Salol, diphenylamine and benzophenone show a small abrupt change in velocity values as the melting point is crossed. These changes are attributed to possible structural changes encountered during transition from the liquid to the super-cooled state, which must be associated with the corresponding change of adiabatic compressibility. Phenol does not show any discontinuity and the gradient is also the same over the whole range. As phenol is highly hygroscopic it is likely to be mixed with certain amount of water and presumably the presence of water masks the small variation in temperature gradient if any.

## INTRODUCTION

The characteristic behaviour of many liquids in passing from the normal state to supercooled state has been studied with respect to the various physical properties such as viscosity (Dodd and Hu,  $\rightarrow$  1949) dielectric constant (Dodd and Roberts, 1950) density (Greenwood and Martin, 1952) specific heat, surface tension (Dodd, 1951) and vapour pressure. Ultrasonic velocity (Barone *et al.*, 1957) and absorption (Hunder, 1951, Parthasarathy and Bindal, 1960) have also been studied to some extent on certain liquids over various ranges of temperatures.

According to Barone, Pisent and Sette some polar liquids which can be easily supercooled show a sudden change of activation energy since viscous flow occurs at a temperature near melting point. They attribute this change to some structural variation inside the liquid.

Hunter (1951) worked on menthol and Petra and Cevolain (1951) in salol. Hunder observed a slight variation of temperature coefficient in menthol but Petra and Cevolain were not able to detect this effect in salol.

Subsequently, Barone, Pisent and Sette (1957) have investigated, menthol, diphenyl ether, *m*-chloronitrobenzene and salol in the normal and supercooled regions. They have discussed the results on the basis of viscosity measurement

and explained that the structural variation, which might be responsible for the variation in temperature co-efficient in the two states of liquid are mainly due to formation of molecular associations

The present work was undertaken to study some more liquids and to investigate their behaviour with respect to ultrasonic propagation in the temperature range of 30°C to 70°C, the melting point of the liquids in question being in the region of 50°C. With the help of a precision interferometer the ultrasonic velocity was measured in salol, thymol, benzophenone, diphenylamine and phenol.

#### EXPERIMENTAL

The work under report was done at a frequency of 6 Mcs. The r.f. generator used consisted of 2 Mcs crystal controlled oscillator in the form of a modified Pierce oscillator. This was followed by an amplifier tripler stage giving 6 Mcs. The r.f. output was fed to the load crystal fixed at the bottom of the interferometer through a condenser coupling. The H.T. current to the output tube was fed through a bridge net-work including a microammeter in such a way that changes in the plate current could be easily observed on the microammeter.

A precision interferometer was used for finding out the velocity at different temperatures by measuring the half wave-length in the liquid under test by shifting the reflector plate with the help of a micrometer screw.

If sound waves proceeding from a vibrating quartz are incident on plane reflector parallel to the source a standing wave pattern is obtained. The plate current of the output tube registers a change depending on the reaction on the transducer produced by a reflected wave. This reaction is maximum when the reflected wave returns 180° out of phase with the out going wave in which case the plate current shows a maximum dip. As the position of the reflecting plate is further changed the reaction on the generator passes through a maximum for each  $\lambda/2$  path difference of sound waves corresponding to movement of the reflector. The reflector movements can be very accurately read with the help of micrometer screw driving it. In the electric circuit, the bridge network is so adjusted for maximum sensitivity that the dips in the current can be easily counted as the reflector plate is moved. The total distance travelled by the reflector divided by the number of dips gives the value of half the wave length. Knowing the frequency of the oscillator the velocity can be calculated.

For the measurement of the velocity at different temperatures, water, from a thermostatically controlled bath was circulated around the liquid under experiment in the interferometer with the help of a centrifugal pump and the temperature was recorded with the help of 1/10°C thermometer, the temperature was constant within 0.1°C.

The arrangement gives .05% as the accuracy in velocity measurement.

## RESULTS AND DISCUSSION

The results obtained in salol, thymol, benzophenone, diphenylamine and phenol are given in Figs. 1, 2, 3, 4 and 5 respectively. They have also been placed in a tabular form for comparison.

It is noticed from the above results that in phenol (Figs. 5) there is no change in ultrasonic velocity as the temperature is reduced below the melting point into the supercooled region. The reason for this may be due to its hygroscopic nature, it is likely to be mixed with certain amount of water. Presumably the presence of this water masks the small variation in temperature gradient if any in phenol.

TABLE I

Comparison of velocity (M/sec) in different liquids at different temperatures

S No.	Temp. °C	Salol m.p. 42°C	Thymol m.p. 51.5°C	Benzophenone m.p. 48°C	Diphenylamine m.p. 54°C	Phenol m.p. 41°C
1	30	1463.00	1406.00	1544.00	1622.00	1485.00
2	33	1453.50	1396.00	1535.00	1611.00	1475.50
3	36	1444.00	1387.00	1526.00	1600.00	1466.00
4	39	1434.00	1378.00	1517.00	1589.00	1457.00
5	42	m.p.	1368.00	1508.00	1578.00	1448.00
6	45	1412.00	1359.00	1499.00	1567.00	1439.00
7	48	1402.50	1350.00	m.p.	1556.00	1429.50
8	51	1393.00	1240.75	1477.00	1545.00	1420.00
9	54	1383.50	1330.00	1465.50	m.p.	1411.00
10	57	1374.00	1320.00	1454.00	1417.75	1401.75
11	60	1364.75	1310.00	1442.50	1507.00	1392.25
12	63	1355.00	1300.00	1431.00	1496.00	1383.00
13	66	1346.75	1290.00	1419.25	1486.00	1374.00
14	69	1337.00	1280.00	1407.75	1475.00	1364.75
15	72	1228.00	1270.00	1396.50	1464.75	1355.50

In the case of thymol (Fig. 2) it is noticed that there is no appreciable abrupt change in the velocity near the melting point but the temperature co-efficient of velocity is different on either side. Benzophenone, (Fig. 3) salol (Fig. 1), and diphenylamine (Fig. 4) show a sudden change in velocity. In salol (Fig. 1) the change is about 11 meter as the temperature is lowered by about 2.5°C in the

neighbourhood of the melting point whereas the normal variation of velocity for  $2.5^{\circ}\text{C}$  change of temperature is found to be about 7 m only.

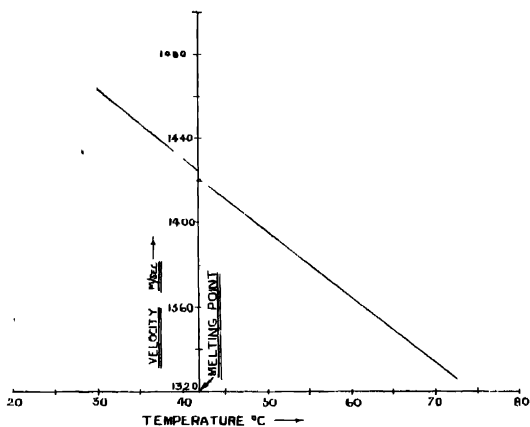


Fig. 1. Ultrasonic velocity in phenyl salicylate (safol).

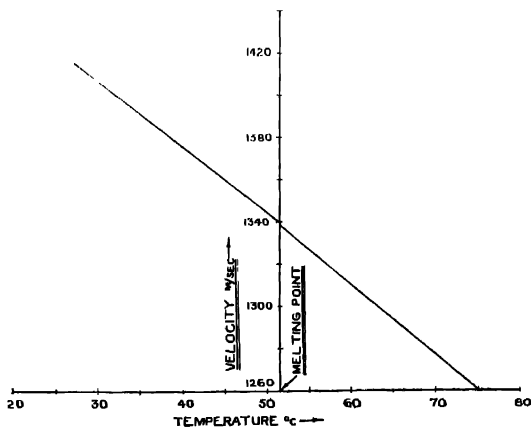


Fig. 2. Ultrasonic velocity in thymol.

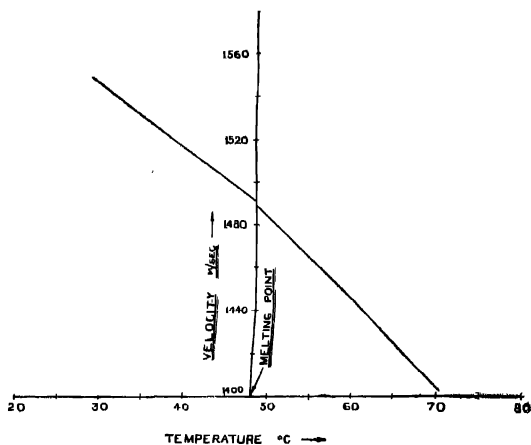


Fig. 3. Ultrasonic velocity in benzophenone

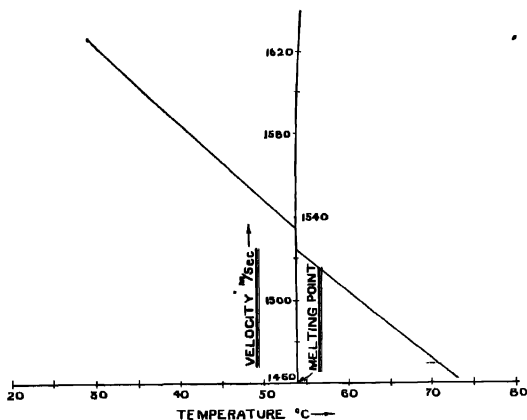


Fig. 4. Ultrasonic velocity in diphenylamine.

The curve obtained in salol (Fig. 1) in the present case does not agree with the curve obtained by Barone and Pisent (1957). They have reported that in the neighbourhood of the melting point, the velocity is changing from higher to lower values as the temperature is lowered to supercooled region whereas in the

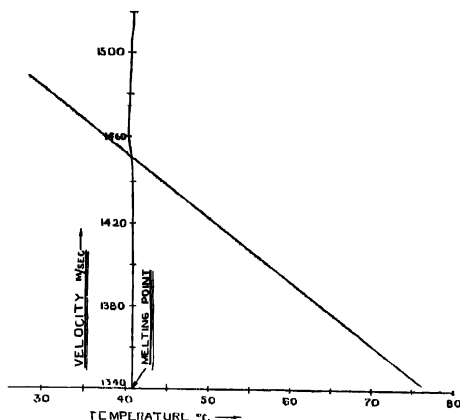


Fig. 5 Ultrasonic velocity in carbolic acid (phenol)

other liquids studied by them give the reverse order. In the work under report not only benzophenone and diphenylamine but also salol show an abrupt increase of velocity as the temperature is lowered to cross the melting point. Presently, it may be explained that the variation in the values in the two regions may be due to structural changes which take place in liquid from normal to supercooled state. Any change in the structure is likely to be associated with a corresponding change of adiabatic compressibility. Dodd (1949) working on measurement of densities of various supercooled liquids observed no detectable change in the temperature-co-efficient of density. This again indicates that the adiabatic compressibility must show an abrupt change at the melting point of the liquids. In the present case if the densities of these liquids are also measured over a similar range of temperature extending into the supercooled region it would be possible to calculate the actual adiabatic compressibility from velocity data already obtained. Work on other lines is in progress.

#### REFERENCES

- Barone, A., Pissin, G. and Sette, D. 1957, *Acoustica*, **7**, 109.  
 Cevoli, S. and Petrait, M. 1951, *Riv. Sci.*, **21**, 1626.  
 Dodd, C. and Hu Pak Mi, 1949, *Proc. Phys. Soc.*, **B62**, 454.  
 Dodd, C. and Roberts, G. N. 1950, *Proc. Phys. Soc.*, **B63**, 814.  
 Dodd, C., 1951, *Proc. Phys. Soc.*, **B64**, 761.  
 Greenwood, N. N. and Martin, R. L. 1952, *Proc. Roy. Soc.*, **A215**, 46.  
 Hunter, A. N., 1951, *Proc. Phys. Soc.*, **B64**, 1086.  
 Parthasarathy, S., Bindal, V. N. 1960 *Nature* **186**, 145.

ULTRAVIOLET BAND SPECTRA OF  $\text{AsO}$  AND  $\text{AsO}^+$ 

S. V. J. LAKSHMAN AND P. TIRUVENGANNA RAO

SPECTROSCOPIC LABORATORIES, DEPARTMENT OF PHYSICS, ANDHRA UNIVERSITY, WALTUR

(Received, April 27, 1960)

## Plate V

**ABSTRACT.** The band spectrum of  $\text{AsO}$  was excited, in a heavy current discharge from a 4 K V transformer, using a quartz discharge tube with internal hollow nickel electrodes fed with a spectro sample of  $\text{As}_2\text{O}_3$ . Two new doublet systems of bands designated as  $C-X^2\Pi$  and  $D-X^2\Pi$ , analogous to those reported by one of the authors (Lakshman 1960) in the case of  $\text{SbO}$ , were observed in the region  $\lambda$  3100– $\lambda$  2400 Å. The spectra were photographed on a Hilger medium quartz and  $\text{LiF}$  quartz Littrow spectrographs. Vibrational analyses of these systems were carried out leading to the following quantum formulae.

$$\begin{aligned}
 C-X^2\Pi : \nu &= \left. \begin{array}{l} 38051.1 \\ 37664.8 \end{array} \right\} \rightarrow 656 \left(3\nu' + \frac{1}{2}\right) - 4 \cdot 85 \left(\nu' + \frac{1}{2}\right) - 964 \cdot 0 \left(\nu'' + \frac{1}{2}\right) + 4 \cdot 50 \left(\nu' + \frac{1}{2}\right)^2 \\
 D-X^2\Pi : \nu &= \left. \begin{array}{l} 38805.9 \\ 37780.5 \end{array} \right\} \rightarrow 611 \left(5\nu' + \frac{1}{2}\right) - 3 \cdot 338 \left(\nu' + \frac{1}{2}\right)^2 - 964 \cdot 0 \left(\nu'' + \frac{1}{2}\right) + 1 \cdot 50 \left(\nu' + \frac{1}{2}\right)^2
 \end{aligned}$$

In addition to the above systems, a singlet system of bands was obtained in the region  $\lambda$  2550– $\lambda$  2200 Å. A vibrational analysis of this system gave the following constants.

$$\begin{array}{lll}
 \nu_e & 12601 \cdot 1 \text{ cm}^{-1} & \omega_e' = 777 \cdot 0 \text{ cm}^{-1} \quad \nu_e' \omega_e' = 6 \cdot 57 \text{ cm}^{-1} \\
 & & \omega_e'' = 1100 \cdot 4 \text{ cm}^{-1} \quad \nu_e'' \omega_e'' = 4 \cdot 878 \text{ cm}^{-1}
 \end{array}$$

From the magnitude of the vibrational constants, it is concluded, that the emitter of this system is the hitherto unknown  $\text{AsO}^+$  ion.

Detailed arguments are presented for assigning this system to  $\text{AsO}^+$ . The observed electronic states of  $\text{AsO}$  and  $\text{AsO}^+$  are compared and discussed with those of the related molecules on the basis of M.O. electron configurations.

## INTRODUCTION

Connelly (1934), Jenkins and Strait (1935), Shawhan and Morgan (1935) reported two doublet systems  $A-X$  and  $B-X$  of  $\text{AsO}$ , in emission, in various sources of excitation in the region  $\lambda$  3450– $\lambda$  2350 Å. Vibrational analyses of these two systems showed that they have a common lower state identified as a  $^2\Pi$  state, with a doublet splitting of  $1026 \text{ cm}^{-1}$ . That this state is the normal state of the  $\text{AsO}$  molecule, is confirmed by the observation of the  $B-X$  bands in absorption by Connelly. Of these two systems the  $A-X$  system consists of red degraded bands in the region  $\lambda$  3450– $\lambda$  2950 Å while the  $B-X$  comprises of violet degraded bands in the region  $\lambda$  2800– $\lambda$  2350 Å. From the observed double-



double headed nature of the bands, each of the two systems was ascribed to a  ${}^2\Sigma \rightarrow {}^2\Pi$  transition.

The present investigations on the spectrum of  $\text{AsO}$  in heavy current discharges were started with a view to obtain possible new systems analogous to the C—X and D—X systems of  $\text{SbO}$  previously reported by one of the authors (Lakshman 1960). This work has led to the analysis and identification of two new doublet systems designated as C— $\text{X}^2\Pi$  and D— $\text{X}^2\Pi$  of the  $\text{AsO}$  molecule and of a band system attributable to the molecule  $\text{AsO}^+$  whose existence is spectroscopically hitherto unknown. We describe below the experimental procedure and the results of detailed analysis of the ultraviolet band systems of  $\text{AsO}$  and  $\text{AsO}^+$ .

#### EXPERIMENTAL

The spectra were excited in a heavy current discharge from a 4K.V. transformer, using a quartz discharge tube with internal hollow nickel electrodes fed with a specpure sample of  $\text{As}_2\text{O}_3$ . Photographs of the spectra were obtained under (a) low pressure stagnant vapour conditions by closing a stop-cock connected in between the discharge tube and the system of evacuating pumps and (b) low pressure flowing vapour conditions. In the former case, the band spectrum of  $\text{AsO}$  was obtained in the region  $\lambda 3500\text{--}\lambda 2400 \text{ \AA}$  while in the latter case, a new group of bands attributed to the  $\text{AsO}^+$  molecule was obtained in addition to the above. Exposures varying from three to ten minutes on Hilger medium quartz and one to two hours on  $\text{E}_1$  quartz littrow spectrographs were found adequate to photograph the spectra on Ilford Selo-chrome and Special Rapid plates. The band heads were measured against iron arc standard lines, using a Hilger comparator.

#### RESULTS

##### $\text{AsO}$ : *New systems*

In addition to the  $\text{A}^2\Sigma \rightarrow \text{X}^2\Pi$  and  $\text{B}^2\Sigma \rightarrow \text{X}^2\Pi$  systems of  $\text{AsO}$  analysed by previous workers, the spectra reproduced in Plate V Figs. 1(a) and 1(b), reveal new groups of red degraded bands in the region  $\lambda 3100\text{--}\lambda 2400 \text{ \AA}$ . The new bands, start from the shorter wavelength side of the A—X system, and partly occur in a region of overlap with the B—X bands. The wave numbers, intensities, and the vibrational assignments for these bands are given in Table I.

Vibrational quantum formulae were derived for the Q—heads of the A—X and B—X systems by Connelly (1934) and also by Jenkins and Strait (1935).

We have observed that the new group of red degraded bands could not be fitted into the vibrational schemes of either of the two components of the A—X system. It seemed, therefore, reasonable to assume that they constitute one or more new doublet systems of  $\text{AsO}$  molecule. A clue to the analysis of the new bands was obtained by the observation of progressions of bands, whose  $\Delta G(v)$

TABLE 1

Wavenumber, intensity and vibrational assignments for the bands of  
 $C-X^2\Pi$  and  $D-X^2\Pi$  systems of AsO and  $A^1\Sigma-X^1\Sigma$  system of AsO<sup>+</sup>

Wave- number cm <sup>-1</sup>	Int.	v',v''	Wave- number cm <sup>-1</sup>	Int.	v',v''	Wave- number cm <sup>-1</sup>	Int.	v',v''
AsO C-X <sup>2</sup> Π <sub>3/2</sub>			AsO D-X <sup>2</sup> Π <sub>3/2</sub>			AsO <sup>+</sup> A <sup>1</sup> Σ-X <sup>1</sup> Σ		
33477	2	1,5	33839	2	0,4	39195	5	0,3
33745	3	0,4	35703	3	0,2	40267	7	0,2
34395	3	1,4	36448	4	0,1	41348	5	0,1
34673	4	0,3	37256	2	1,1	42113	8	1,1
35028	1	2,1	37602	4	0,0	42439	4	0,0
35609	7	0,2	38209	4	1,0	42866	2	2,1
35958*	—	2,3	38807	2	2,0	43205	6	1,0
36257	2	1,2	39402	2	3,0	43957	5	2,0
36558	7	0,1	AsO D-X <sup>2</sup> Π <sub>1/2</sub>			44693	3	3,0
37202	6	1,1	36727	2	0,2	45420	3	4,0
37843	4	2,1	37674	4	0,1			
38159	9	1,0	38280	3	1,1			
38794	4	2,0	38630	3	0,0			
39422	2	3,0	39236	5	1,0			
AsO C-X <sup>2</sup> Π <sub>1/2</sub>			39834	6	2,0			
34716	3	0,4	40424	4	3,0			
35644	4	0,3	41010	3	4,0			
36583	0	0,2	41588	3	5,0			
37531	8	0,1						
38180	2	1,1						
38487	4	0,0						

\* Coincides with an atomic line.

intervals agree closely with those of the ground state  $X^2\Pi$  of the AsO molecule. A detailed analysis, has shown that the new group of bands in the region  $\lambda 3100-\lambda 2400\text{\AA}$  could be interpreted on the basis of two overlapping doublet systems of bands, having a common lower state, identified as the  $X^2\Pi$  state of the AsO molecule. On this basis, the bands have been arranged into two vibrational schemes shown in Tables II and III. Table II refers to the scheme of classification of a doublet system designated as C-X<sup>2</sup>Π. As the bands appear

single headed, they may be either the Q heads of a  ${}^2\Delta(a) - {}^2\Pi(a)$  transition or the R-heads of a  ${}^2\Pi(a) - {}^2\Pi(a)$  transition. Of the two possibilities, the former appears more likely as the upper state can be identified to be a  ${}^2\Delta_a$  state from a comparison of this state with similar levels identified in NS, SiF and SbO. (See discussion below). As the corresponding bands of the two component systems are separated by  $\sim 970 \text{ cm}^{-1}$  the upper state is a regular state and has a doublet splitting equal to  $1026 - 970 = 56 \text{ cm}^{-1}$ . The C-X  ${}^2\Pi_1$  component system consists of only the strong  $v' = 0$  progression of bands. The bands heads of C-X  ${}^2\Pi$  system could be represented by the quantum formula

$$v = \left. \begin{array}{l} 38637.1 \\ 37664.8 \end{array} \right\} + 656.3(v' + \frac{1}{2}) - 4.85(v' + \frac{1}{2})^2 - 964.0(v'' + \frac{1}{2}) + 4.50(v'' + \frac{1}{2})^2$$

to within an accuracy of  $3 \text{ cm}^{-1}$ .

TABLE II  
Vibrational scheme of band heads of the C-X ${}^2\Pi$  system of AsO

$v'$ \ $v''$	0	1	2	3	4	5
0	38487	37531	36583	35644	34716	—
		956	948	939	928	—
		36558	35609	34673	33745	—
			949	936	928	—
		649	—	—	—	—
		644	648	—	650	—
1	—	38180	—	—	—	—
	38159	37202	36257	—	34395	33177
		957	915	—	—	918
		—	—	—	—	—
	635	641	—	—	633	—
2	—	—	—	—	—	—
	38791	37843	—	35958	35028	—
		951	—	—	930	—
	628	—	—	—	—	—
3	—	—	—	—	—	—
	39422	—	—	—	—	—

Table III shows the scheme of classification of band heads of the other doublet system designated as D-X  ${}^2\Pi$ . The analysis shows that the upper state D belongs to Hund's Case (b) and the lower state has a doublet splitting of  $1026 \text{ cm}^{-1}$ , which is identical with the doublet splitting of the  ${}^2\Pi$  ground state. The bands

of this system also appear single headed and may be either the R-heads of a  ${}^2\Pi(b) \rightarrow {}^2\Pi(a)$  transition, or the Q-heads of a  ${}^2\Delta(b) \rightarrow {}^2\Pi(a)$  transition.

The band heads of the two component systems could be represented by the quantum formula,

$$\nu = \left. \begin{array}{l} 38805.9 \\ 37780.5 \end{array} \right\} + 611.5(v' + \frac{1}{2}) - 3.338(v' + \frac{1}{2})^2 - 964.0(v'' + \frac{1}{2}) + 4.50(v'' + \frac{1}{2})^2$$

to within an accuracy of  $3 \text{ cm}^{-1}$ .

AsO: *A singlet system*

TABLE III  
Vibrational scheme of Band heads of the  $D \rightarrow X^2\Pi$  system of AsO

$v'$ \ $v''$	0	1	2	3	4
0	38630 37602 606 606	956 36648 954 606 606	37674 947 35703 945	36727 — —	33839
1	39236 38209 598 598	956 37256 953	38280	—	—
2	39834 38807 590 595	—	—	—	—
3	40424 39402 586 —	—	—	—	—
4	41010 — 578 —	—	—	—	—
5	41588 —	—	—	—	—

As was mentioned previously this system of bands was obtained in the region  $\lambda 2550\text{--}\lambda 2200\text{\AA}$  when the vapour of a sample of  $\text{As}_2\text{O}_3$  was kept flowing under low pressure conditions. It is reproduced in Fig 1(c) of Plate V. The wave numbers, intensities, and the vibrational assignments for these bands are shown in Table I. The analysis of this system presented no difficulty. The two

progressions of bands  $v'' = 0$  and  $v' = 0$  were easily identified leading to the vibrational scheme displayed in Table IV. The following vibrational constants have been derived.

$$\begin{aligned} \omega_e &= 42601.1 \text{ cm}^{-1} & \omega_e' &= 777.0 \text{ cm}^{-1} \\ \omega_e'' &= 1100.4 \text{ cm}^{-1} & \omega_e''' &= 6.57 \text{ cm}^{-1} \\ x_e'' &= 4.878 \text{ cm}^{-1} \end{aligned}$$

TABLE IV  
Vibrational scheme of  $\text{AsO}^+$  bands

$v''$	0	1	2	3
0	42439 766	1091 705	1081 40267	1072 39195
1	43205 752	1092 753		
2	43957 736	1091 42866		
3	44693 727			
4	45420			

The singlet structure of this system and a comparison of the vibrational constants of this system with those of  $\text{NO}^+$  and  $\text{PO}^+$  indicate that the emitter of this system is the hitherto unknown  $\text{AsO}^+$  ion. A detailed discussion on this is given in a later section.

#### DISCUSSION OF RESULTS

$\text{NO}$ ,  $\text{PO}$ ,  $\text{NS}$ ,  $\text{PS}$ ,  $\text{SiF}$ ,  $\text{AsO}$  and  $\text{SbO}$ .

We may now discuss the nature and properties of the electronic states of the  $\text{AsO}$  molecule in relation to those identified so far in the spectra of the related molecules  $\text{NO}$ ,  $\text{PO}$ ,  $\text{NS}$ ,  $\text{PS}$ ,  $\text{SiF}$  and  $\text{SbO}$ . Fig. 2 gives the term scheme of electronic levels identified till now. The ground state of these molecules is well known to be a  $^2\Pi$  state and is represented as  $X^2\Pi$ . The levels A, B, C, D etc., are arranged in the order of increasing energy. However, the designation of the levels in  $\text{PO}$  and  $\text{NO}$  is not strictly in the order X, A, B, C etc. We notice for instance, that the first and second excited states of  $\text{PO}$  are represented by  $B^2\Sigma$  and  $A^2\Sigma$  respectively, while the  $B'^2\Delta_1$  term in  $\text{NO}$  occurs in between the D and E levels, and the new C and D levels in  $\text{AsO}$  fall in between A and B. The ratio



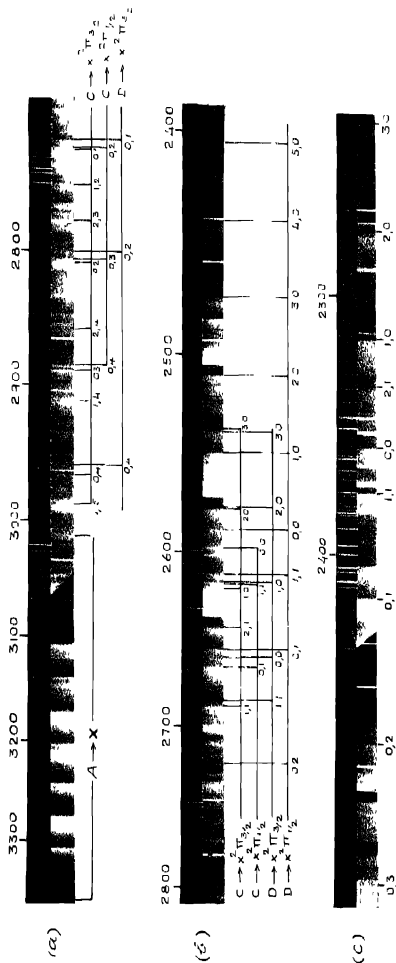


Fig 1. Medium quartz spectrograms.  
 (a) and (b) - The new C-N and D-X systems of AsO  
 (c) - The A  $1\Sigma-X 1\Sigma$  system of AsO $^{+}$   
 (The violet degraded bands in (b) and (c) belong to the B-N system of AsO)





The observed molecular electronic states of NO, NS, PO, PS were previously discussed on the basis of expected molecular electron configurations by Dressler (1955), and of NS and SiF by Barrow (1954 and 1958). Leaving the completed *K* and *L* shells, the ground state configuration in these molecules, in Mulliken's notation, is represented as

$$\dots(\sigma\sigma)^2(y\sigma)^2(w\pi)^4(x\sigma)^2(v\pi) \dots {}^2\pi_r \quad \dots (1)$$

The results of a recent rotational analysis of PO by Singh (1959) and SiF by Johns and Barrow (1957) definitely show that the *B* level in PO  $\left( \frac{\omega'_e}{\omega''_e} = 0.94 \right)$

and *A* level in SiF  $\left( \frac{\omega'_e}{\omega''_e} = 0.84 \right)$  belong to a  ${}^2\Sigma$  term. These states appear analogous to the  ${}^4\Sigma$  level in AsO  $\left( \frac{\omega'_e}{\omega''_e} = 0.71 \right)$  and *B*  ${}^2\Sigma$  in SbO  $\left( \frac{\omega'_e}{\omega''_e} = 0.71 \right)$  and belong to the excited configuration

$$\dots(\sigma\sigma)^2(y\sigma)^2(w\pi)^4(x\sigma)^2 \dots {}^2\Sigma^+, {}^2\Sigma^-, {}^2\Delta, {}^1\Sigma^- \quad \dots (2)$$

The reduction in the vibrational frequency in the excited state of each of the molecules is due to the transition of an electron from the bonding  $x\sigma$  orbital to the anti-bonding  $v\pi$  orbital. However, as was mentioned by Dressler, the reduction in the vibrational frequency of the *B*  ${}^2\Sigma$  state in PO is not so large as in others, indicating that the  $x\sigma$  orbital in PO is practically non-bonding.

In addition to the  ${}^2\Sigma$  state discussed above, the above configuration also gives rise to a  ${}^2\Delta$  term. This state was identified with the *B'* level in NO by Miescher (1956) and with *A* level in NS by Barrow, Drummond and Zeeman (1954). A comparison of the values of  $\omega'_e/\omega''_e$  for these states with the observed *C* levels in AsO and SbO (Lakshman, 1960) reveal that all of them are analogous. We may thus assign the *C* levels in AsO and SbO to a  ${}^2\Delta$  term arising from configuration (2).

The vibrational analyses of the *C*—*X*  ${}^2\Pi$  in PO and of the *D*—*X*  ${}^2\Pi$  system of AsO indicate that the upper state belongs to Hund's case (b). But the  $\Lambda$ —value of the state remains unknown, in the absence of the results of a rotational analysis.

The *B* level in AsO, *E* in SbO, *C* in NS and *B* in SiF are analogous states. Each of these states is characterised by an increase in the vibrational frequency and thereby the force constant with respect to the ground state. These states belong to the configuration

$$\dots(\sigma\sigma)^2(y\sigma)^2(w\pi)^4(x\sigma)^2 \dots (\sigma) \dots {}^2\Sigma^+ \quad \dots (3)$$

corresponding to the transition of an electron from a  $\pi$  anti-bonding orbital to a non-bonding  $\sigma$  orbital.

$\text{NO}^+$ ,  $\text{NS}^+$ ,  $\text{PO}^+$ ,  $\text{PS}^+$  and  $\text{AsO}^+$ .

In this section, we propose to give detailed reasons for assigning the singlet system reproduced in strip (c) of Plate V to the  $\text{AsO}^+$  ion. The arguments presented in the following discussion are closely similar to those used by Dressler (1955) in the spectroscopic identification of the ions  $\text{NS}^+$ ,  $\text{PO}^+$  and  $\text{PS}^+$ . The justification for attributing this singlet system to the  $\text{AsO}^+$  ion can be seen from the fact that there is a considerable increase in the vibrational frequency of the ground state term of the ion arising from the removal of the last  $\pi$  anti-bonding electron of configuration (1) representing the ground state of the neutral  $\text{AsO}$  molecule.

We compare in Table IV the values of  $\frac{\omega_e''(\text{Ion})}{\omega_e''(\text{Molecule})}$  and  $\frac{k_e''(\text{Ion})}{k_e''(\text{Molecule})}$  for the pairs of molecules  $\text{NO}^+$ ,  $\text{NO}$ ,  $\text{NS}^+$ ,  $\text{NS}$ ,  $\text{PO}^+$ ,  $\text{PO}$ ,  $\text{PS}^+$ ,  $\text{PS}$ , and  $\text{AsO}^+$ ,  $\text{AsO}$ .

We observe from the Table V that the values of  $\frac{\omega_e''(\text{Ion})}{\omega_e'(\text{Molecule})}$  and  $\frac{k_e''(\text{Ion})}{k_e'(\text{Molecule})}$  are exactly equal in the case of the three pairs of molecules given in the last three columns.

TABLE V

Comparison of the values of  $\frac{\omega_e''(\text{Ion})}{\omega_e''(\text{Molecule})}$  and  $\frac{k_e''(\text{Ion})}{k_e''(\text{Molecule})}$  for the pairs of molecules  $\text{NO}^+$ ,  $\text{NO}$ ;  $\text{NS}^+$ ,  $\text{NS}$ ;  $\text{PO}^+$ ,  $\text{PO}$ ;  $\text{PS}^+$ ,  $\text{PS}$ , and  $\text{AsO}^+$ ,  $\text{AsO}$ .

	$\text{NO}^+$ $\text{NO}$	$\text{NS}^+$ $\text{NS}$	$\text{PO}^+$ $\text{PO}$	$\text{PS}^+$ $\text{PS}$	$\text{AsO}^+$ $\text{AsO}$
$\frac{\omega_e''(\text{Ion})}{\omega_e''(\text{Molecule})}$	$\frac{2377}{1904} = 1.25$	$\frac{1219}{1219} = 1$	$\frac{1405}{1233} = 1.14$	$\frac{845}{740} = 1.14$	$\frac{1100}{964} = 1.14$
$\frac{k_e''(\text{Ion})}{k_e''(\text{Molecule})}$	1.56	—	1.30	1.30	1.30

A similar comparison of the values of  $\nu_e$  and  $\frac{\omega_e'}{\omega_e''}$  and  $\frac{k_e'}{k_e''}$  (given in Table VI) for the ions  $\text{NO}^+$ ,  $\text{NS}^+$ ,  $\text{PO}^+$ ,  $\text{PS}^+$  and  $\text{AsO}^+$  also shows that there is a similar decrease in the strength of binding of the upper state relative to the ground state. The  $\nu_e$  values of the singlet systems show the expected shift towards red with

TABLE VI

The values of  $\nu_e$ ,  $\omega_e''$ , and  $\frac{k_e'}{k_e''}$  for the molecules  $\text{NO}^+$ ,  $\text{NS}^+$ ,  $\text{PO}^+$ ,  $\text{PS}^+$  and  $\text{AsO}^+$

	$\nu_e$ $\text{cm}^{-1}$	Transition	$\frac{\omega_e'}{\omega_e''}$	$\frac{k_e'}{k_e''}$
$\text{NO}^+$	73470	$A^1\Pi - X^1\Sigma$	0.68	0.46
$\text{NS}^+$	42000	$A^1\Pi - X^1\Sigma$		
$\text{PO}^+$	49940	$A - X$	0.73	0.53
$\text{PS}^+$	40620	$A^1\Sigma - X^1\Sigma$	0.72	0.52
$\text{AsO}^+$	42600	$A^1\Sigma - X^1\Sigma$	0.71	0.50

increasing value of  $\mu$ , the reduced mass, as we pass from  $\text{NO}^+$  and  $\text{PO}^+$  to  $\text{AsO}^+$ . Since the ground state arises from the configuration

$$\dots (z\sigma)^2(y\sigma)^2(w\pi)^1(x\sigma)^2 \dots {}^1\Sigma^+$$
(4)

the upper state should therefore correspond to the excitation of an electron from either a bonding  $w\pi$  or  $x\sigma$  orbital to the  $v\pi$  antibonding orbital. For molecules with small internuclear distance like  $\text{NO}^+$  and  $\text{NS}^+$  we may expect  $x\sigma$  orbital to be higher in energy than  $w\pi$ . Thus the observed first excited  ${}^1\Pi$  state arises from the configuration

$$\dots (z\sigma)^2(y\sigma)^2(w\pi)^1(x\sigma)(v\pi) \dots {}^1\Pi$$
(5)

However, for molecules with large internuclear distance like  $\text{PO}^+$ ,  $\text{PS}^+$  and  $\text{AsO}^+$  for which the ratios are observed to be almost equal, we would then expect the  $x\sigma$  orbital to be lower in energy than the  $w\pi$  orbital. Thus the first observed excited state in these molecules may be represented by the configuration

$$(z\sigma)^2(y\sigma)^2(x\sigma)^2(w\pi)^2(v\pi) \dots {}^1\Sigma^+$$
(6)

Thus the singlet system of the  $\text{AsO}^+$  ion may be represented by the transition  $A^1\Sigma - X^1\Sigma$ . This assignment of the transition is supported by the observed simple rotational structure of the bands consisting of only  $R$  and  $P$  branches when photographed under the high dispersion of a  $\text{Fe}_2$  quartz Littrow spectrograph. ( $2\text{\AA}/\text{mm}$  at  $\lambda 2300\text{ \AA}$ )

In his discussion of the electronic states of  $\text{NO}^+$ ,  $\text{NS}^+$ ,  $\text{PO}^+$  and  $\text{PS}^+$  Dressler (1955) has made the interesting observation that the vibrational frequencies of the ground states of  $\text{NO}^+$  and  $\text{PO}^+$  agree closely with those of the excited states  $A^2\Sigma$  and  $A^2\Sigma$  respectively of  $\text{NO}$  and  $\text{PO}$  as shown below

$$\begin{array}{ll} \text{NO}^+ : \omega_e'' = 2377\text{ cm}^{-1} & \text{NO} : \omega_e'(A^2\Sigma) = 2375\text{ cm}^{-1} \\ \text{PO}^+ : \omega_e'' = 1405\text{ cm}^{-1} & \text{PO} : \omega_e'(A^2\Sigma) = 1391\text{ cm}^{-1} \end{array}$$

We have also observed that the vibrational frequency  $1100\text{ cm}^{-1}$  of the ground state of  $\text{AsO}^+$  agrees closely with the vibrational frequency  $1098\text{ cm}^{-1}$  of the excited  $B^2\Sigma$  state of  $\text{AsO}$ . Now, the  $B^2\Sigma$  state of  $\text{AsO}$  was previously assigned to the configuration

$$\dots (z\sigma)^2(y\sigma)^2(w\pi)^1(x\sigma)^2 \dots (\sigma) \dots {}^2\Sigma$$

in which the last electron is in a non-bonding orbital. If this electron is removed in the process of ionization of  $\text{AsO}$  molecule in the  $B^2\Sigma$  excited state, we should expect no change in the vibrational frequency of the ground state of the ion thus formed. This plausible explanation of the near equality of the vibrational frequency of the  $B$  state with the ground state of the ion gives additional support to the assumption that the emitter of this singlet band system is the  $\text{AsO}^+$  ion.

#### ACKNOWLEDGMENTS

The authors wish to express their thanks to Prof. K. R. Rao for his kind interest in this work. One of the authors (S. V. J. L.) is grateful to the C. S. I. R. (Delhi) for the award of a Research Fellowship.

#### REFERENCES

- Barrow, R. F., Drummond, G. and Zeeman, P. A., 1951, *Proc. Phys. Soc. London*, A, **67**, 365.  
 Connolly, F. C., 1934, *Proc. Phys. Soc. London*, A, **46**, 790.  
 Dressler, K., 1955, *Helv. Phys. Acta.*, **28**, 563.  
 Jenkins, F. A. and Stuart, L. A., 1935, *Phys. Rev.*, **47**, 136.  
 Johns, J. W. C. and Barrow, R. F., 1958, *Proc. Phys. Soc. London*, A, **71**, 176.  
 Lakshman, S. V. J., 1960, *Zeit. fur. Phys.*, **158**, 367.  
 Miescher, E., 1956, *Helv. Phys. Acta.*, **29**, 401.  
 Morgan, F. and Shawhan, E. N., 1935, *Phys. Rev.*, **47**, 192.  
 Morgan, F. and Shawhan, E. N., 1935, *Phys. Rev.*, **47**, 199.  
 Singh, N. L., 1959, *Can. Jour. Phys.*, **37**, 136.  
 Srinivasan Rao, K., 1958, *Can. Jour. Phys.*, **36**, 1526.

# Letters to the Editor

The Board of Editors will not hold itself responsible for opinions expressed in the letters published in this section. The notes containing reports of new work communicated for this section should not contain many figures and should not exceed 500 words in length. The contributions must reach the Assistant Editor not later than the 15th of the second month preceding that of the issue in which the letter is to appear. No proof will be sent to the authors.

9

## THE NEAR ULTRAVIOLET ABSORPTION SPECTRA OF THE THREE ISOMERIC METHYL PHENETOLES

K. V. KAMESWARA RAO AND V. RAMAKRISHNA RAO

DEPARTMENT OF PHYSICS, ANDHRA UNIVERSITY, WALTAIR

(Received, May 2, 1960)

The near ultraviolet absorption spectra of ortho-, meta-, and para-methyl phenetoles were investigated in the vapour, liquid and solid phases

### *Ortho-methyl phenetole*

In absorption in vapour about 20 bands were measured and the intense band at  $2751.6 \text{ \AA}$  ( $36332 \text{ cm}^{-1}$ ) was taken as the (0, 0) band. The spectrum could be interpreted on the basis of four fundamental frequencies in the upper state (534, 734, 956 and  $1275 \text{ cm}^{-1}$ ) and one fundamental in the ground state ( $428 \text{ cm}^{-1}$ ).

In absorption in solid state three bands were obtained and the intense band at  $2787 \text{ \AA}$  ( $35870 \text{ cm}^{-1}$ ) was taken as the (0, 0) band. The spectrum could be interpreted on the basis of two upper state fundamentals (830 and  $1952 \text{ cm}^{-1}$ )

### *Meta-methyl phenetole.*

In absorption spectrum of vapour about 23 bands were measured and the intense band at  $2775.7 \text{ \AA}$  ( $36016 \text{ cm}^{-1}$ ) was taken as the (0, 0) band. The spectrum could be interpreted on the basis of five fundamental frequencies in the upper state (683, 741, 912, 1102 and  $1279 \text{ cm}^{-1}$ ).

In absorption in liquid state three bands were obtained and the intense band at  $2807 \text{ \AA}$  ( $35615 \text{ cm}^{-1}$ ) was taken as the (0, 0) band. The spectrum could be interpreted on the basis of one upper state fundamental  $897 \text{ cm}^{-1}$ .

In absorption in solid state three bands were obtained and the intense band at  $2805 \text{ \AA}$  ( $35640 \text{ cm}^{-1}$ ) was taken as the (0, 0) band. The spectrum could be interpreted on the basis of one upper state fundamental  $886 \text{ cm}^{-1}$ .

*Para-methyl phenetole*

In absorption spectrum of the vapour about 35 bands were measured and the intense band at  $2826.9 \text{ \AA}$  ( $35364 \text{ cm}^{-1}$ ) was taken as the (0, 0) band. The spectrum could be interpreted on the basis of six fundamental frequencies in the upper state (563, 635, 801, 989, 1120 and  $1263 \text{ cm}^{-1}$ ) and one fundamental in the ground state ( $235 \text{ cm}^{-1}$ ).

In absorption in liquid state two bands were obtained and the intense band at  $2873 \text{ \AA}$  ( $34797 \text{ cm}^{-1}$ ) was taken, as the (0, 0) band. The other band was interpreted as the upper state fundamental  $830 \text{ cm}^{-1}$ .

In absorption spectrum of the solid eleven bands were obtained and the intense band at  $2880 \text{ \AA}$  ( $34712 \text{ cm}^{-1}$ ) was taken as the (0, 0) band. The spectrum was interpreted on the basis of three upper state fundamentals ( $452$ ,  $814$  and  $1197 \text{ cm}^{-1}$ ).

The details will be published shortly

## 10

STRUCTURE OF NAPHTHAZARIN,  $\text{C}_{10}\text{H}_8\text{O}_2(\text{CH}_3)_2$ 

P. SRIVASTAVA

INDIAN ASSOCIATION FOR THE CULTIVATION OF SCIENCE, CALCUTTA-32

(Received, April 18, 1960)

Naphthazarin exists in three different modifications. The results of X-ray study on all these different forms have been summed up by Borgen (1956) and by Golder and Zhdanov (1958). A preliminary X-ray investigation on modification II, in the notations of Borgen, was made by Srivastava (1958) and later by Billy (1958) also. Billy has given the rough atomic positions which she estimated from three dimensional Patterson's synthesis and the projections obtained with the help of von Eller's photosummator.

In the present communication the molecular structure of naphthazarin has been determined by means of two-dimensional  $F_0$ -synthesis along [010]. The crystallographic data are :

$$a = 7.90 \text{ \AA}, \quad b = 7.30 \text{ \AA}, \quad c = 16.91 \text{ \AA} \quad \text{and} \quad \beta = 124^\circ 38'$$

The crystal belongs to space group No.  $14P_{21/a} - C_{2h}^{16}$  and contains four molecules in a unit cell.

The molecular orientation was known from the study of magnetic anisotropies in the crystal by Banerji (1938). He further suggests that the intersections of the four molecular planes with (010) cannot all be along the same direction,

but should lie along two different directions in the (010) plane. This leads us to infer that the four molecules should exist in the unit cell, as two pairs, not related by any symmetry and that half-molecule should be taken as the asymmetric unit. This also supports the interpretation made by Billy on the basis of Patterson's function.

Accordingly, two molecules were placed in the unit cell with their centres at 0, 0, 0 and  $\frac{1}{2}, 0, 0$  which, after symmetry operations assigned to the space-group  $P_{21/c}$ , gave rise to two more molecules with their centres at  $0, \frac{1}{2}, \frac{1}{2}$  and  $\frac{1}{2}, \frac{1}{2}, \frac{1}{2}$ , respectively. Atomic positions were found out from the electron density projection in the plane (010) and are given in the Table 1. Molecules were well resolved in the plane (010) but much overlapping was found in (100) projection. Positions of the atoms in the projection (010) are shown in Fig. 1

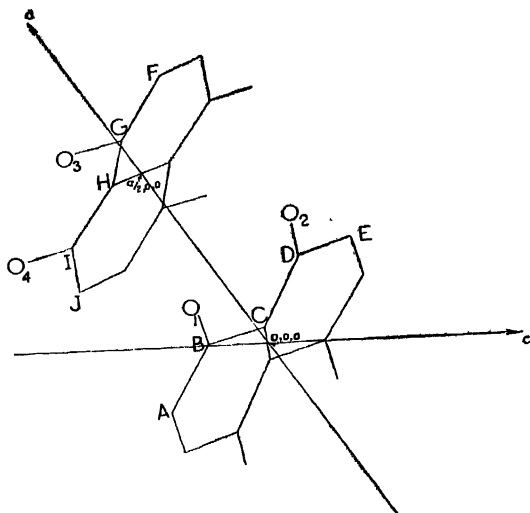


Fig. 1

In the calculation of the structure factors, Hoerni and Ibers' (1954) atomic form factors for oxygen and carbon have been used and an isotropic  $B$ -factor of  $2.5 \times 10^{-3}$  has been imposed upon them. The reliability index

$$R_{(hol)} = \frac{\sum | |F_o| - |F_c| |}{\sum |F_o|}$$

came out to be 0.23

TABLE 1

Molecule at 0,0,0			Molecule at $\frac{1}{2},0,0$		
Atom	X in Å	Z in Å	Atom	Z in Å	Z in Å
A	-1.46	-2.57	F	6.04	1.02
B	0.00	-1.10	G	4.70	0.07
C	0.32	0.12	H	3.75	-0.61
D	1.98	1.72	I	2.35	-2.25
E	2.29	2.93	J	1.28	-2.76
O <sub>1</sub>	0.71	-0.85	O <sub>3</sub>	4.46	-0.90
O <sub>2</sub>	2.67	2.00	O <sub>4</sub>	2.02	-3.25

The complete structure of naphthazarin with Fourier and low temperature refinements will be published shortly.

The author is very thankful to Prof. B. N. Srivastava, D.Sc., F.N.I., for his keen interest throughout the progress of the work and to Dr. B. V. R. Murty, D. Phil., and Dr. S. C. Chakraborty, D. Phil. for their helpful discussions and suggestions. The award of the C.S.I.R. Junior Research Fellowship is also gratefully acknowledged.

## REFERENCES

- Banerji, S., 1938, *Zeit.f. Kristallogr.*, **100**, 316.  
 Billy, C., 1958, *Comp. Rend.*, **247**, 1019.  
 Borgen, O., 1956, *Acta Chem. Scandinavica*, **10**, 867.  
 Golder, G. A. and Zhdanov, G. S., 1958, *Trans. Acad. Sc., U.S.S.R.*, **118**, 1131.  
 Hoerni, J. A. and Ihors, J. A., 1954, *Acta. Cryst.*, **7**, 744.  
 Srivastava P., 1908, *Zeit. f. Kristallogr.*, **111**, 77.



# TRANSISTOR DRIVE CIRCUITS FOR DEKATRONS

K. S. PATEL AND B. M. BANERJEE

SAHA INSTITUTE OF NUCLEAR PHYSICS, CALCUTTA

(Received, March 26, 1960)

**ABSTRACT.** Transistor drive circuits have been described for GC10/4B dekatrons by Chaplin and Kandiah (1958). These apply paired pulses of 80  $\mu$  sec duration and 80 volts amplitude to the dekatron guides and claim a resolving time of 300 microseconds.

A transistor circuit suitable for the faster GC10D dekatron that attains a resolving time of 40  $\mu$  sec has been described by the authors. This supplies a 20  $\mu$  sec, 150 volt pulse and is essentially a blocking oscillator pulser using a ferrite core transformer. The transformer design details have also been described. The circuit is simple and reliable and works over a supply voltage range of 7.5 volts to 18 volts. The current drain at pulse rate of 5000 is only 2.0 mA at 12 volts. This is strikingly low when one remembers that the current drain for a paired pulse drive circuit is 10 mA at a pulse rate of 500 only.

Following this, a similar circuit for GC10B, that needs 60  $\mu$  sec pulses was developed. At 5000 pulse rate its current drain is 12 mA at 12 volts supply. This circuit also works over a range of 7.5 volts to 18 volts. It is essentially more simple and reliable compared to the paired pulse drive circuits and shows a resolving time (200  $\mu$  sec) that is better than the manufacturers figure for this dekatron.

## INTRODUCTION

Of all devices used for decade counting, the glow transfer type dekatrons appear to be the most simple. Extremely low operating power (0.15 watts) and reliability are its further attractions. Combined with a transistor drive circuit and transistorized high tension and extra high tension, perhaps the last word is reached in the development of a portable nuclear counting system that is simple and reliable, efficient and elegant.

Transistor drive circuits have been described by Chaplin and Kandiah (1958). These are for use with the neon-filled GC10/4B dekatrons that have 250  $\mu$  sec resolving time. Paired pulses of 80  $\mu$  sec duration and 80 volts amplitude with adequate overlap, are applied by these circuits to the two guide electrodes of these dekatrons. Resolving time of 300  $\mu$  sec has been claimed for these circuits, which use five crystal diodes, five resistors, two capacitors and a special transformer using a ferrite core. These circuits are adequate for nuclear counting system using G.M. Counters that have dead times in the range of 100 microseconds.

The scintillation detector, which gives a very great improvement in detection efficiency for  $\gamma$ -rays, is however capable of much faster counting. Scintillation



second, and the trigger pulse width must be more than  $5 \mu$  sec. This limitation in the repetition rate is probably due to the increase in the average  $d-c$  level of the drive pulses at higher pulse rate so that higher amplitude drive pulses will be needed for a glow transfer. Also for a constant value of  $C$ , reduction in the supply voltage necessitates a longer duration trigger pulse for maintaining regeneration in the circuit. The current drain at 12 volts is only 2 mA with a pulse rate of 5000 per second. The trigger pulse need have a width of 2 microseconds and a little over 1.5 volts\* in amplitude. Such a pulse is readily obtained from the preceding transistor binary.

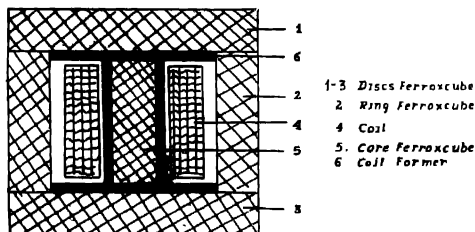


Fig 2(a). Design of the blocking oscillator transformer.

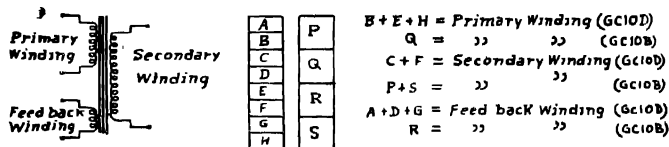


Fig. 2(b). Details of the coil winding of transformer in the GC10D and GC10B circuits.

The resolving time (and other performance data reported here) was measured in the arrangement of Fig. 3 and was found better than 50 microseconds. The

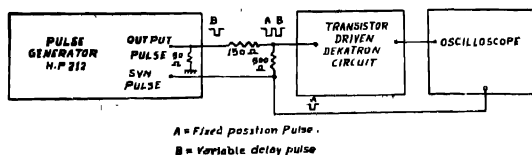


Fig. 3. Arrangement for the measurement of the resolving time of the circuits.

\*The amplitude of the trigger pulse should be a little greater than the base bias. Smaller bias makes the circuit more sensitive.

oscillograms may be seen in Fig. 4a. The large overshoot that follows each drive pulse in it (and also in Fig. 4b) rules out the possibility of glow resting on any of the transfer electrodes. Furthermore, an appreciable overlap is automatically maintained in these circuits (Fig. 1 and Fig. 5). Overlap ensures smooth transfer of the glow from the cathode to the first, second and third guides successively and adds to the inherent reliability of the operation of the tubes.

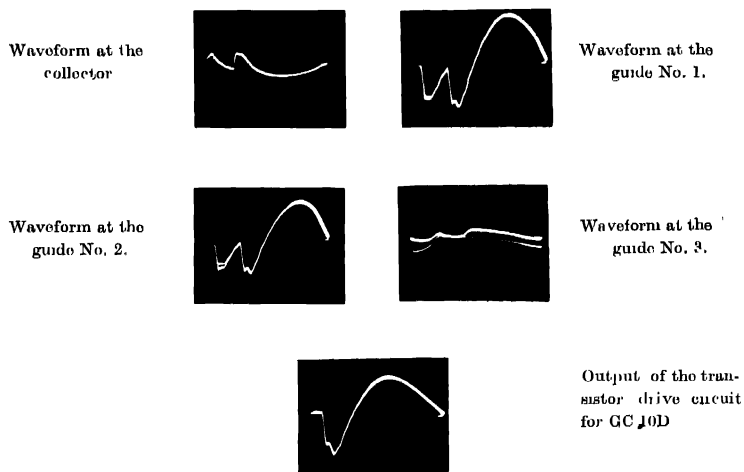


Fig. 4(a). Oscillograms showing the response of the transistor drive circuit for GC 10D, to two input pulses separated by an interval of about  $50\mu$  sec.

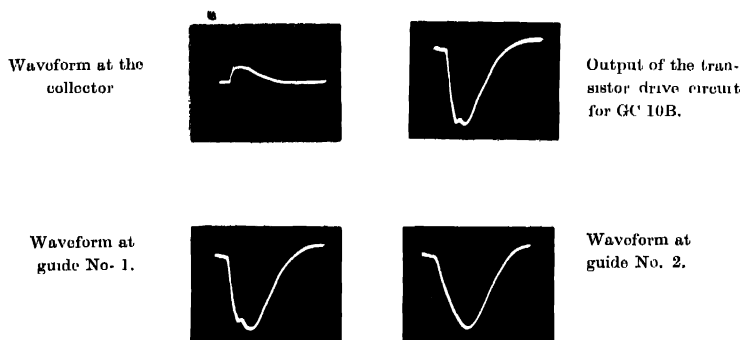


Fig. 4(b). Oscillograms showing the response of the transistor drive circuit for GC 10B.

The surprisingly low current drain of this circuit prompted an enquiry if a circuit for GC 10 B could be developed on these lines which would have much lower current drain. It was felt that the larger current drain of the paired pulse drive circuits (Chaplin, Kandiah) was due to two causes. First, one has to supply the power for storing adequate energy in the magnetic fields of the core, so that a large overshoot, necessary for generation of the second pulse, is produced. Secondly, one has to supply the power dissipated in the back resistance of the crystal diodes that switch the pulses on the dekatron guide electrodes. It was felt that an integrated pulse drive circuit (Eriessson Handbook) instead of the paired pulse, would have greatly reduced current drain. The circuit, as finally developed, is shown in Fig. 5. The resolving time has not been sacrificed in the least, in as much as the circuit counts correctly up to 5000 pulses per second, whereas the manufacturers specification is only 4000 pulses per second. The current drain at 5000 pulse rate is only 12mA at 12 volts which represents tremendous improvement.

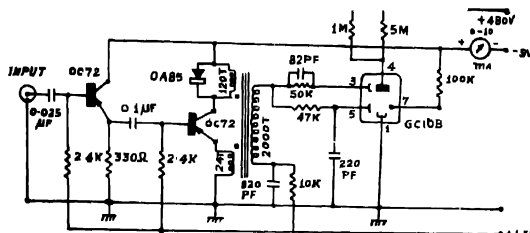


Fig. 5. GC 10B drive circuit.

The circuit works reliably over a supply voltage range of 7.5 volts to 18 volts and it will be seen (Fig. 5) that it is simpler than the paired pulse circuit. In the paired pulse circuits of Chaplin and Kandiah, high back voltages to which the switching diodes across dekatron guides are subjected, introduce a likely cause of failure. Reliability is further endangered in these circuits as the transistor is also subjected to the extremes of its ratings.

The design of the ferrite core transformer, the most important component of these transistor circuits, is actually simpler than the paired pulse circuits, and is given in Fig. 2. A pulse width of 60 microseconds is needed by GC 10B and this is adjusted again by choosing a suitable value for C. The oscillograms may be seen in Fig. 4b. The crystal diode across transformer primary (Fig. 5) not only clips overshoot, but also conserves current drain, as it returns a good part of the magnetic energy back into the supply.

## REFERENCES

- Action, J., 1952, *Electronic Engineering*, **24**, 48.  
Bacon, R., and Pollard, J., 1950, *Electronic Engineering*, **22**, 173.  
Chaplin and Owens, 1956, *Proc. I.E.E.*, **B103**, 510.  
Chaplin and Williamson, 1958, *Proc. I.E.E. B.* **105**, 231.  
Cold Cathode Tubes Handbook- ETELCO Limited (Ericsson) 22 Lincoln's Inn Fields,  
London, W.C.2.  
Kandiah, K., 1958, *Nuclear Instruments*, **2**, 109  
Kandiah, K., 1954, *Electronic Engineering*, **26**, 56.  
Roy, R., 1959, Proc. of the Department of Atomic Energy Conference on Low Energy  
Nuclear Physics.  
Wolfdale, 1958, "The Junction Transistor and its Applications", Heywood and Com-  
pany, London Publication

# X-RAY STUDY OF CRYSTALLITE ORIENTATION IN AGAVE AMERICANA

ANAND PRAKASH AND V. D. GUPTA

PHYSICS DEPARTMENT, UNIVERSITY OF ALLAHABAD, ALLAHABAD

(Received, May 26, 1960)

## Plate VI

**ABSTRACT.** Following the method outlined by P. H. Hermans and others, a quantitative study of crystallite orientation in agave americana fibre under various physical conditions is carried out. It is found that unlike many other cellulose fibres, the orientation of the crystallites in agave americana shows improvement on treatment with NaOH. This is ascribed to the removal of some intercrystalline constituents.

Because of their textile importance cellulose fibres of different kinds and origin are probably the most extensively investigated of all the natural materials. They are known to occur as Natural, Bast and Leaf fibres. The determination of crystallite orientation in a particular type of leaf fibre-agave americana forms the subject matter of the present investigation.

The problem of crystallite orientation in fibres is not only of theoretical interest but also of practical importance as many of their physical and chemical properties are correlated with it. A quantitative investigation of the problem has been attempted by Sisson and Clark (1933), Berkley (1939), R. Hosemann (1937) and Hermans and Hermans (1946). The problem has been studied both from X-ray and optical methods. The X-ray method is more useful because optical methods furnish information merely as to the average orientation of the entire fibrous substance, whereas the X-ray method gives orientation of only the crystallite components. It is in this restricted sense of orientation that a quantitative estimation by means of X-ray methods is made.

The intensity distribution along an X-ray interference circle from a polycrystalline specimen in which crystallites are oriented in some way, offers a possibility to investigate the orientation properties of the material. This was first pointed out and the foundations for such investigation were laid by Polanyi (1921). Since that time a very large number of orientation investigation has been published dealing with inorganic and organic materials of crystalline and semi-crystalline nature. Following Hermans, and Hermans, the orientation factor is determined by the equation

$$f_x = 1 - \frac{3}{2} (\overline{\sin^2 \beta_1} + \overline{\sin^2 \beta_2}) \quad \dots (1)$$

where  $\beta_1$  and  $\beta_2$  are the angular distances along the equator for two paratropic interferences arising from planes approximately at right angles to each other. In taking averages along the arcs we assign weights  $G(\beta) \cos \beta_1$  and  $G(\beta) \cos \beta_2$  the value of  $\beta$  according to the shape of the intensity distribution  $I = G(\beta)$ . Thus

$$\overline{\sin^2 \beta} = \frac{\int I \sin^2 \beta \cos \beta d\beta}{\int I \cos \beta d\beta}$$

However, since in those cases where  $(10\bar{1})$ ,  $(021)$  overlap the intensity curve for  $(10\bar{1})$  alone can not be determined, the following formula is used instead of (1)

$$f_z = 1.245 - 1.72 \sin^2 \beta - 2.06 \overline{\sin^2 l}$$

where  $l$  is the angle along the  $(10\bar{1})$ — $(021)$  circle relating to the total intensity of two overlapping interferences. This is based on  $K = 0.83$

#### EXPERIMENTAL

Raw leaves of agave americana were retted as usual and the fibres obtained were thoroughly washed, dried and combed to ensure parallelism. Filtered  $\text{CuK}_\alpha$  radiation from a Seifert's sealed tube working at 38 KV, and 18 mA was used with a specimen to film distance of 5 cm. and the specimen size, exposure time and photographic technique were standardised as far as possible. The photometer used was Moll's recording type. The film was cut into a circular disc of 4.5 cm diameter and it was mounted on a rotatable holder fixed to the stage of the microphotometer so that the rotation which could be made in steps of  $2^\circ$  are took place about the centre of the photograph. At each setting the film was scanned radially by traversing the holder. Since the films were of low photographic density it was assumed in the calculations that the X-ray intensity was proportional to blackening and was thus linearly related to the logarithm of the intensity of transmitted light. The results obtained are given in Table I.

TABLE I

Sample	$\sin^2 \beta_1$	$\sin^2 \beta_2$	$f_z$
Native Fibre	.041	.055	.85
When treated with 18% NaOH and dried without tension	.026	.0406	.90
Treated with 18% NaOH and dried under tension	.016	.014	.96

Native fibre boiled with 2%  $\text{H}_2\text{SO}_4$  and mercerised with 18% NaOH = 0.75

#### DISCUSSION

Agave americana fibres are stiff, bright and comparatively thicker than jute in the native form. On treatment with caustic soda solution the strength



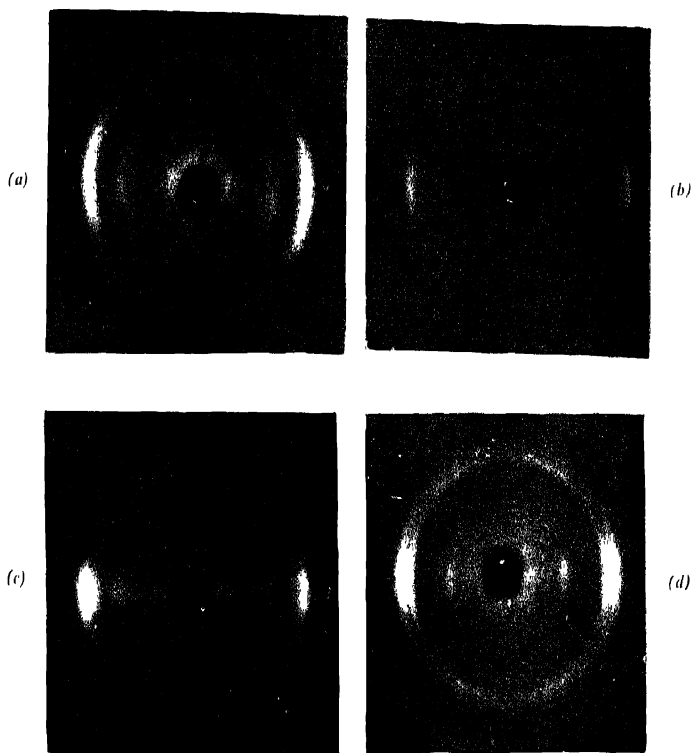


Fig. 1. X-ray photograph of the fibre

- (a) Native fibre
- (b) Treated with 17% NaOH, washed and dried  
without tension
- (c) Same as above when dried under tension
- (d) Boiled with 2% H<sub>2</sub>SO<sub>4</sub> and then  
mercerised.



of the fibre gradually decreases which is evidently due to the removal of lignin and other intercrystalline materials which may also be responsible for an incomplete mercerisation. This is clearly seen from the X-ray photograph of the fibre treated with 18% NaOH (Plate VI). The photograph is a mixed one. The partial reconversion of the cellulose to the native modification can as well be ascribed to the formation of crosslinks between cellulose chains in the neighbourhood of the crystallites and thus creating a disposition in favour of the return to the original configuration after swelling. This seems to be supported by the fact that the degree of mercerisation is more pronounced in a sample which is boiled with 2%  $H_2SO_4$  before being mercerised because it loosens the crosslinks. There is, however, also the possibility of the removal of some intercrystalline constituents which effect mercerisation. Another interesting observation made about agave americana is that the crystallites are better oriented as a result of the treatment with NaOH. This may again be due to the removal of those intercrystalline materials which impede the rotation and alignment of the crystallites. However when the fibre is first boiled with  $H_2SO_4$  and then mercerised, the orientation decreases. This shows that the damage done on  $H_2SO_4$  treatment far outweighs the improvement in orientation when NaOH alone is employed.

A detailed study of agave americana from the scattering of X-rays at small angles and by employing the techniques of electron microscopy is also being made and will be shortly reported.

#### ACKNOWLEDGMENTS

The authors are extremely grateful to Prof. K. Banerjee, D.Sc., F.N.I., for his constant encouragement and guidance throughout the progress of this work. One of the authors (A.P.) is also thankful to the Council of Scientific and Industrial Research for the financial aid.

#### REFERENCES

- Borkley, E. E., 1939, *Textile Research Journal*, **9**, 335.  
Hosemann, R., 1937, *Z. Physik. Chem.*, **179A**, 356.  
Hormans, J. J., Hermans, P. H., et al., 1946, *Rec. Trav. Chim.*, **65** 427,  
Polanyi, M., 1921, *Z. Physik.*, **7**, 149.  
Sisson, W. A. and Clark, G. L., 1933, *Ind. Eng. Chem., Anal. Ed.* **5**, 296.

# SOME OBSERVATIONS ON THE ENERGY SPECTRUM OF LOW ENERGY BREMSSTRAHLUNG FROM ELECTRONS OF ENERGY $\leq 10^{12}$ eV

P. K. ADITYA

DEPARTMENT OF PHYSICS, PANJAB UNIVERSITY, CHANDIGARH

(Received, May 4, 1960)

**ABSTRACT.** Observations have been made on the energy spectrum of photons of energy greater than 30 MeV emitted by bremsstrahlung from high energy electrons of  $10^{11}$  eV to  $10^{12}$  eV. This observation is of importance from the point of view of checking the influence of the density of the medium. No significant departure from the conventional theory has been observed.

## INTRODUCTION

In the past few years, a new aspect of the electrodynamic theory of radiation has evolved from the theoretical prediction of the Russian physicists Landau and Pomeranchuk (1953) and Ter-Mikaelian (1954), according to whom the probability of bremsstrahlung of low energy photons depends upon the density of the medium. In the conventional theory due to Bethe and Heitler (Heitler, 1954) there is no such dependence. According to the new effect, abbreviated as L-P-T, the cross section for the emission of low energy photons is predicted to decrease in media of higher density, as higher initial energies for the primary electron are approached. This influence results from the multiple scattering of the electron and due to the polarisation of the medium. On the basis of quantum mechanical considerations, Migdal (1957) has worked out the details of the effect. Curves suitable for comparison with experiment have been given by Varfolomeev *et al* (1958, 1959)\*

Nuclear emulsions have a density of  $\sim 4 \text{ g.cm}^{-3}$  and electromagnetic cascades initiated by isolated electrons or photons and by the photons from the  $\pi^0$ -mesons created in very high energy interactions are readily available. For primary electron energies greater than or  $\sim 10^{11}$  eV and secondary electron pairs due to photons of a few MeV, one expects to check the validity of the theoretical predictions. This article is meant to describe the results of our work and discuss these in the light of the other results available on the subject.

\* Thanks are due to Professor Varfolomeev for the communication of the preprint and the reprint.

## STATEMENT OF THE PROBLEM

It is important to consider the problem in the light of the experimental observations that can be made. One normally observes a soft shower and obtains its energy from parameters that involve the growth of the shower which is derived from the longitudinal development as given by the cascade theory or from the lateral spread (Pinkau, 1956). There are also alternative methods such as the suppression of ionisation near pair origin (Iwadare 1958) or the true opening angle of the pair (Lohrmann 1955; Aditya 1959 a). The second problem is to detect the secondary pairs and determine the energy of each one of them. When both these quantities are known, the theory can in principle be put to test.

It is well known that the intrinsic fluctuations (Aditya 1959 b) involved in the nature of the processes do not always permit a precise estimation of the primary energy. Results derived from one or a smaller number of cascades are thus subject to uncertainties. This limitation can be overcome to a great extent by collecting together a large number of cascades of about the same energy. Another factor that plays a decisive role, is the probability for the detection of low energy electron pairs. In nuclear emulsions the critical energy is  $\sim 20$  MeV so that one is not likely to detect pairs of energy smaller than this value with as good an efficiency as the high energy pairs. The detection efficiency is strongly dependent upon the experimental conditions of observation.

There is yet another factor that influences our conclusions on the effect, as follows: The lack of low energy pairs is strongly dependent on the primary energy, so that one would like to take account of only the first generation pairs due to the bremsstrahlung from the primary electron and not those created from the secondary electrons. This distinction between the pairs of the various generations is not straightforward, but has been attempted by some workers (Benisz *et al.*, 1959; Fenyves *et al.*, 1959). In such a procedure there is a possibility of introducing a bias towards the removal of more low energy pairs than the high energy ones. In the light of the considerations given above, the results of the present investigation are given.

## EXPERIMENTAL DETAILS

Out of a large number of soft showers picked out from two stacks of stripped emulsions exposed in the stratosphere (Aditya 1959 c), 17 cascades have been selected, the criteria for selection being good conditions of experimental observation. There is apparently no bias likely to affect the conclusions on the subject. 3 cascades are associated with a nuclear disintegration (Aditya 1959 d), 5 are initiated presumably by a single electron entering the stack and 9 originate from a single pair. In each case the development has been normalised to a primary electron and the cascades grouped into two bunches: high energy (650, 625, 550, 500, 500, 475, 350, 325) and low energy (250, 225, 200, 125, 50, 50, 40, 40, 40) groups.

The figures in the brackets give for each cascade the energy per electron in GeV. In the case of cascades initiated by a pair, the energy has been assumed to have been equipartitioned between the two electrons. These energies have in most of the cases been determined by the application of different procedures and the most probable value estimated. The individual errors in the energy estimation are expected to have been smoothed out as the cascades of about the same energy have been grouped together.

In order to keep the detection efficiency presumably constant over the entire energy region, we have not attempted to consider the electron pairs of energy less than 30 MeV. The resulting energy spectrum up to a distance of 1.5 cascade unit has been plotted in the Figs. 1a and 1b, for the two energy intervals. The expected curves for the Bethe-Hertler and Migdal calculations have been included for comparison. We have made no attempt to separate the pairs of various generations on account of the reasons already mentioned. In order to decrease the influence of the pairs of further generations, the measurements have been limited to only the first 1.5 cascade unit from the origin.

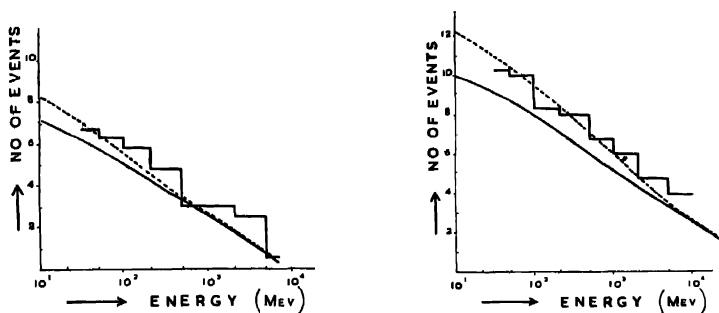


Fig. 1. Energy spectrum for electron pairs observed over the first 1.5 cascade length.

The lower limit for acceptable pair energy has been set at 30 MeV (see text)

(a) 9 cascades of median energy 50 GeV per electron.

(b) 8 cascades of median energy 500 GeV per electron.

From the figure, it may be seen that subject to the experimental fluctuation a conclusive statement might not be made in favour or against one or the other theory. Since our energies are not extremely high, allowance has to be made for the possibility of the suppression being genuine at higher energies, there being no measurable departure up to  $\sim 500$  GeV energy for primary electrons.

#### DISCUSSION

It appears useful to compare our results with those of other workers in the field. Varfolomeev *et al.*, (1958, 1959), have studied the spectra for primary

energies from  $10^{11}$  eV to  $10^{13}$  eV, and secondary pair energies up to 1.5 MeV. They have found a significant departure from the Bethe-Heitler theory and agreement with L-P-T. It is worth considering that their lower limit of  $\sim 1$  MeV is too low to guarantee uniform detection efficiency over the entire range. In view of this it may not be fair to consider their measurements as having established the existence of the effect.

The second investigation is that of the Polish group (Benisz *et al.*, 1959) who have studied 4 photon-initiated cascades out of which three are associated with a high energy disintegration and the fourth one is that of Miesowicz *et al.*, (1957). The mean energy per electron is  $\sim 500$  GeV, and they have attempted at the separation of the pairs of the first generation from the rest. The lack of low energy pairs might well be accounted for the introduced bias. Their energy region is the same as ours and since our statistics is relatively larger with no effect observed, it may be concluded that the effect if present at these energies is not at least of the order suggested by L-P-T.

There is yet another work by the Czech-Hungary group (Fenyves *et al.*, 1959) in which they have studied the energy spectrum up to 1.5 cascade unit for a cascade initiated by a photon of  $\sim 2000$  GeV. In spite of the fact that this energy is fairly high (in fact higher than our energies and of Benisz *et al.*) no departure has been noted. The authors have attempted at the separation of the various generation pairs and still observed no divergence from the conventional theory.

In view of the present investigation and of the investigation of other workers mentioned above, it may be concluded that the decrease of bremsstrahlung cross section for low energy photons is not appreciable. This work however does not prove whether the departure would exist at higher energies.

After this work had been finished, the results of the Bristol group (Fowler *et al.*, 1959) have come to our notice\*. The method is based upon measuring the average distance of materialisation of the first pair for two groups of cascades of different energies. From the distribution of these distances and the mean value for two groups of primary energy  $10^{11}$  eV and  $10^{12}$  eV, they found better agreement with L-P-T than with B-H. Their energy of  $10^{13}$  eV per electron is much higher than most of the other investigations and in view of the large statistics give evidence on the existence of the effect at  $\lesssim 10^{12}$  eV. The actual magnitude of the suppression, whether it is as much as predicted, will have to be determined from the availability of larger statistics.

\*Thanks are due to Professor M. G. K. Menon for pointing out this paper at the Ahmedabad Symposium, where these results were reported: Annual Cosmic Ray Symposium of the Department of Atomic Energy, March 1959.

## REFERENCES

- Aditya, P. K., 1959a, *Ind. J. Phys.*, **33**, 357.  
 Aditya, P. K. 1959b, *Nuovo Cimento*, **13**, 1013.  
 Aditya, P. K., 1959c, *Nuovo Cimento*, **11**, 546.  
 Aditya, P. K., 1959d, *Nuovo Cimento*, **13**, 219.  
 Benisz, J., Chylinaki, Z., and Wolter, W., 1959, *Nuovo Cimento*, **11**, 525.  
 Fenyves, E., Frenkel, A., Tolbisz, I., Pernegr, J., Potzilkka, V., Sedlak, J., and Vrana, J., 1959, *Nuovo Cimento*, **14**, 1249.  
 Fowler, P. H., Perkins, D. H., and Pinkau, K., 1959, *Phil. Mag.*, **4**, 1030.  
 Heitler, W., 1954, *Quantum Theory of Radiation*, (Oxford Press).  
 Iwadar, J., 1958, *Phil. Mag.*, **3**, 680.  
 Landau, L. D., and Pomoranchuk, I. A., 1953, *Dokl Akad. Nauk.*, **92**, 535.  
 Lohrmann, E., 1955, *Nuovo Cimento*, **2**, 1029.  
 Miesowicz, M., Stanicz, O., and Wolter, W., 1957, *Nuovo Cimento*, **5**, 513.  
 Migdal, A. B., 1957, *J. E.T.P.*, **5**, 527.  
 Pinkau, K., 1957, *Phil. Mag*, **2**, 1389.  
 Tor-Mikaelyan, M. L., 1954, *Dokl Akad. Nauk*, **94**, 1033.  
 Varfolomeev, A. A., Gerasimova, R. I., Gurevic, I. I., Makarina, L. A., Romantseva, A. C., Svetlobov, I. A., and Chueva, S. A., 1958, *Proceedings of the International Conference on High Energy Physics at CERN, Geneva, July 1958*, Page 297.  
 Varfolomeev, A. A., Gerasimova, R. I., Gurevic, I. I., Makarina, L. A., Romantseva, A. C., and Chueva, S. A., 1959, *Atomic Energy Institute of the Academy of Sciences of the USSR, Moscow*.



# A HIGH INTENSITY NEUTRON GENERATOR

S. K. MUKHERJEE, N. K. MAJUMDER AND A. GANGULY

SAHA INSTITUTE OF NUCLEAR PHYSICS, CALCUTTA

(Received, May 26, 1960)

**ABSTRACT.** A 400 KV deuteron D.C. accelerator of Cockcroft-Walton type, for production of neutrons by  $d-d$  and  $d-t$  reactions, is described. Special features and principal operating characteristics of this generator are discussed.

## 1. INTRODUCTION

A 400 KV Cockcroft-Walton type deuteron accelerator, designed for delivering 5 mA of deuteron ion beam, had been planned, fabricated and installed in this institute and been operating regularly and efficiently for the last eighteen months. The exothermic nature of ( $d, d$ ) and ( $d, t$ ) reaction and its high cross section made this type of generator compact and low voltage one. The development and easy availability of the targets of deuterium and tritium gas absorbed in Zirconium or Titanium, have given a strong impetus for building this compact low voltage unit for producing fairly strong sources of monoenergetic  $\gamma$ -free neutrons in the 3.5 MeV and 14 MeV range. In fact, several reports (Peck and Eubank, 1955; Bergstrahl, *et al.*, 1953; Loirani, *et al.*, 1957; Bonner, *et al.*, 1959) of such generators have appeared in recent years in the literature. In our case, the aim was to produce and accelerate the most intense beam of deuteron ion that can be brought to bear on the target of absorbed gas quite safely. To achieve this end, we have developed the ion source and the lens system in such a way as to focuss an unanalysed deuteron beam of 2.5 mA. Also the cooling of the target was thoroughly investigated so that in the end we could focuss on the target a beam current of more than 1 mA. The principal characteristics of our generators are (i) its high ion beam consisting of more than 90% of monatomic ions, obtained by suitable modifications of ion source. (ii) The high voltage is obtained by multiplying a high frequency voltage in a cascade column. This is done both for the purpose of economy and reduction in size as also for reduction in ripples and load effect. The filament supply of the rectifier column is separate and also of high frequency. (iii) The cooling of the absorbed gas target is directly by refrigerant or liquid nitrogen, with an eye to the maximum possible heat transfer, so as to bear as high an ion beam as possible on the target without exceeding its safe temperature of 70° at any time even locally.

## II. C-W VOLTAGE GENERATOR

The voltage generator is, as usual, a voltage multiplying circuit based on the original Greinacher (1921) circuit, as improved progressively by Cockcroft-Walton (1932), Gradstein (1936), Arnold (1950), Lorrain (1949), etc. Particularly the masterly analysis of voltage multiplying circuits, by Bowers (1939), and by Mitchell (1945) have contributed handsomely towards the understanding and improvements of this type of voltage generator. Following the development by Douma and Brekoo at the Philips laboratory and the suggestions made by Lorrain, radio frequency was adopted for both the main High Voltage and also for heating the filaments. We discarded the practice of using power frequencies or other near frequencies. In addition to the marked economy in cost and equipments, a considerable reduction in size was achieved by the use of radio-frequencies. Also a decided improvement in the matters of ripples on the output voltage and of voltage drop with load, was achieved through its use. Although the presence of voltage ripple is not a serious handicap to its use as a neutron generator, still the smallest value of ripple voltage is an advantage in achieving a sharply defined energy. In fact, the higher the frequency and the larger the capacity, the smaller will be the ripple and load effect.

The output voltage of a *c-w* multiplier unit can be written as

$$\begin{aligned}
 V &= 2nE - \Delta V - \delta V, \\
 &= 2nE - \frac{i}{fc} \left( \frac{2}{3} n^3 + \frac{1}{2} n^2 - \frac{1}{6} n \right) - \frac{i}{fc} \left[ \frac{n(n+1)}{2} \right] \\
 &= 2nE - \frac{i}{fc} \left[ \frac{2}{3} n^3 + n^2 - \frac{n}{6} + \frac{1}{2} \right] \\
 &= 2nE - \frac{i}{fc} \cdot \frac{n}{3} (2n+1)(n+1) \quad \dots (1)
 \end{aligned}$$

where  $n$  = number of stages in the multiplier column

$E$  = peak input voltage

$\Delta V$  = voltage drop due to load

$\delta V$  = ripple voltage

$i$  = current drain on the high voltage

$f$  = operating frequency

$C$  = condenser value

The effect of higher condenser and frequency values is apparent. So also the desirability of limiting the  $n$  value. In practice, there is an upper limit to the frequency that can be usefully employed. Also the value of the condenser is decided by the bulk and the cost. Some compromise is made between these conflicting factors and it was found that 100 Kc/s and 400 Kc/s are two of the best practical values for the mains and filament heating frequencies. The theo-

retical values of ripple voltage is 3.5 V per mA of load current, and of voltage drop due to load is 22 volt per mA, assuming the value of  $n = 7$  and  $c = .05 \mu f$ .

The unit of a multiplying circuit of our generator is shown as in the Fig. 1. The C-W generator has several pairs of Eimac 100 R radiation cooled rectifier arranged in cascade supported by equal numbers of condensers arranged in column. The tubes are encased in leaklight perspex tubes coupled to each other by aluminium domes. The other arrangements of the column are not far different from that adopted at Philips laboratory. The filaments of the tubes are heated by 350 Kc/s power coupled by ferroxcube core transformer. Plate power supply frequency is 75 Kc/s. The isolation of the two frequencies from each other was obtained by means of LC circuits resonant at the filament heating frequency. The multiplier circuit is supplied by a master oscillator and power amplifier -- the output of which is amplified by a very high  $Q$  resonant coil, which in turn feeds the multiplier column. The bleeder resistance is a chain of five resistances of 100 meg ohms each, which draws a current of 800  $\mu A$  at maximum voltage of 400 KV. This column of resistances is also encased in a perspex tube to be filled with silicone oil for better stability.

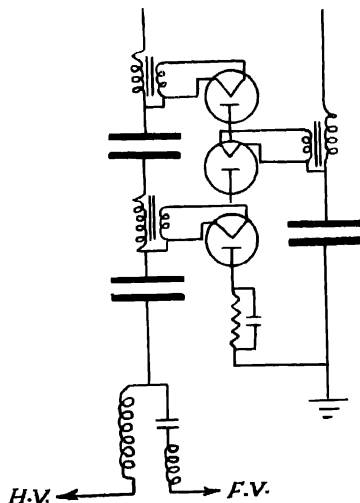


Fig. 1.

The total resistance of the column was measured within an error of 0.1%. It was observed that the resistance column value remained fairly constant over a long period of time. Percentage of ripple was determined by means of an

oscilloscope, taking the output from the low voltage end of the resistance column. The measured value was found to be 7 volt per mA of load current. The voltage drop with 7 mA of load current is 140V. This agrees within close limits with our theoretical value as calculated from the formulae shown in Eq. 1. The stabilisation of the high voltage was achieved by the stabilisation of the input R.F. voltage from the oscillator. This in turn was done by taking a small fraction of the voltage output and using them to correct any change in the D.C. plate voltage of the oscillator. The power to the filaments of the transmitter tubes was fed through a magnetic voltage stabiliser. The actual stabilisation achieved in this way was better than 0.1%.

#### GENERAL ARRANGEMENTS

The plan of the general arrangements of the high tension set, the accelerating unit and the power supplying alternator is shown in the Fig. 2. The accelerator column consists of three numbers of silica tubes. Detailed description of the accelerating tube is given in the following section. The accelerating column

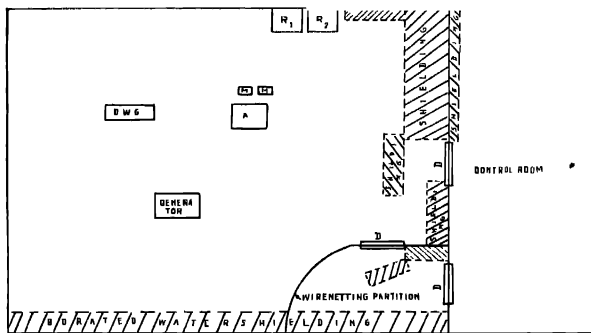


Fig. 2. General plan of layout of C-W Generator

is placed vertically in our case— though we considered the advantages accruing from the horizontal alignment of the column which is very often followed in the case of low voltage accelerator. We are guided in this respect by the ease of assembly and alignment in the vertical system as also the case of automatically providing high voltage insulation from the ground. The units for supplying power to the ion source and the focussing lens—all should be at high voltage and hence placed in a housing well insulated from ground. The high voltage terminal housing is a polished aluminium dome rounded at corners to prevent corona loss. The four insulating columns for supporting this high voltage terminal are all made of 3" dia. perspex tube sealed at both ends to prevent penetration of dust and moisture. The outside surface of these tubes are treated and polished

with silicone fluid D. C. 200 to prevent any adhesion of moisture on them. Inside the high voltage terminal are located (a) the radio-frequency ion source oscillator and its power supply, (b) the extracting voltage supply (0–5 KV), (c) the focussing voltage supply (0–15 KV) and (d) the cooling fans and light arrangements. The precision leak valve and its control together with the gas reservoir are also located inside this dome. Appropriate meters to indicate operation of the above circuits are suitably placed in the dome with clear perspex windows. Control rods in the form of perspex tubes come out of the housing from each circuit. The tubes are operated by remotely controlled system. Mirror and telescope arrangements were made to obtain remote view of the H.V. terminal operation. An alternator for supplying power to the units in the high voltage terminal, is placed in a dome similar to the above. The alternator generates 110 V. A C. single phase, 800 cycles frequency. The alternator body is made of aluminium alloy, thereby ensuring a light weight. The alternator rotates at 3000 r.p.m. and is driven by a motor placed at ground end and the driving system requires careful designs and high insulations.

In our case this is driven by a 3 H.P. A.C. 3 phase motor with speed of 3000 rpm. The coupling system is a  $2\frac{1}{2}$ " dia. perspex tube, 4 ft. long, suitably joined at the ends by means of universal couplings. No speed reduction gears are employed now. This arrangement is marked by simplicity and directness, though it required very careful adjustments at the beginning. An alternate arrangement involving the reduction of speed of rotation of perspex shaft by a factor of 10, is in progress.

#### ION SOURCE

Several types of ion sources were examined for suitability of their uses in this particular instrument. Of these, two types immediately recommended themselves by reasons of stability, long life and ease of maintenance. One of them is the Radio-frequency ion source and the other the Penning Cold Cathode ion gauge type. For low power consumption, circuit simplicity and compactness, the penning type source seemed better. But for high ion yield, and for high percentage of atomic ion in the beam, R. F. type source has hardly any equal. Since our instrument requirement is for highest atomic ion beam consistent with low gas consumption, R. F. ion source became our obvious choice.

In our design, we adopted the Oak Ridge type with some modifications for higher ion yield. The discharge tube is a 1" dia. Pyrex glass tube, 6" long, sealed to the metal plate by means of gasketed flanged joints. The Extraction canal is of pure aluminium  $1/16$ " dia.  $\times$   $3/16$ " long. The cover glass for the canal is of pyrex, —its top grounded flat and polished (Fig. 4). A triode 3/300 tube was used in an ultra-audion circuit to provide a maximum power output of 300 watts at 75 mc/s. The coupling was done by quarter wave transmission lines, glass

leak to the tube was controlled by a finely adjustable leak valve. A strong magnetic field was provided around the canal tip. The life of the glass tip and the aluminium canal depends greatly on the beam current extracted throughout it. In our case the average life of the canal and the tip is more than 200 hrs. The part played by cleaning of the discharge tube can not be over emphasised. The method of cleaning by diluted hydrofluoric acid was found to be good and occasional cleaning by this method tended to increase the ion output.

Deuteron currents approaching 4.5 mA at 4 KV extraction potential could be obtained from this ion source. The beam divergence was small enough to be focussed by an electro static lens within a spot of 3.4 mm at a distance of 1 meter. Of course this required increased gas feed to the source and a longer canal diameter. Experiments on monatomic ion percentage in the deuteron beam current showed that quality of glass of the ion source and its annealing conditions have a strong influence on the high monatomic ion percentage. It was also found that after more than 200 hours running, the ion source tended to produce a lesser yield of atomic ion percentage. This is probably due to vitrification of the glass material.

#### VACUUM SYSTEM

The pumping unit initially consisted of one 4" oil diffusion pump backed by a rotary mechanical pump having a free air displacement capacity of 140 lit/min. The oil diffusion pump was designed and fabricated by us and it developed an unbaffled pumping speed of 275 lit/sec at  $10^{-5}$  mm Hg. The mechanical pump developed a backing pressure of  $6 \times 10^{-4}$  mm Hg and speed of 0.7 lit/sec when the system was running with no gas load. A refrigerated optical baffle using Freon-22, was employed to trap all the back streaming oil vapour and keep the accelerating tubes and target chamber free from traces of oil vapour. The actual pumping speed developed with this baffle and system was 140 l/sec at  $1 \times 10^{-5}$  mm Hg. To handle increased gas feed to the ion source at the time of increasing ion beam current, and also to handle occasional gas bursts, provision of another 4" diffusion pump was made. This later pump was designed with an eye to its ability to handle larger throughput. The baffle system of this pump was made in two stage. One was a water baffle and the second a freon cooled refrigerated baffle. The temperature of the water baffle was designed to be of  $35^\circ\text{C}$ .

The vacuum measuring gauges consist of one thermo-couple gauge for low vacuum range (1 mm to  $10^{-3}$  mm) and one hot cathode ionisation gauge for high vacuum range ( $10^{-4}$  to  $10^{-6}$  mm Hg). Adequate provisions of ion gauge control, interlock system of high vacuum with ion gauge, water flow, refrigerating cooling unit and diffusion pump heater, were arranged. Weston sensitrol relays were freely used for these control. The r.f. ion source at its normal operation consumes nearly 10-15 cc. of gas at atmospheric pressure per hour. This means a leak

load on the high vacuum side of the accelerator tube. The ultimate vacuum in the accelerator tube with no gas load, as measured by the ionisation gauge at the ground end of the tube, was  $2 \times 10^{-6}$  mm Hg and the vacuum with the ion source and the system running, was better than  $1 \times 10^{-5}$  mm Hg.

#### ACCELERATING COLUMN

The accelerating column forms the most important item in the neutron generator. This consists of three silica tubes each of  $6\frac{1}{4} \times 10$ " long with wall thickness of  $\frac{1}{4}$ " and flanged at each end. These are joined together by means of aluminium plates having grooved gasket on each face. The plates and the silica tubes are clamped together and covered by means of ring shaped polished aluminium domes. Each aluminium plate carries a lens. These lenses are formed of spun copper tube, heavily chromium plated. The shape, gap width, diameter and other configuration of the lenses are given in the Fig. 3. Each gap is screened from the silica tubes wall to avoid any accumulation of electrostatic charge by

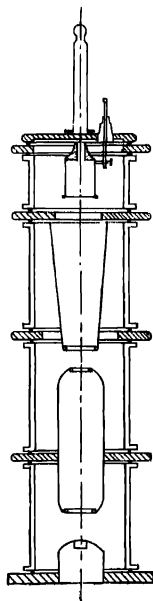


Fig. 3. Ion acceleration column.

the insulator wall. Because of the particular mechanical set up of the lense system, good alignment is automatically assured at the time of assembly. Fig. 4 is a

sketch of the focussing electrode together with the ion source assembly. The ion source is mounted on a gasket in a plate on the other side of which the focussing system is integrally mounted by means of a high voltage ceramic seal. The ion

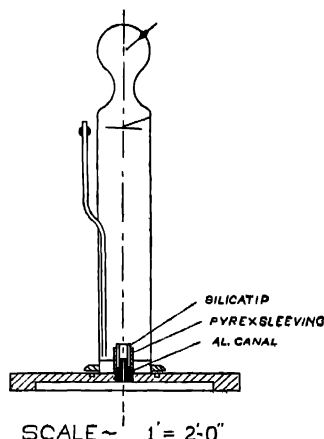


Fig. 4 R. W. ion source.

source can be aligned with respect to the probe canal and the focussing lens by means of a set of removable adjusting screws. These adjustments are to be made when the system is running. The arrangements of the lens system is such that the major part of the accelerating voltage is developed across the last lens gap. As a result the beam is focussed on the target, at a distance of 1.8 metres from the ion source, under all values of high voltage exceeding a certain minimum value. The focal length of the last lens is almost constant irrespective of the voltage on it as it falls on the asymptotic region of the  $f$ - $v$  curve (Fig. 5).

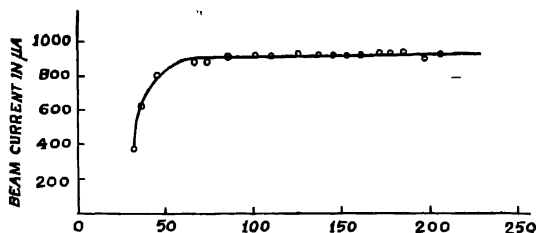


Fig. 5. Deuteron energy in KV.



## TARGET ASSEMBLY

As this instrument is a high current one and meant for high neutron flux, the design of the target system, particularly its cooling, calls for careful attention and examination of details. Our instrument is designed to operate with either tritium or deuterium target. For  $(D, T)$  reaction, Tritium gas absorbed in titanium and mounted by evaporation on copper, was used. Both the thick and the thin types were employed, depending on the necessity of particular experiments. The useful life of a target depends on the efficiency of the cooling system and its ability to transfer the maximum amount of heat without allowing the target to exceed the safe temperature of  $70^{\circ}\text{C}$  even momentarily. The development of hot spot on the target is to be carefully avoided.

We have used several types of target mountings and cooling arrangements. First one we used is shown in Fig 6(i). The cooling was done by pre-cooled water forced directly on the underside of the target in a jet at a maximum pressure of 30 lbs/sq. in. The target intercepts the beam at an angle of  $45^{\circ}$ , and also there is an arrangement to rotate the target at a slow rate by means of motor and gear assembly. An offset in the target manifold enabled one to bring the sample for bombardment within 4 cm from the target. The performance of the target is such that at 200 Kv up to  $450\ \mu\text{A}$  of unanalysed deuteron beam can be brought to bear on the target. The neutron yield under this condition is about  $4 \times 10^{10}$  n/sec. The target temperature rose up to  $70^{\circ}\text{C}$ . The mechanical pump output was monitored for traces of degassed tritium. The target life was understandably short under this condition.

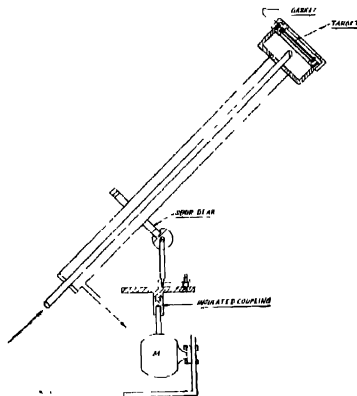


Fig. 6(i). Water-cooled oscillating target.

We changed this target arrangements in favour of another in which cooling is done by means of a refrigerant. The arrangement is shown in Fig. 6(ii). The minimum temperature that the target attains is 8°F. The gas used is Freon-20, and the capacity of the refrigerating unit is more than 4000 BTU/hr. ; under this condition more than 850 $\mu$ A of deuteron beam at 200 KV, was put on the target and continuously operated. For short run not exceeding 1 hr. at a time more

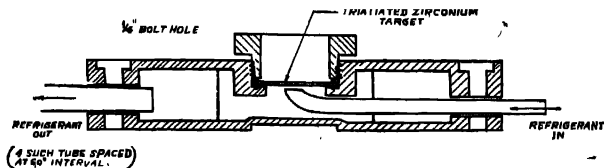


Fig. 6 (ii). Target cooling system. Refrigerant-cooled target

than 1.5 mA was tolerated without exceeding the safe limit of target temperature of 75°C. Temperature measurement was done by means of a pair of differential thermocouple attached to the target. The maximum neutron yield obtained was more than  $3 \times 10^{11}$  n/sec. The beam on this target which is not a rotating type, is purposely defocussed on an area of approximately 3/4", and is thus designed to cover the entire useful area of the target. In this target the bombarding sample can be brought within less than one cm of the target.

Still another type of target cooling was designed for use with liquid nitrogen coolant, but this was discarded in favour of the refrigerant cooled unit in view of the frequent attention that the former type requires. In all these types the main source of trouble is the deposition of carbon, the target assembly due to the traces of oil vapour present from the diffusion pump. This trouble was eliminated in the refrigerant cooled unit by providing a cooler guard ring around the target on which most of the vapour deposit, thus keeping the target free from contamination.

#### ADJUSTMENT

The ion acceleration system needs very careful adjustments and precise alignment in order to obtain the maximum ion beam on the target. This is important, otherwise several undesirable characteristics will appear. Some of the more important of such unwanted characteristics are :

- (i) the radial and axial drift of the focal point of the ion beam, with change in acceleration voltage,
- (ii) change or fluctuations of accelerating voltage with variation in load.

These factors were eliminated with proper care in design and alignment. The ion acceleration systems were first mechanically aligned to a high degree of

precision with respect to the last lens. This was supplemented by a further adjustment in the running condition. The adjustment was made to make the ion beam maximum and by this method the ion optical axes of the ion source, focussing lens and extraction probe lens were brought in one line.

#### MEASUREMENT OF ION CURRENT

Accurate measurement of ion beam current free from all ambiguities due to secondary electron emission and additional secondary ion collection, is very important. Due care and precautions were exercised to measure this. The most direct way is to use a Faraday cage and this cage was used in preliminary stages to measure the current. When ion beam current is high, the colorimetric method is convenient. We have measured the rise in temperature at target, by means of a differential thermocouple. The ion beam current could only be held steady to within 0.5 to 1% under good conditions. The ion current was found to be very sensitive to any change in pressure in the ion acceleration tube and steady beam current could only be obtained if occasional gas bursts in the accelerator tube is kept to a minimum. To this end, twofold means were employed -

(i) keeping the vacuum system scrupulously clean and chromium plating the lens system,

and (ii) using a diffusion pump unit of high enough speed, capable of handling a large throughput without undue rise in ambient pressure

#### NEUTRON FLUX AND SPECTRUM

The neutron flux was measured by three methods .

(i) by means of a calibrated neutron counter

(ii) by means of threshold detectors

and (iii) by means of nuclear emulsion plates.

In the first method, we used a  $\text{BF}_3$  counter (containing enriched  $\text{B}^{10}$ ) in a long counter geometry. This counter was previously calibrated very carefully. Its advantage is that it is insensitive to  $\gamma$ -ray and inherently stable and has very low background, and disadvantages are that it is sensitive to neutrons of lower energy and hence could not discriminate against scattered neutron background.

In most of our experiments, the fast neutron flux measurements were made by activation of some selected element, based on neutron threshold reaction. Its main advantages are (i) it is insensitive to neutrons of energy below the threshold, (hence to most of the scattered neutrons) and (ii) it is capable of measuring flux without causing significant perturbation in flux distribution. In our case  $9.9 \text{ min}$  activity of  $\text{Cu}^{63}$  ( $n, 2n$ )  $\text{Cu}^{62}$  was used for this flux measurement. The threshold of this reaction is 10.65 MeV and the adopted value of its cross-section

is taken to determine any 5.1 min activity of  $\text{Cu}^{65}(n, \gamma)\text{Cu}^{66}$  if it was produced, since the presence of low energy neutron or thermal neutron may cause this later activity to contribute to the total activity and cause errors. However, since  $\text{Cu}^{62}$  is positron emitter the separation of this activity from that of  $\text{Cu}^{66}$  is not

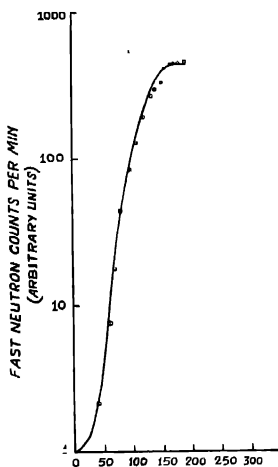


Fig. 7. Neutron yield curve as function of deuteron energy

difficult. Where bombardment time is longer (i.e. more than 30 min) we have used the 14.8 hr. activity of  $\text{Al}^{27}(n, \alpha)\text{Na}^{24}$  having an effective energy of 8.1 MeV for calibration.  $\text{Na}^{24}$  being both  $\beta$  and  $\gamma$  active, we have measured the  $\beta$ -activity by means of an end window G.M. counter and the  $\gamma$  activity by means of a  $\gamma$ -spectrometer. The results from the two measurements agree closely.

The nuclear emulsion plates were used to measure the neutron fluxes as well as the spectrum of neutrons emerging from  $D-T$  reactions. We used Ilford  $\text{C}_2$  plate of emulsion thickness of  $200\mu$  and these are exposed at an angle of  $5^\circ$  to the incident neutron. The measurement of the proton tracks released by the incoming neutrons in the emulsion, yielded the fast neutron spectra [Figs. 8(i) & 8(ii)] with plate both shielded and unshielded are given in the figure. The spectra from an old target is also given. The presence of  $D-D$  neutrons (of 3.5 MeV energy) can be seen.

The degree of reproducibility and accuracy in flux determination by the above methods, have been checked by several independent measurements. A typical determination of the flux by means of several methods is given in Table I.

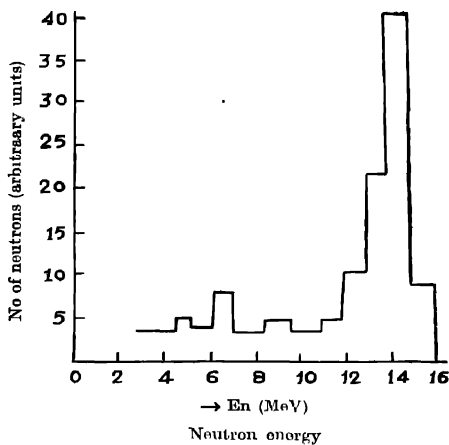


Fig. 8 (i) Spectrum of neutrons from  $Tt_3$  (d,n,  $He^4$  detector in a channel of water and paraffin shield).

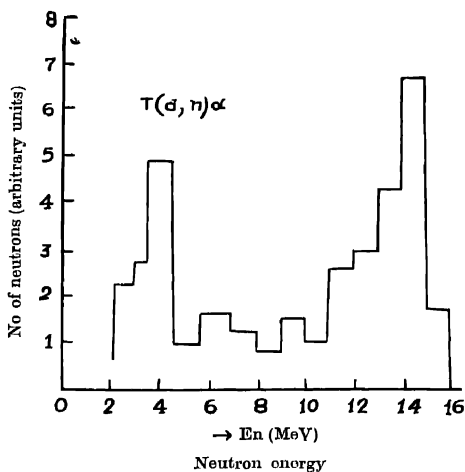


Fig. 8(ii). Spectrum of D-T neutron from an old target, Detector unshielded.

TABLE I

Operational condition	Method of measurement	Value of neutron flux in n/sec.
Deuteron beam Energy - 190 KeV	irradiated <i>Cu</i> foil and measurement of $\beta^+$ activity of $Cu^{62}$ from $Cu^{63}(n, 2n)Cu^{62}$ reaction	
Deuteron beam Current - 580 $\mu$ a	irradiated <i>Al</i> foil and measurement of $\beta^-$ activity of $Na^{24}$ from $Al^{27}(n, \alpha)Na^{24}$ reaction	$8.5 \times 10^{10}$
	irradiated <i>Al</i> foil and measurement of 1.38 MeV $\gamma$ -activity of $Na^{24}$ from the above reaction	$8.3 \times 10^{10}$
	Nuclear emulsion plate Ilford C2 200 $\mu$ thick	$8.5 \times 10^{10}$
	Calibrated <i>BF</i> <sub>3</sub> long counter	$9.2 \times 10^{10}$
	Calibrated fast neutron counter	$8.9 \times 10^{10}$

## ACKNOWLEDGMENT

The authors wish to express their thanks to Dr. B. D. Nagechaudhuri, Director, for his interest and guidance, and to Dr. D. N. Kundu, for valuable criticism and advice. They also express their gratitude to Sri B. M. Banerjee, Sri G. N. Sarkar and Sri B. B. Baliga for their unstinted help in the construction of the R. F. Power units, mechanical fittings and in the measurements of neutron flux, respectively. They also thank Sri B. Chatterjee and Sri N. C. Sen for their wholehearted help in the work.

## REFERENCES

- Allen, W. D. and Fergusson, A. T. G., 1957, *Proc. Phys. Soc. Lond.*, **70A**, 639.  
 Arnold, W. R., 1950, *R.S.I.*, **21**, 796.  
 Borgstrahl T. A., *et al.*, 1953, *R.S.I.* **24**, 417  
 Bounes, W. L. *et al.*, (1959), *Nucleonics*, **17**, 94  
 Bowers, A., 1939, *Electrische Hochspannungen*, Berlin.  
 Cockroft, J. D. and Walton, E. T. S., 1932, *Proc. Roy. Soc. A* **136**, 619.  
 Gradstein, S., 1936, *Philips Tech. Rev.*, **1**, 6.  
 Gromacher, H., 1921, *Z. Physik* **4**, 195.  
 Hanson and McKibbin, 1947, *Phys. Rev.*, **72**, 673.  
 Lorrain, P. *et al.*, 1957, *Canad. Jour. Phys.*, **35**, 299.  
 Tj. Douma and Brekoo, H. P. J., 1949, *Philips Tech. Rev.*, **11**, 123.  
 Mitchell, R. G., 1945, *Wireless Engineers* **22**, 474.  
 Moak, C. D., Reese, H. J. and Good, W. M., 1951, *Nucleonics*, **9**, 18.  
 Peck, R. A. and Eubank, H. P., 1955, *R.S.I.* **26**, 444.

# INFRARED SPECTRA OF URANYL PHOSPHATE, OXALATE, AND SALICYLATE IN THE SOLID STATE

K. V. NARASIMHAM

DEPARTMENT OF APPLIED PHYSICS, MADRAS INSTITUTE OF TECHNOLOGY, CHROMEPET,  
MADRAS

(Received, April 8, 1960)

**ABSTRACT.** The infrared spectra of three compounds, uranyl phosphate, uranyl oxalate, and uranyl salicylate have been studied in the region  $2-24\mu$  using potassium bromide disc and nujol mull methods. About 35 bands in the case of phosphate, 25 in the case of oxalate and 40 in the case of salicylate are obtained from both these methods. The vibrational frequencies obtained from the infra-red work are correlated with those obtained from fluorescence experiments.

## INTRODUCTION

Corn and Wu (1938) are the first to study the infra-red and Raman spectra of uranyl acetate, nitrate, chloride and sulphate and establish the frequencies 860, 210, and  $930\text{ cm}^{-1}$  characterising the uranyl ion. The infra-red spectra of a number of simple and double uranyl salts were studied later by Lecomte and Freymann (1941) who confirmed the above frequencies. Sevchenko and Stepanov (1949) studied the spectra of the uranyl acetate, nitrate, sulphate and potassium sulphate in the region of overtones of the above frequencies and came to the conclusion that the uranyl ion is linear in the case of acetate and nitrate and bent in the case of sulphate and potassium sulphate. All the above workers confined their investigations to the NaCl prism region only i.e., up to  $15\mu$ .

In the present investigation, the infra-red spectra of three compounds, uranyl phosphate ( $\text{H}_2\text{UO}_2\text{PO}_4 \cdot 4\text{H}_2\text{O}$ ), uranyl oxalate [ $\text{UO}_2(\text{COOH})_2 \cdot 3\text{H}_2\text{O}$ ] and uranyl salicylate,  $\text{UO}_2[\text{C}_6\text{H}_4(\text{OH})\text{COO}]_2$  have been studied in the region  $2-24\mu$ . The phosphate has been studied for the first time. The oxalate and salicylate were also studied by Lecomte and Freymann who, however, obtained bands, only in the region  $800-1600\text{ cm}^{-1}$ . Even in this region, the positions of the absorption bands have been indicated in a table but the actual values of the frequencies were not given.

## EXPERIMENTAL TECHNIQUE

The infra red spectra are recorded using two different methods : (1) potassium bromide disc method and (2) nujol mull method. In the case of KBr disc method

(Ford and Wilkinson, 1954), a Hilger automatic double beam prism spectrometer has been used with a rock salt prism for the region  $2\text{--}15\ \mu$ . The wavelength scale is linearly calibrated in microns and the dispersion is  $4.5\text{ cm per micron}$ . Calibration marks are made on the recorder chart, at regular intervals by a small and rapid deflection of the pen. A mixture of between 0.1 and 1.0 per cent of the sample and chemically pure potassium bromide is grinded into a fine powder and then pressed under vacuum to produce clear and transparent disc. The advantage of this method is a better distribution of very small particles in the suspending medium and the elimination of the obscuring bands which occur with mulling agents.

In the case of nujol mull method, spectra are recorded on a single beam Perkin Elmer infrared spectrometer (Model 122) with substances suspended in the nujol mull, in the region  $2\text{--}24\ \mu$  using the sodium chloride and potassium bromide prisms. To obtain the absorption only due to substance, the transmission curve of the nujol is also recorded on the same record chart with the same experimental conditions. After subtracting the absorption due to nujol, the transmission coefficients have been calculated for each point and a graph is drawn between the percentage transmission and wavenumbers.

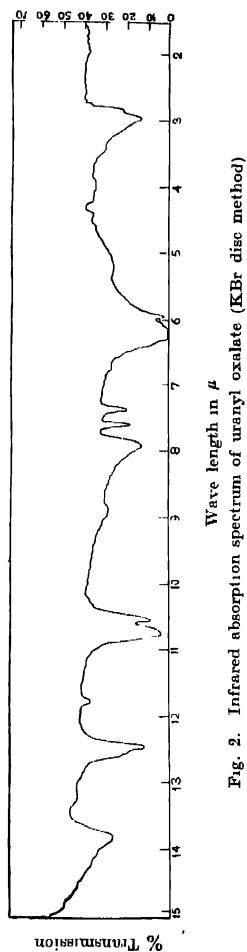
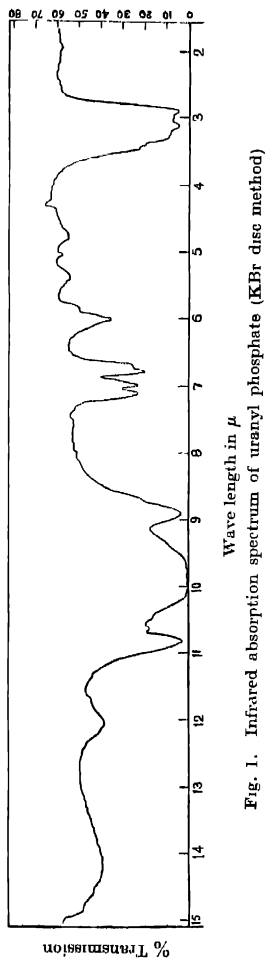
## RESULTS

A comparison of the frequencies of bands obtained from the potassium bromide disc and nujol mull methods, shows that there is reasonable agreement between the two data. However, the absorption bands with the potassium bromide disc method are sharper and better resolved than in the case of nujol mull method.

The frequency values of the bands are given in Tables I, II and III and the curves are given in Figs. (1 to 9). The  $\text{UO}_2^{++}$  ion fundamentals are recorded in all cases. A few bands could be also combination bands. The large number of other bands may consist of combinations of  $\nu_1$ ,  $\nu_2$  and  $\nu_3$  of  $\text{UO}_2^{++}$  ion or fundamentals, combinations and overtones of other radicals of the salts. Prominent examples are the bands due to water of hydration in the  $3400\text{--}3500\text{ cm}^{-1}$  region and the  $\text{C}=\text{O}$  frequencies in oxalate and salicylate occurring in the region  $1600\text{--}1700\text{ cm}^{-1}$ .

The fluorescence and absorption spectra of these compounds are also studied by the author at liquid air temperature with powder samples (Details of these results will be published elsewhere). It is found that the phosphate and oxalate are fluorescent and the salicylate has not shown any fluorescence at all. The ground state frequencies obtained from the analyses of the fluorescence spectra are given in the third column of Table I, II, and III for correlation of the results. It is seen that there is good agreement between the various data.





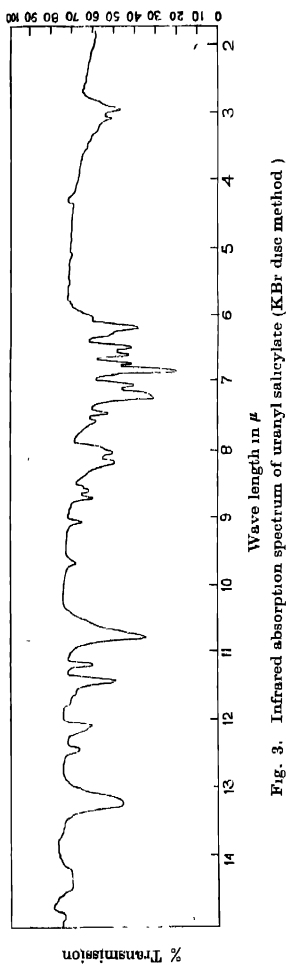


Fig. 3. Infrared absorption spectrum of uranyl salicylate (KBr disc method )

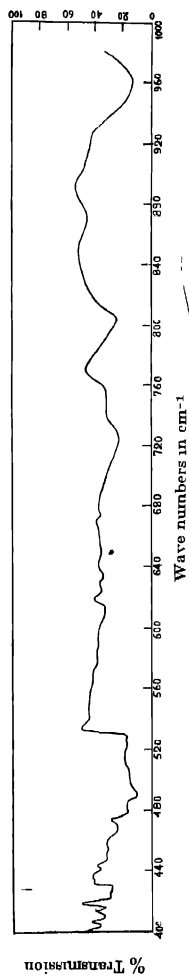


Fig. 4. Infrared absorption spectrum of uranyl phosphate (Nujol mull method.)

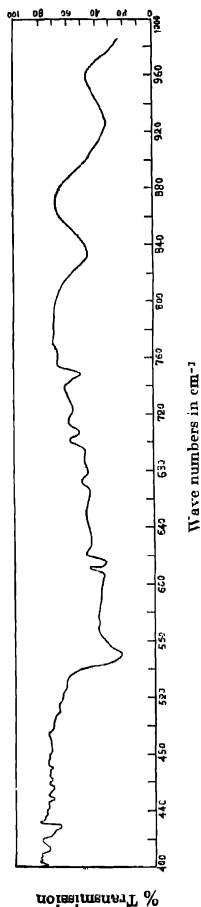


Fig. 5. Infra-red absorption spectrum of uranyl oxalate (Nujol mull method.)

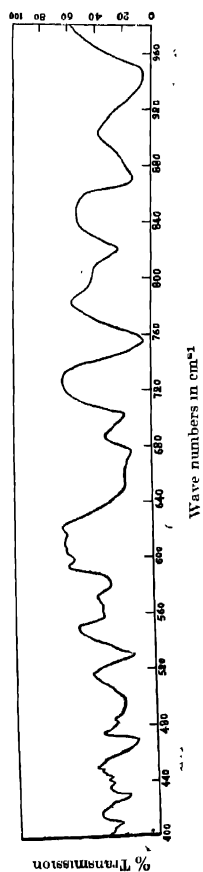


Fig. 6. Infra-red absorption spectrum of uranyl salicylate (Nujol mull method)

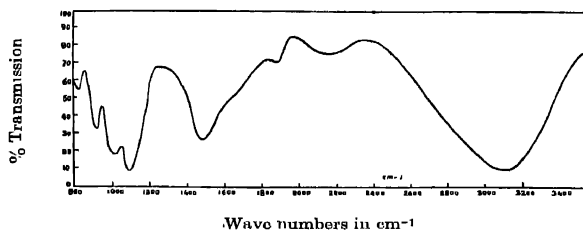


Fig. 7. Infrared absorption spectrum of uranyl phosphate (Nujol mull method)

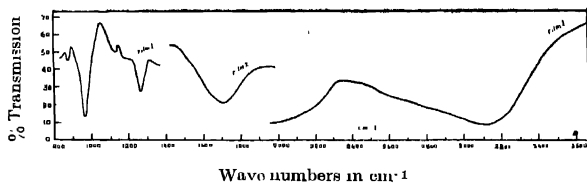


Fig. 8. Infrared absorption spectrum of uranyl oxalate (Nujol mull method)

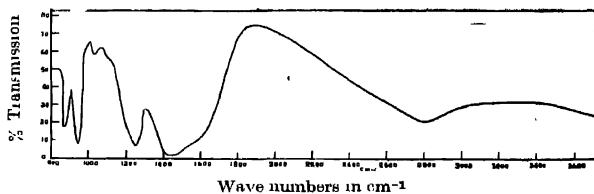


Fig. 9. Infrared absorption spectrum of uranyl salicylate (Nujol mull method)

TABLE I  
Infrared absorption bands of uranyl phosphate

Wavenumber of the band in $\text{cm}^{-1}$			
Potassium bromide disc method	Nujol mull method	Fluorescence	Remarks
1	2	3	4
	550 (vs) 607 (w) 615 (m) 666 (w) 671 (w) 680 (w) 704 (m) 707 (m)		
	723 (w) 749 (s)		
818 (w)			
828 (m) 852 (w) 877 (w)	834 (s)	828	$\nu_1$ fundamental
921 (vs) 938 (w) 954 (w)	926 (vs)	909	$\nu_2$ fundamental
1011 (vs) 1119 (vs) 1359 (w)	1020 (s) 1110 (vs)		$182 + 828 = 1010$ $182 + 921 = 1103$
1401 (s) 1429 (s) 1468 (s)			
1484 (m) 1656 (s) 1712 (w)	1500 (vs)		$2 \times 828 = 1656$
1848 (m)			$2 \times 921 = 1842$
1972 (w)	1900 (m)		
2079 (m)	2180 (m)		
2278 (w)			
2841 (w) 2985 (w) 3067 (w)			
3155 (vs) 3425 (vs)	3130 (vs)		Water of hydration Water of hydration

*w*—weak; *m*—medium; *s*—strong; *vs*—very strong; *b*—broad.

TABLE II  
Infrared absorption bands of uranyl oxalate

Wavenumber of the band in $\text{cm}^{-1}$			
Potassium bromide disc method	Nujol mull method	Fluorescence	Remarks
1	2	3	4
		257	$\nu_2$ fundamental
	625 (w)	609	Oxalate frequency
	635 (w)		
672 (w)	675 (w)		
710 (w)			
723 (s)	725 (m)		
755 (w)			$3 \times 257 = 771$
796 (w)			
803 (s)	806 (s)		
849 (w)	870 (m)	875	$\nu_1$ fundamental
928 (vs)			
947 (s)	961 (vs)	961	$\nu_3$ fundamental
1123 (w)	1130 (w)		$849 + 257 = 1106$
1259 (s)	1250 (s)		
1316 (m)			
1355 (m)			$849 + 2 \times 257 = 1366$
1383 (w)			
1473 (w)			
1606 (s)			
1629 (vs)		1672	C = O frequency
1686 (s)	1700 (s)		
1920 (m)	1950 (w)		$2 \times 947 = 1894$
2907 (w)	3210 (s)		
3378 (s)			Water of hydration
3546 (w)			

TABLE III  
Infrared absorption bands of uranyl salicylate

Wavenumber of the band in $\text{cm}^{-1}$			
Potassium bromide disc method	Nujol mull method	Remarks	
	530 (s)		
	557 (w)		
	580 (s)		
	597 (w)		
	616 (w)		
	652 (w)		

TABLE III (contd.)

Infrared absorption bands of uranyl salicylate

Wavenumber of the band in $\text{cm}^{-1}$		
Potassium cromide disc method	Nujol mull method	Remarks
1	2	3
669 (w)	675 (m)	
695 (b)	700 (s)	
756 (vs)	755 (vs)	
803 (m)		
827 (m)	819 (s)	
848 (w)		
859 (w)		
875 (m)	870 (s)	$\nu_1$ fundamental
892 (m)		
929 (vs)	945 (vs)	$\nu_1$ fundamental
1033 (w)	1035 (w)	
1101 (m)		
1147 (m)		
1160 (w)		
1219 (m)		
1242 (m)	1250 (vs)	
1309 (w)		
1319 (w)		
1340 (m)		
1385 (vs)		
1393 (w)		
1420 (m)	1440 (vs)	
1466 (vs)		
1488 (m)		
1517 (m)		
1546 (m)		
1597 (w)		
1616 (s)	1600 (m)	C=O frequency
1653 (w)		
1805 (w)		
1949 (w)		
	2800 (s)	
3215 (m)		Water of hydration
3307 (s)		

## ACKNOWLEDGMENTS

This work has been carried out under the inspiring guidance of Dr. V. Ramakrishna Rao, Reader, Andhra University. The infra-red spectra with the nujol mull method were taken at the Indian Institute of Science, Bangalore. In this connection, thanks are due to Mr. C. K. Narayanaswamy and Prof. R. S. Krishnan. Thanks are also due to the authorities of National Physical Laboratory, New Delhi, where the infra-red spectra were taken with the pressed disc technique.

## REFERENCES

- Corn, G. K. T. and Wu C. K., 1938, *Trans. Farad. Soc.*, **34**, 1483.  
Ford, M. A. and Wilkinson, G. D. 1954, *J. Sci. Inst.* **31**, 338  
Lecomte, J. and Freymann R., 1941, *Bull. Soc. Chim.*, **8**, 622.  
Sevchenko, A. N. and Stopanov, B. I., 1949, *Znhr. Exptl. teoret. Fiz.* **19**, 1113.



# SINGLET→TRIPLET ABSORPTION IN HALOGEN SUBSTITUTED TOLUENES\*

J. K. ROY

OPTICS DEPARTMENT, INDIAN ASSOCIATION FOR THE CULTIVATION OF SCIENCE,  
CALCUTTA-32

(Received, May 27, 1960)

**ABSTRACT.** Continuous singlet→triplet absorption in the near ultraviolet region due to orthobromotoluene, parachlorotoluene and metafluorotoluene in the liquid state has been investigated. It has been observed that the region of absorption shifts gradually towards the red with the increase in the atomic weight of the substituent halogen atom. The luminescence spectrum due to metafluorotoluene in the solid state at  $-180^{\circ}\text{C}$  has also been studied, and the luminescence bands have been found to be weaker than those due to chloro- and bromotoluene.

## INTRODUCTION

It is well known that Lewis and Kasha (1944) first suggested that the phosphorescence exhibited by many pure substances are due to transitions from the triplet state of the molecules to the lowest singlet state. Lewis and Kasha (1945) also observed singlet→triplet (S→T) absorption in pure para dichlorobenzene, dibenzalacetone, nitrobenzene and phenazine. Reid (1950a) next observed (S→T) absorption bands in pyridine in the liquid state at room temperature and in ethylene in the vapour state (Reid, 1950b). Later, Kasha (1952) demonstrated that the singlet→triplet absorption in aromatic compounds is strengthened not only by heavy substituent atoms in the molecule but also by such atoms in surrounding solvent molecules in any solution. McClure *et al.* (1954) observed S→T absorption in para diiodobenzene, para dibromobenzene, bromobenzene,  $\beta$ -iodochloro- and  $\beta$ -iodobromo naphthalenes, 1, 3, 5-tribromobenzene and 1, 2, 4, 5-tetrabromobenzene, but they did not find any such absorption in para dichlorobenzene, para iodobiphenyl and nitrobenzene either at the room temperature or at liquid nitrogen temperature. The apparent non-appearance of any S-T bands in the above cases was attributed by them to the difficulties of separating the very weak and diffuse S→T absorption spectra from the normal singlet→singlet absorption. Biswas (1954, 1955a & b, 1956a & b) and Sirkar and Biswas (1956) observed luminescence bands in some halogen substituted toluenes and although Biswas (1956) looked for the absorption band responsible for the emission he was

\*Communicated by Prof. S. C. Sirkar

unable to detect any strong  $S \rightarrow T$  absorption. Recently, it has been shown by the present author (Roy, 1959) that the luminescence in parachlorotoluene in the solid state at  $-180^{\circ}\text{C}$  takes place after direct  $S \rightarrow T$  transition.

It was thought worthwhile to investigate whether any singlet  $\rightarrow$  triplet absorption is exhibited by these compounds and whether the intensity of such absorption depends on the atomic weight of the heavy substituent atom in the molecule as reported by previous workers in other cases (McClure, *et al.* 1954). In the present investigation the singlet  $\rightarrow$  triplet absorption in metafluorotoluene, parachlorotoluene and ortho bromotoluene have been studied using a long absorbing path.

The luminescence spectrum of pure metafluorotoluene in the solid state at  $-180^{\circ}\text{C}$  has also been investigated and it has been compared with the spectra due to chlorotoluenes and bromotoluenes reported by previous workers (Biswas, 1956a & b).

#### EXPERIMENTAL

The liquids orthobromotoluene, parachlorotoluene and metafluorotoluene of chemically pure quality supplied by British Drug House (England), were distilled several times under reduced pressure and fractionated to remove traces of impurities. For studying the absorption spectra of the above substances in the liquid state at  $24^{\circ}\text{C}$ , a 10 cm. long pyrex glass cell provided with plane parallel quartz windows was used. A 250 watt straight filament lamp in glass envelope was employed as the source of continuous radiation in the near ultraviolet region. The absorption spectra of the substances were photographed on Ilford HP3 films using a Hilger medium quartz spectrograph having a dispersion of  $22 \text{ \AA}/\text{mm}$  in the  $3500 \text{ \AA}$  region. The time of exposure varied from a few seconds to half a minute and the width of the slit was about  $0.10 \text{ mm}$ . Iron arc spectrum was recorded on each spectrogram as comparison. The absorption spectrum of benzene was also recorded for comparing it with the spectra of the disubstituted benzenes mentioned above. The microphotometric records of the spectrograms were obtained with a self-recording Moll microphotometer supplied by Kipp and Zonen. The absorption spectra were calibrated with the help of the microphotometric records of the iron lines after drawing a thin and straight reference line across the spectra, coinciding with a known iron line.

The luminescence spectrum of pure meta fluorotoluene in the solid state at  $-180^{\circ}\text{C}$  was investigated with the arrangements used previously by Biswas (1956a).

#### RESULTS AND DISCUSSION

The microphotometric records of the absorption spectra due to pure orthobromotoluene, parachlorotoluene, metafluorotoluene and benzene are reproduced

in Figs. 1(a), 1(b), 1(c) and 1(d) respectively. The reference line in the records is the 4046 Å line of mercury.

The main bands in the luminescence spectrum due to metafluorotoluene in the solid state at  $-180^{\circ}\text{C}$  with their widths and estimated intensities (*s*—strong, *m*—medium, *w*—weak, etc.) are given in Table I.

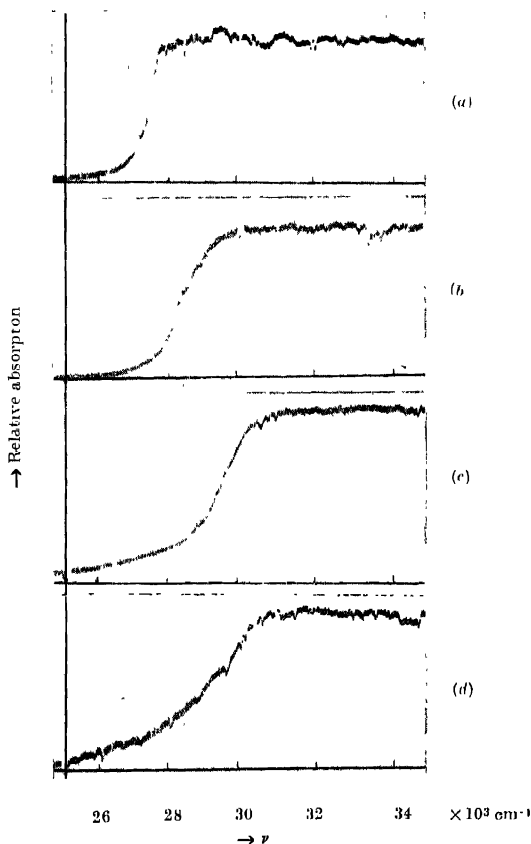


Fig. 1. (a) *o*-Bromotoluene (b) *p*-Chlorotoluene  
(c) *m*-Fluorotoluene, (d) Benzene

TABLE I  
luminescence spectra of metafluorotoluene

Position of the bands $\nu$ in $\text{cm}^{-1}$	Width of the bands in $\text{cm}^{-1}$	Differences from the 1st band in $\text{cm}^{-1}$
24968 (w)	436	
24072 (w)	725	896
23413 (s)	603	1555
22521 (m)	558	2447
21761 (s)	948	3207
20910 (vw)	765	4058

## DISCUSSION

(a) *Absorption spectra due to singlet  $\rightarrow$  triplet transition.*

It is well known (Lewis and Kasha, 1945) that benzene shows a weak  $S \rightarrow T$  absorption in the region (3300-3700)Å. This is evident from Fig. 1(d). The absorption due to metafluorotoluene reproduced in Fig. 1(c) appears to be similar to that due to benzene (Fig. 1(d)). This similarity indicates the existence of very weak  $S \rightarrow T$  absorption in metafluorotoluene. Fig. 1(b) and 1(a) show that as the fluorine atom is replaced successively by chlorine and bromine atoms, the  $S \rightarrow T$  absorption becomes much stronger and the region where the absorption starts shifts gradually towards red. Further, absorption curves due to orthobromotoluene and parachlorotoluene show steeper rise in this region than in the case of either metafluorotoluene or benzene. These results are similar to those reported by McClure *et al.* (1954) for substituted naphthalenes. It is evident from results of the present investigation that in the case of substituted benzenes also the perturbation due to substituent halogen atom increases with the increase in the atomic weight of the substituent atom and the  $S \rightarrow T$  transition becomes allowed.

The strong  $S \rightarrow T$  absorption observed in the cases of orthobromotoluene and parachlorotoluene also explains the intense luminescence in the visible region exhibited by these compounds in the solid state at  $-180^\circ\text{C}$  (Biswas, 1956a, 1956b).

(b) *Luminescence spectrum of metafluorotoluene.*

It would be interesting to compare the intensities of luminescence spectrum of metafluorotoluene with that due to orthobromotoluene or parachlorotoluene excited under similar conditions. It can be seen from the results obtained by Biswas (1956 a & b) that the intensity of luminescence spectrum of orthobromo-

toluene is larger than that due to parachlorotoluene. The intensity of the luminescence spectrum due to metafluorotoluene recorded under similar conditions has been found to be lower than that due to para chlorotoluene. This agrees with the fact that the strength of S→T absorption is small in this case and shows further that the luminescence is produced by the transition from the triplet to the singlet state.

## ACKNOWLEDGMENT

The author is highly indebted to Professor S. C. Sirkar, D.Sc., F.N.I., for constant help and guidance throughout the progress of the work.

## REFERENCES

- Biswas, D. C. (1954), *Ind. J. Phys.*, **28**, 423.  
Biswas, D. C. 1955a, *Ind. J. Phys.*, **29**, 257.  
Biswas, D. C. 1955b, *Ind. J. Phys.*, **29**, 503.  
Biswas, D. C. 1956a, *Ind. J. Phys.*, **30**, 143.  
Biswas, D. C. 1956b, *Ind. J. Phys.*, **30**, 255.  
Biswas, D. C. 1956, Unpublished result.  
Kashu, M., 1952, *J. Chem. Phys.*, **20**, 71.  
Lewis, G. N. and Kashu, M., 1944, *J. Am. Chem. Soc.*, **66**, 2100.  
Lewis, G. N. and Kashu, M., 1945, *J. Am. Chem. Soc.*, **67**, 991.  
McClure, D. S., Blake, N. W. and Hansl, P. L., 1954, *J. Chem. Phys.*, **22**, 255.  
Reid, C., 1950a, *J. Chem. Phys.*, **18**, 1277.  
Reid, C., 1950b, *J. Chem. Phys.*, **18**, 1677.  
Roy, J. K. 1959, *Ind. J. Phys.*, **33**, 209.  
Sirkar, S. C. and Biswas, D. C. 1956, *J. Chem. Phys.*, **24**, 470.

# *Letters to the Editor*

*The Board of Editors will not hold itself responsible for opinions expressed in the letters published in this section. The notes containing reports of new work communicated for this section should not contain many figures and should not exceed 500 words in length. The contributions must reach the Assistant Editor not later than the 15th of the second month preceding that of the issue in which the letter is to appear. No proof will be sent to the authors.*

11

## LIGHT ABSORPTION IN PARAMAGNETIC $\text{Co}^{++}$ IONS IN STATE OF SOLUTION

A. MOOKHERJI AND N. S. CHHONKAR

PHYSICS LABORATORY, AGRA COLLEGE, AGRA

(Received, May 7, 1960)

In a recent paper Chakravarty and Chatterji (1959) assuming an approximate tetragonal axis of symmetry for the octahedron of water cluster about  $\text{Co}^{++}$  ion and following the method of Abragam and Pryce (1951) have developed general expressions for the magnetic susceptibilities along and normal to the axis of symmetry of the water cluster about  $\text{Co}^{++}$  ion in crystal in terms of the tetragonal splitting  $\Delta$ , the effective Lande-splitting factor and the spin-orbit coupling coefficient. In order to get a fit with the experimentally observed data of magnetic susceptibility measurements by Bose (1948), they required a small value of  $\Delta$  varying with temperature and a value of the coefficient of spin-orbit coupling which is the same as that for the free ion, for the salts studied.

An examination of the energy level expressions Owen (1955) shows that if  $\Delta$  is small, then the number of absorption bands of  $\text{Co}^{++}$  ion salts in crystalline state or in state of solution will be limited to three instead of six. Absorption measurements of about fifteen cobalt salts in state of aqueous solution by us, show a single band at about  $19,550 \text{ cm}^{-1}$  and two discernable bands at about  $20,900 \text{ cm}^{-1}$  and  $21,800 \text{ cm}^{-1}$  which point out clearly that  $\Delta$  should be extremely small in them, in agreement with the theoretical findings of Chakravarty and Chatterji. The second findings by these authors that the spin-orbit coupling coefficient in crystalline state is the same as the free ion value, will mean that the covalent overlap of  $3d$ -orbitals and the  $s$ - and  $p$ -orbitals of water cluster about  $\text{Co}^{++}$  ion can be neglected (Owen 1955). Consequently the term separation  $E$  for the free ion will be the same as  $E'$ , that for the crystal. From our optical absorption

measurements we have evaluated  $E'$  for about a dozen of  $\text{Co}^{++}$  salts in state of aqueous solution. We find that  $E'/E \sim 0.95$  which is in complete agreement with the findings of Chakravarty and Chatterji.

## REFERENCES

- Abragam, A. and Pryce, M. H. L., 1951, *Proc. Roy. Soc. A*, **205**, 135.  
" " " 1951, *Proc. Roy. Soc. A*, **206**, 173.  
Bose, A., 1948, *Ind. Jour. Phys.*, **22**, 276.  
Chakravarty, A. S. and Chatterji, R., 1959, *Ind. Jour. Phys.*, **33**, 531.  
Owen, J., 1955, *Proc. Roy. Soc.* **227**, 183.





# NUCLEAR SPIN ECHOES AND MOLECULAR SELF-DIFFUSION IN LIQUIDS

S. K. GHOSH AND S. K. SINHA

SAHA INSTITUTE OF NUCLEAR PHYSICS, CALCUTTA

(Received July 8, 1960)

**ABSTRACT.** The nuclear spin-echo phenomenon and the effect of molecular self-diffusion in liquids on the spin-echoes have been treated on the basis of a new stochastic model. The physical and mathematical inconsistencies of similar treatments reported earlier have also been discussed. A spin-echo method for measuring the co-efficient of molecular self-diffusion  $D$  directly, using the "image echo" has been developed, which completely eliminates the relaxation damping of the echo signal. It has also been shown that the diffusion damping co-efficient  $k$  thus determined can be utilized for an independent measurement of transverse relaxation time  $T_2$  even in presence of appreciable diffusion. These methods have been used in the case of water, and the values of  $D$  and  $T_2$  obtained agree well with other measurements. Further, a direct experimental check has been furnished to compare the validity of different theoretical approaches to this problem.

## 1. INTRODUCTION

The mechanism of formation of nuclear spin-echoes and the effect of molecular self-diffusion on the echo-amplitudes have been discussed previously by various authors [Hahn (1950), Das and Saha (1954), Carr and Purcell (1954), Herzog and Hahn (1956), Torrey (1956) and Douglass and McCall (1958)]. The equilibrium (thermal) magnetization of a substance when placed in a steady magnetic field, is deflected from the direction of the magnetic field by a short radio frequency ( $rf$ ) pulse and during the absence of the pulse the nuclear magnets execute Larmor precession ( $Lp$ ) about the steady field with different Larmor frequencies ( $Lf$ ) because of inhomogeneity in the magnetic field. After a certain time-interval  $\tau$ , if a second short  $rf$  pulse is used to reverse the phase accumulated by the nuclear magnets, the nuclei will recluster completely at the end of the next interval  $\tau$  and give the echo signal. This complete reclustering will be possible only when the phase accumulations of individual groups are equal in the two intervals. If, however, there be any process that makes these phase accumulations unequal, the reclustering at the end of the interval  $2\tau$  will not be complete and the echo amplitude will diminish. The diminution will depend on  $\tau$  if the phase accumu-

\* One should note that the random motion of the molecules will also average out the "local field" and give rise to relaxation damping of the nuclear induction signals.  $T_1$  and  $T_2$  in Bloch equations (1) take account of this effect.

lation due to that process is time dependent. The random (Brownian) motion of the molecules in a liquid is such a process\*. This process carries the molecules along with the resonating nuclei to different sites in the inhomogeneous magnetic field, thereby changing their  $Lf$  and hence the phase of their  $Lp$ . Since this is a Markoffian process, the phase-accumulations will not be proportional to first power of time, and as a result they will not be equal in the two intervals. Thus, there will be damping of the echo-amplitude which has been called the diffusion damping by Hahn. If instead of two pulses, three pulses are used to form the echoes the above effect of molecular self-diffusion will manifest itself in the different echoes in different ways. This effect has been discussed by Hahn and later corrected by Herzog and Hahn and by Das and Saha in the three-pulse echo system. Their methods have been examined in some details at the end of Section II.

The present work considers the following model. The random molecular motion is described by the motion of any representative molecule with proper initial distribution in Larmor frequencies (conforming with the actual physical situation). Such a distribution can be represented by Dirac's  $\delta$ -function as in the case of liquid molecules executing Brownian motion [Green (1952)]. The whole time-interval in which we are interested is divided into a large number of small sub-intervals, and the damping of the echo signal due to random phase-accumulations in the successive short intervals, that arise through random change in Larmor frequency has been taken into account through the change in Larmor frequency which follows a Markoff process\* [Chandrasekhar (1943), Wang and Uhlenbeck (1945), Anderson (1954), Herzog and Hahn (1956)], satisfying Chapman-Kolmogoroff equation. The results of such calculation agree with those from the straightforward treatments of Carr and Purcell and of Torrey when extended to echoes for Carr-Purcell pulse sequence.

On the basis of this formulation, experimental methods for the determination of self-diffusion constant,  $D$ , and the transverse relaxation time  $T_2$ , have been developed. In these methods the diffusion-damping co-efficient  $k$  ( $= \gamma^2 G^2 D$ , where  $\gamma$ ,  $G$  and  $D$  have the usual meaning) can be obtained without previous determination of  $T_2$ . This value of  $k$  is then used to obtain  $T_2$  from Carr-Purcell method in general cases, which has been described in details in Section IV. Besides obtaining a satisfactory value for  $D$  and  $T_2$ , an independent experimental check of the physical basis of the theoretical formulation has also been described.

In Section II, the theoretical formulation is presented with criticism of Das and Saha's and of Herzog and Hahn's treatments. In Section III, the apparatus used is briefly described. The Section IV contains the experimental methods for

\* A collection of the relevant papers on Markoff Process can be found in "Noise and Stochastic Processes", edited by N. Wax., Dover Publications, New York, (1954).

measurement of  $D$  and  $T_2$ , and the results. In the last Section I', the different experimental methods for measuring  $D$  and  $T_2$  have been critically examined.

## II THEORETICAL FORMULATION

Let us start with the Bloch equations (Bloch, 1946) which have been proved satisfactory in describing the dynamical behaviour of nuclear magnetization. The equations can be written in a co-ordinate system rotating with the pulsed-rf frequency,  $\omega$  as [Bloch, 1946. Rabi *et al.*, 1954]

$$\frac{du}{dt} + \eta v = -\frac{u}{T_1}$$

$$\frac{dv}{dt} = \eta u + Rv = -\frac{v}{T_2}$$

and

$$\frac{dw}{dt} = Rv = -\frac{w}{T_1} - \frac{w_0}{T_1} \quad (1)$$

Here  $u$ ,  $v$ ,  $w$ ,  $w_0$  and  $\eta$  have a slightly different meaning than the usual. The molecules carrying the nuclear magnets execute random (Brownian) motion in an externally applied inhomogeneous magnetic field. To take account of the effect of this random motion on the spin-echo phenomenon, the Bloch equations have been assumed to be true for the average magnetization of a molecule at a point  $(x, y, z)$  inside the sample.  $u$ ,  $v$  and  $w$  are the  $x'$ ,  $y'$  and  $z'$  components, respectively of the average molecular magnetization  $M_{mol}$ .  $w_0$  is the equilibrium value of magnetization at thermal equilibrium and is given by  $w_0 = \chi_{mol} H_z(x, y, z)$ ,  $\chi_{mol}$  being the static molecular susceptibility,  $R = \gamma H_1$  and  $\eta = \gamma H_z(x, y, z) - \omega$ ;  $H_1$  is the half amplitude of the applied linearly polarised rf field,  $2H_1 \cos \omega t$ .

One of the two circularly polarized components of the rf field is actually effective in producing resonance.  $H_z(x, y, z)$  is the value of the externally applied magnetic field at the point  $(x, y, z)$ .  $T_1$  and  $T_2$  are the usual longitudinal and transverse relaxation times respectively as introduced by Bloch. The random change of position of the molecule causes a corresponding change in the value of  $\eta$ . This random motion is of the nature of the stationary Markoff process. On the average this motion is well represented by the Langevin equation (Kirkwood, 1946 & Green, 1952).

In order to find out the magnetization under study at any subsequent time from its initial value we have to follow the motion of such a molecule. In following the motion of the molecule we shall have to keep in mind that the magnetization must satisfy the Bloch equations whereas its position co-ordinates and hence  $\eta$  will be obtained from the Langevin equation. For the solution of the

Bloch equations under such conditions we divide the whole time interval from the start of the pulse sequence into a large number of small sub-intervals. These sub-intervals are of such magnitude that the root mean square change in  $\eta$  is very small. Under such conditions we can solve the Bloch equations during these sub-intervals taking  $\eta$  to be constant; the stochastic nature of  $\eta$  is taken into account through the inclusion of a transition probability corresponding to the change in  $\eta$  from its initial value at the beginning of the sub-interval to the final value at the end of the sub-interval. The integration over the initial value of  $\eta$  for the interval will give us the value of magnetization at the time we are interested in, and it is a function of  $\eta$  corresponding to that time.

Analytically, let  $\Phi(\eta_s, t_s)$  be the solution of the Bloch equations for a certain value of  $\eta (= \eta_s)$ . Since  $\eta$  is a stochastic variable, the value of magnetization with a certain value of  $\eta (= \eta_s)$  must be expressed as

$$F[\eta_s, t_s] = \Phi(\eta_s, t_s) W(\eta_s, t_s)$$

where  $W(\eta_s, t_s)$  expresses the probability that at time  $t_s$  we have the value of  $\eta$  as  $\eta_s$ . As  $\eta$  follows a Markoff process  $F[\eta_s, t_s]$  can be related with its value at any other time by a relation like the Chapman-Kolmogoroff equation:

$$F[\eta_s, t_s] = \int_{-\infty}^{\infty} F[\eta_i, t_i] T(\eta_s, t_s | \eta_i, t_i) d\eta_i$$

Here  $T(\eta_s, t_s | \eta_i, t_i)$  denotes the transition probability of the change of  $\eta_i$  to  $\eta_s$  in time  $t_s - t_i$ . This transition probability, in general, will be product of two transition probabilities, namely  $B(\eta_s, t_s | \eta_i, t_i)$  and  $P(\eta_s, t_s | \eta_i, t_i)$ . The first one is obtainable from the solution of Bloch equations if we could treat  $\eta$  also to be varying during the period. The second one can be obtained from the solution of Langevin equation. Now, if the time-interval  $t_s - t_i$  is considered to be very small such that the change in  $\eta$  during the interval is small, but is of sufficient magnitude such that the force causing the displacements of the particles and hence the change of  $\eta$  fluctuates a large number of times, we have

$$B(\eta_s, t_s | \eta_i, t_i) \simeq B(\eta_i, t_s | \eta_i, t_i)$$

$$\text{and} \quad P(\eta_s, t_s | \eta_i, t_i) \simeq \left\{ \frac{1}{4\pi k(t_s - t_i)} \right\}^{\frac{1}{2}} \exp \left\{ -\frac{(\eta_s - \eta_i)^2}{4k(t_s - t_i)} \right\}$$

(see expression (6))

with these assumptions,

$$\begin{aligned} F[\eta_s, t_s] &= \int_{-\infty}^{\infty} \Phi(\eta_i, t_i) B(\eta_i, t_s | \eta_i, t_i) W(\eta_i, t_i) P(\eta_s, t_s | \eta_i, t_i) d\eta_i \\ &= \int_{-\infty}^{\infty} \Phi(\eta_i, t_s) W(\eta_i, t_i) P(\eta_s, t_s | \eta_i, t_i) d\eta_i \end{aligned}$$

This relation shows that if we know the initial value of  $F$ , we can deduce its value at any other time

Let us now consider a particle situated initially at the point  $(x_0, y_0, z_0)$ . The magnetization at  $t = 0$  can be represented by

$$u(0, \eta) = u(0)W(\eta, 0) = 0$$

$$v(0, \eta) = v(0)W(\eta, 0) = 0$$

$$\text{and} \quad w(0, \eta) = w(0)W(\eta, 0) = w_0\delta(\eta - \eta_0) \quad \dots (2)$$

The initial distribution has been taken in the form of Dirac  $\delta$ -function as the position of the particle is definite at the point  $(x_0, y_0, z_0)$ , and hence  $\eta_0 = \gamma H_z(x_0, y_0, z_0) = \omega$ . For the most general field distribution

$$H_z(x_0, y_0, z_0) = H_z(0) + x_0 \left( \frac{dH_z}{dx} \right)_0 + y_0 \left( \frac{dH_z}{dy} \right)_0 + z_0 \left( \frac{dH_z}{dz} \right)_0 + \dots$$

terms with higher derivatives of  $H_z$ .  $H_z(0)$  is the value of the steady magnetic field at the origin. For simplicity the field gradient can be taken to be constant and unidirectional (in the direction of  $z$ ), and  $\eta_0$  can be written as

$$\eta_0 = \gamma H_z(0) = \omega + \gamma G z_0 \quad \dots (3)$$

where  $G = \frac{dH_z}{dz}$ . At exact resonance  $\gamma H_z(0) = \omega = 0$ . The treatment, which

has been followed here for this simple case, can be easily shown to be valid for multi-directional field gradients as well as for off-resonance conditions\*.

Hence, considering any time-interval  $t$ , we divide it into a large number, say  $n$  of small and equal sub-intervals of  $\Delta t$  each, such that  $n\Delta t = t$  and assign values to  $\eta$  at the beginning and at the end of each sub-interval. For example,  $\eta_{m-1}$  and  $\eta_m$  are these values for the  $m$ -th sub-interval. For the  $m$ -th sub-interval the Bloch equations are solved taking  $\eta_{m-1}$  to be constant, and we obtain  $\phi(\eta_{m-1})$ ,

\* Since the results of this formulation (taking the field gradient in the  $z$ -direction as constant, and neglecting the field gradients in other directions) are used to interpret data obtained with a magnet where these conditions are not strictly valid, it is interesting to investigate the effects due to (a)  $G$  being not constant, and (b) the gradients in the  $x$  and  $y$  directions are not zero. It can be easily shown that none of these affects the result appreciably. Both the situations, described above, introduce small error in the value of  $k$ , but the time-dependence of the signal amplitudes remains almost unaffected. To test these points experimentally, the time dependence of the amplitude of the image echo was recorded without applying any field gradient in  $z$ -direction externally. Even in this case (where the field-gradient is multidirectional) the time dependence was found to be parabolic as the equation (14) predicts.

$m\Delta t$ ) where  $\phi$  stands for  $u, v$  and  $w$  components.  $F[\eta_m, m\Delta t]$  is then obtained by using the relation

$$F[\eta_m, m\Delta t] = \int_{-\infty}^{\infty} F[\eta_{m-1}, m\Delta t] P(\eta_m, \Delta t | \eta_{m-1}) d\eta_{m-1} \quad \dots (4)$$

where  $P(\eta_m, \Delta t | \eta_{m-1})$  is the probability of  $\eta_{m-1}$  changing to  $\eta_m$  in the time-interval  $\Delta t$ . Using the relation

$$\eta_m - \eta_{m-1} = \gamma G(z_m - z_{m-1}) \quad \dots (5)$$

$P(\eta_m, \Delta t | \eta_{m-1})$  can be obtained from the solution of Langevin equations, and the expression for it comes out as

$$P(\eta_m, \Delta t | \eta_{m-1}) = \left( \frac{1}{4\pi k \Delta t} \right)^{\frac{1}{2}} \exp \left\{ -\frac{(\eta_m - \eta_{m-1})^2}{4k \Delta t} \right\} \quad \dots (6)$$

where  $k = \gamma^2 G^2 D$ ,  $D$  being the co-efficient of molecular self-diffusion. The Eq. (1) take different forms in the presence and in the absence of the  $\pi$ -pulse, and the usual solutions in the two cases are each treated as  $\phi$  as discussed above. The thermal equilibrium value of  $w$ -component can be shown to be given by

$$w_0[\eta_n, n\Delta t] = w_0 \int_{-\infty}^{\infty} \delta(\eta - \eta_0) P(\eta_n, n\Delta t | \eta) d\eta = w_0 P(\eta_n, n\Delta t | \eta_0) \quad \dots (7)$$

The final value of  $F(t)$  is then obtained from the relation

$$F(t) = \int_{-\infty}^{\infty} F[\eta_n, n\Delta t] d\eta_n \quad \dots (8)$$

This is the value of magnetization for a single particle. We obtain the total magnetization  $M(t)$  due to the whole sample by using the relation

$$M(t) = N \iiint F(t) dV \quad \dots (9)$$

where the integration extends over the whole sample volume and  $N$  is the number density of the molecules.

For a cylindrical sample-holder and for the constant field gradient in the  $z$ -direction, the volume integral gives an expression of the form

$$\frac{2M_0 J_1(p)}{p} \quad \dots (10)$$

where for primary echo,

$$p = \gamma G a(t - 2\tau_1) \quad \dots (11)$$

Expressions for the echoes and the free induction signals for three pulses of nutational angles  $\xi_1$ ,  $\xi_2$  and  $\xi_3$  applied at times  $t = 0$ ,  $\tau_1$  and  $\tau_2$  respectively, as obtained by the present treatment.

Position of the signals	Time independent part of the amplitudes at signal maxima	Time dependent part of the amplitudes at the signal maxima	Part dependent on molecular self diffusion
0	$-M_0 \sin \xi_1$	1	1
$\tau_1$	$-M \sin \xi_2$	$1 - (\cos \xi_1 - 1) \exp \left( -\frac{\tau_1}{T_1} \right)$	1
$\tau_2$	$-M_0 \sin \xi_3$	$1 + \left\{ 1 - (\cos \xi_1 - 1) \exp \left( -\frac{\tau_1}{T_1} \right) \right\} \times \cos \xi_2 - 1 \left[ \exp \left( -\frac{\tau_2 - \tau_1}{T_1} \right) \right]$	1
$2\tau_1$	$M_0 \sin \xi_1 \sin^2 (\xi_2, 2)$	$\exp \left( -\frac{2\tau_1}{T_2} \right)$	$\left[ \exp \left( -\frac{2}{3} k \tau_1 \right) \right]$
$2\tau_2$	$M_0 \sin \xi_1 \cos^2 (\xi_2, 2) \sin^2 (\xi_3, 2)$	$\exp \left( -\frac{2\tau_2}{T_2} \right)$	$\left[ \exp \left( -\frac{2}{3} k \tau_2 \right) \right]$
$\frac{2(\tau_2 - \tau_1)}{\text{(Image echo)}}$	$-M_0 \sin \xi_1 \sin^2 (\xi_2/2) \sin^2 (\xi_3, 2)$	$\exp \left[ -\frac{2(\tau_2 - \tau_1)}{T_2} \right]$	$\left\{ \exp \left[ -\frac{2}{3} k \tau_1 + (\tau_2 - 2\tau_1) \right] \right\}$
$[2\tau_2 - \tau_1]$	$[M_0 \sin \xi_2 \sin^2 (\xi_3, 2)]$	$\left[ 1 + (\cos \xi_1 - 1) \exp \left( -\frac{\tau_1}{T_1} \right) \right] \times \exp \left[ -\frac{2(\tau_1 - \tau_1)}{T_2} \right]$	$\exp \left[ -\frac{2}{3} k(\tau_2 - \tau_1) \right]$
$\tau_2 + \tau_1$	$\frac{1}{2} M_0 \sin \xi_1 \sin \xi_2 \sin \xi_3$	$\exp \left[ -\frac{2\tau_1}{T_2} - \frac{\tau_2 - \tau_2}{T_1} \right]$	$\exp \left[ -\lambda \left\{ \frac{2}{3} \tau_1^2 - \tau_1(\tau_2 - \tau_1) \right\} \right]$
$2n\tau$	$(-1)^{n-1} M_0$	$\exp \left[ -\frac{2n\tau}{T_2} \right]$	$\exp \left[ -\frac{2}{3} k n \tau_2 \right]$
(Carr-Parcell echoes*)			

\* Echoes obtained at time  $t=2n$  after the application of a series of  $n$   $180^\circ$  pulses at times  $t=(2n-1)$  following a  $90^\circ$  pulse applied at  $t=0$ .

$a$  is the internal radius of the sample holder,  $J_1$  is the first order Bessel function of the first kind. This represents the shape of the echo and of the free induction signals. For constant field gradients in the three directions, this is given by

$$\frac{2M_0 J_1(p)}{p} \cdot \frac{\sin q}{q} \quad \dots \quad (12)$$

where for primary echo,

$$p = \gamma \left\{ \left( \frac{dH_z}{dz} \right)^2 + \left( \frac{dH_z}{dr} \right)^2 \right\}^{\frac{1}{2}} a(t - 2\tau_1)$$

and

$$q = \gamma \left( \frac{dH_z}{dy} \right) b(t - 2\tau_1) \quad \dots \quad (13)$$

$b$  is the effective length of the sample

Using the above scheme and the usual technique of matching the Bloch equations, the different free induction signals and the different echo signals for any number of pulses of arbitrary nutational angles can be obtained. The results of such calculations for three pulses applied at time  $t = 0, \tau_1$  and  $\tau_2$  are shown in Table I. Table I also contains the expressions for the amplitudes of the echoes occurring at  $t = 2\tau_1$ , when a first  $90^\circ$ -pulse followed by a series of  $n$   $180^\circ$ -pulses are applied at times  $t = \tau_1, 3\tau_1, \dots (2n-1)\tau_1$ . This expression agrees with that obtained by Carr and Purcell and later by Torrey for such pulse sequences. The expressions for the image echo at maximum amplitude, as obtained by different theoretical approaches, have been shown in Table II. The disagreement observed is expected since some of the earlier methods were not rigorously correct, and we discuss them below.

Herzog and Hahn (1956) have extended their method, used in solids, to the case of liquids. If, however, one uses the Eqns (23) and (25) of their paper to calculate the amplitude of the free precession signals in liquids, one obtains infinite amplitude for the signals\*. The reason for this can be seen to be the assumption

$$P(\eta_0) = \text{constant.}$$

Moreover, the above assumption does not represent the physical situation. Also the diffusion-process in liquid can not be described in exactly the same way as

\* The equations in the appendix of Herzog and Hahn's paper giving the signal amplitudes in liquids show finite amplitude since the integration was not fully carried out. Actually they should get, for example,  $E_{max} \sim \exp[-\frac{1}{2}k\tau^2] \delta(0)$  for the primary echo, where  $\delta(0)$  is the Dirac's  $\delta$ -function for the zero value of the parameter i.e. at  $t = 2\tau_1$ . Similar will be the case with other signals.



TABLE II

Expressions for the amplitude of the image echo at echo maximum, according to different theoretical approaches.  $\theta$  denotes the time of occurrence of the echo maximum, measured from the third pulse i.e.,  $\theta = \tau_2 - 2\tau_1 - \tau - \tau_2 - \tau_1$  where  $\tau_1$  and  $\tau_2$  are positions of the second and the third pulses respectively. Echo maximum occurs at  $t = 2(\tau_2 - \tau_1)$  and  $\xi_1$ ,  $\xi_2$  and  $\xi_3$  are the nutational angles of the applied pulses as in Table I

	Common part of the echo-amplitude, as given by different theoretical approaches	Part dependent on diffusion
1. Hahn	$-M_0 \sin \xi_1 \sin^2 (\xi_2/2) \sin^2 (\xi_3/2)$ $\propto \exp \left[ -\frac{2(\tau_2 - \tau_1)}{T_2} \right]$	$\exp \left( -\frac{8}{3} k \tau \right)$
2. Das and Saha	..	$\exp \left[ -k \left\{ \frac{5}{3} \tau^3 - 4\tau^2 \theta + 5\tau \theta^2 - \theta^3 \right\} \right]$
3. The present treatment*	..	$\exp \left[ -2k \left\{ \frac{1}{3} \tau^3 - \tau^2 \theta + \tau \theta^2 \right\} \right]$

\* The same results can be also derived from Torrey's (1956) treatment based on the solution of diffusion equation.

they have done in the case of solid. The stationary distribution as obtained from "the probability distribution for the frequency" (see Eq. (31) of their paper) reduces to zero as  $t \rightarrow \infty$ . Their treatment will be valid in the case of liquid also if the probability distribution for the frequency is taken in such a way that it conforms with the actual stationary distribution in liquids. We, however, note that the damping terms in equations for the free precession signals in liquids as given in their paper are identical with ours. This is because the damping terms depend on the probability distribution for the frequency (transition probability) and on the phase factor coming through the solution of the Bloch equations; and these are the same both in our treatment and in Herzog and Hahn's.

The treatment of Das and Saha contains the following important points —

(1) They assigned definite phase (as they termed) and the Larmor frequency change for each of the free precession intervals. In essence it is equivalent to the splitting up of the actual phase accumulated in any free precession interval into two parts :-

- (a) the phase accumulated when the Larmor frequency remains constant in the interval considered, and
- (b) the difference between the total phase accumulated and the part described in (a).

In averaging these phase accumulations, they have separately averaged over the two parts considering them to be following independently the Gaussian distribution law. The justification for such treatment is yet to be shown.

(2) They separately considered the phase accumulations in the different free precession intervals. This is not justified for the following reasons :

(a) since the accumulated phase does not follow the Markoff process, the averaging of phase in successive free precession intervals comprising the total interval is not justified.

(b) since the echo signals are made possible due to the preservation of the phase-memory by the nuclear magnets, the consideration of the phase accumulations in different free precession intervals as completely independent does not conform with the physical situation.

Since they considered phase averaging in this way, the phase-reversal could not be taken into account in their treatment

### III. APPARATUS

The apparatus used has been reported earlier by Banerjee *et al.* in this journal (Banerjee *et al.*, 1957). The addition to the apparatus is a trigger generator of conventional type. In order to use Carr-Purcell method for determining relaxation time  $T_2$ , a Carr-Purcell sequence generator has been constructed. This is based on the principle of running an one-shot multivibrator with arrangement for a proper positive triggering feed-back through a feed-back amplifier. The total delay is, however, distributed over two such multivibrators in series which also makes it possible to arrange such that the multivibrators return to their initial conditions each time before being triggered. The sequence can be stopped by closing down the feed-back loop by another pulse synchronized with the repetition period generator. This is a very simple method of getting such pulse sequence with fairly good stability of pulse separations. The stability of the multivibrators can be easily improved by increasing the value of the grid-resistor (returning to high tension) in comparison to the plate-load. The circuit for Carr-Purcell sequence generator is shown in Fig. 1.

### IV. EXPERIMENTAL PROCEDURE AND RESULTS

#### (a) Measurement of Molecular Self-diffusion Co-efficient $D$ :

For the measurement of  $D$ , we observe the amplitude of the "image echo" which is formed at time,  $t = 2(\tau_2 - \tau_1)$  with a  $90^\circ$ — $180^\circ$ — $180^\circ$  pulse sequence, and as seen from the expressions in Table II, the relaxation damping of the echo-amplitude will not change with variation of  $\tau_1$ , if  $(\tau_2 - \tau_1)$  is kept constant, whereas the diffusion damping will change. Thus we can isolate the diffusion damping from that due to relaxation. The diffusion damping of this echo can be displayed on the oscilloscope screen by triggering the sweep with a trigger-pulse which changes its



position on the time-scale as the value of  $\tau_1$  is varied. In practice, the sweep was triggered just before the third pulse by introducing a fixed delay between the second pulse and the triggering pulse. Hence as  $\tau_1$  was changed keeping  $(\tau_2 - \tau_1)$  constant, the triggering pulse also correspondingly changed its position, the small delay between the triggering and the third pulse, however, always remained the same. One can now obtain a multiple exposure of this echo with variation of  $\tau_1$ . With the above arrangement, where the position of the image-echo is kept constant (by keeping  $(\tau_2 - \tau_1)$  constant), and the position of the triggering pulse is shifted exactly by the same amount as the variation in  $\tau_1$ , we get a plot of the echo-amplitude *vs.*  $\theta [-2(\tau_2 - \tau_1) \quad \tau_2 - \tau_2 - 2\tau_1]$ ,  $\theta$  denoting the time measured from the 3rd pulse. The triggering of the sweep was done by a pulse from a trigger-generator which is itself triggered by the second pulse such that the delay between the second and the triggering pulse can be kept constant. Fig. 2 shows such a multiple exposure.

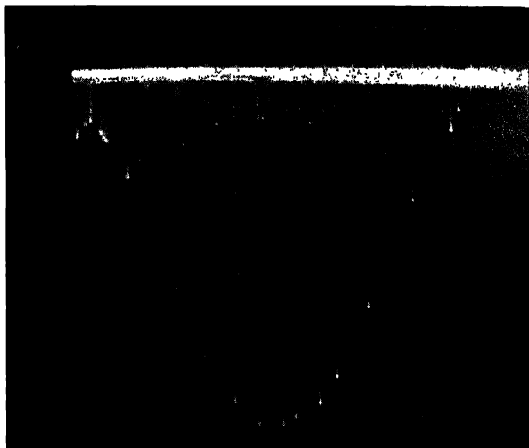


Fig. 2.—Multiple exposure of the image echo from protons in water, with variation of  $\tau_1$ , keeping  $(\tau_2 - \tau_1)$  constant. A sequence of three pulses ( $90^\circ$ - $180^\circ$ - $180^\circ$ ) applied at times  $t=0$ ,  $\tau_1$  and  $\tau_2$  respectively has been used. The sweep calibration with 2ms marker can be seen below the base-line.

The use of  $90^\circ$ - $180^\circ$ - $180^\circ$  pulse sequence with exact values of these angles is not critical, but the angle adjustments are done as accurately as possible in order to minimise the amplitudes of all other echoes which may interfere on the multiple-exposure photograph. A preliminary check is made to see that the resonance condition is reached (Ghose *et al.*, 1957a), the maintenance of the resonance condition being also not essential. It is, however, essential to maintain the mag-

netic field  $H_0$  at a constant value. This was done in our case with the help of a fluorine signal, obtained by steady NMR method

As seen in Table II, the plot of  $\log_e A$  vs  $\theta (= \tau_2 - 2\tau_1)$  where  $A$  is the echo-amplitude, is a parabola satisfying the equation

$$\log_e A = \text{constant} - 2k\tau^2\theta - 2k\tau\theta^2 \quad (14)$$

where  $\tau = \tau_2 - \tau_1 = \text{constant}$ . Thus  $k$  can be obtained from the experimental data fitting them to an equation of parabola by the standard method (Johnson, 1952) and comparing the latter with relation (14). Such a parabola is shown in the Fig. 3,  $k$  can also be evaluated from the gradients of (14) at  $\theta = 0$  and  $\theta = \tau$ , since

$$\left[ \frac{d}{d\theta} \log_e A \right]_{\theta=0} - \left[ \frac{d}{d\theta} \log_e A \right]_{\theta=\tau} = -2k\tau^2 \quad \dots (15)$$

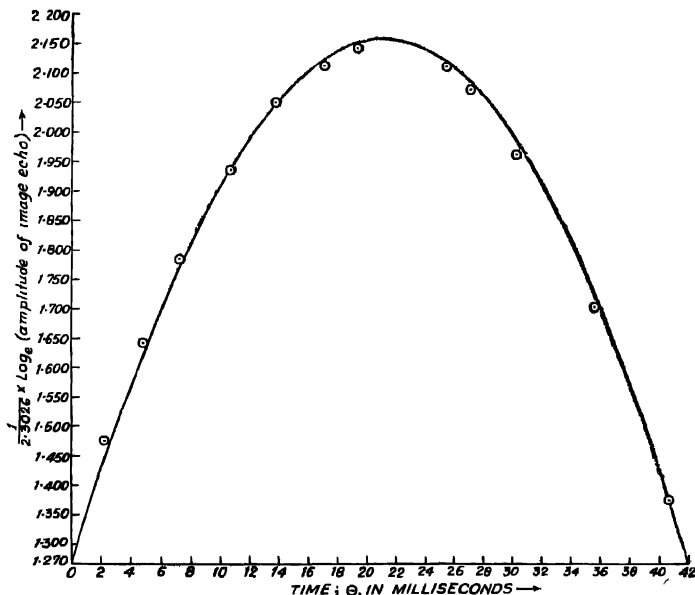


Fig. 3. The logarithm of the amplitudes of the image echo is plotted against  $\theta$ , given by  $\theta = \tau_2 - 2\tau_1$ , where  $\tau_1$  and  $\tau_2$  give the position of the second and the third pulse respectively. The parabola fitting the experimental points are also shown (in solid line).

From the geometry of the parabola, this gradient can be evaluated simply from the relation

$$\left[ \frac{d}{d\theta} \log_e A \right]_{\theta=0} = - \frac{2\{(\log_e A)_{\theta=\tau/2} - (\log_e A)_{\theta=0}\}}{\tau/2} \quad \dots (16)$$

Combining (15) and (16)

$$k = \frac{2\{(\log_e A)_{\theta=\tau/2} - (\log_e A)_{\theta=0}\}}{\tau^3} \quad \dots (17)$$

To obtain  $D$  from the value of  $k$ , the magnitude of the magnetic field gradient,  $G$ , is required. The magnetic field gradient was applied as was suggested by Carr and Purcell by two co-axial coils of 170 turns each wound on a perspex form, the common axis of the coils being in the direction of  $H_0$ . The value of  $G$  was experimentally determined from the echo modulation. By considering in some cases six or seven such maxima or minima it was found that the maximum deviation from the average value of  $G$  as determined from the different maxima or minima was 3 to 4% at most, which indicates that the over-all field gradient along the axis of the sample holder was negligible.

The rf field  $H_1$  used was approximately 5 gauss, and the proton resonance was observed at about 14 mc/sec.

$D$  was measured with three different field gradients, 1.19, 1.71 and 2.18 gauss/cm, and was found to be the same within experimental error, the average

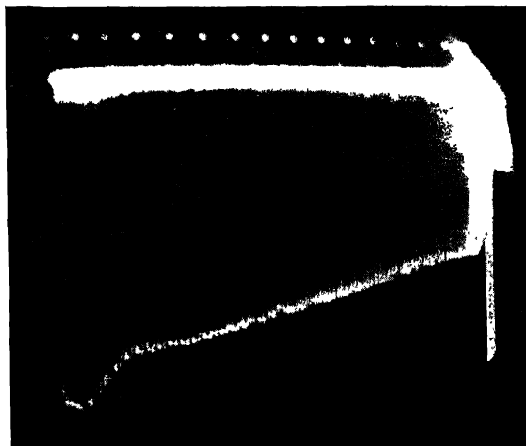


Fig. 4.—Carr-Purcell echoes from protons in water, with the magnetic field gradient 1.71 gauss/cm, almost from the beginning of the sequence. The value of  $\tau$ , the separation between the first 90° and the next 180° pulses, used was 3.3 ms. Sweep calibrator marker separation was 40 ms.

value being  $2.6 \times 10^{-5} \text{ cm}^2/\text{sec}$  for water at room temperature ( $30^\circ\text{C}$ ). The sample was doubly distilled water sealed in a pyrex glass-tube. The value of  $D$  thus determined agrees well with other measurements [Carr and Purcell (1954), Orr and Bulter (1935), Wang *et al.* (1953)]

(b) *Measurement of  $T_2$*

If  $k$  is known the value of  $T_2$  can be determined in principle by Hahn's method, where the two pulse echo amplitude is corrected for diffusion damping and plotted against  $\tau_1$ , the slope of the resulting straight line giving  $1/T_2$ . In case of protons in water the value of  $T_2$  is comparatively large, and thus the slope will be small. Thus in this case time considered should be made large. But it was found that for large values of time, the corrected echo-amplitudes do not fall on a straight line, the expected straight line showing oscillatory tendencies (giving maxima and minima with increase of time). The origin and the nature of this phenomenon is being investigated in greater details.

$T_2$  can, however, be determined accurately from Carr-Purcell decay constant after correcting it for diffusion damping. Even for large field gradient, this correction gives good result for the value of  $T_2$ . Fig. 4 shows a photograph of Carr-Purcell sequence of echoes for water, the magnetic field gradient used was 1.71

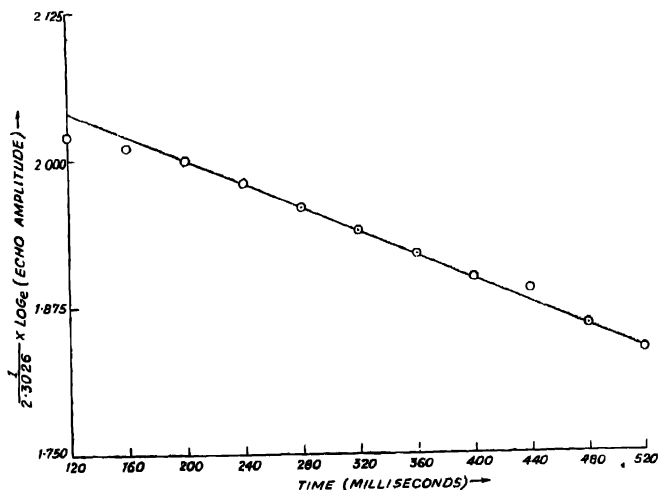


Fig. 5.—The logarithms of the echo amplitudes obtained from the Carr-Purcell sequence (Fig. 4) are plotted against time. The slope of the straight line gives  $\frac{1}{T_2} + \frac{1}{4\tau^2} + \frac{1}{3} k\tau^2$  where  $k = \gamma^2 G^2 D$  and  $\tau$  is the separation between the first  $90^\circ$  and the next  $180^\circ$  pulses. From this,  $T_2$  can be obtained, if  $k$  and  $\tau$  are determined separately.

gauss/cm In Fig. 5 the logarithms of the echo-amplitudes are plotted against time. The value of the envelope decay constant,  $T_2^*$  as obtained from Fig. 5, which is related to  $T_2$  by the following relation

$$\frac{1}{T_2^*} = \frac{1}{T_2} + \frac{1}{3} k\tau^2 \quad \dots (18)$$

where  $\tau$  is the separation between the 1st  $90^\circ$  pulse and the next  $180^\circ$  pulse, is found to be 1.99 seconds. Using the previously determined value of  $k$  and  $\tau$ , the value of  $T_2$  comes out as 2.5 seconds.

With the same sample of water,  $T_1$  also was determined by null method (Ghose *et al.*, 1957b), and was found to be 2.88 seconds, thus the ratio of  $T_1/T_2$  agrees well with BPP theory (Bloembergen *et al.*, 1948).

In the above determinations the error creeps in mainly because of the following causes

(1) Very high degree of stability in the delays introduced by the multi-vibrators, in our pulsing system, cannot be expected, because of inherent instability of such systems

(2) The accuracy in time measurement is also limited as we had to calibrate the oscilloscope sweep by an external marker (Hewlett Packard, Model 100D and 202A). Even with very stable marker the time-measurement will not be correspondingly accurate since one has to measure time from the calibration of the oscilloscope sweep.

(3) The noise-figure of the apparatus limits the accuracy of measurement of the signal amplitudes and the error due to this cause is difficult to estimate exactly.

The use of scalar-type pulsing arrangement with stable oscillators as time-generators will remove the causes (1) and (2) to a large extent, and thus will improve the accuracy of measurement.

It is, however, expected that the maximum error in all our determinations was less than 5%.

### (c) *Experimental check of the different theoretical approaches*

So far, the value of  $D$ , as obtained using the different theoretical formulations, was considered as a check of the theoretical approaches. This is, however, indirect. The "image" echo considered in the present work affords a direct check since the nature of variation of its amplitude with  $\theta$ , is predicted to be different in different approaches. According to Hahn's approach the amplitude of this echo should not change at all. This approach is then obviously not correct, which was modified later by Herzog and Hahn\*. According to Das and Saha's treatment the amplitude of this echo follows the following equation

$$\log A = \text{constant} + 4k\tau^2\theta - 5k\tau\theta^2 + k\theta^3 \quad \dots (19)$$

\* However, their results for liquids are not considered here for reasons explained in Section II.



and the maximum of  $\log_e A$  will occur at

$$\theta = 0.465(\tau_2 - \tau_1)$$

According to the present approach, the above maximum will be at

$$\theta = 0.5(\tau_2 - \tau_1)$$

There is thus about 7% difference in the predicted positions of the maximum. Experimental results on the determination of the position of this maximum favour the conclusion of the present paper. In Fig. 6 Eqs. (14) and (19) are plotted in a scale such that they are closest to each other. The experimental points are then reduced to the same scale to observe which of the two curves they follow. It is found that they follow the Eq. (14) more closely than the Eq. (19) showing that the present approach is more acceptable.

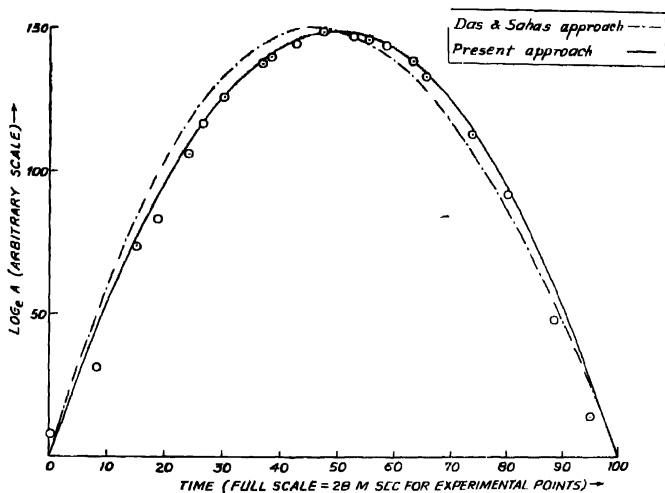


Fig. 6.—The theoretical Eqs. (14) and (19), giving the logarithms of the amplitude of the image echo, as derived from Das and Saha's and from the present treatment are drawn in the same scale for comparison with the experimental data, which are also plotted here in the same scale. The Eqs. (14) and (19) are brought to the same scale by coinciding any two points of the two curves. The two corresponding experimental points are then brought to those common points for reducing the experimental points to the common scale of the two curves.

## V. DISCUSSION

Let us now examine the various different NMR methods for the measurement of  $D$  and  $T_2$ . Of all such methods\*, those developed by Hahn and by Carr and Purcell are mostly used

Hahn's method of measurement of  $T_2$  is seriously handicapped in most cases where the liquids have comparatively small viscosity. In these cases even in most homogeneous magnets ordinarily available, the diffusion effect will seriously interfere with the measurement of  $T_2$ .

Carr-Purcell's method removes this difficulty by minimizing the diffusion-effect, for which one has to use a large number of  $180^\circ$   $\pi$ -pulses. If the adjustment of the angles of the  $180^\circ$   $\pi$ -pulses is not exact, the error produces a cumulative effect and the amplitude of the echo formed after a large number of pulses becomes seriously affected. It can, however, be shown that if the echoes after a large number of pulses are considered the above effect introduces an extra damping such that the total damping remains still exponential. This extra damping can be made negligibly small if the error in the adjustment of the angle of the  $180^\circ$   $\pi$ -pulses is kept within 1-2%. This can be easily obtained. One should, however, note that Meiboom and Gill (1958), have suggested a method by which the above cumulative error can be reduced. But in general case, the overall field inhomogeneity and the values of relaxation time  $T_2$  may prevent the use of a large number of  $\pi$ -pulses, which thus limits the application of the method in such cases. One can, however, adjust the field gradient such that the exponential decay of the Carr-Purcell echo sequence contains only the diffusion and the relaxation damping, the relaxation time can then be accurately determined from that decay constant, if the diffusion damping at the field gradient is ascertained independently. This is exactly what is done in the present method as described in Section IV.

We also note that while determining  $D$  from Hahn's plot (after finding out  $T_2$  previously) Carr and Purcell found that with large field gradients there is departure from the expected straight line. This effect also limits the use of Carr-Purcell method for measuring  $D$  in general cases. Similar departure from the straight line was also observed when we attempted to evaluate  $T_2$  from Hahn's plot, after finding out  $k(= \gamma^2 G^2 D)$  previously. As mentioned earlier in Section IV, we obtained a curve showing maxima and minima, instead of a straight line. This effect shows itself at large time  $t$  and increases with the increase in the value of the field gradient. Both the Carr-Purcell and the Douglas-McCall methods of measuring  $D$  from Hahn's plot will be seriously affected by the above phenomenon. In the present method this effect can be made very small even for large magnetic

\* A brief account and the references of different methods of measuring  $T_2$  can be found in "Nuclear Magnetic Resonance" by E. R. Andrew, Cambridge University Press, London (1955).

field gradient by properly adjusting the separation between the second and the third pulses, such that diffusion-damping becomes predominant in comparison with the above effect.

Though the effect of chemical shift and J-coupling (Hahn and Maxwell, 1952) will affect the amplitude of the image echo, their effect can be minimized in the present method by properly choosing the value of the magnetic field gradient. It may be mentioned here that the previous determination of  $D$  can be profitably used in the evaluation of  $J$  by the spin-echo technique (Hahn and Maxwell, 1952 and Crawford and Foster, 1956)]

## ACKNOWLEDGMENTS

The authors wish to thank Prof. A. K. Saha and Mr. B. M. Banerjee for their encouragement and interest during the progress of the work. They also appreciate many helpful discussions and criticism from Dr. D. K. Roy and Mrs. T. Roy.

## REFERENCES

- Anderson, P. W., 1954, *J. Phys. Soc. Japan*, **9**, 316.  
 Banerjee, B. M., Ghosh, S. K. and Saha, A. K., 1957, *Ind. J. Phys.*, **31**, 211.  
 Bloch, F., 1946, *Phys. Rev.*, **70**, 460.  
 Bloembergen, N., Purcell, E. M. and Pound, R. V., 1948, *Phys. Rev.*, **73**, 673.  
 Carr, H. Y. and Purcell, E. M., 1954, *Phys. Rev.*, **94**, 630.  
 Chandrasekhar, S., 1943, *Rev. Mod. Phys.*, **15**, 1.  
 Crawford, G. J. R. and Foster, J. S., 1956, *Canad. J. Phys.*, **34**, 653.  
 Das, T. P. and Saha, A. K., 1954, *Phys. Rev.*, **93**, 749.  
 Douglas, D. C. and McCall, D. W., 1958, *J. Phys. Chem.*, **62**, 1102.  
 Ghose, T., Ghosh, S. K. and Roy, D. K., 1957a, *J. Phys. Soc., Japan*, **12**, 816.  
 Ghose, T., Ghosh, S. K. and Roy, D. K., 1957b, *Nuovo Cimento Series X*, **6**, 1771.  
 Green, H. S., 1952, "The Molecular Theory of Fluids," North-Holland Publishing Company, Pages 195 ff. and 151 ff.  
 Hahn, E. L., 1950, *Phys. Rev.*, **80**, 580.  
 Hahn, E. L. and Maxwell, D. E., 1952, *Phys. Rev.*, **88**, 1070.  
 Herzog, B. and Hahn, E. L., 1956, *Phys. Rev.*, **103**, 148.  
 Inc., New York, Chapter Nine.  
 Johnson, Lee H., 1952, *Nomography and Empirical Equations*. John Wiley & Sons.  
 Kirkwood, J. G., 1946, *J. Chem. Phys.*, **14**, 180.  
 Meiboom, S. and Gull, D., 1958, *Rev. Sci. Instr.*, **29**, 688.  
 Orr, W. J. C. and Butler, J. A. V., 1935, *J. Chem. Soc.*, 1273.  
 Rabi, I. I., Ramsey, N. F. and Schwinger, J., 1954, *Rev. Mod. Phys.*, **26**, 167.  
 Torrey, H. C., 1956, *Phys. Rev.*, **104**, 563.  
 Wang, J. H., Robinson, C. V. and Edelman, I. S., 1953, *J. Amer. Chem. Soc.*, **75**, 466.  
 Wang, M. C. and Uhlenbeck, G. E., 1945, *Rev. Mod. Phys.*, **17**, 323.

# ABSORPTION OF MICROWAVES IN CYCLOHEXANOL AND CYCLOPENTANOL AND THEIR SOLUTIONS

T J BHATTACHARYYA

OPTICS DEPARTMENT, INDIAN ASSOCIATION FOR THE CULTIVATION  
OF SCIENCE, JADAVPUR, CALCUTTA 32.

(Received, June 20, 1960)

**ABSTRACT.** The absorption of 3.18 cm microwaves in cyclohexanol, cyclopentanol, and their solutions in heptane and carbon tetrachloride was studied at different temperatures. The solution in  $\text{CCl}_4$  did not show any absorption. The temperature-attenuation curves show maxima at 105°C, 96°C, 14°C and 8°C respectively in the cases of cyclohexanol, cyclopentanol and 10% solutions of the substances in heptane. The values of the radius of the rotor calculated from Debye's theory are 1.41, 1.42, 1.40 and 1.43 Å respectively. The rotor has been identified with the OH group.

The attenuation coefficients for the solutions in heptane were found to be greater than those of the pure liquids. This has been explained on the assumption that in pure liquids there exist dimers formed through intermolecular OH...O bond which break up in the solutions.

The absence of any absorption in the solutions of  $\text{CCl}_4$  has been attributed to the formation of OH...Cl bond between the solvent and the solute molecules.

## INTRODUCTION

The study of the absorption of microwaves of wavelength 3.18 cms in *o*-chlorophenol (Ghosh, 1955) and in solutions in  $\text{CCl}_4$  (Bhattacharyya, 1958) and similar investigations in ethylene chlorhydrin (Bhattacharyya, 1959) furnished evidence for the formation of hydrogen bond between neighbouring molecules in the pure liquids and breaking up of such associated groups into single molecules in solutions in suitable solvents. In the case of solution of ethylene chlorhydrin in methyl cyclohexane it was found that of the two types of dimers present in the liquid only those formed through the intermolecular OH...O bond break up into single molecules in the solution. There was no further interaction between solvent and the solute molecules, but in the case of the solution in  $\text{CCl}_4$  it was found that an intermolecular OH...Cl bond is formed between the solvent and the solute molecules so that the C—Cl group at the other end of the latter molecule possesses freedom of rotation about the C—Cl bond. These results confirmed the conclusions drawn by Mazumder (1959) from the results of investigations of the infrared spectra of the solution of ethylene chlorhydrin in  $\text{CCl}_4$ .

It was thought worthwhile to extend the investigation to other substances containing OH group as a substituent. Cyclopentanol and cyclohexanol which are two typical alicyclic alcohols were chosen for this purpose and the absorption of 3.18 cm microwaves in solutions of these two compounds in heptane and carbon tetrachloride has been investigated.

# EXPERIMENTAL

The experimental arrangements and procedure were similar to those used in a previous investigation (Bhattacharyya, 1958)

In order to verify whether the absorption observed with any particular cell was genuine or spurious, two cells of different thicknesses were used successively and the strengths of absorption in the two cells were compared. The absorption was studied in the pure liquids and also in 10% solutions of the liquids in  $\text{CCl}_4$  and in heptane. The values of the static dielectric constants, the refractive indices and the coefficients of viscosity for the pure liquids were obtained from the standard tables. As the data for solution in heptane were not available they were determined experimentally. In the case of the solutions in  $\text{CCl}_4$  no absorption of the microwaves was observed.

The radius of the rotor  $a$ , was calculated in the case of the pure liquids with the help of the Debye's formulae

$$\omega\tau = \frac{\epsilon_0 + 2}{\epsilon_1 + 2} \sqrt{\frac{\epsilon_1}{\epsilon_0}} a^3 = \frac{KT}{4\pi\eta} \quad \dots (1)$$

where  $\epsilon_0$ , the dielectric constant at very high frequencies has been taken to be the square of the refractive index of the liquid,  $\epsilon_1$  and  $\eta$  are the dielectric constant and the coefficient of viscosity of the liquid at the temperature  $T^\circ\text{K}$  at which the maximum absorption of the 3.18-cm waves takes place.

In the case of the solution in heptane also the same formulae and the constants determined experimentally were used.

# RESULTS AND DISCUSSION

The temperature-dependence of the attenuation coefficient for the pure liquids has been shown in Fig. 1. Curves I and II are for two different cells filled with pure cyclopentanol. Similarly, curves III and IV show the absorption in pure cyclohexanol in the two cells.

Fig. 2. shows the relation between temperature and the attenuation coefficient for the 10% solutions of the cyclopentanol and cyclohexanol in heptane. In calculating attenuation coefficient for the solutions, the equivalent thickness of the substance in the cell instead of the real thickness of the cell has been taken into consideration.

The radius of the rotor calculated for the different samples are given in Table I. It is found to be about  $1.4 \times 10^{-8}$  cm in each case. The temperatures at which the maximum absorption take place in cyclopentanol and cyclohexanol are  $96^\circ\text{C}$  and  $105^\circ\text{C}$  respectively. From Fig 1 it is observed that the two cells of different thickness give identical results which show that the absorption is genuine.

TABLE I

Substances	$\omega/2\pi\text{Mc/sec.}$	$\epsilon_1$	$\sqrt{\epsilon_0}$	$\tau \times 10^{11}/\text{sec}$	$100\eta$	$T^\circ\text{K}$	$a \times 10^8 \text{ cm}$
Cyclopentanol	9415	9.00	1.45	1.31	1.90	369	1.42
Cyclohexanol	„	8.00	1.46	1.35	2.06	379	1.41
10% soln. of cyclopentanol in heptane	„	6.00	1.43	1.48	1.70	281	1.40
10% soln. of cyclohexanol in heptane	„	5.00	1.44	1.51	1.65	287	1.43

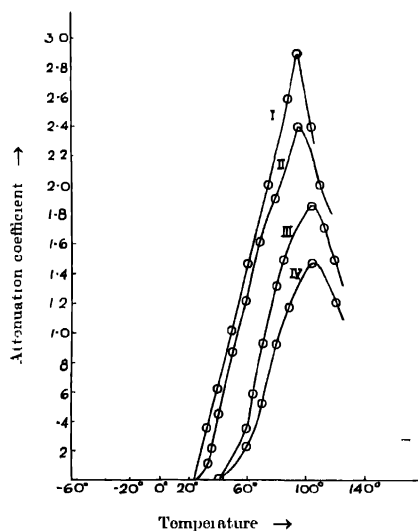


Fig. 1. Curve I—Pure cyclopentanol, thickness of the liquid : 1.4 cm.  
 Curve II— „ „ „ „ „ „ : 1.0 cm.  
 Curve III—Pure cyclohexanol, thickness of the liquid : 1.4 cm.  
 Curve IV— „ „ „ „ „ „ : 1.0 cm.

The fact that the solutions in heptane show the maximum absorption of the microwaves at much lower temperatures also lends additional support to the conclusions that the absorption is genuine and that it is dependent on the viscosity of the liquid, as postulated in Debye's theory. These results further show that Debye's formula is applicable in these cases.

From Fig. 2 it is observed that the values of the maximum attenuation coefficient for the solutions of cyclohexanol and cyclopentanol in heptane are 8.9 and 12.0 respectively. Fig. 1 on the other hand shows the maximum values in the case of pure cyclohexanol and cyclopentanol to be 1.84 and 2.88 respectively. The increase of absorption in the case of the solutions indicates the increase of the free OH group in solutions. Hence it can be concluded that the OH group in large number of molecules in the pure substances have no freedom of orientation. This can only happen if associated pairs of molecules are formed through intermolecular OH...O bonding. It can therefore be concluded that in the pure alcohols loose dimers are formed through intermolecular OH...O bond and they break up into single molecules in solutions.

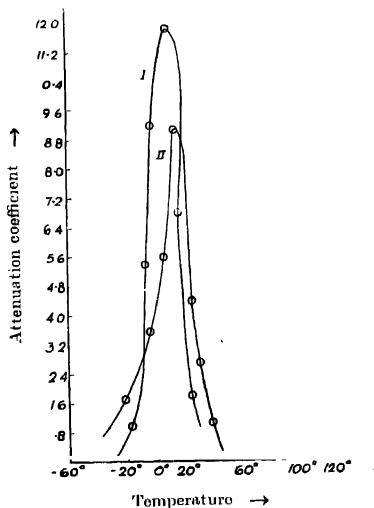


Fig. 2. Curve I—10% solution of cyclopentanol in heptane, (thickness of the cell = 1.4 cm.)

Curve II—10% solution of cyclohexanol in heptane, (thickness of the cell = 1.4 cm.)

In solutions in carbon tetrachloride, however, no absorption was observed though the viscosity of the solution in  $\text{CCl}_4$  is nearly the same as that of the

solution in heptane. It might be expected that the OH...O bond should break up in these solutions. Hence the absence of absorption indicates the formation of a new type of hydrogen bond due to the action of the solvent molecules. It is quite probable that the OH group of the molecule of either of the compounds forms virtual linkage with the chlorine atom of the  $\text{CCl}_4$  molecule in the solutions. This newly formed OH...Cl bond prevents the free orientation of the OH group and consequently, no absorption of the microwaves can take place in these solutions. Evidence for the formation of such OH...Cl bond between the solvent and solute molecules in the solution of ethylene chlorhydrin in  $\text{CCl}_4$  was observed earlier (Bhattacharyya, 1959). Study of the infrared absorption of the solution of ethylene chlorhydrin in  $\text{CCl}_4$  (Mazumder, 1959) also led to these conclusions.

The results of these investigations thus throw much light on the nature of influence of intermolecular fields in such polar liquids and their solutions in suitable solvents.

#### ACKNOWLEDGMENT

The author is indebted to Professor S. C. Sirkar, D.Sc. F.N.I., for his constant guidance throughout the progress of the work.

#### REFERENCES

- Bhattacharyya, T. J., 1958, *Ind. J. Phys.*, **32**, 573.  
" " 1959, *Ind. J. Phys.*, **33**, 498.  
Ghosh, D. K., 1955, *Ind. J. Phys.*, **29**, 450.  
Mazumder, M. M., 1959, *Ind. J. Phys.*, **33**, 346.



# LIGHT ABSORPTION IN PARAMAGNETIC IONS IN STATE OF SOLUTION. PART II— $\text{Ni}^{++}$ ION

A. MOOKHERJI AND N. S. CHHONKAR

PHYSICS LABORATORIES, AGRA COLLEGE, AGRA

(Received, June 10, 1960)

**ABSTRACT.** The light absorption in aqueous solution of nickel salts are studied in the range 10,000 Å to 3900 Å by a Hilger Uvispek spectrophotometer and the results are discussed in the light of crystalline electric field theory.

The cubic field coefficient has almost the same value in all the salts except the amino-salts.

It is observed that the term separation comes to be smaller for the ion in crystal than for the free ion. From this lowering the covalency factor  $f^2$  was evaluated.  $f^2$  tends to a value of 0.9 for all the salts except the amino-salts pointing that  $f_{\pi}^2$  is unity in them. In amino-salts  $f^2$  arises from  $\sigma$  and  $\pi$ -orbital overlap.

Excellent agreement with the measured values of magnetic anisotropy was obtained by attributing the bands at 13,900  $\text{cm}^{-1}$  and 15,200  $\text{cm}^{-1}$  as due to the splitting by a crystal field of tetragonal symmetry.

The effect of long range field was observed to be very pronounced in single sulphate and selenate, double sulphates and selenates of K and Rb, while this was less pronounced in double sulphates and selenates of  $\text{NH}_4$  and Tl.

## INTRODUCTION

In the previous part of this paper (Mookherji & Chhonkar, 1959) which we shall refer as part I hereafter, a systematic optical investigation of the consequences of the crystalline electric fields on cupric ions in about twenty different salts in state of aqueous solution has been reported. A number of interesting results that have been obtained are:

- 1) At least some of the co-ordinating members of the octahedral cluster about the  $\text{Cu}^{++}$  ion in some salts are very probably other than water molecules.
- 2) The complex,  $[\text{Cu}(\text{H}_2\text{O})_6]^{2+}$ , in different salts in aqueous solution is not truly ionic but possesses some amount of covalent bonding.
- 3) In some salts appreciable  $\sigma$ -bonding prevails and  $\pi$ -bonding is neglected, while in others there are both  $\sigma$ -orbital and  $\pi$ -orbital overlap.
- 4) The position of the absorption bands in state of solution does not vary much from salt to salt amongst sulphates, nitrates, chlorides etc.; while there are appreciable variations amongst others (i.e. acetate, propionate and formate).

For free  $\text{Cu}^{++}$  ion, the ground state is  $^2D$ , no other terms of the same multiplicity lie very close, whereas for free  $\text{Ni}^{++}$  ion the ground state is  $^3F$  and a term of the same multiplicity  $^3P$  lies  $16,900\text{ cm}^{-1}$  above it (Moore, 1952). Naturally the crystalline field splitting of the ground state of the two free ions will be very different. Just like  $\text{Cu}^{++}$  ion, in octahedrally co-ordinated salts of  $\text{Ni}^{++}$  ion, an orbitally non-degenerate level lies lowest in the Stark-pattern, but weaker spin-orbit coupling in  $\text{Ni}^{++}$  ion makes the contribution from the upper levels to the  $g$ - and  $\mu$ -values appreciably smaller than that for  $\text{Cu}^{++}$  ion (Owen, 1955. Bose and Mitra, 1952).

Dreisich *et al.* (1937, 1939) working on the selective optical absorption spectra of  $\text{Ni}^{++}$  ion in  $[\text{Ni}(\text{H}_2\text{O})_6]^{2+}$  and  $[\text{Ni}(\text{NH}_3)_6]^{2+}$  salts observed broad absorption bands with centres at about  $8,497\text{ cm}^{-1}$ ,  $15,370\text{ cm}^{-1}$  and  $25,510\text{ cm}^{-1}$  and  $10,804\text{ cm}^{-1}$ ,  $17,200\text{ cm}^{-1}$  and  $27,900\text{ cm}^{-1}$  respectively. They reported a fine structure of the band at  $8,497\text{ cm}^{-1}$ . Owen *et al.* (1957) were unable to find any such fine structure of this band, using much higher resolving power instruments.

Jorgensen (1955) has shown that in a series of  $\text{Ni}^{++}$  complexes the lowest singlet state intermixes strongly with triplet states giving rise to double bands.

The present communication deals with the measurements of absorption spectra of about twenty nickel salts in aqueous solution. The results are discussed in the light of the theories developed by Hartmann and Muller (1958), Orgel (1955), Jorgensen (1955), Griffiths and Owen (1952) and Owen (1955).

## EXPERIMENTAL

The measurements were carried out by Hilger's Uvispek spectrophotometer and the same procedure as in part I of this paper (Mookherji and Chhonkar, 1959) was adopted. Chemicals used were of Merck's gravimetric reagent quality. Triple distilled water was used for making solutions.

The measurements were centred round about  $27^\circ\text{C}$ , but no observable change in the position of the absorption bands was noted for small room temperature variations.

## RESULTS

The results of the measurements are collected in Tables Ia and Ib. In order to get prominent absorption peaks for the salts studied, the solutions had to be diluted. Just like cupric salts (part I), progressive dilution from that concentration at which the prominent peak is obtained, does not change the position of the absorption peak. The variations of absorption in different salt solutions are shown graphically in figs. 1 to 18.

TABLE Ia

Salts	Concentrations %	Maximum absorption at					
		$\lambda$ in Å			Wavenumbers in $\text{cm}^{-1}$		
		II	III	IV	II	III	IV
$\text{NiSO}_4$	3	7190	6580	3950	13,910	15,200	25,320
$\text{NiSeO}_4$	4	7220	6570	3950	13,850	15,220	25,320
$\text{Ni}(\text{NH}_4\text{SO}_4)_2$	3	7200	6560	3945	13,890	15,240	25,350
$\text{Ni}(\text{KSO}_4)_2$	4	7190	6570	3945	13,910	15,220	25,350
$\text{Ni}(\text{RbSO}_4)_2$	4	7225	6600	3950	13,850	15,150	25,320
$\text{Ni}(\text{TlSO}_4)_2$	sat.	7195	6560	3945	13,900	15,240	25,350
$\text{Ni}(\text{NH}_4\text{SeO}_4)$	4	7230	6580	3950	13,830	15,200	25,320
$\text{Ni}(\text{KSeO}_4)_2$	4	7230	6580	3950	13,830	15,200	25,320
$\text{NiCl}_2$	4	7180	6550	3950	13,980	15,270	25,320
$\text{NiBr}_2$	2	7220	6580	3950	13,850	15,200	25,320
$\text{Ni}(\text{NO}_3)_2$	2	7190	6570	3950	13,910	15,220	25,320
$\text{Ni}_2\text{Br}_2(\text{NO}_3)_{12}$	4	7240	6600	3945	13,810	15,150	25,350
$\text{Ni}(\text{CH}_3\text{COO})_2$	2	7225	6600	3950	13,850	15,150	25,320
$\text{Ni}(\text{CH}_3\text{COO})_2$	3	7200	6580	3950	13,890	15,200	25,320

TABLE Ib

Salts	Concentration %	Maximum absorption at						
		$\lambda$ in Å				Wavenumbers in $\text{cm}^{-1}$		
		I	II	III	IV	I	II + III	IV
$[\text{Ni}(\text{NH}_3)_4](\text{SO}_4)$	2.25 1:1	NH <sub>4</sub> OH	9500	5785	3600	10,530	17,280	27,780
$[\text{Ni}(\text{NH}_3)_4](\text{OH})$	1.5 1:1		9525	5775	3600	10,490	17,310	27,780
$[\text{Ni}(\text{NH}_3)_4](\text{Cl})$	2.0 1:1		9350	5750	3600	10,700	17,390	27,780
$[\text{Ni}(\text{NH}_3)_4](\text{CH}_3\text{COO})$	2.0 1:1		9325	5750	3600	10,720	17,390	27,780

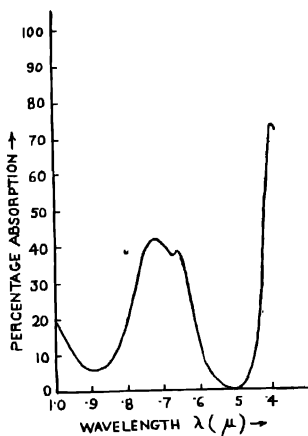


Fig. 1. Stark splitting of ground state of  $\text{Ni}^{2+}$  ion.

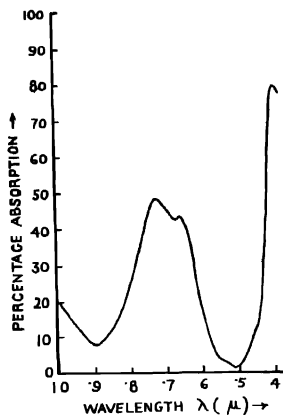


Fig. 2. Absorption curve of 3%  $\text{NiSO}_4$  solution.

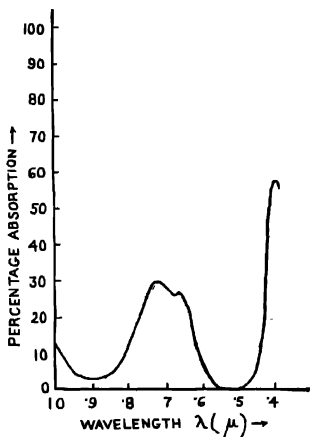


Fig. 3. Absorption curve of 4%  $\text{NiSeO}_4$  solution.

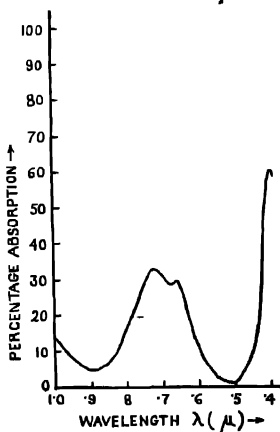


Fig. 4. Absorption curve of 3%  $\text{Ni}(\text{NH}_4\text{SO}_4)_2$  solution.

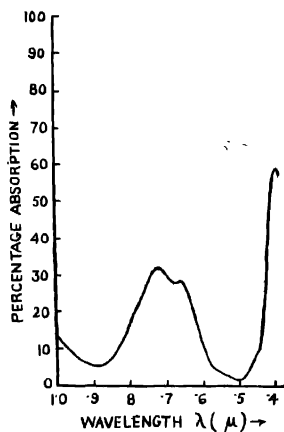


Fig. 5. Absorption curve of 4%  $\text{Ni}(\text{K}_2\text{SO}_4)_2$  solution

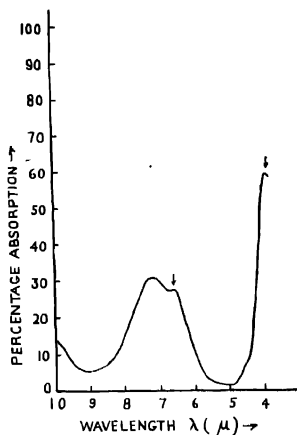


Fig. 6. Absorption curve of 4%  $\text{Ni}(\text{Rh}_2\text{S}_4\text{O}_4)_2$  solution

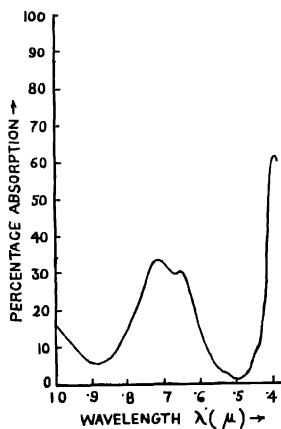


Fig. 7. Absorption curve of sat.  $\text{Ni}(\text{Tl}_2\text{SO}_4)_2$  solution

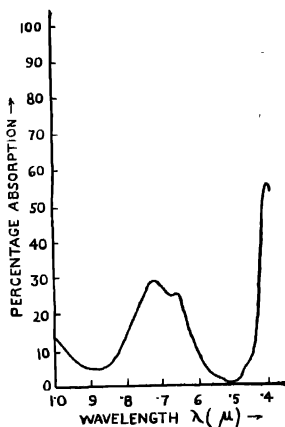


Fig. 8. Absorption curve of 4%  $\text{Ni}(\text{NH}_4)_2\text{SeO}_4$  solution

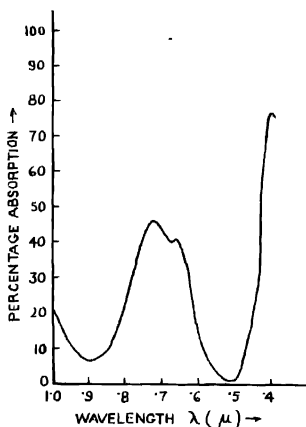


Fig. 9. Absorption curve of 4%  $\text{Ni}(\text{K}_2\text{SO}_4)_2$  solution

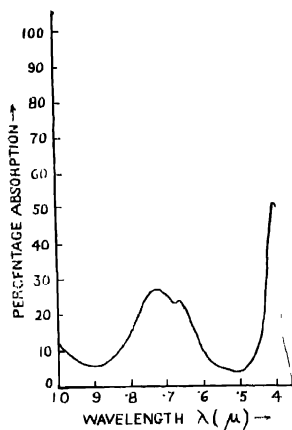


Fig. 10. Absorption curve of 3%  $\text{NiCl}_2$  solution

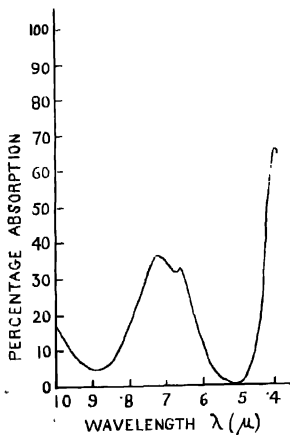


Fig. 11. Absorption curve of 2%  $\text{NiBr}_2$  solution

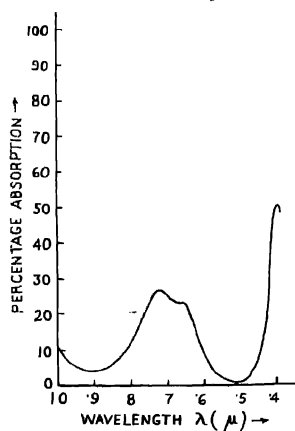


Fig. 12. Absorption curve of 2%  $\text{Ni}(\text{NO}_3)_2$  solution

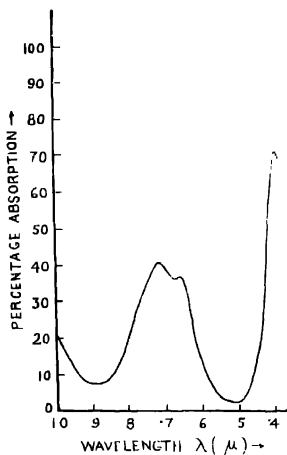


Fig. 13. Absorption curve of 4%  $\text{Ni}_3\text{Bi}_2(\text{NO}_3)_{12}$  solution

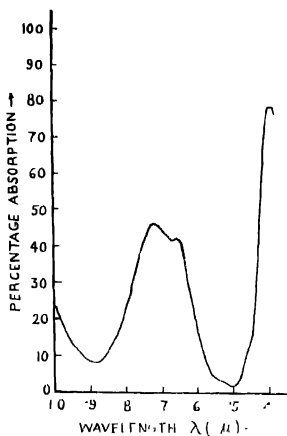


Fig. 14. Absorption curve of 2%  $\text{Ni}(\text{HCOO})_2$  solution

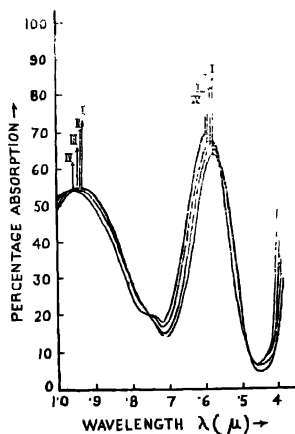


Fig. 15. Absorption curve of 3%  $\text{Ni}(\text{CH}_3\text{COO})_2$  solution

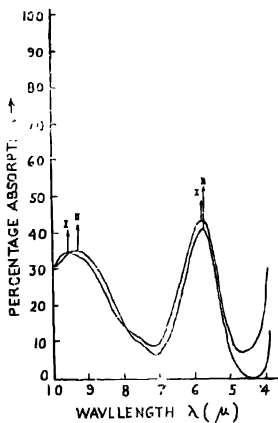


Fig. 16. Absorption curve of 2.25%  $[\text{Ni}(\text{NH}_4)_4](\text{SO}_4)$

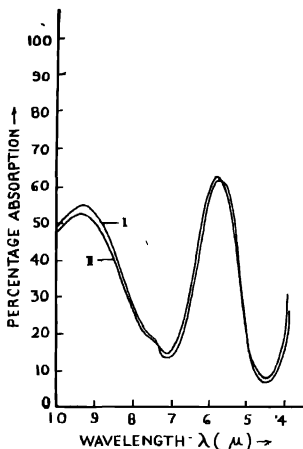


Fig. 17 Absorption curve of 1.5 %  $[\text{Ni}(\text{NH}_3)_6](\text{OH})_2$  solution

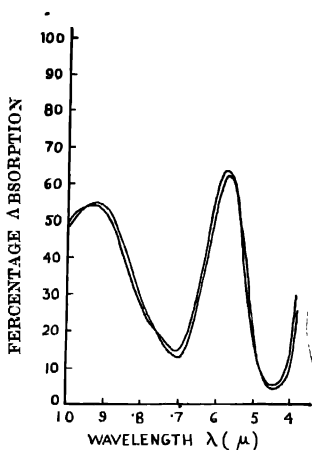


Fig. 18. Absorption curve of 2%  $[\text{Ni}(\text{NH}_3)_6](\text{Cl})_2$  solution

## DISCUSSION

### (a) The absorption spectra

For all the salt solutions studied in Table Ia, the absorption spectra consist of three maxima at about  $13,900\text{ cm}^{-1}$ ,  $15,200\text{ cm}^{-1}$  and  $25,350\text{ cm}^{-1}$  within the range of our studies. We shall designate them by II, III and IV respectively. The first maximum observed by Dreisch *et al.* (1937, 1939), which lies in the infra-red region for all the salts ( $\sim 8500\text{ cm}^{-1}$ ) except amino-salts (Table Ib, for which it lies in the visible range  $10,800\text{ cm}^{-1}$ ) will be known as I.

The maximum at about  $15,370\text{ cm}^{-1}$  was detected by Dreisch and Trommer (1937) and was later identified by Owen (1955) as arising due to the transition from Stark-level  $\Gamma_2$  to  $\Gamma_4$  (Fig. 19). This is almost identical with our III. The maximum II was not detected by them but has recently been observed by Owen, Holmes and McClure (1957) in  $\text{NiSO}_4 \cdot 7\text{H}_2\text{O}$ ,  $\text{NiSiF}_6 \cdot 6\text{H}_2\text{O}$  and  $\text{K}_2(\text{Zn.Ni})(\text{SO}_4)_2 \cdot 6\text{H}_2\text{O}$  (1% Ni) crystals and also in state of dilute aqueous solution of nickel sulphate using a spectrophotometer. The bands II and III were named as 'red band' by them. Hartmann and Muller (1958) using three glass prism spectrograph and infra-red sensitized plates found this 'red band' to be single. But on enlargement of the photographs this band showed a fine structure (four peaks named by them as C, D, E and a). Three of them are of almost equal intensity, while



the fourth one is very feeble. They then interpreted some of these structures in the light of the theory put forward by Hartmann (1954) and Furlan (1957). They attributed the first two peaks (*C* and *D*) as due to tetragonal splitting, while the fourth peak (*a*) was assigned to the transition due to mixing but failed to account for the third peak (*E*) on the basis of the energy level diagram derived from ligand field splittings. According to Jorgensen (1958) also the occurrence of the peak (*E*) is a very puzzling problem. The assignment of Hartmann and Muller can not be correct for reasons to follow.

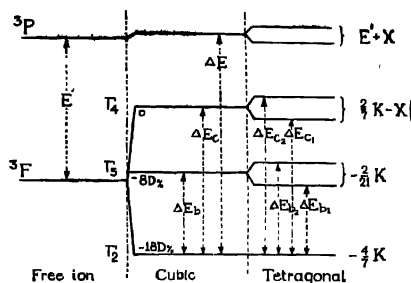


Fig. 19

This third peak can not be due to vibrational level because then it would have been much affected by solvent, solute and dilution (Freed, 1942) and also this separation ( $\sim 1300 \text{ cm}^{-1}$ ) is too high (Schultz, 1957). The intensity of this band is almost equal to the transitions from other Stark-levels and hence can not be also due to mixing (Orgel, 1955). According to Balhausen (1955) the occurrence of II and III bands is either due to tetragonal field effects or to (*L, S*) coupling effects. Jorgensen (1955) has pointed out that (*L, S*) coupling alone can not explain the occurrence of these bands.

#### b) The crystal field and energy levels

The ground state of  $\text{Ni}^{2+}$  ion ( $3d^8 \text{ } ^3F$ ) under the influence of a crystalline electric field conforming to a potential of the type,

$$V = K' \left( x^4 + y^4 + z^4 - \frac{3}{5} r^4 \right) + T'_2 (2z^2 - x^2 - y^2) + T'_4 \left( z^4 + 6x^2y^2 - \frac{3}{5} r^4 \right), \dots \quad (1)$$

where  $K = \frac{2}{5} e r^4 K'$ ,  $T'_2 = e r^2 T_2$ ,  $T_4 = e r^4 T'_4$  and  $\bar{r}^4$  is the average value for the radius of  $3d$ -electrons, splits energy levels as shown in Fig. 19.

The so split levels will be approximately, taking the lowest as zero, given by (Owen, 1955)

$$\begin{array}{l}
 {}^3P \left\{ \begin{array}{l} p_1 \quad E' + X + \frac{4}{7} K + \frac{4}{5} T_2 - \frac{16}{105} T_4 \\ p_2 \quad E' + X + \frac{4}{7} K - \frac{2}{5} T_2 - \frac{16}{105} T_4 \\ c_2 \quad \frac{6}{7} K - X + \frac{4}{35} T_2 - \frac{44}{105} T_4 \\ c_1 \quad \frac{6}{7} K - X - \frac{8}{35} T_2 - \frac{4}{105} T_4 \end{array} \right\} \dots (2) \\
 {}^3P' \left\{ \begin{array}{l} b_2 \quad \frac{10}{21} K + \frac{10}{105} T_4 \\ b_1 \quad \frac{10}{21} K - \frac{60}{105} T_4 \\ a \quad 0 \end{array} \right\}
 \end{array}$$

From the experimental observations of Owen, Holmes and McClure (1957) on single crystals of  $\text{NiSO}_4 \cdot 7\text{H}_2\text{O}$ ,  $(\text{Zn}, \text{Ni}) \cdot \text{K}_2(\text{SO}_4)_2 \cdot 6\text{H}_2\text{O}$  and  $\text{NiSiF}_6 \cdot 6\text{H}_2\text{O}$  and on aqueous solution of  $\text{NiSO}_4$ , it is seen that  $\Delta E_p \approx 3\Delta E_{b_2}$  (Fig. 19). This will be evident from the Table II., and hence  $\left( \frac{10}{105} T_4 \right)$  is very very small compared to  $\Delta E_p$ . It is seen also that we are more correct if we take  $\Delta E_p \approx 3\Delta E_b$ .

TABLE II

Crystals	$\Delta E_{b_2} = \frac{10}{21} K + \frac{10}{105} T_4$ in $\text{cm}^{-1}$	$\Delta E_p$ in $\text{cm}^{-1}$	$3\Delta E_{b_2} - \Delta E_p = \frac{10}{105} T_4$ in $\text{cm}^{-1}$
$\text{NiSO}_4 \cdot 7\text{H}_2\text{O}$	8600	25,500	300
$\text{K}_2 \cdot (\text{Zn}, \text{Ni}) \cdot (\text{SO}_4)_2 \cdot 6\text{H}_2\text{O}$	8550	25,500	150
$\text{NiSiF}_6 \cdot 6\text{H}_2\text{O}$	8550	25,500	150
$\text{NiSO}_4(\text{soln})$	8500	25,300	200

Let us assign the band I due to transition  $\frac{10}{21} K + \frac{10}{105} T_4 \rightarrow 0$  and call it as  $\Delta E_{b_2}$ . Then

$$\Delta E_b = \frac{10}{21} K - \frac{1}{3} \Delta E_p$$

and hence

$$\Delta E_{b_2} - \Delta E_b = \frac{10}{105} T_4 \quad \dots (3)$$

From the expression (3) the value of  $T_4$  can be calculated which comes out of the right order as suggested by Owen (1955). This also supports our argument that we are correct to take  $\Delta E_p = 3\Delta E_b$ .

Let us assign the other two bands II and III as due to transitions

$$\begin{aligned} C_1 &\rightarrow 0 \\ &\text{(as given by Eq. 2)} \\ C_2 &\rightarrow 0 \end{aligned}$$

and designate them by  $\Delta E_{i_1}$  and  $\Delta E_{i_2}$  respectively (Fig. 19) then following Owen, Holmes and McClure (1957) the band III can be taken as  $\Delta E_{e_1}$  or

$$\Delta E_{e_2} \approx \Delta E_e - \frac{6}{7} K - X \quad \dots (4)$$

if the effect of  $T_2$  and  $T_4$  are neglected (in this we are justified as  $T_2$  and  $T_4$  are themselves small and are of opposite sign in the expression for energy). From expression (4)  $X$  comes out as  $100 \text{ cm}^{-1}$ . This  $X$  may be neglected compared to  $\frac{6}{7} K$  while fitting the optical data. Hence we get

$$\Delta E_p = 3\Delta E_b - \frac{10}{7} K - \frac{5}{3} \Delta E_i \quad \dots (5)$$

So from a measurement of either of  $\Delta E_p$  or  $\Delta E_b$  or  $\Delta E_e$  one can evaluate  $K$  which are shown in Table III.

In nickel-amino-salts  $K$  is calculated directly without any approximation since the transition  $\Delta E_b$  is known.

$K$ -values (Table III) indicate that in state of solution all the six members of the cluster about the  $\text{Ni}^{2+}$  ion may be the same in Tutton-salts and halides etc. but in amino-salts they will be different.

c) *Evaluation of the term separation ( $E'$ )*

For ions where  ${}^4F$ -term lies lowest, the term separation  $E'$  in crystals, which is an important spectroscopic constant, can be evaluated if at least two out of the three transitions are observed (Owen, 1955). From Fig. 1 it is seen that

$$E' = \Delta E_p + \Delta E_c - 3\Delta E_b \quad (6)$$

(neglecting the small tetragonal terms)

From which we have

$$E' = \Delta E_c \quad (\text{a very good approximation}) \quad (7)$$

In amino-salts  $E'$  can be evaluated without any approximation however small they might be since all the three transitions have been observed. These are given in Table III.

TABLE III

salts	K-values cm <sup>-1</sup>	E-values cm <sup>-1</sup>	F-values cm <sup>-1</sup>	$\mu$ -values (soln.) at 300°K		$g$ -values at 300°K	
				Opti- cal	Magne- tic	Calcu- lated	Observed
NiSO <sub>4</sub>	17,725	15,200	0.900	3.278	3.319	2.280	2.20*
NiSeO <sub>4</sub>	17,725	15,220	0.901	3.278	3.258	2.280	
Ni(NH <sub>4</sub> SO <sub>4</sub> ) <sub>2</sub>	17,745	15,240	0.902	3.277	3.249	2.277	2.25**
Ni(KSO <sub>4</sub> ) <sub>2</sub>	17,745	15,220	0.901	3.277	3.314	2.277	2.25**
Ni(Rb <sub>2</sub> SO <sub>4</sub> ) <sub>2</sub>	17,725	15,150	0.896	3.268		2.276	
Ni(TlSO <sub>4</sub> ) <sub>2</sub>	17,745	15,240	0.902	3.277	3.321	2.277	2.25**
Ni(NH <sub>4</sub> SeO <sub>4</sub> ) <sub>2</sub>	17,725	15,200	0.900	3.278	3.184	2.280	
Ni(K <sub>2</sub> SeO <sub>4</sub> ) <sub>2</sub>	17,725	15,200	0.900	3.278	3.193	2.280	
NiCl <sub>2</sub>	17,725	15,270	0.904	3.278	3.245	2.280	2.21***
NiBr <sub>2</sub>	17,725	15,200	0.900	3.277	3.286	2.280	
Ni(NO <sub>3</sub> ) <sub>2</sub>	17,725	15,220	0.901	3.278	3.326	2.280	
Ni <sub>3</sub> Br <sub>2</sub> (NO <sub>3</sub> ) <sub>12</sub>	17,745	15,150	0.896	3.277		2.280	
Ni(CHOO) <sub>2</sub>	17,725	15,150	0.896	3.268		2.276	
Ni(CH <sub>3</sub> COO) <sub>2</sub>	17,725	15,200	0.900	3.278	3.322	2.280	
Ni[(NH <sub>3</sub> ) <sub>4</sub> ](SO <sub>4</sub> )	22,115	13,470	0.797				
Ni[(NH <sub>3</sub> ) <sub>4</sub> ](OH)	22,030	13,020	0.805				
Ni[(NH <sub>3</sub> ) <sub>4</sub> ](Cl)	22,470	13,070	0.773				
Ni[(NH <sub>3</sub> ) <sub>4</sub> ](CH <sub>3</sub> COO)	22,512	13,010	0.770				

\* Oio (1953)

\*\* Griffiths and Owen (1952)

\*\*\* Ting and Williams (1951)

It is observed that there is a lowering of the term separation  $E'$  for  $\text{Ni}^{++}$  ion in crystal from the free ion value of  $E = 16,900 \text{ cm}^{-1}$  (Moore, 1952)

Following Owen (1955) this lowering may be attributed to the covalency factor  $f^2$  arising from partial overlap of the  $3d$ -orbitals with  $\sigma$ - and  $\pi$ -orbitals of the surrounding atoms

$$\text{Hence} \quad \frac{E'}{E} = f^2 \quad (8)$$

where  $f^2 = f_{\sigma}^2 + f_{\pi}^2$ .

In ordinary nickel salts  $f_{\pi}^2$  is unity. From the above relation one can calculate  $f^2$  which are given in Table III

Primarily this covalency factor should not be different for all the salts in which  $\text{Ni}^{++}$  ion is similarly coordinated with six water molecules, but there might be appreciable change in the overlap between  $\text{Ni}^{++}$  ion and that of oxygen and hence in the covalency factor from salt to salt arising from the effect of distant atoms. In state of solution distant atom effect will be negligible and hence covalency factor should not vary appreciably from salt to salt with similar coordination.

An examination of the  $f^2$ -values shows that in all the nickel salts  $f^2 \approx 0.9$  except for the ammo-salts, where it tends to be 0.78. This suggests that  $f_{\pi}^2$  may not be negligible in nickel ammo-salts. As a result both  $\sigma$ - and  $\pi$ -orbital overlap may exist so that  $f_{\sigma}^2 \approx 0.9$  and  $f_{\pi}^2 \approx 0.85$  making  $f^2 = 0.76$  nearly as observed.

#### d) Evaluation of the mean magnetic moment $\mu$

Following Schlapp and Penney (1932), Griffiths and Owen (1952) the principal magnetic moments  $\mu_{||}$  and  $\mu_{\perp}$  along and normal to the axis of symmetry of the water cluster about the  $\text{Ni}^{++}$  ion are given by

$$\left. \begin{aligned} \mu_{||}^2 &= 8 \left[ \left\{ 1 + 8\lambda\alpha'_{||} + \frac{\theta_{||}}{kT} + \dots \right\} - 3kT\alpha'_{||} \right] \\ \mu_{\perp}^2 &= 8 \left[ \left\{ 1 + 8\lambda\alpha'_{\perp} + \frac{\theta_{\perp}}{kT} + \dots \right\} - 3kT\alpha'_{\perp} \right] \end{aligned} \right\} \quad \dots (9)$$

where  $\theta_{||} = 4/3\lambda^2 \cdot (\alpha'_{\perp} - \alpha'_{||})$  and  $\theta_{\perp} = 2/3\lambda^2 \cdot (\alpha'_{||} - \alpha'_{\perp})$ ,  $\lambda$  is the spin-orbit coupling constant for the free ion and is equal to  $-324 \text{ cm}^{-1}$  (Sheenstone and Willets 1951),  $\alpha'_{||}$  and  $\alpha'_{\perp}$  are the coefficients of the crystal field.

From the relation (9)

$$\mu^2 = \frac{\mu_{||}^2 + 2\mu_{\perp}^2}{3} = 8\{1 + (8\lambda - 3kT)\alpha'\} \quad \dots (10)$$

where

$$\alpha' = \frac{\alpha'_1 + 2\alpha'_2}{3} - \frac{f^2}{\Delta E_b} = -2.1 \frac{f^2}{K}.$$

Hence utilising our  $K$ -values and  $f^2$ -values  $\mu$  for  $\text{Ni}^{2+}$  ion in different salts in state of solution are evaluated and given in Table IV. In order to check these deduced values we have measured the magnetic susceptibilities of nickel salts in state of aqueous solution at concentrations of optical measurements by modified Curie balance (unpublished, D. Neogy). These are also given in Table IV. There is a close agreement between these two sets of values.

(e) *Calculation of the splitting factor 'g'.*

According to Owen (1955) the splitting factor for  $\text{Ni}^{2+}$  ion is given by the relation

$$g = 2 - \frac{128\lambda}{K} \cdot f^2 \quad \dots (14)$$

where the symbols have their usual meaning.

Thus one can calculate  $g$ -values in state of solution from the optically observed  $K$  and  $f^2$ -values. These are given in Table IV. Directly measured  $g$ -values in state of solution are not available for comparison. However, it is interesting to note that  $g$ -values for some of the nickel salts in crystalline state do not differ much from our evaluated values.

(f) *Anisotropy of the cluster about the  $\text{Ni}^{2+}$  ion in state of solution.*

For the octahedrally coordinated  $\text{Ni}^{2+}$  ion, in the salts studied the predominant cubic component of crystalline electric field acting upon it from the surrounding charges splits its original  $J$ -multiplet state  $3d^8 {}^3F$  into an orbital singlet lying at about  $10^4 \text{ cm}^{-1}$  below the two triplets. A very small rhombic component of the field removes the orbital degeneracy of the triplets. Van Vleck (1932), Schlapp and Penney (1932), Griffiths and Owen (1952), Bleaney and Stevens (1953) and Stevens (1953) have calculated the three principal susceptibilities under the above conditions. Bose *et al.* (1958) have shown that on the assumption of an approximate tetragonal symmetry and since in nickel salts  $K_{\perp}$ , susceptibility normal to the tetragonal axis is greater than  $K$ , that along the tetragonal axis, the anisotropy of the individual paramagnetic unit is given by

$$\left. \begin{aligned} \Delta K = K_{\perp} - K_{\parallel} &= \frac{8N\beta^2}{3kT} \left\{ 8\lambda - 3kT - \frac{2\lambda^2}{kT} + G \right\} \times (\alpha_{\perp} - \alpha_{\parallel}) f^2 \\ \text{where } G &= 16\lambda^2 (\alpha_{\perp} + \alpha_{\parallel}) f^2 + \frac{2\lambda}{3kT} [(\alpha_{\perp} + 2\alpha_{\parallel}) f^2 + 2\lambda \{\alpha_{\perp}^2 + 2\alpha_{\parallel}^2\} f^4] \end{aligned} \right\} \dots (12)$$

and  $\alpha_{\perp}$  and  $\alpha_{\parallel}$  are the principal field coefficients related to the splittings of the orbital levels in a tetragonal field.

$\alpha_{\perp}$  and  $\alpha_{\parallel}$  must be known from optical observations before one can calculate  $\Delta K$ . This is done in the following manner

As shown in Fig. 20 the split levels in a tetragonal field are named as  $\Delta E_{e_2}$ ,  $\Delta E_{e_1}$ ,  $\Delta E_{b_2}$  and  $\Delta E_{b_1}$ . Then we will have

$$\left. \begin{aligned} \frac{1}{\alpha_{\parallel}} &= \Delta E_{e_2} \quad \text{and} \quad \frac{1}{\alpha_{\perp}} = \Delta E_{e_1} \\ \text{further} \quad \frac{1}{\alpha_{\parallel}} &= \Delta E_{b_2} \quad \text{and} \quad \frac{1}{\alpha_{\perp}} = \Delta E_{b_1} \end{aligned} \right\} \dots (13)$$

When the tetragonal components are absent the mean centres are  $\Delta E_a$  and  $\Delta E_b$  which are related as

$$\Delta E_r = 1.8 \Delta E_b \quad (14)$$

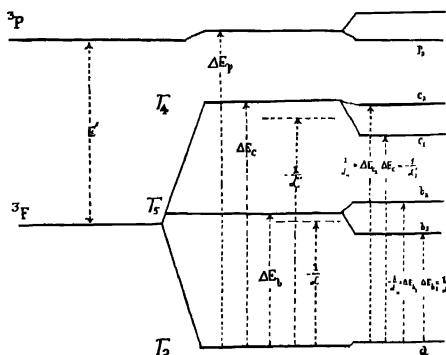


Fig. 20. The effect of tetragonal field on  $\alpha$  and  $\alpha''$ .

The effect of the tetragonal field is to make the mean centres as  $-\frac{1}{\alpha''}$  and  $\frac{1}{\alpha}$ , where

$$\alpha'' = \frac{\alpha_{\parallel} + 2\alpha_{\perp}}{3}, \quad \alpha = \frac{\alpha_{\parallel} + 2\alpha_{\perp}}{3}$$

and

$$\alpha = 1.8\alpha''$$

Since we have observed  $\Delta E_{e_2}$  and  $\Delta E_{e_1}$ , hence  $\alpha''$  can be calculated.

From the expression (2) it can be seen that

$$\alpha = 1.8\alpha'' = \frac{1}{3} \left[ \frac{1}{A+B} + \frac{2}{A-6B} \right]$$

where  $A = \frac{10}{21} K$  and  $B = \frac{10}{105} T_4$

Thus the value of  $T_4$  for different salts can be evaluated. These are included in Table IV. Hence using the values of  $K$  and  $T_4$  for different salts in Eq. (13)  $\alpha_{\perp}$  and  $\alpha_{\parallel}$  are immediately obtained and from which  $\Delta K$ . These values are shown in Table IV.

We have included  $\Delta K$ -values so calculated in Table IV and for comparison given the  $\Delta K$ -values from magnetic measurements by Bose *et al.* (1958). The difference that is observed between the anisotropies of the paramagnetic unit in state of aqueous solution and in crystalline state can be well understood follow-

TABLE IV

Salts	$T_4$	$\alpha_{\perp} \times 10^5$	$-\alpha_{\parallel} \times 10^5$	Optical $\Delta K \times 10^6$	Magnetic
(a) Sulphate Series					
Heptahydrate	1315	13.005	11.675	204	258
NH <sub>4</sub>	1315	13.007	11.675	204.8	210*
K	1351	13.987	11.666	204	261.7
Rb	1430	13.123	11.660	223	280.1
Tl	1365	13.038	11.654	211.8	221.1
(b) Selenate Series					
Hexahydrate	1386	13.072	11.665	215.3	370
NH <sub>4</sub>	1339	13.020	11.671	208	212**
K	1339	13.020	11.671	208	234.5
(c) Halide Series					
Cl <sub>2</sub>	1290	12.987	11.679	201	
Br <sub>2</sub>	1315	13.012	11.665	212	
(d) Nitrate Series					
(NO <sub>3</sub> )	1315	13.005	11.675	204	
Bi	1733	13.405	11.609	274	
(e) Organic Base Series					
(C <sub>12</sub> H <sub>22</sub> O <sub>11</sub> )	1430	13.123	11.660	223	
(CH <sub>3</sub> ) <sub>2</sub> COO	1315	13.005	11.675	204	370***

Krishnan *et al.* (1933.)

\*\* Mookherji (1946.)

\*\*\* Muthur (unpublished)



ing Van Vleck (1939), Bose *et al.* (1958) and Bose and Mitra (1952). According to them the major cubic field arises from the water cluster about the  $\text{Ni}^{++}$  ion in the hydrated salts and hence leaves an orbital singlet lowest in the Stark-pattern. The primary Jahn-Teller effect can very feebly distort the water cluster resulting in the feeble anisotropy of the electric field about the  $\text{Ni}^{++}$  ion. In order to explain 5% to 8% anisotropy of the cluster there must be an additional distortion of the  $[\text{Ni}(\text{H}_2\text{O})_6]^{++}$  cluster. This is supplied by the field of charges or dipoles outside the cluster i.e. by the effect of the distant atoms. Now in state of solution this effect of distant atoms will be very small and hence the additional distortion. As a result magnetic anisotropy  $\Delta K$  of  $[\text{Ni}(\text{H}_2\text{O})_6]^{++}$  cluster in state of solution should differ from that of crystalline state. It is observed that this distant atom effect is very much pronounced in the double sulphates and selenates of *K*, *Rb* and single sulphate and not so much pronounced in double sulphates and selenates of  $\text{NH}_4$  and  $\text{Li}$ .

We have made measurements with a single crystal of  $\text{Ni.K}_2(\text{SO}_4)_2.6\text{H}_2\text{O}$ . The observed bands are at  $14,145\text{ cm}^{-1}$ ,  $15,550\text{ cm}^{-1}$  and  $26,000\text{ cm}^{-1}$ . The calculated value of  $K$  is  $18,197\text{ cm}^{-1}$ ,  $E'$  is  $15,550\text{ cm}^{-1}$  and hence  $f^2 = 0.92$ . Taking this  $f^2$  value and  $K$  we have calculated  $\mu$ ,  $g$  and  $\Delta K$  values. These are as follows.

	Calculated	Observed
$\mu$	3.27	3.18
$g$	2.28	
$\Delta K$	240	261.4

The agreement between the observed values and calculated values is very good.

If one accepts the findings of Hartmann and Müller (1958) that the tetragonal splitting in  $\text{NiSO}_4.7\text{H}_2\text{O}$  and  $\text{NiSO}_4.6\text{H}_2\text{O}$  crystals is  $\sim 400\text{ cm}^{-1}$  as correct and calculate  $\Delta K$  then one gets a very absurd value of  $\Delta K$ . For heptahydrate  $\Delta K$  comes out as  $530 \times 10^{-6}$  as against 254 (magnetic measurements) and for hexahydrate the same value as against 354 (magnetic measurements). Thus the findings of Hartmann and Müller can not be correct.

#### ACKNOWLEDGMENTS

The work was carried out at the Physics Laboratories of Agra College, Agra. We wish to express our sincere thanks to University Grants Commission due to whose generous grant it was possible to purchase the 'Unispek' spectrophotometer which enabled us to carry out this piece of work.

Our sincere thanks are also due to Professor A. Bose, D.Sc., F.N.I., for his helpful criticisms and concrete suggestions.

## REFERENCES

- Bethe, H., 1929, *An. Physik*, **8**, 133.  
 Bethe, H., 1930, *Z. Physik*, **60**, 218.  
 Bloaney, B. and Stevenson, K. W. H., 1953, *Rep. Progr. Phys.*, **16**, 108.  
 Bose, A. and Mitra, S. K., 1952, *Ind. Jour. Phys.*, **26**, 393.  
 Bose, A., Mitra, S. K. and Datta, S. K., 1958, *Proc. Roy. Soc.*, **A248**, 153.  
 Ballhaussen, 1955, C. J. Kgl Danske Vindenskab., Selskab, Mat. fgs. Medd. No. 8, 29  
 Dreisch, Th. and Trommer, W., 1937, *Z. Phys. Chem.*, **B 37**, 40.  
 Dreisch, Th. and Kallscheuer, O., 1939, *Z. Phys. Chem.*, **B 45**, 19.  
 Freed, S., 1942, *Rev. Mod. Phys.*, **14**, 105.  
 Furlanot, 1957, *Z. Physik Chem.*, **10**, 291.  
 Gorter, C. J., 1932, *Phys. Rev.*, **42**, 437.  
 Griffiths, J. H. and Owen, J., 1952, *Proc. Roy. Soc.*, **A213**, 451.  
 Hartmann, H., 1954, *Theorie der chemischen Bindung auf quantentheoretischer Grundlage*. Springer verlag.  
 Hartmann, H. and Muller, 1958, *Discussions of Farad., Soc.*, **26**, 49.  
 Jorgensen, CHR. Kluxbull, 1955, *Acta. Chem. Scand.*, **9**, 1362.  
 „ 1958, *Discussions of Farad. Soc.*, **26**, 90.  
 Krishnan, K. S., Chakravorty, N. C. and Banerjee, S., 1933, *Philos Trans.*, **232**, 99.  
 Mookherji, A., 1946, *Ind. Jour. Phys.*, **20**, 9.  
 Mookherji, A. and Chhonkar, N. S., 1959, *Ind Jour. Phys.* **42**, 74.  
 Moore, C. E. 1952, Atomic Energy Levels—Nat. Bur. Stand. circ. 467, Vol. II.  
 Orgul, L. E., 1955, *J. Chem. Phys.*, **23**, 1004.  
 Owen, J., 1955, *Proc. Roy. Soc.*, **227**, 183.  
 Owen, G. Holmes and Donald S. McClure, 1957, *J. Chem. Phys.*, **26**, 1686  
 Ono, 1953, *J. Phys. Soc. Japan*, **8**, 802.  
 Polder, D., 1942, *Physika*, **9**, 709.  
 Schlapp, R. and Penney, W. G., 1932, *Phys. Rev.*, **42**, 1666.  
 Schultz, M. L., 1942, *J. Chem. Phys.*, **10**, 194.  
 Stevenson, K. W. H., 1953, *Proc. Roy. Soc.*, **A219**, 542.  
 Schonstone and Willets, 1951, *Phys. Rev.*, **41**, 208.  
 Ting and Williams, 1951, *Phys. Rev.*, **82**, 507.  
 Van Vleck, J. H., 1932, *Phys. Rev.*, **41**, 208.  
 Van Vleck, J. H., 1939, *J. Chem. Phys.*, **61**, 72.

# ON THE ELECTRONIC SPECTRA OF 2-BROMO-AND 3-BROMOPYRIDINE IN DIFFERENT STATES AND IN SOLUTIONS

T N MISRA

OPTICS DEPARTMENT, INDIAN ASSOCIATION FOR THE CULTIVATION  
OF SCIENCE, CALCUTTA 32.

(Received, May 30, 1960)

**ABSTRACT.** The ultraviolet absorption spectra of 2-bromo- and 3-bromopyridine in all the three phases and also of their solutions have been investigated and a tentative assignment of the bands of the vapours has been made

In the vapour phase, 3-bromopyridine exhibits two systems of discrete bands, one due to the  $n \rightarrow \pi^*$  transition (Transition I) and the other due to  $\pi \rightarrow \pi^*$  transition (Transition II). In the liquid state, in the solid state at  $-180^\circ\text{C}$  and in solution in alcohol, the  $n \rightarrow \pi^*$  transition is absent and only one system of bands due to  $\pi \rightarrow \pi^*$  transition is observed. In the spectrum due to the solution in 3-methyl pentane, however, the  $n \rightarrow \pi^*$  transition persists. It is suggested that the molecules of 3-bromopyridine form associated groups through the nitrogen  $sp^2$  electron and the hydrogen atom of neighbouring molecules in the states of aggregation of the pure substance.

In the case of 2-bromopyridine it is confirmed that the  $n \rightarrow \pi^*$  transition is absent not only in the state of aggregation and in solution in alcohol but also in its spectra due to the vapour phase and solution in 3-methyl pentane probably due to the intramolecular inductive influence of the bromine atom on the  $sp^2$  electron of the adjacent nitrogen atom as suggested by earlier workers.

## INTRODUCTION

It is now an established fact (Kasha, 1950, Rush and Sponer, 1952) that in the near ultraviolet absorption spectrum of *N*-heterocyclic compounds in the vapour state there is a second system of bands due to the excitation of a nonbonding  $sp^2$  electron of the nitrogen atom to the first unfilled  $\pi$ -molecular orbital of the ring called  $n \rightarrow \pi^*$  transition besides the system due to  $\pi \rightarrow \pi^*$  transition.

Recently, Banerjee (1956, 1957) studied the absorption spectra of pyridine and the three isomeric picolines in the liquid state and in the solid state at low temperature and observed that the second system of bands due to the  $n \rightarrow \pi^*$  transition disappears with liquefaction of the vapour and it is absent also in the spectrum due to the substances in the solid state. The absence of the  $n \rightarrow \pi^*$  transition in the liquid and solid states was explained by him on the assumption that in these states of aggregation the molecules are associated through weak

virtual bonds formed by the non-bonding electron of the nitrogen atom and the hydrogen atom of neighbouring molecules

Roy (1958) studied the absorption spectra of solutions of pyridine in different solvents and obtained both  $n \rightarrow \pi^*$  and  $\pi \rightarrow \pi^*$  transitions in solutions in cyclohexane, 3-methyl pentane and carbon tetrachloride. But in the spectrum due to the solution in isobutyl alcohol, the  $n \rightarrow \pi^*$  transition was found to be absent and this was attributed to the formation of a bond between the pyridine molecule and the OH group of alcohol molecule through the non-bonding electron of the nitrogen atom.

Stephenson (1954) studied the absorption spectra of some substituted pyridine compounds including 2-bromopyridine and 3-bromopyridine dissolved in iso-octane and ethyl alcohol. In the case of solution of 3-bromopyridine in ethyl alcohol the  $n \rightarrow \pi^*$  transition was found to be absent, but it appeared in the spectrum due to the solution in iso-octane. In the case of 2-bromopyridine, however, no change in intensity was observed in the low energy region when the solvent was changed from iso-octane to alcohol. The  $n \rightarrow \pi^*$  transition was found to be absent also in the spectrum due to vapour of this substance. He concluded from these results that the  $n \rightarrow \pi^*$  transition was absent in the spectrum due to 2-bromopyridine. He explained this absence of the  $n \rightarrow \pi^*$  transition on the assumption that inductive attraction of halogen atom attached to the adjacent carbon atom increases the binding energy of the nonbonding electrons of the nitrogen atom and consequently the bands due to the  $n \rightarrow \pi^*$  transition are shifted to the region of the bands due to  $\pi \rightarrow \pi^*$  transition.

The present work was undertaken to investigate the ultraviolet absorption spectra of 2-bromo- and 3-bromopyridine in the vapour state and to analyse the bands, if possible, because Stephenson (1954) had not analysed these bands. It was also intended to find out whether the  $n \rightarrow \pi^*$  transition is actually absent in the case of 2-bromopyridine in the vapour state.

The absorption spectra of these compounds in the solid and liquid states and in solutions in different solvents have also been studied in order to compare these spectra with those due to the substances in the vapour state.

## EXPERIMENTAL

Chemically pure samples of 2-bromo- and 3-bromopyridine supplied by Fluka, Switzerland, were fractionated and the proper fractions were distilled under reduced pressure before use. To study the spectra due to the vapour absorption, cells of length 50 cm and 10 cm were used. The cell was filled up with the vapour at saturation vapour pressure at different temperatures and the spectra due to the vapour at different densities were photographed. Two separate electrical heaters, one for the absorption cell and the other for the bulb containing the liquid and

attached to the absorption cell, were used to control the temperature. The reservoir containing the liquid was always kept at a temperature about 5°C lower than that at any part of the absorption cell. To produce a low pressure in the vapour in the absorption tube, the tube was kept at the room temperature while the bulb containing the liquid was immersed in a suitable low temperature bath.

To record the bands due to  $\pi \rightarrow \pi^*$  transition in 3-bromopyridine, the 10 cm cell was used and it was kept at the room temperature while the reservoir was kept at 0°C. The 50-cm cell under similar conditions was used to record the bands due to the  $n \rightarrow \pi^*$  transition. In the case of 2-bromopyridine an absorption cell of length 50 cm was used and the reservoir was kept at 0°C for studying the  $\pi \rightarrow \pi^*$  transition and at 50°C for studying  $n \rightarrow \pi^*$  transition.

Very thin films of thickness of the order of a few microns of the substances in the liquid and solid states were required to produce absorption bands due to  $\pi \rightarrow \pi^*$  transition. Thicker films of the liquids were also used to find out whether bands corresponding to  $n \rightarrow \pi^*$  transition were present.

The solvents used to study the absorption spectra of the substances in the solutions were ethyl alcohol and 3-methyl pentane. The solvents were found to produce no absorption band in the region under consideration. In this case, a brass cell 5mm thick provided with quartz windows was used and the strength of the solution was varied from .01% to .08% by weight. Spectrograms were taken on Agfa Isopan film with a Huger E 1 spectrograph giving a dispersion of the order of 3Å per mm in the region of 2600Å. Iron arc spectrum was taken on each spectrogram as a comparison.

Microphotometric records were taken with a Kipp and Zonen self-recording microphotometer. The absorption spectra were calibrated with the help of microphotometric records of the iron lines using the method described in an earlier paper (Sirkar and Misra, 1959).

As the Raman and infrared spectra of these two substances had not been studied by previous workers, infrared absorption spectra of very thin films of the substances were recorded with a Perkin-Elmer Model 21 spectrophotometer using rock salt optics in order to find out the ground state vibrations and these were used to verify the excited state frequencies derived from the ultraviolet absorption spectra.

## RESULTS AND DISCUSSION

Microphotometric records of the absorption spectra of 3-bromo- and 2-bromopyridine in different states and in solutions are reproduced in Figs. 1-6. The wave numbers of the bands in  $\text{cm}^{-1}$ , approximate intensities and their probable assignments are given in Tables I, II, III and IV.

### 3-Bromopyridine

#### (a) Spectrum of the vapour phase.

The absorption spectrum of 3-bromopyridine in the vapour phase (Fig. 1) shows two distinct systems of bands under different conditions of pressure and length of absorbing column of the vapour. With the vapour at the saturation pressure at 4°C and with an absorption tube 50 cm long, a system of absorption bands starting at about 35000  $\text{cm}^{-1}$  followed by region of complete absorption is observed. The bands of this system are sharp and narrow and following Kasha (1950), they have been attributed to the  $n \rightarrow \pi^*$  transition (Transition I). At lower pressure of the vapour in a shorter cell, the second band system appears in the region 36000  $\text{cm}^{-1}$  to 39000  $\text{cm}^{-1}$  and the broad bands of this system resemble those due to other substituted benzenes arising from the  $\pi \rightarrow \pi^*$  transition (Transition II). The analysis of the bands of these two systems is discussed separately in the following sections

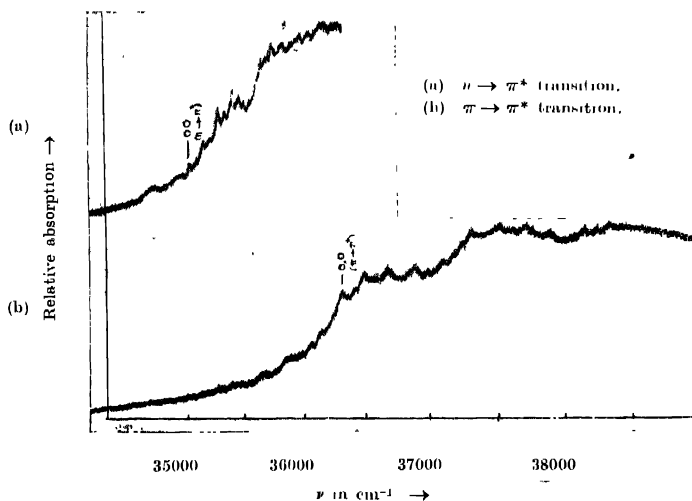


Fig. 1. Microphotometric records of the ultraviolet absorption spectra of 3-bromopyridine in the vapour state.

#### i) $\pi \rightarrow \pi^*$ transition (Transition II)

The strong band at 36300  $\text{cm}^{-1}$  in this system has been taken as the 0, 0 band. Most of the remaining strong bands represent transitions involving excited state

TABLE I  
Ultraviolet absorption bands of 3-bromopyridine in the vapour phase

Wave no. (cm <sup>-1</sup> ) and intensity	Assignment	Wave No. (cm <sup>-1</sup> ) and intensity	Assignment
Transition I ( $n \rightarrow \pi^*$ )		Transition II ( $\pi \rightarrow \pi^*$ )	
34778 (wb, diffuse)	?	35866 (mw)	0-434
34925 (wb, diffuse)	'	35986 (w)	0-314
35080 (w)	0, 0	36064 (mw)	0-236
35183 (s)	0   103	36123 (w)	0-177
35238 (w)	0   158	36300 (s)	0, 0
35310 (s)	0   230	36458 (s)	0-158
35359 (s)	0   279	36526 (w)	0   226
35412 (w)	0+103+230	36579 (s)	0-279
35429 (s)	0   349	36672 (s)	0   372
35460 (s)	0   158   230	36835 (s)	0   158+372
35517 (ms)	0   2   103   230	36875 (s)	0   575
35564 (ms)	0+2   103+279	36971 (w)	0   671
35621 (w)	0+2   158   230	37081 (m)	0   781
35659 (m)	0   579	37163 (m)	0   863
35702 (w)	0   158+2   230	37246 (m)	0   946
35752 (m)	0   2   103+2   230	37309 (s)	0   1009
35857 (s, b)	0+2   158+2   230 ( $\pi \rightarrow \pi^*$ )	37532 (s)	0+372+863
35986 (ms, b)	0+2   279+349 ( $\pi \rightarrow \pi^*$ )	37721 (s)	0-1421
36062 (ms, b)	0+2   349+279 ( $\pi \rightarrow \pi^*$ )	37884 (s)	0   375   1009
		38171 (s)	0   863   1009
		38247 (m)	0-946   1009
		38324 (m)	0+2   1009

vibrational frequencies 158, 226, 279, 372, 575, 671, 781, 863, 946, 1009 and 1421 cm<sup>-1</sup> and also ground state frequencies 177, 236, 314 and 430 cm<sup>-1</sup> as shown in Table I. In order to find out the ground state vibrational frequencies, the infrared absorption spectrum of a very thin film of 3-bromopyridine with NaCl optics was studied. The wave numbers of the observed infrared bands are 695(s),

785(s), 870(vw), 1002(s), 1082(s), 1090(h)\*, 1188(vw), 1319(vw), 1416(s), 1462(ms), 1558(h) and 1572(ms). The strength of the absorption at the bands are given in parentheses.

The infrared absorption bands at  $695\text{ cm}^{-1}$ ,  $785\text{ cm}^{-1}$ ,  $870\text{ cm}^{-1}$ ,  $1002\text{ cm}^{-1}$  and  $1082\text{ cm}^{-1}$  may be the ground state frequencies corresponding to the excited state frequencies  $671\text{ cm}^{-1}$ ,  $781\text{ cm}^{-1}$ ,  $863\text{ cm}^{-1}$ ,  $946\text{ cm}^{-1}$  and  $1009\text{ cm}^{-1}$  respectively. The absorption band apparently arising from the excited state frequency  $1421\text{ cm}^{-1}$  may have actually been produced by two excited state vibrations, the corresponding ground state frequencies being  $1416\text{ cm}^{-1}$  and  $1462\text{ cm}^{-1}$  observed in the infrared and thus may explain why this band is broader than the other bands.

The ground state values of the excited state frequencies  $158\text{ cm}^{-1}$ ,  $226\text{ cm}^{-1}$ ,  $279\text{ cm}^{-1}$  and  $372\text{ cm}^{-1}$  may probably be  $177\text{ cm}^{-1}$ ,  $236\text{ cm}^{-1}$ ,  $314\text{ cm}^{-1}$  and  $430\text{ cm}^{-1}$  respectively observed on the longer wavelength side of the 0,0 band as  $v \rightarrow 0$  transitions.

(ii)  $n \rightarrow \pi^*$  transition (Transition I)

The  $n \rightarrow \pi^*$  transition of 3-bromopyridine lies in the region  $35000\text{ cm}^{-1}$  to  $36000\text{ cm}^{-1}$ . Assuming the band at  $35080\text{ cm}^{-1}$  as the 0,0 band of this system, the other bands can be assigned as progression of frequencies 103, 158, 230, 279, 349 and  $579\text{ cm}^{-1}$  and their combinations as shown in Table I. The bands at  $35857\text{ cm}^{-1}$ ,  $35986\text{ cm}^{-1}$  and  $36062\text{ cm}^{-1}$  are not narrow line-like bands unlike the other bands of this system. The high intensity and large breadth of these bands may be due to superposition of bands due to  $n \rightarrow \pi^*$  on the bands of the  $\pi \rightarrow \pi^*$  transition. Thus the band at  $35857\text{ cm}^{-1}$  may be assigned as an  $n \rightarrow \pi^*$  transition  $(0 + 2 \times 158 + 2 \times 230)$  superimposed on the  $(0 - 434)$  band of the  $\pi \rightarrow \pi^*$  transition. Similarly, the other two bands are formed by superposition of the bands  $(0 + 2 \times 279 + 349)$  and  $(0 + 2 \times 349 + 279)$  of  $n \rightarrow \pi^*$  system on the bands  $(0 - 314)$  and  $(0 - 236)$  of the  $\pi \rightarrow \pi^*$  system respectively.

No attempt has been made to assign the two broad diffuse bands at  $34778\text{ cm}^{-1}$  and  $34925\text{ cm}^{-1}$  since they have structures entirely different from those of bands due to both  $n \rightarrow \pi^*$  and  $\pi \rightarrow \pi^*$  transitions.

(b) Spectra of the solutions

In the spectrum of .01% solution of 3-bromopyridine in ethyl alcohol (Fig. 2) only three broad bands are observed in the region  $36000\text{ cm}^{-1}$  to  $38000\text{ cm}^{-1}$ , the 0,0 band being assumed to be at  $36197\text{ cm}^{-1}$ . The other two bands form progression of excited state frequency  $966\text{ cm}^{-1}$  and its harmonics. The nature and position of these bands suggest that they belong to the  $\pi \rightarrow \pi^*$  system. With increased concentration, the long wavelength side was photographed, but no

\* 'h' indicates a hump in the absorption curve.



band system corresponding to the  $n \rightarrow \pi^*$  transition observed in the vapour could be detected.

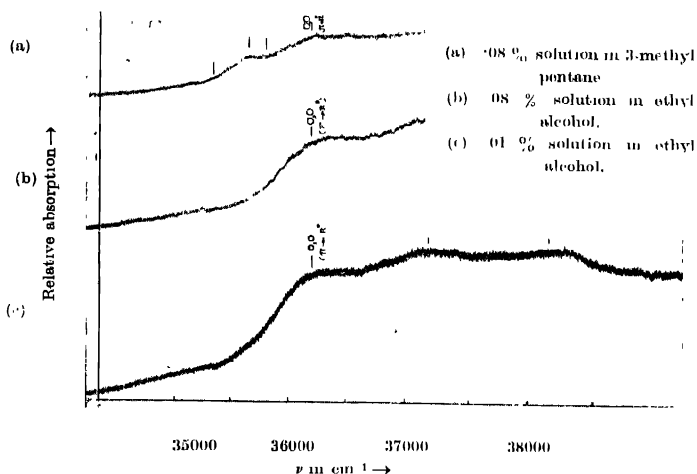


Fig. 2. Microphotometric records of the ultraviolet absorption spectra of solutions of 3-bromopyridine

In the spectrum due to the solution in 3-methyl pentane a broad band extending from  $35327 \text{ cm}^{-1}$  to  $35806 \text{ cm}^{-1}$  with the peak at  $35650 \text{ cm}^{-1}$  was observed which probably corresponds to the  $n \rightarrow \pi^*$  transition. The structure was, however, not resolved. The result is in agreement with that reported by Roy (1958) who observed the  $n \rightarrow \pi^*$  transition in solution of pyridine in 3-methyl pentane and it was found to be absent in the solution in isobutyl alcohol. This absence of  $n \rightarrow \pi^*$  transition in solution in alcohol was explained by Stephenson (1954) and Roy (1958) by assuming that in the solution in alcohol, the non-bonding  $sp^2$  electrons of the nitrogen atom become involved in formation of a hydrogen bond while in the solution in 3-methyl pentane no such bond-formation takes place.

(c) *Spectra in the solid and liquid states*

Both in the liquid and solid states (Fig. 3a and 3b) only one system of broad bands corresponding to the  $\pi \rightarrow \pi^*$  transition is produced by this substance and the system due to  $n \rightarrow \pi^*$  transition did not appear even when a thick film was used as the absorber

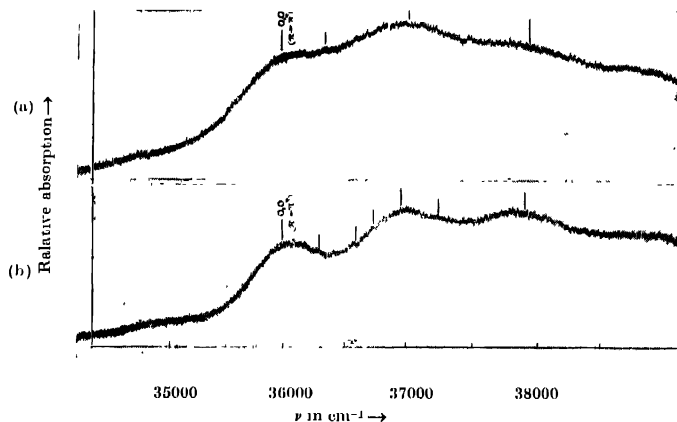


Fig. 3. Microphotometric records of the ultraviolet absorption spectra of 3-bromopyridine

(a) Liquid at 32°C.

(b) Solid at -180°C.

TABLE II

Ultraviolet absorption bands of 3-bromopyridine

Liquid at 32°C		Solid at -180°C		Solution at 32°C	
Wave No. (cm <sup>-1</sup> ) and intensity	Assignment	Wave No. (cm <sup>-1</sup> ) and intensity	Assignment	Wave No. (cm <sup>-1</sup> ) and intensity	Assignment
Transition I					
Absent		Absent		.08% sol. in alcohol	.08% sol. in 3-methyl pentane
				Absent	Broad band extended from 35327 cm <sup>-1</sup> to 35806 cm <sup>-1</sup>
Transition II					
35973 (s) 0, 0		35986 (s) 0, 0		.01% sol in alcohol	
		36268 (w) 0+282		36197 (s) 0, 0	
36329 (m) 0+356		36570 (mw) 0+584			
		36713 (m) 0+727			
36943 (s) 0+970		36951 (s) 0+965		37163 (s) 0+966	
		37247 (m) 0+1261			
37913 (s) 0+2×970		37920 (ms) 0+2×965		38134 (s) 0+2×966	

In the spectrum due to the liquid the 0,0 band has been identified with that at  $35973\text{ cm}^{-1}$  and the other bands indicate a progression of vibrational frequencies  $356$  and  $970\text{ cm}^{-1}$  in the excited state. The 0,0 band of this system thus shifts by about  $327\text{ cm}^{-1}$  towards red with the change from the vapour to the liquid state.

When the liquid is solidified and cooled to  $-180^{\circ}\text{C}$ , the bands become sharper and assuming the 0,0 band to be at  $35986\text{ cm}^{-1}$ , the spectrum can be analysed into a progression of the excited state frequencies  $282$ ,  $584$ ,  $726$ ,  $965$  and  $1261\text{ cm}^{-1}$ . With the solidification of the liquid and lowering of temperature to  $-180^{\circ}\text{C}$ , the 0,0 band does not show any further appreciable shift. It is thus evident that the major shift in the position of the 0,0 band occurs when the change of vapour to liquid state takes place.

Similar disappearance of bands due to  $n \rightarrow \pi^*$  transition in the liquid and solid states was observed in the case of pyridine and the isomeric picolines (Banerjee, 1956 and 1957). This was explained by assuming that in the condensed phases, the molecules of these compounds form associated groups through the nitrogen non-bonding electron and hydrogen atom of the neighbouring molecules. The results observed in the case of 3-bromopyridine also seem to corroborate the view mentioned above and indicate a similar association of molecules in the liquid and solid states.

It can be seen from Table II that a single excited state frequency  $970\text{ cm}^{-1}$  occurs in the case of the liquid and  $965\text{ cm}^{-1}$  in the case of the solid state in place of two such frequencies  $946\text{ cm}^{-1}$  and  $1016\text{ cm}^{-1}$  observed in the spectrum due to the vapour. This is evidently due to broadening of the bands in the former cases caused by the intermolecular field and to consequent overlapping which gives a mean frequency.

## *2-bromopyridine*

### *(a) Spectrum in the vapour phase*

The spectrum due to the 2-bromopyridine in the vapour state yields only one system of discrete bands in the region  $37000\text{ cm}^{-1}$  to  $39000\text{ cm}^{-1}$ , as can be seen from Figs. 4a and 4b. With the increase in the length of the absorbing path and in the pressure of the absorbing vapour, unlike in the case of 3-bromo isomer, no sharp, narrow and line-like bands due to  $n \rightarrow \pi^*$  transition were observed in this case. The weak continuous absorption extending up to about  $900\text{ cm}^{-1}$  on the long wavelength side of the 0,0 band due to the  $\pi \rightarrow \pi^*$  transition at higher temperature and pressure observed in this case may be due to  $v \rightarrow 0$  transition coupled to the electronic transition in  $\pi \rightarrow \pi^*$  system. Thus the  $n \rightarrow \pi^*$  system is absent in this case. These results thus agree with those reported by Stephenson (1954).

(i)  $\pi \rightarrow \pi^*$  transition (Transition II)

The strong band at  $36958 \text{ cm}^{-1}$  has been taken to be the 0,0 band and the analysis of the other bands has yielded the excited state vibrational frequencies 136, 280, 653, 742, 954, 1053 and  $1554 \text{ cm}^{-1}$  as shown in Table III.

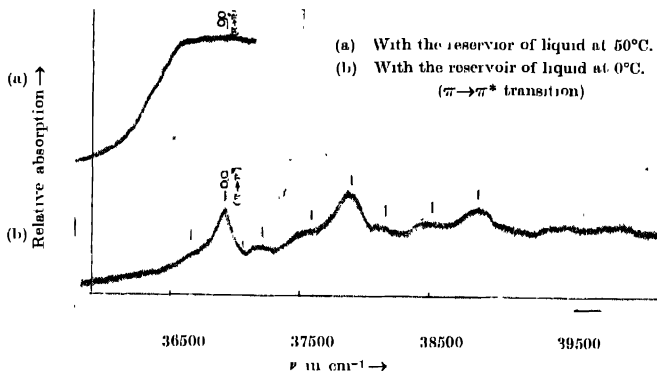


Fig. 4 Microphotometric records of ultraviolet absorption spectra of 2-bromopyridine in the vapour state.

The infrared absorption spectra of a very thin film of 2-bromopyridine was studied with rocksalt optics in order to find out the ground state vibrational frequencies. The wave numbers of the observed infrared bands are 698 (ms), 756 (s), 988(ms), 1040(w), 1075(s), 1103(s), 1148(vw), 1282(vw), 1418(s), 1451(ms) and  $1563(s)$ , the strengths of absorption being given in the parentheses.

The upper state vibrational frequencies 653, 742 and  $954 \text{ cm}^{-1}$  can be correlated to the ground state frequencies 698, 756 and  $988 \text{ cm}^{-1}$  observed in the infrared absorption. The vibrational frequencies  $1053 \text{ cm}^{-1}$  and  $1554 \text{ cm}^{-1}$  in the excited state probably correspond to the infrared frequencies  $1075 \text{ cm}^{-1}$  and  $1563 \text{ cm}^{-1}$  respectively.

As regards the band at a distance of  $280 \text{ cm}^{-1}$  on the shorter wavelength side of the 0,0 band, a band at  $292 \text{ cm}^{-1}$  on the longer wavelength side has been recorded. This band which probably represents the ground state frequency has not been observed in the infrared absorption because of limitation of NaCl optics used. The band at  $136 \text{ cm}^{-1}$  on the shorter wavelength side of the 0,0 band might represent a  $0 \rightarrow v'$  transition. The assignment is not improbable for such low frequency transition is observed in the case of 3-bromo isomer and other substituted pyridine compounds (Rush and Spomer, 1952).

TABLE III

Ultraviolet absorption bands of 2-bromopyridine in the vapour state

Wave No. ( $\text{cm}^{-1}$ ) and intensity	Assignment	Wave No. ( $\text{cm}^{-1}$ ) and intensity	Assignment
Transition I		Transition II	
Absent		36006 (w)	0-292
		36958 (s)	0, 0
		37094 (w)	0   136
		37238 (m)	0   280
		37611 (m)	0   653
		37700 (w)	0   742
		37912 (s)	0   954
		38011 (vw)	0   1053
		38178 (m)	0   1220
			0   280   954 }
		38512 (ms)	0   1554
		38870 (s)	0   2   954

A comparison of the absorption spectra of 2-bromopyridine and pyridine in the vapour state shows that the 0,0 band of 2-bromopyridine is shifted by about  $1392\text{ cm}^{-1}$  towards red with respect to that of the latter compound. A similar substitution by  $\text{CH}_3$  group in  $\alpha$ -picoline shifts the 0,0 band only by  $730\text{ cm}^{-1}$ .

(b) *Spectra of solutions*

When 2-bromopyridine is dissolved in alcohol, at a concentration of .01% by weight and a path length of 5 mm, the band system due to  $\pi \rightarrow \pi^*$  transition appears with the 0,0 band at  $36753\text{ cm}^{-1}$  and the other bands are represented by progression of frequencies  $971\text{ cm}^{-1}$  and  $655\text{ cm}^{-1}$  in the excited state (Fig. 5c). It can be seen that in the case of .01% solution in alcohol the 0,0 band is shifted by about  $200\text{ cm}^{-1}$  towards long wavelengths from the 0,0 band due to the vapour.

On gradually increasing the concentration of the solution from .01% to .08% by weight, a continuous absorption due to  $v \rightarrow 0$  transition of  $\pi \rightarrow \pi^*$  system is observed in the region  $35500\text{ cm}^{-1}$  to  $36700\text{ cm}^{-1}$  as is evident from the absorption curve reproduced in Fig. 5. A similar absorption is also observed in case of .08% solution in 3-methyl pentane, but no band system due to  $n \rightarrow \pi^*$  transition as observed in the case of 3-bromopyridine could be detected in this case.

This is an agreement with the conclusions of Stephenson (1954) who earlier studied the absorption spectra of solution of 2-bromopyridine in alcohol and in iso-octane and from the similarity of the two absorption curves concluded that the  $n \rightarrow \pi^*$  transition is absent in the spectrum due to the 2-bromopyridine molecule.

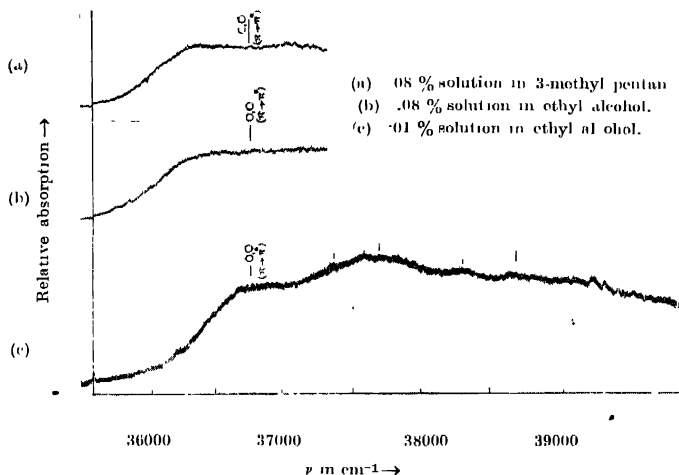


Fig. 5. Microphotometric records of the ultraviolet absorption spectra of solutions of 2-bromopyridine.

(c) *Spectrum in the liquid and solid states*

In the spectrum of 2-bromopyridine in the liquid state only one system of discrete bands consisting of three broad bands due to Transition II is observed (Fig. 6), the band at  $36571 \text{ cm}^{-1}$  being taken as the 0,0 band of this system. Thus the 0,0 band shifts by about  $387 \text{ cm}^{-1}$  towards longer wavelengths with liquefaction of the vapour. The other bands can be assigned to a progression of the excited state frequency  $918 \text{ cm}^{-1}$ . When the liquid is frozen and cooled to about  $-180^\circ\text{C}$ , these bands become a little sharper, but the bands are not resolved into sharper components. The shift of the bands with liquefaction of the vapour is much larger than that observed in spectrum due to the solution in alcohol. The 0,0 band in this case is at  $36479 \text{ cm}^{-1}$  and the other two bands are assigned to a progression of the upper state vibrational frequency  $971 \text{ cm}^{-1}$ . Thus with

solidification and cooling the substance to about  $-180^{\circ}\text{C}$ , the 0,0 band undergoes a small shift of  $92\text{ cm}^{-1}$  towards red.

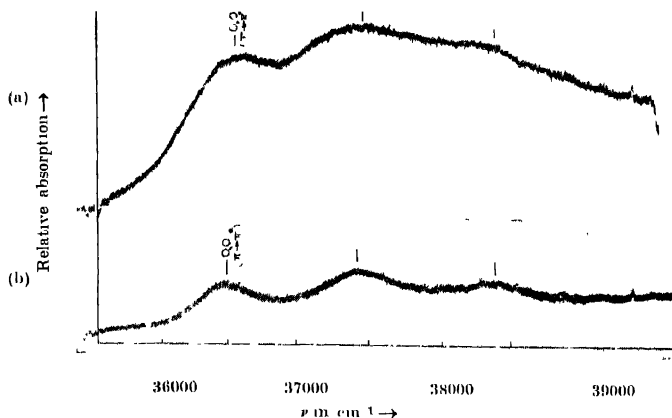


Fig. 6. Microphotometric records of the ultraviolet absorption spectra of 2-bromopyridine.

(a) Liquid at  $32^{\circ}\text{C}$ .

(b) Solid at  $-180^{\circ}\text{C}$ .

TABLE IV

Ultraviolet absorption bands of 2-bromopyridine

Liquid at $32^{\circ}\text{C}$		Solid at $-180^{\circ}\text{C}$		Solution at $32^{\circ}\text{C}$	
Wave No. ( $\text{cm}^{-1}$ ) and intensity	Assignment	Wave No. ( $\text{cm}^{-1}$ ) and intensity	Assignment	Wave No. ( $\text{cm}^{-1}$ ) and intensity	Assignment
Absent		Absent		.08% sol. in alcohol	
Absent		Absent		.08% sol. in 3-methyl pentane	
Absent		Absent		.01% sol. in alcohol	
Transition I				36753 (s)	0, 0
				37408 (m)	0+655
				37724 (s)	0+971
				38379 (s)	0+971+655
Transition II				38406 (ms)	0+2×918
				38697 (s)	0+2×971

When thicker film of thickness of the order of 10 microns is used, the  $\pi \rightarrow \pi^*$  system produces continuous total absorption but no other band system in the low energy region corresponding to  $n \rightarrow \pi^*$  transition is produced by the substance either in the liquid state or in the solid state at  $-180^\circ\text{C}$ .

It is concluded that in the case of 2-bromopyridine the  $n \rightarrow \pi^*$  transition is absent whether the substance is in the vapour phase, in solutions or in the states of aggregation. As postulated by Stephenson (1954) this may be due to the inductive attraction of the halogen atom attached to the carbon atom adjacent to the nitrogen atom which increases the binding energy of the non-bonding electron over that existing in pyridine, thereby shifting the  $n \rightarrow \pi^*$  transition into the spectral region of  $\pi \rightarrow \pi^*$  transition and the situation is not altered when the molecules are in solutions and also in the state of aggregation.

#### ACKNOWLEDGMENT

The author is indebted to Professor S. C. Sirkar, D.Sc., F.N.I., for his kind interest and guidance in the work.

#### REFERENCES

- Banerjee, S. B., 1956, *Ind. J. Phys.*, **30**, 480.  
.. 1957, *Ibid.*, **31**, 11.  
Kasha, M., 1950, Discussion of the Faraday Society, No. 9, 14  
Misra, T. N., 1959, *Ind. J. Phys.*, **33**, 276  
Roy, S. B., 1958, *Ind. J. Phys.*, **32**, 323.  
Rush, J. H. and Sponer, H., 1952, *J. Chem. Phys.*, **20**, 1847  
Sirkar, S. C. and Misra, T. N., 1959, *Ind. J. Phys.*, **33**, 45.  
Stephenson, H. P., 1954, *J. Chem. Phys.*, **22**, 1077.



# Letters to the Editor

*The Board of Editors will not hold itself responsible for opinions expressed in the letters published in this section. The notes containing reports of new work communicated for this section should not contain many figures and should not exceed 500 words in length. The contributions must reach the Assistant Editor not later than the 15th of the second month preceding that of the issue in which the letter is to appear. No proof will be sent to the authors.*

12

## ON THERMAL CONDUCTIVITY OF ALUMINIUM AT LOW TEMPERATURES

H N PATIL

GUJARAT COLLEGE, AHMEDABAD

(Received, June 25, 1960)

There are two mechanisms conducting the heat in a metal. As in non-conductors there is transfer of heat by the lattice waves and in addition a transfer by the electrons. The total heat conductivity is thus made up of two components  $K_g$  the lattice conduction, and  $K_e$  the electronic conduction. The electronic heat resistance  $W (= 1/K_e)$  can be written as  $W = W_0 + W_i$ , where  $W_0$  is the resistance due to impurity scattering and  $W_i$  is the resistance due to the scattering of the conduction electrons by the lattice waves and imperfections.  $W_0$  is of the form  $\beta/T$ , and  $W_i$  at temperatures below about  $\theta/10$ , is of the form  $\alpha T^2$ .

Thus neglecting the lattice conduction  $K_g$  in the case of pure metals, we have for total thermal resistance  $W = \alpha T^2 + \beta/T$ . A plot of  $WT$  against  $T^3$  over a certain range of temperature should be a straight line with a slope  $\alpha$ .

In case of experimental curve for Al drawn by Andrews and his coworkers (1951), it is seen that such plot has two linear sections instead of one having slopes  $\alpha = 2.470 \times 10^{-5} \text{ cm}^2 \text{ Watt}^{-1} \text{ } ^\circ\text{K}^{-1}$  for the range of temperature 3.5°K to 12.5°K, and  $\alpha = 6.00 \times 10^{-5} \text{ cm}^2 \text{ Watt}^{-1} \text{ } ^\circ\text{K}^{-1}$  for the range 2° to 4°K.

This observed variation in slope is explained on how  $\theta$  the Debye characteristic temperature changes with  $T$ . Rosenberg (1957) and others have observed such variations in slope in case of Cd, Zn and Hg, etc.

Semi-analytic method has been used in the case of Al to study the temperature dependence of  $\theta$  at low temperatures (Seitz and Trunbull, 1956). The values of  $\theta$  in the region where it first departs from  $\theta_0$ , and the value of  $\theta$  at 0°K, are given

by  $\theta^3 = \theta_0^3[1 - f'(s, t) (T/\theta_0)^2]$ . The parameters  $s$  and  $t$  are determined from the values of elastic constants at 0°K and values of  $f'$  for *bcc* and *fcc* lattices are determined from tables (Seitz and Turnbull, 1956). Using the elastic constants at 0°K for Al,  $c_{11} = 1.226$ ,  $c_{12} = 0.708$ ,  $c_{44} = 0.306$ , the characteristic temperature, in case of central forces plus electron gas model is given by  $\theta = 426.6 - 0.0544 T^2$ .

From this expression, it is seen that the temperature region in which  $\theta$  starts changing with temperature approximately corresponds to the region in which the value of slope,  $\alpha$  changes. But from the ratio of values of  $\alpha$  it seems necessary, in addition to the study of variation in  $\theta$  to consider lattice conductivity because of impurities in the specimen and scattering by boundaries, the dominant source of thermal resistance at very low temperature. The lattice component would cause the curve  $WT$  against  $T^3$  to dip below (Handbuch der Physik XIV p. 247)

Author's thanks are due to Principal Y. G. Naik for useful discussions.

#### REFERENCES

- Andrews, F. A. Webber, R. T. and Spohr, D. A. 1951, *Physical Review*, **84**, 904.  
 Dekker, A. J. 1957, *Solid State Physics*, p. 295.  
 Rosenberg, H. M. 1957, *Phil. Mag.*, **2**, 541.  
 Seitz and Turnbull, 1956, *Solid State Physics*, Vol. 2, p. 285.

# ESTIMATION OF $(\Delta r_e)$ OF AN ELECTRONIC BAND SYSTEM—A NEW METHOD

N. R. TAWDE AND A. P. WALVEKAR

DEPARTMENT OF PHYSICS, KARNATAK UNIVERSITY, DHARWAR

(Received June 23, 1960)

**ABSTRACT** A new method of constructing the Morse potentials associated with an electronic band system without the knowledge of internuclear distances and estimating therefrom the difference  $(\Delta r_e)$  in the equilibrium distances in the two states has been suggested. The knowledge of this latter quantity  $(\Delta r_e)$  is an essential parameter in the theories of vibrational transition probabilities in molecular spectra.

## 1

Morse potential becomes defined when equilibrium internuclear distances are known. But there are a number of band systems for which  $r_e$  values are not known, because of the difficulties of analysing the rotational structures. As such distances, or at least the difference between them for a transition, are essential for the problems of vibrational transition probabilities in electronic band spectra of diatomic molecules, it was thought worthwhile to explore the possibility of an indirect method, independent of rotational structure analysis to get a clue to the nearest, if not the precise estimate of the difference in internuclear equilibrium distances. The method and procedures are outlined in the following sections.

## 2

The usual Morse expression for potential energy

$$U = D_e(1 - e^{-a(r-r_e)})^2 \quad \dots (1)$$

can be converted to a slightly modified form

$$\frac{1}{a} \log_e \left( 1 + \sqrt{\frac{u}{D_e}} \right) = (r - r_e) \quad \dots (2)$$

For  $r_e = 0$ , the Eq. (2) above becomes

$$\frac{1}{a} \log_e \left( 1 + \sqrt{\frac{u}{D_e}} \right) = -r \quad \dots (3)$$

If  $a$ ,  $u$  and  $D_e$  are assumed known, then the left hand side of Eqns. (2) or (3) above can be evaluated. These quantities are expressed as

$$a = 0.2454 \sqrt{\mu \omega_e x_e}$$

$$U(=E_v) = \omega_e(v + \frac{1}{2}) - \omega_e x_e(v + \frac{1}{2})^2$$

$$D_e = \frac{\omega_e^2}{4\omega_e x_e}$$

Of these the quantity  $E_v$  is calculated for different values of  $v$ , i.e. 0, 1, 2, 3... and substituted in Eq. (2). We then get from it a set of values of  $(r_e - r)$  corresponding to  $E_0, E_1, E_2, E_3...$  etc. which we could designate as  $r_0, r_1, r_2, r_3, \dots$  etc. These are taken as one set of values about the equilibrium distance and are used for plotting the relevant part of the potential energy curve. It is then necessary to obtain points for other extremities of the vibrational levels for plotting the complementary part of the curve. This means another set of  $r$  values corresponding to  $E_0, E_1, E_2$  and so on. For this purpose, since we are concerned with a harmonic oscillator the expression of Pillow (1951) can be made use of. According to Pillow, the centres of vibrational energy levels of an anharmonic oscillator lie at a distance of  $(v+1)(x/a)$  from centres of the vibrational energy levels of the harmonic oscillator. Using this expression, the other set of  $r$  values will become

$$r_0 + 2(v_0 + 1) \frac{x}{a}$$

$$r_1 + 2(v_1 + 1) \frac{x}{a}$$

$$r_2 + 2(v_2 + 1) \frac{x}{a}$$

$$\dots \dots \dots \text{etc}$$

The method of arriving at the above type of expressions is indicated below.

The vertical axis is at a distance of  $r_0$  (for  $v = 0$  level) from the point of intersection of the potential energy curve and the vibrational energy level. As the centre of the vibrational energy level of the anharmonic oscillator lies at a distance  $(v_0 + 1) \frac{x}{a}$  from the vertical axis, the centre of the vibrational energy level of the anharmonic oscillator is at the distance  $r_0 + (v_0 + 1) \frac{x}{a}$  from the same point of intersection. So the distance from the vertical axis up to the point of intersection to the right will be

$$r_0 + (v_0 + 1) \frac{x}{a} + (v_0 + 1) \frac{x}{a}$$

or,

$$r_0 + 2(v_0 + 1) \frac{x}{a}$$

Now starting with  $r_e = 0$ , which may be taken as the origin and making use of these two sets of  $r$ -values and the vibrational energy  $E_v$ , the potential energy curves both for the upper and lower states of transition can be drawn. Some of these  $r$ -values for the  $A^3\Pi$  state of the  $\text{Cl}_2$  molecule have been derived and shown in Table I.

TABLE I  
Derived  $r$ -values for  $C_2$ ,  $A^3\Pi$  state.

$v$	$(v+1)x/a \text{ \AA. u.}$	$E_v(\text{cm}^{-1})$	$(-r) \text{ \AA.}$	$(+r) \text{ i.e. } r+2(v+1)(x/a) \text{ \AA.}$
0	0.003784	889.9	0.05206	0.05963
1	0.00757	2645.3	0.08596	0.10109
2	0.01135	4367.8	0.1074	0.1301
3	0.01514	6057.3	0.1241	0.15438
4	0.01862	7713.9	0.1374	0.17464
10	0.04162	16963.5	0.1902	0.27344

The assumption made above about the origin, i.e.  $r = 0$  means that the two curves for the pair of the states involved are drawn about a common vertical axis. This is not enough as the curves need to be disposed with respect to the position of the minimum as well as with respect to their energy difference, i.e. the horizontal shift as well as the vertical shift. The steps for obtaining these relative dispositions are indicated below.

It is an established fact that if  $\omega_e' > \omega_e''$  then  $r_e' < r_e''$  and vice versa. So from the  $\omega_e$  values, we know the direction in which the curve for the upper state is to be shifted with respect to the lower curve on the horizontal axis.

If the intensities of the bands are known fairly accurately or could be estimated, then it is possible to fix the Condon parabola or the most probable transitions. By trial the curve is shifted in the proper direction along horizontal axis until the most probable transitions known as above, are reached. When this is achieved carefully, one could get the nearest approximation to the quantity  $(\Delta r_e)$ .

To test the performance of the method outlined above, some well-established band systems were selected for study. Experimental intensity data as well as  $r_e$ -values in both the states are accurately known for these systems. One could construct the potential energy curves and derive the  $(\Delta r_e)$  value in the manner shown above. On the other hand, there is the knowledge of the exact value of this quantity from the rotational structure analysis constants. Both these values for the band systems chosen are recorded in Table II. How far the estimated values depart from exact experimental data is shown by calculating the percentage departure.

TABLE II  
Comparative study

Molecule	Transition	$\Delta r_e$	$\bar{A}$	Percentage departure from expl. value
		Present	Expl. value (Herzberg, 1950)	
C <sub>2</sub> (Swan)	A $^4\pi - X^3\pi$	0.04	0.046	-13.0
AlO	A $^2\Sigma - X^2\Sigma$	0.045	0.049	- 8.2
BO- $\alpha$	A $^3\pi - X^2\Sigma$	0.160	0.1475	-  8.8
BO- $\beta$	B $^2\Sigma - X^2\Sigma$	0.095	0.1061	-10.4
CN-violet	B $^2\Sigma' - X^2\Sigma'$	0.0226	0.0212	6.1
N <sub>2</sub> (HP)	C $^1\pi - B^3\pi$	0.055	0.0641	- 14.2
MgO	B $^1\Sigma - X^1\Sigma$	0.011	0.012	- 8.3

For certain band systems, estimates have been made by earlier workers on the basis of empirical relations or other methods. We can pick up one of these systems to see how far the forecast of ( $\Delta r_e$ ) from the present method stands in relation to other estimates. The system to which we would refer is the ( $C'-B$ ) transition of BO. Katti (1957) by applying 4 different methods or rules has estimated the  $\Delta r_e$ -difference for this system. These estimates are recorded in Table III in which also, is included the value predicted from the present method.

TABLE III

Relation or method used	$\Delta r_e$ -estimates	$\bar{A}$
Morse (1929)	0.1204	Katti (1957)
Birge (1932) and Mecke (1925)	0.1035	„
Wu and Chao (1947)	0.0720	„
Nicholls (1955)	0.1503	„
<i>Present method</i>	0.095	

It is evident from the results of Table III that the value derived from the method suggested here compares favourably with the data derived from other methods and particularly Birge and Mecke's relation. Although Katti is inclined to favour the value from Morse's relation, the approach made by the present method is the next best like Birge and Mecke's among the few methods or relations that are available. The true situation with regard to any of these methods will not be gauged unless we have in our possession the measured  $r_e$ -values from rotational structure analysis.

## *Estimation of $(\Delta r_e)$ of an Electronic Band System, etc. 401*

The advantage of the method is that it is entirely independent of any of the two  $r_e$ -values of the electronic states involved and requires the parameters, viz.,  $\omega_e$  and  $\omega_e x_e$  which are generally provided by vibrational analysis and the knowledge of the most probable transitions from vibrational intensity data.

### REFERENCES

- Birge, R. T., 1932, *Phys. Rev.*, **42**, 437  
Herzberg, G., 1950, *Spectra of Diatomic Molecules*, D. Van Nostrand Co., New York  
Katti, M. R., 1957, M.Sc. Thesis, Karnatak University, Dharwar  
Meeke, R., 1925, *Z. Physik*, **32**, 823  
Morse, P. M., 1929, *Phys. Rev.*, **34**, 57.  
Nicholls, R. W., 1955, *Molecular Band Intensities and their Interpretation*, Proc. Airglow Aurora Conference.  
Pillow, M. E., 1951, *Proc. Roy. Soc.*, **64**, 772.  
Wu and Chao, 1947, *Phys. Rev.*, **71**, 118.

# RAMAN SPECTRA OF FLUOROBENZENE AT DIFFERENT LOW TEMPERATURES

DEB KUMAR MUKHERJEE

OPTICS DEPARTMENT, INDIAN ASSOCIATION FOR THE CULTIVATION  
OF SCIENCE, CALCUTTA 32

(Received, May 30, 1960)

## Plate VII

**ABSTRACT.** The Raman spectra of fluorobenzene in the solid state at  $-60^{\circ}\text{C}$  and at  $-180^{\circ}\text{C}$  have been investigated and compared with the spectrum due to the liquid. At  $-60^{\circ}\text{C}$  the crystals produce a new low-frequency line at  $95\text{ cm}^{-1}$  and the line shifts to  $100\text{ cm}^{-1}$  when the temperature is lowered to  $-180^{\circ}\text{C}$ . This new line has been attributed to the formation of dimers at low temperature. Further, the Raman shifts of some prominent lines have been observed to change with solidification of the compound and lowering of temperature and these changes also have been attributed to the formation of dimers.

The polarisation of the Raman lines of the compound has been reinvestigated and it has been observed that the line  $517\text{ cm}^{-1}$  is not totally depolarised and although the value of factor of depolarisation is quite large it is actually less than  $6/7$ .

## INTRODUCTION

The Raman spectra of many mono- and disubstituted benzenes in the solid state at different low temperatures were studied by many previous workers. The Raman spectra of chlorobenzene and bromobenzene studied earlier by Ray (1950) and Biswas (1955) respectively showed that in the spectrum of frozen chlorobenzene at  $-60^{\circ}\text{C}$  there are five new lines in the low frequency region the intensities and frequency-shifts of which increase when the temperature is lowered to  $-180^{\circ}\text{C}$ . In the case of crystalline bromobenzene at  $-60^{\circ}\text{C}$  only two new lines appear in the low frequency region while the number increases to three with lowering of temperature to  $-180^{\circ}\text{C}$ . These results were interpreted on the hypothesis that the lines are due to small groups of molecules formed through virtual linkages in the solid state and the changes with temperature were attributed to the strengthening of these bonds and formation of fresh bonds at lower temperatures. The fluorobenzene molecule contains a highly active fluorine atom and the behaviour of this molecule in the solid state was not known. The Raman spectra of this compound at  $-60^{\circ}\text{C}$  and at  $-180^{\circ}\text{C}$  have, therefore, been investigated to find out the number of new low-frequency lines which may be produced by this compound in the solid state and the dependence of intensity and positions of the lines on temperature.



As regards the assignment of the Raman lines to different modes of vibration of the molecule as given in the Tables by Landolt-Börnstein (1951) the line  $518\text{ cm}^{-1}$  has been assigned to a totally symmetric mode but the line has been described as a totally depolarised one. This is anomalous and therefore the polarisation of the Raman lines of this compound has been re-investigated to find out whether the discrepancy is genuine or not.

#### EXPERIMENTAL

Chemically pure sample of fluorobenzene obtained from Eastman Organic Chemicals Co of New York was used in the present investigation and it was repeatedly distilled under reduced pressure before each exposure. The Raman spectra due to the substance in the liquid state and in the solid state at  $-60^{\circ}\text{C}$  and at  $-180^{\circ}\text{C}$  were photographed with the arrangements used by previous workers in this laboratory (Biswas, 1954). The intermediate temperature of  $-60^{\circ}\text{C}$  was obtained by using as a refrigerant a mixture of alcohol and liquid oxygen in proper proportion in a Dewar vessel of Pyrex glass. All the Raman spectra were photographed on Ilford Zenith plates using a Fuess glass spectrograph giving a dispersion of about  $11\text{ Å}$  per mm in the  $4000\text{ Å}$  region. Iron arc spectrum was also recorded on each spectrogram as comparison.

In order to study the polarisation of the Raman lines light from two horizontal mercury arcs was focussed with cylindrical condensers on the horizontal pyrex glass tube containing the liquid and the two components of the scattered light were focussed on the slit of the spectrograph one above the other with the help of a double image prism. With this arrangement the convergence of the merident light made the horizontal component of the totally depolarised line more intense than the vertical component. So, it was easy to find out the totally depolarised lines in the spectrum.

#### RESULTS AND DISCUSSION

Spectrograms showing the Raman lines due to fluorobenzene in the liquid state and in the solid state at different temperatures are reproduced in Figs. 1(a)-1(c) and the polarised Raman spectrum of the liquid is shown in Fig. 1(d), Plate V. The low frequency line due to the solid at  $-60^{\circ}\text{C}$  and  $-180^{\circ}\text{C}$  is shown in the enlarged spectrograms in Figs. 2(a) and 2(b) respectively in the same plate.

The Raman frequencies due to the substance in the liquid and solid states are given in Table I. The Raman shifts due to the liquid reported by previous workers (Magat, 1936) are also given in the same table for comparison.

##### (a) New Raman lines in the low frequency region

It can be seen from Figures 2(a) and 2(b) and from Table I that only one broad new line at  $95\text{ cm}^{-1}$  appears in the Raman spectrum due to the frozen fluorobenzene at  $-60^{\circ}\text{C}$ , and the line becomes sharper and is shifted to  $100\text{ cm}^{-1}$  when

TABLE I  
Fluorobenzene,  $C_6H_5F$   
 $\Delta\nu$  in  $cm^{-1}$

Liquid		Solid	
Magat, 1936	Present author at 30°C	at -60°C	at -180°C
		95 (7b) o, k	100 (7) o, k
243 (8) 6/7	242 (8b) $\pm$ o, k, D	255 (5) o, k	260 (2) o, k
424 (1)			
500 (0)			
518 (3) 6/7	517 (3) o, k ; P	510 (0) o, k	510 (1b) o, k
615 (2) 0/7	615 (2) o, k ; D	615 (0) o, k	615 (1b) o, k
705 (1)			
755 (1)	755 (1) o, k		
806 (9) 0,5	806 (6) o, k ; P	806 (5) o, k	806 (6) o, k
830 (1)			
883 (0) 6/7			
997 (2)	998 (1) o, k	996 (4) o, k	996 (5) o, k
1010 (10) 0,1	1009 (10) o, k ; P	1010 (4) o, k	1010 (4) o, k
1025 (1)			
1068 (1)	1068 (ob) o, k		
1157 (3) 6/7	1158 (4) o, k, D	1158 (0) o, k	1158 (1) o, k
1220 (4) 0,5	1222 (3) o, k ; P	1214 (1) o, k	1214 (3) o, k
1280 (0)			
1413 (0)			
1498 (1)	1499 (2) o	1499 (0) o	1499 (1) o
1601 (4) 6/7	1602 (3b) o, k ; D	1603 (0b) o	1603 (1b) o
1625 (0)	1625 (0) o, k		
2615 (1)			
2917 (1)			
2986 (1)	2990 (0) k ?		—
3027 (1)			
3074 (10) 0,1	3075 (12b) o, k, P	3082 (5b)	3088 (7b) k
3090 (-)			
3180 (-)			
3677 (-)			

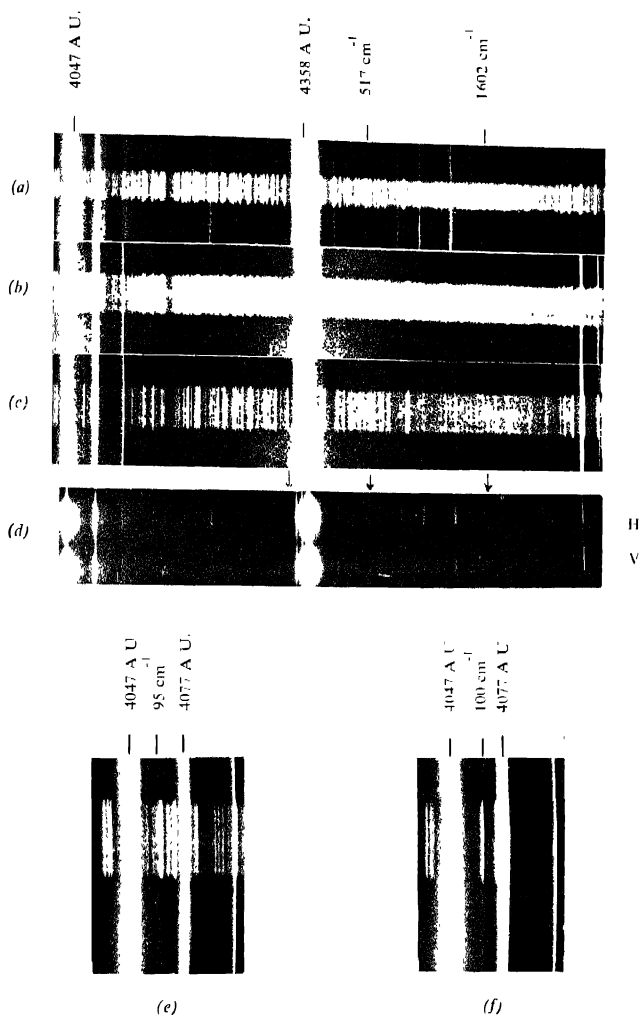


Fig. 1. Raman spectra of fluorobenzene

- (a) Liquid at 30°C  
 (b) Solid at -60°C  
 (c) Solid at -180°C

- (d) Polarisation of Raman lines  
 (e) Showing low frequency Raman lines at -60°C  
 (f) Showing low frequency Raman lines at -180°C



the temperature is further lowered to  $-180^{\circ}\text{C}$ . The changes in the Raman shifts of the low frequency lines due to chlorobenzene and bromobenzene were reported previously by Ray (1950) and Biswas (1955) respectively. Ray (1950) observed five new lines in the case of chlorobenzene in the solid state both at  $-60^{\circ}\text{C}$  and  $-180^{\circ}\text{C}$ , while bromobenzene showed (Biswas, 1955) two such lines at  $-60^{\circ}\text{C}$  and three new lines at  $-180^{\circ}\text{C}$ . The crystal structures of the compounds were not known at that time but recently Biswas (1958) has reported that both the crystals of chlorobenzene and bromobenzene at  $-180^{\circ}\text{C}$  belong to the same space group  $Q_h^{13}$  and also contain the same number of molecules per unit cell. If the new lines were due to lattice oscillations depending on the symmetry of the lattice the number of such lines would be the same in both these cases, but actually it is not so. The space group of fluorobenzene crystals is not known but the fact that other monosubstituted benzenes produce more than one line in the solid state while only one new line is observed in the case of fluorobenzene cannot be explained by the hypothesis put forward by Bhagavantam (1941) and Kastler and Rousset (1941) independently that angular oscillations of the molecules pivoted in the crystal lattice give rise to these new lines. Moreover, the amplitude of angular oscillation would decrease and consequently the intensity of the new line would diminish at lower temperatures, but actually the intensity of the line does not diminish with lowering of temperature from  $-60^{\circ}\text{C}$  to  $-180^{\circ}\text{C}$ .

Ray (1950) and Biswas (1955) concluded from the changes observed in the intensities and frequency-shifts of the low frequency lines in the case of crystals of chlorobenzene and bromobenzene respectively with lowering of temperature of the crystals that these lines might be due to oscillations in groups of molecules formed by virtual intermolecular linkages in the solid state as proposed by Sirkar (1936). Kastha (1958) recently found evidence of formation of such groups even in the liquid state just above the freezing point. The replacement of a bromine atom by the chlorine atom in the benzene ring may appreciably increase the affinity of the molecule to form intermolecular linkages with more distant neighbours increasing thereby the size of the associated groups and the number of the new Raman lines given by such groups. The situation is different in the case of fluorobenzene because fluorine being more reactive than chlorine the molecules may form dimers even in the liquid state just above the freezing point with a structure of the dimer in which the fluorine atom of each of the two molecules is attached to a hydrogen atom of the other molecule.

(b) *Shift of Raman lines of the molecule with solidification*

Table I shows that most of the Raman frequencies reported by Magat (1936) in the case of fluorobenzene in the liquid state have been observed in the present investigation. The line  $242\text{ cm}^{-1}$  due to the liquid is found to shift to  $255\text{ cm}^{-1}$  when the liquid is frozen and the temperature is lowered to  $-60^{\circ}\text{C}$  and to  $260\text{ cm}^{-1}$  at  $-180^{\circ}\text{C}$ . The line  $517\text{ cm}^{-1}$  shifts to  $510\text{ cm}^{-1}$  when the liquid is frozen and

cooled to  $-180^{\circ}\text{C}$ . The spectrum due to the liquid shows a feeble line with Raman shift  $998\text{ cm}^{-1}$  and an intense line  $1009\text{ cm}^{-1}$ . The line  $998\text{ cm}^{-1}$  shifts to  $996\text{ cm}^{-1}$  and becomes stronger with the solidification of the liquid and lowering of temperature to  $-60^{\circ}\text{C}$ . This can be explained on the assumption that the line  $996\text{ cm}^{-1}$  is due to dimers the number of which increases with solidification of the liquid. The line  $1222\text{ cm}^{-1}$  observed in the liquid is shifted to  $1214\text{ cm}^{-1}$  when the liquid is solidified. Further the Raman line  $3075\text{ cm}^{-1}$  shifts to  $3082\text{ cm}^{-1}$  with the solidification of the liquid and to  $3088\text{ cm}^{-1}$  when the crystal is further cooled to  $-180^{\circ}\text{C}$ .

On comparing the results with those due to bromobenzene (Biswas, 1955) it is found that the line  $242\text{ cm}^{-1}$  of fluorobenzene behaves in the same way with solidification of the liquid and lowering of temperature as the line  $182\text{ cm}^{-1}$  of bromobenzene. Biswas assigned the latter line to the vibration of type corresponding to the  $\epsilon_u^+$  mode of the benzene ring given in Figure 1, No. 16 by Sponer and Kirby-Smith (1941) and the shift was attributed to the formation of virtual linkages between neighbouring molecules. In the present case also similar explanation holds good. The shift of the other lines mentioned above also lend support to the hypothesis that dimers are formed in the solid state of the substance.

(c) *Polarisation of the line  $517\text{ cm}^{-1}$*

The polarised Raman spectrum of liquid fluorobenzene shows that the horizontal component of the totally depolarised line  $1602\text{ cm}^{-1}$  is more intense than the vertical component while the vertical component of the  $517\text{ cm}^{-1}$  line is slightly more intense than the horizontal component. Hence the latter line is not totally depolarised and although the value of factor of depolarisation is quite large it is certainly less than  $6/7$ .

#### ACKNOWLEDGMENT

The author is indebted to Professor S. C. Sirkar, D.Sc., F.N.I., for his kind interest and valuable guidance throughout the progress of the work.

#### REFERENCES

- Bhagavantam, S., 1941, *Proc. Ind. Acad. Sci.*, **13A**, 543.
- Biswas, D. C., 1955, *Ind. J. Phys.*, **29**, 503.
- Biswas, S. G., 1958, *Acta Crystallographica*, **2**, 882.
- Kastha, G. S., 1958, *Ind. J. Phys.*, **32**, 473.
- Kastler, A. and Rouset, A., 1941, *Comptes Rendus*, **212**, 645.
- Landholt and Börnstein, 1951, *Molekeln* I, Teil 2, 304.
- Magat, M., 1936, *Annual Tables of Constants and Numerical Data*, p. 26-75.
- Ray, A. K., 1950, *Ind. J. Phys.*, **24**, 111.
- Sirkar, S. C., 1936, *Ind. J. Phys.*, **10**, 189.
- Sponer, H. and Kirby-Smith, J. S., 1941, *J. Chem. Phys.*, **9**, 667.

# A TWO-DIRECTIONAL FOCUSSED HIGH-INTENSITY MASS-SPECTROMETER

S. B. KARMOHAPATRO

SAHA INSTITUTE OF NUCLEAR PHYSICS, CALCUTTA

(Received, July 8, 1960)

**ABSTRACT.** A two-directional focusing high-intensity mass-spectrometer of focusing angle  $\sqrt{2}\pi$  with mean radius 381 mm, variable 20 KV accelerating voltage, is described. Focusing properties and performance with a magnetic oscillation type ion source for gases are studied so that the instrument may be useful for studies of collision of ions in gases and solids, for preparation of isotopic targets and  $\beta$ -sources by direct deposition method.

## INTRODUCTION

High-intensity mass-spectrometers or low-intensity electromagnetic isotope separators have recently become very important tools for research and many such instruments with ion currents ranging from 10  $\mu$ A to 100  $\mu$ A have been constructed in different laboratories. Koch (1958) has reviewed these instruments, constructed so far and their application in laboratories for nuclear research. In the present paper we shall describe the constructional details of the development of a high-intensity mass-spectrometer consisting of a two-directional focussed magnetic analyser with a preliminary report of its performance.

## THE MAGNETIC ANALYSER

The magnetic analyser, the main component of the mass-spectrometer, is designed after the  $\beta$ -ray spectrometer, originally constructed by Sieghan and Svartholm (1946) with some modifications. The choice of such two directional focussed  $\sqrt{2}\pi$  magnet over other types for high-intensity mass spectrometry was dictated by the following considerations

- 1) The axial focusing property of the analyser is of great advantage since it enables the direct deposition of  $\beta$ -ray sources or targets without any appreciable loss of the source materials used in the ion source.
- 2) The dispersion of such magnetic analysers is higher than that of the homogeneous magnetic analysers or the inhomogeneous ones as used by Zilversehoon (1954) and Artsimovich *et al* (1957)
- 3) In spite of the disadvantages of the aberration factor which is higher for the two directional focussed magnetic analysers than the third order focussing, one, used by Zilversehoon (1954) the simplified conical shape of the pole faces

used by Arhman and Svartholm (1955) for a  $\beta$ -ray spectrometer or by Snyder *et al.* (1950) for a nuclear spectrometer could more easily be attained than shaping the inhomogeneity in the pole faces for third order focussing

4) The accommodation of the ion source would have been convenient with a  $180^\circ$ -two directional focussing magnetic analyser described by Snyder *et al.* (1950). However with a  $\sqrt{2}\pi$  focussing angle, the loss of ions is minimum and without any special device, space charge elimination can be accomplished with the electrons produced by the ion beam in collision with the residual gas as has been discussed by Zilver Schoon (1954), since ions do not travel any distance out of the magnetic field.

The dimensions and the constructional details of the analyser with the focus-

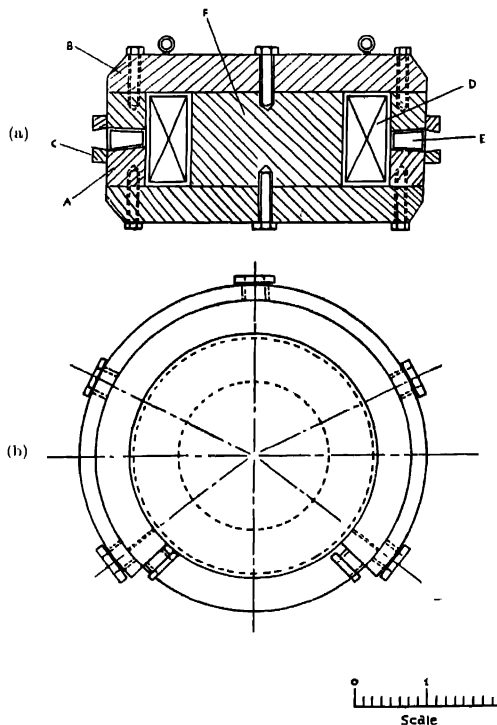


Fig 1 - (a) Vertical section of the magnetic analyser with chamber; A and C—pole pieces with extension, B—yoke; D—coil; E—chamber.

(b) Horizontal section of the magnetic analyser with the vacuum chamber.



smg properties of the pole faces were previously described by the author (1959). The mean radius for the ions is kept at 381 mm at a gap width 5 cm as shown in Fig. 1(a) and 1(b). The vertical and horizontal sections of the magnetic analyser are shown in 1(a) and 1(b) respectively, along with the vacuum chamber.

In addition to the vacuum system described by the author (1959), a four-inch diffusion pump is now used on the ion source side for differential pumping of the residual gases and vapours. Both the diffusion pumps are operated with freon cooled baffles, so that the pressure of the chamber is maintained at  $\sim 1 \times 10^{-6}$  mm Hg. when the ion source is operated with a gas. Liquid air traps are also provided to reduce the condensable vapours. The pressure is measured with thermocouple, penning and ionisation gauges.

#### THE ION SOURCE

A magnetic oscillation type ion source for gases is used with axial extraction as described by Nielsen (1957). The ion source (Fig. 2) consists of a ribbon filament (G), tips of which are water cooled, a cylindrical anode (H) of graphite with a 3/16 inch hole for the outlet of ions and outlet side is tapered at an angle of

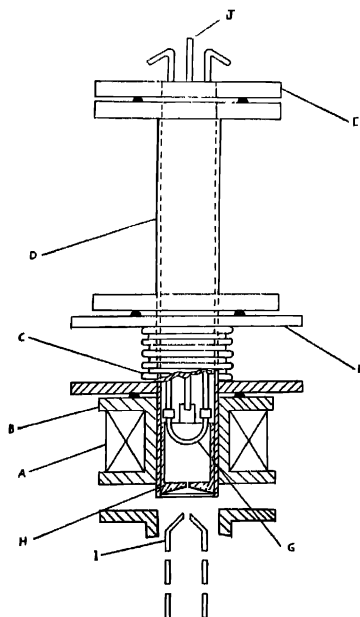


Fig. 2. Diagram of the ion source and the focussing electrodes.

55°. The whole system is on a brass flange (*E*) with electrical leads hermetically sealed. The tubular lead (*J*) connecting the anode serves as gas inlet adjustable through a needle valve. The source with flange is placed within a double-flanged specially made vitreous tube (*D*) and made vacuum tight with rubber O-rings. One flange of the vitreous tube is connected to the main vacuum chamber through a bellow (*C*) for slight adjustment of the system in space and a brass cylinder (*B*) containing the solenoid (*A*) for producing an axial magnetic field  $\sim 200$  gauss for operating the ion source.

Three co-axial iron cylinders over the solenoid have to be used with spacers for screening the magnetic field of the main analyser, which might disturb the arc of the ion source. The ions are extracted through an electrode system consisting of three graphite cylinders, the first one (*I*) kept at a potential  $\sim 1500$  V, which can be varied for attaining the optimum condition. The second one is kept at a potential  $0.75$  V, where *V* is the accelerating voltage and the third cylinder is at earth potential. Ions are electrostatically focused through this lens system and deflected by the magnetic analyser. The operating pressure in the source chamber is kept at  $\sim 10^{-2}$  to  $10^{-3}$  mm Hg approximately

#### ELECTRONIC EQUIPMENTS

Resolving power of a mass-spectrometer greatly depends upon the stability of the magnetic field and the accelerating voltage. For attaining a specified resolution, the order of voltage stability required is only half of that of the magnetic field i.e.  $\frac{\Delta H}{H} = \frac{\Delta V}{2V}$ . So, it was decided to stabilise the magnetic field to 1/2000 and the accelerating voltage power supply to 1/1000. In stabilising the magnetic field, the current passing through the exciting coil is usually stabilised. For high impedance coils (D.C. 800  $\Omega$  resistance) of our magnetic analyser, a stabilised

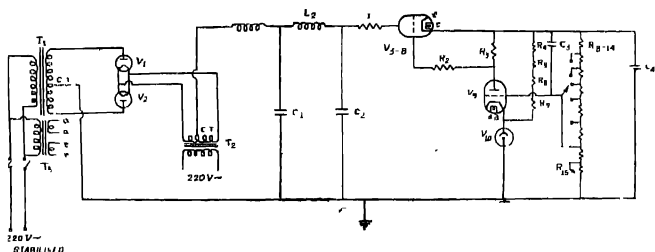


Fig. 3. Stabilised power supply for the magnet coils :

$T_1$ —Pri 220v, Sec 2000—0—2000v; 1 5A;  $T_2$ —Pri 220v, Sec 2.5—0—2.5v, 30A;  $T_3$ —Pri 220v, Sec 6 3v, 3A; 2.5v, 5A;  $L_1, L_2$ —20H, 1.5A ms. 2KV;  $C_1, C_2$ —16  $\mu$ fd, 2500v D.C.;  $C_3$ —1  $\mu$ fd, 2KV D.C.;  $C_4$ —4  $\mu$ fd, 1500V D.C.;  $V_1, V_2$ —872A,  $V_3$ —8—6336 (6);  $V_6$ —2C53,  $V_{10}$ —5651;  $R_1$ —100 $\Omega$ ,  $R_2$ —2K $\Omega$ ,  $R_3$ —4M $\Omega$ ,  $R_4$ —100K $\Omega$ ,  $R_{8-14}$ —100K $\Omega$ ,  $R_{16}$ —100K $\Omega$  Helipot (ten turns).

power supply was considered sufficient to attain short period stability of the magnetic field. Fig. 3 shows the circuit diagrams of the stabilised power supply  $\pm 200$  to  $\pm 1500$  V at 1.25A used for exciting the magnet coils. The use of 6336 (Chattham) series control tubes, high  $\mu$  triode 2C53 as amplifier and 5651 as reference tube gives a stability of  $\sim 1/2000$  to the magnetic field over the mains fluctuations stabilised to 0.2%, with an a.c. stabiliser (G.R.). For a better stabilisation, a second feedback stage similar to that used by Pelchowich (1954) or to avoid long time instability a current stabilisation device will be required. For the present, neither of these improvements have been considered.

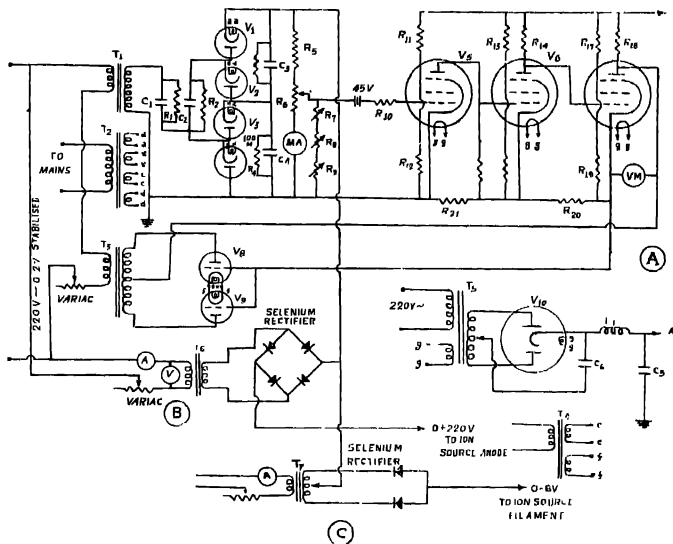


Fig. 4. Power supply for the ion source :

(A) Accelerating voltage 0.20KV (stabilised), (B) Arc voltage, (C) Filament heating supply,  $T_1$ —Pr1 220v, Sec 0.5KV, 50 mA (ms. 25KV),  $T_2$ —Pr1 220v, Sec 2.5–2.5, 10A (4) (ms. 25KV),  $T_3$ —Pr1 90v, Sec 400–0–400, 100mA,  $T_4$ —Pr1 220v, Sec 0–2 5v, 5A (2),  $T_6$ —Pr1 220v, Sec 350–0–350, 6 3v, 5A,  $T_8$ —Pr1 220v, Sec 0–8v, 100A,  $T_7$ —Pr1 220, Sec 0–220v, 2A,  $L_1$ —5H, 100mA,  $C_1$ ,  $C_2$ ,  $C_3$ ,  $C_4$ —0.5  $\mu$ fd, 10 KV D.C.,  $C_5$ ,  $C_6$ —2  $\mu$ fd, 500V, D.C.,  $V_{1-4}$ —8020,  $V_{5-7}$ —6J7,  $V_{8-10}$ —2A3,  $V_{11}$ —6X5,  $R_{1-5}$ —100M $\Omega$ ,  $R_6$ —1K $\Omega$ , pot,  $R_{7,8}$ —1M $\Omega$ , pot,  $R_9$ —125 $\Omega$ , pot,  $R_{10,11}$ —0.4M $\Omega$ ,  $R_{12,13}$ —0.1M $\Omega$ ,  $R_{14}$ —0.4M $\Omega$ ,  $R_{15}$ —0.1M $\Omega$ ,  $R_{16}$ —30K $\Omega$ ,  $R_{17}$ —10K $\Omega$ ,  $R_{18}$ —100 K $\Omega$ ,  $R_{19}$ —2.5K $\Omega$ ,  $R_{20-21}$ —2K $\Omega$ ,

The 0 to +20 KV accelerating voltage power supply (Fig. 4) is a quadrupler rectifier from a 5 KV transformer, the primary of which is supplied with 0.2%

For oscilloscope detection of the ion beam, a special type of transformer with proper air gap in the core and the secondary voltage variable from 0 to 1000V is connected in series with the accelerating voltage output for modulating it at 50 c/sec with other arrangements similar to described by Zilver Schoon (1954).

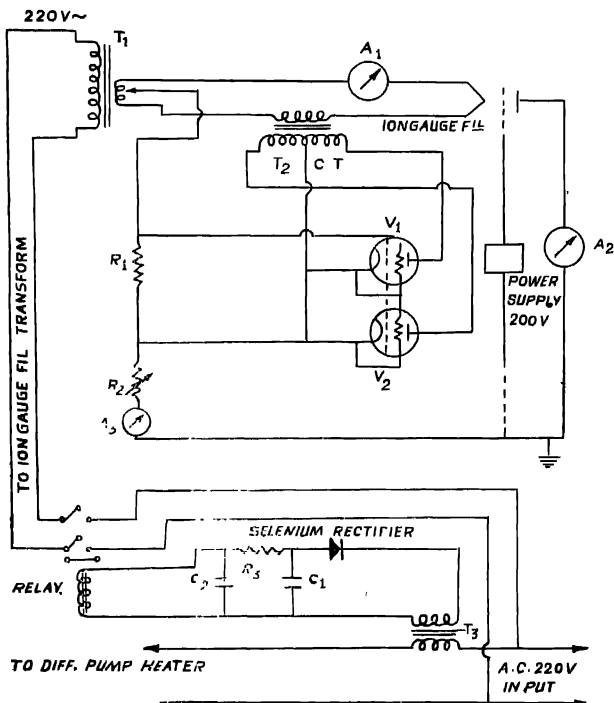


Fig. 5.—Circuit diagram for ionisation gauge with interlock for the diffusion pump.  
 $T_1$ —Pr1 220V, Sec—6.3V, 10A,  $T_2$ —Pri 6.3V, Sec, 110—0—110V,  $T_3$ —Pri 12V—Sec  
 220V,  $C_{1,2}$ —50  $\mu$ fd, 500V D.C.,  $R_1$ —2K $\Omega$ ,  $R_2$ —1K $\Omega$  pot.,  $R_3$ —200 $\Omega$ ,  $A_1$ —0—10A  
 $A_2$ —0—10 $\mu$ A,  $A_3$ —0—10mA.

Fig. 5 shows the ion gauge circuit with devices for emission regulation, modified from a circuit used by Richard and Tuthill (1951).

For the safety of the ion gauge, its filament supply is interlocked with the heater supply of the diffusion pump by a circuit (Fig. 5) so that the ion gauge is protected when the heater supply breaks down. The backing mechanical pump is connected with the diffusion pump through a magnetic valve with air-admittance, which protects the diffusion pump oil from contamination with mechanical pump oil.

Fig. 6 shows a functional diagram of the mass-spectrometer with its different components.

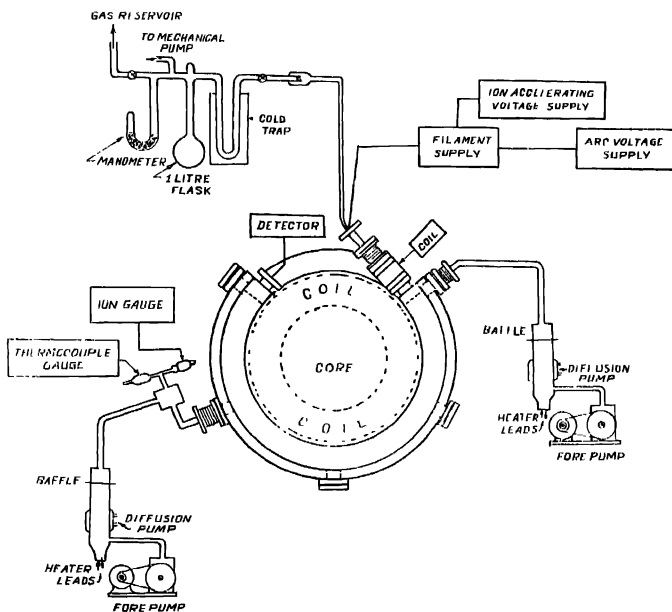


Fig. 6.—Functional diagram of the mass spectrometer.

#### PERFORMANCE

The performance of the mass spectrometer was tested by introducing neon and krypton gas in the ion source. Fig. 7 shows the photograph of the mass-spectrum of krypton from the oscilloscope screen, obtained by sweeping the ion-beam over a slit 1/32 inch wide by modulating the accelerating voltage with the

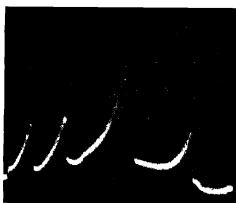


Fig. 7.—Oscillograph record of the mass spectrum of Krypton isotopes.  
( $M=82, 83, 84 \ \& \ 86$ ).

following operating conditions : filament power  $\sim 230$  Watts, arc voltage  $\sim 70$  Volts, arc current  $\sim 400$  mA, accelerating voltage  $\sim 6$  KV.

The oscillograph record shows some distortion due to the back-ground noise, when arc strikes and which can not be eliminated with the oscilloscope available. The current for the highest peak is estimated as  $\sim 10^{-7}$  amp. The resolving power is measured to be  $\sim 125$ , from the equation

$$R = \frac{x}{W_1} \cdot M$$

where  $x$  is the distance between two masses,  $W_1$  is the half width,  $M$  is the mass number. The resolving power is found to be constant with the ions of neon and krypton for the accelerating voltage up to 8 KV, above which no reliable data at present were taken, because of the sparking between the ion source and negative electrode for extraction. Since the extraction of ions behaves as space charge limited current with this type of ion source, high accelerating voltage will enhance the focused ion beam. Moreover, the influence of the field of the main magnetic analyser over the focusing electrode, which are not fully shielded, may be somewhat responsible for the loss of the extracted current.

It is observed that the sparking is due to the rise in pressure on the ion source side and a diffusion pump of higher speed than the present one may improve the situation. Furthermore, better stabilisation of the accelerating voltage and the magnetic field, regulation of the arc, will be necessary to improve the resolving power of the instrument and the transmission may increase by modifying the ion source, extraction system and the vacuum system.

#### ACKNOWLEDGMENT

The author is grateful to Prof. B. D. Nag Choudhury for his keen interest, guidance and constant encouragement in course of this work. I also thank Prof. D. N. Kundu for helpful discussions and to Mr. B. M. Banerjee for valuable suggestions about the design of some of the electronic circuits. Thanks are also

due to Mr. S. Guha for his help in fabrication of some of the electronic equipments and to the workshop staff for mechanical construction of the ion-source

## REFERENCES

- Arbman, E., and Svartholm, N., 1955, *Arkiv For Fysik*, **10**, 1  
Artsimovich, L. A., *et al.*, 1957, *Soviet journal of atomic energy (Atomya Energiya)* **3**, 12, 1301.  
Hanson, A. O., 1944, *Rev. Sci. Inst.*, **5**, 57.  
Karmohapatro, S. B., 1950, *Ind. J. Phys.*, **33**, 139  
Koch, J., 1958, *Electromagnetic Isotope Separators and Applications of Electromagnetically Enriched Isotopes* (North Holland).  
Nielsen, K. O., 1957, *Nuclear Instruments*, **I**, 289.  
Pelchowich, I., 1954, *Philips Reserch Report*, **9**, 1.  
Richard, P. I., and Tuthil, W. Ansel, 1951, *Rev. Sci. Inst.*, **22**, 841.  
Siegbalm, K. and Svartholm, N., 1946, *Arkiv, Math. Astron, Fysik*, **33A**, No. 21  
Snyder, C. W., Rubin, S., Fowler, W. A., and Lauritsen, C. C., 1950, *Rev. Sci. Inst.*, **21**, 852.  
Zilver Schoon, C. J., 1954, Thesis, Amsterdam

# THERMAL EXPANSION OF SOME ALKALI HALIDES BY X-RAY DIFFRACTION

P. D. PATHAK

DEPT. OF PHYSICS, GUJARAT UNIVERSITY, AHMEDABAD

N. V. PANDYA

M. G. SCIENCE INSTITUTE, AHMEDABAD

(Received, June 16, 1960)

**ABSTRACT** In this paper the X-ray data on the thermal expansion of KBr, KI and CsBr upto their melting points is reported for the first time. The contribution of lattice defects to the thermal expansion is discussed. The applicability of the Debye-Grüneisen theory to explain the variation of thermal expansion with temperature is examined. An explanation of the difference in the observed values by the X-ray and the macroscopic methods is given, and an application of it to obtain a quantitative measure of the Schottky defects is indicated.

## INTRODUCTION

In the field of solids, the study of the alkali halides has provided us with a number of most interesting properties. But when the literature about the variation of lattice constants with temperature by X-ray method is examined, we find that the crystals are not studied as a group. Scattered data are available on lattice constant variation (and hence on thermal expansion variation) with temperature, in some cases up to the melting point and in others within a limited range of temperature.

Reliable data on KBr and KI especially at high temperature are not available. Gott (1942) studied these salts between 20°C and 190°C but the X-ray expansion values obtained by him differ by about 5 per cent in the case of KBr and about 15 per cent in the case of KI from his values determined by the macroscopic methods, thus indicating a large concentration of defects (especially in KI). Connell and Martin (1951) repeated the observations under identical conditions and found their X-ray values agreeing closely with the macroscopic values of Gott.

The only X-ray data available so far up to the melting point of CsBr is that of Johnson, Agron and Breiding (1955). But their value of  $\alpha$  at 25°C is about 20 per cent lower than that of Krishnan and Srinivasan (1950) obtained by precision interferometric method.

The present measurements were, therefore, undertaken (i) to provide accurate



X-ray data on the thermal expansion of KBr, KI and CsBr by employing a diffractometer, Geiger counter, ratemeter and an automatic chart recorder, (ii) to study the role of lattice defects on the thermal expansion and (iii) to examine the validity of the Debye-Grüneisen equations.

The diffractometer disc had a diameter of 500 mm. and was calibrated in degrees ( $2\theta$ , each degree divided into four parts). The Geiger counter could be moved over the graduated scale either by means of a spherometer (whose disc had a diameter of about 70 mm.) or by a synchronous motor. The disc of the spherometer carried graduations so that readings of the counter positions could be read up to 1 minute of arc and by estimation up to  $\frac{1}{2}$  minute.

## OBSERVATIONS AND RESULTS

A special small furnace (Pathak and Pandya, 1959) which was fitted in the centre of the diffractometer was constructed in the laboratory. The temperatures were measured by a platinum-platinum plus 10% rhodium thermocouple. The furnace was calibrated by observing the meltings of (i) acetanilide (115°C), (ii)  $\text{NaNO}_3$  (310°C), (iii)  $\text{K}_2\text{Cr}_2\text{O}_7$  (400°C), (iv)  $\text{CsCl}$  (616°C), (v)  $\text{KCl}$  (790°C) and  $\text{NaCl}$  (800°C). The results on  $\text{NaCl}$  (Pathak and Pandya, 1959) and  $\text{CsI}$  (Pathak and Pandya, 1960) obtained by using the furnace have already been reported. Since the earlier results agreed with those of the most reliable workers, it was decided to extend the observations to other alkali halides. The results now obtained are given in Table I.

TABLE I

KBr		KI		CsBr	
Temperature degree C	Cell constant $a$ , Å	Temperature degree C	Cell constant $a$ , Å	Temperature degree C	Cell constant $a$ , Å
30	6.579	28	7.052	31	4.292
72	6.589	78	7.066	81	4.303
110	6.601	118	7.081	120	4.312
170	6.618	159	7.092	182	4.327
226	6.631	204	7.105	263	4.346
281	6.652	261	7.125	295	4.353
350	6.670	320	7.143	340	4.364
415	6.686	376	7.160	368	4.371
497	6.714	432	7.182	389	4.376
553	6.732	495	7.204	442	4.391
611	6.753	542	7.224	495	4.407
		601	7.244	540	4.422
				601	4.445

TABLE II

KBr		KI		CsBr	
Temperature degree C	$\alpha \times 10^6$	Temperature degree C	$\alpha \times 10^6$	Temperature degree C	$\alpha \times 10^6$
30	38.6	28	40.4	31	47.8
72	39.4	78	41.6	81	50.0
110	40.0	118	42.5	120	51.6
170	41.1	159	43.4	182	54.1
226	42.2	204	44.5	263	57.3
281	43.1	261	45.7	295	58.6
350	44.3	320	47.1	340	60.4
415	45.5	376	48.4	368	61.4
497	46.9	432	49.6	389	62.3
553	48.0	495	50.9	442	64.4
611	48.9	542	51.9	495	66.4
		601	53.2	540	68.1
				601	70.3

TABLE III

$\alpha \times 10^6$					
Substance	Temperature range °C	Connell band Martin (X-ray values)	Gott (X-ray values)	Gott (Macro- scopic) values)	Authors' (X-ray values)
KBr	18-100	40.5	38.8	40.8	39.2
	18-190	41.7	40.5	41.4	40.0
KI	20-100	40.6	37.2	40.8	41.2
	20-190	42.1	36.1	42.7	42.4

TABLE IV  
Caesium bromide

Temperature degree C	$\alpha \times 10^6$		
	Authors' (X-ray values)	Krishnan & Srinivasan (Macroscopic values)	Johnson <i>et al</i> (X-ray values)
0	46.6	46.6	37.2
31	47.8	48.0	39.5
81	50.0	50.3	43.0
120	51.6	51.9	45.7
182	54.1	54.5	50.0
263	57.3	57.6	55.5
295	58.6	58.7	57.7
340	60.4		60.8
368	61.4		62.7
389	62.3		64.1
442	64.4		67.6
495	66.4		71.0
540	68.1		74.0
601	70.3		77.8

The equations satisfying the smooth curves drawn from the observed points are given below.

$$\text{KBr} \quad -a_t = 6.5725 + 2.499 \times 10^{-4}t + 6.557 \times 10^{-8}t^2.$$

$$\text{KI} \quad -a_t = 7.0436 + 2.801 \times 10^{-4}t + 8.780 \times 10^{-8}t^2$$

$$\text{CsBr} \quad -a_t = 4.2870 + 1.998 \times 10^{-4}t + 9.378 \times 10^{-8}t^2$$

The coefficient of thermal expansion  $\alpha$  was calculated from the equation  $\alpha = \frac{1}{a_t} \cdot \frac{da_t}{dt}$ . The values of  $\alpha$  thus obtained for the three salts are given in Table II.

Our results are compared with those of the earlier workers in Table III and IV.

The satisfactory agreement between our values and those of Connell and Martin as well as with the macroscopic values of Gott at comparatively low temperatures indicates not too large a concentration of the migrated defects at the surface at these temperatures. (vide section 4)

It can be seen from Table IV that our results with CsBr agree quite satisfactorily with those of Krishnan and Simivasan but disagree widely with those of Johnson *et al*

# DEBYE GRUNEISEN EQUATIONS

Debye-Gruneisen theory gives (Roberts, 1951)

$$\frac{V_T - V_0}{K_0} \left\{ 1 - \frac{n+m+1}{2} \frac{V_T - V_0}{V_0} \right\} = \gamma E \quad \dots (1)$$

In this equation  $V_T$  and  $V_0$  are the volumes of the crystal at  $T^\circ K$  and  $0^\circ K$  respectively,  $K_0$  the compressibility at  $0^\circ K$ ,  $E$  the vibrational energy of the crystal,  $\gamma$  the Gruneisen constant and  $m$  and  $n$  are constants obtained from the potential energy of the crystal,

$$W(V_0) = \frac{A}{V_0^n} + \frac{B}{V_0^m} \quad \dots (2)$$

The thermal expansion of a solid is always small so that  $\frac{n+m+1}{2} \frac{V_T - V_0}{V_0}$

is small compared with unity. Neglecting it the Eq. (1) can be written as

$$V_T - V_0 = \gamma K_0 E \quad \dots (3)$$

Dividing both sides of the equation (1) by  $V_0$  and transposing we obtain

$$\frac{V_T - V_0}{V_0} = \frac{\gamma E K_0 / V_0}{\left\{ 1 - \frac{n+m+1}{2} \frac{V_T - V_0}{V_0} \right\}} \quad \dots (4)$$

Writing  $Q = V_0 / \gamma K_0$  and  $p = \frac{n+m+1}{2}$  in equation (4) we get

$$\frac{V_T - V_0}{V_0} = \frac{E/Q}{\left\{ 1 - p \cdot \frac{V_T - V_0}{V_0} \right\}} \quad \dots (5)$$

Substituting for  $V_T - V_0$  in the small correction term from Eq. (3), Eq. (5) becomes

$$\frac{V_T - V_0}{V_0} = \frac{E/Q}{1 - p \cdot E/Q} \quad \dots (6)$$

Remembering that

$$\frac{V_T}{V_0} \cdot \frac{V_0}{a_0} = 3 \cdot \frac{a_T - a_0}{a_0}$$

where  $a_T$  and  $a_0$  are the lattice constants at  $T^\circ K$  and  $0^\circ K$  respectively, Eq. (6) can be written as

$$3 \cdot \frac{a_T - a_0}{a_0} = \frac{V_T - V_0}{V_0} = \frac{E/Q}{\rho \cdot E/Q} \quad \dots (7)$$

In the case of alkali halides,  $E$  the vibrational energy is given by  $E = 6RT \cdot D(\theta/T)$ . Putting this value of  $E$  in Eq. (7) and transposing we get

$$\frac{a_0}{a_T - a_0} = \frac{Q}{2R} \cdot \frac{1}{T \cdot D(\theta/T)} - 3\rho \quad \dots (8)$$

This equation shows that the graph of  $\frac{a_0}{a_T - a_0}$  against  $\frac{1}{T \cdot D(\theta/T)}$  should be

a straight line. If for a given crystal the above graph is really a straight line, we can (i) show that the substance obeys Gruneisen's law and (ii) determine the Gruneisen's parameters  $Q/2R$  and  $3\rho$  from the graph.

The value of  $a_0$  can be estimated from the low temperature approximation to Eq. (7)

$$\begin{aligned} 3 \cdot \frac{a_{273} - a_0}{a_0} &\approx \left( \frac{E}{Q} \right)_{273} \approx \left( \frac{3\alpha E}{C_v} \right)_{273} \\ &= \frac{3\alpha_{273} \cdot 273 \cdot D(\theta/273)}{C(\theta/273)} \end{aligned}$$

where  $C(\theta/273)$  is the specific heat function and  $\frac{C_v}{3\alpha} = Q = \text{constant}$  for low temperatures.

In the case of alkali halides investigated in the present experiments the graphs of  $\frac{a_0}{a_T - a_0}$  against  $\frac{1}{T \cdot D(\theta/T)}$  are straight lines, as predicted by the Gruneisen theory. The Gruneisen's parameters  $Q/2R$  and  $3\rho$ , therefore, assume great importance. The parameters determined from the above graphs for the different halides are compiled in Table V. The values of these parameters for CsBr calculated from the X-ray measurements of Johnson *et al.*, are given for comparison.

TABLE V  
Grüneisen parameters

Substance	$(Q/2R) \times 10^3$	$\beta p$	Reference
KBr	28.81	7.25	Present values
	28.60	—	Eq. 9
KI	27.12	6.50	Present values
	25.20	—	Eq. 9
CsBr	23.56	7.25	Present values
	27.10	10.80	Johnson <i>et al.</i> , (1955)
	23.20	—	Eq. 9

The value of  $Q$  can also be obtained from the relation

$$Q = \frac{V_0}{\gamma \cdot K_0} \quad \dots \quad (9)$$

where  $K_0$  and  $V_0$  are the compressibility and molar volume at 0°K. The values of  $Q/2R$  calculated from this equation are also given in Table V, the values of  $V_0$ ,  $\gamma$  and  $K_0$  being taken from Born and Huang (1954).

#### ROLE OF LATTICE DEFECTS IN THE EXPANSION OF IONIC CRYSTALS

The fact that the ionic crystals conduct an electrolytic current which obeys Ohm's law at high temperatures shows that these crystals possess imperfections at elevated temperatures. It has been found that the ionic conductivity increases as the temperature increases showing that the concentration of the defects increases with temperature. Schottky (1935) and Jost (1933-37) have shown that it is exceedingly unlikely that interstitial ions occur in any appreciable quantity in alkali halides. Mott and Littleton (1938) have refined the calculations and have shown in the case of Sodium chloride, for example, that the energy required to take a  $Na^+$  ion from a normal lattice position to an interstitial position is 2.9 eV, whereas the energy required to form a pair of vacancies is 1.86 eV. Thus the number of interstitial ions is very much less than the number of vacancies indicating that in alkali halides the Frankel defects are practically absent while the Schottky defects predominate.

As the temperature increases more and more ion pairs which were forming the part of the Schottky defects migrate to the surface. At the surface these ions are not surrounded by the bulk of the lattice and they cease to be defects. Now they could be reasonably expected to behave as fresh ions which are

deposited on the surface of an ionic crystal, forming the same structure as the bulk of the crystal. This happens because the ions are of the same type as constitute the crystal. These fresh deposits will increase the total volume of the crystal but will not modify the cell size. The cell size will alone be measured in the X-ray pictures, while in the macroscopic measurement of volume we measure the total volume (due to thermal expansion of the cell and that due to the surface deposits).

We are thus led to believe that the difference in the measured values of  $\alpha$  by the X-ray and the macroscopic methods may be due to the fresh deposits at the surface due to the migration of the ions forming the Schottky defects. If this is correct we could expect the divergence in the two values to increase with the temperature. It thus appears plausible that we could estimate the degree and the extent of the migration of the defects by carrying out accurate measurements of  $\alpha$  by the X-ray and the macroscopic methods. This work has been started by us and appears hopeful.

#### ACKNOWLEDGMENT

It is a pleasure to record our sincere thanks to Professor K. R. Dixit for useful discussion and help in preparing this paper.

#### REFERENCES

- Born, M. and Huang, K., 1954, *Dynamical Theory of Crystal Lattices*, pp. 52-54, Clarendon Press, Oxford.
- Connell, L. F. and Martin, H. C., 1951, *Acta Cryst.*, **4**, 75.
- Gott, A., 1942, *Ann. Phys. Leipzig*, **41**, 520.
- Johnson, J. W., Agron, P. A. and Bredig, M. A., 1955, *J. Amer. Chem. Soc.*, **77**, 2734.
- Jost, W., 1933, *J. Chem. Phys.*, **1**, 466; 1934, *Z. Phys. Chem.*, **A169**, 129; 1936, *Ibid.*, **B32**, 1; 1937, *Diffusion und Chemische Reaktion in festen Stoffen*, Stenckopf, Leipzig.
- Krishnan, R. S. and Srinivasan, R., 1956, *Proc. Phys. Soc.*, **B69**, 679.
- Mott, N. F. and Littleton, M. J., 1938, *Trans. Farad. Soc.*, **34**, 485, 500.
- Pathak, P. D. and Pandya, N. V. 1959, *Curr. Sc.*, **28**, 320; 1960, *Ibid.*, **29**, 14.
- Roberts, J. K., 1951, *Heat and Thermodynamics*, p. 543, Blackie and Son, Ltd., London.
- Schottky, W. 1935, *Z. Phys. Chem.*, **B29**, 335.

# CHOICE OF SAMPLED WAVES FOR TIME-DIVISION MULTIPLEX TELEPHONE SYSTEMS

P. N. DAS

READER IN TELECOMMUNICATION ENGINEERING UNIVERSITY OF ROORKEE

(Received, December 12, 1959; after revision, May 25, 1960)

**ABSTRACT.** We can have multiplex telephone systems by using sampled voice signals on time division basis. These sampled voice signals may be used to operate the telephone receivers directly. The paper deals with the choice of the optimum frequency and width at which the voice signals are to be sampled in order that the telephone receivers may give the maximum output without having any appreciable distortion.

## INTRODUCTION

Recently time-division principles have been applied to multiplex radio relay systems (Grieg and Levine, 1946) and pulse code modulation methods have been used in many of them (Black, 1947 and Fieldman 1948). The use of sampled waves in time-division working has some advantages in telephone systems and although their use in telephone systems has not yet been established, work is being carried on in this direction (Chattermole, 1958 and Price, 1958). Sampling frequencies of different values and of different width have been tried but no investigation appears to have been made with regard to the determination of the optimum values of the sampling frequency and its width. Sampled voice signals are just like pulse amplitude modulated signals but in them as the modulations are unidirectional, no demodulation is required and they can be used to operate the telephone receivers directly. An attempt has been made in this paper to determine the optimum values of the sampling frequency and its width when sampled voice signals are used to operate the telephone receivers directly.

## TELEPHONE RECEIVER AND SAMPLED VOICE SIGNALS

In the case of sampled voice signals with square-topped pulses separated by spaces of no pulses, not only will the original voice signal be present but there will also be a very large number of beat frequencies formed by the frequencies of the original wave with the fundamental and odd harmonics of the sampling frequency. When the sampling frequency is greater than twice the highest frequency component present in the voice signal, all the frequency components of the voice signal will be present in the sampled wave according to Shannon's sampling theorem, but when a telephone receiver is subjected to such sampled voice signals, it will be subjected not only to the original voice signal but also to a very large



number of beat frequency components referred to above. It is, therefore, clear that if the telephone receiver is to give an exact reproduction of a voice signal from a sampled wave, the sampling frequency should not only be greater than double the highest frequency component present in the voice signal, but the sampling frequency should be such that none of the other wave packets associated with sampled wave may affect the telephone receiver.

When the number of channels to be worked on sampled voice signals on time-division basis is increased, the duration of the samples are to be necessarily decreased in proportion. Thus for a 100 channel system, the duration of the samples must at least be decreased to 1/100th part of the time between consecutive samples. When the duration of the samples is very small, however compared to the time between consecutive samples, the telephone receiver may be assumed to be subjected to a series of impulses at the sampling points and the diaphragm may be assumed to be displaced to distances proportional to the total sum of the amplitudes of the impulses. In this case also the frequencies in the signal will be reproduced exactly when the sampling frequency is an exact multiple of them. This can be shown very easily mathematically. When they are not exact multiples, the sum total of the amplitudes due to the same frequency component will be different in different half cycles and sub-harmonics of the frequencies will be introduced. These have been illustrated in Figs 1(a), 1(b), 1(c) and 1(d) for a few cases. As the voice signal consists of a band of frequencies, any one sampling frequency cannot be exact multiple of all the components. Therefore distortions are liable to be introduced. This distortion, however, decreases as the sampling frequency is increased and it is negligible when the sampling frequency is many times the highest frequency component present in the voice signal.

#### MATHEMATICAL TREATMENT

Suppose  $p$  is the angular frequency of the original wave and  $W$  is the angular frequency of the sampling rate.

Further, let  $yW = xp$  where  $y$  and  $x$  are the two minimum possible integral numbers.

Then the angular distance between two consecutive samples will be given by

$$\theta = 2\pi \frac{y}{x}$$

If  $m$  samples correspond to  $n$  cycles of the wave

Then  $\theta.m. = n.2\pi$  ( $m$  and  $n$  are integral numbers)

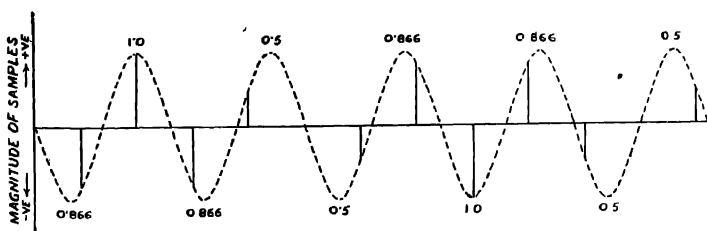
or 
$$n = \frac{\theta.m.}{2\pi} = \frac{2\pi y}{x} \frac{m}{2\pi} = \frac{y}{x} \cdot m$$

Thus for given values of  $y/x$ ,  $m$  will be of such value that  $n$  becomes an integer.

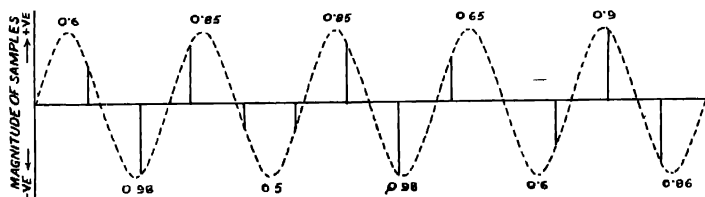
When  $W = 2p, 3p, 4p$  etc,  $n$  will become equal to 1. Therefore in each cycle there will be a definite number of samples and it can be shown that the total magnitude of the samples in each half portion is also equal. Therefore if a telephone receiver be subjected to each sampled waves instead of the continuous wave, it will give the same reproduction.

When, however,  $y/x$  has a value such that  $y$  has got a value other than 1,  $n$  will also have a value other than 1. In such a case a fixed number of samples cannot be contained in each cycle of the wave and so the samples in each cycle will be differently distributed but a definite number of samples will be repeated after every few and definite number of cycles of the wave, this number of cycles being given by the value of  $n$ . Further, the sum total magnitude of the samples in each half cycle will not be of the same value and a sub harmonic of the order of the value  $n$  will be introduced.

If a band of frequencies, say, voice frequencies are, therefore, sampled and a receiver is subjected to such a sampled wave, a few frequency components whose direct multiples will be the sampling frequency, will be correctly reproduced and others will be distorted. It is to be noted, however, that higher the values of sampling rates, greater will be the number of samples present in each half cycle of each component and less will be the differences in total magnitude of the samples. These will be evident from Figs. 1(a), 1(b) 1(c) and 1(d). Therefore, for good



(a)  $\theta = 150^\circ$ ;  $p = \frac{5}{12}\omega$ ;  $\omega = 2\frac{2}{5}p$ .



(b)  $\theta = 140^\circ$ ;  $p = \frac{7}{8}\omega$ ;  $\omega = 2\frac{4}{7}p$ .

Fig. 1(a) & 1(b). Total magnitude of pulses in different half cycles when sampling done at a frequency which is not an exact multiple of the frequency of the wave.

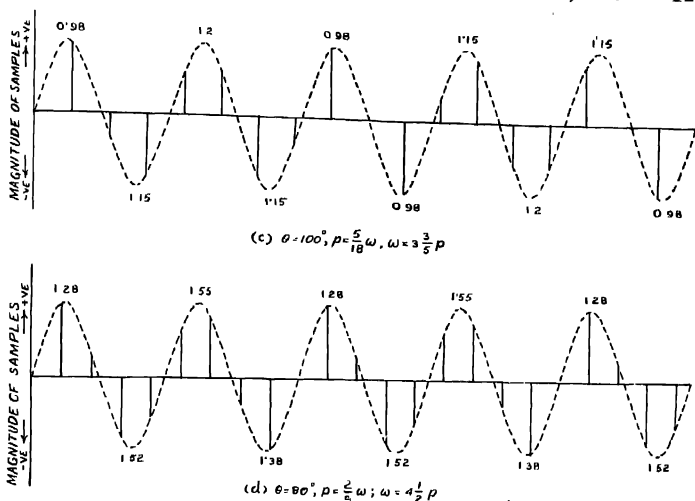


Fig. 2(c) & (d). Total magnitude of pulses in different half cycles when sampling is done at a frequency which is not an exact multiple of the frequency of the wave.

reproduction purposes, the sampling frequency should be quite a number of times the highest frequency component present in the voice signal. As discussed afterwards, it has been experimentally found that the sampling frequency should be at least 4 times the highest frequency component present in the voice signal, in order that the distortions in the output of the telephone receiver may be negligible.

#### METHODS OF PRODUCING SUITABLE SAMPLED WAVES

Germanium diodes in the form of a bridge have been used by the author elsewhere (Das, 1957) in producing sampled waves as shown in Fig. 2. The bridge shows a low resistance between the points *A* and *B* when *C* is at a higher potential than *D* and it shows a very high resistance when *C* is at a lower potential than *D*. If an alternating voltage referred to as the switching voltage be applied between *C* and *D*, then the bridge will be made conducting and non-conducting alternately between the points *A* and *B* and the bridge will behave like a switch between *A* and *B*. If pulses are used as switching voltage in series with a bias voltage as shown, then also the bridge will be conducting during pulse periods only if the pulse voltage is greater than the bias voltage. Pulses of varying frequency and varying width are obtained by triggering a monostable multivibrator

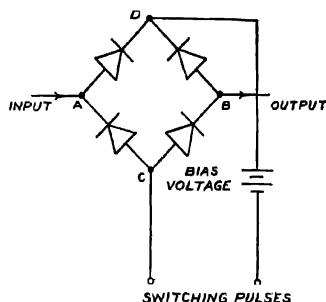


Fig. 2. Bridge switching circuit with Bias voltage.

with a blocking oscillator. The frequency of pulses is changed by changing the frequency of triggering pulses with the help of the blocking oscillator and the duration of the pulses is changed with the help of the monostable multivibrator used. Thus using such pulses as switching voltages, we can get the sampled waves of different sampling frequency and of different width.

### EXPERIMENTAL

#### (i) Optimum sampling frequency

The experimental arrangement is shown in Fig. 3. The switching voltage obtained in the way described above is applied to the bridge circuit consisting of four germanium diodes in series with a bias battery voltage of 5 volts. The audio signal was obtained from an audio oscillator and the sampled

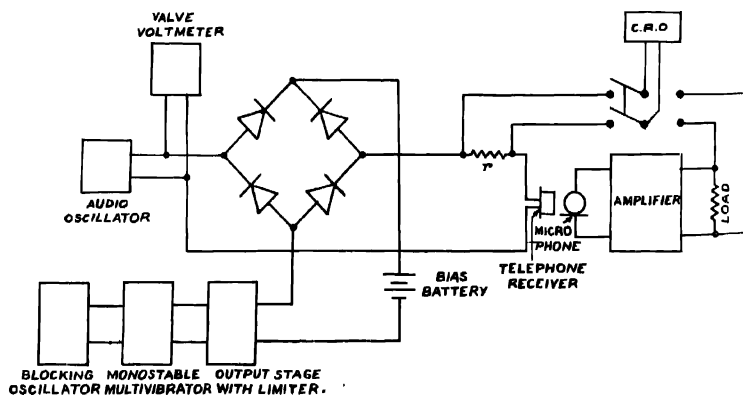


Fig. 3. Experimental arrangement.

wave obtained was connected directly to a telephone receiver. The output of the telephone receiver is fed to a microphone and the output signal from the microphone is amplified by means of an amplifier whose output was studied with a C.R.O. When the sampling frequency was above 10 Kc/s, the output of the telephone receiver was found to be an exact reproduction of the audio signal over the entire voice signal range up to 3 Kc/s irrespective of the width of the samples. When the sampling frequency was lower than 10 Kc/s, but an exact multiple of the audio signal, then also the output was found to be an exact reproduction of the signal which was sampled. When, however, the sampling frequency was less than 10 Kc/s and not an exact multiple of the audio signal frequency, distortions were found to be present in the output and these distortions varied as the sampling frequency was changed evidently due to the different sub-harmonics that were present in the different cases. One such distorted signal as seen in C.R.O. for a sinusoidal wave is shown in Fig. 4(a). When, however, the sampling frequency was 10 Kc/s and above, the output of the same audio wave as seen in C.R.O. is as shown in Fig. 4(b).

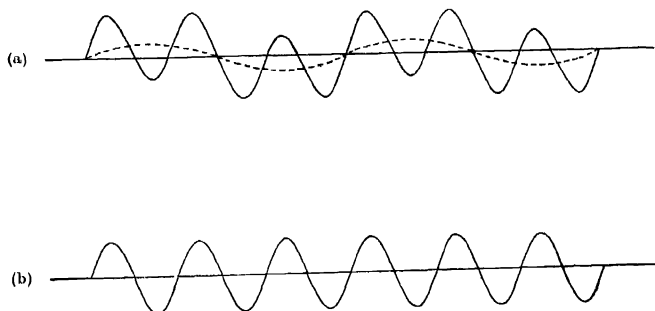


Fig. 4. (a) Output of a sinusoidal signal when sampling frequency is not an exact multiple of the signal and much below 10 Kc/s.

(b). Output of the same sinusoidal signal when the sampling frequency is 10 Kc/s.

#### (ii) *Optimum width of samples*

The power of the original wave is theoretically proportional to  $t^2/T^2$  in the sampled wave where  $t$  is the width of the sample and  $T$  is the time interval between consecutive samples. Therefore, if keeping the sampling frequency constant, its width is decreased, the power of the original wave in the sampled wave will also be decreased and in order to get the same power output the power of the original wave has to be increased before it is sampled. This has been experimentally determined with the same experimental arrangement, with the slight modification by which the output can be measured. The results obtained are

shown in Fig. 5. Excess power in *db* required in audio signals of 1000 c.p.s. before it is sampled in order that the sampled waves may give the same audio signal output in a telephone receiver, has been plotted against width of samples of different sampling frequency. It is seen that smaller the width of the samples, larger the power required in the audio signals for giving the same output from

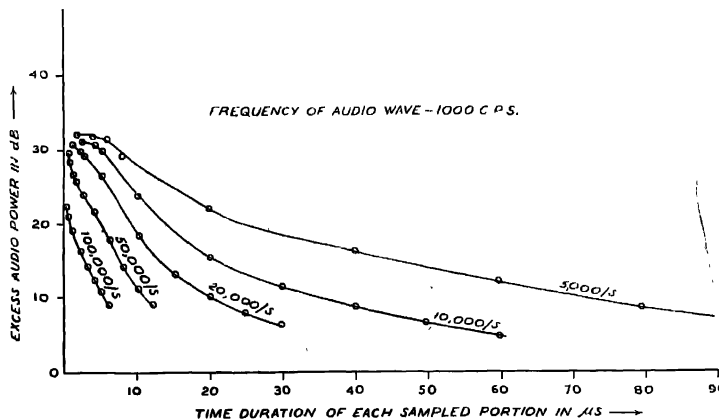


Fig. 5.

the sampled waves. The maximum width of samples is, however, determined by the sampling frequency and the number of channels in the system. With 10 Kc/s as the sampling frequency, the value of  $T$  is fixed i.e. 100  $\mu$ -secs. Thus for a 10-channel system, the maximum theoretical value of the width of the sample can be 10  $\mu$ -secs. If we are to give a margin of 100 p.c. distortion, the width of the samples will be limited to 5  $\mu$ -secs only. With such samples the audio signal has to be increased in power by about 30 db before sampling if the telephone receiver is to give the same output as the original audio signal.

#### DISCUSSION

When a telephone receiver is directly operated by sampled voice signals, the sampling frequency having a value equal to double the highest frequency component present in voice signals, the reproduction is not satisfactory because of the beat frequency components formed by the fundamental and odd harmonics of sampling frequency. For instance, if the sampling frequency is three times a particular frequency component in the voice signal, then the second harmonic will be introduced by the lower beat. For this reason although 3 Kc/s may be taken as the highest frequency component of the voice signals, a sampling frequency of 6 Kc/s does not reproduce the original signal faithfully. The beat frequencies

formed by higher harmonics present in the square-topped signals may be negligible but the beat frequency formed by the fundamental of the sampling frequency cannot be neglected. An ordinary telephone receiver is not very sensitive above 7 Kc/s. Hence if the beat frequency formed by any component of the voice signal with at least the fundamental of the sampling frequency does not come within 7 Kc/s, the reproduction is not distorted. As the highest frequency component present in voice signals may be taken as 3 Kc/s, the lowest sampling frequency necessary is 10 Kc/s as experimentally determined.

When the samples are of very short durations, distortion due to the sampling frequency being not an exact multiple of any voice signal frequency, is also negligible when the sampling frequency is at least 10 Kc/s. The maximum width of the samples that can be used is limited by the number of channels for a particular sampling frequency. It is to be noted, however, that when the number of channels is increased and the width is necessarily decreased it is not necessary to increase the power of the audio signal proportionately as shown by the flat nature of curves of Fig 6 towards the smaller width regions. As it is desirable to use the lowest value of sampling frequency, 10 Kc/s is the optimum value for sampling voice signals to be used for working telephone receivers and the optimum width of the samples is determined by the number of channels in the system.

#### ACKNOWLEDGMENT

The author is very much grateful to Prof. C. S. Ghosh, Head of Electrical Engineering Department, University of Roorkee, Roorkee, for his encouragement in carrying out the work.

#### REFERENCES

- Black, H. S., 1947, *Bell Labs. Record*, **257**, 265.  
Chattermole, K. W., 1958, *Proc. I. E. E.*, **105**, Part B, 499.  
Chattermole, K. W., 1958, *Proc. I. E. E.*, **105**, Part B, 471.  
Das, P. N., 1957, *Journal of Technology*, **11**, 18.  
Grieg and Lavino, 1946, *Electrical Communication*, **23**, 159.  
Fieldman, C. B., 1948, *Bell Labs. Record*, **299**, 364.  
Prico, J. C., 1958, *Proc. I. E. E.*, **105**, 463.

# Letters to the Editor

*The Board of Editors will not hold itself responsible for opinions expressed in the letters published in this section. The notes containing reports of new work communicated for this section should not contain many figures and should not exceed 500 words in length. The contributions must reach the Assistant Editor not later than the 15th of the second month preceding that of the issue in which the letter is to appear. No proof will be sent to the authors.*

13

## FORCE CONSTANTS OF THE URANYL ION BY WILSON'S F-G MATRIX METHOD

K. V. NARASIMHAM

(APPLIED PHYSICS DEPARTMENT, MADRAS INSTITUTE OF TECHNOLOGY, CHROMPET, MADRAS)

(Received, April 2, 1960)

The force constants of the  $\text{UO}_2^{++}$  ion in caesium uranyl nitrate have been calculated by the Wilson's normal coordinate treatment (1939 and 1941) for both the bent and linear structures ( $C_{2v}$  and  $D_{\infty h}$  point groups respectively). The vibrational frequencies, bond length and bond angle are taken from the data reported by Dieke and Duncan (1949). They are as follows .

Symmetric stretching frequency	883.98 $\text{cm}^{-1}$
Symmetric bending frequency	213.16 „
Antisymmetric stretching frequency	956.20 „
Bond length 1.58 Å.	Bond angle 135°.

For the bent uranyl ion, four constants  $F_a$ ,  $F_{ad}$ ,  $F_d$  and  $F_a$  are to be calculated and there are only three frequencies for the ion. Therefore, the value of  $F_d$  calculated by Satyanarayana (1942) using the equations given by the valence force field theory has been taken. The value is  $6.97 \times 10^5$  dynes/cm. Assuming this value of  $F_d$ , the other potential constants are calculated by the F-G matrix method.

For the linear uranyl ion, the G matrix elements are obtained from the tables of Decius (1948). But a deficiency occurs in his tables when a molecule contains three or more collinear nuclei as in the expressions for the s-vectors given by Wilson for bending coordinates, the denominator becomes zero. Therefore, Fongle and Meister (1951) have given alternate expressions for the kinetic energy



matrix elements of the bending co-ordinates for linear molecules, from which the  $g$  matrices of the bending coordinates of the  $\text{UO}_2$  ion are calculated.

TABLE

Force constant	Description	Bent $\text{UO}_2$ ion ( $C_{2v}$ ) ( $\times 10^5$ dynes/cm.)	Linear $\text{UO}_2$ ion ( $D_{\infty h}$ ) ( $\times 10^5$ dynes/cm.)
$f_d$	O-U stretching	16.97	17.49
$f_{dd}$	Interaction between the two bonds	-0.77	-0.12
$f_a$	O-U-O bending	0.47	0.20
$l_{da}$	Interaction between the bond and angle	-2.31	0

The author is thankful to Dr. V. Santhamma for her help in the course of the calculations and to Dr. V. Ramakrishna Rao for his interest in the work.

## REFERENCES

- Decius, J. C., 1948, *J. Chem. Phys.*, **16**, 1025.  
 Dieke, G. H. and Duncan, A. B. F., 1949, *Spectroscopic Properties of Uranium Compounds* (McGraw Hill publication).  
 Feigle and Meister, 1951, *J. Chem. Phys.*, **19**, 982.  
 Satyanarayana, B. S., 1942, *Proc. Ind. Acad. Sci.*, **15A**, 414.  
 Wilson, E. B., 1939, *J. Chem. Phys.*, **7**, 1047.  
 Wilson, E. B., 1941, *J. Chem. Phys.*, **9**, 76.

## 14

PHASE-TRANSITIONS IN  $\text{Cu}[(\text{NH}_4)\text{SO}_4]_2 \cdot 6\text{H}_2\text{O}$ 

(Miss) GOURI BHOWMIK

DEPARTMENT OF MAGNETISM, INDIAN ASSOCIATION FOR THE CULTIVATION OF SCIENCE,  
 JADAVPUR, CALCUTTA-32.

(Received, August 8, 1960)

Magnetic measurements showed (Bose, *et al.*, 1957 & 58) that the single crystals of many Tutton salts (composition  $\cdot \text{M}(\text{AXY})_2 \cdot 6\text{H}_2\text{O}$ ) lost their magnetic anisotropies in the range  $65^\circ$ – $120^\circ\text{C}$ , probably due to a phase transition taking place which caused the single crystal to become polycrystalline. As a preliminary to studying the change in magnetic properties of the substance with change in structures, a study of the thermal dehydration of a typical case—that of  $\text{Cu}[(\text{NH}_4)\text{SO}_4]_2 \cdot 6\text{H}_2\text{O}$ , was undertaken which shows that there is a loss of 4 molecules of water at  $67^\circ\text{C}$ . The crystal structure of the dehydrated product was then

studied from X-ray powder photograph. It is found that the dehydrated product consists of the double salt  $\text{Cu}(\text{NH}_4)\text{SO}_4\cdot 2, 2\text{H}_2\text{O}$ . Application of Lipson's method (Lipson, 1949) shows that it has an orthorhombic unit cell having dimensions:  $a = 14.84\text{\AA}$ ,  $b = 12.52\text{\AA}$ ,  $c = 10.69\text{\AA}$  containing 8 molecules per cell. Conditions of reflection suggest the possibility of assigning to the dihydrate either of the space-group  $\text{P}_{mn}2_1$  or  $\text{P}_{mmm}$ .

Since direct X-ray data on  $\text{Cu}(\text{NH}_4)\text{SO}_4\cdot 6\text{H}_2\text{O}$  single crystal is lacking, we also undertook to study it and find that the hexahydrate which belongs to the space-group  $\text{P}2_1/a$  and contains 2 molecules in the unit cell (Hofmann, 1931), has the following cell dimensions.  $a = 9.27\text{\AA}$ ,  $b = 12.50\text{\AA}$ ,  $c = 6.33\text{\AA}$ ,  $\beta = 106.5^\circ$ .

It is interesting to note that the  $b$  axis in both the hexa- and dihydrate has the same length. It is, therefore, probable that the transition from the monoclinic to the orthorhombic system has taken place after merely a loss of 4 water molecules and a rearrangement of the molecules with reference to two vertical planes i.e., the transition is "topotactic" in nature.

Phase transition study for further dehydration and a more detailed study of structural changes by growing single crystals at high temperatures are under progress.

The author expresses her sincere thanks to Prof. A. Bose, D.Sc., F.N.I., for his kind interest and constant guidance and to Mr. S. Ray, M.Sc., for many helpful discussions during the progress of the work.

#### REFERENCES

- Bose, A., Mitra, S. C. and Dutta, S. K., 1957, *Proc. Roy. Soc., A* **239**, 165.  
 Bose, A., Mitra, S. C. and Dutta, S. K., 1958, *Proc. Roy. Soc., A* **248**, 153  
 Hofmann, W., 1931, *Zeits f. Krist.*, **78**, 279.  
 Lipson, H., 1949, *Acta Cryst.*, **2**, 43

#### 15

### F-G MATRIX ELEMENTS FOR PYRAMIDAL $\text{XY}_2\text{Z}$ MOLECULES

P. BABU RAO AND K. SREERAMAMURTY

PHYSICS DEPARTMENT, S. V. UNIVERSITY COLLEGE, TIRUPATI

(Received July 7, 1960)

Using Wilson's F-G matrix methods (1939, 1941), Pistorius (1959) obtained the elements for the planar  $\text{XY}_2\text{Z}$  type molecules employing the most general harmonic force field. These were recalculated by the authors (1960) and utilised to calculate the potential constants for certain specific cases. Venkateswarlu and Sundaram (1957) carried out a normal coordinate treatment for the pyramidal

$XY_2Z$  type molecules neglecting a number of force constants. As a large number of these molecules are known and as their structural constants are being found by microwave techniques, it is felt desirable to carry out a similar calculation for this type of molecules employing the most general harmonic force field.

The following symmetry coordinates are set up which transform according to the characters of the corresponding vibration types.

$$A' \quad R_1 = \frac{1}{\sqrt{3}} (\Delta D + \Delta d_1 + \Delta d_2)$$

$$R_2 = \frac{1}{\sqrt{6}} (2\Delta D - \Delta d_1 - \Delta d_2)$$

$$R_3 = \frac{d}{\sqrt{3}} (\Delta\alpha_1 + \Delta\alpha_2 + \Delta\beta)$$

$$R_4 = \frac{d}{\sqrt{6}} (2\Delta\beta - \Delta\alpha_1 - \Delta\alpha_2)$$

$$A'' \quad R_5 = \frac{1}{\sqrt{2}} (\Delta d_1 - \Delta d_2)$$

$$R_6 = \frac{d}{\sqrt{2}} (\Delta\alpha_1 - \Delta\alpha_2)$$

Here  $\Delta D$  and  $\Delta d$  represent the  $X \cdots Z$  and  $X-Y$  stretchings,  $\Delta\alpha$  and  $\Delta\beta$  the valence angle bendings of  $Y-X-Z$  and  $Y-X-Y$  respectively

The potential energy  $V$  is given by

$$\begin{aligned} 2V = & f_D \cdot \Delta D^2 + f_d \sum_i \Delta d_i^2 + 2f_{Dd} \cdot \Delta D \sum_i \Delta d_i \\ & + 2f'_{dd} \Delta d_1 \Delta d_2 + 2f_{Da} \Delta D \cdot d \sum_i \Delta\alpha_i + 2f_{da} \cdot d \cdot \sum_i \Delta d_i \Delta\alpha_i \\ & + 2f'_{aa} \cdot d \sum_{i \neq j} \Delta d_i \Delta\alpha_j + 2f_{d\beta} d \Delta\beta \sum_i \Delta d_i \\ & + 2f_{D\beta} \Delta D \cdot d \Delta\beta + f_a d^2 \sum_i \Delta\alpha_i^2 + 2f_{a\alpha} d^2 \Delta\alpha_1 \Delta\alpha_2 \\ & + 2f_{a\beta} d^2 \Delta\beta \sum_i \Delta\alpha_i + f_\beta d^2 \Delta\beta^2 \end{aligned}$$

The following  $F$  matrix elements are obtained :

$$A' \quad F_{11} = \frac{1}{3} (f_D + 4f_{Dd} + 2f_1)$$

$$F_{12} = \frac{1}{3\sqrt{2}} (2f_D + 2f_{Dd} - 2f_1)$$

$$F_{13} = \frac{1}{3} (2f_{D\alpha} + f_{D\beta} + 2f_2 + 2f_{d\beta})$$

$$F_{14} = \frac{1}{3\sqrt{2}} (2f_{D\beta} + 4f_{d\beta} - 2f_{D\alpha} - 2f_2)$$

$$F_{22} = \frac{1}{6} (4f_D - 8f_{D\alpha} + 2f_1)$$

$$\frac{1}{3\sqrt{2}}$$

$$F_{24} = \frac{1}{6} (4f_{D\beta} - 4f_{D\alpha} + 2f_2 - 4f_{d\beta})$$

$$F_{33} = \frac{1}{3} (2f_3 + 4f_{\alpha\beta} + f_\beta)$$

$$F_{34} = \frac{1}{3\sqrt{2}} (2f_{\alpha\beta} + 2f_\beta - 2f_3)$$

$$F_{44} = \frac{1}{6} (4f_\beta + 2f_3 - 8f_{\alpha\beta})$$

Where  $f_1, f_2$  and  $f_3$  stand for

$(f_d + f_{dd}), (f_{d\alpha} + f'_{d\alpha})$  and  $(f_\alpha + f_{\alpha\alpha})$  respectively.

$$A'' : \quad \begin{aligned} F_{55} &= f_d - f_{dd} \\ F_{56} &= f_{d\alpha} - f'_{d\alpha} \\ F_{66} &= f_\alpha - f_{\alpha\alpha} \end{aligned}$$

The elements of the inverse kinetic energy ( $G$ ) matrix are given below using the following abbreviations :

$$\begin{aligned} d/D - \cos \alpha &= K & 1 + \cos \alpha - \cos \beta &= Q \\ 1 - d/D \cos \alpha &= L & 1 + \cos \beta - 2 \cos \alpha &= T \\ 1 - \cos \alpha &= M_\alpha & 1 - \cos \beta - 2 \cos^2 \alpha &= V \\ 1 - \cos \beta &= M_\beta & \cos \alpha = c_\alpha, \quad \sin \alpha = S_\alpha \\ 1 + \cos \beta &= N & \cos \beta = C_\beta, \quad \sin \beta = S_\beta \\ 1 + 2 \cos \alpha &= P \end{aligned}$$

$\mu_i$  = Reciprocal mass of the atom  $i$

$A'$  :

$$G_{11} = \frac{1}{3} \left[ \mu_x \{2(N+P)-1\} + 2\mu_y + \mu_z \right]$$

$$G_{12} = \frac{\sqrt{2}}{3} \left[ \mu_x (P-Q) - \mu_y + \mu_z \right]$$

$$G_{13} = -\frac{2}{3} \mu_x \left[ \frac{KQ + LP}{S_\alpha} + \frac{2M_\beta Q}{S_\beta} \right]$$

$$G_{14} = -\frac{\sqrt{2}}{3} \mu_x \left[ \frac{KQ + LP}{S_\alpha} + 2 \frac{S_\beta^2}{S_\beta} \frac{C_\alpha M_\beta}{S_\beta} \right]$$

$$G_{22} = \frac{1}{3} [\mu_x(2T + M_\beta) + \mu_y + 2\mu_z]$$

$$G_{23} = \frac{\sqrt{2}}{3} \mu_x \left[ \frac{KT - 2LM_\alpha}{S_\alpha} + \frac{M_\beta T}{S_\beta} \right]$$

$$G_{24} = \frac{1}{3} \mu_x \left[ \frac{KT - 2LM_\alpha}{S_\alpha} + \frac{2M_\beta T}{S_\beta} \right]$$

$$G_{33} = \frac{2}{3} \left[ \mu_x \left\{ \frac{K^2 N + 2L^2 + 4C_\alpha K L}{S_\alpha^3} + M_\beta + \frac{2M_\beta N K + 8C_\alpha M_\beta L}{S_\alpha S_\beta} \right\} \right. \\ \left. + 2\mu_y \left( 1 + \frac{C_\alpha M_\beta}{S_\alpha S_\beta} \right) + \mu_z \frac{d^2}{D^2} \frac{V}{S_\alpha^2} \right]$$

$$G_{34} = \frac{\sqrt{2}}{3} \left[ \mu_x \left\{ 2M_\beta + \frac{S_\beta^2 K + 2C_\alpha M L}{S_\alpha S_\beta} - \frac{N L^2 + 2L^2 + 4C_\alpha K L}{S_\alpha^2} \right. \right. \\ \left. \left. + \mu_y + \mu_z \frac{d^2}{D^2} V \right\} \right]$$

$$G_{44} = \frac{1}{3} \left[ \mu_x \left\{ 4M_\beta + \frac{M_\beta K^2 + 2L^2 + 4C_\alpha K L}{S_\alpha^2} - 4 \frac{S_\beta^2 K + 2C_\alpha M L}{S_\alpha S_\beta} \right\} \right. \\ \left. + \mu_y \left( 5 - \frac{4C_\alpha M_\beta}{S_\alpha S_\beta} \right) + \mu_z \frac{d^2}{D^2} \frac{V}{S_\alpha^2} \right]$$

$$G_{55} = \mu_x M_\beta + \mu_y$$

$$G_{56} = -\mu_x \frac{M_\beta K}{S_\alpha}$$

$$G_{66} = \mu_x \frac{M_\beta K}{S_\alpha^2} + \mu_y + \mu_z \frac{d^2}{D^2} \frac{M_\beta}{S_\alpha^2}$$

## REFERENCES

- Babu Rao, P. and Sreeramamurty, K., 1960, *Zeits. f. Phys. Chemie*, Communicated.  
 Pistorius, C. W. F. T., 1959, *J. Chem. Phys.*, **30**, 332.  
 Venkateswarlu, K., and Sundaram, S., 1957, *J. Chem. Physique*, 202.  
 Wilson, Jr., E. B. 1939, *J. Chem. Phys.*, **7**, 1041.  
 „ 1941, *J. Chem. Phys.*, **9**, 76.

## BOOK REVIEWS

THE CHEMISTRY OF NATURAL PRODUCTS, Edited by K. W. Bentley,  
Volume I. "The Alkaloids" by K. W. Bentley. Interscience Publishers,  
New York. 1957. pp. 237.

The "Alkaloids" is the first of a series to be published and this is expected to have a wide coverage on the chemistry of natural products. In fact during the last three years a few volumes have already appeared. The aim of these publications as stated in the "Introduction" particularly the present one, is to have a golden mean between exhaustive treatises like "The Alkaloids" edited by Manske and Holmes and "The Plant Alkaloids" by Henry, primarily meant for the benefit of graduate students in British Universities.

It becomes extremely difficult for the author, who has however made notable contributions towards our knowledge of alkaloids, to apply his discretion with judgment consistent with clarity of expression, when he has to deal with an already vast and a rapidly expanding subject in such a short span of about 225 pages. Naturally many important topics of current interest had to be omitted in this book. Particular mention may be made of the absence of any chapter on Rauwolfia and curare alkaloids. Another aspect which merits considerable attention is that sufficient emphasis has been placed on biogenesis for better understanding of the formation of and correlation amongst different groups of alkaloids. It may be mentioned that these half-tested truths and plausible assumptions are now-a-days being accepted as absolutes and realities and this shows some unscientific tender-mindedness on the part of some authors.

Coverage of the book is quite commendable and it is a pleasant reading because of profusely neat and hand-drawn structures in every alternate page of the book. The only criticism that can be made is that some errors have crept into the book which are, of course, trivial in nature. Lot of credit goes to the author in presenting this volume at such a low price thereby making it available to a wide circle of readers and from these considerations, purpose of writing this book has been fully justified.

*P. C. D.*

PRINCIPLES OF PHYSICAL SCIENCE—By F. T. Bonner and M. Phillips,  
August, 1957, pp. 716, Addison-Wesley Publishing Co., Inc., Reading,  
Massachusetts, U.S.A. Price \$ 7.50.

It is now a well recognised fact that science has become such an integral part of our life that a basic knowledge of it is essential even for persons who are not

directly connected with science. It is a difficult task to give in the compass of a single volume the fundamentals of the physical sciences in a form which can be understood by the readers having no scientific background. In the present book the authors have performed this task very creditably. They have been able to give a coherent picture of the physical sciences from the astronomy of ancient Greeks to the modern chemistry, nuclear physics, geophysics etc. The topics for discussion have been very carefully chosen from the different branches of science so as to represent a good overall picture. The treatment of the various scientific phenomena is very clear and interesting. A large number of carefully designed illustrations is given which makes it easier to grasp the fundamentals. The book may be useful to fresh college students of science as additional reading. The large number of instructive examples at the end of each chapter will help to clarify the physical ideas. The get-up of the book is excellent.

B.N.S.

PROCEEDINGS OF THE INTERNATIONAL SYMPOSIUM ON ISOTOPE SEPARATION", edited by Kistemaker, Bigeleisen and Nier. (North-Holland Publishing Co.)

This volume is a compilation of the papers read at the first international symposium on isotope separation held in Amsterdam in 1957, organised by the Netherlands Physical Society in collaboration with the International Union of Pure and Applied Physics. There are at present not many standard books on the theory and method of isotope separation. The publication of this volume giving the latest achievements in this field is most welcome.

The study of the science of isotope separation has received great impetus during the last two decades with the discovery of nuclear fission and the use of separated isotopes as a tool for investigation of problems in chemistry, physics, biology and production technology. The book deals with both the science and the technology of production of isotopes, their purification and properties and covers a wide ground. All the papers are conveniently grouped according to the method of separation employed, under the following nine parts :

1) Chemical Engineering, 2) Molecular Interactions, (3) Chemical Exchange, 4) Electromigration, 5) Distillation, 6) Thermal Diffusion, 7) Diffusion, 8) Electro-magnetic Separation, 9) Ultra-centrifuges.

The chemical engineering section deals mainly with the design procedure for large scale isotope separation units starting from basic laboratory data while the second section deals with the physical properties of isotope mixtures whose knowledge is essential for the understanding of the different processes. In the section on "Diffusion" also various aspects of design theory for large diffusion

plants have been discussed. Reports on plants for large scale separation of nitrogen, hydrogen and boron isotopes as well as discussions on the theory of the process of isotope separation by chemical exchange have been included under the section "Chemical Exchange", while separation of isotopes of oxygen, lithium, hydrogen and boron by distillation process, and the economic considerations of a fractional distillation plant have been presented in "Distillation" section. The theory and performance of multi-stage thermal diffusion columns, have been discussed in the section on "Thermal Diffusion" and the production of  $U^{235}$  for the Manhattan District programme has been described. The operational experience of electromagnetic separators in Harwell and Oak-ridge has been described in the section on "Electromagnetic Separation". The progress in the practical aspects of isotope separation by the two comparatively new methods of electromigration and gas centrifuge has been reported in another two sections.

From the brief resume of the different sections given above it will be clear that the papers presented at the symposium cover a very wide spectrum of methods now available for isotope separation. The book will be very useful to all those who have some acquaintance with the subject and want to keep themselves abreast of the existing literature and the present trends. Sufficient details about design and construction have been given at several places to make the study more useful and realistic. The editors and the publishers are to be thanked for providing such a collection of up-to-date information about this very modern and developing subject.

*B. N. S.*



# AN ISOTOPE EFFECT IN THE COLLECTION ON CHARGED PLATES OF (n, $\gamma$ ) RECOIL PRODUCTS OF BROMINE

H. J. ARNIKAR AND A. LAL

LABORATORY OF NUCLEAR AND PHYSICAL CHEMISTRY, BANARAS HINDU UNIVERSITY, BANARAS

(Received, June 16, 1960)

**ABSTRACT.** A study of the relative yields of  $\text{Br}^{80}$ ,  $\text{Br}^{80m}$  and  $\text{Br}^{82}$  following an irradiation of  $\text{C}_6\text{H}_5\text{Br}$  for a duration of 9 days, by an analysis of the time-decay curves, show that the apparent yield of  $\text{Br}^{80}$  on the anode plate is roughly twice that of  $\text{Br}^{82}$ . These results are discussed, *vis-a-vis*, standard data for the thermal neutron capture cross sections of corresponding target atoms,  $\text{Br}^{79}$  and  $\text{Br}^{81}$  and their relative abundances. These findings, considered along with the probable counting efficiency for the resulting radioactive products and their decay characteristics, point to the existence of a small but definite net isotope effect in the overall process of (i) recoil, (ii) charge acquisition and (iii) collection on the charged plate.

## INTRODUCTION

Results of early workers (Fermi *et al.*, 1935; Libby and Vault, 1939, 1941 and Goldsmith and Bluerer, 1950) on the use of charged plates for collecting the (n,  $\gamma$ ) recoil products show marked differences in respect of relative yields collecting on the plates of either sign and of a separation or otherwise of isotopic and isomeric products. Fermi *et al.* (1935) found in the case of methyl or ethyl iodide vapour under neutron irradiation, the polarity of the collecting electrode was not significant. Similarly Libby and de Vault (1939 & 1941) find equal enrichment of  $\text{Br}^{80}$  isomers on the anode and cathode. On the contrary, the results of Paneth and Fay (1935 and 1936) on the separation of radioisotopes of As as well as of bromine and iodine forming under the Szilard-Chalmers' process showed a marked dependence of the yield not only on the sign of the electrode but on its chemical nature and physical condition of the surface. With Pt electrodes, for instance, no activity collects in the case of irradiation of aliphatic halogen compounds, while with smooth Ag or Cu electrodes the active products are deposited exclusively on the anode. In the case of bromobenzene, however, products collect on both anode and cathode in the ratio of roughly 2:1. The results of Capron (1946) are at further variance, more activity collects on the cathode than on the anode in the case of  $\text{C}_2\text{H}_4\text{Br}_2$ , while it is the reverse in the case of  $\text{C}_6\text{H}_5\text{Br}$ . This last finding of preferential collection on the anode appears to be of more frequent occurrence as, for instance, also in the separation of  $\text{In}^{114}$  isomers (Goldsmith and Bluerer, 1950).

There is a similar lack of agreement in respect of whether or not an isotopic and isomeric enrichment occurs in the products of the recoil process collecting on the charged plates. Fox and Libby (1952) Roul and Libby (1953) and Chien and Willard (1954) find no isotopic effect in the retention (fraction of active products left in the original organic medium unrecovered) in the case of *iso*- and *n*-propyl bromide, while Shaw (1951 and 1956) as well as Capron and co-workers (1946, 1952 and 1953) find important isotopic and even isomeric effects at least in the case of aromatic bromo-compounds. No agreed mechanism is available for the secondary reactions following the ( $n, \gamma$ ) recoil reaction, to account for the relative yields on the charged plates of the different isotopic and isomeric products as in the case of bromobenzene. The following work has been undertaken with the object of obtaining experimental data under controlled conditions which would help in understanding the role of ionization in the above, an aspect relatively less studied hitherto. The present paper reports results for the collection on charged plates of radioisotopes of bromine in a state of high specific activity and of the associated isotope effect.

#### EXPERIMENTAL

About 500 ml of bromobenzene were irradiated in a pyrex beaker by a 50mC source of (Ra+Be) plunged in the liquid. The neutron source was surrounded by 2 cm of paraffin and a thin walled glass tube. This glass sheath was necessary as both paraffin and polythene were found to be acted upon by bromobenzene under the action of the accompanying high energy gamma radiation. The

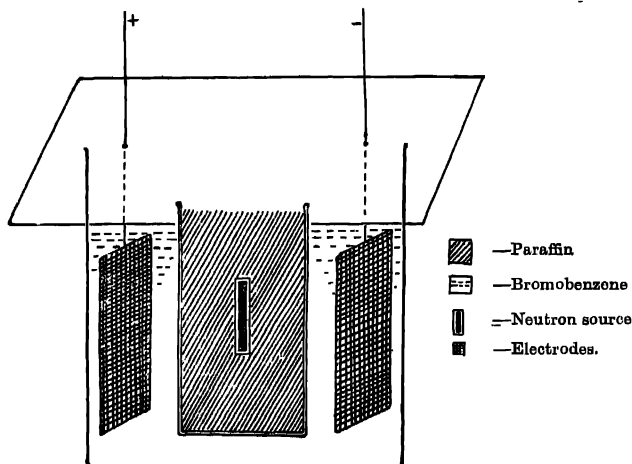


Fig. 1. Arrangement for the collection of ( $n, \gamma$ ) recoil products of bromine on charged plates.

electrodes consisting of two parallel plates of either (1) copper with a thin coat of agar-agar gel containing 0.1% of NaOH or (2) silver with or without a trace of AgBr, were placed 6 cms apart and symmetrically with respect to the neutron source, as shown in Fig. 1. The field was provided by a battery of 90 volts connected across the electrodes. Irradiations were conducted for a period of 9 days corresponding to about six-times the half-life of the longest lived isotope, viz. 36 hr Br-82. Sometimes a field of 1050 volts was applied during the last 5 hours of irradiation. The radio-isotopes were recovered in the end from the two charged plates separately as follows. In the case of the gel-coated copper electrodes, the gel was melted by warming and the liquid collected was evaporated directly in a counting tray and in the case of the Ag electrodes, the isotopes were recovered by washing the surface with a small amount of ammonia and evaporating the liquid to dryness in a counting tray. Separated in this way, the product was in a state of high specific activity, the amount of inactive bromine being negligible.

## RESULTS

The activities collected on the positive and negative electrodes were measured separately with a thin end-window G. M. counter under conditions of constant geometry. From an analysis of the corresponding time-decay curves the relative yields of different radioisotopes present in the fraction collected were computed. From two measures of the total activity produced in the liquid, with and without the electric field, determined with a liquid counter, the percentage retention was calculated. This varied between 60 to 70% for all the isotopes considered together. Decay curves (Figs. 2 and 3) which are typical of numerous observations show that three activities Br-82 (36 hr) and the metastable Br-80 $m$  (4.4hr) and her ground state Br-80 (18 mm) are produced. Also some of the last activities were directly formed from the target Br-79.

The use of extremely thin end-window counter permitted the counting of 80 KcV gammas, of which about 45% are internally converted, with an efficiency comparable to the counting of the betas from Br-80 and Br-82. Countings with a scintillation counter with and without filters for the betas justified this.

The relative yields given in Table I of the different activities collecting on the two electrodes are typical of a series of experiments.

TABLE I

Activity	Anodo	Cathodo
Total	450	220
36-hour	115	88
18-min	200	100
4.4-hour	135	32

The periods of the two isomers are such that they reach transient equilibrium during the duration of the experiment and the shorter lived (18 min) Br-80 decays with the same period, viz., 4.4 hours as its parent Br-80m. Hence of the total 4.4. hour activity measured one half is due to the daughter product.

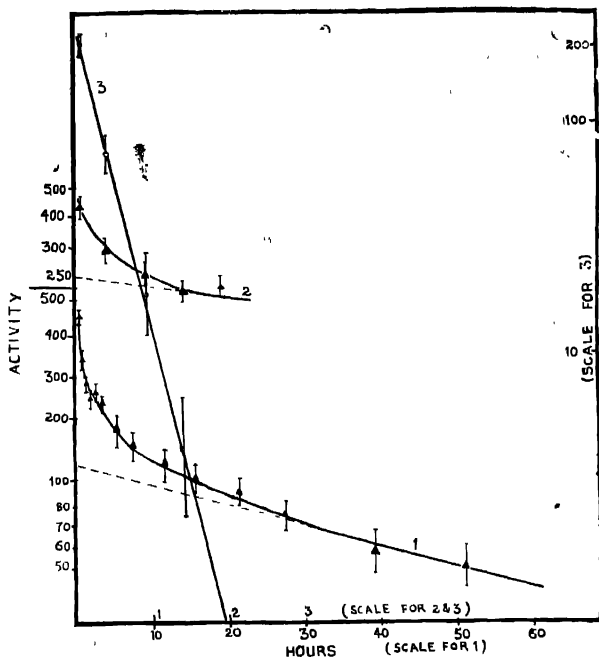


Fig. 2. Analysis of the decay curves of the activity collecting on the anode.

Positive Plate 1. Decay curve - Br-80, Br-80m, Br-82, 2. Decay curve : Br-80 & Br-80m, 3. Half-life line - Br-80.

This 'half' value together with the 18 min. activity directly formed from the target represents the total Br-80 collected. Table II shows the net values of the different radiostopes directly formed from the target.

TABLE II

Isotope	Anode	Cathode
Br-82	115	88
Br-80	200	100
Br-80 m.	68	16

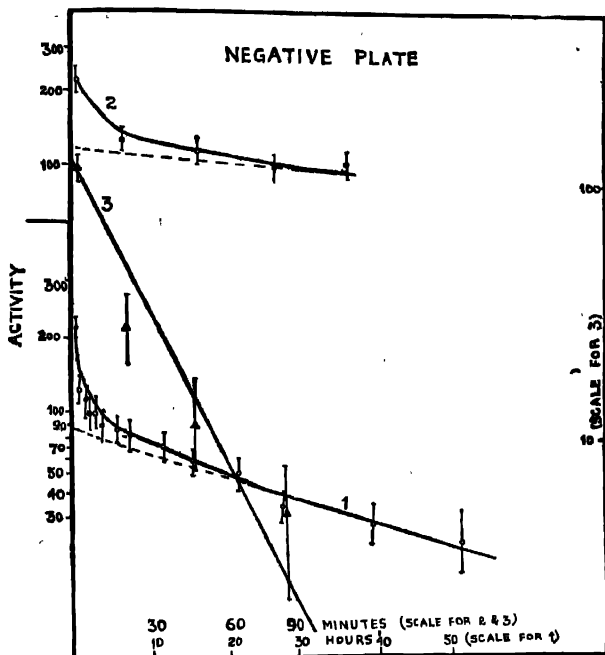


Fig. 3. Analysis of the decay curve of the activity collecting on the anode.  
 1. Decay curve: Br-80, Br-80 $m$  & Br-82, 2. Decay curve: Br-80 & Br-80 $m$ ,  
 3. Half-life line: Br-80.

#### DISCUSSION

In the formation of Br-80 by the  $(n, \gamma)$  reaction the maximum energy of the gamma emitted is 7.88 MeV (Groshev *et al.*, 1959) which gives 416 eV as the corresponding maximum recoil energy of the Br-80 nucleus, which is adequate for its rupture from the parent molecule. The initial recoil-rupture reaction



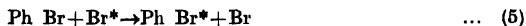
is, according to Libby (1947), followed by



As a recombination of these high energy particles may not be readily possible, Shaw (1956) suggests the following secondary reactions:



Reactions (3) and (4) tend to increase the Szilard-Chalmers' extraction yield while the isotope exchange reaction Eq.(5).



leads to increased retention. This is the basis of concentrating radioisotopes by the Szilard-Chalmer technique.

In the above mechanism, it is to be noted, that ionization is not referred to as a necessary stage. As against this, the results presented above as well as those reported earlier by Capron *et al* (1958) point to the appearance of ionization at some stage in the process. In our experiment, both positively and negatively charged particles have been collected (*vide* Table II). With a high factor of internal conversion ( $\sim 45\%$ ) associated with the transition  $\text{Br-80} \rightarrow \text{Br } 80m$ , a fraction of the initially formed Br 80 is to be expected to be in the  $\text{Br}^+$  state, following considerable electron loss due to Auger effect. This accumulation of charge, Goldsmith and Bluerer (1950) have shown, may lead to molecular dissociation. Earlier, Cooper (1942) had worked out the theoretical basis for the occurrence of such molecular dissociations occurring as a consequence of the Franck-Condon principle.

These considerations account for the positively charged particles collecting on the cathode and of the concentration of the ground state isomer Br-80 on the cathode. The extreme instability of the  $\text{Br}^+$ , however, leads to a greater fraction of it to be changed to  $\text{Br}^-$  finally during transit through the bromobenzene medium. A value of 5.4 for the dielectric constant of the medium is considered high enough to bring about this conversion. These results finally lead to a greater yield on the anode than on the cathode as observed. It is clear that other modes of ionization have to be contemplated, in addition to the Auger consequence following internal conversion, for explaining the collection on charged plates of the metastable isomer and, more specially the isotope Br-82 which does not undergo isomeric transition.

The other observation of interest is the occurrence of an isotope effect in the relative yields of the radio-isotopes Br-80, Br-80 m and Br-82 collecting on either electrode. The relative yield ( $\gamma$ ) for a given species is directly related to the capture cross-section ( $\sigma$ ) of the corresponding target nucleus and its amount ( $n$ ) in the path of the neutron beam. We may thus write for the yield,

$$\gamma_i = \theta_i \sigma_i n_i$$

Here  $\theta$  is the fraction of the given product finally collecting on a given charged plate. In the absence of an isotope effect this fraction ( $\gamma/\sigma n$ ) should be the same for all the species. Table III shows the relative yields together with known data for the percentage natural abundance ( $n$ ) and the capture cross-section ( $\sigma$ ) of the corresponding target nuclei Br-79 and Br-81.

TABLE III

Target data			Product yields			
			Anode		Cathode	
$\sigma$ (barns)		$n(\%)$	$\gamma$	$\gamma/\sigma n$	$\gamma$	$\gamma/\sigma n$
Br-79 (18 min.)	8.5	50.5	200	0.466	100	0.233
Br-79 (4.4 hr.)	2.9	50.5	68	0.466	16	0.109
Br-81	3.5	49.5	115	0.665	88	0.507

Results for the positive plate show the occurrence of a marked isotope effect in the formation and the collection of the isotopes, Br 80 and Br 82 in contrast with its absence as between the two isomers Br-80 *m* and Br-80 as shown by the characteristic  $(\gamma/\sigma n)$  values. In the case of the negative plate however, an additional enrichment of the isomers is also apparent. This undoubtedly arises from the predominance of Br<sup>+</sup> in the ground state of Br-80 following the internal conversion—ionization mechanism discussed above. The value for  $(\gamma/\sigma n)$  for Br-80 is over twice that for Br-80 *m* on the negative plate, while the two values are the same for positive plate.

The earlier results of Shaw (1956) indicate a similar order of retention as between the two isomers. Our results however differ from those of Shaw in respect of the order of the yield as between the lighter and heavier isotopes. The formation of active water-soluble compounds, other than HBr and elementary bromine, during accompanying radiolysis is considered one of the causes for the variable yields reported by earlier workers, employing aqueous extraction to concentrate the recoil products. It would thus appear that the method adopted in the present work of collecting the products on dry charged plates would minimize these variables. A more detailed investigation in respect of the influence of field intensity, nature of the target substance and possibly temperature, would be helpful in understanding some of the secondary reactions following the  $(n, \gamma)$  reaction.

## REFERENCES

- Capron, 1946, *Nature*, **157**, 806.  
 Capron and Oshima, 1952, *J. Chem. Phys.*, **20**, 1403.  
 Capron and Crevecoeur, 1952, *J. Chim. phys.*, **49**, 20.  
 Capron and Crevecoeur, 1953, *J. Chem. Phys.*, **21**, 1843.  
 Capron *et al.*, 1958, Proc. Second Int. Conf. (Peaceful Uses of Atomic Energy), Geneva, Sept., 1958.  
 Chien and Willard, 1954, *J. Am. Chem. Soc.*, **76**, 4735.  
 Cooper, 1942, *Phys. Rev.*, **61**, 1.  
 Fay and Paneth, 1935, *Nature*, **135**, 820.  
 Fay and Paneth, 1936, *J. Chem. Soc.*, 384.

- Fermi, Amaldi and others, 1935, *Proc. Roy. Soc.*, **A149**, 522.  
Fox and Libby, 1952, *J. Chem. Phys.*, **20**, 487.  
Groshev, *et al.*, 1959, "Atlas of  $\gamma$ -Ray Spectra for Radiative Capture of Thermal Neutrons" (Pergamon Press, London).  
Goldsmith and Bluerer, 1950, *J. Phy. & Colloid Chem.*, **54**, 717.  
Libby and de Vault, 1939, *Phys. Rev.*, **55**, 322.  
Libby and de Vault, 1941, *J. Am. Chem. Soc.*, **63**, 3216.  
Libby, 1947, *J. Am. Chem. Soc.*, **69**, 2523.  
Millman and Shaw, 1956, *J. Chem. Soc.*, 2101.  
Roulard and Libby, 1953, *J. Chem. Phys.*, **21**, 1495.  
Shaw, 1951, *J. Chem. Soc.*, 443.  
Shaw and Collie, 1951, *J. Chem. Soc.*, 434.



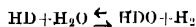
# THERMAL DIFFUSION FACTOR FOR HYDROGEN AND WATER MIXTURES

S. C. SAXENA

CHEMISTRY DIVISION, ATOMIC ENERGY ESTABLISHMENT Trombay, Bombay

(Received, August 1, 1960)

**ABSTRACT.** The thermal diffusion factor for the system hydrogen and water-vapour, has been calculated from an equation which utilises only the experimental data on transport properties and their temperature derivatives and is independent of any particular form for the inter-molecular potential. The thermal diffusion factor has also been computed for other systems which emerge out of the different isotopic species of these two principal components. These values are of particular interest in interpreting the data obtained on the enrichment of hydrogen isotopes, in a thermal diffusion column, using the following chemical exchange reaction :



## INTRODUCTION

Considerable interest centres around the equilibrium and non-equilibrium properties of water and its mixtures with other gases. This is because of the presence of water vapour all around us in the atmosphere and design-engineers need all such data in connection with their problems involving heat transfer etc. References to such data are found in the work of Keenan and Keyes (1954), Hirschfelder, Curtiss and Bird (1954a), Powell (1958), and Liley (1958). In recent years, some success has been achieved in computing the properties of non-polar molecules from the theoretical results of statistical mechanics in conjunction with spherically symmetric intermolecular potentials. Unfortunately, the position for polar molecules is far from satisfactory. For such molecules, the complicated angle-dependent potentials make it very difficult, if not impossible, to calculate the various collision cross-sections. There is an additional interest in the thermal diffusion factor for the hydrogen and water system, for thermal diffusion coupled with chemical exchange has been tried by Pierce (1959) to enrich the hydrogen isotopes in a thermal diffusion column. The theoretical calculations of the thermal diffusion factor, in particular, are more complicated because of the following two reasons : Firstly, the infinite determinants which represent the thermal diffusion factor have been expanded into an infinite series by two different methods, viz., Chapman-Cowling (1952) and Kihara (1949), Mason (1957). Secondly, both these infinite series have in general rather poor convergence and consequently, to arrive at reliable results for actual systems elaborate numerical calculations

have to be performed for the specific intermolecular potential. In this paper all these difficulties have been successfully surmounted and the values of the thermal diffusion factor for the various combinations of the stable isotopes of hydrogen with normal and heavy hydrogen water have been calculated in the temperature range 307°K to 350°K for both the ends of the concentration range.

#### FORMULAE FOR THE THERMAL DIFFUSION FACTOR

The general formula for the thermal diffusion factor,  $\alpha_T$ , is given in the books of Chapman-Cowling (1952) and Hirschfelder, Curtiss and Bird (1954) as the ratio of infinite determinants. Various approximations are then obtained by expanding these infinite determinants according to the procedure of either Chapman-Cowling (1952) or Kihara (1949). Mason (1957) has studied in detail the convergence errors involved in  $\alpha_T$  on various intermolecular potentials and for specific types of mixtures. Recently, Weissman, Saxena and Mason (1960) have shown that for a binary mixture, where the heavy component is in trace and the ratio of the molecular masses  $\approx 0.1$  or less,  $\alpha_T$  can be calculated within one to two percent by the following formula

$$[\alpha_T] = (6C_{12}^* - 5)(-S_2/Q_2)(1+K), \quad \dots (1)$$

where the subscript 2 represents the lighter component and for a mixture consisting of polar and nonpolar components (being designated by the subscripts  $p$  and  $n$  respectively) we have:

$$S_2 = -S_n = \frac{15M_p(M_p - M_n)}{2(M_p + M_n)^2} + \frac{4M_p M_n A_{p-n}^*}{(M_p + M_n)^2} - \frac{M_n}{M_p} \left( \frac{2M_n}{M_n + M_p} \right)^{\frac{1}{2}} \left( \frac{\sigma_{n-n}^2 \Omega_{n-n}^{(2,2)*}}{\sigma_{p-n}^2 \Omega_{p-n}^{(1,1)*}} \right), \quad \dots (2)$$

$$Q_2 = Q_n = \frac{2}{M_p(M_p + M_n)} \left( \frac{2M_p}{M_p + M_n} \right)^{\frac{1}{2}} \left( \frac{\sigma_{n-n}^2 \Omega_{n-n}^{(2,2)*}}{\sigma_{p-n}^2 \Omega_{p-n}^{(1,1)*}} \right) (3M_p^2 + M_n^2 + (8/5)M_p M_n A_{p-n}^*), \quad \dots (3)$$

$$A_{p-n}^* = \Omega_{p-n}^{(2,2)*} / \Omega_{p-n}^{(1,1)*}, \quad \dots (4)$$

$$C_{12}^* = C_{p-n}^* = \Omega_{p-n}^{(1,2)*} / \Omega_{p-n}^{(1,1)*}, \quad \dots (5)$$

$$K = \frac{1}{42} (8E_{n-n}^* - 7)^2 + \frac{2}{21} \left( 1 - \frac{M_n}{M_p} \right) (8E_{n-n}^* - 7) \left[ 1 - \frac{3}{2} (5 - 4B_{p-n}^*) (6C_{p-n}^* - 5)^{-1} \right], \quad \dots (6)$$

$$B_{p-n}^* = [5\Omega_{p-n}^{(1,2)*} - 4\Omega_{p-n}^{(1,3)*}] / \Omega_{p-n}^{(1,1)*}, \quad \dots \quad (7)$$

$$E_{n-n}^* = \Omega_{n-n}^{(2,3)*} / \Omega_{n-n}^{(2,2)*} \quad \dots \quad (8)$$

where  $M$  represents the molecular mass,  $\Omega^{(i,j)*}$  are the reduced Chapman-Cowling collision integrals and  $\sigma$  is the collision diameter. Here, we have arbitrarily chosen the subscript 2 for the nonpolar component, hydrogen, in order to be consistent with the convention of assigning the subscript 1 to the heavier component. In case, the lighter component is polar, correct values will be obtained, if the subscripts representing the molecular species are interchanged.

A straightforward calculation of  $\alpha_T$  is not possible from these expressions, for the various collision cross-sections have not been evaluated for such an intermolecular potential which takes into account the polar nature of the molecules. The labour involved in the evaluation of these collision integrals is formidable and as yet this has not been accomplished. However, all these collision integrals (except  $A_{p-n}^*$ ) can be replaced by the absolute values of the transport coefficients or their temperature derivatives. The required relations are:

$$(6C_{p-n}^* - 5) = 2 \left[ 2 - \left( \frac{\partial \ln D_{p-n}}{\partial \ln T} \right)_{pr} \right], \quad \dots \quad (9)$$

$$(5 - 4B_{p-n}^*) = 5 - \frac{4}{3} \left[ 2 \left( \frac{\partial \ln D_{p-n}}{\partial \ln T} \right)_{pr} - 1 \right]$$

$$\left[ 9 - 2 \left( \frac{\partial \ln D_{p-n}}{\partial \ln T} \right)_{pr} \right] - \frac{4}{3} \frac{d^2 \ln D_{p-n}}{d(\ln T)^2}, \quad \dots \quad (10)$$

$$(8E_{n-n}^* - 7) = 2 \left[ 1 - \frac{\partial \ln \eta_{n-n}}{\partial \ln T} + \frac{\partial \ln f_n}{\partial \ln T} \right], \quad \dots \quad (11)$$

$$-S_n = \frac{15M_p(M_p - M_n)}{2(M_p + M_p)^2} + \frac{4M_p M_n A_{p-n}^*}{(M_p + M_n)^2} - \frac{5}{3} \frac{M_n^2}{(M_p + M_n)} \frac{p D_{p-n} f \eta}{\eta_{n-n} R T}, \quad \dots \quad (12)$$

$$Q_n = \frac{10}{3} \frac{M_n}{(M_n + M_p)} \left( \frac{pr D_{p-n}}{\eta_n R T} \right) \left( (3M_p^2 + M_n^2 + \frac{8}{5} M_p M_n A_{p-n}^*) \right), \dots \quad (13)$$

$$f \eta = 1 + \frac{3}{196} (8E_{n-n}^* - 7). \quad \dots \quad (14)$$

In the above equations  $pr$  stands for the pressure. When the light component is in trace following Mason (1957)  $\alpha_T$  can be calculated thus:

$$\alpha_T = \left[ 2 - \left( \frac{\partial \ln D_{p-n}}{\partial \ln T} \right)_{pr} \right] \left[ 1 - \mu_1 \left( \frac{M_n}{M_p} \right) \right], \quad \dots \quad (15)$$

where

$$\mu_1 = \frac{(16A^*_{p-n} - 10) - 3(5 - 4B^*_{p-n})}{10 + 3(5 - 4B^*_{p-n})} \quad \dots (16)$$

Thus, if we know  $D_{p-n}$  and  $\eta_{p-n}$  as a function of temperature and  $A^*_{p-n}$  is assumed,  $\alpha_T$  can be calculated.  $A_{p-n}$  is known to be fairly constant (1.10) over a long range of temperature, [Saxena, 1960] and does not vary much from the nature of the potential. Further, it is shown later that  $\alpha_T$  is insensitive to the value of  $A_{p-n}$  and so an approximate guess will serve our present purpose. In this way the form of the intermolecular potential is completely removed from the expression for  $\alpha_T$  in favour of measureable quantities and their temperature derivatives. The only limitations of these formulae are the basic assumptions involved in the derivation of the kinetic theory of gases. The one of special interest here, rigorously speaking, is that these formulae hold only for spherically symmetric molecules. This assumption is rather serious for the case of water which is polar, but as the transport properties are less sensitive to molecular orientations and as Krieger (1951) had some success for polar molecules with an angle-independent potential, we will continue to assume the applicability of central forces.

#### CALCULATION OF THE THERMAL DIFFUSION FACTOR

The diffusion coefficients have been experimentally measured for the hydrogen and water system by Winkelmann (1884, 1889), Schwartz and Brow (1951) and Crider (1956). The results of Winkelmann and Crider agree with each other but are systematically lower than those of Schwartz and Brow. The reason of this disparity probably lies in the effect of supercooling at the vapour-liquid interface (Le Blanc and Wuppermann, 1916) and in the difference in the solubility of hydrogen in water. Schwartz and Brow have avoided this difficulty and I feel their data is the most reliable one at the moment. This latter data can be represented by a linear plot of  $\log D$  vs.  $\log T$  in the entire temperature range (307.3—352.7°K), with the average standard deviation of 0.6% only. Consequently, we will treat  $(\partial \ln D / \partial \ln T)_{pr}$  as constant in the formulae of the previous section and then to this approximation,  $\partial^2 \ln D / (\ln T)^2$  can be neglected in this temperature range.

The data for the viscosity of hydrogen in this temperature range is given by Trautz and Binkelc (1930), Trautz and Heberling (1931), Trautz and Hussein (1934), Johnston and McCloskey (1940) and Wobser and Nuller (1941). All this data can again be represented by a linear plot of  $\log \eta$  vs.  $\log T$  in this temperature range with an average deviation of 0.1% only. The value of the term,  $\partial \ln f_n / \partial \ln T$ , was found to be negligible in this temperature range [Saxena, 1956].

Table I lists the values of the thermal diffusion factor for the two limiting ends of the composition range and for the three temperatures at which the experimental diffusion data are available. In column 2 are tabulated the  $\alpha_T$  values, calculated according to Eq. (1) in conjunction with Eq. (6) and from (9) to (14) while the column 4 values emerge out of the use of Eqs. (15), (16) and (10). These values, designated as first set, utilise the diffusion data of Schwartz and Brow (1951). The second set of  $\alpha_T$  values listed in columns 3 and 5 of Table I have similarly been calculated, except that the diffusion data of Winkelmann (1884, 1889) has been used. In these calculations a constant value of 1.10 for  $A^*$  was used. However, these calculations are insensitive to the  $A^*$  value, in as much as a change of 20% in  $A^*$  changes  $\alpha_T(X_1 = 0, \text{ at } 328.6^\circ\text{K})$  only by 0.2%.  $\alpha_T$  values, calculated using the diffusion data of Schwartz and Brow, are always higher than those obtained using the data of Winkelmann. The author feels that the first set of  $\alpha_T$  values is more reliable.

TABLE I  
Thermal diffusion factor for  $\text{H}_2$  -  $\text{H}_2\text{O}$  system

Temp. °K	$\alpha_T$ calculated, $X_1 = 0$		$\alpha_T$ calculated, $X_2 = 0$	
	First set	Second set	First set	Second set
307.3	1.21	1.04	0.812	0.61
328.6	1.24	1.07	0.812	0.61
352.7	1.30	1.08	0.812	0.61

In Table II, are tabulated the diffusion coefficients and the thermal diffusion factors at 300°K and 350°K for the various systems, permuting out of the isotopes of hydrogen ( $\text{H}_2$ , HD and  $\text{D}_2$ ) and heavy hydrogen substituted water ( $\text{H}_2\text{O}$ , HDO and  $\text{D}_2\text{O}$ ). The diffusion coefficients have been calculated from the measured values for  $\text{H}_2$ - $\text{H}_2\text{O}$  system, by applying the mass correction factor.  $\alpha_T$  values are calculated in the same way as that of Table I. The  $\eta$  values also were generated from the experimental values available for hydrogen and by multiplying these with appropriate mass correction factors. The  $\alpha_T$  values for those system, where the mass ratio is considerably more than 0.1 will be somewhat inaccurate because of the use of Eq.(6). However, even for the worst case of  $\text{D}_2$ - $\text{H}_2\text{O}$ , K has only a value of 0.0145 and consequently the values given in Table II can be treated as fairly reliable. These values of  $\alpha_T$  are very useful in assessing the data obtained in connection with the enrichment of hydrogen in a thermal diffusion column, using the following chemical exchange

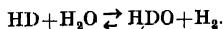


TABLE II

Diffusion coefficients and thermal diffusion factors

System	$D_{2-n}$ in cm <sup>2</sup> /sec.		$\alpha_T$ at 300°K		$\alpha_T$ at 350°K	
	300°K	350°K	$X_1 = 0$	$X_2 = 0$	$X_1 = 0$	$X_2 = 0$
H <sub>2</sub> -H <sub>2</sub> O	0.996	1.195	1.193	0.812	1.290	0.812
H <sub>2</sub> -HDO	0.994	1.192	1.206	0.812	1.303	0.812
H <sub>2</sub> -D <sub>2</sub> O	0.991	1.189	1.217	0.813	1.316	0.813
HD-H <sub>2</sub> O	0.834	1.000	1.078	0.807	1.167	0.807
HD-HDO	0.830	0.996	1.104	0.808	1.187	0.808
HD-D <sub>2</sub> O	0.828	0.993	1.112	0.809	1.203	0.809
D <sub>2</sub> -H <sub>2</sub> O	0.739	0.886	0.970	0.803	1.052	0.803
D <sub>2</sub> -HDO	0.735	0.882	0.993	0.803	1.076	0.803
D <sub>2</sub> -D <sub>2</sub> O	0.732	0.878	1.012	0.804	1.097	0.804

In fact, the present work was undertaken out of the need to interpret such results.

Unfortunately, at present there is no rigorous procedure for calculating the transport properties of mixtures consisting of a polar and a non-polar component. Hirschfelder, Curtiss and Bird (1954b) have advanced an approximate procedure, which also has not been extensively tested so far. This approach is based on the concept that the effective potential between a polar and a non-polar molecule has the same form as that between two non-polar molecules. An attempt is being made to assess such semi-empirical approaches proceeded by a redetermination of the force constants for pure polar gases from the upto date data.

## ACKNOWLEDGMENTS

It is a pleasure to thank Dr. J. Shankar for his interest and encouragement and to Mr. P. A. Pardeshi for his help with some of the calculations.

## REFERENCES

- Chapman, S. and Cowling, T. G., 1953, *The Mathematical Theory of Non-Uniform Gases*, Cambridge University Press, England.
- Crider, W. L., 1956, *J. Am. Chem. Soc.*, **78**, 924.
- Hirschfelder, J. O., Curtiss, C. F. and Bird, R. B., 1954, *Molecular Theory of Gases and Liquids*, John Wiley and Sons, Inc., New York, (a) Chapters 3 and 8; (b) p. 600-604.
- Johnston, H. L. and McCloskey, K. E., 1940, *J. Phys. Chem.*, **44**, 1038.
- Keenan, J. H. and Keyes, F. G., 1954, *Thermodynamic Properties of Steam*, John Wiley and Sons, Inc., New York.
- Kihara, T., 1949, *Imperfect Gases*, originally published in Japanese by Asakusa Bookstore, Tokyo, Japan, and translated into English by the U.S. Office of Air Research, Wright-Patterson Air Force Base. See also *Revs. Modern Phys.*, 1953, **25**, 831.

- Krieger, F. J., 1951. The Viscosity of Polar Gases, Project Rand Report RM-646.
- Lawson, A. W., Lowell, R., and Jain, A. L., 1959, *J. Chem. Phys.*, **30**, 643
- Le Blanc, M. and Wuppermann, G., 1916. *Z. physik. Chem.*, **91**, 143.
- Liley, P. E., Thermodynamic and Transport Properties of Gases, Liquids and Solids, published by the American Society of Mechanical Engineers, New York, pages 211-219.
- Mason, E. A., 1957, *J. Chem. Phys.*, **27**, 75, 782
- Pierson, R. W., 1959. Doctoral Dissertation, Columbia University, New York, U.S.A.
- Powell, P. E., 1958. *Advanced in Phys.*, **7**, 276
- Saxena, S. C., 1956, *J. Phys., Soc. Japan.*, **11**, 367.
- Saxena, S. C., 1960, To be published in *Physica*.
- Schwartz, F. A. and Brow, J. E., 1951, *J. Chem. Phys.*, **19**, 640.
- Trautz, M. and Binkele, H. E., 1930, *Ann. Physik*, **5**, 561.
- Trautz, M. and Heberling, R., 1931, *Ann. Physik.*, **10**, 155
- Trautz, M. and Husseni, I., 1943, *Ann. Physik.*, **20**, 121.
- Weissman, S. Saxena, S. C. and Mason, E. A., 1960. *Phys. Fluids*, July-August issue.
- Winkelmann, A., 1884, *Wied. Ann.*, **22**, 152.
- Winkelmann, A., 1889, *Wied. Ann.*, **36**, 93
- Wobser, R., and Muller, F., 1941, *Kolloid-Beih.*, **52**, 165

## A NOTE ON HEAT TRANSFER AND FILM BOILING

R. D. RAO, H. S. DESAI AND D. V. GOGATE

PHYSICS DEPARTMENT, M. S. UNIVERSITY, BARODA

(Received May 31, 1960)

**ABSTRACT.** Heat transfer between electrically heated metal wires and different boiling liquids has been studied and characteristic boiling curves are obtained by plotting the heat flux  $q/A$  against the excess of temperature  $\Delta t$  of the wire over the boiling point. The relation between the heat transfer coefficient  $h$  and  $\Delta t$  has also been studied. The values of maximum heat flux and critical temperature difference are calculated for the different wires and liquids used in this investigation.

## INTRODUCTION

It is a matter of common experience that when a red hot metal is quenched in water, the metal first cools slowly, then rapidly and then slowly again. This can be taken as a good illustration of the three possible types of boiling, viz.—film boiling, nucleate boiling and natural convection boiling. Film boiling is that type of boiling which occurs when a vapour film exists between a heated surface and a boiling liquid. In nucleate boiling, vapour bubbles originate from different parts of the heated surface. Natural convection boiling takes place when the difference of temperature between the heated surface and the liquid is small. In the operations of jets and rockets, there are frequent contacts between a boiling liquid and a hot surface and this is the condition for film boiling. In an electrically heated boiler or an atomic power plant where the heat input is the controlled variable, there is always a danger that the temperature of the heated object may rise abruptly if the heat input is near the critical heat flux ( $q/A$ ). This danger becomes much more pronounced if the value of the heat input is above the maximum heat flux ( $q/A$ )<sub>max</sub>. If the abrupt temperature rise is sufficiently large, it may give rise to sudden expansion and weakening of certain parts of the system, sometimes causing breakage.

In view of the above importance of film boiling and nucleate boiling, we have tried (1) to investigate the effect of quenching electrically heated wires in different liquids and (2) to study the heat transfer, by means of characteristic boiling curves (incorporating free convection boiling, nucleate boiling and film boiling) between cylindrical metal wires and boiling liquids.

Drew and Mueller (1937) and others have studied heat transfer to boiling liquids by steam condensing method. Nukiyama (1934) succeeded in obtaining almost complete boiling curves by electrically heating thin platinum wires submerged



in boiling water. Natural convection boiling and nucleate boiling of water for different pressures have been studied by Addoms (1948) using thin platinum wires. Extensive study of film boiling was made by Bromley (1950) using various organic liquids.

During our study of heat transfer, we have obtained characteristic boiling curves for a number of liquids and the results of our experiments on heat transfer between cylindrical metal wires and boiling liquids have been described in this note. The complete boiling curves [plots of  $\log(q/A)$  against  $\log \Delta t$ ] for the various liquids used have been obtained for different wires, and the maximum heat flux and the critical temperature difference have been calculated. The heat flux ( $q/A$ ) for unit difference of temperature between the wire and the surrounding liquid is known as the heat transfer coefficient  $h$ . Thus  $h = \frac{q}{A \cdot \Delta t}$ . The relation between this coefficient  $h$  and the temperature difference  $\Delta t$  has also been studied for liquids such as water, carbon tetrachloride, turpentine, etc. and some typical results have been graphically illustrated (Fig. 2).

#### EXPERIMENTAL

The experimental arrangement consisted of a simple Wheatstone bridge with ratio arms of 1000 ohms each. A thin platinum wire which was submerged in the boiling liquid was included in the third arm of the bridge in series with an ammeter, while a small rheostat and a Eureka wire bridge with a sliding contact formed the fourth arm of the bridge.

The platinum wire was allowed to remain in the boiling liquid for some time before passing a current through it so that it attained the temperature of the boiling liquid. The resistance of the wire could then be calculated at this temperature, if  $R_0$ , the resistance of the wire at  $0^\circ\text{C}$  and  $\alpha$ , the temperature coefficient of resistance for the wire are known. A very small current which does not heat the wire appreciably, was then passed through the wire and a balance was obtained by adjusting the rheostat and by sliding the contact on the Eureka wire bridge. The current through the wire was then increased so as to raise its temperature. This increases the resistance of the wire, thus disturbing the balance previously obtained. The contact is now shifted so as to restore the balance. Knowing the value of this shift and also the resistance per unit length of the Eureka wire, the change in resistance  $\Delta R$  of the platinum wire could be calculated. The excess of temperature of the wire above the boiling point of the liquid could then

be determined by means of the relation  $\Delta t = \frac{\Delta R}{R_0 \alpha}$ .

## RESULTS AND DISCUSSION

The input power  $q$  is equal to  $\frac{C^2 R}{J}$  where  $C$  is the current passing through the wire,  $R$  is its resistance and  $J$  is the mechanical equivalent of heat. The heat

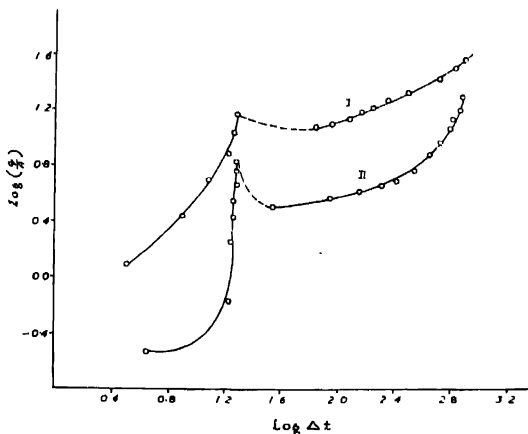


Fig. 1. Curves showing the variation of  $q/A$  with the excess of temperature.  
Curve I—Platinum-water. Curve II—Platinum-carbontetrachloride.

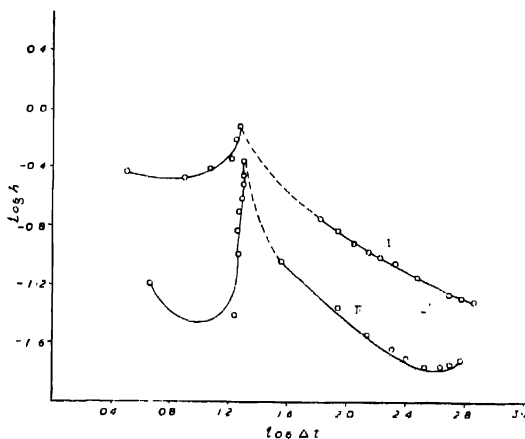


Fig. 2. Curves showing the variation of  $h$  with the excess of temperature.  
Curve I—Platinum-water. Curve II—Platinum-carbontetrachloride.

flux is given by  $q/A$  where  $A$  is the surface area  $2\pi rl$  of the wire of length  $l$  and radius  $r$ . Typical curves showing the variation of  $q/A$  with the excess of temperature  $\Delta t$  as also the relation between the heat transfer coefficient  $h$  ( $= \frac{q}{A\Delta t}$ ) and  $\Delta t$  for water and carbon-tetrachloride are exhibited in Figs. (1) and (2) respectively.

The values of the maximum heat flux  $(q/A)_{max}$  and critical temperature difference  $\Delta t_{crit}$  for the different wires and liquids used as also the values of the slopes calculated for natural convection boiling and nucleate boiling together with the heat transfer coefficient ( $h$ ) at the peak value are shown in Table I.

TABLE I

Liquid	Wire	Slopes for		$\left(\frac{q}{A}\right)_{max}$ cal/sec. cm <sup>2</sup>	$\Delta t_{crit}$	$(h)_{max}$ cal/cm. <sup>2</sup> sec°C
		Nat. conv. boiling	Nucl. boiling			
Water (B.P. 100°C)	Platinum	0.91	3.26	15.8	19°C	0.800
Turpentine (B.P. 166°C)	-do- $r = 0.005$ cm.	1.2	3.6	12.02	39.8°C	0.302
	Copper $r = 0.0026$ cm.	1.0	4.66	10.96	36.3°C	0.302
	Tungsten $r = 0.0028$ cm.	0.9	1.6	12.6	43.6°C	0.275
Naphthalene (B.P. 215°C)	Platinum	0.77	2.8	11.48	39.8°C	0.288
	Copper	0.83	2.75	10.72	39.8°C	0.263
	Tungsten	1.0	1.7	12.59	38.02°C	0.331
Carbontetrachloride (B.P. 77°C)	Platinum	0.6	2.57	6.9	19.95°C	0.355
	Tungsten	0.71	3.0	8.7	22.9°C	0.355

When the heat flux exceeds  $(q/A)_{max}$  the system passes from nucleate boiling regime to film boiling regime after passing through a transient state of unstable film boiling. This unstable (transient) state is shown by the dotted curve in Figs. (1) and (2). In the state of stable film boiling a vapour film is formed between the wire and the liquid. This film acts as a barrier in which the heat flow is due more to conduction than to convection. The formation of this barrier (vapour blanket) naturally diminishes the heat flow from the wire to the liquid and hence the value of heat transfer coefficient  $h$  is also decreased as indicated by the graphs in Fig. 2. These graphs also indicate that if the heat flux is still further increased, the value of  $h$  goes on decreasing further.

## CONCLUSIONS

(a) The material and dimensions of the wire do not seem to affect the value of the maximum heat flux  $(q/A)_{max}$  so much as the properties of the liquid, especially the latent heat of vaporisation.

(b) The continued decrease in the value of  $h$  with the increase of heat flux in the film boiling regime seems to be due to a slight increase in the thickness of the vapour film.

## REFERENCES

- Addoms J. N., 1948, "Heat Transmission" by William H. McAdams, McGraw-Hill  
Third Edition 1954 page 382 in Asian students' Edition.  
Bromley, L. A., 1950, *Chem. Eng. Progr.*, **46**, 221.  
Drew, T. B. and Mueller, A. C., 1937, *Trans. Am. Inst. Chem. Engrs.*, **33**, 449.  
Nukiyama, S., 1934, *J. Soc. Mech. Engrs., (Japan)*, **37**, 367, S53-54.

## THE DIELECTRIC PROPERTIES OF COPAL ESTER

A. K. SEN and G. N. BHATTACHARYA

DEPARTMENT OF APPLIED PHYSICS, CALCUTTA UNIVERSITY

(Received, July 27, 1960)

**ABSTRACT.** The dielectric properties of copal ester have been measured over a wide range of temperature and frequency viz., from 25°C to 160°C and from 400 c/s to 300 kc/s. Within the temperature range of investigation copal ester behaves as a typical polar resin in the anomalous dispersion range. The loss curves have unusually broad peaks which suggest a highly distributed relaxation time of its orientating polar units. This is corroborated from the shape of the  $\epsilon''/\epsilon_m''$  vs  $\log f/f_m$  curve as well as a high value of the distribution factor calculated from the Cole and Cole diagram. With the help of melt viscosity data of this resin the size of its rotating unit has been calculated following Debye's relation and the calculated radius comes out to be about 1.5 Å, which is the same as that of a hydroxyl group. The presence of the hydroxyl group is clearly indicated in the infrared absorption spectrum of this resin, which suggests these groups to be its actual rotating units.

## INTRODUCTION

Copals are a general name for various fossil and semi-fossil resins found in some tropical countries. They are usually named after their places of origin. Like rosin, copals have a high acid value and they differ somewhat in their chemical and physical properties depending upon their composition. Copal esters, however, are important as they are widely used in the preparation of insulating varnishes, impregnating compounds, moulded insulation etc.

Bhattacharya (1946) studied the dielectric properties of Manila Copal, while Clare (1949) reported the dielectric properties of Kauri copal. But recently the application of Debye's equation for obtaining the size of the rotating unit in a few natural resins has revealed some interesting fact. In the case of rosin (Sen and Bhattacharya, 1958a) the radius obtained is equal to the effective radius of abietic acid molecule, the chief constituent of rosin, whereas in the case of ester gum (Sen and Bhattacharya, 1958b) which has a much bigger molecule, a similar calculation yields a much smaller value for the radius, viz., that of the hydroxyl group. The fact that ester gum contains hydroxyl group has been corroborated later from the infrared absorption curve.

It was concluded, therefore, that perhaps the unesterified hydroxyl groups of mono- and di-abietates in ester gum were the actual rotating units. If now mono- and di-abietates are formed during the esterification of rosin, it is natural to expect

a similar formation of mono- and di-glycerides during the esterification of similar other resins with glycerol. If in these esters too the value of the radius comes out to be that of the hydroxyl group our conclusions regarding the rotating unit in ester gum can be justified to some extent. With this end in view the measurement of the dielectric properties of the glycerol esters of copal has been undertaken.

#### THEORETICAL AND EXPERIMENTAL

The theoretical aspects of dielectric measurement have been fully discussed before (Sen and Bhattacharya, 1958a and 1958b) and the procedure for the measurement of permittivity, power factor, resistivity and viscosity are the same as reported earlier (Sen and Bhattacharya, 1957, 1958a & b).

#### *Infrared absorption curves*

##### (1) *Recording of absorption curves*

Absorption measurements were done on a Hilger infrared spectrophotometer, model H 800, using a rock-salt prism as the dispersion element in the range of 1 to 15 microns. The instrument was used in the double beam position, where the transmission through the test medium was automatically balanced with the transmission through air. A Brown-Electronik recording potentiometer was used for obtaining the absorption-wavelength curve. This curve was photographically reduced to convenient size.

##### (2) *Preparation of test-pieces.*

Wires of 28 S.W.G. were made into rectangular frames of dimensions approximately  $1" \times \frac{1}{4}"$ . Films were formed on the wire frames from molten resin having appropriate viscosity and surface tension depending upon temperature. Sufficient care was taken in preparing the films of required thickness making a compromise between maximum transmission and mechanical stability.

#### DISCUSSION

The results of measurement of dielectric constant  $\epsilon'$ , dielectric loss  $\epsilon''$ , and power factor  $\tan \delta$  for various temperatures and frequencies are shown graphically in Figs. 1, 2, and 3 respectively.

These curves also indicate the characteristics of a typical polar substance in the anomalous dispersion range. The power factor as well as the dielectric loss curves begin to rise from about 50°C. The loss maxima for 10 kc/s, 50 kc/s, 100 kc/s and 300 kc/s are more or less of the same value and it is about 0.09 while for 400 c/s and 1 kc/s they are slightly higher. The range of temperature over which the different peaks are distributed is about 42°C.

The striking feature of these loss curves is their unusually broad peaks. The dielectric constant curves are also flat. The nature of these curves indicates

the effects of distributed relaxation time in a greater degree. From Fig. 4 it may also be seen that the region of dispersion spreads over at least 5 to 6 decades

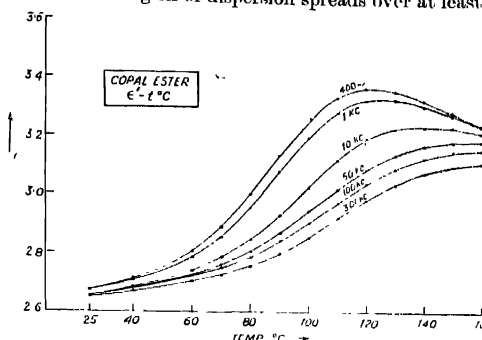


Fig. 1

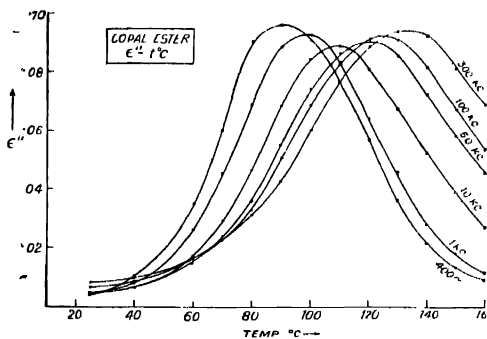


Fig. 2.

of frequency. The Cole and Cole diagram for this resin is shown in Fig. 6. Although the experimental curve is a circular arc its centre lies considerably below the abscissa signifying a wide distribution of relaxation times. The value of the distribution factor  $h$  calculated from the diagram is 0.69 compared to 0.52 for ester gum. The  $\epsilon''/\epsilon'_m$  vs  $\log f/f_m$  curve in Fig. 7 also reveals this high degree of distribution.

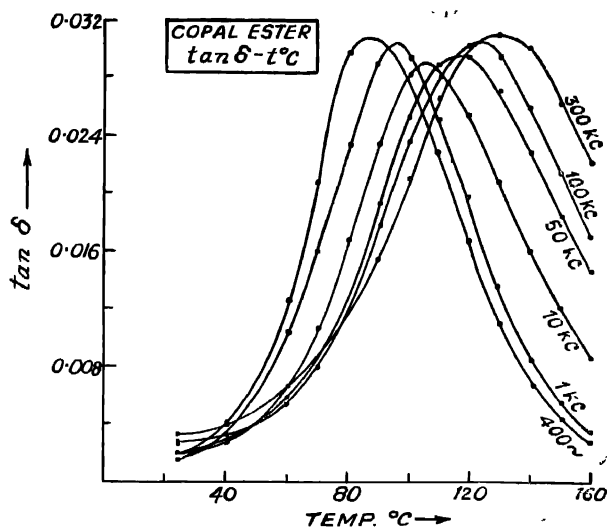


Fig. 3.

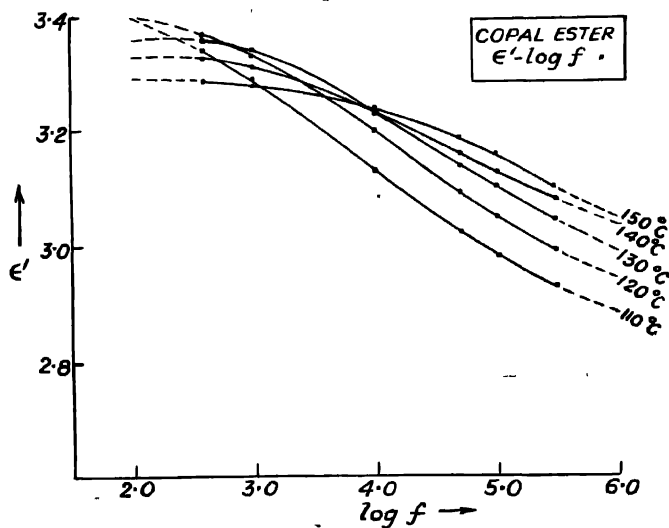


Fig. 4.



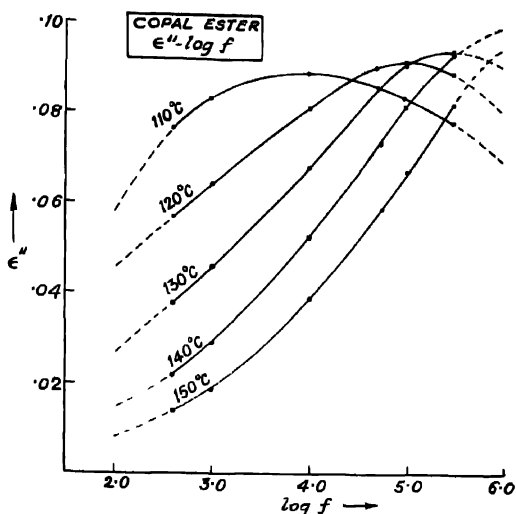


Fig. 5.

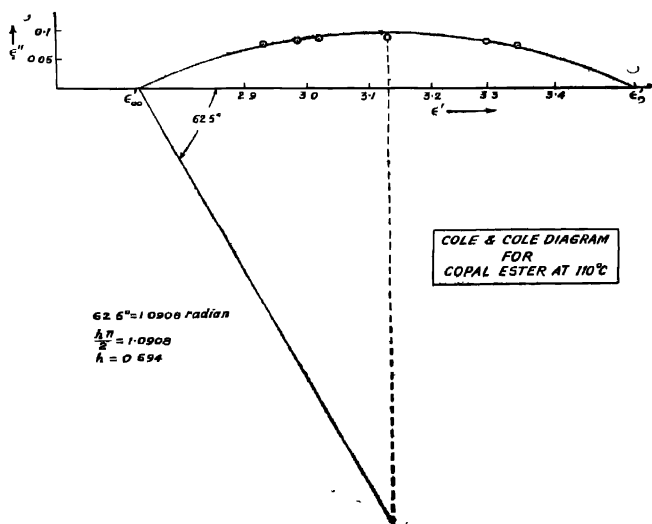


Fig. 6.

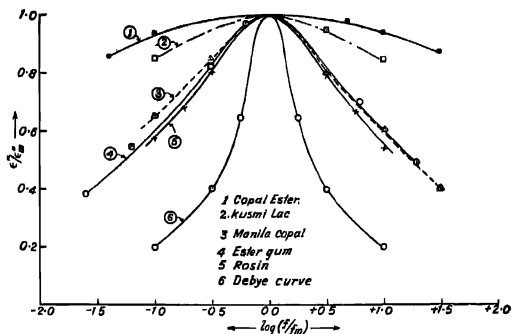


Fig. 7.

We may now calculate the value of the radius of the rotating unit in this resin from the relaxation time at the temperature of a loss-maximum and its melt viscosity at that temperature

The melt viscosity of copal ester was determined in the same way as in the case of other resins. The results are shown in Table 1 and the graph of  $\log \eta$  against  $1/T$  is shown in Fig. 8.

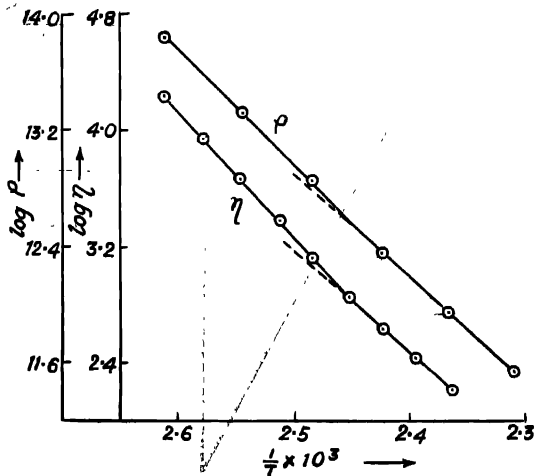


Fig. 8.

TABLE I  
Viscosity—temperature data

Temperature		$\frac{1}{T} \times 10^3$	Viscosity $\eta$ in poise	log $\eta$
t°C	T°K			
110	383	2.611	10,630	4.2208
115	388	2.577	8,710	3.9400
120	393	2.545	4,480	3.6513
125	398	2.513	2,400	3.3802
130	403	2.481	1,320	3.1205
135	408	2.451	680	2.8325
140	413	2.421	420	2.6232
145	418	2.392	260	2.4150
150	423	2.364	100	2.2041

For comparing the internal friction involved in viscosity and resistivity, the curve of log  $\rho$  plotted against  $1/T$  is incorporated in the same figure. Resistivity and conductivity data are given in Table II.

TABLE II  
D.C. conductivity or resistivity—temperature data

Temperature		$\frac{1}{T} \times 10^3$	Conductivity $k$ in mho cm <sup>-1</sup>	Resistivity $\rho$ in ohm cm	log $\rho$
t°C	T°K				
110	383	2.611	$0.152 \times 10^{-12}$	$6.575 \times 10^{12}$	13.8179
120	393	2.545	$0.475 \times 10^{-12}$	$2.104 \times 10^{12}$	13.3231
130	403	2.481	$0.146 \times 10^{-12}$	$6.837 \times 10^{12}$	12.8349
140	413	2.421	$0.437 \times 10^{-12}$	$2.289 \times 10^{12}$	12.3595
150	423	2.364	$0.112 \times 10^{-11}$	$8.940 \times 10^{11}$	11.9513
160	433	2.309	$0.284 \times 10^{-11}$	$3.525 \times 10^{11}$	11.5471

The slopes of both the viscosity and resistivity curves are identical signifying that the same energy of activation is involved in both the processes. As in the case of ester gum (Sen and Bhattacharya, 1957) a transition point is also seen in this resin near about 130°C. The slopes of both the viscosity and resistivity curves change abruptly at this temperature in a similar way signifying some change of state at this temperature.

The radius of the rotating unit is computed using Debye's equations and the results are shown in Table III.

TABLE III  
Calculated relaxation time and radius of the rotator

Frequency in kc/s	Loss maximum temperature $t_m$ in °C	Relaxation time $\tau$ in sec.	$\log \eta$ at $t_m$	Radius of the rotator $a$ in Å
10	110	$1.424 \times 10^{-5}$	4.22	1.53
50	121	$2.859 \times 10^{-6}$	3.00	1.45
100	127	$1.434 \times 10^{-6}$	3.26	1.50
300	135	$4.808 \times 10^{-7}$	2.82	1.48

The chemical composition of manila copal has been studied by various workers and according to them it consists of several acids. According to Tschirch and Koch (1902) the major constituents of manila copal (comprising about 75% of the total) are two isomeric forms of mancopalic acid, viz.,  $\alpha$  and  $\beta$ -mancopalic acid having the chemical formula  $C_{19}H_{17}COOH$ . Other constituent acids have more or less similar chemical formula. Therefore, glycerol esters of these acids should—even on a moderate estimate, be big molecules—much bigger than the values shown in Table III. Therefore, rotation of the entire molecule seems improbable in this resin also. A segment or a part of the molecule or some groups attached to it may be the actual rotator here.

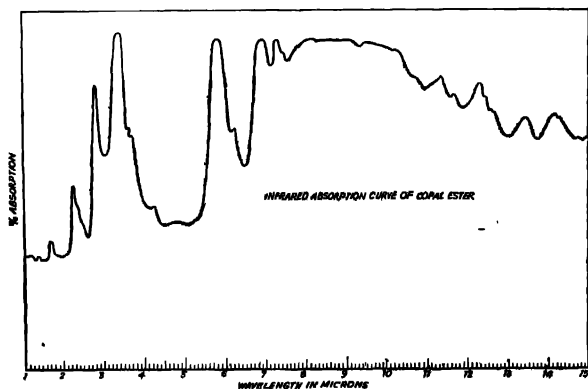


Fig. 5.

The values of the radii obtained are the same as in the case of ester gum, viz., that of a hydroxyl group. The presence of hydroxyl groups in ester gum has been conclusively proved and they can be explained as due to the presence of mono- and di-glycerides formed during the esterification of rosin with glycerol. In copal ester also the presence of hydroxyl groups can be similarly expected. But this view can be justified if their presence can be similarly demonstrated on the basis of other evidences.

From the infrared absorption curve shown in Fig. 9 it may be seen that an absorption peak occurs at the wavelength of  $2.78\mu$  signifying the presence of hydroxyl groups also in this resin as in the case of ester gum.

#### ACKNOWLEDGMENTS

The authors are grateful to the Director, Central Glass and Ceramics Research Institute, Calcutta, under the Council of Scientific and Industrial Research Government of India, for providing them with the facilities available there for obtaining the infrared absorption spectrogram of this resin. They also wish to express their thanks to Messrs. Jenson and Nicholson (India) Ltd. for the supply of a sample of copal ester.

#### REFERENCES

- Bhattacharya, G. N., 1946, *J. Sc. & Ind. Res.*, **4B**, 713.  
Claro I. C., 1949, *Elastomers and Plastomers* (Elsevier Publishing Co., New York), **2**, 371.  
Sen, A. K. and Bhattacharya, G. N., 1957, *J. Assoc. App. Physicists.*, **4**, 72.  
Sen A. K. and Bhattacharya G. N., 1958a, *Ind. J. Phys.*, **32**, 556.  
Sen A. K. and Bhattacharya, G. N., 1958b, *Ind. J. Phys.*, **32**, 49.  
Tschirch and Koch, 1902, *Arch. Pharm.*, **240**, 202.

## THE LIFETIME OF HYPERFRAGMENTS\*

G. C. DEKA

DEPARTMENT OF PHYSICS, COTTON COLLEGE, GAURATI

(Received, May 19, 1960)

**ABSTRACT.** Available data on the time of flight of hyperfragments have been used to deduce a lifetime for light hypernuclei, and the value thus obtained is discussed.

During recent years a large number of nuclear fragments, so-called hyperfragments (HF) which contain a  $\Lambda^0$  hyperon have been observed in nuclear emulsions and their proper analysis has also been made. Along with other properties the  $\Lambda^0$  hyperon binding energy of most of the low charged ( $Z \leq 3$ ) HFs have been measured. An extensive search on the subject was also made by the author (Thesis 1959), and the results have been published in *Nuovo Cimento* (1959). A detailed survey of the available data was reported by Levi-Setti *et al.* (1958). An interesting aspect of the subject which is not yet attempted by any previous worker is the measurement of the lifetime of such HFs and a comparison with that of a free  $\Lambda^0$  hyperon decay. The latter is however fairly well known from different chamber experiments. Several authors using statistical procedures have estimated the mean lifetime of the free  $\Lambda^0$  particle. A value reported by Blumenfeld *et al.* (1956) is  $2.8 \pm .4 \cdot 10^{-10}$  sec obtained on the basis of 65 events observed in a 36" multiplate cloud chamber exposed to a  $\pi$ -meson beam at Brookhaven. A recent value quoted by Raman (1960) in his book is  $2.6 \pm .16 \cdot 10^{-10}$  sec which includes data upto 1959.

When measuring the lifetime of HFs there are a number of experimental difficulties e.g.

- i) Most of the HFs decay at rest permitting thereby only the measure of moderation time which is a lower estimate of the mean life.
- ii) Decays in flight which yield information about the mean life are difficult to detect and identify due to the similar events recorded in emulsions.
- iii) Non mesonic decays are very often missed in observations.
- iv) Heavy HFs, which are usually short evaporation tracks, cannot be identified nor their velocity at production can be calculated.

The experiments made and the procedures adopted by the author are briefly as follows :

---

\*The preliminary result of this paper was reported in the Cosmic Ray symposium held at Ahmedabad, 1960.

A stack of Hford G5 emulsions exposed to an intense beam of 4.5 BeV  $\pi^-$  mesons from Berkeley Bevatron was area scanned under low magnification. All double stars which may be possible HFs were picked up. Another stack of K5 emulsions exposed to a beam of 300 MeV/c  $K^-$ -mesons from the same machine was line scanned for double stars. All the secondary particles emitted from the second stars were followed to their ends, and their energy and momentum were determined from the observed ranges.

Out of 51,000 pion interactions 98 double stars and of 1300  $K^-$  interactions at rest 61 double stars were picked up and analysed by applying a few selection criteria in order to minimise the bias, arising out of similar events like nuclear collisions, captures of negatively charged particles and chance coincidences.

The interconnecting track of every star was closely examined for its multiple scatterings and the thinning down near the second star, the features which usually indicate the stopping of a particle. For a flat interconnector of range  $\geq 20\mu$  it may be possible to exclude  $\pi^-$  meson-capture, as the high multiple scatterings of such a track is distinctive. In a very few cases the charge  $Z$  of the HF could also be determined from  $\delta$ -ray observation or by profile measurements on the tracks. The non mesonic decays in flight of heavy HFs were indicated by the presence of  $\delta$ -rays closed to the second star. Sometimes the mass of a long ranged HF can be determined from multiple scatterings by a constant sagitta method. To define a HF decay the information from the detailed analysis of the second star was taken. A HF which decays into two charged particles producing two collinear tracks or, into three charged particles producing three co-planar tracks could be uniquely defined. Others, for which are obtained a sensible  $\Lambda$ -binding energy when the unbalanced momentum is given to one neutron only, are also considered to be nearly unique. Besides, there are a number of events which



Fig. 1.  $H^+$ -hypernucleus ejected from a  $K^-$ -capture star, decaying in flight into  $H^+ + \pi^-$ .

cannot be interpreted from such analysis, but may not show any feature which can exclude them from being HF decay.

The time of flight or the moderation time of the well defined HFs are determined from their observed range by using the recent range-energy relations given by Barkas (1957).

Two HF decays in flight have been reproduced in Figs. 1 and 2.



Fig. 2.  $B^{10}_{11}$ —hypernucleus ejected from a 4.5 BeN  $\pi^-$  meson decaying in flight into  $He^4 + p + n$  (2).

The available data has been listed in the Tables I and II

TABLE I  
Events observed by the author

	HFs	No. of events observed		Total time of flight in $10^{-10}$ sec.
		At rest	In flight	
Mesonic decays	$He^4$	4	1	0.64
	$He^4$	4		0.07
	$He^6$	6		1.50
	$Li^7$	1		0.04
	$Be^8$	1		0.07
Non-mesonic decays	$He^4$	1	...	0.08
	$Li^{6,7}$	...	1	0.18
	$B^{10}_{11}$	...	1	0.03



TABLE II  
Events observed by other authors

	HFs	Time of flight in $10^{-10}$ sec.	Reference
Mesonic decays	H <sup>3</sup> (f)	1.30	Friedlander <i>et al.</i> , 1956.
	H <sup>3</sup> (,,)	0.06	Filipkowski, <i>et al.</i> , 1958.
	H <sup>4</sup> „	0.22	-do-
	He <sup>4</sup> „	0.77	Fowler and Hansen, 1956.
	H <sup>3</sup> „	1.10	Cloud Chamber expt.
	He <sup>4</sup> „	5.00	-do-
	H <sup>3</sup> „	0.02	Sorensen, <i>et al.</i> , 1956.
	He <sup>4</sup> „	5.40	Sorrel, <i>et al.</i> , 1955.
	Li <sup>3</sup> (r)	1.30	Castagnoli, <i>et al.</i> , 1955.
	H <sup>3</sup> „	0.45	Herman Yagoda, 1955.
	H <sup>3</sup> „	0.15	Imaeda, <i>et al.</i> , 1958.
	H <sup>3</sup> „	0.15	-do-
	H <sup>3</sup> „	0.22	-do-
	He <sup>5</sup> „	0.50	Hill, <i>et al.</i> , 1956.
	Li <sup>7</sup> „	1.00	Filipkowski, <i>et al.</i> , 1956.
Non-mesonic decays	H <sup>4</sup> (f)	0.11	Fry, <i>et al.</i> , 1958.
	Be (r)	0.11	Castagnoli, <i>et al.</i> , 1955.
	B „	0.76	-do-

Ignoring the biases against detecting decays in flight and the non mesonic decays, a life time has been deduced from the above data. Such values are the following :

(1)  $2.7 \pm 0.9 \times 10^{-10}$  sec for the mesonic decay,

(2)  $0.4 \pm 0.2 \times 10^{-10}$  sec for the non-mesonic decay.

This shows that there is little difference between the lifetime for HFs decaying mesonically and that for a free  $\Lambda^0$  decay. The much lower value for the non-mesonic decay is apparently due to the considerably fewer events.

It is however to remark that as the experimental materials may contain bias and the events cannot be selected in controlled conditions the above results cannot therefore be given an unambiguous physical interpretation. It is more an indication of the interest to collect data in a well controlled unbiased manner.

## ACKNOWLEDGMENTS

The author expresses his gratitude to Prof. C. F. Powell F.R.S. for his hospitality and the use of the facilities of the H. H. Wills Physical Laboratory, Bristol where the experimental work included in this paper was done. He also likes to thank Dr. D. Evans of Bristol for his helpful suggestions. He thanks the Govt. of Assam for providing facilities for such a piece of research work in Cotton College, Gauhati.

## REFERENCES

- Blunfield, H., Chonowsky, W. and Lederman, L. N., 1958, *Il Nuovo Cim.*, **2**, 296.  
Barkas, W. H., Report UCRL 2426, Rev. 1957.  
Deka, G. C., 1959, *Il Nuovo Cim.*, **6**, 1217.  
Filipkowski, A. and Skrzypczar, E., 1956, Pol. Akademi Report no. 24/vi.  
Filipkowski, A., Gierula, J. and Zioliński, P., 1957, *Acta. Phys. Polon.*, **16**, 159.  
Levi Setti, R., Slater, W. E., and Telegdi, V. L., 1958, *Il Nuovo Cim. Suppl.*, **1**, 10.  
Raman, P., 1960, "The theory of elementary particles".

# IMPEDANCE MATCHING BY RE-ENTRANT STUB LINE

G. S. SANYAL

INDIAN INSTITUTE OF TECHNOLOGY, KHARAGPUR

(Received, August 23, 1960)

**ABSTRACT.** This article describes a new method of matching a load to a transmission line. This is suitable for narrow band matching when the load V.S.W.R. is greater than 4.

## INTRODUCTION

It is well known that for efficient transfer of power and for other considerations, a transmission line is required to be matched to the load. In many cases, however, the load presents an impedance different from the characteristic impedance of the transmission line necessitating some device to match the load to the line. At frequencies where lumped networks are not suitable, the devices normally employed for narrow band matching are stub lines, quarter-wave transformers, or dielectric sleeves. To these may be added a re-entrant stub line matching section as shown in Fig. 1.

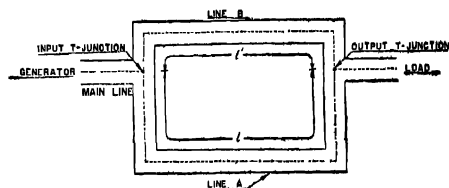


Fig. 1. Re-entrant stub line matching section using coaxial line.

Two transmission lines *A* and *B* are connected in parallel to form a re-entrant double stub line. It will be shown that if the two line lengths  $l$  and  $l'$  are appropriately selected the impedance at the output *T*-junction is transformed to the desired value at the input junction. The range of impedances at the output *T*-junction that can be matched to the input line depends upon the characteristic impedances of lines *A* and *B* relative to the main line. Theoretically, by proper choice of the characteristic impedances of lines *A* and *B*, it is possible to make the main line flat for any load V.S.W.R. at the output junction. In practice, however, the case of importance will be when the characteristic impedance of all the lines are identical. Only this case will, therefore, be considered. This consideration restricts the use of the re-entrant stub line section as a matching device to load V.S.W.R. equal to or higher than 4. The analysis together with some experimental results are presented in this article.

## MATRIX PARAMETERS OF TRANSMISSION LINES

The input and output currents  $I_1$  and  $I_2$  of a uniform, loss-less transmission line of length  $l$  shown in Fig. 2(a) can be expressed in terms of the corresponding voltages  $E_1$  and  $E_2$  by

$$\left. \begin{aligned} I_1 &= -j Y_0 (\cot \beta l) E_1 + j Y_0 (\operatorname{cosec} \beta l) E_2 \\ I_2 &= j Y_0 (\operatorname{cosec} \beta l) E_1 - j Y_0 (\cot \beta l) E_2 \end{aligned} \right\} \quad \dots (1)$$

where  $Y_0$  and  $\beta$  ( $= 2\pi/\lambda$ ) are the characteristic admittance and the phase constant respectively of the line and  $\lambda$  is the wavelength.

In matrix notation Equ. (1) is written as

$$\begin{bmatrix} I_1 \\ I_2 \end{bmatrix} = \begin{bmatrix} -j Y_0 \cot \beta l & j Y_0 \operatorname{cosec} \beta l \\ j Y_0 \operatorname{cosec} \beta l & -j Y_0 \cot \beta l \end{bmatrix} \times \begin{bmatrix} E_1 \\ E_2 \end{bmatrix} \quad \dots (2)$$

i.e.,  $[I] = [Y] \times [E]$

We can, therefore, represent a given length of transmission line by a two-terminal pair network, shown in Fig. 2(b), provided their admittance matrices

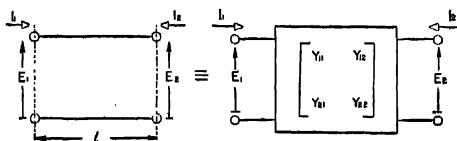


Fig. 2(a). Loss-less transmission line of length  $l$  and characteristic admittance  $Y_0$ .

Fig. 2(b). Equivalent network representation of the transmission line.

are identical. For the equivalent network the elements of the admittance are obtained from

$$[Y] = j Y_0 \begin{bmatrix} -\cot \beta l & \operatorname{cosec} \beta l \\ \operatorname{cosec} \beta l & -\cot \beta l \end{bmatrix} = \begin{bmatrix} Y_{11} & Y_{12} \\ Y_{21} & Y_{22} \end{bmatrix}$$

i.e.,  $\left. \begin{aligned} Y_{11} &= Y_{22} = -j Y_0 \cot \beta l \\ Y_{12} &= Y_{21} = j Y_0 \operatorname{cosec} \beta l \end{aligned} \right\} \quad \dots (3)$

Let us now consider the two lines  $A$  and  $B$ , one ( $A$ ) of length  $l$  and the other ( $B$ ) of length  $l'$ , each of characteristic admittance  $Y_0$  connected as shown in Fig. 1. The equivalent network representation is shown in Fig. 3 where the unprimed quantities refer to line  $A$  and the primed quantities to line  $B$ .

The resultant  $[Y]$  matrix of the parallel combination of the two networks is thus from Equ. (3).

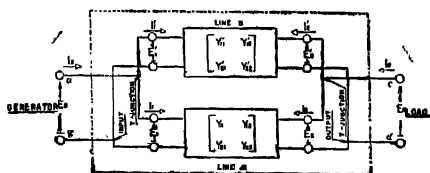


Fig. 3. Equivalent network representation of the re-entrant stub line

$$\begin{aligned} \text{Resultant } [Y] &= \begin{bmatrix} Y_{11} + Y'_{11} & Y_{12} + Y'_{12} \\ Y_{21} + Y'_{21} & Y_{22} + Y'_{22} \end{bmatrix} \\ &= jY_0 \begin{bmatrix} -(\cot \beta l + \cot \beta l') & (\operatorname{cosec} \beta l + \operatorname{cosec} \beta l') \\ (\operatorname{cosec} \beta l + \operatorname{cosec} \beta l') & -(\cot \beta l + \cot \beta l') \end{bmatrix} \end{aligned} \quad (4)$$

The matrix representation (4) now leads us to a single equivalent network of the re-entrant stub line section as far as the input (terminals  $a-b$ ) and output (terminals  $c-d$ ) are concerned. This is shown in Fig. 4.

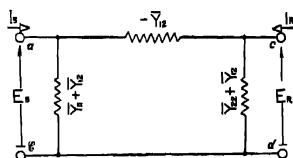


Fig. 4. Resultant network configuration of the re-entrant stub line.

In the above representation,

$$\left. \begin{aligned} \bar{Y}_{11} &= Y_{11} + Y'_{11} = \bar{Y}_{22} = Y_{22} + Y'_{22} \\ &= -jY_0(\cot \beta l + \cot \beta l'); \\ \bar{Y}_{12} &= (Y_{12} + Y'_{12}) = (Y_{21} + Y'_{21}) \\ &= jY_0(\operatorname{cosec} \beta l + \operatorname{cosec} \beta l') \end{aligned} \right\} \quad \dots \quad (5)$$

If the value of the load admittance at  $c-d$  is  $\bar{Y}_R = -(I_R/E_R)$ , it is easy to show that the input admittance at  $a-b$  looking into the terminals is

$$Y_{in} = \bar{Y}_{11} - [\bar{Y}_{12}^2 / (\bar{Y}_{22} + Y_R)] \quad \dots \quad (6)$$

## IMPEDANCE MATCHING

We now propose to show that for  $Y_R$  lying within a certain range defined later, it is possible to make  $Y_{in} = Y_0$  by appropriate choice of the lengths of the lines  $A$  and  $B$ . The condition required for matching is  $Y_{in} = Y_0 + j(0)$ . The desired line lengths  $\theta (= \beta l)$  and  $\theta' (= \beta l')$  are then obtained from Eq (5) and (6) and are governed by the following two simultaneous equations:

$$\left. \begin{aligned} g_R (\operatorname{cosec} \theta + \operatorname{cosec} \theta')^2 &= g_R^2 + (b_R + \cot \theta + \cot \theta')^2 \\ \frac{(b_R + \cot \theta + \cot \theta') (\operatorname{cosec} \theta + \operatorname{cosec} \theta')^2}{g_R^2 + (b_R + \cot \theta + \cot \theta')^2} &= \cot \theta + \cot \theta' \end{aligned} \right\} \dots (7)$$

where

$$g_R - jb_R = Y_R/Y_0 = y_R.$$

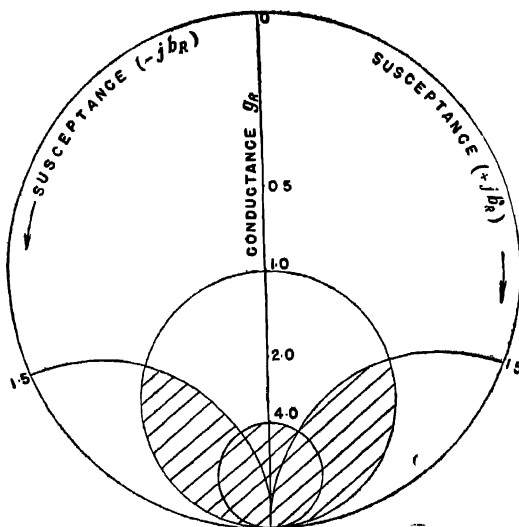


Fig. 5. Smith chart showing the range of impedance (shaded region) that can be matched.

Equ. (7) on simplification yields

$$\left. \begin{aligned} \cot \theta + \cot \theta' &= a \\ \operatorname{cosec} \theta + \operatorname{cosec} \theta' &= \pm b \end{aligned} \right\} \dots (8)$$

where

$$a = b_R/(g_R - 1)$$

$$b = \sqrt{g_R(1 + a^2)}$$

The solutions of Equ. (8) are :

$$\left. \begin{aligned} \text{(i)} \quad \cot \frac{\theta}{2} &= \frac{1}{2} (d_1 \pm \sqrt{d_1^2 - 4c_1}), \quad \cot \frac{\theta'}{2} = \frac{1}{2} (d_1 \mp \sqrt{d_1^2 - 4c_1}) \\ \text{(ii)} \quad \cot \frac{\theta}{2} &= \frac{1}{2} (d_2 \pm \sqrt{d_2^2 - 4c_2}), \quad \cot \frac{\theta'}{2} = \frac{1}{2} (d_2 \mp \sqrt{d_2^2 - 4c_2}) \end{aligned} \right\} \dots \quad (9)$$

where

$$c_1 = (b+a)/(b-a), \quad c_2 = 1/c_1$$

$$d_1 = a+b, \quad d_2 = a-b.$$

It can be easily shown that solutions for  $\theta$  and  $\theta'$  may also be obtained from the alternative forms of Eq. (8) given below in Eq. (10) and (11) :

$$\left. \begin{aligned} \operatorname{cosec}^2 \theta \mp b \operatorname{cosec} \theta + \left( \frac{a^2}{b^2 - a^2} + \frac{b^2 - a^2}{4} \right) &= 0 \end{aligned} \right\} \dots \quad (10)$$

and an identical equation for  $\operatorname{cosec} \theta'$ .

$$\left. \begin{aligned} \cot^2 \theta - a \cot \theta + \left( \frac{b^2}{b^2 - a^2} - \frac{b^2 - a^2}{4} \right) &= 0 \end{aligned} \right\} \dots \quad (11)$$

and an identical equation for  $\cot \theta'$ .

Physically realisable solutions for  $\theta$  and  $\theta'$  are obtained provided the inequality  $g_R + b_R^2/(g_R - 1) \geq 4$  is satisfied. The range of  $g_R$  where it is possible to get an impedance match is thus shown by the shaded region in the Smith chart (Fig. 5). It would be seen that whenever load V.S.W.R.  $\geq 4$ , an impedance match at the input  $T$ -junction can always be obtained by locating the putput  $T$ -junction at any appropriate point inside the shaded region.

A similar analysis for the case when the characteristic admittances of lines  $A$  and  $B$  are each half the input and output lines, shows that all load V.S.W.R.'s can be matched.

#### V. S. W. R. IN EACH LINE

The normalised values of the output admittances  $y_{A0}$  and  $y_{B0}$  terminating the

lines *A* and *B* respectively (see Fig. 3), are dependent upon the line lengths and the load admittance and are given by

$$\begin{aligned} y_{A0} &= -(I_2/E_2) \\ &= \frac{y_{12}(y_R + y'_{22}) - y_{22}y'_{12}}{y_{12} + y'_{12}} \\ &= \frac{y_R \operatorname{cosec} \theta - j \operatorname{cosec} \theta \cot \theta' + j \cot \theta \operatorname{cosec} \theta'}{\operatorname{cosec} \theta + \operatorname{cosec} \theta'} \quad \dots (12) \end{aligned}$$

$$\begin{aligned} y_{B0} &= -(I'_2/E'_2) \\ &= \frac{y'_{12}(y_R + y_{22}) - y_{22}'y_{12}}{y'_{12} + y_{12}} \\ &= \frac{y_R \operatorname{cosec} \theta' - j \operatorname{cosec} \theta' \cot \theta + j \cot \theta' \operatorname{cosec} \theta}{\operatorname{cosec} \theta + \operatorname{cosec} \theta'} \quad \dots (13) \end{aligned}$$

In the above all admittances denoted by lower case symbols are normalised with respect to  $Y_0$ .

Once the complex values of  $y_{A0}$  and  $y_{B0}$  are obtained from Eqns. (12) and (13), the reflection coefficients  $\Gamma_{A0}$  and  $\Gamma_{B0}$  at the output ends of lines *A* and *B* respectively are readily determined. Thus

$$\left. \begin{aligned} \Gamma_{A0} &= (1 - y_{A0})/(1 + y_{A0}) \\ \Gamma_{B0} &= (1 - y_{B0})/(1 + y_{B0}) \end{aligned} \right\} \quad \dots (14)$$

The V.S.W.R.'s set up in each line are then :

$$\left. \begin{aligned} \rho_A &= (1 + |\Gamma_{A0}|)/(1 - |\Gamma_{A0}|) \text{ for line } A \\ \rho_B &= (1 + |\Gamma_{B0}|)/(1 - |\Gamma_{B0}|) \text{ for line } B \end{aligned} \right\} \quad \dots (15)$$

#### SPECIAL CASE OF RESISTIVE LOADS ( $g_R \geq 4$ )

Let us consider the case when the load V.S.W.R.  $\geq 4$ . If now the load presented at the output *T*-junction is resistive,  $b_R = 0$  and  $y_R = g_R (\geq 4)$ . For such a situation, assumed to be brought about by proper location of the matching device along the load side of the transmission line, Eqns. (8), (12) to (15) are very much simplified and are respectively given below :

$$\cot \theta + \cot \theta' = 0$$

$$\operatorname{cosec} \theta + \operatorname{cosec} \theta' = \pm b$$

$$\text{whence } \theta + \theta' = \pi$$

$$\text{and } \operatorname{cosec} \theta = \pm b/2$$



$$\left. \begin{aligned} y_{A0} &= (g_R/2) + j \cot \theta \\ y_{B0} &= (g_R/2) - j \cot \theta \end{aligned} \right\}$$

$$\Gamma_{A0} = \Gamma_{B0} = [(g_R - 3)/(g_R + 5)]^{\frac{1}{2}}$$

$$\rho_A = \rho_B = (\sqrt{g_R + 5} + \sqrt{g_R - 3})/(\sqrt{g_R + 5} - \sqrt{g_R - 3})$$

The last one shows that when the load V.S.W.R.  $\gg 5$ ,  $\rho_A$  and  $\rho_B$  are each approximately half the load V.S.W.R.

#### EXPERIMENTAL VERIFICATION

Three re-entrant line matching sections were made with two *T*-junctions and lengths of rigid air dielectric coaxial lines (outer 5/8" OD  $\times$  1/32" wall tubing and inner 0.244" dia) of characteristic impedance 50 ohms having the following electrical lengths :

- (i)  $l = 26.34$  cm,  $l' = 99.90$  cm
- (ii)  $l = 16.34$  cm,  $l' = 89.90$  cm.
- (iii)  $l = 15.04$  cm,  $l' = 89.90$  cm

Calculated performances of each of these when the output *T*-junction is placed at a voltage minimum (resistive load) show that the input should be matched at

- (i)  $\lambda = 252.48$  cm, frequency = 118.82 Mc/s  
when load V.S.W.R. = 10.75, i.e.,  $g_R = 10.75$
- (ii)  $\lambda = 212.48$  cm, frequency = 141.19 Mc/s  
when load V.S.W.R. = 18.51, i.e.,  $g_R = 18.51$
- (iii)  $\lambda = 209.88$  cm, frequency = 142.94 Mc/s  
When load V.S.W.R. = 21.13, i.e.,  $g_R = 21.13$

Measurement of admittance at the input *T*-junction with an U.H.F. Admittance Meter (General Radio Co., type 1602B) showed perfect agreement in each case within the accuracy of the instrument.

#### ACKNOWLEDGMENTS

Author's thanks are due to Prof. H. Rakshit and Mr. R. C. Ganguly for several helpful discussions.

# SOME STUDIES ON THE SPREAD-F, DOUBLE-F AND FORKED-F TRACES AS OBSERVED AT HARINGHATA (CALCUTTA)

R. N. DATTA

INSTITUTE OF RADIOPHYSICS AND ELECTRONICS, UNIVERSITY OF CALCUTTA, CALCUTTA-8

(Received, August 19, 1960)

**ABSTRACT.** The paper deals with the occurrence and origin of the Spread-F phenomena including 'double' and 'forked' F-traces. From the spread-F records and from the theoretical relation of the spread-F index with the critical frequency and the velocity of irregularities, it is found that the percentage of occurrence of spread-F depends both on the electron density and the velocity of the irregularities. The night-time appearance of this phenomenon and its sharp decrease at sunrise lend support to this conclusion.

## INTRODUCTION

Irregular and diffuse reflections from the night-time  $F'$  layer, commonly known as the spread- $F'$  or  $F$ -scatter phenomena, have received considerable attention in recent years particularly in relation to its diurnal and seasonal variations and its dependence on magnetic activities. In this paper, a study of the spread-F phenomena has been made from the  $h'f$  records of Haringhata (Geomag. lat.  $12.5^\circ\text{N}$ , long.  $88^\circ 31'\text{E}$ , lat.  $22^\circ 56'\text{N}$ ) for low sunspot years 1955-56, and the characteristics obtained at this latitude are compared with those reported from other places. Theoretical consideration on the origin of spread- $F'$  and its relation with  $F_2$  region irregularities have been examined.

The study of the observed characteristics includes diurnal and seasonal variations of the nature and occurrences of spread- $F'$  in different seasons and on magnetically quiet and disturbed days. An index of scale zero to three as suggested by Briggs (1957) has been followed for indicating the degree of spreading (scale zero referring to normal trace and scales one, two and three to the weak, medium and intense types of scattering respectively). The relations between  $f_oF_2$  with the occurrence of spread- $F'$  and its latitude variation have also been discussed. A study of the nature and occurrences of double- $F'$  and forked- $F'$  traces has been made, as, both the said traces are usually found to precede or follow the scattering phenomena. According to Briggs (1957), the spread in critical frequency is due to the presence of the ionospheric irregularities in the  $F'$  region and according to Voge (1955) these irregularities are dependent on the velocities. It is shown that if account is taken of both these factors, that is, when

the velocity term is included in the expression for the spread in critical frequency, the characteristics of the diurnal and seasonal variations are better understood.

# CHARACTERISTICS OF THE SPREAD-F PHENOMENON

The night-time  $F$  echoes in the ionograms, leaving aside the simple traces can be classified broadly into three types : (a) Spread- $F$ , (b) Double- $F$  and (c) Forked- $F$  traces (Fig. 1).

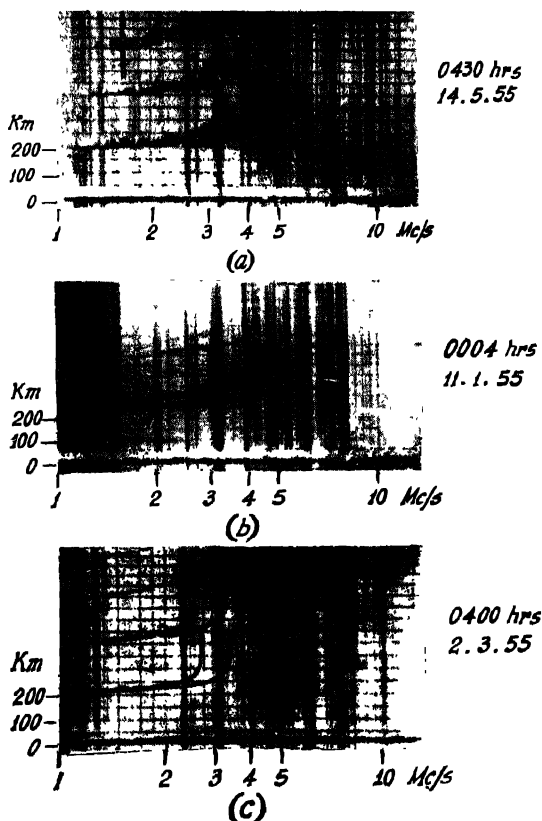


Fig. 1. Typical  $h$ - $f$  record obtained at Haringnata showing  
(a) Spread- $F$ ,  
(b) Double- $F$ ,  
and (c) Forked- $F$  traces.

(a) *Spread-F trace*: This is a thickening and diffusiveness of both the  $O$  and  $X$  components of the regular  $F$ -echoes which become more marked near the critical frequencies. Appearing at any part of the night, usually some time after sunset, it becomes more prominent with the progress of the night and decays sharply at sunrise. During the same night the variation in the degree of the spread may pass through one or two peaks. The spread also exhibits seasonal variations in the frequency of occurrence. There is a general agreement in the diurnal variations in the degree of spread obtained at different stations, but the seasonal variations as reported from different places appear to be different. From the analysis of data done by Reber (1954), Briggs (1956), Kasuya *et al.* (1955), Wells (1954), Dagg (1957), Wright *et al.* (1956) and Lyon *et al.* (1958), it is found that leaving aside the auroral type of spreading, the characteristics of spread- $F$  are of two types, namely, (i) middle or temperate latitude type and (ii) low latitude or equatorial type. The occurrences of temperate latitude type of spreading have a tendency to increase during winter whereas those of equatorial type increase during summer in low sunspot years. McNicol and Bowman (1957), after examining the data for a number of stations, observed that a reasonable smooth distribution of occurrences of spread- $F$  exists in the range of geomagnetic latitudes between  $20^{\circ}N$  or  $S$  and  $45^{\circ}N$  or  $S$ , and that the existence of equatorial type is comparatively small. No suggestion for the change over latitude from equatorial to temperate latitude type of spreading has been given there. Lyon *et al.* (1958) from a study of spread- $F$  and magnetic activity suggested, from the results of two stations, Koroia and Johannesburg, situated at the temperate latitudes, that the transition from equatorial to temperate type of spreading is at some latitude between these two stations and at about  $20^{\circ}S$  (Geo. lat.) or  $35^{\circ}S$  (Geomag. lat.). Recently Kotadia (1959) after examining the data of some northern stations has suggested the change over latitude to be at  $31.2^{\circ}N$  (Geo. lat.). But the suggested belt for the types of spreading cannot explain the non-seasonal variation of the occurrence of spread- $F$  at Washington ( $50.3^{\circ}N$  Geomag. lat.) and at Rarotonga ( $21.7^{\circ}S$  Geomag. lat.). In our case, however, it is found that percentage of occurrence of spread- $F$  traces, of all the three degrees, is more marked in summer than in winter and is minimum during the autumnal equinox. The observational results are depicted in Figs. 2(a), (b), (c) and (d).

Hourly per cent counts of spread- $F$  occurrence have been made separately for the magnetically quiet and disturbed days from the Haringhata data for the summer season in the low sunspot year 1955-56. Variations of the counts are shown in Fig. 3. It will be seen that percentage of occurrences is higher on the magnetically quiet than on the disturbed days. Similar effect, i.e., decreased scatter with increased magnetic activity, has been observed for summer at Ibadan (Geomag. lat.  $10.4^{\circ}N$ ), Kodaikanal (Geomag. lat.  $0.6^{\circ}N$ ), Singapore (Geomag. lat.  $10^{\circ}S$ ) and Ahmedabad (Geomag. lat.  $13.6^{\circ}N$ ).

Some anomalies also exist regarding the occurrence of spread-F echoes in relation to  $f_oF_2$ . Reber (1954) at Hawaii found a clear inverse correlation, whereas Dagg (1957) did not find it as clearly at Slough. The night-time  $f_oF_2$  and its association with spreading phenomena has been studied for Haringhata. The critical frequencies are grouped as shown in Table I and in each range of frequencies, percentage of occurrences of spread-F has been observed.

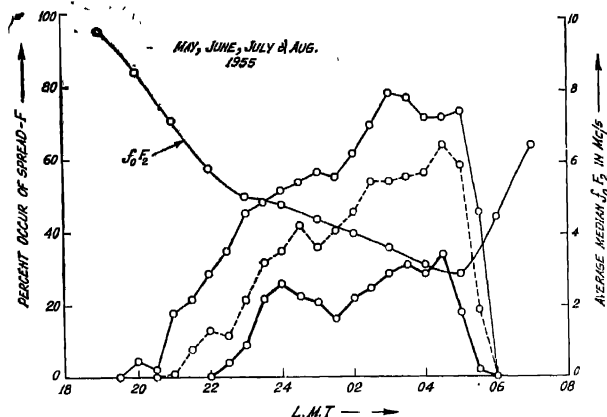


Fig. 2 (a). Diurnal variation of percent count of occurrences of spread-F in summer.  
..... weak, - - - medium, . . . . intense.

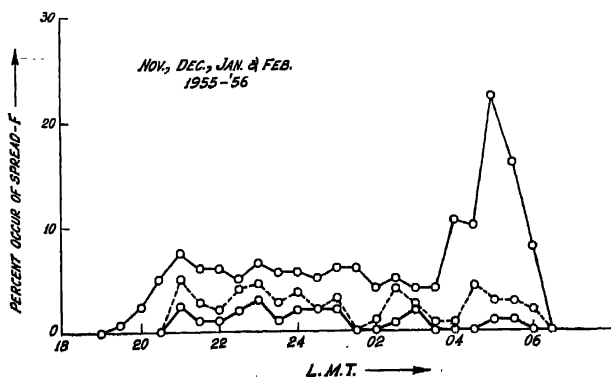


Fig. 2 (b). Diurnal variation of percent count of occurrences of spread-F in winter.  
..... weak, — medium, ——— intense.

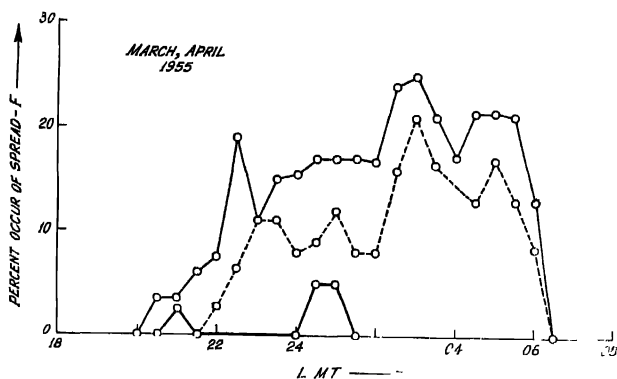


Fig. 2 (c). Diurnal variation of percent count of occurrences of spread- $F$ , in vernal equinox.  
 .....weak, ----- medium, ——— intense.

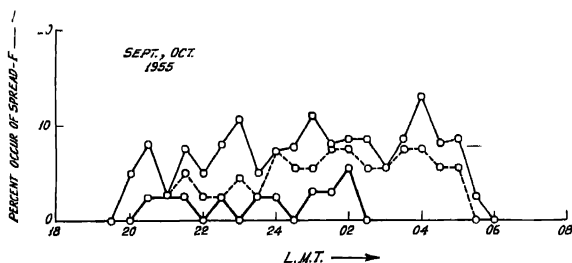


Fig. 2(d). Diurnal variation of percent count of occurrences of spread- $F$  for Haringhata for the three different degree in autumnal equinox.  
 .....weak, ----- medium, ——— intense.

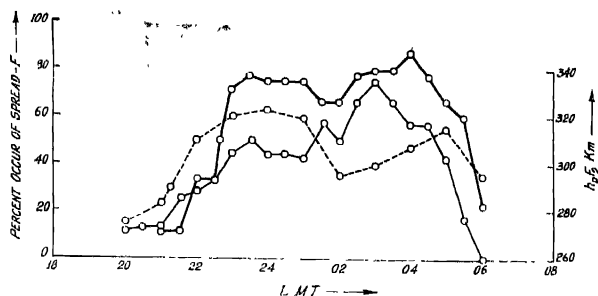


Fig. 3. Diurnal variation of percent count of occurrences of spread-F for magnetically quiet and disturbed days and variation of hourly median values of  $h_p F_2$  at Haringhata. Heavy line represents mag. quiet days light line represents mag. disturbed days and dashed line represents  $h_p F_2$ .

TABLE 1

Frequency range in Mc/s	Percentage of occurrence of spread F
1 5—2 0	84
2 1—2 5	80
2 6—3 0	75
3 1—3 5	71
3 6—4 0	45
4 2—4 5	27
4 5—5 0	30
5 1—5 5	11
5 6—6 0	2
6 0—7 0	0
7 0—8 0	0

The graph drawn from the above results in the form of histogram (Fig. 4), shows that percentage of spread-F becomes prominent as the critical frequency is lowered, and is thus a decreasing function of  $f_o$ . The same conclusion can be drawn from Fig. 2(a), showing the nature of variation of percent count of spread-F with the hourly average median  $f_o F_2$ . The ionograms for the summer months have only been taken for this analysis, as, during these days the missing records are least.

Variation of hourly median values of  $h_p F_2$  and appearance of spread-F at Haringhata show that there is fairly parallel relationship between the two. Maximum of  $h_p F_2$  coincides with the peak of the frequency of occurrence of spread-F (Fig. 3). The result supports those obtained by Kasuya *et al.* (1954) and Bowman (1960) and suggests that spread-F is originated from the upper F region.

(b) *Double F-traces* and (c) *Forked-F traces* : Night time  $h'f$  records sometimes contain two parallel  $F$  layer traces each showing the usual magnetoionic splitting with some degree of spreading. These are too close to each other to admit of any explanation in terms of multiple reflections. It is believed that the upper trace is due to oblique reflections from some moving folds or deformities in the  $F'$  region.

Sometimes, instead of broadening, each of the two components of the  $F$  layer trace assumes a forked appearance near the critical frequency.

Typical examples of double- $F$  and forked- $F$  traces from our records are shown in Fig. 1(b) and 1(c).

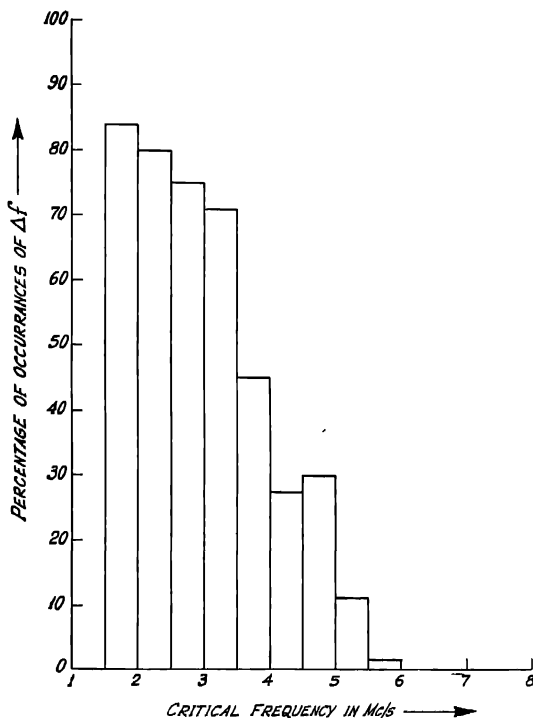


Fig. 4. Variation of percent count of occurrences of Spread- $F$  with  $f_oF_2$  for summer quiet days at Haringhata.

From the study of ionograms it is found that these are invariably associated with some degree of spreading either preceding or following the simple traces. Moreover, the diurnal variations of their occurrences for summer season (Fig. 5)



follow the same pattern as that of the spread- $F$  occurrence. This suggests that the causes of spread- $F$ , double- $F$  and forked- $F$  traces are likely to be the same, the particular picture depending probably on the size and orientation of the said irregularities.

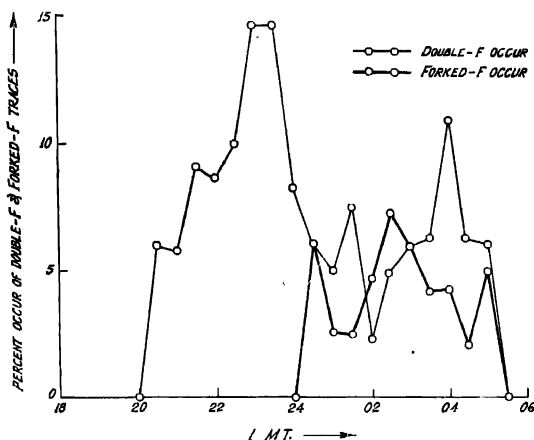


Fig. Diurnal variation of double- $F$  and forked- $F$  traces for summer seasons as found at Haringhata.

#### THEORETICAL INTERPRETATION OF OBSERVATIONAL RESULTS

A considerable amount of work has been done to explain the observed characteristics of the Spread- $F$  phenomenon. According to the present state of knowledge, the most prominent cause of the phenomenon appears to be the irregularities which are known to exist in the electron density distribution in the  $F$  region. These irregularities have been found to correlate positively with magnetic activity at high latitudes and negatively at low latitudes. According to the above hypothesis Spread- $F$  condition should exhibit similar correlation with magnetic activity. This indeed is what is found from the observations of Hertz (1959) and Lyon *et al.* (1958) and also from our result.

The effect of irregularities on the spread- $F$  has been examined theoretically by Briggs. According to this author, the relation between the irregularity  $\Delta N$ , the critical frequency  $f_0$ , and the spread  $\Delta f_0$ , is given by

$$\Delta N \propto f_0 \Delta f_0$$

Also, it has been shown by Voge (1955) that if  $v$  is the velocity with which the

irregularity is drifted then  $\Delta N$  is proportional to  $v^2$ . Hence, combining the above relation with Voge's proportionality

$$\Delta N \propto v^2$$

we may write

$$f_0 \Delta f_0 \propto v^2$$

or

$$\Delta f_0 \propto \frac{v^2}{f_0}, \text{ i.e., } \frac{v^2}{\sqrt{N}}$$

This shows that the night-time increase in velocities of the irregularities and simultaneous decrease in electron density can intensify the degree of spreading. That the velocity changes considerably is well known from the measurement of drift movement by radio astronomical techniques. Drift speeds of 60 m/sec at 19 hr, 290 m/sec at 01 hr and 170 m/sec at 05 hr, have been recorded (Maxwell, 1954). Moreover, the decrease in electron density may cause the enhancement of scattering, for, such decrease in electron density reduces the electromagnetic damping of the turbulence on which the production of the irregularities depends (Booker, 1958). It has been suggested (Booker and Wells, 1938, Maxwell, 1954, Martyn, 1955 and Dagg 1957) that the irregularities may have their origin in the  $E$  layer turbulence created in the Dynamo region at night, the turbulence effect being communicated to the  $F$  region by the presence of earth's magnetic field. It is to be noted that  $v$  in the term  $v^2/f_0$  varies considerably at the same place and also from place to place. This may explain the anomalies of the seasonal variations of spread- $F$  occurrences at different places. Also,  $\Delta f_0$  depends inversely on  $f_0$ . This inverse dependence may perhaps be associated with the observed relation of  $f_0 F_2$  and the percentage occurrence of spread- $F$ .

#### CONCLUDING REMARK

Occurrence of spread- $F$  is a night-time phenomenon and becomes more prominent at Haringhata during summer, during magnetically quiet days and during periods of low critical frequency. The observed results are in agreement with those obtained at equatorial stations like Ibandan, Singapore and Ahmedabad during low sunspot years. The change over latitude from the temperature type of spread to the equatorial type is not yet definitely known. Washington (Geomag. lat. 50°.3N) and Rarotonga (Geomag. lat. 21.7°S) may lie in the change over region. The anomaly of clear inverse correlation of spread- $F$  occurrence with critical frequency at different places may be attributed to the possible fluctuations in the velocity of the irregularities. The ionograms, where the spread in critical frequency is measurable accurately (as in the case of weak spreading), may be used to estimate the velocity of the irregularities from the observed critical frequency and its spreading.

# ACKNOWLEDGMENTS

The work forms part of the programme of the Radio Research Committee of the Council of Scientific and Industrial Research, Government of India. The author is indebted to Professor J. N. Bhar, D.Sc., F.N.I., for his keen interest and encouragement. Thanks are also due to Dr. A. K. Saha for valuable suggestions.

# REFERENCES

- Booker, H. G. and Wells, H. W., 1938, *Terr. Mag.*, **43**, 249.  
 Booker, H. G., 1956, *J. Geophys. Res.*, **61**, 673  
 Booker, H. G., 1956, *J. Atmos. Terr. Phys.*, 8, Suppl. Part II, **52**.  
 Booker, H. G., 1958, *Proc. I.R.E.*, **46**, 298.  
 Bowman, G. G., 1960, *Aust. J. Phys.*, **13**, 69.  
 Briggs, B. H., 1957, *J. Atmos. Terr. Phys.*, **12**, 34.  
 Briggs, B. H., 1957, *J. Atmos. Terr. Phys.*, **12**, 89.  
 Dagg, M., 1957, *J. Atmos. Terr. Phys.*, **11**, 133 & 139.  
 Eckersley, T. L., 1958, *Proc. Phys. Soc.*, **56**, 1025.  
 Hartz, T. R., 1959, *Canadian Jour. of Phys.*, **37**, 1137.  
 Kasuya, I., Kataho, S. and Taguchi, S., 1955, *J. R.R.L. (Japan)*, **2**, 329.  
 Katodia, K. M., 1959, *Proc. Ind. Acad. of Sciences*, **1**.  
 Lyon, A. J., Skinner, N. J. and Wright, R. W., 1958, *Nature*, **181**, 1724.  
 Maxwell, A., 1954, *Phil. Mag.*, **45**, 1247.  
 McNicol and Bowman, G. G., 1957, *Aust. J. Phys.*, **10**, 588.  
 Reber, G., 1954, *J. Geophys. Res.* **59**, 257 & 445.  
 Voge, J., 1955, *L'Onde Electrique*, **35**, 565.  
 Wells, H. W., 1954, *J. Geophys. Res.*, **59**, 273.  
 Wright, R. W., Koster, J. R. and Skinner, N. J., 1956, *J. Atmos. Terr. Phys.*, **8**, 240.

# APPENDIX

If  $\rho$  is the density of air at the ionospheric region producing scattering and  $N$  is the number of electrons per unit volume then

$$N \propto \rho$$

$$\text{Hence} \quad \frac{\Delta N}{N} = \frac{\Delta \rho}{\rho} \quad \dots (1)$$

For perfect gas, where fluctuation of temperature is negligible it can be written that

$$\frac{\Delta \rho}{\rho} \simeq \frac{\Delta p}{p} \quad \dots (2)$$

where  $p$  is the pressure of air at that region.

The variation of atmospheric temperature with height during daytime and night-time (Fig. 6) shows that temperature gradient at night is comparatively low. So the Eqn. (2) is applicable in the ionospheric region at night.

Now  $\Delta p \propto v^2$  (Bernoulli's principle).  
 $\Delta N \propto v^2$

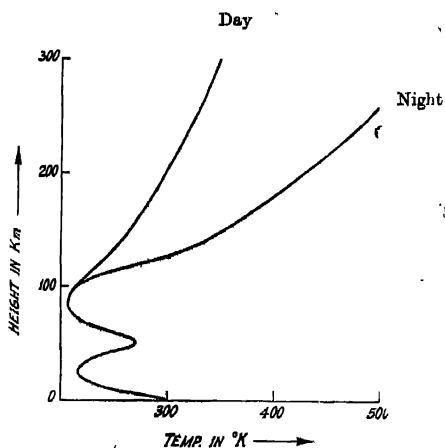


Fig. 6.

# DAY TO DAY CHANGES IN THE DAILY MEAN INTENSITY OF COSMIC RAYS

R. P. KANE, S. R. KANE AND B. A. HOLLA

PHYSICAL RESEARCH LABORATORY, AHMEDABAD

(Received, August 12, 1960)

**ABSTRACT.** Data obtained at Kodaikanal (geomag. lat.  $1^{\circ}\text{N}$ , altitude 2300 meter) for cosmic ray mesons and the nucleonic component are analysed for the first 12 months of the I.G.Y. (July 1957-June 1958). Day to day changes of the mean intensity and their relationship with geomagnetic phenomena are studied. Comparison is made with neutron monitor data at Huancaayo, Ottawa and Resolute. A variation spectrum of the type  $\delta D(E)/D(E) \propto E^{-1}$  is obtained.

## I. INTRODUCTION

During the I.G.Y. period, several workers in the world have operated cosmic ray meson telescopes and neutron monitors on a continuous basis. The Physical Research Laboratory, Ahmedabad, India, also participated in this effort and contributed data for neutron monitors and cubical meson telescopes for the stations at Ahmedabad and Kodaikanal. Besides these instruments, a narrow angle telescope of semi-angles  $10^{\circ}$  in the E-W plane and  $20^{\circ}$  in the N-S plane was also operated at Kodaikanal during the I.G.Y. period. Since meson telescopes and neutron monitors at different latitudes and altitudes have different energy responses to the primary cosmic ray intensity, a comparison of data from these gives an idea about the energy dependence of cosmic ray variations.

In this communication we have described the results of an analysis of results obtained with five different cosmic ray measuring instruments. Details of these are given in Table I.

TABLE I  
Details of the stations

Instrument	Situation	Alt. (met.)	Geomagnetic		Cut off energies (BeV)
			Lat.	Long.	
Meson telescope ( $10^{\circ} \times 20^{\circ}$ )	Kodaikanal	2343	$1^{\circ}$	$147^{\circ}$	15
Neutron pile	Kodaikanal	2343	$1^{\circ}$	$147^{\circ}$	15
	Huancaayo	3400	$-1^{\circ}$	$354^{\circ}$	13
	Ottawa	101	$57^{\circ}$	$351^{\circ}$	2
	Resolute	17	$83^{\circ}$	$289^{\circ}$	0

## II. ENERGY RESPONSE OF THE VARIOUS INSTRUMENTS

Before proceeding with an examination of the results of analysis of the data from the various instruments, it is advisable to get an idea of the differences in their energy responses. This was attempted by following Dorman's (1957) method, which is outlined below :

The number  $N(h)$  of secondary cosmic ray particles at a latitude  $\lambda$  and at an atmospheric depth ( $h$ ) is given by

$$N_{\lambda}(h) = \int_{E_{\lambda}^c}^{\infty} D(E) \cdot M(E, h) dE \quad \dots (1)$$

where  $D(E)$  represents the primary energy spectrum at the top of the atmosphere and  $M(E, h)$  is the "multiplicity function" which gives the number of secondary particles produced by a primary particle of energy  $E$ . The lower limit of integration  $E_{\lambda}^c$  is the minimum (critical) energy for arrival of primary cosmic rays in the vertical direction at latitude  $\lambda$ .

Dividing Eq. (1) by  $N_{\lambda}(h)$  and multiplying by 100, we get

$$100\% = 100 \int_{E_{\lambda}^c}^{\infty} \frac{D(E)M(E, h)dE}{N_{\lambda}(h)} = \int_{E_{\lambda}^c}^{\infty} W(E, h)dE \quad \dots (2)$$

where  $W(E, h)$  represents the percentage contribution to the secondary component at depth  $h$ , due to primaries of energy  $E$ .  $W(E, h)$  is known as the "coupling constant". A knowledge of its functional relationship with  $E$  is necessary to get an idea of the energy response of any particular instrument.  $W$  involves the product of the primary energy spectrum  $D(E)$  and the multiplicity function  $M(E, h)$ . The primary energy spectrum of cosmic ray intensity is now fairly well established. But the multiplicity function  $M(E, h)$  is difficult to calculate theoretically because of many complex processes involved in the interactions of primary cosmic ray particles with air nuclei. Dorman (1957) has pointed out that the coupling constants  $W$  can also be evaluated from a knowledge of the latitude dependence of cosmic ray intensity, as follows :

Differentiating (1) partially with respect to  $E_{\lambda}^c$ , we get

$$\frac{\partial N_{\lambda}(h)}{\partial E_{\lambda}^c} = -\partial E_{\lambda}^c \frac{D(E) \cdot M(E, h)}{N_{\lambda}(h)} = -\partial E_{\lambda}^c \cdot W_{\lambda}(E, h) \quad \dots (3)$$

It is clear, therefore, that  $W(E, h)$  is directly related to the latitude effect of the secondary component observed at a depth  $h$ . Since the latitude effects of the

various secondary components have been precisely obtained experimentally, the coupling constants  $W(E, h)$  can be easily calculated for energies between 0 and 15 BeV which is the maximum vertical cut-off energy (at  $\lambda = 0$ ). For higher energies, Dorman suggests extrapolation methods which are based partly on experimental results and partly on theoretical considerations.

The coupling constants  $W(E, h)$  are different for different secondary components and for different altitudes and latitudes and have been calculated by Dorman from experimental latitude effect data. Fig. 1 gives the coupling constants as percentage per BeV for the various secondary components mentioned in Table I. Since the latitude dependence of the meson component at the altitude of Kodai-kanal is not known, the coupling constants for the same are obtained by averaging the coupling constants for lon-chamber measurements at 10 Km altitude and hard component measurements at sea-level.

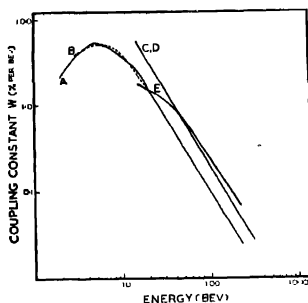


Fig. 1. Coupling constant  $W$  (percentage per BeV) for various secondary components. A-Resolute neutrons, B-Ottawa neutrons, C-Huancayo neutrons, D-Kodaikanal neutrons, E-Kodaikanal mesons. All plots are normalised to give  $\int W.dE = 100$ .

Knowing the value of  $W$  for all energies between  $E$  and  $\infty$ , it should be possible to calculate the mean energies to which the various instruments respond. A statistical method of obtaining the same would be to calculate mean energy  $\bar{E}$  by the formula

$$\bar{E} = \frac{\int_{E_{\lambda}^0}^{\infty} W(E) \cdot E \cdot dE}{\int_{E_{\lambda}^0}^{\infty} W(E) \cdot dE} \quad \dots (4)$$

However, this method does not succeed for any of the curves given in Fig. 1 because of the following reason. For high energies, the plots in Fig. 1 can be

approximated to a relation of the type  $W = k.E^{-\nu}$ . However, the values of  $\nu$  are all less than 2 whereas the integral in the numerator of Eq. (4) is convergent only if  $\nu > 2$ . Hence, Eq. (4) does not yield finite values for the mean energy  $\bar{E}$ .

Fonger *et al.* (1953) have avoided this difficulty by assuming an arbitrary definition of mean energy  $\bar{E}$  as,

$$\frac{1}{1+\bar{E}} = \frac{\int_{E_{\lambda}^0}^{\infty} \frac{W(E) \cdot dE}{1+E}}{\int_{E_{\lambda}^0}^{\infty} W(E) dE} \quad \dots (5)$$

Using this formula, the mean energies for the various secondary components referred to in Table I would be as follows:

Kodaikanal meson	54 BeV
Kodaikanal neutron	34 „
Huancayo „	34 „
Ottawa „	12 „
Resolute „	11.5 „

One may also view the energy response qualitatively by calculating the percentage of particles contributed by primaries confined to an energy range 0 to  $E$  for various values of  $E$ . Fig. 2 gives the percentages for the various secondary components.

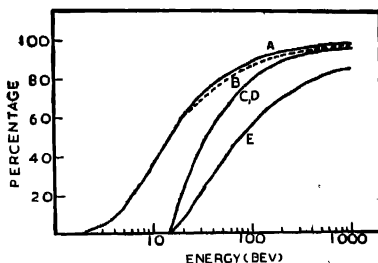


Fig. 2. Percentage of secondary particles contributed by primaries of energies below  $E$ . Symbols A, B, C, D & E have the same meaning as in Fig. 1.

It can be seen from Fig. 2 that for the neutron monitors at Ottawa and Resolute, almost 50% of the secondaries are due to primary energies between



0 to 15 BeV while for the nucleonic component at Huancayo and Kodaikanal the corresponding energy range is 15 to 35 BeV. For Kodaikanal meson intensity, the range is still higher viz. 15 to 75 BeV.

### III. DAILY MEAN INTENSITY OF COSMIC RAYS

The daily mean intensities of the nucleonic component and meson component of cosmic ray intensity at the various places corrected for barometric effect only are plotted in Fig. 3 for the period July 1957 to June 1958. The daily means of  $H$ , the horizontal component of earth's magnetic field at Kodaikanal, are also plotted.

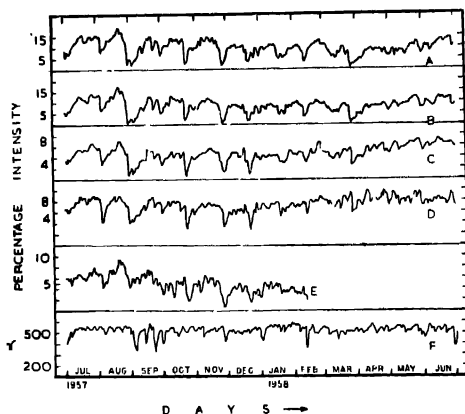


Fig. 3. Plot of daily mean intensities. Symbols A, B, C, D, E are as in Fig. 1.  $H$  represents the horizontal component of earth's magnetic field at Kodaikanal..

It can be seen from Fig. 3 that the daily mean intensity shows large fluctuations during the period under consideration. Variations as high as 5% at the equatorial stations and 10% or more at high latitude stations are observed frequently. Many of the sharp minima indicate Forbush type decreases.

To find out the extent to which these variations are simultaneous at the various stations, correlation coefficients are calculated for the various pairs. They are given in Table II.

It can be seen from Table II that

- (a) Kodaikanal neutrons and Huancayo neutrons are very highly correlated with each other but not so much with either Kodaikanal mesons or Ottawa and Resolute neutrons.

TABLE II

Correlation coefficients between the various components

	Kodaikanal meson	Kodaikanal neutron	Huancayo neutron	Ottawa neutron	Resolute neutron
Kodaikanal meson	1.00	0.68	0.70	0.70	0.59
Kodaikanal neutron	0.68	1.00	0.91	0.73	0.66
Huancayo neutron	0.70	0.91	1.00	0.86	0.71
Ottawa neutron	0.70	0.73	0.86	1.00	0.97
Resolute neutron	0.59	0.66	0.71	0.97	1.00

(b) Ottawa and Resolute neutrons are very highly correlated with each other.

It seems, therefore, that the mean intensity variations are broadly parallel at all the stations indicating a world wide nature of the variations, but there are differences also between stations at different latitudes as also between mesons and nucleonic component. It is also observed that the average ranges of the variations for Kodaikanal neutron and Huancayo neutron are about the same, while the ranges of neutron intensity at Ottawa and Resolute are more than twicet hose at Kodaikanal or Huancayo. Kodaikanal meson intensity has a range somewhat lesser than Kodaikanal neutron intensity. This indicates a strong energy dependence where lower energies have larger variations.

It must be noted, however, that the meson intensity is not corrected for upper air temperature effect and is not, therefore, directly comparable to the neutron intensities. The lower correlation between neutron and meson intensities could be due to this fact. Unfortunately, upper air radio-sonde data for Kodaikanal are not available and hence it is not possible to estimate and correct for the upper air temperature effect at Kodaikanal.

#### IV. RECURRENCE TENDENCIES IN THE DAILY MEAN INTENSITY VARIATIONS

To study the recurrence tendencies in the daily mean intensity, the days on which Ottawa neutron intensity showed maxima and minima were chosen as epoch days and Chree diagrams were drawn for the various intensities for  $n = -60$  to  $+60$  about the epoch day  $n = 0$ . These are shown in Fig. 4.

Fig. 4(a) and 4(b) refer to Ottawa neutron intensity maxima and minima respectively as epochs. It will be seen that there is a 27-day recurrence tendency for both the maxima and minima. Chree diagram for  $H$ , the horizontal component of earth's magnetic field at Kodaikanal is also plotted in Fig. 4. It will be seen from Fig. 4(b) that  $H$  has a minimum at  $n = 0$  which means that on cosmic ray minima days, value of  $H$  is also minimum. However, the magnitude of the minimum in  $H$  is rather small ( $\sim 70$  gamma). This is discussed further in Section V.

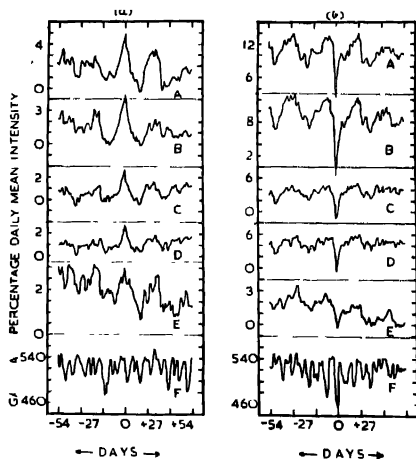


Fig. 4. Three diagrams of daily mean intensities of cosmic rays and earth's magnetic field for Ottawa neutron intensity (a) Maxima and (b) Minima as epoch days.

A-Ottawa neutron, B-Resolute neutron, C-Huancayo neutron, D-Kodaikanal neutron, E = Kodaikanal meson, F = Horizontal component of earth's magnetic field.

# V. RELATIONSHIP WITH GEOMAGNETIC DISTURBANCES

As a measure of the geomagnetic disturbance of any particular day, a character figure  $C_p$  is evolved, which takes into account deviations from averages of the

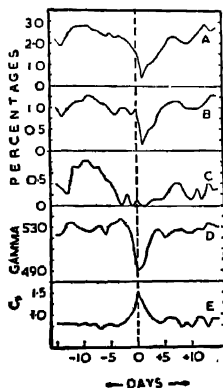


Fig. 5. Three diagrams of daily mean intensities of cosmic rays and earth's magnetic field for  $C_p$  maxima as epoch days. A-High latitude neutrons, B-Equator neutrons, C-Equator mesons, D-Horizontal component of earth's magnetic field, E- $C_p$  values.

variations in the various magnetic elements at several locations all round the world. Values of  $C_p$  range from 0 to about 2.0. To study the relationship between  $C_p$  and cosmic ray variations, days of maxima of  $C_p$  values were chosen as epoch days and Chree diagrams were drawn for the daily mean intensity of cosmic rays. These are shown in Fig. 5.

It seems that  $C_p$  maxima are followed within a day or two by cosmic ray minima. This is in agreement with earlier observations of similar nature by workers elsewhere (e.g. Simpson 1954).

However, it is found that the changes in the mean cosmic ray intensity associated with  $C_p$  maxima are not very large. Thus, the changes at equator are of the order of 1% only whereas it is seen from Fig. 1, that the mean intensity variations are sometimes as large as 5% for equatorial stations. It is obvious, therefore, that there is no one-to-one relationship between  $C_p$  maxima and cosmic ray minima. Apart from the possibility that some of the cosmic ray changes have apparently no connection with  $C_p$  maxima at all, it is also possible that all  $C_p$  maxima are not on the same footing so far as their effects on cosmic ray intensity are concerned. It is worthwhile, therefore, to see whether a criterion could be decided, upon which one could separate out those  $C_p$  maxima which are better related to cosmic ray changes than the others. In the past, attempts have been made (Sekido *et al.*, 1955) to study separately cosmic ray storms which are, and are not, associated with geomagnetic disturbances. However, the selection criterion there is the effect on cosmic ray intensity itself. We have adopted a criterion which was first introduced by Allon (1944). The  $C_p$  maxima are divided into 4 groups according to whether they are preceded and/or succeeded by significant maxima at 27 day interval. Thus, the four groups are:—

Group A:  $C_p$  maxima preceded and succeeded by  $C_p$  maxima at  $\pm 27$  days.  
 $+C_p^+$

Group B:  $C_p$  maxima succeeded by  $C_p$  maxima at  $\pm 27$  days but not preceded at  $\pm 27$  days.  
 $^{\circ}C_p^+$

Group C:  $C_p$  maxima preceded by  $C_p$  maxima at  $\pm 27$  days but not succeeded at  $\pm 27$  days.  
 $+C_p^{\circ}$

Group D:  $C_p$  maxima having no preceding or succeeding maxima at  $\pm 27$  days.  
 $^{\circ}C_p^{\circ}$

Taking  $C_p$  maxima in each group separately as epoch days, Chree diagrams were drawn for the various cosmic ray intensities as also for the horizontal component of earth's magnetic field. In Table III, we have summarised the main features of the Chree diagrams. For comparison, the main features as revealed by Fig. 5 for all  $C_p$  maxima as epochs are also included in Table III.

It is clearly seen from Table III that though all types of  $C_p$  maxima produce cosmic ray minima at about  $n = 0$  to  $+2$ , the magnitude of the drop in cosmic

TABLE III  
Relationship between  $C_p$  maxima and cosmic ray intensity

Epoch days ( $n = 0$ )	Range of $C_p$ minima at	Cosmic ray minima at	Magnitude of cosmic ray intensity drop				Ratio of range high lat : equator (neutrons)	Horizontal component of magnetic field at Kodaikanal		Remarks
			Equator		High lat.			Min. at	Intensity drop	
			Meson	Neutron	Neutron	Neutron				
All $C_p$ max.	About 0.5 to 1.5	$n = +1$ day	0.5%	1.0%	2.0%	2.0	$n = 0$	45 gamma	Maximum at $n = 0$ very prominent.	
$^*C_p^+$ max.	"	About $n = +1$	0.5%	0.5%	1.5%	3.0	About $n = +1$	40 gamma	Large fluctuation of $H$ values on days on either side of $n = 0$ .	
$^oC_p^+$ max.	"	"	0.5%	0.5%	1.5%	3.0	$n = 0$	55 gamma	"	
$^*C_p^o$ max.	"	"	1.2%	1.5%	3.0%	2.0	$n = +1$	60 gamma	"	
$^oC_p^o$ max.	"	"	1.2%	1.5%	4.5%	3.0	$n = 0$	70 gamma	Effect at $n = 0$ very prominent.	

ray intensity is not the same for all. Thus,  $+C_p^0$  and  $^0C_p^0$  maxima which are characterised by either a fading or an absent recurring tendency have the largest effect on cosmic rays. The effect is about 1.5% at equator and 4% at high latitude for neutrons. The ratio of these two is, however, about the same for all types of  $C_p$  maxima.

It seems, therefore, that  $C_p$  maxima which do not have recurring tendencies produce the greatest reduction in cosmic ray intensity. From the last two columns of Table III, it is seen that the association of all  $C_p$  maxima with characteristics of  $H$  variation is not the same. Thus the  $C_p$  maxima of the  $+C_p^0$  or  $^0C_p^0$  type show a larger range in the value of  $H$  as compared to the range due to other  $C_p$  maxima.

It is now well-known that geomagnetic disturbances of the recurring type are associated with coronal activity and C.M.P. of weak coronal emission. On the other hand, the non-recurring type disturbances are associated with S. C. type of magnetic storms and also with sunspot groups of complex magnetic field, and with C.M.P. of sunspot groups having high activity in solar radio noise. It seems, therefore, that cosmic ray events have a better association with phenomena of the latter type.

There are, however, two major apparent discrepancies in these observations. They are as follows :

- (a) Through  $C_p$  maxima having little or no 27 day recurrence tendencies are better associated with cosmic ray minima, the Chree diagrams for cosmic ray intensity minima as epochs show prominent recurrence tendencies as shown in Fig. 4(b).
- (b) Though the non-recurring type  $C_p$  maxima are also associated with S. C. type magnetic storms, there is no one-to-one relationship between cosmic ray storms (viz. sharp minima of cosmic ray intensity) and the S.C. type storm decreases of the horizontal component of earth's magnetic field.

These discrepancies can, however, be understood if the following assumptions are made:

- (i) The recurring type geomagnetic disturbances do have some effect on cosmic ray intensity though the effects are not so prominent as in the case of effects of non-recurrent type storms. This is borne out by results given in Table III.
- (ii) The non-recurring type disturbance need not be assumed to be directly responsible for cosmic ray minima but both may have a common source of origin. The effects of the common source may persist longer in cosmic ray intensity than in geomagnetic disturbances.

- (iii) As stated earlier, all cosmic ray intensity minima are not associated with minima of horizontal component of earth's magnetic field. However, when a Chree diagram is drawn for intensity minima of the horizontal component of magnetic field at Kodaikanal as epoch days, it is found that the cosmic ray intensity shows a prominent minimum on or about the epoch days and the magnitude of this minima is quite large, about half of the general range of variation in cosmic ray intensity (Fig. 6). Thus, all cosmic ray storms are not associated with magnetic storms of the S.C. type. But many of the S.C. type magnetic storms are associated with cosmic ray storms. This is not incompatible with (a) and (b) above.

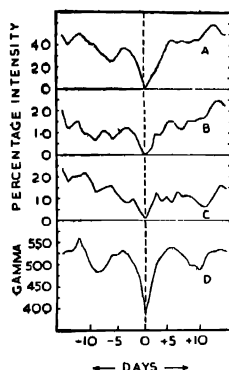


Fig. 6. Chree diagrams of daily mean intensities of cosmic rays for minima of horizontal component of earth's magnetic field as epoch days. A-High latitude neutrons, B-Equator neutrons, C-Equator mesons, D-Horizontal component of earth's magnetic field.

## VI. ENERGY DEPENDENCE OF THE VARIATIONS IN PRIMARY INTENSITY

As has been shown so far, fluctuations as high as 5% at equator and 10-15% at high latitudes are observed in cosmic ray intensity. It is obvious, therefore, that the variations of cosmic ray intensity have energy spectra significantly different from the primary energy spectrum. Referring to Eq. (1), we obtain by differentiating partially with respect to  $D(E)$ ,

$$100 \cdot \frac{\partial N_{\lambda}(h)}{N_{\lambda}(h)} = \int_{E_{\lambda}^0}^{\infty} \frac{\partial D(E)}{D(E)} \cdot W_{\lambda}(E, h) dE \quad \dots (8)$$

For the L.H.S., the experimental values are about 3—4% for Kodaikanal mesons, about 5% for Kodaikanal and Huancayo neutrons and about 10-15% for Ottawa and Resolute neutrons.

It is found that a variation spectrum of the type  $\partial D(E)/D(E) \propto E^{-1}$  fits the experimental values reasonably well.

It should be noted, however, that such a spectrum fits only to the gross effects mentioned above. In individual events and for smaller time intervals, far too large effects (100% or more) have been observed at high latitudes. The energy spectrum involved there should be far more steep. Values as high as  $E^{-5}$  have been suggested (Sekido and Murakami, 1955).

## VII. CONCLUSION

The broad conclusions of the above analysis may be summarised as follows

- (1) The daily mean intensities of cosmic rays as observed by meson telescope and neutron monitors at the stations of Kodaikanal, Huancayo, Ottawa and Resolute show large fluctuations during the period July 1957 to June 1958. The range of fluctuations is about 3—5% and 5% for mesons and neutrons respectively at equatorial stations and 10—15% for neutrons at high latitudes.
- (2) The maxima and minima of the daily mean intensity of cosmic rays exhibit strong 27-day recurrence tendencies.
- (3) An analysis with  $Cp$  maxima as epochs indicates that  $Cp$  maxima are followed by cosmic ray minima with a probable lag of 1 or 2 days. Amongst the  $Cp$  maxima, the non-recurrent types seem to be better associated with cosmic ray minima.
- (4) Cosmic ray storms are not invariably associated with magnetic storms but magnetic storms of the S.C. type are many times associated with cosmic ray minima.
- (5) Large cosmic ray intensity decreases are world-wide in nature but their magnitude seems to be more than double at high latitudes as compared to that at equator.
- (6) The day to day variations of cosmic ray intensity are energy dependent. The variation spectrum  $\partial D(E)/D(E)$  is of the type  $E^{-1}$  where  $D(E)$  is the primary energy spectrum.

## ACKNOWLEDGMENTS

The authors are grateful to Professor V. A. Sarabhai for valuable guidance during the course of this investigation. Thanks are due to various research groups who have contributed neutron monitor data during the I.G.Y. The co-operation of the staff of the Solar Physics Observatory Kodaikanal, is greatly appreciated.



Thanks are due to S. R. Thakore and others for computational help and to the Atomic Energy Commission of India for financial assistance.

# REFERENCES

- Allen, 1944, *Month. Notices of Roy. Astro. Soc.*, **104**, 13.  
 Dorman, I. L., 1957, "Cosmic Ray Variations" published by State Publishing House for Technical & Theoretical Literature, Moscow.  
 Fonger, W. H., 1953, *Phys. Rev.*, **91**, 351.  
 Sekido, Y., Wada, M., Kondo, I. and Kawabata, K., 1955, *Rep. Ionosph. Res. Japan.*, **2**, 174.  
 Sekido, Y. and Murakami, K., 1955, *Proc. IUPAP Cosmic Ray Congress, Mexico*, 253.  
 Simpson, J. A., 1954, *Phys. Rev.*, **94**, 426.

# APPENDIX

Epoch dates for the various Chree diagrams

Month	Ottawa maxima	Ottawa minima	$^{\circ}C_p^{+}$ max.	$^{\circ}C_p^{+}$ max.	$^{\circ}C_p^{0}$ max.	$^{\circ}C_p^{+0}$ max.	H minima
Jul. 57	27					19	
Aug.	21	5,30		3,6	29	13	
Sep.	20	3,14 23,30	2	23	29	4,13	5,13, 23,30
Oct.	10	23		14	21		
Nov.	13	27	9,18	7		26	27
Dec.	6,10,28	22	6		11,31	1	31
Jan. 58	10	18	21			18	
Feb.	5,23	12		6,21	17	11	11
Mar.	20	15,26			5,19	12,25	
Apr.	25	30	3,29	17			
May	26	31	14,26			29,31	
Jun.				7			

## AN X-RAY STUDY OF SILVER-CADMIUM ALLOYS\*

MD. ABDUL QUADER

DEPARTMENT OF GENERAL PHYSICS AND X-RAYS,  
INDIAN ASSOCIATION FOR THE CULTIVATION OF SCIENCE, CALCUTTA-32

(Received, August 24, 1960)

**ABSTRACT.** An X-ray investigation of the silver-cadmium system of alloys has been carried out to determine the phase boundaries at temperatures below 300°C with particular attention to the  $\beta$ -field. The presence of the  $\beta'$  phase, which occurs in the  $\beta$ -field at temperatures below 228°C has been confirmed. The lattice parameter and structure of the  $\alpha$ ,  $\beta'$  and  $\zeta$  phases have been determined. An approximate boundary of the  $\beta'$  phase has been obtained. The boundaries of the other phases as obtained by us agree with those of Owen *et al.* The results are discussed in the light of the Hume-Rothery rule and the zone-theory.

## INTRODUCTION

The equilibrium diagram of the silver-cadmium system of alloys, published in Metals Handbook (1948) is based on the thermal and microscopical work of Durrant (1931, 1935). In this diagram a phase  $\beta'$  (ordered body-centred cubic with CsCl type of structure) is given in the  $\beta$ -field. The diagram presented by Owen *et al.* (1939) from the X-ray investigation of the system differs from that given in Metals Handbook in respect of the exact position of the phase boundaries, though the arrangement of the different phases is similar. They, however, could not get the  $\beta'$ -phase at the lower temperature as their samples, according to them, could not be brought to a satisfactory state of equilibrium by annealing within a reasonable time.

The earlier X-ray investigations of the alloys by Astrand and Westgren (1928) and Natta and Freri (1928) revealed only the  $\beta$  and  $\zeta$  phases. The only evidence of the  $\beta'$  phase from the X-ray study was given by Kosolapov and Trapeznikov (1936) who studied a single 51 atomic percent cadmium alloy in a high temperature camera and got the  $\beta'$  phase at 270°C and  $\zeta$  phase at 500°C. Later work (Owen *et al.*), however, proved that the temperatures recorded by them were incorrect. Thus at present there is no satisfactory confirmation of the boundaries of the  $\beta'$  phase by X-ray methods. In the present work an attempt has been made to determine the phase boundaries of the silver-cadmium alloys at temperatures below 300°C with particular attention to the  $\beta$ -field where the  $\beta'$  phase occurs. The  $\zeta$  to  $\beta'$  transformation was studied in detail by taking X-ray

\*Communicated by Prof. B. N. Srivastava.

powder diffraction photographs of the alloys in the high temperature camera and also by taking photographs of quenched specimens of the alloys.

#### EXPERIMENTAL PROCEDURE

X-rays are intensively used to study the equilibrium diagram of metallic systems and are extremely valuable for the identification of phases in alloys. They may be used for this purpose even when it is not possible to index the diffraction lines or to solve the crystal structure. There are two general ways of applying X-rays to study the equilibrium diagrams : (a) the lattice parameter method and (b) the method of vanishing lines.

(a) *The lattice parameter method :*

In general the lattice parameter of pure metals changes, either decreases or increases, with the addition of a second metal i.e. on alloying. If the system does not form a continuous range of solid solutions, a break will occur in the lattice parameter composition curve, from which the limit of solid solubility can be determined. In the same way the limit of other intermediate phases, if any, can be established. Thus by applying this lattice parameter method the interphase boundaries between two phases, when they occur due to the change in composition, can be determined at any temperature.

(b) *The method of vanishing lines :*

If a standard film of a particular phase has been obtained, a simple visual examination of X-ray films is often sufficient to establish the existence of that particular phase in a polyphase alloy. The boundaries of the phase fields are determined by a method of X-ray bracketing, in which, if the diffraction lines due to a phase are present on one film and absent in another, the boundary is drawn between the temperatures or compositions to which the two films refer. The sensitivity of this method, however, depends on the width of the two-phase region and also whether the phases give rise to strong diffraction lines which do not overlap. In a favourable case as little as 1% of a given phase can be determined visually on a Debye-Scherrer film.

#### PREPARATION OF ALLOYS

Small amounts of silver-cadmium alloys up to 68 per cent by weight of cadmium were prepared from spectroscopically pure metals obtained from Johnson Matthey & Co., London. Accurately weighed quantities of silver and cadmium in the form of turnings (cleaned and dried) were taken in pyrex tubes, evacuated and sealed under very low pressure of helium, and heated in an electric furnace. The mixture was first heated for an hour at 500°C, when cadmium melted and got absorbed in silver by diffusion thereby lowering the melting point of silver. The temperature of the furnace was then raised till the alloy melted, when it was made

homogeneous by shaking and quenched in water to prevent segregation and inhomogeneity which might occur during slow cooling.

The prepared alloys were weighed to ensure that no loss had occurred during heating. The alloys were again sealed in evacuated pyrex tubes and homogenized at 600°C for 24 hours and then examined for homogeneity by taking filings from different parts of the lump. From the homogeneous lumps, powdered samples were prepared and taken in small pyrex tubes, evacuated and sealed. The tubes were suspended by means of a fine copper wire in a vertical tube furnace and annealed at different temperatures. The tubes could be dropped into cold water placed just below the furnace by opening the bottom door and cutting the suspension. The method yielded very efficient quenching. Specimen for the high temperature camera was prepared by taking the powder in thin-walled pyrex capillaries.

#### APPARATUS

Philips precision cameras with 57.3 and 114.5 mm diameter were used to take the powder photograph of the quenched alloys. High temperature X-ray photographs were taken in Unicam 19 cm high temperature camera, which was calibrated by measuring the lattice spacing of pure silver up to 500°C.  $\text{CuK}_\alpha$  radiations from a sealed off Philips X-ray tube were used to obtain the diffraction photographs.

#### EXPERIMENTAL RESULTS

Powders of the silver-cadmium alloys situated within the range of composition from 47 to 58% by weight of cadmium were quenched from different temperatures and X-ray pictures were taken. A preliminary survey shows that this region contained a single body-centred cubic  $\beta'$  (ordered) phase below about 228°C bordered on either side by double phase regions. The alloy 47\* is in  $(\alpha + \beta')$  field below 228°C and in  $(\alpha + \zeta)$  above it (See Fig.1). Both the alloys 56.4 and 58 are mixtures of  $\beta'$  and  $\gamma$ , a complex body-centred cubic with 52 atoms per unit cell, below 220°C, above which they are in  $(\zeta + \gamma)$  region. All the four alloys included between 50.8 to 53% by weight of cadmium are in the  $\beta'$ -field below about 228°C, and in the  $\zeta$  phase above it. A second transformation from  $\zeta$  to  $\beta$  (body-centred cubic with same lattice parameter as that of  $\beta'$ ) was also observed with these alloys. Thus when 51.57 alloy was quenched from 450°C it yielded  $\beta$  phase. The  $\beta$  phase was also obtained with 51.3 alloy when an exposure was given at 440°C in the high temperature camera. According to Owen this transformation occurs at 427°C for the alloys with compositions from 43.7 to 50% by weight of cadmium, and 445°C for the alloys from 56 to 60% cadmium. No attempt has been made here to redetermine this transformation

\*Alloy 47 indicates an alloy with 47% by weight of cadmium.

temperature, but the observation on the two alloys mentioned above, confirmed their results.

(i) *The  $\alpha/(\alpha+\beta')$  and  $\alpha/(\alpha+\zeta)$  phase boundaries.*

Three  $\alpha$  phase alloys with 25.1, 30.1 and 34.7% by weight of cadmium were prepared. In order to get a relation between lattice parameter and composition in the  $\alpha$  phase, the lattice parameter of these alloys were measured. Powders of alloy 47 were annealed at 235°C for five days and quenched in water and X-ray powder photograph was taken. Sharp lines of  $\alpha$  and  $\zeta$  phases were obtained. The lattice parameter of  $\alpha$  phase was calculated from (511) lines and those of  $\zeta$  were obtained from (21 $\bar{3}$ 3), (30 $\bar{3}$ 2) and (0006) lines (the wave length used for CuK $\alpha$  radiations are CuK $\alpha_1$  = 1.54051 and K $\alpha_2$  = 1.54433 Å). The alloy was again quenched from 224°C after annealing for five days, which yielded  $\alpha$  and  $\beta'$  lines, from which the lattice parameters for  $\alpha$  and  $\beta'$  phases were calculated. The results are given in the Table I. The  $\alpha$  phase in the 47% alloy corresponds to 43.5 and 43.4% by weight of cadmium at 235 and 224°C respectively, as obtained by extrapolating the lattice parameter composition curve for  $\alpha$  phase alloys. These gave the limit of the  $\alpha$  phase. By narrowing the limits of annealing temperatures a temperature of 228°C $\pm$ 1 was obtained for this alloy at which  $\beta'$ - $\zeta$  transformation occurs.

TABLE I  
Lattice parameter of  $\alpha$ -phase alloys

Alloy composition in wt. % of Cd.	Lattice parameter at 30°C in Å	Quenching temperature °C
25.1	4.1400	—
30.1	4.1518	—
34.7	4.1635	—
47.0	4.1839	235
47.0	4.1837	224
47.0	4.1835	180

(ii) *The  $(\alpha+\zeta)/\zeta$  and  $(\alpha+\beta')/\beta'$  phase boundaries*

The four alloys included between 50.8 and 53% cadmium by weight are all in the  $\beta'$  field below the transformation temperature and in the  $\zeta$  phase above it. Alloy 51.3 was studied in the high temperature camera up to 440°C. The photograph taken at 440°C shows that the alloy again changed to body-centred cubic phase.

The  $\beta'$ - $\zeta$  transformation was studied in detail for the 51.3 alloy using the high temperature camera. For that purpose exposures in the high temperature camera were made at several temperatures between 220 to 240°C. A temperature hysteresis was observed in course of taking these photographs. Thus it has been observed that  $\beta'$  transforms to  $\zeta$  at about 225°C when photographs were taken at successive increasing temperatures i.e. when going from  $\beta'$  to  $\zeta$  field, and  $\zeta$  transforms to  $\beta'$  at about 220°C in the reverse process. But when the specimen was annealed in the camera for six hours before recording the pictures at every temperature, no such temperature hysteresis was observed. This revealed that  $\beta'$ - $\zeta$  transformation is not rapid and requires time to be completed. This phenomenon was also observed in the case of quenched alloys. An alloy, originally in the  $\zeta$  state, when annealed at 220°C for two hours and quenched, gave  $\zeta$  phase only, whose diffraction lines were not sharp but diffuse. This shows that the atoms of the  $\zeta$  phase have started moving and are slightly displaced from the normal positions still-keeping the hexagonal symmetry i.e. the lattice is strained. However, the results obtained with the high temperature camera are that the alloy 51.3 is in the  $\zeta$  phase at 230°C and in  $\beta'$  at 225°C. The mean value 227.5°C was accepted as the approximate transformation temperature for this alloy.

Powders of the 51.3 alloy were annealed at temperatures of 224°C, 227°C, 230°C and 234°C for five days and quenched in water and their diffraction photographs were taken. The results are that at 224°C the alloy is in the  $\beta'$  phase, at 227°C both  $\beta'$  and  $\zeta$  are present, and at 230 and 234°C there is only the  $\zeta$  phase. Hence 227°C was accepted as the transformation temperature.

The lattice parameter of the  $\beta'$  and  $\zeta$  phases corresponding to all the four alloys were determined. The variation of the lattice parameter of  $\beta'$  phase with composition was rather small. No variation in the 'c' parameter of the hexagonal  $\zeta$  phase was observed and only the 'a' parameter changed with composition. The lattice parameter of  $\beta'$  and  $\zeta$  phases as well as the annealing temperatures are included in the Table II.

TABLE II  
Lattice parameter of  $\beta'$  and  $\zeta$  phases

$\beta'$			$\zeta$				c/a
Composi- tion wt. % of Cd.	Annealing temp.°C.	Lattice paramo- ter in Å	Composi- tion wt. % of Cd.	Annealing temp. in °C	Paramo- ter 'c' in Å	Paramo- ter 'a' in Å	
47.0	224	3.3314	47.0	235	4.8236	2.9835	1.617
50.8	224	3.3315	50.8	234	4.8240	2.9835	1.617
51.3	224	3.3316	51.3	235	4.8238	2.9840	1.616
51.57	224	3.3318	51.57	235	4.8238	2.9843	1.616
53.0	216	3.3323	53.0	226	4.8239	2.9854	1.615
56.4	215	3.3325	56.4	224	4.8238	2.9860	1.615
58.0	210	3.3326	58.0	230	4.8234	2.9862	1.614

The transformation temperatures of all the other alloys were established by examining the quenched powders. The results are given in the Table III. Alloy 53 when annealed for 15 days at 220°C, the accepted transformation temperature for this alloy, yielded both  $\beta'$  and  $\zeta$  phases.

TABLE III

 $\beta'$ - $\zeta$  transformation temperatures

Composition of alloys; wt. % of cadmium	$\beta'$ - $\zeta$ transformation temperature °C.	Phases
47.0	228	$(\alpha + \beta') - (\alpha + \zeta)$
50.8	228	$\beta' - \zeta$
51.3	227	"
51.57	226	"
53.0	222	"
56.4	220	$(\beta' + \gamma) - (\zeta + \gamma)$
58.0	220	"

An approximate value of thermal expansion for the  $\beta'$  and  $\zeta$  phases were obtained from the high temperature photographs. For  $\beta'$  phase a value of  $24 \times 10^{-6} \text{ }^\circ\text{C}^{-1}$ , and for  $\zeta$  phase values of  $\alpha_c = 22 \times 10^{-6} \text{ }^\circ\text{C}^{-1}$  and  $\alpha_a = 36 \times 10^{-6} \text{ }^\circ\text{C}^{-1}$  corresponding to the  $c$  and  $a$  axes respectively were obtained. The axial ratio  $c/a$  for the  $\zeta$  phase changes from 1.617 to 1.614 with increasing cadmium concentrations. The value of  $c/a$  also decreases with increasing temperature.

The lattice parameter of  $\beta'$  and  $\zeta$  phases were plotted against composition, and by extrapolation it was observed that the  $\beta'$  and  $\zeta$  phases in 47% alloy correspond to 50.6 and 50.7% by weight of cadmium respectively. These gave the composition of the  $(\alpha + \zeta)/\zeta$  and  $(\alpha + \beta')/\beta'$  boundaries.

(iii) *The  $\zeta/(\zeta + \gamma)$  and  $\beta'/(\beta' + \gamma)$  phase boundaries*

The alloys 56.4 and 58% by weight of cadmium were studied by quenching method. A transformation temperature of  $220^\circ\text{C} \pm 1$  was obtained for both the alloys. The alloy 56.4 was also studied up to  $400^\circ\text{C}$  in the high temperature camera. The high temperature study of the alloy yielded  $219^\circ\text{C} \pm 1$  as the transformation temperature. The lattice parameters of the phases were calculated from the high angle lines. Lattice parameter of  $\gamma$  was  $9.9704 \text{ \AA}$  for both the alloys. By extrapolating the lattice parameter for  $\beta'$  and  $\zeta$  corresponding to these two alloys, the boundary between  $\beta'/(\beta' + \gamma)$  and  $\zeta/(\zeta + \gamma)$  was obtained. Alloys 47 and 56.4 were annealed for more than 15 days at  $180^\circ\text{C}$  and yielded an approximate boundary composition at that temperature. The results are included in the Table IV.

## DISCUSSION OF RESULTS

The presence of the  $\beta'$  phase, which was suspected by Durrant and others from thermal and microscopical studies of the silver-cadmium alloys, has been confirmed by our X-ray investigation of the system. The  $\beta'$  phase boundaries determined by us are found to differ considerably from those given in Metals Handbook, these latter being based on the microscopical work of Durrant. The boundaries of the  $\alpha$  and  $\zeta$  phases obtained in the present work agree with those found by Owen *et al.* The boundary compositions of the different phases, as obtained in course of the present work along with those obtained by Owen, are given in Table IV.  $\beta' - \zeta$  transformation temperatures of all the alloys examined are given in the Table III. These differ from those given in Metals Handbook by about 12°C.

TABLE IV  
Boundaries in the silver-cadmium system of alloys

Temp. °C.	Boundary composition (cadmium weight percent)							Author
	$\alpha/(\alpha+\beta')$	$(\alpha+\beta')/\beta'$	$\beta'/(\beta'+\gamma)$	$\alpha/(\alpha+\zeta)$	$(\alpha+\zeta)/\zeta$	$\zeta/(\zeta+\gamma)$	$(\zeta+\gamma)/\gamma$	
180	43.3	50.6	53.6					1
215		50.6	53.65					1
224	43.4			43.5	50.7			1
235				43.5	50.7	53.75		1
250				43.5	50.75	54.0		2
270					50.75	54.0		2
300				43.6			59.6	2
210							59.6*	2
180							59.6*	2

1 Present work.      2 Owen, Roger and Guthrie (1939).      \*Corresponds to  $(\beta'+\gamma)/\gamma$ .

With the help of these data the equilibrium diagram of the Ag-Cd system between the compositions of 40 to 60% by wt of cadmium and up to 300°C was constructed and is given in Fig. 1. The complete diagram of the system, shown in Fig. 2 was obtained by combining the results of Owen *et al.* with those of the present observations. This represents a complete diagram for the silver-cadmium system obtained from the X-ray study of the alloys in the solid state. However, the liquids and solids curves were not determined in the present investigation.

A duplex ( $\beta'+\zeta$ ) phase region is also included in the diagram, based on the observations on three alloys as mentioned earlier. It has not been possible to determine the extent of this duplex region precisely, but observations show that



it is confined within  $\pm 2^\circ\text{C}$  of the corresponding ( $\beta'$ - $\zeta$ ) transformation temperature. The general arrangement of the phase fields is similar to that in the silver

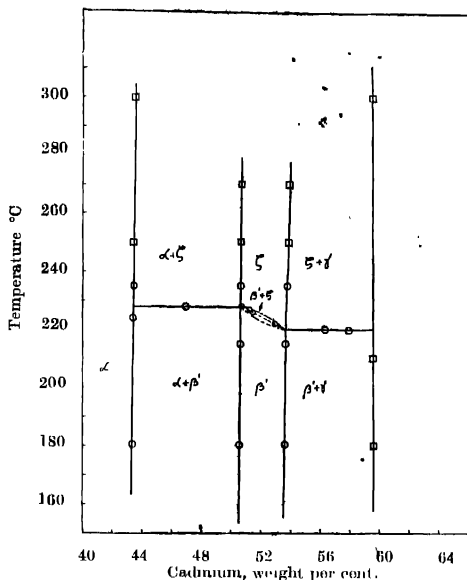


Fig. 1. Boundaries of the  $\beta'$ -phase in the Ag-Cd system

zinc system except that in the case of Ag-Zn there is only one ( $\beta$ - $\zeta$ ) transformation at about  $260^\circ\text{C}$ , whereas in Ag-Cd system there are two transformations in the  $\beta$ -field.

The structures of the different phases in the diagram are:  $\alpha$  phase, face-centred cubic,  $\beta$  phase, body-centred cubic;  $\beta'$  phase, ordered body-centred cubic with CsCl type of structure;  $\gamma$  phase, complex body-centred cubic with 52 atoms to the unit cell; and  $\zeta$ ,  $\delta$  and  $\epsilon$  phases are close-packed hexagonal. It is not possible to get evidence of long range order in  $\beta'$  phase from x-ray investigations in this case as the super-lattice lines cannot be recorded on account of the nearly equal scattering powers of silver and cadmium atoms. However, there is evidence from nuclear magnetic resonance experiments (Drain, 1959) that the silver and cadmium atoms strongly attract each other which shows that unlike atom pairs will be favoured in this alloy. It may be concluded that the  $\beta$  to  $\zeta$  and again  $\zeta$  to  $\beta'$  transformations are probably controlled by the order parameters and energy considerations.

The alloy 68% by weight of cadmium, which is in the  $\delta$  phase field, was studied. The lattice parameters of the  $\delta$  phase are:  $a = 3.037 \text{ \AA}$ ,  $c = 4.824 \text{ \AA}$  and  $c/a = 1.588$ .

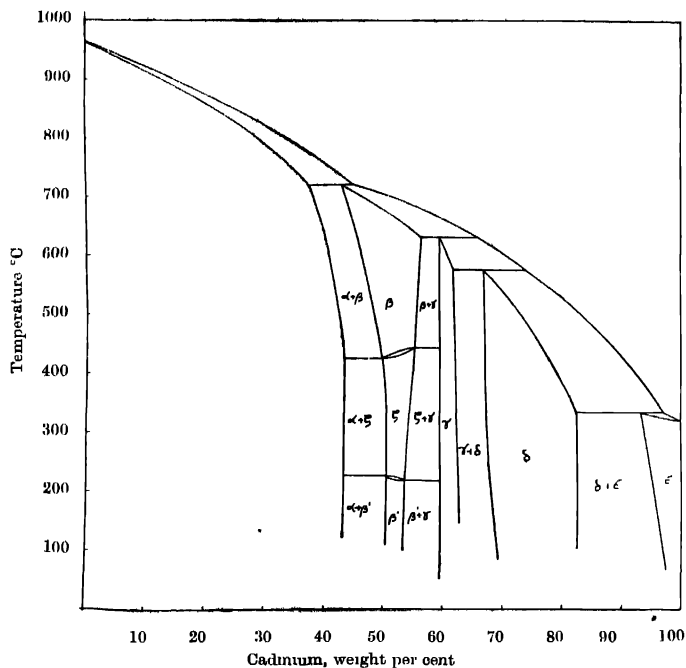


Fig. 2. Equilibrium Diagram of silver-cadmium alloys based on the work of Owen *et al.*, and the present investigations.

The formation of the intermediate phases  $\beta$ ,  $\zeta$  and  $\gamma$  can be explained by the Hume-Rothery rule for electron compounds. Assuming that the electrons are nearly free and the Fermi energy is the most significant factor determining the stability of these phases, Jones (1934, 1937) has given a theoretical explanation of the Hume-Rothery rule from the zone theory of metals. According to this rule the  $\alpha$  phase having f.c.c. structure should become unstable at the electron concentration 1.4 while from the equilibrium diagram (Fig. 1) of Ag-Cd alloys it comes out to be 1.425. Similarly, for the  $(\alpha + \beta')/\beta'$  boundary the Hume-Rothery rule gives 1.5 as against 1.496 found here. For the  $\beta'/( \beta' + \gamma)$  and  $(\beta' + \gamma)/\gamma$  boundaries we find the electron concentrations 1.528 and 1.586 as against 1.5 and 1.6 from the Hume-Rothery rule.

#### ACKNOWLEDGMENT

The author is indebted to Prof. B. N. Srivastava, D.Sc., F.N.I., for suggesting the problem and for his valuable guidance throughout the progress of the work.

REFERENCES

- Astrand, H. and Westegren, A., 1928, *Z. anorg allgen chem.*, **175**, 90.  
Drain, L. E., 1959, *Phil. Mag.*, **4**, 484.  
Durrant, P. J., 1931, *J. Inst. Metals.*, **45**, 99.  
Durrant, P. J., 1935, *J. Inst. Metals*, **56**, 155.  
Jones, J., 1934, *Proc. Roy. Soc.*, **144**, 225.  
Jones, H., 1937, *Proc. Phys. Soc.*, **49** 250.  
Kosolapov, G. F., and Trapeznikov, A. K., 1936, *J. Tech. Phys. (USSR)*, **6**, 1131.  
*Metals Handbooks*, 1948, American Society for Metals.  
Natta, G., and Freri, M., 1928, *Atti accad Lincei.*, **7**, 422.  
Owen, E. A., Roger, J. and Guthrie, J. C., 1939, *J. Inst. Metals.*, **65**, 457.

# IONIZATION OF E-LAYER BY X-RAYS

S. N. GHOSH AND SHARDA NAND

J. K. INSTITUTE OF APPLIED PHYSICS, UNIVERSITY OF ALLAHABAD, ALLAHABAD

(Received, August 16, 1960)

**ABSTRACT.** In this paper, the transmission curves for solar radiations in the X-ray and ultraviolet regions through the earth's atmosphere, obtained from rocket data and absorption coefficients have been utilized for determining the radiation responsible for E-layer ionization. It is found that only X-rays between the wavelength region 5 to 100Å are absorbed in the region of the atmosphere occupied by E-layer. The amount of energy absorbed is  $0.19 \text{ erg cm}^{-2} \text{ sec}^{-1}$ . The number of ions produced by (1) absorbed X-rays, (2) ejected photoelectrons produced by X-rays, and (3) Auger Effect induced by X-rays has been calculated and found to be  $4 \times 10^8$ ,  $5.6 \times 10^9$ , and  $2.5 \times 10^8 \text{ cm}^{-2} \text{ sec}^{-1} \text{ column}^{-1}$  respectively or the total rate of production of ions in the E-layer is  $6.2 \times 10^8 \text{ cm}^{-2} \text{ sec}^{-1} \text{ column}^{-1}$ . Remembering the error in the measurements of energy from a rocket, this value agrees with that obtained from substituting the value of effective recombination coefficient and electron density for E-layer in the expression  $q = \alpha N_e^2$ .

The temperature of the sun corresponding to different wavelength regions are calculated from data obtained from rocket-borne experiments. The calculated values agree with those given by Nicolet.

## 1. INTRODUCTION

E. O. Hulburt (1938) was the first to propose that soft X-rays may produce the E-region. Bates and Hoyle (1948) supported Hulburt's proposal. In considering auroral phenomena, Vegard (1923, 1938) also suggested that soft X-rays are a major contributor to the ionization at high altitudes. Also, from solar energy measurements by rocket-borne experiments, it appears that ionization of the E-layer is due to soft X-ray emissions from solar corona. Recently, Friedman (1959) suggested that E-region is produced by X-rays and Lyman- $\beta$  (1025Å), and D-region by Lyman- $\alpha$  (1216Å).

In this paper, the total amount of solar X-ray energy absorbed within the E-layer is calculated from the energy at the top of the earth's atmosphere obtained from rocket-borne experiments and the transmission curves for these radiations through the atmosphere. The rate of ionization produced by absorbed energy is then calculated and compared with other available value.

The temperatures of the sun at different spectral regions in the ultraviolet and X-rays are also calculated from the amounts of solar energy at the top of the earth's atmosphere, obtained from rocket-borne experiments.

## 2. TRANSMISSION CURVES FOR X-RAYS AND ULTRA-VIOLET RADIATIONS

Fig. 1 shows the transmission of different wave-lengths through the earth's atmosphere. The solid curves (Friedman, 1959) represent the penetration of solar radiations into the atmosphere for vertical incidence obtained from rocket-borne experiments. The dot-dash curves (Byrau *et al.*, 1954) show the penetration of certain radiations computed from absorption coefficients given by Compton and Allison (1953). Dotted line curves (Friedman *et al.*, 1951) represent the transmission of solar radiations observed from V-2 49 rocket using photon counters.

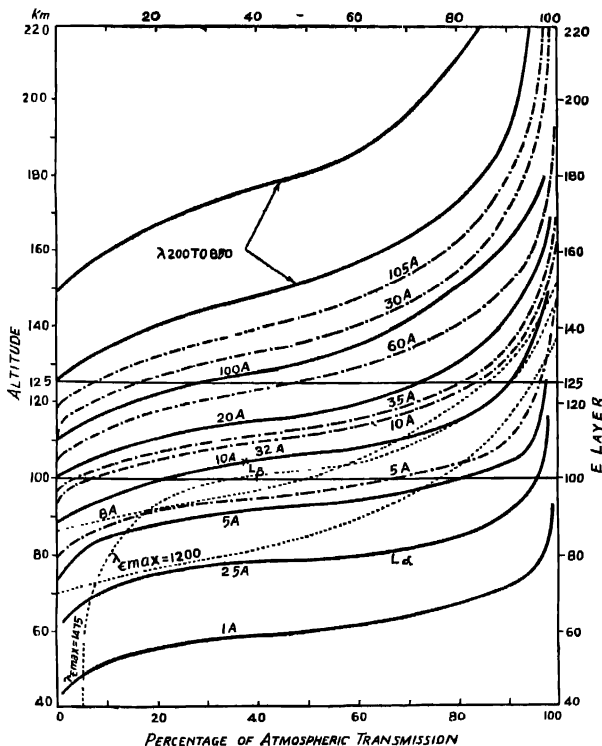


Fig. 1. Atmospheric transmission for different wavelengths in the X-ray and ultraviolet regions. The solid curves (Friedman, 1959) are obtained from rocket-borne experiments. Dotted line curves (Friedman, 1951) are also obtained using photon counters in V-2 49 rocket. Dot-dash curves are computed from absorption coefficients given by Compton and Allison.

It will be seen from above curves that, in general, radiations penetrate deeper into the atmosphere as the wavelength decreases. There are, however, certain departures. Wavelengths 1475Å, Lyman- $\alpha$ , 1200Å and Lyman- $\beta$  penetrate much deeper into the earth's atmosphere. In the dot-dash curves, wavelength 30 Å penetrated to a lesser depth compared to wavelengths 35Å, 60Å and 100Å. Also, it may be noted that Lyman- $\alpha$ , and 2.5Å, and wavelengths 10Å and 32Å have the same penetrating characteristics.

From the nature of these transmission curves, one can easily conclude that different amounts of energy corresponding to different wavelengths are absorbed at different altitudes of the atmosphere. Wavelengths from 200 Å to 850 Å are absorbed above 125Km, whereas those between 5Å and 100Å are absorbed in the region 90-125 Km. The Lyman- $\alpha$  radiation (Byram *et al.*, 1953) penetrates upto  $74 \pm 2$  Km. Also, Lyman- $\beta$  is absorbed between altitudes 90 and 125 Km. Wavelength 2.5Å penetrates below 70 Km and 1Å well below 60 Km.

From rocket data, 50 per cent transmission of energy at different wavelengths in the X-ray region is calculated and is shown in Fig. 2. The values given by Leo Goldberg (1954) for 50 per cent transmission of energy for higher wavelengths are also given in the same figure.

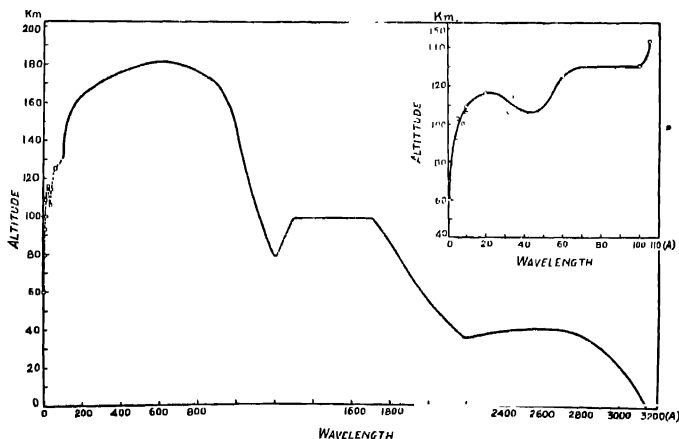


Fig. 2. Altitudes for 50 per cent transmission of solar energy in the X-ray region. Solid line curve is drawn by Leo Goldberg and the dashed curve (shown in a magnified scale on the right side) is obtained from the present work.

### 3. ABSORPTION OF X-RAYS IN E-LAYER

The results of measurements of electron density as obtained from different rocket flights at White Sands Proving Ground, New Mexico, are given in Table 1.

These measurements show that the height of the maximum ionization of the *E*-layer lies between 100 and 110 Km. It has also been observed that under normal conditions of the sun there is not much variation in electron density up to 125 Km, although during solar activity there is considerable variation. Therefore, for calculating the number of ion  $\text{cm}^{-2} \text{sec}^{-1} \text{column}^{-1}$ , the *E*-layer may be assumed to lie between 100 and 125 Km.

TABLE I

*E*-layer ionization from rocket data at white sands proving ground,  
New Mexico

Rocket flight, date and time	Authors	Altitude of maximum ionization Km	Remarks
May 7, 1947; 11-25 hrs. MST		About 110	Rapid increase in electron density from 85 Km to 110 Km; no measurement was made above 110 Km.
Jan. 22, 1948; 13-14 hrs. MST		100	Electron density increases from 92 Km to 100 Km. No data available above 100 Km.
V-2 No. 49, Sept. 29, 1949; 10-00 hrs. MST		107	Peak electron density at 107 Km. Between 110 and 125 Km, there is not much variation in electron density.
Viking No. 5, Nov. 21, 1950; 10.18 hrs. MST		110	Electron density gradient becomes steep from about 92 Km. Peak electron density is observed at 110 Km. There is not much variation in electron density between 110 and 125 Km.
Viking No. 10, May 7, 1954; 10-00 hrs. MST	<i>b</i>	Peaks at 101, 112 and 129	Measurements show a rapid increase in electron density at 91 and 101 Km.
Aerobee-38, June 26, 1953; 12.10 hrs. MST	<i>c</i>		A sharp maxima at 110 Km.
Aerobee-HI NRL-50, June 29, 1956; 12-09 hrs. MST	<i>d</i>	Sharp maxima at 101	Electron density increases from 92 to 160 Km. Between 100 and 125 Km, the electron density is practically constant.

*a*—Jackson, 1954 & Seddon, 1954; *b*—Seddon *et al.*, 1954; & Jackson, 1956; *c*—Pfister *et al.*, 1958; *d*—Jackson *et al.*, 1958.

Solar energy values at the top of the earth's atmosphere for different wavelengths were obtained from rocket flights and are shown in Section 5 (Table 4). The percentage of absorption of these radiations in the *E*-layer was calculated from Fig. 1. Assuming the *E*-layer to lie between altitudes 100-125 Km, the energy absorbed in this layer corresponding to different wavelengths is then calculated and is given in Table II. A graph is drawn between the absorbed energy and wavelengths and is shown in Fig. 3. The integrated area gives the total

amount of X-ray energy absorbed in the *E*-region. Its value is estimated to be  $0.19 \text{ erg cm}^{-2} \text{ sec}^{-1}$ . [The Lyman- $\beta$  ( $\lambda 1025$ ) radiation is also absorbed between

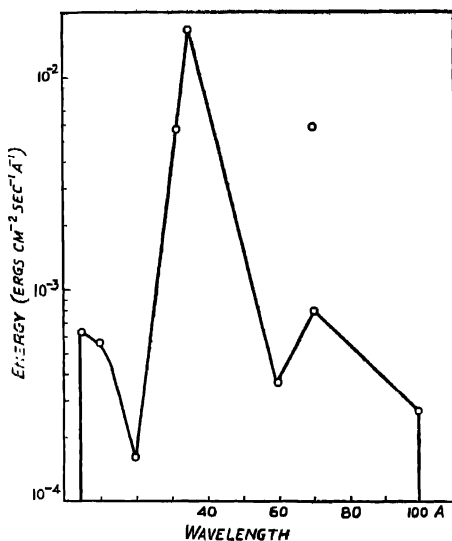


Fig. 3. The solar energy in the X-ray region absorbed in the *E*-layer as calculated from Fig. 1. The *E*-layer is assumed to lie between altitudes 100 and 125 Km. Corresponding to  $70 \text{ Å}$  two energy values,  $2 \times 10^{-3}$  and  $1.5 \times 10^{-2} \text{ ergs cm}^{-2} \text{ sec}^{-1} \text{ Å}^{-1}$  were obtained by Friedman (1959). In the present calculations only the lower value is taken.

the altitudes 100-125 Km. However, it does not produce *E*-layer ionization because it requires radiations of wavelength less than  $1019 \text{ Å}$ ].

TABLE II

Solar energy in the X-ray region absorbed between altitudes 100 and 125 Km

Wavelength (Å)	Percentage of energy absorbed	Energy absorbed ( $\text{erg cm}^{-2} \text{ sec}^{-1} \text{ Å}^{-1}$ )
5	25	$6.25 \times 10^{-4}$
10	75	$5.63 \times 10^{-4}$
20	75	$1.62 \times 10^{-4}$
32	70	$5.81 \times 10^{-3}$
35	85	$1.70 \times 10^{-2}$
60	50	$3.75 \times 10^{-4}$
70	40	$8.00 \times 10^{-4}$
100	30	$2.70 \times 10^{-4}$



#### 4. IONIZATION IN E-LAYER BY X-RAYS

Assuming that X-rays absorbed in the E-layer are responsible for its ionization, the number of ions produced in this layer has been calculated as follows :

The amount of energy absorbed in the E-layer in an interval of 5Å has been obtained from Fig. 3. The mean photon energy in the interval is then calculated. Dividing the former by the latter gives the number of photons. Knowing the number of photons in the interval of 5Å, the rate of production of ions\* in the E-layer by X-rays emitted by the sun has been calculated.

The rate of production of  $O^+$  ions,  $q(O^+)$ , will depend upon the product of absorption coefficient,  $\alpha_o$ , of O atoms corresponding to frequency  $\nu$  and its concentration,  $n(O)$ . Therefore,

$$q(O^+) \propto \alpha_o n(O). \quad \dots (1)$$

Similarly, in the case of nitrogen atoms

$$q(N^+) \propto \alpha_N n(N). \quad \dots (2)$$

Therefore,

$$\frac{q(N^+)}{q(O^+)} = \frac{\alpha_N n(N)}{\alpha_o n(O)} \quad \dots (3)$$

$$\text{or,} \quad q(O^+) = \frac{\alpha_o n(O)[q(O^+) + q(N^+)]}{\alpha_o n(O) + \alpha_N n(N)} \quad \dots (4)$$

Substituting  $A$  for  $[q(O^+) + q(N^+)]$  which is the total rate of production of ions in the E-layer or the number of photons absorbed, the Eqn. (4) becomes

$$q(O^+) = \frac{\alpha_o n(O)}{\alpha_o n(O) + \alpha_N n(N)} \times A.$$

$$\text{Similarly,} \quad q(N^+) = \frac{\alpha_N n(N)}{\alpha_o n(O) + \alpha_N n(N)} \times A.$$

The absorption coefficients of atomic oxygen and nitrogen have been taken after Compton and Allison (1953) and the particle concentration after Nicolet (1959). The ejected photoelectrons are loaded with excess energy and cause valence ionization of other atoms. Also, from Auger Effect for K-L shell transition for O and N atoms there exists 50 per cent probability of electron ejection and

\* The photons corresponding to wavelengths  $\leq 23.58 \text{ \AA}$  and  $31.18 \text{ \AA}$ , eject K electrons from oxygen and nitrogen atoms respectively, while those corresponding to wavelengths greater than the above values eject L electrons.

50 per cent for X-ray emission. The rates of ion production by the above processes are given in Table III.

TABLE III

Ion production due to X-rays in the *E*-layer by different processes

	K-shell ionization	L-shell ionization	Valence shell ionization	Ionization by Auger Effect	
	( $\text{cm}^{-2}\text{s}^{-1}\text{col}^{-1}$ )	( $\text{cm}^{-2}\text{s}^{-1}\text{col}^{-1}$ )	( $\text{cm}^{-2}\text{s}^{-1}\text{col}^{-1}$ )	Direct electron ejection ( $\text{cm}^{-2}\text{s}^{-1}\text{col}^{-1}$ )	From X-ray emission ( $\text{cm}^{-2}\text{s}^{-1}\text{col}^{-1}$ )
Oxygen	$2.5 \times 10^6$	$1.6 \times 10^8$	$2.2 \times 10^9$	$1.2 \times 10^6$	$2.4 \times 10^7$
Nitrogen	$1.8 \times 10^7$	$2.2 \times 10^8$	$3.4 \times 10^9$	$8.8 \times 10^6$	$2.2 \times 10^8$
Total	$2.0 \times 10^7$	$3.8 \times 10^8$	$5.6 \times 10^9$	$1.0 \times 10^7$	$2.4 \times 10^8$

Therefore, the average rate of ion production in the *E*-layer is  $6.2 \times 10^9 \text{ cm}^{-2} \text{ sec}^{-1} \text{ column}^{-1}$ .

Another value for the rate of production of ions can be obtained by substituting the values of  $\alpha$  and  $Ne$  in the expression for the rate of production of ions at equilibrium condition, namely,

$$q = \alpha Ne^2 \quad \dots (5)$$

where,

$q$ —rate of ion production,

$\alpha$ —effective recombination coefficient,

and  $Ne$ —ionization density.

The value of  $\alpha$  as given by different investigators (Appleton, 1959; Landmark, 1956) ranges from  $1 \times 10^{-8}$  to  $4 \times 10^{-8} \text{ cm}^3 \text{ sec}^{-1}$ . The calculated value of the rate of total ion production due to X-rays agrees with the value obtained from the expression (5) if  $\alpha = 6 \times 10^{-8} \text{ cm}^3 \text{ sec}^{-1}$  and  $Ne = 2 \times 10^5 \text{ cm}^{-3}$ . It may, however, be noted that the transmission curves (Fig. 1) were plotted from the data obtained from rocket-borne experiments by using photon counters and thermoluminescent phosphor technique. These data are liable to be in error. The measurements with photographs and ion chambers give more accurate values for the energy (Friedman, 1959; Jager, 1959).

#### 5. TEMPERATURE OF SUN IN X-RAY AND ULTRA-VIOLET REGIONS

We have already seen in Section 3 that the energy values at the top of earth's atmosphere corresponding to different wavelengths from ultraviolet to X-rays are obtained from rocket-borne experiments. From these energy values and considering the sun as a black body radiator, the coronal temperatures corres-

ponding to the emission of X-rays and ultraviolet radiations have been computed following the method of Nicolet (1952) as follows.

If  $\rho(\nu)$  be the density of radiation emitted by the sun, then from Planck's formula

$$\rho(\nu) = \frac{8\pi h \nu^3}{C^3} (e^{h\nu/kT} - 1)^{-1},$$

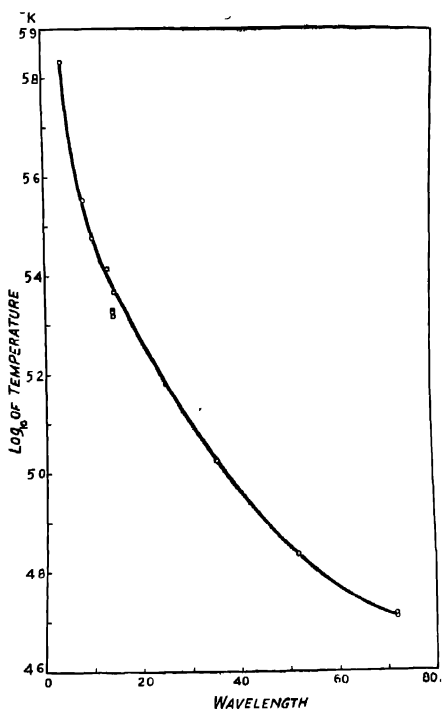


Fig. 4. Variation of temperature of the sun with wavelength in the X-ray region obtained from rocket data.

where the symbols have their usual significance. The radiation density  $\rho'(\nu)$  at the top of the atmosphere is given by the relation

$$\rho'(\nu) = \beta_s \cdot \rho(\nu),$$

TABLE IV

Equivalent black body temperatures of the sun obtained from rocket-borne experiments in the X-ray and ultraviolet regions

Wavelength region (Å)	Author	Condition of the sun	Energy (ergs cm <sup>-2</sup> sec <sup>-1</sup> )	Equivalent black body temperature (°K)
Below 8	a	late in class I flare	$5 \times 10^{-3}$	$6.8 \times 10^5$
6—10	b	160 minutes after class I flare	$10^{-4} - 10^{-3}$	$3.5 \times 10^5$
8—12	c	quiet	$3 \times 10^{-3}$	$3.0 \times 10^5$
8—18	d	high coronal activity	0.6	$2.6 \times 10^5$
8—20	c	-do-	0.1	$2.3 \times 10^5$
8—20	a	quiet	$1.5 \times 10^{-3}$	$2.1 \times 10^5$
8—20	a	-do-	$1.3 \times 10^{-3}$	$2.1 \times 10^5$
8—20	a	-do-	$1.2 \times 10^{-4}$	$2.1 \times 10^5$
8—20	a	-do-	$0.4 \times 10^{-3}$	$2.1 \times 10^5$
10—60	d		1.0	$1.1 \times 10^5$
44—60	e	minimum solar activity	$1.4 \times 10^{-2}$	$6.8 \times 10^4$
44—100	e	-do-	$3.5 \times 10^{-2}$	$5.2 \times 10^4$
44—100	e	-do-	$2.9 \times 10^{-2}$	$5.2 \times 10^4$
1050—1240	f	normal	0.4	5330
1200	b	-do-	$6.2 \times 10^{-2}$	(6000)*
1216	g	no unusual solar activity	6.3	7730
1150—1340	b	-do-	1—10	5630
1230—1340	b	-do-	0.2	4840
1500	b	-do-	$5.4 \times 10^{-3}$	(4500)*
2050	h	-do-	3.7	(5000)*

a—Chubb *et al.*, 1957; b—Friedman *et al.*, 1951

c—Burnight, 1952; d—Byram *et al.*, 1954;

e—Byram *et al.*, 1956; f—Tousey *et al.*, 1951.

g—Jager, 1959 & h—Byram *et al.*, 1952.

For figures marked with \* the amounts of energy have been calculated from the given temperatures.

where the dilution coefficient  $\beta_s$  is given by

$$\begin{aligned}\beta_s &= \frac{R^2}{4r^2} = \frac{(\text{sun radius})^2}{4(\text{sun-earth distance})^2} \\ &= 5.41 \times 10^{-6}.\end{aligned}$$

The temperatures thus calculated are given in Table 4. Comparing these values with the equivalent black body temperatures calculated by Nicolet (1952) from the coronal radiation of the quiet sun given in Table V, we find that there is a fair agreement between the two sets of values. The variation of temperature with wavelengths in the X-ray region is shown in Fig. 4. It may, however, be pointed out that the emission from the sun may be of grey body type (Byram *et al.*, 1956). If such be the case, the actual temperature will be higher than those given in Table IV.

TABLE V

Equivalent black body temperatures of quiet sun in the X-ray and ultraviolet regions obtained by Nicolet

Wavelength (Å)	Equivalent black body temperature (°K)
4	$5.0 \times 10^5$
10	$3.0 \times 10^5$
14	$2.0 \times 10^5$
20	$1.6 \times 10^5$
21.5	$1.5 \times 10^5$
29.6	$1.2 \times 10^5$
50	$7.5 \times 10^4$
75	$5.0 \times 10^4$
200	$2.0 \times 10^4$
228	$1.9 \times 10^4$
250	$1.8 \times 10^4$
500	$7.0 \times 10^3$
910	$5.0 \times 10^3$
1000	$5.0 \times 10^3$

## REFERENCES

- Appleton, E. V., 1959, *Proc. I.R.E.*, **47**, 155.
- Burnight, T. R., 1952, *Physics and Medicine of the Upper Atmosphere*, pp. 233, University of New Mexico Press.
- Byram, E. T., Chubb, T., Friedman, H., and Lichtman, S. W., 1952, *J. Opt. Soc. Amer.*, **42**, 876.
- Byram, E. T., Chubb, T., Friedman, H. and Gailar, N., 1953, *Phys. Rev.*, **91**, 1278.
- Byram, E. T., Chubb, T. and Friedman, H., 1954, *Solar X-rays and E-layer Ionization, Rocket Exploration of the Upper Atmosphere*, pp. 274, Pergamon Press Ltd., London.
- Byram, E. T., Chubb, T. A. and Friedman, H., 1956, *J. Geophys. Res.*, **61**, 251.
- Chubb, T. A., Friedman, H., Kroplin, R. W. and Kupperian, J. E. Jr., 1957, *J. Geophys. Res.*, **62**, 389.
- Compton, A. H. and Allison, S. K., 1953, *X-rays in Theory and Experiment*, Macmillan and Co.
- Friedman, H., Lichtman, S. W. and Byram, E. T., 1951, *Phys. Rev.*, **83**, 1025.
- Friedman, H., 1959, *Rocket Observations of the Ionosphere*, *Proc. I.R.E.*, **47**, 272.
- Goldberg, L., 1954, *The Absorption Spectrum of the Atmosphere. The Earth as a Planet*, Edited by G. P. Kuiper, pp. 434. The University of Chicago Press, Chicago, Illinois.
- Hoyle, F. and Bates, D. R., 1948, *Terr. Mag.*, **53**, 51.
- Hulburt, E. O., 1938, *Phys. Rev.*, **53**, 344.
- Jackson, J. E., 1954, *J. Geophys. Res.*, **59**, 377.
- Jackson, J. E., 1956, *J. Geophys. Res.*, **61**, 107.
- Jackson, J. E. and Seddon, J. C., 1958, *J. Geophys. Res.*, **63**, 197.
- Jager, C. D., 1959, *Handbuch Der Physik*, Published by Springer-Verlag, Berlin. Göttingen, Heidelberg.
- Landmar, B., 1956, *Solar Eclipses and the Ionosphere*, Pergamon Press, London.
- Nicolet, M., 1952, *Annales de Geophysique*, Tome 8, fascicule 2, 141.
- Nicolet, M., 1952, *Physics and Medicine of the Upper Atmosphere*, pp. 201, University of New Mexico Press.
- Nicolet, M., 1959, *La Thermosphere*, *Annales de Geophysique*, Tome 15, N° 1, 1-21.
- Pfister, W. and Ulwick, J. C., 1958, *J. Geophys. Res.*, **63**, 315.
- Seddon, J. C., 1954, *J. Geophys. Res.*, **59**, 463.
- Seddon, J. C., Pickar, A. D. and Jackson, J. E., 1954, *J. Geophys. Res.*, **59**, 513.
- Tousey, R., Watanabe, K. and Purcell, J. D., 1951, *Phys. Rev.*, **83**, 792.
- Vagard, L., 1923, *Skr. Vid. Selsk.*, I, Nos. 8, 9 and 10.
- Vogard, L., 1938, *Geofys. Publ.*, **12**, 23, 2pls.

## ANALYSIS OF RANDOM FADING RECORDS

S. R. KHASTGIR

CALCUTTA UNIVERSITY

AND

R. N. SINGH

BANARAS HINDU UNIVERSITY

(Received, September 3, 1960)

**ABSTRACT.** The analysis of the three-spaced-receiver fading records taken at Banaras from November, 1956 to March, 1958, with vertically-directed pulse transmission on 3.8 Mc/s has yielded the following results :

(i) The ratio of the drift velocity  $v_\omega$  to the r.m.s. line-of-sight velocity  $v_0$  of the ionospheric irregularities is not found to be constant, as is expected from theory. The ratio increases with the increasing drift velocity.

(ii) The ratio of the drift velocity  $v_\omega$  to the product of the frequency of fading  $N$  and the wavelength  $\lambda$  is not found to be constant, as is expected from theory. The ratio decreases with the increasing drift velocity.

(iii) The angle of spread of the scattered components from the ionospheric irregularities obtained from  $\theta_0 = \sin^{-1} (N \cdot \lambda / 2v_\omega)$  is found to increase with the increasing drift velocity.

## THEORETICAL CONSIDERATIONS

Ratcliffe (1948) developed a theory of the randomly fading radio waves. According to the theory, the irregularities in the ionosphere are the scattering centres which may be regarded as gas molecules under thermal agitation. The distribution of velocity (in one dimension) can then be expressed as:

$$P(v) = A \cdot \exp \left( - \frac{v^2}{v_0^2} \right) \quad \dots (1)$$

where  $\int_{-\infty}^{\infty} P(v)dv = 1$  and  $v_0$  is the r.m.s. line-of sight velocity of the irregular scattering centres.

The frequency of the scattered components suffers a Doppler shift of frequency due to the line-of-sight velocity of the scattering centres. Considering the frequency-shift,  $f-f_0$ , the power-spectrum is given by

$$W(f) = B \cdot \exp \left[ - \frac{\lambda^2 (f-f_0)^2}{8v_0^2} \right] \quad \dots (2)$$

where  $\lambda$  is the wavelength of the wave.

The auto-correlation function of the fading pattern may be written as

$$P_R(\tau) = \frac{\overline{R(t) \cdot R(t+\tau)} - [\overline{R(t)}]^2}{[\overline{R(t)}]^2 - [\overline{R(t)}]^2} \quad \dots (3)$$

where  $R(t)$  and  $R(t+\tau)$  are the amplitudes of the fading signals at instants  $t$  and  $t+\tau$ . Since the auto-correlation function is proportional to the Fourier transform of the distribution of power in the power spectrum, it can be shown

$$P_R(\tau) = C. \exp. \left[ -\frac{16\pi^2 v_0^2 \tau^2}{\lambda^2} \right] \quad \dots (4)$$

The theory can be tested by finding whether the auto-correlation function of the fading pattern obeys this law, and if it does, the magnitude of  $v_0$  can be obtained from the value of  $\tau$ , where  $P_R(\tau)$  falls to  $e^{-1}$  in the auto-correlogram. Thus

$$v_0 = \frac{\lambda}{4\pi\tau} \quad \dots (5)$$

If the spatial auto-correlation of the fading pattern is plotted as a function of distance in one direction from a fixed origin, it is possible that it would fall in a smooth manner. Ratcliffe and Pawsey (1933), Pawsey (1935) had shown that the spatial auto-correlation function falls to about 0.8 in a distance of one wavelength. If now the irregular ionosphere producing this pattern were to move with a velocity  $v_\omega$ , the diffraction produced on the ground would move with velocity  $2v_\omega$ . Therefore the spatial auto-correlation function would fall to about 0.8 in time  $\lambda/2v_\omega$ .

If now we assume the space and time auto-correlation to be similar (say, Gaussian), then the space auto-correlation function will fall to  $e^{-1}$  in time

$$\tau = \frac{0.8\lambda}{2v_\omega \cdot e^{-1}} = \frac{2.2\lambda}{2v_\omega} \quad \dots (6)$$

Then comparing the relations (5) and (6) we obtain

$$v_0 = \frac{v_\omega}{4.4\pi}$$

or

$$v_\omega / v_0 \approx 14 \quad \dots (7)$$

McNicol (1949) developed a quick method of determining the r.m.s. line-of-sight velocity  $v_0$  by counting the number of maxima  $N$  of the fading pattern per sec. The approximate relation was given by

$$v_0 = \frac{N \cdot \lambda}{5} \quad \dots (8)$$



Considering (7) and (8) we have

$$v_{\omega} = 14v_0 = 14 \frac{N\lambda}{5} = 2.8N\lambda \quad \dots (9)$$

Further Briggs (1951) assuming that the horizontal movement of the reflecting layer to be the main cause of fading deduced the relation :

$$N = \frac{2v_{\omega}}{\lambda} \sin \theta_0 \quad \dots (10)$$

where  $\theta_0$  is the semi-angle of the cone of the down-coming waves. It will be noticed that this relation is the same as the relation (9) given by McNicol except for the constants.

#### RESULTS OF THE ANALYSIS OF THE FADING RECORDS

A number of three-spaced-receiver fading records taken at Banaras from November 1956 to March 1958 with vertically-directed pulse-transmission on 3.8 Mc/s has been analysed. The cross-correlation method has given the drift velocity. The same sets of records have been used to find the r.m.s. line-of-sight velocity  $v_0$  of the irregularities in the ionosphere by finding the time at which the auto-correlation function falls to a value  $e^{-1}$  and using relation (5). Table I shows the results of the analysis. The various values of the drift velocities have been arranged in groups of 0-10, 10-20, 20-30 metres/sec. and the averages of these have been estimated.

TABLE I  
Frequency 3.8 Mc/Sec.

Drift velocity $v_{\omega}$ metres/sec.	r.m.s. line-of-sight velocity of the ionospheric irregularities $v_0$ metres/sec.	$v_{\omega}/v_0$
12	1.23	9.75
26	2.46	10.60
37	2.70	13.70
48	3.20	15.00
56	3.40	16.40
67	3.50	19.00
78	4.10	19.00
86	4.60	18.60
	mean	15.25

It is evident from the data given in Table I that the ratio of the drift velocity  $v_{\omega}$  to the r.m.s. line-of-sight velocity  $v_0$  of the ionospheric irregularities varies with

the magnitude of the drift velocity, the ratio being smaller for the lower values of the drift velocity and larger for the higher values. Clearly the results show a departure from the theoretical relation (7).

The relation between the drift velocity  $v_w$  and the frequency of fading  $N$  has also been found by analysing the random fading records. In Table II are given the values of the frequency of fading  $N$  and of the ratio of the drift velocity  $v_w$  to  $N\lambda$  for the different groups of the drift velocity. It is clear that the ratio  $v_w/N\lambda$  decreases with the increase of the drift velocity. This variation is a departure from the theoretical relation (9). Using the relations (9) and (10), the angles of spread of the scattered components from the ionospheric irregularities for the various values of the drift velocity have been calculated. The calculated values of the spread angle are also entered in Table II. It is interesting to note that the spread angle increases with the increase of the drift velocity.

TABLE II

$v_w$ meters/sec.	60N in cycles/min	$v_w/N\lambda$ = const.	$\theta_0 = \sin^{-1} \frac{N\lambda}{2v_w}$
12	1.8	5.83	4° 50'
26	4.2	4.64	6° 19'
37	7.7	3.60	8° 2'
48	10.5	3.43	8° 20'
56	13.0	3.23	8° 55'
67	16.7	3.00	9° 35'
78	20.8	2.81	10° 23'
86	27.2	2.40	12° 7'
mean		3.62	

It may be mentioned that the angle of spread of the scattered components is of the same order as that obtained by Briggs (1951) and Rao and Rao (1958). The values of the spread-angle are also in agreement with the values obtained by Briggs and Philips (1950) and by Khastgir and Singh (1960) from the three-spaced-receiver fading records.

## REFERENCES

- Briggs, R. H., 1951. *Proc. Phys. Soc. (Lond.)*, **64B**, 255.  
 Briggs, R. H. and Philips, G. J., 1950. *Proc. Phys. Soc. (Lond.)*, **63B**, 907.  
 Khastgir, S. R. and Singh, R. N., 1960. *Jour. Atmos. and Terr. Physics*, **18**, Nos 2 and 3.  
 McNicol, R. E. W., 1949. *Proc. Inst. Elec. Engrs.* **96**, Part III, 517.  
 Pawsey, J. L., 1935. *Proc. Camb. Phil. Soc.*, **31**, 125.  
 Rao, B. R. and Rao, M. S., 1958, *Jour. Brit. IRE*, **18**, No. 8, 493.  
 Ratcliffe, J. A., 1948. *Nature*, **162**, 9.  
 Ratcliffe, J. A. and Pawsey, J. L., 1933. *Proc. Camb. Phil. Soc.*, **20**, 301.

# Letters to the Editor

*The Board of Editors will not hold itself responsible for opinions expressed in the letters published in this section. The notes containing reports of new work communicated for this section should not contain many figures and should not exceed 500 words in length. The contributions must reach the Assistant Editor not later than the 15th of the second month preceding that of the issue in which the letter is to appear. No proof will be sent to the authors.*

16

## LATITUDE DEPENDENCE OF NUCLEONIC INTENSITY DURING AUGUST 24 – SEPTEMBER 20, 1957

LEKH VIR AND P. S. GILL

GULMARG RESEARCH OBSERVATORY, GULMARG).

As early as 1933, Messerschmidt (1933) and Steinmaurer and Graziadei (1933) observed a decrease in cosmic ray intensity during a magnetic storm. However, Forbush (1937) incorporating Cheltenham and Huancayo data with that of Hafelekar obtained by Hess and Demmelmair (1937) established the world-wide character of the decrease in cosmic ray intensity with magnetic storm. Since then various reports of such decreases have appeared in literature.

Various methods for measuring the amplitude of the decreases have been adopted by different workers. In this note, we have followed the method suggested by McCracken and Johns (1959). According to it, where the correlation coefficient between any two sets of data  $R_1$  and  $R_2$  is greater than 0.8, the measure of relative amplitude is defined as  $(\sigma_1/R_1)/(\sigma_2/R_2)$  where

$$\sigma_1 = \sqrt{\frac{1}{N-1} \sum (R_i - \bar{R}_1)^2} \text{ and } \bar{R}_1 = \frac{1}{N} \sum R_i$$

and  $R_i$  is the daily mean intensity.

During the period considered, a large Forbush type decrease in intensity occurred. Using the definition given above, and comparing daily mean data, the relative amplitude of the decrease in the intensity of nucleonic component of cosmic radiation for ten sea-level stations with respect to Huancayo data has been computed. The results are plotted in Fig. 1.

The striking feature of this decrease, as is obvious from the Fig. 1, is that the curve does not flatten out beyond the latitude knee. Instead the relative amplitude goes on increasing even up to 82.9°N. Also the relative amplitude is not symmetrical about the geomagnetic equator.

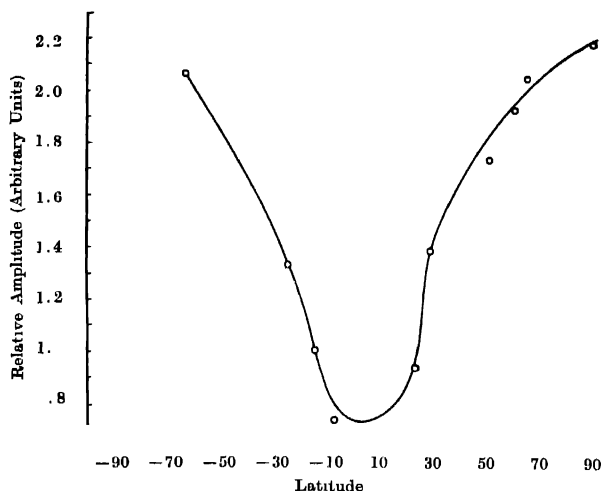


FIG. 1. Latitude dependence of a Forbush-type decrease. The relative amplitude is in arbitrary units.

#### REFERENCES

- Forbush, S. E., 1937. *Phys. Rev.*, **51**, 1108.  
 Hees, V. F. and Demmelmaier, A. 1937. *Nature*, **140**, 316.  
 McCracken K. G. and Johns, D. H., 1959. *Nuovo Cimento*, **13**, 96.  
 Messerschmidt, W., 1933. *Z. Phys.*, **85**, 332.  
 Stienmeurer, R., and Graziadei, H. T., 1933. *Akad. Wiss. Wien*, **22**, 672.

#### 17

### DEBYE $\Theta$ OF SOME CRYSTALS

S. K. JOSHI AND S. S. MITRA\*

PHYSICS DEPARTMENT, ALLAHABAD UNIVERSITY, ALLAHABAD-2,

(Received, June 25, 1960)

Because of its inherent relationship with lattice vibrations, Debye characteristic temperature,  $\Theta$  enters into a large number of solid state problems. The importance of this parameter and the scarcity of the available data have prompted us (Joshi and Mitra, 1960) to calculate and tabulate the Debye temperature of a large number of solids utilising the recent values of their elastic constants. In

\* Now at Ontario Research Foundation, Canada,

TABLE I  
Debye characteristic temperature and elastic constants for some crystals  
(1) Cubic system

Formula	Substance	Elastic constants in units of $10^{11}$ dynes/cm <sup>2</sup>				Debye Temp. in °K	
		$c_{11}$	$c_{44}$	$c_{12}$	Source	Calculated	Exptl.
CsBr	Cesium bromide	3.097	0.7500	0.903	Reinitz and Huntington (1960)	136	
CsI	Cesium iodide	2.434	0.6316	0.636	Reinitz and Huntington (1960)	120	
Nb	Niobium	19.2	5.68	13.4	Bolef and Menes (1960)	283	
RbBr	Rubidium bromide	3.15	0.384	0.493	Reinitz and Huntington (1960)	127	
RbI	Rubidium iodide	2.54	0.276	0.407	Reinitz and Huntington (1960)	99	100-118
Ta	Tantalum	26.5	8.31	15.9	Bolef and Menes (1960)	259	246
V	Vanadium	22.9	4.38	11.7	Bolef and Menes (1960)	394	338

## (2) Hexagonal system

Formula	Substance	Elastic constants in units of $10^{11}$ dynes/cm <sup>2</sup>					Debye Temp. in °K	
		$c_{11}$	$c_{33}$	$c_{44}$	$c_{22}$	$c_{13}$	Source	Exptl.
CdS	Cadmium sulphide	8.432	9.397	1.489	5.212	4.638	Bolef <i>et al.</i> (1960)	214

## (3) Trigonal system

Formula	Substance	Elastic constants in units of $10^{11}$ dynes/cm <sup>2</sup>						Debye Temp. in °K	
		$c_{11}$	$c_{33}$	$c_{44}$	$c_{66}$	$cc_{13}$	$c_{14}$	Source	Exptl.
Bi	Bismuth	6.17	3.63	1.074	1.379	2.38	-0.699	Eckstein <i>et al.</i> , (1960)	107

\* Now I.C.I. Fellow, University of Aberdeen.

the present communication it is intended to calculate the Debye  $\Theta$  of some additional crystals belonging to the cubic, hexagonal and trigonal systems.

Only the lattice waves of nearly infinite wavelength contribute to the specific heat at very low temperatures, and  $\Theta$  values derived from elastic constants are equal to those obtained from calorimetric data near 0°K.  $\Theta$  is given by

$$\Theta = \frac{h}{k} \left( \frac{9N}{4\pi VI} \right)^{1/3}$$

where

$$I = \sum_0 \frac{1}{v_i^3} \frac{d\Omega}{4\pi}$$

$h$  is Plack's constant,  $k$  is Boltzmann's constant,  $N$  is the number of vibrating units in volume  $V$  of the specimen and  $v_i$  are velocities of propagation for low frequency vibrations and as such are functions of direction. The subscript  $i$  numbers the solutions of the Christoffel equation for plane wave motion. It has been evaluated using Houston's series expansion method as modified by Betts *et al.* (1956).

For an accurate evaluation of  $\Theta$  the values of elastic constants measured at about 0°K should be used (Alers and Neighbours, 1959). But in the absence of such data elastic constants measured at ordinary temperatures have been utilised, which yield an approximate value of  $\Theta$ .

The values of  $\Theta$  and the elastic constants from which they have been calculated for a number of substances belonging to the various symmetry classes are presented in Table I. The experimental  $\Theta$  values derived from calorimetric measurements are also included, wherever available.

The authors are deeply indebted to Prof. K. Banerjee and Prof. S. N. Ghosh, for their interest in the investigation.

#### REFERENCES

- Alers, G. A. and Neighbours, J. R., 1959, *Revs. Mod. Phys.*, **31**, 675.  
 Betts, D. D., Bhatia, A. B. and Wyman, M., 1956, *Phys. Rev.*, **104**, 37.  
 Betts, D. D., Bhatia, A. B. and Horton, G. K., 1956, *Phys. Rev.*, **104**, 43.  
 Bolof, D. I., Melamed, N. T. and Menes, M., 1960, *Bull. Am. Phys. Soc.*, **5**, 169.  
 Bolef, D. I. and Menes, M., 1960, *Bull. Am. Phys. Soc.*, **5**, 40.  
 Eckstein, Y., Lawson, A. W. and Reneker, D. H., 1960, *Bull. Am. Phys. Soc.*, **5**, 170.  
 Joshi, S. K. and Mitra, S. S., 1960, *Proc. Phys. Soc. (London)*, **76**, 295.  
 Reinitz, K. and Huntington, H. B., 1960, *Bull. Am. Phys. Soc.*, **5**, 40.

# MAGNETISM OF THE IRON PARTICLES AS REVEALED BY ELECTRON DIFFRACTION

S. YAMAGUCHI

THE INSTITUTE OF PHYSICAL AND CHEMICAL RESEARCH, 31 KAMIFUJI (HONGO)  
TOKYO, JAPAN

(Received, September 21, 1960)

The path of an electron beam is deflected in a magnetic field as the result of the Lorentz effect. This effect is observable in the diffraction pattern obtained from a ferromagnetic substance.

The rather soft electrons (about 50 KV) graze the surface of matter, whereas the hard electrons (about 200KV) are able to tunnel through a thick particle (thickness: about 3000 Å) (Yamaguchi, 1957, Yamaguchi and Takeuchi, 1957).

These two experiences imply that the alternative use of the soft and the hard electrons is of use for studying the surface magnetism of a given particle as compared with the interior magnetism of itself by means of diffraction.

Iron powder was here employed as a specimen for the experiment. The iron particles were magnetically attracted at the sharp edge of a razor blade acting as permanent magnet (remanence: about 10000 gauss). In this way these iron particles were kept in the saturation induction. An electron beam grazed these magnetized particles to give rise to a diffraction pattern.

A process of double exposure was carried in order to measure the Lorentz effect caused by the specimen. The diffraction pattern of a non-ferromagnetic gold foil was first photographed, and then that of the specimen was superimposed upon it. In this process, the position of the photographic plate as well as the wavelength of the incident beam were kept constant. Fig. 1 is a double diagram obtained in this process with the soft electrons (wavelength: 0.0479 Å). It is remarkable in this diagram that the diffraction rings from the reference gold foil and those of the specimen are eccentric as the result of the Lorentz effect. The ring eccentricity measurable in Fig. 1 makes it possible to calculate the magnetic induction at the surface of the specimen. Fig. 2 is a double diagram obtained with the hard electrons (wavelength 0.0277 Å) from the same spot of the specimen as for Fig. 1. There is again the ring eccentricity in this diagram. This diagram informs us of the magnetic induction found in the interior of the particle specimen. We have a relation between Figs. 1 and 2 :

$$\frac{Z_1}{Z_2} = \frac{\lambda_1 B_s}{\lambda_2 B_i} \quad \dots (1)$$

where  $Z_1$  and  $Z_2$  mean the ring eccentricity in Fig. 1 and that in Fig. 2,  $\lambda_1$  and  $\lambda_2$  mean the wavelength in Fig. 1 and that in Fig. 2 ( $0.0479$  and  $0.0277 \text{ \AA}$ ), and  $B_s$  and  $B_i$  mean the surface and the interior inductions of the iron particles. From Figs. 1 and 2 we measure  $Z_1/Z_2 = 1.59$ . According to Eq. (1), therefore, we obtain

$$B_s/B_i = 0.92$$

or

$$B_s < B_i.$$



FIG. 1. A double diagram from the magnetized specimen and gold, taken with the soft electrons. Wavelength:  $0.0479 \text{ \AA}$ . Camera length:  $495 \text{ mm}$ . Positive enlarged 2.3 times.



FIG. 2. A double diagram taken with the hard electrons. Wavelength:  $0.0277 \text{ \AA}$ .



The diffraction rings characteristic of the oxide ( $\text{Fe}_3\text{O}_4$ ) in Fig. 1 with the soft electrons are distinctly more intense than those in Fig. 2 with the hard electrons. This fact verifies readily that the surface of the iron particles is covered with the oxide. The induction of this oxide is lower than that of pure iron. It is, therefore, reasonable for the present specimen that the surface induction  $B_s$  is lower than the interior induction  $B_i$ . A model of the iron particle under question is illustrated in Fig. 3.

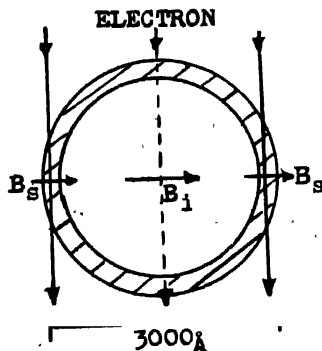


FIG. 3. The magnetic structure of the iron particle as revealed by electron diffraction.  $B_i$  and  $B_s$  mean the interior and the surface induction respectively.

#### REFERENCES

- Yamaguchi, S. and Takeuchi, T., 1957, *J. Colloid Sci.*, **12**, 263.  
Yamaguchi, S., 1957, *J. Chem. Phys.*, **27**, 1114.

## BOOK REVIEW

**FRONTIERS IN SCIENCE** ; Edited by Edward Hutchings, Jr., pp.362+vi.  
George Allen Unwin Ltd, Ruskin House, Museum Street, London, 1960,  
Price 25 s. net.

Science is a continuous advance to new frontiers. Although, the geographic frontiers are disappearing, frontiers of Science are never ending. In the thirty-five most illuminating and exciting research reports that make up this volume frontiers of Science have been well explored by world renowned scientists like Linus Pauling, Robert Oppenheimer, Fred Hoyle, Sir Charles Darwin and twenty-eight other stalwarts of scientific researches.

The present volume has been divided into three main sections : the Physical Science, the Biological Sciences and Science and Society introduced respectively by George Beadle, Harrison Brown and Hunter Mead. Among many problems the interesting ones dealt with in this volume are the origin of life, growing population of the world and how to feed them, growth and reproduction of viruses, the structure of living matters, radiation, the life cycles of stars, natural disturbances, its cause and effects, place of technology in civilization and the relation of science and religion.

It is needless to mention that the present volume will be extremely helpful not only to scientists who are carrying on researches in the subjects discussed in this book, but also to non-scientists who want to keep themselves in contact with the current scientific developments.

The get-up of the volume is quite good.

(Dilip Kumar Ghosh)

# INTERMOLECULAR POTENTIAL AND PROPERTIES OF ARGON

I. B. SRIVASTAVA

INDIAN ASSOCIATION FOR THE CULTIVATION OF SCIENCE, CALCUTTA-32

(Received, September 23, 1960)

**ABSTRACT.** By utilising the recent compressibility data, the potential field of argon has been determined on the Lennard-Jones (12:6) and (9:6) models. The force constants thus determined on the L-J (12:6) model give a better correlation of the various properties of argon than those obtained previously. A consideration of the equilibrium properties of argon lends support to the suggestion of Kihara that the potential bowl of the spherical molecules should be wider than that given by the L-J (12:6) model

## INTRODUCTION

Considerable progress has already been made in correlating the various bulk properties of molecules and particular success has been achieved in the case of spherical molecules. One of the most common forms of the intermolecular potential used for this purpose is the Lennard-Jones ( $n : m$ ) potential

$$\phi(r) = \epsilon \left[ \frac{m}{n-m} \left( \frac{r_m}{r} \right)^n - \frac{n}{n-m} \left( \frac{r_m}{r} \right)^m \right] \quad \dots (1)$$

where  $r$  is the distance between the two molecules and  $\epsilon$  is the potential minimum at  $r = r_m$ . The quantity  $r_m$  is related to  $\sigma_n$ , the value for which  $\phi(r) = 0$ , by the relation

$$\sigma_n = r_m \left( \frac{m}{n} \right)^{\frac{1}{n-m}} \quad \dots (2)$$

Theoretical considerations lead us to assume  $m = 6$ , but it is impossible to fix  $n$  from theory and it is usual to determine  $n$  from best empirical fit.

Even for spherical molecules, there remains some uncertainty about the best value of the index  $n$ . Several workers, Hirschfelder, *et al.* (1948), Srivastava and Madan (1953a, 1953b) and others have shown that the transport properties can be represented reasonably well with  $n = 12$ . Unfortunately due to difficulty in evaluating the complicated collision integrals for the transport properties, these have till now been evaluated only for  $m = 6$ ,  $n = 12$  (Hirschfelder, *et al.*, 1954) and for  $m = 4$ ,  $n = 8$  (Clark-Jones, 1940).

It has been found that amongst the equilibrium properties the second virial coefficient  $B(T)$  is rather insensitive to the form of potential chosen. The reason

for this may be found in the recent work of Kellar and Zumino (1959) which shows that  $B(T)$  alone can determine only the repulsive part and the width of the intermolecular potential as a function of its depth. So it appears that from a consideration of  $B(T)$  data at sufficiently high temperatures (where the repulsive part of the potential is more important), it should be possible to find the best value of  $n$ . Unfortunately, no such data exist. A serious disadvantage in using the third virial coefficient,  $C(T)$  (which is sensitive to the potential form chosen), for determining the intermolecular potential is the difficulty of obtaining accurate values of  $C(T)$ , unless the compressibility data are very accurate. However, Bahadur and Madan (1960) have tried to obtain the force parameters on the  $L-J$  (12 : 6) potential from  $C(T)$  data by drawing smooth curves. Very recently, Guggenheim and McGlashan (1960) have obtained a five parameter potential for argon by utilising mainly the various crystal properties. It has however been shown by Jansen and McGinnies (1956) that in the crystalline state the assumption of pairwise additivity of the molecular forces is not strictly valid. The three-body long range forces in a crystal have been found to contribute a sizeable portion of the total Van der Waals interaction energy which becomes greater, the heavier the atom and the higher the density of the crystalline medium. Consequently, the treatment of Guggenheim *et al.*, which is based on two-body forces, is somewhat uncertain.

Kihara (1953, 1955), from a consideration of  $B(T)$  and  $C(T)$  values suggested that at least for the spherical molecules, the potential bowl should be wider than that given by  $L-J$  (12 : 6) potential, and  $L-J$  (9 : 6) model might give better representation of the various molecular properties. However, some of the  $C(T)$  values used by Kihara were not very reliable. Other workers Hirschfelder, *et al.*, (1954), Beattie (1952) and Michels (1958), have also found that the  $L-J$  (12 : 6) potential is incapable of giving a completely satisfactory representation of the various equilibrium properties and have suggested that the discrepancies may be due to incorrectness of the potential form. It appears therefore that Kihara's suggestion requires further investigation. For this purpose we have chosen to consider the case of argon for which compressibility and other experimental data exist in the literature in the hope that a thorough consideration of various properties of argon may clear up some of the uncertainties. Attempts have also been made to get a set of force constants on the  $L-J$  (12 : 6) model which will give a better correlation of the various properties of argon than that obtained hitherto.

#### DETERMINATION OF THE PARAMETERS

We have followed the procedure of Whalley and Schneider (1955) in fitting the experimental second virial data to the Lennard-Jones (12 : 6) and (9 : 6) potentials. The data used are those recently published by Michels *et al.* (1958) together

with their earlier determinations (1949) in the temperature range from  $-150^{\circ}\text{C}$  to  $+150^{\circ}\text{C}$ . The second virial coefficient  $B(T)$  may be written as

$$B(T) = \rho B^*(T^*) \quad \dots (3)$$

where  $\rho$  is a constant depending on  $\sigma$  and  $B^*(T^*) = B(T)/B(T)_{\text{rig. sph.}}$ . The tables of  $B^*$  as a function of  $T^*$  have been obtained for the  $L-J(12:6)$  model by Hirschfelder, *et al* (1954) and for  $L-J(9:6)$  model by Epstein and Hibbert (1952). First the parameter  $\rho$  (which gives  $\sigma$ ) and  $c/k$  have been obtained approximately by following the graphical procedure of Lennard-Jones (1924). In order to determine  $\rho$  and  $\epsilon/k$  more accurately the method of least squares (Deming 1943) has been applied as follows:

Let the approximate values of  $\rho$  and  $\epsilon/k$  determined graphically be  $\rho_0$  and  $(c/k)_0$  and

$$\epsilon/k = (\epsilon/k)_0 - K \quad \dots (4)$$

$$\rho = \rho_0 - L \quad \dots (5)$$

where  $K$  and  $L$  are small correction terms. Then the normal equations for computing the correction terms are written as

$$\Sigma(KF_{\epsilon/k} + LF_{\rho} + F_0)F_{\rho} = 0 \quad \dots (6)$$

$$\Sigma(KF_{\epsilon/k} + LF_{\rho} + F_0)F_{\epsilon/k} = 0 \quad \dots (7)$$

with

$$F_0 = B(T) - \rho B^*(T^*)$$

$$F_{\epsilon/k} = -[\rho/(\epsilon/k)] \cdot T^* \left( \frac{dB^*}{dT^*} \right)$$

$$F_{\rho} = B^*(T^*).$$

TABLE I  
Parameters on  $L-J(12:6)$  and  $(9:6)$  potentials

Authors	L-J (12:6) model		L-J (9:6) model	
	$\sigma \text{\AA}$	$\epsilon/K^{\circ}\text{K}$	$\sigma \text{\AA}$	$\epsilon/K^{\circ}\text{K}$
Present work	3.418	120.23	3.584	89.59
Michels, <i>et al.</i> (1949)	3.405	119.8	—	—
Whalley and Schneider (1955)	3.409	119.49	3.567	89.64
Hirschfelder, <i>et al.</i> from viscosity (1954)	3.418	124	—	—
Behadur and Madan (1960)	3.419	120.5	—	—

Here  $F_0$ ,  $F_{e/k}$  and  $F_\rho$  are to be calculated using the absolute values  $(\epsilon/k)_0$  and  $\rho_0$ . Eqs. (6) and (7) are then solved for  $K$  and  $L$ . If the difference between  $(\epsilon/k)_0$  and  $\rho_0$ , and  $\epsilon/k$  and  $\rho$  comes out to be more than a few percent the fitting is done by using better approximations.

The force constants thus determined on  $L-J$  (12:6) and (9:6) models are shown in Table I, together with the values obtained by other workers.

## COMPARISON WITH EXPERIMENT

### (a) Equilibrium Properties

#### (i) Second Virial and Third Virial Coefficients

The experimental and calculated values of second virial coefficient  $B(T)$  and the third virial coefficient  $C(T)$  on Lennard-Jones (12:6) and (9:6) models are shown in Table II. For  $B(T)$  it is not possible to determine the superiority of the  $L-J$  (12:6) or the  $L-J$  (9:6) potential over the other. It is, however, to be noted that Michels, *et al.* (1958) could not fit their  $B(T)$  data at lower temperatures on the  $L-J$  (12:6) models with the force constants previously determined by them (1949). It will be seen that with the force constants deter-

TABLE II

Experimental and calculated values of  $B(T)$  and  $C(T)$  on the  $L-J$  (12:6) and  $L-J$  (9:6) models

T °K	B(T) (c.c./mole)				C(T) (c.c./mole) <sup>2</sup>		
	Expt.	L-J (12:6) calc.	L-J (12:6) from Michels <i>et al.</i>	L-J (9:6) calc.	Expt.	L-J (12:6) calc.	L-J (9:6) model
133.2	-107.98	-106.79	-104.95	-104.79	2656	1426	1976
138.2	-100.88	-99.69	-98.13	-98.04	2418	1478	1964
143.2	-94.43	-92.86	-92.22	-92.19	2417	1503	1943
148.2	-88.45	-87.95	-87.36	-86.77	2357	1505	1913
150.7	-85.64	-85.34	-83.68	-84.20	2313	1504	1899
153.2	-82.97	-82.81	-81.26	-81.79	2278	1499	1882
163.2	-73.25	-73.31	-72.23	-72.77	2104	1468	1810
173.2	-65.21	-65.63	-63.68	-65.05	2015	1416	1740
188.2	-54.83	-55.40	-54.16	-55.11	1791	1336	1637
203.2	-46.83	-47.14	-45.95	-46.93	1711	1255	1571
223.2	-37.43	-38.36	-37.27	-37.91	1541	1175	1451
248.2	-28.57	-30.61	-28.46	-28.96	1365	1085	1340
273.2	-21.45	-21.95	-21.49	-21.92	1270	1020	1279
298.2	-15.75	-15.83	-15.93	-15.98	1160	977	1241
323.2	-11.24	-11.65	-11.16	-11.38	1130	935	1176
348.2	-7.25	-7.48	-7.28	-7.36	1040	905	1139
373.2	-4.0	-4.10	-3.98	-3.94	1000	883	1110
398.2	-1.18	-1.34	-1.14	-1.046	970	866	1084
423.2	+ 1.38	+ 1.23	+ 1.31	+ 1.34	880	852	1062

mined in this paper, the low temperature  $B(T)$  values of argon can also be represented satisfactorily on the  $L-J(12:6)$  model.

The agreement between the experimental and the calculated values of  $C(T)$  is not good either for the  $L-J(12:6)$  or  $L-J(9:6)$  potential, but is definitely better on  $L-J(9:6)$  model.

(ii) *Joule-Thomson coefficient*

The Joule-Thomson Coefficient at zero pressure  $\mu^0$  may be written on the  $L-J(12:6)$  model as

$$\mu^0 C_p^0 = b_0(B^*_{11} - B^*) \quad \dots \quad (8)$$

TABLE III

Experimental and the calculated values of the J—T coefficient of argon  
at zero pressure in °C atm<sup>-1</sup>

T °K	$\mu^0 \times 10^3$ Expt. (a)	$\mu^0 \times 10^3$ on the L-J (12:6) model	$\mu^0 \times 10^3$ on the L-J (9:6) model
123.2	1.750	1.648	1.527
137.7	1.293	1.386	1.311
148.2	1.075	1.217	1.155
160.7	0.935	1.070	1.026
173.2	0.835	0.988	0.9022
185.7	0.756	0.884	0.8034
198.2	0.695	0.736	0.7211
223.2	0.578	0.632	0.587
248.2	0.4905	0.522	0.492
273.2	0.418	0.445	0.419
298.2	0.360	0.388	0.362
323.2	0.312	0.330	0.314
348.2	0.270	0.304	0.2745
373.2	0.236	0.245	0.239
398.2	0.204	0.214	0.207
423.2	0.178	0.186	0.181
473.2	0.134	0.140	0.129

(a) J. R. Roebuck and H. Osterberg, (1934)

where  $C_p^0$  is the zero pressure value of the molar specific heat,  $b_0 = \frac{3}{2}\pi N\sigma^3$  and  $B_1^* = T^* \frac{dB^*}{dT^*}$ . The  $B_1^*$  and  $B^*$  have been tabulated as a function of  $T^*$  (Hirschfelder *et al.*, 1954).

On the  $L-J$  (9 : 6) model Epstein and Hibbert (1952) have calculated the values of  $B^*$  as a function of  $1/T^*$ . From these tables the values of  $B^*$  and  $B_1^*$  as functions of  $T^*$ , required for calculating  $\mu^0(C_p^0)$  were obtained graphically. The values thus obtained are given in appendix which may be utilized for the calculation of  $\mu^0$  on the  $L-J$  (9 : 6) model. The experimental and the calculated values of  $\mu^0$  on different molecular models are given in Table III. It is interesting to note that Hirschfelder (1938) could not fit the experimental  $\mu^0$  data for argon on the  $L-J$  (12 : 6) model. Table III shows that the  $L-J$  (9 : 6) potential gives a better agreement with the experimental values of  $\mu^0$  than the  $L-J$  (12 : 6) model.

### (iii) Crystal properties

The heat of sublimation,  $\Delta H_v(0)$  and the lattice spacing,  $R$ , both at 0°K are simply correlated with the inter-molecular potential provided the substance crystallises in the cubic system. The equations for the lattice spacing including the effect of zero point energy have been given by Corner (1948) for ( $n$  : 6) potential which have been reduced for the  $L-J$  (12 : 6) and  $L-J$  (9 : 6) potential as follows :

For the  $L-J$  (12 : 6) potential,

$$C_0 = 2C_{12} \left( \frac{\sigma}{R} \right)^6 + \left\{ \frac{h^2}{8\pi^2 m c \sigma^2} \right\}^{\frac{1}{2}} \cdot \frac{77C_{14} \left( \frac{\sigma}{R} \right)^6 - 10C_8}{\left\{ 22C_{12} \left( \frac{\sigma}{R} \right)^{10} - 5C_8 \left( \frac{\sigma}{R} \right)^4 \right\}^{\frac{1}{2}}} \quad \dots (9a)$$

and for  $L-J$  (9 : 6) potential

$$C_0 = C_9 \left( \frac{r_m}{R} \right)^3 + \left\{ \frac{h^2}{3\pi^2 m e r_m^2} \right\}^{\frac{1}{2}} \cdot \frac{11C_{11} \left( \frac{r_m}{R} \right)^3 - 5C_7}{4C_{11} \left( \frac{r_m}{R} \right)^7 - \frac{5}{2} C_8 \left( \frac{r_m}{R} \right)^4} \quad \dots (9b)$$

where  $r_m$  = value of  $r$  at potential minimum

$h$  = Planck's constant

$m$  = mass of the molecule



and  $C_n$  for  $n = 1, 2$ , etc. are numerical constants calculated by Lennard-Jones and Ingham (1925). Using the force constants determined in the present paper, the value of  $R$  was evaluated from Eqn. (9). This value of  $R$  was used for calculating the  $\Delta H_p^{(0)}$  with the help of equation given below for ( $n : 6$ ) potential,

$$\Delta H_v^{(0)} = \frac{1}{2} N \epsilon \left[ 6 C_n \left( \frac{r_m}{R} \right)^n - n C_6 \left( \frac{r_m}{R} \right)^6 \right] \quad (n=6) \quad \dots \quad (10)$$

The values of  $\Delta H_v^{(0)}$  and  $R$  thus obtained together with the experimental values are given in Table IV. It is to be noted that the crystal data cannot give any definite information about the suitability of any particular form of potential as it has been shown by McGinnes and Jansen (1956) that the assumption of the additivity of molecular force is not possibly valid in the crystalline state. Consequently, equations (9) and (10) which are based on this assumptions are somewhat uncertain.

TABLE IV  
Experimental and calculated values of  $\Delta H_v^{(0)}$  and  $R$  for argon

Authors	$H_v^{(r)}$ in cal./mole			$R$ in Å		
	Expt.	Calculated		Expt.	Calculated	
		L-J (12:6)	L-J (9:6)		L-J (12:6)	L-J (9:6)
Present work	<sup>a</sup> 1998 ± 40	2010	1722	<sup>b</sup> 3.81	3.73	3.908
Whalley and Schneider		2033 ± 6	1718 ± 5		3.767	3.929

(a) Whalley and Schneider, (1955)

(b) Simon and Von Simon, (1924)

### (b) *Transport properties*

(i) *Viscosity*

The experimental and the calculated values of viscosity of argon on  $L-J$  (12.6) model have been given in Table V. The agreement of calculated values with the experimental data is better than that obtained by using Michels' force constants. It has long been known that the high temperature viscosity data of argon cannot be represented well by the  $L-J$  (12.6) potential. This may be due to the increasing importance of the repulsive part of the intermolecular potential at high temperature which should vary exponentially rather than obey an inverse power law.

(ii) *Thermal conductivity*

The experimental and calculated values of the thermal conductivity of argon is given in Table VI. The theoretical values were calculated to the first approxi-

TABLE V

Experimental and calculated values of viscosity of argon (in  $10^{-7}$  gm/cm.sec)

T °K	Expt.	Calculated from our constants	Calculated from force constants of Michels, <i>et al.</i>	Calculated from force constants from viscosity	Ref for Expt. data
80	688	660	666	649	a
120	993	997	1005	979	a
160	1298	1319	1332	1300	a
200	1594	1620	1636	1601	a
240	1878	1902	1920	1882	a
280	2145	2166	2182	2143	a
298	2228	2274	2279	2267	b
375	3685	3704	3737	3682	c
676	4115	4133	4169	4111	c
800	4621	4662	4698	4641	a
1200	5947	6066	6113	6083	a
1500	8778	8953	7161	6983	a

(a) Johnston and Grilly, (1942)

(b) Kestin and Lidenpost (1959)

(c) Trautz Molster and Zink, (1930)

mation on the Chapman-Enskog theory (Hirschfelder, *et al.*, 1954). It may be seen that the force constants determined in the present work from the second virial coefficient can represent the thermal conductivity of argon almost as satisfactorily as those determined from viscosity.

TABLE VI

Experimental and calculated values of the thermal conductivity  $K$  (in  $10^{-7}$  cal. cm $^{-1}$ . sec $^{-1}$ . deg $^{-1}$ .) for argon.

T °K	Expt (a)	Calculated from our force constants	Calculated from force constants of Michel, <i>et al.</i>	Calculated from force constants from viscosity
90.23	141	139	140	137
194.7	293	295	298	292
273.2	394	395	399	392
373.2	506	505	509	504
491.2	614	618	623	619
579.2	684	694	700	696

(a) Kannuluk and Carman, (1952)

## CONCLUSIONS

(1) A consideration of the equilibrium properties of argon lends support to the suggestion of Kihara that the potential bowl of the spherical molecules should be wider than that given by the  $L-J$  (12 : 6) model. The fact that the high temperature transport properties require a value of index of repulsion higher than 12 may be due to the inadequacy of inverse power repulsion at higher temperature. Hence at moderate temperature a  $L-J$  (9 : 6) model may possibly give a better representation of the potential field, than a  $L-J$  (12 : 6) potential.

(2) The set of force constants obtained on the  $L-J$  (12:6) potential in this paper gives a more consistent representation of the various properties of argon than those hitherto obtained.

#### ACKNOWLEDGMENTS

The author is thankful to Prof. B. N. Srivastava, D.Sc., F.N.I., for his valuable guidance and discussions throughout the progress of this work. He also wishes to express his thanks to Mr. A. K. Barua for suggesting the problem and many helpful discussions.

#### REFERENCES

- Bahadur, J., and Madan, M. P., 1960. *Proc. Nat. Inst. of Sci. of India*, **27**, 64.  
 Beattie, J. A., Brerley, J. S., and Barrault, R. J. 1952. *J. Chem. Phys.*, **20**, 1615.  
 Deming, W. B., 1943. *Statistical Adjustment of Data*, John Wiley & Sons, Inc., New York.  
 Epstein, L. F., and Hibbert, C. J., 1952. *J. Chem. Phys.*, **20**, 752.  
 Epstein, L. F., Hibbert, C. J., Power, M. D. and Roo, G. M. 1954. *J. Chem. Phys.*, **22**, 464.  
 Guggenheim, E. A., and Mc Glashan, M. L., 1960. *Proc. Roy. Soc.*, **225**, 456.  
 Hirschfelder, J. O., Bird, R. B., and Spotz, E. L., 1948. *J. Chem. Phys.*, **16**, 908.  
 Hirschfelder, J. O., Curtiss, C. F. and Bird, R. B., 1954. *Molecular Theory of Gases and Liquids*, John Wiley & Sons, Inc., New York.  
 Jansen, L. and Mc Ginnies, R. T. 1956. *Phys. Rev.*, **104**, 961.  
 Johnston, H. L., and Gilly, E. R. 1942. *J. Phys. Chem.*, **46**, 948.  
 Jones, L. C. 1940. *Phys. Rev.*, **58**, 111.  
 Kannulank, W. G., and Carman, E. H. 1952. *Proc. Phys. Soc. (London)*, **65B**, 701.  
 Kollar, J. B. and Zunino, B., 1959. *J. Chem. Phys.*, **30**, 1351.  
 Kostin, J. and Lidenpost, W., 1950. *Physica*, **26**, 1033.  
 Kihara, T., 1953. *Revs. of Modern Phys.*, **25**, 831.  
 Kihara, T., 1955. *Revs. of Modern Phys.*, **27**, 412.  
 Lennard-Jones, J. E. and Ingham, A. E., 1925. *Proc. Roy. Soc. (London)*, **A107**, 636.  
 Michels, A., Wijker, H. and Wijker, H.K., 1949. *Physica*, **15**, 627.  
 Michels, A., Lovelt, J. M., and de Graeff, W., 1958. *Physica*, **22**, 659.  
 Roebuck, J. R. and Osterberg, H., 1934. *Phys. Rev.*, **46**, 785.  
 Simon and von Simon 1926. *Z. Physik*, **25**, 160.  
 Srivastava, B. N. and Madan, M. P., 1953a. *Proc. Roy. Soc. (London)*, **A66**, 277.  
 Srivastava, B. N. and Srivastava, K. P., 1957. *Ind. Jour. Phys.*, **31**, 404.  
 Trautz, M., Molster, A. and Link, R., 1930. *Ann. Physik*, **7**, 1644.  
 Whalley, E., and Schneider, W. G. 1955. *J. Chem. Phys.*, **23**, 1644.

#### APPENDIX

The values of  $B^*$  and  $T^* \frac{dB^*}{dT^*}$  on the  $L-J$  (9:6) model were obtained graphically from the table given by Epstein and Hibbert (1952). The values thus obtained are given in Table VII. This table may be used to calculate the Joule-Thomson Coefficient at zero pressure on the  $L-J$  (9:6) model.

TABLE VII

Table for  $B^*$  and  $B_1^* = \frac{dB^*}{dT^*} \cdot T^*$  for calculating  $\mu^0$ , the zero-pressure Joule-

Thomson Coefficient on  $L-J$  (9:6) model

$T^*$	$B^*$	$B_1^*$	$T^*$	$B^*$	$B_1^*$
0.5	-11.19	17.25	3.1	-0.355	1.085
0.55	-9.40	16.51	3.2	-0.322	1.043
0.60	-7.94	13.80	3.3	-0.275	1.010
0.65	-6.98	11.70	3.4	0.248	0.975
0.70	-6.17	10.15	3.5	-0.220	0.940
0.75	-5.52	9.00	3.6	-0.188	0.923
0.85	-4.52	7.31	3.7	-0.163	0.882
0.90	-4.04	6.58	3.8	-0.134	0.857
0.95	-3.74	6.03	3.9	-0.110	0.835
1.0	-3.46	5.3	4.0	-0.085	0.810
1.1	-2.97	4.62	4.1	-0.068	0.788
1.2	-2.56	4.03	4.2	-0.052	0.765
1.3	-2.25	3.62	4.3	-0.033	0.740
1.4	-2.00	3.23	4.4	-0.017	0.72
1.5	-1.78	2.91	4.5	-0.002	0.695
1.6	-1.58	2.69	4.6	+0.012	0.680
1.7	-1.42	2.49	4.7	+0.028	0.665
1.8	-1.29	2.29	4.8	+0.042	0.650
1.9	-1.15	2.12	4.9	+0.053	0.638
2.0	-1.05	1.96	5.0	+0.063	0.620
2.1	-0.958	1.84	6.0	+0.161	0.568
2.2	-0.868	1.702	7.0	+0.23	0.426
2.3	-0.787	1.602	8.0	+0.28	0.356
2.4	-0.714	1.502	9.0	+0.317	0.302
2.5	-0.646	1.410	10.0	+0.346	0.245
2.6	-0.585	1.338	11.0	+0.365	0.187
2.7	-0.530	1.27	12.0	+0.381	0.150
2.8	-0.477	1.21	13.0	+0.395	0.104
2.9	-0.435	1.165	14.0	+0.405	0.084
3.0	-0.390	1.11	15.0	+0.416	0.0675

## A NOTE ON SOME TUNABLE OSCILLATORS

N. B. CHAKRABORTY\* and K. D. DIXIT

J. K. INSTITUTE OF APPLIED PHYSICS, UNIVERSITY OF ALLAHABAD,  
ALLAHABAD

(Received, July 1, 1960)

**ABSTRACT.** Some arrangements of voltage tunable two-path oscillators capable of large frequency deviation are discussed. Possible combinations of the transfer functions of the individual paths together with the tuning equation and the constraints for stable amplitude of oscillation are given. In some circuit arrangements the variation of frequency with modulating voltage is found to be linear over a wide range.

The present note discusses some circuit arrangements of voltage tunable oscillators which are theoretically capable of very large frequency deviation. In practical arrangements a frequency tuning ratio of two to one and in some cases five to one have been achieved. Tuning is accomplished by means of variation of the gains of the individual paths of a two-path oscillator.

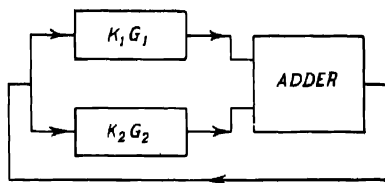


Fig. 1. Schematic diagram of a two-feedback loop.

If  $G_1(p)$  and  $G_2(p)$  are the transfer functions of the two paths of the feedback loop in Fig. 1 the characteristic equation of the loop is given by

$$K_1 G_1 + K_2 G_2 = 1 \quad \dots (1)$$

Here  $K_1$  and  $K_2$  are the gain multiplying factors and are in general variable in accordance with the tuning voltage. If the adder is non-ideal and has a transfer function  $F(p)$  then Eq. (1) is modified to

$$K_1 G_1 + K_2 G_2 = \frac{1}{F} \quad (1.a)$$

The condition for proper working is that the imaginary axis be the root locus with unity feedback.

In Table I some possible combinations of transfer functions together with the tuning equation and the constraints for stable amplitude of oscillation are

\* Now at the Institute of Radio Physics and Electronics, University of Calcutta.

presented. All the circuits have the property that in theory it should be possible to tune their frequency of operation electronically from very low to very high frequencies. Furthermore the magnitude of their positive feedback voltage should be independent of the frequency of resonance. In some arrangements the curve of frequency versus modulating voltage is linear over a wide range. In a few arrangements where the stray capacitances can be taken into account in forming the transfer functions the tuning range can obviously be extended to figure of merit of the tubes employed or a fraction of it depending on the gain required

It will be observed that types 1-6 are practical at audio frequencies, types 1, 5 and 6 at low and very low frequencies, while types 1, 6, 7 and 8 are useful at radio frequencies. In Fig. 2(a) and Fig. 2(b) are presented circuit arrangements

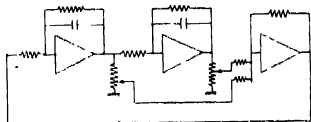


Fig. 2(a). Schematic diagram of the circuit arrangement of type 1 for low and very low frequencies

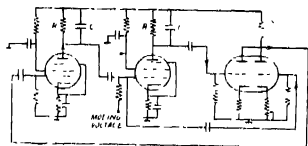


Fig. 2(b) Schematic diagram of the circuit arrangement of type 1 for A. F. and R. F.

of oscillator of type 1 for use at low and at radio frequencies. For *RF* an interesting form derived from type 6 making use of delay lines can be made as shown in Fig. 3(a) and (b). Its tuning equation is

$$\pi\delta = \cos^{-1}(-K_1/2) \quad (2)$$

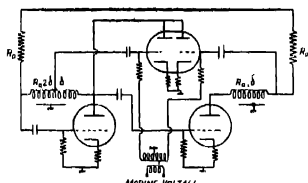


Fig. 3(a). Schematic diagram of a circuit arrangement of type 6.

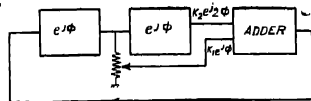


Fig. 3(b). Functional diagram of type 6.

The frequency of excursion in this case is limited to  $\frac{1}{2\delta}$ . The linearity of modulation around  $\frac{1}{4\delta}$  has been observed to be quite good. It is to be noted that

TABLE I

Type	$G_1(j\omega)$	$G_2(j\omega)$	Constraint	Tuning equation	Differential equation	Working frequency
1	$\frac{1}{1+j\omega}$	$-\frac{1}{(1+j\omega)^2}$	$K_1=2$	$\omega = \sqrt{K_2-1}$	$\frac{d^2x}{dt^2} - 2\frac{dx}{dt} + x - K_2x - \frac{d}{dt}F(x) - F(x)=0$	L.F., A.F. & R.F.
2	$\frac{\omega}{1+j\omega}$	$-\left(\frac{j\omega}{1+j\omega}\right)^2$	$K_1=2$	$\omega = \frac{1}{\sqrt{K_2-1}}$	$\frac{d^2x}{dt^2} (1+K_2) - 2\frac{dx}{dt} + x - \frac{d^2}{dt^2}F(x) - \frac{d}{dt}F(x)=0$	A.F.
3	$\frac{1}{1+j\omega}$	$\frac{j\omega}{(1+j\omega)^2}$	$K_1-K_2=2$	$\omega = \sqrt{K_2-1}$	$\frac{d^2x}{dt^2} + 2\frac{dx}{dt} - x - F(x) - \frac{d}{dt}F(x) - K_2\frac{dx}{dt}=0$	A.F.
4	$\frac{1}{1+j\omega}$	$\frac{1-j\omega}{(1+j\omega)^2}$	$K_1-K_2=2$	$\omega = \sqrt{2K_2-1}$	$\frac{d^2x}{dt^2} - 2\frac{dx}{dt} + x - K_2x - K_1\frac{dx}{dt} - F(x) - \frac{d}{dt}F(x)=0$	L.F., A.F. & low R.F.
5	$\frac{1-j\omega}{1+j\omega}$	$\left(\frac{1-j\omega}{1+j\omega}\right)^2$	$K_2=-1$	$\omega = \sqrt{\frac{2-K_1}{2-K_1}}$	$\frac{d^2x}{dt^2} - 2\frac{dx}{dt} - x - K_1x - K_1\frac{d^2x}{dt^2}$ $-\frac{d^2}{dt^2}F(x) + 2\frac{d}{dt}F(x) - F(x)=0$	L.F., A.F. & low R.F.
6	$e^{j2F(x)}$	$e^{j2F(x)}$	$K_2=-1$	$F(\omega) = \cos^{-1} \frac{K_1}{2}$	$x(t) - K_1x(t-\delta) + F(x(t-\delta)) = 0$ if $F(\omega) = -\omega\delta$ .	R.F.
7	$\frac{1-e^{-j\omega\delta}}{1-e^{-j\omega}}$	$-\left(\frac{1-e^{-j\omega\delta}}{1-e^{-j\omega}}\right)^2$	$K_1=0$	$\omega = \frac{2}{\delta} \tan^{-1} \sqrt{\frac{1}{K_2}}$	$x(t-2x(t-\delta)) - x(t-2\delta)$ $-F(x(t)) - 2F(x(t-\delta)) + F(x(t-2\delta)) = 0$	R.F.
8	$\frac{1+e^{-j\omega\delta}}{1-e^{-j\omega\delta}}$	$-\left(\frac{1+e^{-j\omega\delta}}{1-e^{-j\omega\delta}}\right)^2$	$K_1=0$	$\omega = \frac{2}{\delta} \cot^{-1} \sqrt{\frac{1}{K_2}}$	$x(t) - 2x(t-\delta) - x(t-2\delta)$ $-F(x(t)) - 2F(x(t-\delta)) + F(x(t-2\delta)) = 0$	R.F.

in arrangements of types 6, 7 and 8, means will have to be adapted to suppress harmonics.

The forms 1—5 have identical characteristic equations. However the way nonlinearities enter into the equation is different and consequently the amplitude stability and other related properties will be different. The nonlinear defining equations in the different cases are also presented in Table I.  $F(x)$  represents the nonlinear parameter basically governing the amplitude of oscillation.

It has been found that the variation of frequency is limited in practice to a ratio of five to one in types 1—5, while in the rest it is about two to one. It is thought that this may be due to the very considerable variation of the slope of the loop phase shift. Another cause is the non-ideal behaviour of the adder.

The disturbing effect of the adder can be removed in the following manner. Supposing that the transfer function of the adder  $\frac{b}{p+b}$ , is the modified loop, equation is

$$(K_1G_1+K_2G_2) \cdot \frac{b}{p+b} = 1 \quad \dots (1c)$$

The characteristic equation of the loop in the oscillating condition will now be

$$(p^2+K)(p+C) = 0 \quad \dots (3)$$

It will be found in this case that both  $K_1$  and  $K_2$  are to be varied. For type 1 for example  $K_1$  and  $K_2$  are related by

$$(2b+1)(2+b) = K_1b(2+b)+b(1-K_1-K_2) \quad \dots (4)$$

#### TUNABLE AMPLIFIERS

It is evident that at a gain setting smaller than that required for self-oscillation all the circuits can be used as tunable amplifiers and hence as spectrum analysers. The nature of the selectivity curve and the variation of the maximum output of the response curve with the tuning frequency will obviously depend on the point of observation of the output as well as the nature of the transfer functions. In the diagram of Fig. 1 for example for inputs  $E_1$ ,  $E_2$  and  $E_A$  applied respectively at the input to  $G_1$  circuit,  $G_2$  circuit and the adder the voltage outputs at the corresponding output points will be given by

$$\frac{e_1}{G_1} = f(K_1G_1E_1+K_2G_2E_2+E_A)+E_1, \quad \dots (5a)$$

$$\frac{e_2}{G_2} = f(K_1G_1E_1+K_2G_2E_2+E_A)+E_2, \quad \dots (5b)$$

$$e_A = f(K_1G_1E_1+K_2G_2E_2+E_A) \quad \dots (5c)$$



where

$$f = \frac{1}{1 - K_1 G_1 - K_2 G_2}.$$

In the arrangement of Fig. 1, for example, if  $E_A$  be the input applied to the adder the output  $e_2$  will be given by

$$e_2 = \frac{G_2}{1 - K_1 G_1 - K_2 G_2} E_A - \frac{1}{(2 - K_1)j\omega_0} E_A, \quad \text{at } p = j\omega_0.$$

The peak of response will therefore depend on the tuning frequency. If on the other hand, the voltage obtained at the output of  $G_1$  circuit is transmitted through a circuit having a transfer function  $\frac{p}{p+1}$  one obtains a transfer characteristic which does not depend on the tuning frequency. It should be noted that a much simpler solution is possible for the arrangement of type 3.

#### REFERENCES

- Anderson, F. B., 1951, *Proc. I. R. E.*, **39**, 881.  
 Delange, O. E., 1949, *Proc. I. R. E.*, **37**, 1328.  
 Stewart, J. L., 1955, *Proc. I. R. E.*, **43**, 589.

RAMAN, INFRARED AND LUMINESCENCE SPECTRA OF  
SOME TRISUBSTITUTED BENZENES

K. K. DEB AND S. B. BANERJEE

OPTICS DEPARTMENT, INDIAN ASSOCIATION FOR THE CULTIVATION OF SCIENCE  
CALCUTTA-32,

(Received, August 24, 1960)

## Plate VIII

**ABSTRACT.** In the present paper tentative assignment of the vibrational frequencies of the molecules of 2, 4- and 3, 4-dichlorotoluene and 1, 2, 4-trichlorobenzene has been proposed from an analysis of the Raman and infrared spectra of the compounds. The Raman spectra of the dichlorotoluenes have been investigated at  $-180^{\circ}\text{C}$  and it has been observed that some of the intramolecular vibrations are affected and a few low frequency lines are exhibited by the compounds at the low temperature. Explanation of these changes has been offered in terms of association of the molecules at the low temperature. It has also been observed that in the solid state at  $-180^{\circ}\text{C}$  both the compounds yield luminescence bands and the  $\text{C}=\text{C}$  valence oscillation appears to be coupled with the electronic transition giving rise to these bands.

## INTRODUCTION

It is known from previous investigations (Biswas, 1954, 1955a,b, Sanyal, 1953) that the Raman spectra of mono- and disubstituted benzene compounds undergo changes and new low frequency Raman lines appear in the spectra with change of state and lowering of temperature, depending on the nature and relative positions of the substituents. In the present work, such investigation has been extended to two trisubstituted benzene compounds, viz., 2, 4- and 3, 4-dichlorotoluene. In order to understand the significance of the changes, it is necessary to assign the molecular frequencies, and both infrared and Raman spectra of the compounds were studied for this purpose. As a comparison with 1, 2, 4-trichlorobenzene would be helpful in making the assignments, the infrared spectrum of this compound was also recorded in the present investigation and the data for the Raman spectra obtained by Mukherjee (1960) have been utilised. The proposed assignments of the frequencies of all the three compounds and the observed changes in the Raman spectra of 2, 4- and 3, 4-dichlorotoluene with solidification have been discussed in this paper.

## EXPERIMENTAL

The liquids were supplied by Fisher Scientific and Co., U.S.A. and were repeatedly subjected to both fractional and vacuum distillation before each exposure. In the case of the dichlorotoluenes two spectrograms, one with suit-

able light filters and another without filters, were obtained both for the liquid and solid states. The experimental arrangement for recording the Raman spectra in the solid state was the same as that reported earlier (Deb, 1960). The polarisation of the Raman lines was also studied by photographing the two components simultaneously with the help of a double image prism. The Raman spectra were photographed on Ilford Zenith plates using a Fuess glass spectrograph giving a dispersion of about  $11\text{ \AA}$  per mm in the  $4046\text{ \AA}$  region.

The infrared absorption spectra were recorded with a Perkin-Elmer Model 21 spectrophotometer with NaCl optics. Thin films of the liquids at the room temperature pressed between two rocksalt plates were used to obtain the absorption spectra.

## RESULTS AND DISCUSSION

The spectrograms showing the Raman lines of 2, 4- and 3, 4-dichlorotoluene in the liquid and solid states are reproduced in Figs. 1 and 2, Plate VIII and the infrared absorption curves of the dichlorotoluenes and 1, 2, 4-trichlorobenzene are shown in Figs. 3, 4 and 5. The frequency shifts of the Raman lines and the observed infrared frequencies in  $\text{cm}^{-1}$  of the three compounds are given in Tables I, II and III, the Raman frequencies for 1, 2, 4-trichlorobenzene being taken from Mukherjee's results (Mukherjee, 1960). The state of polarisation of Raman lines are indicated by the letters 'P' and 'D' which mean 'polarised' and 'totally depolarised' respectively. The frequencies lower than  $600\text{ cm}^{-1}$  could not be studied in the infrared because of the limitation of the NaCl optics used.

### (a) Assignment of molecular frequencies of 2, 4- and 3, 4- dichlorotoluene and 1, 2, 4- trichlorobenzene.

The strong Raman lines at  $705\text{ cm}^{-1}$ ,  $685\text{ cm}^{-1}$  and  $675\text{ cm}^{-1}$  observed in the case of 2,4-dichlorotoluene, 3,4-dichlorotoluene and 1,2,4-trichlorobenzene respectively ( $698$ ,  $682$  and  $675\text{ cm}^{-1}$  in the infrared) may be assigned to a C—Cl vibration arising from  $a_{1g}$ ,  $b_{1u}$ ,  $e_{2g}$  and  $e_{2u}$  vibrations in benzene, all of which become  $a'$ -type vibration in these compounds having  $C_2$  symmetry. The polarisation data support this assignment which is also in agreement with the results for mono- and dichlorobenzenes (Sponer and Kirby-Smith, 1941). There would also be components arising from these modes with frequencies of C—H valence oscillation of  $a'$ -type. They are likely to be represented by the lines  $3062$ ,  $3062$  and  $3066\text{ cm}^{-1}$  for the three compounds. We should also expect a corresponding C—CH<sub>3</sub> stretching oscillation in the case of the dichlorotoluenes and actually the Raman spectra of the two dichlorotoluenes show lines at  $1203$  and  $1211\text{ cm}^{-1}$  which should represent this vibration, there being no corresponding line in the spectrum of 1, 2, 4-trichlorobenzene. The depolarised lines  $2926\text{ cm}^{-1}$  of 2, 4-dichlorotoluene and  $2938\text{ cm}^{-1}$  of 3, 4-dichlorotoluene have also no counter-

TABLE I

Raman and infrared spectra of 2,4-dichlorotoluene

Raman shift in $\text{cm}^{-1}$			Infrared bands	
Liquid at 30°C			Wave No. in $\text{cm}^{-1}$	
Landolt-Bornstein (1951)	Present authors		and intensity	
			28 (3)	
			42 (1)	
			84 (4b)	
			101 (1)	
122 (3)	127 (2)	o, k D		
181 (7)	181 (6)	$\perp$ o, k D	160 (1b)	
202 (8)	202 (8)	$\perp$ o, k D	205 (4b)	
265 (0)	269 (0)	k	208 (1)	
311 (5)	312 (6)	+o, k D	318 (3)	
378 (7)	380 (8)	$\perp$ o, k P	380 (3)	
400 (3)	402 (3)	o, k P	401 (1)	
462 (4)	464 (4)	o, k P	464 (2)	
542 (0)				
645 (3)	646 (3)	o, k D	653 (1)	
704 (6)	705 (8)	o, k P	706 (6)	698 (w)
				799 (s)
832 (6)	834 (8)	o, k P	833 (6)	825 (s)
				852 (w)
				983 (w)
1046 (0)	1049 (1)	o, k	1048 (0)	1044 (ms)
				1088 (mb)
1105 (5)	1108 (4)	o, k P	1107 (2)	
				1122 (vw)
1143 (3)	1145 (4)	o, k P	1148 (0)	
1203 (5)	1204 (6)	o, k P	1210 (6)	
1251 (1)	1255 (1)	o, k P	1257 (0)	
	1302 (1)	o, k P	1301 (0)	
1378 (4)	1382 (6)	o, k P	1383 (5)	1372 (m)
1437 (0)	1438 (0)	o, k	1440 (0)	1438 (w)
				1460 (s)
				1538 (vw)
1590 (5b)	1592 (6b)	o, k D	1591 (1)	1580 (vw)
2029 (1)	2025 (4b)	o, k D	2026 (1)	
3061 (0)	3062 (1)	o, k	3060 (0)	

TABLE II

Raman shift in $\text{cm}^{-1}$		Infrared bands Wave No in $\text{cm}^{-1}$ and Intensity
Liquid at $30^\circ\text{C}$	Solid at $-180^\circ\text{C}$	
	46 (1)	
	76 (1)	
127 (2b) + c, k D	145 (2)	
202 (6b) $\pm$ c, D	202 (3)	
269 (0) e, k D	269 (0b)	
312 (6) $\perp$ c, k D	316 (1)	
368 (4) $\pm$ c, k P	366 (2)	
435 (6) $\pm$ c, k P	433 (4)	
463 (6) $\pm$ c, k P	461 (3)	
557 (obb) e, k		
624 (obb) e, k		
645 (ob) c, k	646 (0)	
686 (7) c, k P	680 (8)	682 (m)
		805 (vs)
870 (4) e, k P	870 (3)	865 (s)
		941 (vw)
		998 (vw)
1030 (4) e, k P	1026 (2)	1030 (s)
1101 (0) c	1100 (0)	
1135 (5) e, k P	1146 (2)	1130 (s)
	1170 (1)	1142 (vvw)
1211 (6) c, k P	1215 (6)	1211 (vvw)
		1258 (w)
1276 (1b) e, k D	1276 (0)	
1381 (4) c, k P	1377 (4)	1381 (s)
1443 (1b) c		1420 (vvw)
1457 (1b) c		
1470 (0) c		1469 (vs)
1598 (6) e, k D	1598 (1)	1592 (w)
2938 (5) c, k D	2938 (0)	
3062 (1) e, k P	3062 (0)	

TABLE III  
Raman and infrared spectra of 1, 2, 4-trichlorobenzene

Raman shift in $\text{cm}^{-1}$ Liquid at $30^\circ\text{C}$ (Mukherjee, 1960)		Infrared bands Wave No. in $\text{cm}^{-1}$ and Intensity
112 (2)	o, k	
182 (2)	s, k	
195 (4)	o, k	
310 (1)	o, k	
332 (3)	$\pm$ e, k	
308 (2)	o, k P	
459 (2)	e, k	
673 (5)	o, k	675 (m)
816 (0)	o, k	810 (vs)
868 (0)*		865 (s)
1034 (3)	e, k P	1052 (s)
		1096 (vs)
1090 (1)	o, k P	1122 (s)
1124 (2)	o, k	1243 (m)
1158 (4)	o, k	1376 (s)
1261 (1)*		1419 (w)
1375 (0)	o, k	1459 (vs)
		1490 (vw)
		1566 (s)
1571 (6h)	o, k	1620 (vw)
		1725 (vw)
3066 (5)	k	3090 (m)

\* These frequencies are taken from Landolt-Börnstein's (1951) tables.

part in the spectrum of 1, 2, 4-trichlorobenzene and are thus expected to arise from a mode of vibration in the methyl group. From analogy with other methylated compounds, these have been attributed to the asymmetric stretching of the C—H bond in the methyl group.

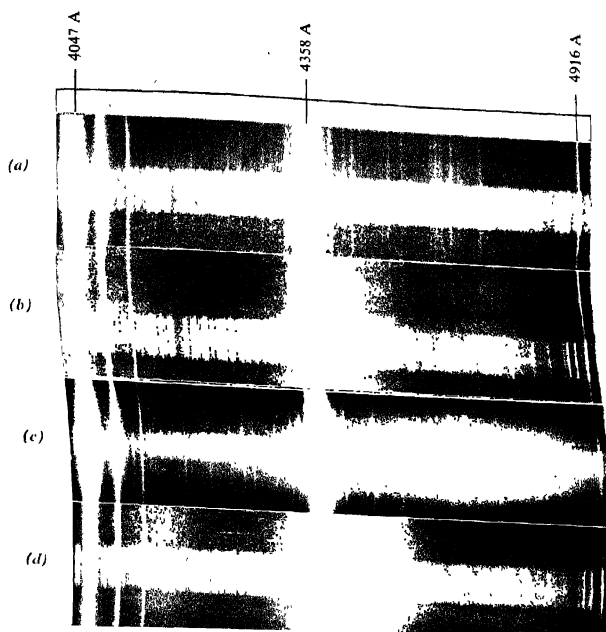
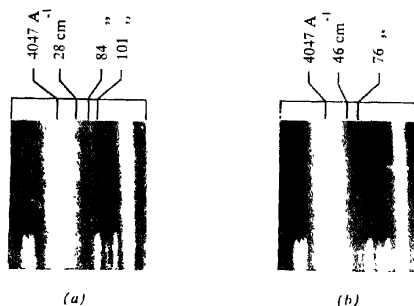


Fig. 1



Raman spectra

- Fig. 1. (a) 2,4 - dichlorotoluene, liquid at 30°C  
 (b) " " " " solid at -180°C  
 (c) 3,4 - dichlorotoluene, liquid at 30°C  
 (d) " " " " solid at -180°C
- Fig. 2. (a) Low-frequency Raman lines of 2,4 - dichlorotoluene at -180°C  
 (b) Low-frequency Raman lines of 2,4 - dibromotoluene at -180°C





The frequencies 1145 and 1108  $\text{cm}^{-1}$  of 2, 4-dichlorotoluene, 1136 and 1101  $\text{cm}^{-1}$  of 3, 4-dichlorotoluene, and 1158 and 1098  $\text{cm}^{-1}$  of 1, 2, 4-trichlorobenzene

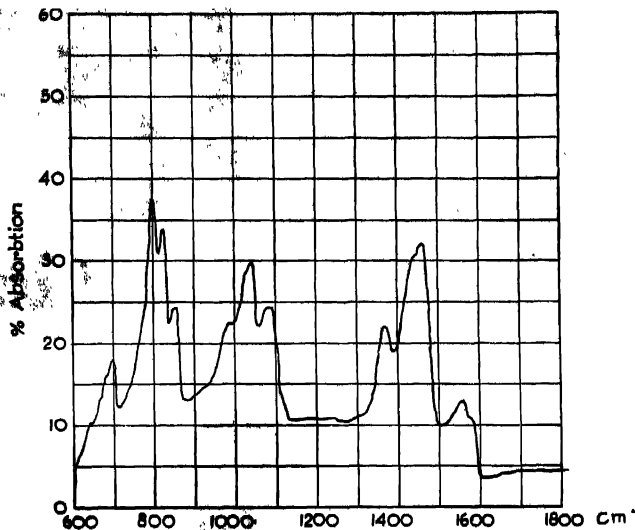


Fig. 3. Infrared spectrum of 2,4-dichlorotoluene (liquid at 26°C)

are probably due to  $a'$ -type vibration originating from  $e_{2g}$  and  $b_{2u}$  modes in benzene, the frequencies representing C—H in-plane deformation vibration. It may be noted that these lines are all polarised and the frequencies are only weakly active in the infrared. The Raman lines 1049, 1030 and 1052  $\text{cm}^{-1}$  respectively of the two dichlorotoluenes and the trichlorobenzene may be due to a component of the  $e_{1u}$  (1035  $\text{cm}^{-1}$ ) mode of benzene.

As can be seen from the tables, that 2, 4- and 3, 4-dichlorotoluene and 1, 2, 4-trichlorobenzene show strong infrared bands at 1460, 1469 and 1459  $\text{cm}^{-1}$  respectively, which are either absent or very weak in the Raman effect, and also bands at 1372, 1381 and 1376  $\text{cm}^{-1}$  respectively. It is well known that within the methyl group in methyl substituted benzenes there are bands due to asymmetric and symmetric C—H bending oscillation falling in the 1450 and 1381  $\text{cm}^{-1}$  regions. But the presence of strong bands at 1459 and 1376  $\text{cm}^{-1}$  in the infrared spectrum of 1, 2, 4-trichlorobenzene clearly indicates that the similar frequencies observed in the dichlorotoluenes cannot be uniquely assigned to vibrations in the  $\text{CH}_3$  group, for they may be due to some other suitable modes of vibration of the molecules themselves. From the discussions of previous workers, the 1460, 1469 and 1459  $\text{cm}^{-1}$  bands due to the three compounds appear to represent a

component of the  $e_{1u}$  mode of frequency  $1485\text{ cm}^{-1}$  in benzene. The frequencies  $1372$ ,  $1381$  and  $1376\text{ cm}^{-1}$  may represent another component of the same mode. In the case of the dichlorotoluenes the bending modes of methyl group may be superposed on these frequencies. The bands near  $1430\text{ cm}^{-1}$  due to the dichlorotoluenes may be attributed to a second component of the asymmetric bending in the methyl group usually observed in the methyl substituted compounds (Sheppard *et al.*, 1953). The Raman lines  $1592\text{ cm}^{-1}$  of 2, 4-dichlorotoluene,  $1598\text{ cm}^{-1}$  of 3, 4-dichlorotoluene and  $1591\text{ cm}^{-1}$  of 1, 2, 4-trichlorobenzene correspond in all probability to a component of  $e_{2g}$  mode in benzene of frequency  $1596\text{ cm}^{-1}$ . The observed infrared frequencies are  $1580$ ,  $1592$  and  $1566\text{ cm}^{-1}$  respectively, the other components in infrared are probably the frequencies  $1558$ ,  $1564$  and  $1550\text{ cm}^{-1}$  respectively.

In all these three molecules with  $C_s$  symmetry, the  $606\text{ cm}^{-1}$   $e_{2g}$  vibration in benzene splits up into two  $a'$  components and these may be identified with

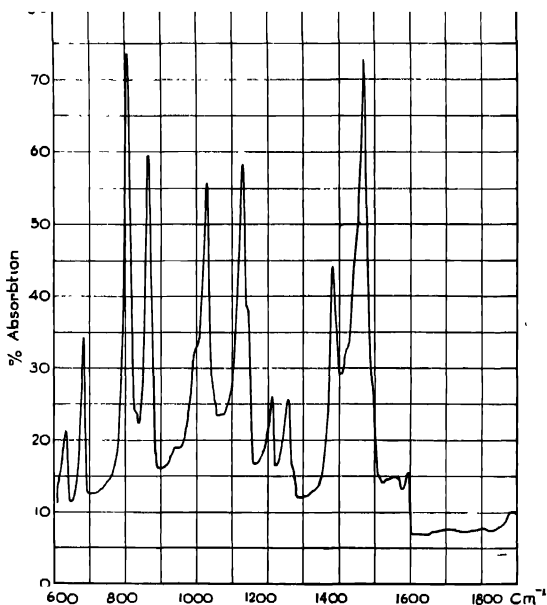


Fig. 4. Infrared spectrum of 3,4- dichlorotoluene (liquid at  $26^{\circ}\text{C}$ )

the polarised Raman lines  $380$  and  $464\text{ cm}^{-1}$  of 2, 4-dichlorotoluene,  $368$  and  $463\text{ cm}^{-1}$  of 3, 4-dichlorotoluene and  $332$  and  $459\text{ cm}^{-1}$  of 1, 2, 4-trichlorobenzene.

In each case, the lower of the two frequencies would correspond to the mode in which all the atoms are displaced.

As discussed above, there are four bending modes in the plane of the benzene molecule viz.,  $a_{2g}$  ( $1298\text{ cm}^{-1}$ ),  $b_{2u}$  ( $1170\text{ cm}^{-1}$ ),  $e_{2g}$  ( $1178\text{ cm}^{-1}$ ) and  $e_{1u}$  ( $1035\text{ cm}^{-1}$ ). These become  $a'$ -type vibrations in the case of  $C_2$  symmetry and are expected to give rise to frequencies corresponding to chlorine bending vibration. The three polarised Raman lines at 402, 435 and  $395\text{ cm}^{-1}$  in the case of the three compounds may correspond to one such mode. At least another component of low frequency should be found near  $200\text{ cm}^{-1}$  (Sponer and Kirby-Smith, 1941) but the depolarisation of the observed lines in this region presents difficulty in assignment of this mode.

Out of the four hydrogen bending vibrations ( $a_{2u}$ ,  $b_{2g}$ ,  $e_{2u}$  and  $e_{1g}$ ) perpendicular to the plane of the ring in benzene, there should result  $a''$  type bending vibrations

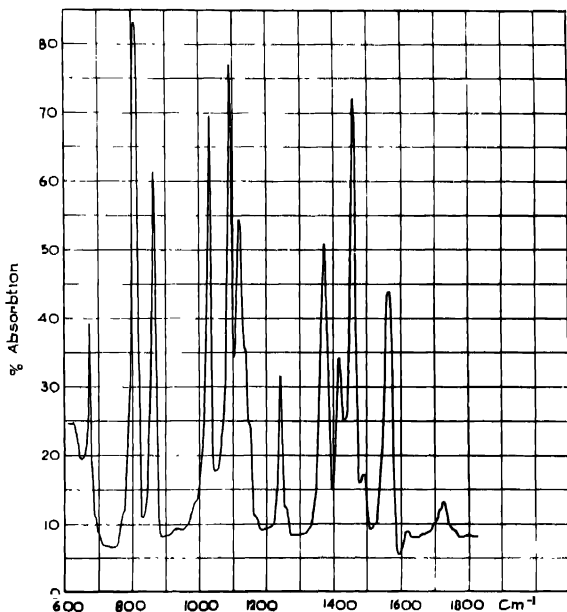


Fig. 5. Infrared spectrum of 1,2,4-trichlorobenzene (liquid at  $26^{\circ}\text{C}$ )

of hydrogen, chlorine and probably of methyl group, giving rise to depolarised Raman lines. It is known from previous results that 1, 2, 4-trisubstituted benzene compounds usually exhibit infrared band corresponding to a C—H out of plane deformation near  $800\text{ cm}^{-1}$  (Bellamy, 1954). Accordingly, the bands 799, 805

and  $810\text{ cm}^{-1}$  observed in the infrared spectra of 2, 4- and 3, 4-dichlorotoluene and 1, 2, 4-trichlorobenzene may be taken to correspond to this vibration, but the absence of any corresponding Raman line in the case of all the three compounds is difficult to interpret as no line is expected to be forbidden in the Raman effect of compounds with  $C_s$  symmetry. The two depolarised low frequency Raman lines  $181\text{ cm}^{-1}$  and  $202\text{ cm}^{-1}$  for 2, 4-dichlorotoluene, and 182 and  $195\text{ cm}^{-1}$  for 1, 2, 4-trichlorobenzene correspond in all probability to components of out of plane chlorine bending modes. The value of  $181\text{ cm}^{-1}$  is probably a little higher in the case of 3, 4-dichlorotoluene as is evident from the broadness of the  $202\text{ cm}^{-1}$  line. Biswas (1958) has proposed the alternative assignment for line near  $202\text{ cm}^{-1}$  observed in chlorotoluenes, that these may be due to dimeric type of associated molecules present in the liquid. This will be taken up while discussing the Raman effect at low temperatures. In both 2, 4- and 3, 4-dichlorotoluene, a depolarised line at  $269\text{ cm}^{-1}$  is observed, while there is no corresponding line in 1, 2, 4-trichlorobenzene. This may indicate that this frequency originates from a motion of the methyl group and we propose to associate it with  $\text{C}-\text{CH}_3$  out of plane deformation.

The  $b_{2g}$  and  $e_{2u}$  modes of out of plane carbon vibration in benzene will produce  $a''$  type vibrations giving depolarised Raman lines. One of the components of the  $e_{2u}$  mode which will be only slightly affected is probably the  $312\text{ cm}^{-1}$  line in the dichlorotoluenes and  $310\text{ cm}^{-1}$  in 1, 2, 4-trichlorobenzene. The other lower component may be detected in the  $127\text{ cm}^{-1}$  line in the dichlorotoluenes and probably the  $112\text{ cm}^{-1}$  line in 1, 2, 4-trichlorobenzene. The  $645\text{ cm}^{-1}$  line may be the contribution of the  $b_{2g}$  mode.

In the Raman spectra of dichlorotoluenes two strong polarised lines at 834 and  $870\text{ cm}^{-1}$  have been observed ( $825$  and  $865\text{ cm}^{-1}$  in the infrared). These may be  $a'$  vibration originating from  $a_{1g}$ ,  $b_{1u}$ ,  $e_{2g}$  and  $e_{1u}$  modes in benzene, though it is difficult to propose any definite interpretation of these bands.

(b) *Changes in the intramolecular oscillations of 2, 4- and 3, 4-dichlorotoluene in the solid state at  $-180^\circ\text{C}$ .*

In the Raman spectra of both 2, 4- and 3, 4-dichlorotoluene a line at  $127\text{ cm}^{-1}$  is observed which is found to disappear in the spectra of the solids. Further, in the case of 2, 4-dichlorotoluene the  $181\text{ cm}^{-1}$  line is also absent and a new line at  $160\text{ cm}^{-1}$  is observed at  $-180^\circ\text{C}$ . In the case of 3, 4-dichlorotoluene the broad band at  $202\text{ cm}^{-1}$  becomes sharp while a new line at  $145\text{ cm}^{-1}$  appears when the compound is solidified. These changes probably indicate that in the solid state at  $-180^\circ\text{C}$ , the molecules of the compounds become associated resulting in restriction of some vibrations of the single molecules. This probably causes the  $\text{C}-\text{Cl}$  out of plane bending vibration of frequency  $181\text{ cm}^{-1}$  in the case of 2, 4-dichlorotoluene and one component of the mode of frequency  $202\text{ cm}^{-1}$  of 3, 4-dichlorotoluene to shift

to lower energies and the lower component of C—C out of plane deformation vibration of frequency  $127\text{ cm}^{-1}$  to disappear. The absence of any appreciable shift of the  $202\text{ cm}^{-1}$  line due to 2, 4-dichlorotoluene and the other component of  $202\text{ cm}^{-1}$  line due to 3, 4-dichlorotoluene may be due to the fact that these lines have their origin in a motion of dimeric molecules present in the liquid state as proposed by Biswas (1958) in the case of monochlorotoluenes.

When 2, 4-dichlorotoluene is solidified and cooled to  $-180^\circ\text{C}$  the lines  $312$ ,  $646$  and  $1204\text{ cm}^{-1}$  are shifted to  $318$ ,  $653$  and  $1210\text{ cm}^{-1}$  respectively without any appreciable changes in the relative intensity. Thus the component of C—C out of plane deformation vibrations of frequencies  $312$  and  $646\text{ cm}^{-1}$  which are largely unaffected by substitution are found to be only slightly influenced by association of the molecules in the solid state. In the case of 3, 4-dichlorotoluene, the lines  $686$  and  $1030\text{ cm}^{-1}$  are shifted to  $680$  and  $1026\text{ cm}^{-1}$  respectively. Further, the strong line at  $1135\text{ cm}^{-1}$  splits up into two lines at  $1146$  and  $1170\text{ cm}^{-1}$  respectively. It is also observed that the relative intensities of lines  $1592$  and  $2926\text{ cm}^{-1}$  of 2, 4-dichlorotoluene and  $1598$  and  $2938\text{ cm}^{-1}$  of 3, 4-dichlorotoluene are reduced in the solid state at  $-180^\circ\text{C}$ . The diminution in intensity of the lines of frequencies  $1592$  and  $1598\text{ cm}^{-1}$  due to a mode involving stretching of the C—C bond may indicate that in the case of both these molecules formation of associated groups takes place at the expense of the C—C bond.

(c) *Low frequency Raman lines in 2, 4- and 3, 4-dichlorotoluene*

In the solid state at  $-180^\circ\text{C}$ , the 2,4-dichlorotoluene exhibits Raman lines at  $28$ ,  $42$ ,  $84$  and  $101\text{ cm}^{-1}$  in the low frequency region, the lines at  $28$  and  $84\text{ cm}^{-1}$  being relatively stronger. On the other hand, 3, 4-dichlorotoluene under similar condition yields only two low frequency Raman lines at  $46$  and  $76\text{ cm}^{-1}$  respectively. Probably the number of types of associated groups in the case

TABLE IV  
Luminescence spectra of 2, 4- and 3, 4-dichlorotoluene in the solid state at  $-180^\circ\text{C}$

2, 4-Dichlorotoluene at $-180^\circ\text{C}$		3, 4-Dichlorotoluene at $-180^\circ\text{C}$	
Position of bands in $\text{cm}^{-1}$ and Intensity	Separation in $\text{cm}^{-1}$ from the first band	Position of bands in $\text{cm}^{-1}$ and Intensity	Separation in $\text{cm}^{-1}$ from the first band
22717 (ms)	0	24180 (w)	0
21197 (ms)	1520	22556 (s)	1632
		21197 (ms)	2983
		20889 (ms)	3291

of 3, 4-dichlorotoluene is smaller than that in 2, 4-dichlorotoluene because of proximity of the chlorine atoms in the 3- and 4 positions in the former molecule.

(d) *Luminescence spectra of 2, 4- and 3, 4- dichlorotoluene at  $-180^{\circ}\text{C}$*

When 2, 4-dichlorotoluene is frozen and cooled to  $-180^{\circ}\text{C}$ , two strong and very broad luminescence bands with centres at about 22717 and 21197  $\text{cm}^{-1}$  are observed and the separation 1520  $\text{cm}^{-1}$  between the components approximates to  $\text{C}=\text{C}$  vibrational frequency. In the case of 3, 4-dichlorotoluene, four broad bands are observed at 24180, 22556, 21197 and 20889  $\text{cm}^{-1}$  respectively. The separation of the last three bands from the first one are 1632, 2983 and 3291  $\text{cm}^{-1}$  respectively. In this case also the  $\text{C}=\text{C}$  vibration is prominent as the 1632  $\text{cm}^{-1}$  frequency, the 3291  $\text{cm}^{-1}$  frequency being approximately the first harmonic of 1632  $\text{cm}^{-1}$ . The other frequency separation 2983  $\text{cm}^{-1}$  may represent a  $\text{C}-\text{H}$  valence oscillation. It may be mentioned here that in the case of other chloro and bromo substituted toluenes, Biswas (1954, 1955) and Sanyal (1953) observed similar broad luminescence bands with a frequency separation approximating to  $\text{C}=\text{C}$  vibrational frequency. Further, in all these compounds the associated groups in the solid state at  $-180^{\circ}\text{C}$  are apparently formed at the expense of the  $\text{C}=\text{C}$  bond as is evident from diminution in intensity of this vibrational frequency at the low temperature. It is, therefore, interesting to note that this particular mode is coupled with the electronic transition giving rise to the luminescence spectra exhibited by these compounds in the solid state at low temperature.

#### ACKNOWLEDGMENT

The authors are indebted to Professor S. C. Sirkar, D.Sc., F.N.I. for his keen interest and valuable suggestions and also to Mr. G. S. Kastha for helpful discussions.

#### REFERENCES

- Bollamy, L. J., 1954, The Infrared Spectra of Complex Molecules.  
 Biswas, D. C., 1954, *Ind. J. Phys.*, **28**, 54.  
 „, 1955a, *Ind. J. Phys.*, **29**, 62.  
 „, 1955b, *Ind. J. Phys.*, **29**, 74  
 „, 1958, D.Sc. Thesis of the Calcutta University  
 Deb, K. K. 1960, *Ind. J. Phys.*, **34**, 247.  
 Landolt-Bornstein, 1951, Zahlenwerte und Funktionen, I Band, Atom und Molekular Physik, pp. 523-24.  
 Mukherjee, D. K., 1960, Unpublished results (private communication).  
 Sanyal, S. B. 1953, *Ind. J. Phys.*, **23**, 447.  
 Sheppard, N. and Simpson, D. M., 1953, *Quant. Rev.*, **7**, 19.  
 Spomer, H. and Kirby-Smith, J. S., 1941, *J. Chem. Phys.*, **9**, 667.

# ULTRASONIC VELOCITY IN SOME AQUEOUS SOLUTIONS OF ELECTROLYTES

P. R. K. L. PADMINI AND B. RAMACHANDRA RAO

(ULTRASONIC LABORATORIES, ANDHRA UNIVERSITY, WALTAIR)

(Received, July 22, 1960)

**ABSTRACT.** The variation of ultrasonic velocity, adiabatic compressibility, apparent molal compressibility and molar sound velocity with concentration is studied in eleven electrolyte solutions. The results are interpreted in the light of Debye-Huckel's theory of electrolytes. The hydration numbers are estimated for all the electrolytes and compared with the data obtained by other methods. Non-linear variations of molar sound velocity with molar concentration observed in some cases is explained in terms of molecular association and ionic solvation.

## 1. INTRODUCTION

Ultrasonic velocity measurements in electrolytic solutions are of considerable importance as they enable us to test the validity of the several theories of electrolyte solutions. Besides it has been possible to estimate the number of water molecules attached to the ions in solution known as hydration number. Following the theory of Debye-Huckel, Gucker (1933) has derived certain limiting laws for the apparent molal compressibility and interpreted his experimental data in the light of this theory. Subsequently Bachem (1936), Scot, Obenhaus and Wilson (1934), Krishnamurthy (1950), Rao and Rao (1958) studied the apparent molal compressibilities in several solutions of electrolytes of different valence types and reported deviations from the limiting laws. While studying variations of ultrasonic velocities in solutions of electrolytes certain unusual features like decrease of velocity with increase of concentration have also been reported by some investigators in a few electrolytes namely, potassium iodide, lead nitrate, lead acetate and uranyl acetate. Very recently, Marks (1960) has calculated the hydration numbers for salts of alkali metals investigated by him.

As very little work has been done particularly on the estimation of hydration numbers and molar sound velocities in the case of solutions of electrolytes, the authors have taken up this investigation by taking measurements for about eleven new electrolytes.

## 2. RESULTS

Aqueous solutions of the following salts are studied.

- |                       |                       |                     |
|-----------------------|-----------------------|---------------------|
| 1. Lithium acetate.   | 5. Cadmium acetate    | 9. Barium bromide.  |
| 2. Sodium acetate.    | 6. Cadmium chloride.  | 10. Cadmium Iodide. |
| 3. Potassium acetate. | 7. Cadmium Bromide    | 11. Zinc Iodide,    |
| 4. Cobaltous acetate. | 8. Strontium Bromide. |                     |

The salts used are of either E. Merck or B. D. H. Solutions of different concentrations are prepared and the ultrasonic velocities are determined by a fixed path variable frequency interferometer accurate to  $\pm 1$  m/sec. The densities ( $\rho$ ) are determined by specific gravity bottle using a Bunge balance accurate to 1 mgm.

The values of adiabatic compressibility  $\beta$  and apparent molal compressibility  $\phi(k_2)$  are calculated by using the relations

$$\beta = \frac{1}{\rho V^2}, \quad \phi(k_2) = \beta \times \frac{1000}{C} - \frac{\beta_1}{d_1} \left( \frac{1000d}{C} - M \right)$$

Where  $\beta_1$  is the adiabatic compressibility of the solvent,  $C$  = Molar concentration and  $M$  = the molecular weight of the solute.

The variation of ultrasonic velocity, adiabatic compressibility and apparent molal compressibility with concentration for all the eleven salts investigated is shown graphically in Figs. 1 to 6.

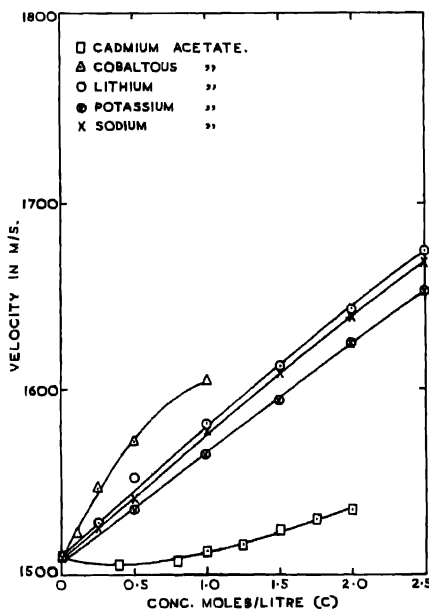


FIG. 1. Variation of ultrasonic velocity with concentration of the electrolyte.



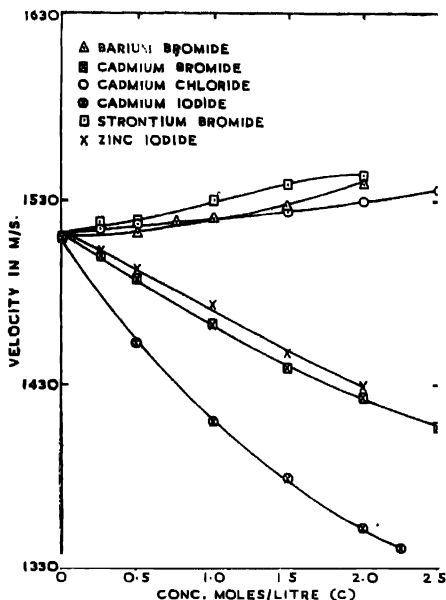


Fig 2 Variation of ultrasonic velocity with concentration of the electrolyte.

#### VARIATION OF ULTRASONIC VELOCITY AND ADIABATIC COMPRESSIBILITY WITH CONCENTRATION

It can be seen from Figs. 1 and 2 that in almost all the salts studied, the velocity is found to increase with concentration except in the cases of zinc iodide, cadmium bromide and iodide. Cadmium acetate solution showed a slight decrease in velocity initially and then showed gradual increase with concentration almost linearly. Although the anomalies of decrease of velocity with increase of concentration are noticed for these four salts, the adiabatic compressibility always showed the normal decrease with increase of concentration as can be seen in Figs. 3 and 4. The non-linear variation of velocity with concentration in the case of cobalt acetate is similar to the non-linear variation exhibited by some ferrous salts. A comparative study of the behaviour in the case of cadmium halides shows that the gradient of velocity-concentration graph decreases progressively from cadmium chloride to iodide. In a similar manner the velocities for barium bromide solutions are lower than those of barium chloride solutions studied by

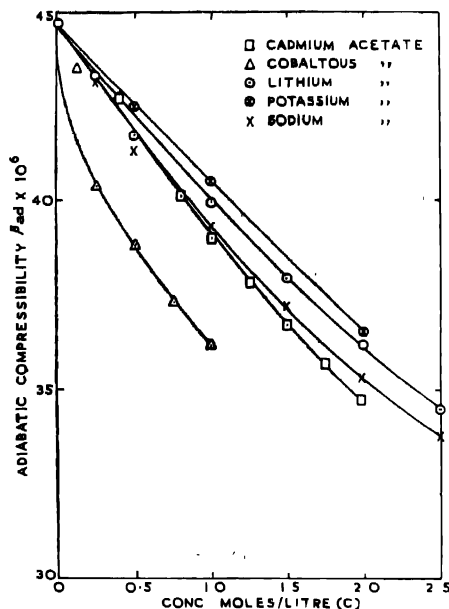


FIG. 3. Variation of adiabatic compressibility with concentration of the electrolyte.

Bachem (1936). It appears from these observations that for a fixed positive radical increase of atomic weight of the negative radical in the halogen group decreases the ultrasonic velocity. This is also borne out by data available for alkali halides studied by earlier works (Bachem, 1936; Krishnamurty, 1950 and Wada *et al.*, 1950).

It may also be noted that solutions of all the iodides studied so far show a decrease of velocity with concentration at first and later on show an increase in some cases.

The compressibility is always found to decrease with increase of concentration following closely the equation.,

$$\beta = \beta_1 + AC + BC^{3/2}$$

given by Gücker (1933).

From a systematic study of a series of aqueous solutions of some sulphates Marks (1944) has drawn the important conclusion that for a fixed anion the com-

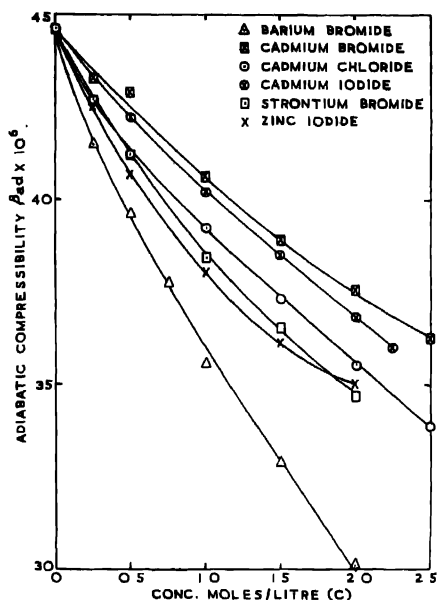


Fig. 4. Variation of adiabatic compressibility with concentration of the electrolyte.

compressibility at a particular concentration decreases with increasing ionic radius of the cation. Here an attempt is made to interpret the results of this investigation in the light of this rule. For this purpose the data available in literature are also utilised. The compressibility data for different electrolyte solutions at a fixed concentration either 0.5 M to 1.0 M are presented in Table I.

Comparing the sodium-fluoride, chloride and nitrate solutions with the corresponding potassium salt solutions for the same concentration it is seen that the compressibility of the potassium salt solutions is always less. This may be attributed to the higher radius of  $K^+$  ion compared to  $Na^+$  ion. Comparing the adiabatic compressibilities of 1M solutions of  $MgCl_2$ ,  $CaCl_2$ ,  $CdCl_2$  it is seen that  $CdCl_2$  and  $CaCl_2$  obey the above rule while  $MgCl_2$  shows deviation from it. This deviation may be due to the partial hydrolysis of magnesium chloride into magnesium hydroxide. All the three bromide solutions studied follow this rule quite well. The two iodides of zinc and cadmium show deviation from this rule. Similar deviations are noticed in the case of nitrates and sulphates of Fe, Co, Ni which hydrolyse in aqueous solutions. It is obvious that the effect of water of

TABLE I

Salt	Formula	Conc. Moles/ litre	$\beta \times 10^{12}$ Cm <sup>2</sup> /dyne	Ionic radius of the Å catio
Sodium fluoride	NaF (1-1)	0.5	42.14	0.95
Potassium fluoride	KF (1-1)	0.5	39.43	1.33
Sodium chloride	NaCl (1-1)	1.0	38.02	0.95
Potassium chloride	KCl (1-1)	1.0	36.46	1.33
Magnesium chloride	MgCl <sub>2</sub> (2-1)	1.0	35.70	0.65
Calcium chloride	CaCl <sub>2</sub> (2-1)	1.0	36.50	0.99
Cadmium chloride	CdCl <sub>2</sub> (2-1)	1.0	39.37	0.97
Sodium nitrate	NaNO <sub>3</sub> (1-1)	0.5	41.73	0.95
Potassium nitrate	KNO <sub>3</sub> (1-1)	0.5	41.03	1.33
Strontium nitrate	Sr(NO <sub>3</sub> ) <sub>2</sub> (2-1)	0.3	41.01	1.13
Barium nitrate	Ba(NO <sub>3</sub> ) <sub>2</sub> (2-1)	0.3	40.52	1.35
Nickel nitrate	Ni(NO <sub>3</sub> ) <sub>2</sub> (2-1)	0.3	41.80	0.69
Barium bromide	BaBr <sub>2</sub> (2-1)	1.0	35.96	1.35
Strontium bromide	SrBr <sub>2</sub> (2-1)	1.0	38.59	1.13
Cadmium bromide	CdBr <sub>2</sub> (2-1)	1.0	39.88	0.97
Zinc iodide	ZnI <sub>2</sub> (2-1)	1.0	37.27	0.74
Cadmium iodide	CdI <sub>2</sub> (2-1)	1.0	39.46	0.97
Magnesium sulphate	MgSO <sub>4</sub> (2-2)	0.5	36.77	0.65
Zinc sulphate	ZnSO <sub>4</sub> (2-2)	0.5	36.34	0.74
Iron sulphate	FeSO <sub>4</sub> (2-2)	0.5	38.80	0.75
Lithium acetate	Li(CH <sub>3</sub> COO)·2H <sub>2</sub> O (1-1)	1.0	39.15	0.60
Sodium acetate	Na(CH <sub>3</sub> COO)·3H <sub>2</sub> O (1-1)	1.0	38.54	0.95
Potassium acetate	K(CH <sub>3</sub> COO) (1-1)	1.0	39.77	1.33
Cadmium acetate	Cd(CH <sub>3</sub> COO) <sub>2</sub> ·2H <sub>2</sub> O (2-1)	1.0	38.32	0.97
Cobaltous acetate	Co(CH <sub>3</sub> COO) <sub>2</sub> ·4H <sub>2</sub> O (2-1)	1.0	35.52	0.72

hydration is to decrease the compressibility of the solution —If we however compare the three salts lithium, sodium and cadmium acetates having nearly the same number of molecules of water of crystallization, it will be seen that the compressibility decrease from lithium to cadmium where as the ionic radius increases from Li<sup>+</sup> to Cd<sup>++</sup> progressively. The deviation from this rule observed in the case of cobaltous acetate may be partly due to hydrolysis and partly due to the large

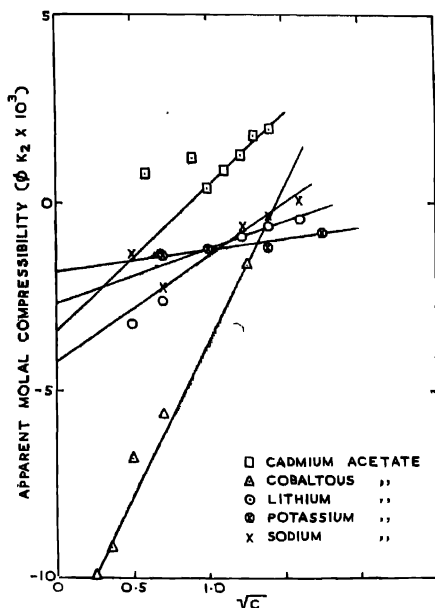


FIG. 5. Relation between apparent molal compressibility and square-root of concentration.

number of molecules of water of crystallisation, the high value of compressibility for solutions of potassium acetate compared to others in spite of its large ionic radius of 1.33 may be attributed to the lack of water of crystallisation.

#### APPARENT MOLAL COMPRESSIBILITIES AND ESTIMATION OF HYDRATION NUMBERS

It can be seen from Figs. 5 and 6 that the apparent molal compressibility  $\phi(k_2)$  varies almost linearly with square root of concentration in all cases except cadmium salts for which deviations are noticed particularly at lower concentrations. The values of  $\phi(k_2)$  for most of the salt solutions are generally negative and there are very few cases for which positive values are reported. In this investigation positive values of  $\phi(k_2)$  are observed for the case of cadmium acetate, bromide and iodide and strontium bromide solutions. The values of the gradients  $\frac{\partial \phi(k_2)}{\partial \sqrt{c}}$  are determined and presented in Table II along with the theoretically computed values.

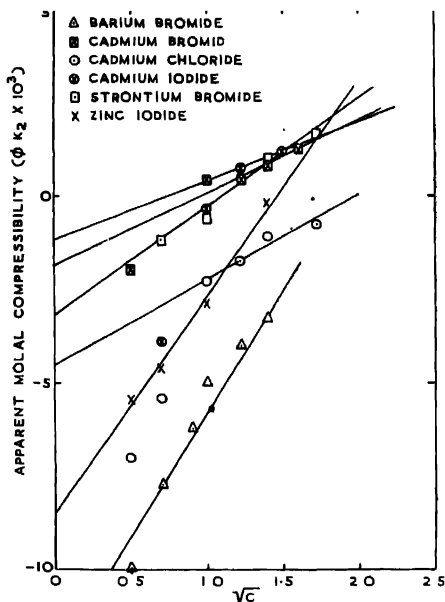


FIG. 6. Relation between apparent molal compressibility and square root of concentration.

TABLE II

Salt	Type of Electrolyte	$(\epsilon r^2 z_+^2 z_-^2)^{1/2}$	$\{\partial \phi(k_2)/\partial c^{1/2}\}$		$(K_2) \times 10^9$ $\alpha = 0$	Hydration number
			$10^{10}$ C.G.S. Theoretical	$10^4$ Exptl.		
Lithium acetate $2H_2O$	1-1	2.828	6.3	29.50	-2.90	3.60
Sodium acetate $3H_2O$	1-1	2.828	6.3	23.00	-3.55	4.40
Potassium acetate	1-1	2.828	6.3	12.50	-3.30	4.20
Cadmium acetate $2H_2O$	2-1	14.700	32.6	40.00	+3.50	4.40
Cubaltous acetate $4H_2O$	2-1	14.700	32.6	110.00	-22.90	28.50
Barium bromide	2-1	14.700	32.6	67.44	-12.20	15.40
Strontium bromide	2-1	14.770	32.6	15.80	-3.66	4.50
Cadmium bromide	2-1	14.700	32.6	43.00	-0.80	—
Cadmium iodide	2-1	14.700	32.6	34.00	-0.38	—
Cadmium chloride	2-1	14.700	32.6	26.66	-5.00	6.20
Zinc iodide	2-1	14.700	32.6	62.10	-9.18	1.40

In the (1-1) type electrolytes studied the slopes of almost all the solutions show deviations from the theoretical values but it is found that the experimental values are always higher. There is a fairly good agreement between experimental and theoretical values in the case of the (2-1) type salts cadmium acetate, bromide and iodide although these solutions showed unusual behaviour in other physical properties. Although strontium bromide and cadmium chloride belong to (2-1) valence type, their gradients are even smaller than the theoretical values of the (1-1) type electrolyte solutions. In general, it may be concluded from the above study of the apparent molal compressibilities that Gucker's limiting law is only in qualitative agreement with the experimental values.

It is well known that the water molecules in the immediate neighbourhood of ions in an electrolyte solution are intimately bound to the ions. This process is known as hydration. The first layer of water molecules attached to the ion is known as primary water of hydration. Estimation of primary hydration numbers of ions is now possible by several methods based on diffusion, ionic mobilities, activity coefficients etc. Hydration numbers can also be estimated from a study of apparent molal compressibility on the assumption that the ion as well as the primary water of hydration are incompressible compared to the free solvent molecules. Wada and Shimbo (1950) have given the following relation from which the hydration number can be calculated

$$\lim_{c \rightarrow 0} \phi(k_2) = -\beta_1 V_h$$

$V_h$  is the volume of primary water of hydration for more of the electrolyte. The limiting value  $\phi(k_2)$  can be obtained by extrapolating  $\phi(k_2)$  versus  $\sqrt{c}$  graph to zero concentration.

Using the experimental values of  $\phi(k_2)$  and  $\beta_1$  the values of  $V_h$  are estimated.

By making the further assumption that the molar volume of the solvent molecules in the primary hydration sheath is the same as that of the pure solvent, the combined primary hydration number for the electrolyte is obtained by dividing  $V_h$  by the molar volume of water. The experimental values thus obtained for all the electrolytes investigated are presented in the last column in Table II. The values of hydration numbers of lithium, sodium and potassium acetates are nearly of the same order of magnitude as the values 4, 5 and 5 for the ions  $\text{Li}^+$ ,  $\text{Na}^+$  and  $\text{K}^+$  respectively available in literature (Bell, 1958). This leads to the conclusion that the contribution due to the acetate radical is very low. The low values of 4.4 obtained for cadmium acetate shows that the hydration number of  $\text{Cd}^{++}$  ion is of the same order as  $\text{Na}^+$  or  $\text{K}^+$  ions although it is doubly ionised. Assuming the contribution of  $\text{Cl}^-$  ion to combined hydration number as unity as obtained from activity coefficients method, it will be seen that the data for  $\text{CdCl}_2$  leads to the same value of about 4 for the primary hydration number

of  $\text{Cd}^{++}$  ion. The abnormally low values of hydration number obtained for  $\text{CdBr}_2$  and  $\text{CdI}_2$  may be attributed to the anomalous variation of ultrasonic velocity with concentration and the non-linear nature of  $\phi(k_2)$  versus  $c^{\frac{1}{2}}$  plot. Cobaltous acetate gives an abnormally high value of 28.5 for the hydration number part of which may be due to hydrolysis. Taking the value for bromine as one, the hydration number for Sr comes out to be approximately 4 which is of the same order as  $\text{Na}^+$  or  $\text{K}^+$  ions. Similarly, the values obtained for  $\text{Ba}^{++}$  and  $\text{Zn}^{++}$  ions are 13 and 9 respectively.

#### MOLAR SOUND VELOCITY AND ASSOCIATION

Rao (1940) has shown that the molar sound velocity  $R$  given by  $\frac{\bar{M}}{\rho} (V)^{1/3}$  is independent of temperature for non-associated liquids. For associated liquids like water and alcohol,  $R$  varies appreciably with temperature and Weissler has utilised this variation for studying the change of relative association with temperature. It is well known that in the case of ideal solutions where there is no association or complex formation, the  $R$  value for the solution estimated by using the relation

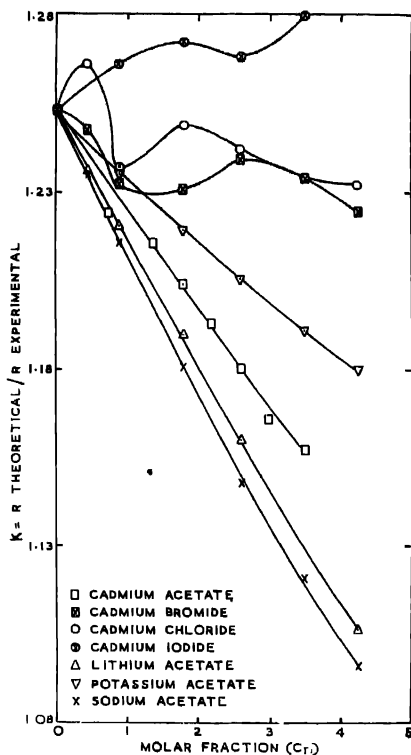
$$R = \frac{\bar{M}}{\rho} (V)^{1/3}$$

where

$$\bar{M} = \frac{n_1 M_1 + n_2 M_2}{n_1 + n_2}, \quad C_m = \frac{n_1}{n_1 + n_2}.$$

varies linearly with molar concentration of the solute  $C_m$  from the value of  $R$  for the solvent to that of the solute. The theoretically computed values of  $R$  from the known molar sound velocity increments for the atoms may be taken to be equal to the values for the ideal solution. The  $R$  values for the various solutions investigated are computed and it is found that the  $R$  variation with molar fraction is nearly linear in all cases except cadmium halides. It is also found that the computed values of  $R$  for the solutions are always higher than the theoretically experimental values. Taking the ratio  $K$  of computed to experimental value of  $R$  as an index of the degree of association and solvation, these values are plotted against molar fraction  $C_m$  as shown in Fig. 7. The value of  $K = 1.253$  obtained for zero concentration gives an idea of the degree of association in pure water which is responsible for the lowering of  $R$ . In the presence of an electrolyte the water molecules will be dissociated, consequently there will be a decrease in the value of  $R$ . Simultaneously there is also the phenomenon of solvation which increases the value of  $K$ . In all the acetates studied  $K$  decreases with increase of concentration showing a decrease of association of water molecules with concentration. In the case of aqueous solutions of cadmium chloride




 FIG. 7. Variation of "K" factor with molar fraction " $C_m$ "

bromide and iodide peculiar variations of the factor  $K$  are observed. The curves show maxima and minima indicating that the process involved is quite complex. This effect is particularly predominant in the case of cadmium iodide for which the  $K$  factor continues to increase with concentration, a feature which is quite unusual.

#### ACKNOWLEDGMENT

The authors are indebted to Council of Scientific and Industrial Research, New Delhi, for financial assistance given to this research project.

## REFERENCES

- Bell, R. P., 1958. *Endeavour*, **17**, 31.  
Buchem, Ch., 1936. *Z. F. Physik*, **101**, 541.  
Dutta, A. K. and Ghosh, B. B., 1943. *Ind. Jour. Phys.*, **17**, 19.  
Gueker, F. T., 1933. *Jour. Amer. Chem. Soc.*, **55**, 2700.  
Krishnamurty, B. 1950. *Jour. Sci. Ind. Res.*, **9B**, 215, **10B** 140 (1951).  
Marks, G. W., 1951. *Jour. Acous. Soc. America*, **31**, 936.  
Marks, G. W., 1960. *Jour. Acous. Soc. America*, **32**,  
Rao, M. R., 1940. *Ind. Jour. Phys.*, **14**, 100.  
Rao, K. S. and Rao, B. R., 1958. *Jour. Sci. Ind. Res.*, **17B**, 444.  
Scott, A. F., Obenhaus, and Wilson, R. W., 1934. *Jour. Phys. Chem*, **38**, 937.  
Wada, Shunbo, Oda., 1950. *Jour. Acous Soc. America*, **22**, 880.

# DIPOLE MOMENT AND RELAXATION TIME OF CERTAIN TRI-SUBSTITUTED BENZENES

J. SOBHANADRI

PHYSICS DEPARTMENT, ANDHRA UNIVERSITY, WALTAIR

(Received, September 12, 1960).

**ABSTRACT.** Using the author's method, dipole moment and relaxation time are determined for six tri-substituted benzenes from measurements at 3.26 cms. Benzene is used as the solvent.

In a previous paper (Sobhandri, 1960), the author has described a method for evaluating relaxation times and dipole moments of certain polar molecules in dilute solution from measurements of the dielectric constant  $\epsilon'$  and loss factor  $\epsilon''$  at a single frequency. This method is adopted in this paper for determining  $\tau$  and  $\mu$  of six tri-substituted benzenes for which no data are available in the literature. Benzene is used as the solvent. The experimental procedure was the same as the one described in an earlier paper (Narasimha Rao, 1956) from this laboratory.  $\epsilon'$  and  $\epsilon''$  are calculated using the standing wave method of Roberts and von Hippel (1946).

Tables I to VI give the values of  $\epsilon'$  and  $\epsilon''$  for different weight fractions along with the values of  $\frac{\epsilon''}{\epsilon' - \epsilon_{\infty}}$ . The mean value of  $\frac{\epsilon''}{\epsilon' - \epsilon_{\infty}}$  is taken to calculate the relaxation time and the dipole moment. The final values of  $\tau$  and  $\mu$  are collected in Table VII.

All the molecules investigated may be taken as rigid and approximately spherical since they are formed by nuclear substitution in the benzene ring. The first four molecules (the toluenes) are of the same molecular weight, the main difference among themselves being in the location of the different groups. The other two are similar.

The dipole moment values obtained agree well with the r.f. values determined by Narasimha Rao (1956). Though the values of  $\tau$  are almost of the same order for the four toluenes, a slight increase with increasing  $\mu$  is evident. A similar feature may also be seen in the case of the other two nitrobenzenes. However, both  $\mu$  and  $\tau$  are considerably higher in the nitro compounds than in the toluenes.

TABLE I  
6-Chloro 3-nitrotoluene  
 $\epsilon_1 = 2.270$

S.NO.	W	$\epsilon'$	$\epsilon''$	$\frac{\epsilon''}{\epsilon' - \epsilon_1}$
1	0 005578	2 296	0 01863	0 7164
2	0 006988	2 298	0 02141	0 7645
3	0 008614	2 300	0 02418	0 8060
4	0 010600	2 304	0 02828	0 8296
5	0 012590	2 314	0 03028	0 6880

$$\text{Mean } \frac{\epsilon''}{\epsilon' - \epsilon_1} = 0.7609$$

$$\tau = 13.19 \times 10^{-12} \text{ Sec.}$$

$$\mu = 3.09 \text{ D}$$

TABLE II  
2-Chloro 4-nitrotoluene  
 $\epsilon_1 = 2.270$

S.NO.	W	$\epsilon'$	$\epsilon''$	$\frac{\epsilon''}{\epsilon' - \epsilon_1}$
1	0 004501	2 299	0 02443	0 8424
2	0 005178	2 301	0 02731	0 8810
3	0 007437	2 312	0 03598	0 8509
4	0 009552	2 322	0 04612	0 8869
5	0 010610	2 327	0 05110	0 8964

$$\text{Mean } \frac{\epsilon''}{\epsilon' - \epsilon_1} = 0.8727$$

$$\tau = 15.14 \times 10^{-12} \text{ Sec.}$$

$$\mu = 4.17 \text{ D}$$

TABLE III  
6-Chloro 2-nitrotoluene  
 $\epsilon_1 = 2.270$

S.NO.	W	$\epsilon'$	$\epsilon''$	$\frac{\epsilon''}{\epsilon' - \epsilon_1}$
1	0 006063	2 294	0 01782	0 7425
2	0 007230	2 300	0 02065	0 6885
3	0 008710	2 304	0 02367	0 6961
4	0 10680	2 310	0 02855	0 7137
5	0 11650	2 316	0 03341	0 7261

$$\text{Mean } = 0.7134$$

$$= 12.37 \times 10^{-12} \text{ Sec.}$$

$$\mu = 3.11 \text{ D}$$

TABLE IV  
4-Chloro 2-nitrotoluene  
 $\epsilon_1 = 2.270$

S NO.	W	$\epsilon'$	$\epsilon''$	$\frac{\epsilon''}{\epsilon' - \epsilon_1}$
1	0.005089	2.296	0.02011	0.7734
2	0.006531	2.304	0.02745	0.8074
3	0.007396	2.310	0.02928	0.7319
4	0.009208	2.317	0.03671	0.7811
5	0.011480	2.329	0.04640	0.7863

$$\text{Mean } \frac{\epsilon''}{\epsilon' - \epsilon_1} = 0.7760$$

$$\tau = 13.46 \times 10^{-12} \text{ Sec.}$$

$$\mu = 3.66 \text{ D}$$

TABLE V  
2, 3-Dichloro nitrobenzene  
 $\epsilon_1 = 2.270$

S NO	W	$\epsilon'$	$\epsilon''$	$\frac{\epsilon''}{\epsilon' - \epsilon_1}$
1	0.00743	2.310	0.03698	0.9458
2	0.01040	2.319	0.04704	0.9601
3	0.01291	2.322	0.05070	0.9750
4	0.01614	2.327	0.05546	0.9729
5	0.01893	2.341	0.06963	0.9806

$$\text{Mean } \frac{\epsilon''}{\epsilon' - \epsilon_1} = 0.9669$$

$$\tau = 16.77 \times 10^{-12} \text{ Sec}$$

$$\mu = 3.82 \text{ D}$$

TABLE VI  
2, 5-Dichloro nitrobenzene  
 $\epsilon_1 = 2.270$

S.NO.	W	$\epsilon'$	$\epsilon''$	$\frac{\epsilon''}{\epsilon' - \epsilon_1}$
1	0.008802	2.306	0.0320	0.8896
2	0.01030	2.311	0.0367	0.8960
3	0.01239	2.316	0.0441	0.9588
4	0.01601	2.325	0.0532	0.9674
5	0.01893	2.329	0.0549	0.9309

$$\text{Mean } \frac{\epsilon''}{\epsilon' - \epsilon_1} = 0.9286$$

$$\tau = 16.11 \times 10^{-12} \text{ Sec.}$$

$$\mu = 3.41 \text{ D}$$

TABLE VII  
Temperature 28°C

Substance	$\tau \times 10^{12}$ sec.	$\mu$	$\mu_r f.D$
6-Chloro 2-nitrotoluene	12.37	3.11	2.93
6-Chloro 3-nitrotoluene	13.19	3.09	3.11
4-Chloro 2-nitrotoluene	13.46	3.66	3.63
2-Chloro 4-nitrotoluene	15.14	4.17	4.05
2, 5-Dichloro nitrobenzene	16.11	3.41	3.45
2, 3-Dichloro nitrobenzene	16.77	3.82	3.86

The author is deeply indebted to Prof. K. R. Rao for his kind and valuable guidance throughout the progress of the work. He is also grateful to the Government of India for the award of a scholarship.

#### REFERENCES

- Narasimha Rao, D. V. G. L., 1956, *Ind. J. Phys.*, **30**, 582.  
 Radhakrishna Murthy, Ch. and Narasimha Rao, D. V. G. L., 1956, *J. Sci. Industr. Res.*, **15B**, 346.  
 Roberts, S. and von Hippel, A., 1946, *J. appl. Phys.*, **17**, 610.  
 Sobhanadri, J., 1960, *Trans. Farad. Soc.*, **56**, 310.

# ON THE SINGLET $\rightarrow$ TRIPLET ABSORPTION IN AROMATIC COMPOUNDS IN GASEOUS STATE

S. C. SARKAR AND J. K. ROY

OPTICS DEPARTMENT

INDIAN ASSOCIATION FOR THE CULTIVATION OF SCIENCE, CALCUTTA-32

(Received, November 4, 1960)

## Plate IX

**ABSTRACT.** The absorption spectra in the near ultraviolet region of benzene and *o*-bromotoluene in the vapour state at the respective saturation pressures at the room temperature with a path length of about 62 feet have been photographed and compared with the spectra due to the substances in the liquid state having equivalent path lengths. It has been observed that although benzene in the liquid state with a path length 1.2 cms shows considerable absorption in the  $3300\text{\AA} - 3400\text{\AA}$  region due to singlet  $\rightarrow$  triplet transition, such absorption in the case of the vapour at 12 mm pressure, with a path length of 62 feet is very much less than that in the liquid. Similar results have been observed in the case of *o*-bromotoluene, the path length being 7 mm for the liquid and 62 feet for the vapour at 55 mm pressure. It has been pointed out that the singlet  $\rightarrow$  triplet absorption and the corresponding luminescence observed by previous workers in these cases are enhanced considerably in the state of aggregation of the molecules.

## INTRODUCTION

The singlet  $\rightarrow$  triplet absorption in some aromatic liquids was first observed by Lewis and Kasha (1945). Kasha also observed later (Kasha, 1952) that this absorption is strengthened when a heavy substituent atom is introduced in the benzene molecule and also when the molecules are dissolved in a solvent, the molecules of which contain such heavy atoms. Sirkar and Biswas (1956) and Biswas (1956) observed that the relative intensities of the bands and their positions in the luminescence spectra of frozen solutions of certain disubstituted benzene compounds depend to some extent on the nature of the solvent. Later, Roy (1959) proved conclusively that the luminescence in such cases was produced after absorption in the process of singlet  $\rightarrow$  triplet transition. As it was suggested by Sirkar and Biswas (1956) and also by Biswas (1956) that the luminescence exhibited by the molecules in the solid state at low temperatures might be due to formation of small groups of molecules it would be of interest to find out whether the singlet  $\rightarrow$  triplet absorption is an intrinsic property of the individual molecules in the gaseous state or it is developed in the state of aggregation. It is difficult to make experimental arrangement for this purpose, because the life time of the

triplet state is large and consequently the absorption is very weak. However, the absorption is exhibited by some of these liquids even when the absorbing path is only about 5 cms. If the absorption could be detected in these cases using absorption cells of thickness about 1 cm, it would be possible to study the absorption in the vapour with equivalent path length.

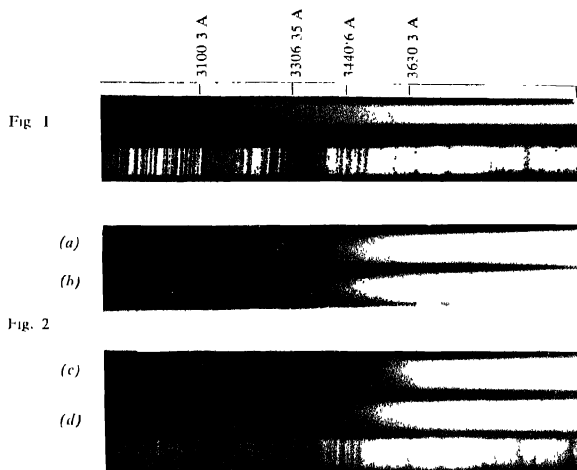
An attempt has, therefore, been made to study the absorption spectra in the near ultraviolet region of vapours of benzene and *o*-bromotoluene at pressures 12 cm and 5.5 cm respectively, the absorbing path being 18.90 metres long in each case. The spectra due to the liquids of equivalent thickness have also been photographed under identical conditions and compared with those due to the vapours. The results have been discussed in the present paper.

#### EXPERIMENTAL

The absorbing path of the vapour about 18.90 metres long was obtained by making two cells of straight pyrex glass tubes each about 32 feet long, provided with quartz windows and placed side by side parallel to each other. The continuous radiation from a tungsten filament lamp in glass bulb was made parallel with a quartz lens and passed through one of the tubes. The rays being then reflected by two right angled quartz prisms, passed through the other tube and were finally focussed on the slit of the spectrograph with another quartz lens. The radiation emitted by the lamp was found to have wavelengths longer than 3000 Å and therefore the absorption due to singlet → singlet transition was not possible in this arrangement. A bulb of Pyrex glass containing the liquid was connected to each of the absorption cells through a greasless stopcock and a side tube. First, the long cells were evacuated and the spectrum of the incident radiation passing through the tubes was recorded. The short empty cell for the liquid was next placed in the path of the rays and the long absorption cells were filled with the vapour of the liquid at the saturation pressure which was measured with a differential manometer. The pressure was found to be 120 mm in the case of benzene and 55 mm in the other case. After photographing the absorption spectrum of the vapour on a photographic film the long cells were evacuated and the short cell was filled with the distilled liquid and the absorption spectrum of the liquid was photographed on the same film with the same exposure and under identical conditions as in the case of the vapour.

The liquids benzene and *o*-bromotoluene used in the investigation were of chemically pure quality and they were first fractionated and then distilled in vacuum before being introduced in the bulb mentioned above. The thickness of the cell for the liquid was 1.2 cm for benzene and 7 mm in the case of *o*-bromotoluene. The spectra were photographed with Hilger medium quartz spectrograph on Agfa Isopan films, the time of exposure being about 10 hours in each case.





## Ultraviolet absorption spectra

Fig. 1. Absorber — evacuated cell, 18.90 metres long

Fig. 2 (a) Absorber — benzene (liquid), 12 mm long cell  
+ above evacuated cell  
(b) Absorber — benzene vapour at 120 mm of Hg,  
18.90 metres long cell  
(c) Absorber — *o*-bromotoluene (liquid), 7.0 mm long cell  
+ above evacuated cell  
(d) Absorber — *o*-bromotoluene vapour at 55 mm of Hg,  
18.90 metres long cell



## RESULTS AND DISCUSSION

The spectrograms for benzene and *o*-bromotoluene are reproduced in Figs. 2(a), 2(b), 2(c) and 2(d) in Plate IX, the spectrum of the incident continuous radiation passing through the evacuated absorption tube being shown in Fig. 1. These spectra show that in the case of benzene in the vapour state (Fig. 2b) there is only a very weak absorption in the region 3400 Å-3300 Å, while in the spectrum due to the liquid of equivalent thickness (Fig. 2a) there is appreciable absorption in this region. In the case of *o*-bromotoluene in the vapour state Fig. 2(d), however, there is weak absorption even in the region 3600 Å-3400 Å and the absorption in this region is very much stronger in the spectrum due to the liquid Fig. 2(c). It is evident, therefore, that even in the vapour state the *o*-bromotoluene molecule shows much stronger absorption due to singlet  $\rightarrow$  triplet transition than the benzene molecule and that such absorption increases enormously when the vapour is liquefied. Thus the substituent bromine atom in the *o*-bromotoluene molecule in the vapour state is responsible for the increase in the strength of singlet  $\rightarrow$  triplet absorption and shift of the region of absorption towards red. When the vapour is liquefied the influence of intermolecular forces increases the strength of the absorption enormously in the case of *o*-bromotoluene, but only slightly in the case of benzene. If in the liquid state the dissipation of energy of the excited state by processes other than radiation would result in the shortening of the life-time of the excited state and consequent increase in the absorption such increase would be of the same order in both the liquids. The increase is, however, much larger in the case of *o*-bromotoluene than in the case of benzene. In the former case the molecule has not only a heavy atom but it also has a permanent electric moment. On comparing the luminescence exhibited by different disubstituted benzenes, it is found that the luminescence produced by chloro- and bromotoluenes is much stronger than that exhibited by dichloro- or dibromobenzenes. It appears, therefore, that not only the presence of heavy atoms but also the formation of groups of associated molecules may be partly responsible for the luminescence and absorption due to singlet  $\rightarrow$  triplet transition.

## REFERENCES

- Biswas, D. C., 1956, *Ind. J. Phys.*, **30**, 143.  
Kasha, M., 1952, *J. Chem. Phys.*, **20**, 71.  
Lewis, G. N. and Kasha, M., 1945, *J. Am. Chem. Soc.*, **67**, 904  
Roy, J. K., 1959, *Ind. J. Phys.*, **33**, 209.  
Sirkar, S. C. and Biswas, D. C., 1956, *J. Chem. Phys.*, **24**, 470.

# Letters to the Editor

*The Board of Editors will not hold itself responsible for opinions expressed in the letters published in this section. The notes containing reports of new work communicated for this section should not contain many figures and should not exceed 500 words in length. The contributions must reach the Assistant Editor not later than the 15th of the second month preceeding that of the issue in which the letter is to appear. No proof will be sent to the authors.*

## 1

### ON THE VARIATION OF ELECTRONIC TRANSITION MOMENT $R_e$ IN CN VIOLET BAND SYSTEM

S. S. PRASAD

DEPARTMENT OF PHYSICS, L. S. COLLEGE, MUZAFFARPUR (BIHAR)

(Received, October 8, 1960)

Nicholls (1956) has discussed the variation of electronic transition moment,  $R_e(r)$ , with  $r$  for a number of band systems including the CN violet band system. He used the experimental transition probability data of Ornstein and Brinkman (1931) and obtained the following expression for the variation of  $R_e(r)$ ,

$$R_e(r) = \text{const. } (-1 + 2.579 r)$$

in the range  $0.95 < r < 1.32\text{\AA}$

Nicholls and Dixon (1958) have also studied the variation of  $R_e(r)$  with  $r$  in the case of CN red system excited in active nitrogen-carbon tetrachloride source and found that the expression

$$R_e(r) = \text{const. } (1 - 0.166 r)$$

represents the variation of  $R_e(r)$  with  $r$  in the range  $1.04 < r < 1.27\text{\AA}$ .

It may be noted that CN red system is due to a transition of the CN molecule from its excited  $A^2\pi_i$  state to  $X^2\Sigma^+$  state, while the violet system is due to one from excited  $B^2\Sigma^+$  to  $X^2\Sigma^+$  state. Now Bates (1949) has suggested that the variation of  $R_e(r)$  with  $r$  will be larger for perpendicular ( $\Delta\Lambda = \pm 1$ ) than for parallel ( $\Delta\Lambda = 0$ ) band system. If Bates' suggestion contains any germ of truth, so larger a variation of  $R_e(r)$  with  $r$  in CN violet system (as compared to that in CN red system) becomes doubtful.

Guided by this doubt, the recent experimental transition probability data for furnace excited CN violet system given by King and Floyd (1955) have been analysed for the trend of variation of  $R_e(r)$  with  $r$ . The method used was the  $r$ -centroid method used by Nicholls in his own analysis. The variation of  $R_e(r)$  with  $r$  has been found to be given in the same range of  $r$  by the expression

$$R_e(r) = \text{const} (1 + 0.03 r)$$

This trend is much slower than the trend reported by Nicholls (1956) and lends a further support to Bates' suggestion

It seems that the actual trend of variation of  $R_e(r)$  with  $r$  in CN violet band system is represented by the above expression. So far as the more rapid variation of  $R_e(r)$  with  $r$  obtained by Nicholls from an analysis of Ornstein and Brinkman's experimental data is concerned, it may possibly be due to some systematic error in the Ornstein and Brinkman's data.

This inference is also supported by a remark of Brinkman quoted by Smit (1946). According to Brinkman himself the accuracy of these results (i.e., of Ornstein and Brinkman's transition probability values) has been estimated to be not high. It was always hoped that the furnace measurements will yield accurate band ratio.

#### REFERENCES

- Bates, D. R., 1949, *Proc. Roy. Soc.*, **A196**, 217.  
 King, R. W. and Floyd, A. L., 1955, *J. Opt. Soc. (America)*, **45**, 249.  
 Nicholls, R. W., 1956, *Proc. Phys. Soc.*, **69A**, 741.  
 Nicholls, R. W. and Dixon, R. N., 1958, *Canad. Jour. Phys.*, **36**, 127.  
 Ornstein, L. S. and Brinkman, JI, 1931, *Proc. Roy. Acad. (Amsterdam)*, **34**, 33.  
 Smit, J. A., 1946, *Physica*, **12**, 697 and 699.

## BOOK REVIEW

PROCEEDINGS OF THE INTERNATIONAL SYMPOSIUM ON TRANSPORT PROCESSES IN STATISTICAL MECHANICS, Edited by I. Prigogine, Interscience Publishers, New York, and London, 1958, pp. 436. Price \$ 10.00

The present volume is a collection of 48 papers presented in the International Symposium on 'Transport Processes in Statistical Mechanics' held in Brussels in Aug. 1956. The volume has been divided into 14 parts, the theoretical papers being grouped in Parts I to XII and experimental papers in Parts XIII and XIV. The division of the book into the different parts is, however, not always quite logical.

In parts I to III the statistical mechanical basis of the steady state has been discussed from several points of view leading to the derivation of Boltzmann equation as used in the kinetic theory of gases, while part IX deals with the quantum-mechanical aspect. The other parts deal with specific problems. Transport phenomena (mainly thermal conductivity and diffusion) in solids are dealt with in Parts IV, V and VII while diffusion in gases and liquids are discussed in Parts VI and VIII respectively. Part X deals with some transport phenomena in liquids, particularly liquid helium. Part XI which covers about seventyfive pages is particularly welcome as it gives a fair idea of the controversial aspects of the basic principles of the thermodynamic theory of irreversible processes. This might stimulate activity in making the fundamentals more sound or in extending the domain of applicability of the theory of irreversible processes. In parts XIII and XIV some special experiments of topical interest are discussed such as viscosity and thermal conductivity of gases at high pressures, diffusion and thermal diffusion in gases and liquids, Soret effect, etc. The parts are followed by discussions which are quite interesting and useful.

The book gives, in a small compass, a good picture of the current effort being made to elucidate the intricate aspects of the Transport Theory from statistical mechanics. In view of the nature of the subject and the form of the book as a mere collection of papers, the present volume is likely to be useful only for research workers in the field.

- B. N. S.